VDA | Verband der Automobilindustrie

FAT | Forschungsvereinigung Automobiltechnik

FAT-Schriftenreihe 379

Dynamische Erfassung und Beurteilung von Situationsbewusstsein im Kontext des automatisierten Fahrens

DySAM – Dynamische Erfassung und Beurteilung von Situationsbewusstsein im Kontext des automatisierten Fahrens

Autoren/Forschungsstellen:

Fei Yan, Ulm University
Mark Eilers, Humatects GmbH
Bertram Wortelen, Humatects GmbH
Andreas Lüdtke, Humatects GmbH
Martin Baumann, Ulm University

Das Forschungsprojekt wurde mit Mitteln der Forschungsvereinigung Automobiltechnik e.V. (FAT) gefördert.

Executive Summary

The report presents the comprehensive development and analysis of the DySAM system, designed to enhance driver monitoring and situation awareness assessment. DySAM (Dynamic Situation Awareness Model) is a driver monitoring system that leverages sensor data to continuously evaluate a driver's situation awareness (SA) in real-time. The system is expected to help improving safety and optimizing human-machine interaction within autonomous vehicles or advanced driver-assistance systems (ADAS).

The report begins with an overview of the DySAM system and its connection to driver monitoring and situation awareness evaluation. By providing continuous SA assessments derived from sensor information, DySAM aims to enhance safety and driver performance in a wide range of driving scenarios.

Chapter 2 delves into the architecture and components of the DySAM system. It outlines three major components: the feature processing pipeline, the inference engine, and the probabilistic model. The feature processing pipeline collects sensor data and extracts indicators for SA assessment. The inference engine utilizes a probabilistic model to infer probability distributions over current SA based on the collected evidence.

Afterwards, chapter 3 details the datasets and annotations used for training and validating the DySAM models. It describes the experimental setup, including trials for different SAE (Society of Automotive Engineers) levels and non-driving related tasks. It explains how the data was divided into training and test sets for model development and evaluation.

Chapter 4 focuses on a detailed description of the implementation of the feature processing pipeline (FCP), which acts as an interface between the driving simulator and the DySAM system. The FCP collects sensor data, processes it into SA indicators, and buffers recent sensor information during runtime.

Finally, chapter 5 elaborates on the modeling of situation awareness using DySAM. It introduces two main types of models: NDRT (Non-Driving Related Task) models and SAGAT (Situation Awareness Global Assessment Technique) Score models. NDRT models assess situation awareness based on behavioral patterns and SA indicators, while SAGAT Score models evaluate SA using observed behaviors and SAGAT scores. The NDRT models are validated via the classification quality for the currently carried out NDRT. The SAGAT score models are validated via the prediction of the recorded SAGAT score. The chapter also discusses latent pattern discovery and model selection strategies.

In conclusion, the report underscores the significance of the DySAM system in advancing driver monitoring and situation awareness assessment. By leveraging sensor data and sophisticated models, DySAM offers valuable insights into driver behavior, which can help to enhance safety in various driving scenarios. Future research may focus on refining model architectures, optimizing feature selection, and integrating DySAM into real-world applications to further improve driver assistance systems and autonomous vehicles.

Zusammenfassung

Der Bericht stellt detailliert die Entwicklung und Analyse des DySAM-Systems zur verbesserten Fahrerüberwachung und insbesondere Situationsbewusstseinsbewertung vor. DySAM (Dynamic Situation Awareness Model) ist ein Fahrerüberwachungssystem, das Sensordaten nutzt, um das Situationsbewusstsein (SA) eines Fahrers kontinuierlich in Echtzeit zu bewerten. Das System soll dazu beitragen, die Sicherheit zu verbessern und die Mensch-Maschine-Interaktion in autonomen Fahrzeugen oder fortschrittlichen Fahrerassistenzsystemen (ADAS) zu optimieren.

Der Bericht beginnt mit einem Überblick über das DySAM-System. Durch die Bereitstellung kontinuierlicher, aus Sensorinformationen abgeleiteter SA-Bewertungen zielt das DySAM-System darauf ab, die Sicherheit in einer Vielzahl von unterschiedlichen Fahrszenarien zu erhöhen.

Kapitel 2 befasst sich mit der Architektur des DySAM-Systems. Es werden drei Hauptkomponenten beschrieben: die Feature-Processing-Pipeline, die Inferenz-Engine und das probabilistische Modell. Die Feature-Processing-Pipeline sammelt Sensordaten und extrahiert Indikatoren für die SA-Bewertung. Die Inferenz-Engine nutzt ein probabilistisches Modell, um auf der Grundlage der gesammelten Indikatoren Wahrscheinlichkeitsverteilungen über das aktuelle Situationsbewusstsein abzuleiten.

Anschließend werden in Kapitel 3 die Datensätze und die Datenannotation beschrieben, die zum Training und zur Validierung der DySAM-Modelle verwendet werden. Es beschreibt den Versuchsaufbau für verschiedene SAE-Automationsstufen und nicht fahrbezogener Aufgaben. Es erklärt, wie die Daten für die Modellentwicklung und -bewertung in Trainings- und Testsätze aufgeteilt wurden.

Kapitel 4 konzentriert sich auf eine detaillierte Beschreibung der Implementierung der Feature Processing Pipeline (FCP), die als Schnittstelle zwischen dem Fahrsimulator und dem DySAM-System fungiert. Die FCP sammelt Sensordaten, verarbeitet sie zu SA-Indikatoren und puffert aktuelle Sensorinformationen während der Laufzeit.

Abschließend wird in Kapitel 5 auf die Modellierung des Situationsbewusstseins mithilfe von DySAM eingegangen. Es werden zwei Haupttypen von Modellen vorgestellt: NDRT-Modelle (Non-Driving Related Task) und SAGAT-Score-Modelle (Situation Awareness Global Assessment Technique). NDRT-Modelle bewerten das Situationsbewusstsein anhand von Verhaltensmustern und SA-Indikatoren, während SAGAT-Score-Modelle SA anhand beobachteter Verhaltensweisen und SAGAT-Scores bewerten. Die Validierung der NDRT-Modelle erfolgt über die Klassifizierungsgüte einer aktuell durchgeführten NDRT und die der SAGAT-Score-Modelle über die Vorhersage des erfassten SAGAT Scores. Zudem werden in diesem Kapitel auch Strategien zur Entdeckung latenter Muster erörtert, sowie Strategien für die Auswahl von Modellvarianten diskutiert.

Der Bericht unterstreicht die Bedeutung des DySAM-Systems für die Weiterentwicklung von Fahrerüberwachungssystemen und der Situationsbewusstseinsbewertung. Durch die Nutzung von Sensordaten und hochentwickelten Modellen bietet DySAM wertvolle Einblicke in das Fahrerverhalten, die dazu beitragen können die Sicherheit in verschiedenen Fahrszenarien zu bewerten. Zukünftige Forschung könnte sich auf die Verfeinerung von Modellarchitekturen, die Optimierung der Indikatorauswahl und die Integration von DySAM in reale Anwendungen konzentrieren, um Fahrerassistenzsysteme und autonome Fahrzeuge weiter zu verbessern.

Table of contents

Abbreviations

2TBN	Two time-slice Bayesian Network
AUC	Area under curve
BN	Bayesian Network
BIC	Bayesian Information Criterion
CPD	Conditional probability distribution (/ density function)
DAG	Directed acyclic graph
DBIC	Discriminative Bayesian Information Criterion
DBN	Dynamic Bayesian Network
EM	Expectation-Maximization
FCP	Feature processing pipeline
FPR	False positive rate
JPD	Joint probability distribution (/density function)
MAP	Maximum a posteriori
MEMM	Maximum entropy Markov model
MLE	Maximum likelihood estimate
NDRT	Non-driving-related task
NIW	Normal Inverse Wishart
PDF	Probability density function
PMF	Probability mass function
ROC	Receiver Operating Characteristic
SA	Situation Awareness
SAGAT	Situation Awareness Global Assessment Technique
SART	Situation Awareness Rating Technique
SURT	Surrogate Reference Task
TPR	True positive rate
VBEM	Variational Bayes Expectation-Maximization

1 Introduction

According to SAE International (2021), drivers need to monitor the road and take over the driving task facing critical events at SAE Level 2. From SAE Level 3, drivers don't need to drive and monitor the traffic situation and only intervene when the automated system requests. Currently, many car manufacturers have introduced SAE Level 2 driving automation systems to the market, such as Telsa's Autopilot, Audi's Traffic Jam Assist, and BMW's Driving Assistant Plus (Teoh, 2020). Concerning SAE Level 3 driving automation system, Honda have released the first vehicle equipped with certified level 3 self-driving feature, namely "Traffic Jam Pilot" in 2021. Nevertheless, within these automation levels, humans still play a central role as system monitors at SAE Level 2 or as fallback-ready users at SAE Level 3 and are necessary for ensuring safety. For this purpose, it must be ensured that drivers can adequately take control of the vehicle, for example, in safety-critical situations or at system limits. For this to happen, drivers must have sufficient situational awareness (SA) when they need to intervene in the driving task. It requires an adequate perception of the elements in the environment, an understanding of their meaning, and a projection to the near future. (Endsley, 1995). This goes clearly beyond simple eye-tracking and can be essential for future driver monitoring in SAE Level 2 and Level 3 automation. The aim of the project "DySAM" was to develop and validate an algorithm for dynamic online assessment of SA in the context of SAE Level 2 / Level 3 vehicle automation.

1.1 Requirements for maintaining and building situational awareness at SAE Level 2 & Level 3

The already partially available assistance systems of driving automation introduce new challenges for maintaining and building situational awareness. These requirements are especially related to Level 2 and Level 3 driving automation according to the SAE classification (SAE, 2021).

Level 2 driving automation requires continuous monitoring of the system by the driver. Regarding the hand position to be adopted, many systems prescribe a "hands-on" (wheel); others explicitly allow a "hands-free" operation. In both cases, the driver's monitoring task requires sufficient situational awareness to adequately assess the vehicle's behavior. HMI approaches, often combined with driver monitoring, can assist the driver in maintaining situational awareness. This idea requires that situational awareness also be detectable or quantifiable during system use.

With Level 3 automation, the monitoring requirement is no longer required. Non-driving-related tasks can be allowed during automated driving within certain limits. Facing a takeover request, however, the driver must take over control of the vehicle and make all associated decisions within a certain takeover time budget. For this purpose, it is necessary to build situational awareness within a comparatively short time (e.g., 5-10 seconds), to continue driving safely. It would make sense to hand over the automation to the driver only after modelling the current situation awareness to ensure that it is sufficiently available. Furthermore, this modelling allows supporting the building of situation awareness by a suitable HMI concept.

2 Overview of the project

2.1 Project goal

The project's central objective is to develop and validate a measurement concept that can dynamically and online assess the current driver's situation awareness at SAE Level 2 or SAE Level 3 or predict it (especially in takeover situations). This will allow the design of future concepts of driver-vehicle interaction for SAE L2 and L3 systems that can adaptively respond to the instantaneous situation awareness state of the driver, e.g., to ensure adequate monitoring of an SAE Level 2 automation or adequate intervention at the system boundary for a SAE Level 3 automation.

2.2 Approach

Building adequate situation awareness requires the coordinated interaction of several cognitive processes. The generation and maintenance of situation awareness is a complex process for which there is no single, non-intrusive, real-time measurable variable that allows reliable assessment of situation awareness across a wide range of driving situations. What is needed, therefore, is a model that accounts for a range of measurable variables that correlate with the establishment and maintenance of situational awareness to enable a robust assessment. In addition, the parameterization of the model must both make do with limited or summarized data from the scientific literature, but also allow for the use of detailed time series of sensor data that may be noisy. This also means that the modeling language must allow for both simple manual model specification based on literature results and machine learning based on time series data, as well as a combination of both. In addition, human behavior generally exhibits high variability. Therefore, when modeling human behavior, it is typically assumed that confounding factors not explicitly accounted for by the model can have a significant impact on model performance. This uncertainty, as well as the uncertainty arising from sensor inaccuracies in the physiological measurement procedures, must be taken into account when choosing the modeling method.

For the aforementioned requirements, Dynamic Bayesian Networks (DBNs) - a model class of probabilistic graphical models (Koller & Friedman, 2009) - are particularly suitable. DBNs allow modeling discrete-time dynamic processes under uncertainty. To do so, the complex joint probability distribution of a time series of random variables is factorized into a product of simpler parameterizable probability distributions based on statistical and/or causal relationships between the variables. This factorization can be visually represented as a direct acyclic graph. Fully parameterized, a DBN can be used to compute probability distributions over (subsets of) non-observable variable(s) given evidence of all observable variables. These DBNs will be used in this project for dynamic, real-time modeling of situation awareness.

2.3 Overview of work packages

The DySAM project was comprised of three work packages (WPs). WP1 focused on the theoretical concept of situation awareness (SA) in the context of automated driving at SAE Level 2 and Level 3, the results of which are documented in section 3. In WP2, the concept for modeling and measuring situation awareness was defined, including the assessment of different measurement principles and the selection of a suitable method (WP 2.1), development and implementation of an algorithm for online assessment of based on the selected measurement principle (WP 2.2), and planning and implementation of a driving simulator study to validate this modeling on the basis of situations or

usage scenarios known to influence SA (WP 2.3). The results of W2 are documented in sections 4 and 5. Lastly, WP3 focused on the documentation of the project results, cumulating in this report.

3 Theoretical concept of Situation Awareness

The theoretical concept of situation awareness identifies not only the psychological processes underlying situation awareness but also their observable correlates (e.g., specific parameters of gaze behavior, hand and body posture, etc.), which can serve as candidates for possible measures of situation awareness. In addition, the different central functions of situation awareness for automated driving are analyzed on SAE L2 and on SAE L3. For this purpose, a task analysis is used to analyze the main tasks involved in driving with SAE L2 and L3 systems, e.g., monitoring the system within and at the system boundaries or taking control in SAE L3 systems after a takeover request.

3.1 Task analysis

The task analysis has been conducted separately for SAE Level 2 and SAE Level 3. The objectives associated with the tasks, situation, the decisions that must be made to achieve the objectives, and the information necessary to make those decisions are considered (see Figure 1).

At SAE Level 2, a driver's task is to continuously supervise the traffic environment, to achieve the goal of maintaining the situation awareness to ensure traffic safety. When a system reaches its limitation, the driver needs to check the system performance and also the HMI to make decisions. If the driver decides to take over the control from the SAE Level 2 system, a take-over action will be executed via putting hands on the steering wheel or using gas/brake pedal. Giving an example, at 8:15 in the morning, David drives 6.5 km stretch of urban roadway with a speed limit of 50 km/h to his company. After 2 minutes, he activates the ACC system. After 3 minutes of turning to the left, a cyclist appears in front of David's car, but the ACC is not able to recognize the relatively small bicycle due to the sensor limitation and keep gradually close to the cyclist. At the same time, a visual warning is shown in the speedometer. After receiving these warnings, David needs to have a look at the HMI and make decisions, and take over control as soon as possible.

At SAE Level 3, driver doesn't need to supervise the environment, but needs to intervene when the system issues a "request to intervene (RtI)" due to the system error or system limitation. For this, driver is actually called "fallback-ready" user and needs to build situation awareness on time to be able to take over the control when needed. When a driver is busy, the NDRT and a takeover request come due to the system limitation in the current scenario, the driver needs to observe the environment first before taking over the control from the SAE Level 3 system. If a driver decides to take over, a take-over action will be executed via putting hands on the steering wheel or using gas/brake pedal. For instance, at 8:15 in the morning, Fiona drives a 30 km stretch of highway at 130 km/h limit to his company. At the beginning, she drives manually. After 2 minutes, she activates the automation mode of her SAE Level 3 system and begins to watch YouTube videos. After 8 minutes, a broken vehicle appears suddenly in front of Fiona's car and the system reaches its boundary. Hence, a TOR is shown to Fiona via visual and acoustic warnings. As Fiona is busy with watching videos and not aware of the surroundings, she needs to check the traffic situations and make decisions. In the end, she takes over the control by putting her hands on the steering wheel and her feet on the gas pedal.

The results of task analysis at SAE Level 2 and Level 3 can be relevant for developing driving scenarios for the validation study in WP 2.3.

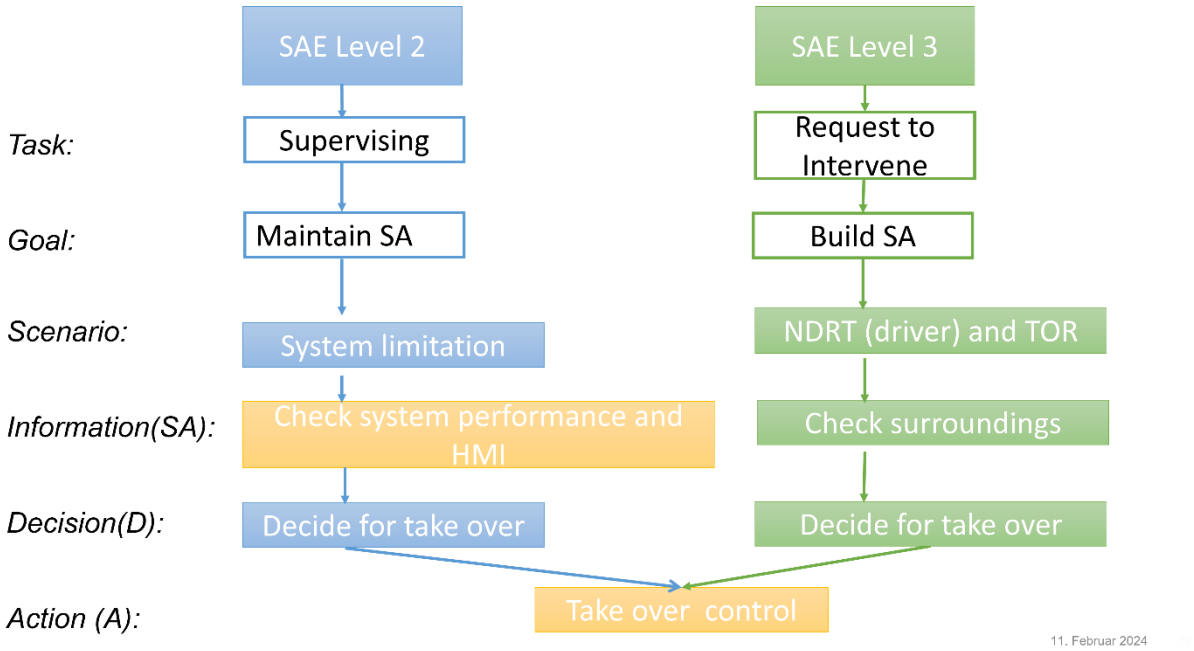

Figure 1: Task analysis for SAE Level 2 and SAE Level 3 associated with task, goal, scenario, information, decision and action (SA: situation awareness; HMI: human- machine interface; NDRT: non-driving related task; TOR: take-over request).

3.2 Psychological processes underlying situation awareness

Oriented on Endsley's situation awareness model (see Figure 2), the relevant psychological processes underlying situation awareness including perceiving the relevant information from the environment, interpreting the perceived information, making decisions and executing actions. The corresponding components (task, goal, situation, information, decision and action) involved in the task analysis at SAE Level 2 and SAE Level 3 can be allocated to the corresponding psychological process. Based on the task analysis and psychological process, some metrics that can be considered measures of situation awareness can be retrieved, especially while identifying the necessary information needed for SAE Level 2 and Level 3. For example, when drivers need to check the traffic environment or the HMI, their gaze behaviors, hand and body postures etc. can serve as candidates for measuring situation awareness. However, the retrieved metrics in this way are limited and therefore a systematic review on the relevant indicators that can measure situation awareness is necessary.

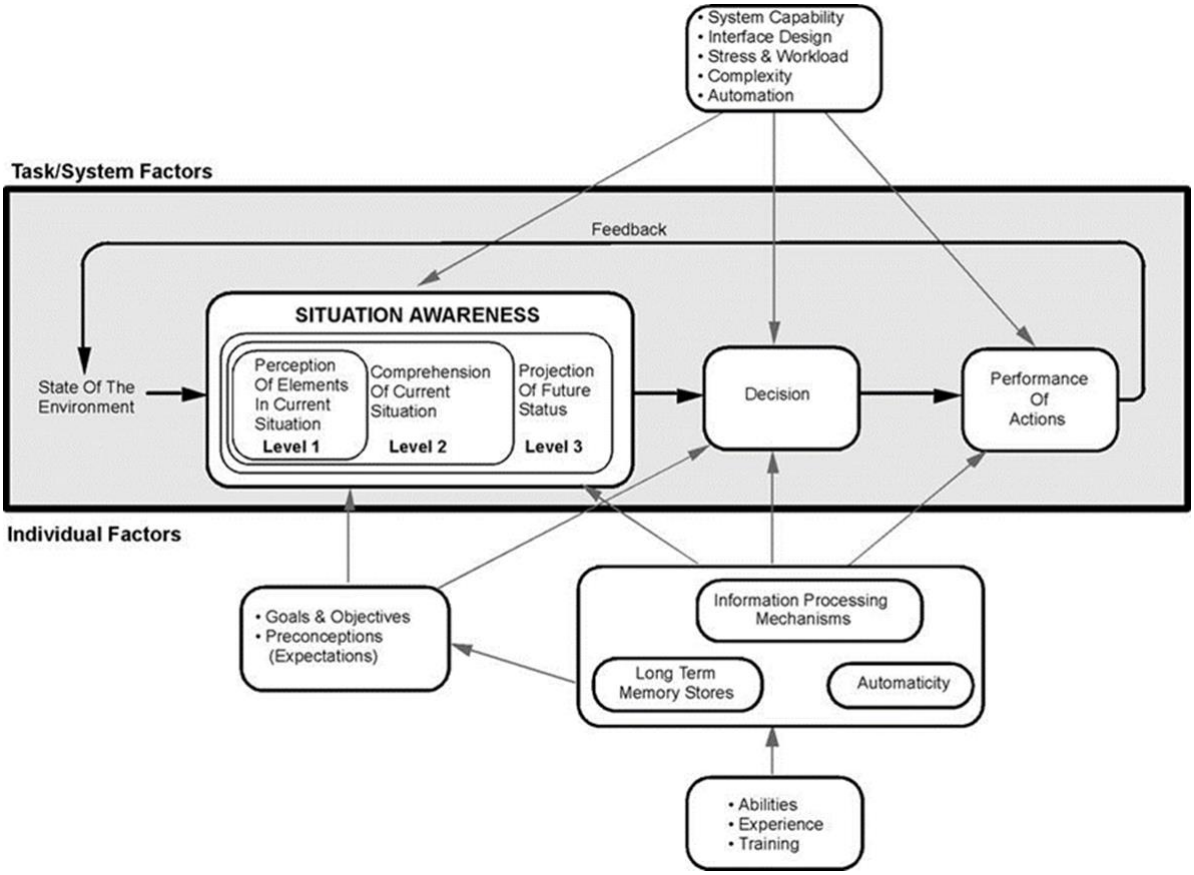

Figure 2: Situation awareness model.

3.3 Metrics for measuring situation awareness

An analysis of current research literature on situational awareness, particularly in the context of automated driving has been conducted on SAE Level 2 and Level 3. Relevant channels of publication of scientific papers (journals such as Transportation Research Part F: Traffic and Transport Psychology, Accident Analysis & Prevention, Human Factors, Safety Science, Ergonomics, Theoretical Issues in Ergonomics Science, etc., as well as proceedings of relevant international meetings, such as International Annual Meeting HFES, Automotive UI, CHI, etc.) has been searched. We first defined the inclusion criteria for the literature review, which should include publications that measure situation awareness or model situation awareness art SAE Level 2 and SAE Level 3. In addition, a review paper "Physiological Measurements of Situation Awareness: A Systematic Review" by Zhang et al. (2023) and its corresponding reference papers are used to guide the literature review. A total of 19 publications were identified after systematic analysis by domain experts. The associated indicators [1]for measuring situation awareness with their assigned categories can be seen in Figure 3.

[1] The list containing relevant publications and the descriptions of metrics has been submitted to FAT in the first project period.

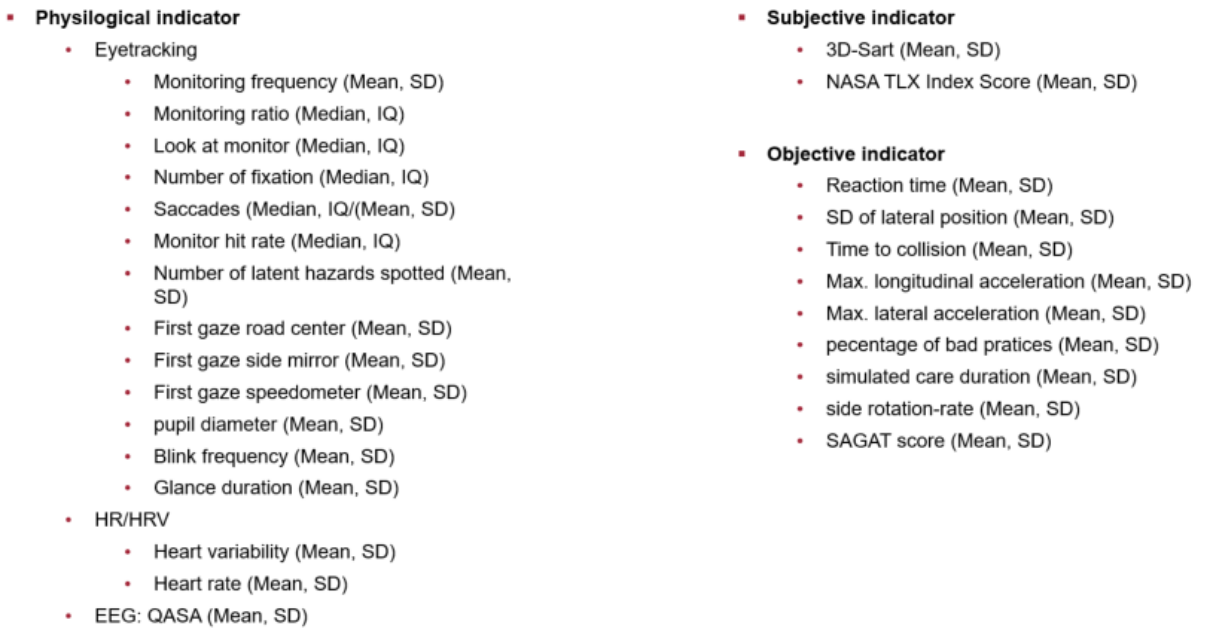

Figure 3: Categories for indicators of situational awareness.

In order to select representative indicators that can dynamically measure situation awareness, three categories of criteria have been considered. Firstly, the measurement-theoretical criteria, such as reliability, validity, sensitivity, specificity, accuracy have been taken into account. Reliability refers to the consistency of a measure (whether the results can be reproduced under the same conditions). Validity refers to the accuracy of a measure (whether the results really do represent what they are supposed to measure). Sensitivity and specificity mathematically describe the accuracy of a test which reports the presence or absence of a condition: Sensitivity (true positive rate) refers to the probability of a positive test, conditioned on truly being positive; specificity (true negative rate) refers to the probability of a negative test, conditioned on truly being negative. Accuracy refers to how close a measurement is to the true value. Each criterion in this category has been set up with three levels: low, medium, and high. After checking in the literature and discussing with domain experts, indicators shown in Figure 3 were filled with the levels for these theoretical criteria respectively. Only the indicators labelled with at least medium level of these criteria are further considered for modelling situation awareness. Secondly, the criteria regarding modeling situation awareness have been used, such as real-time capability, scenario (in)dependence, operationalizability, relevance/suitability for predicting SA. For this category of criterion, indicators should not require knowledge about the full driving session (real-time capability) and don't require specific knowledge about the environment or context (scenario (in)dependence). Knowledge about the environment and driving context would require a set of suitable vehicle sensors and an interpretation of the driving context with respect to SA. These aspects would largely increase the system complexity. In addition, indicators related to time intervals must be implementable via sliding windows (operationalizability) and relevant to predict situation awareness (relevance/suitability for predicting SA). At last, statistical significance test and priority of indicators have also been considered. The indicators that have significant influence on situation awareness empirically are considered. Also, indicators that have priority in predicting situation awareness are selected, such as pupil diameter, monitoring frequency, saccade frequency (Zhou, Yang, & De Winter, 2021). After considering these criteria and discussing with domain- experts, eight specific indicators have been suggested: Pupil diameter, blink frequency, glance duration,

monitoring frequency, saccade frequency, yaw movement of head, heart rate variability, and hands on detection. In the following, the definitions provided in the respective literature are provided. For the practical utilization of these indicators in DySAM, we occasionally rely on alternative definitions, better suited for the scenarios and use cases addressed in DySAM (c.f., Section 5.1.3)

- *Pupil diameter* is defined as the average pupil size in each condition in relation to the average pupil size during the entire experiment in mm, which can indicate changes in a person's cognitive workload (Klingner, Kumar, & Hanrahan, 2008).
- *Blink frequency* is measured in numbers per minute, and the eyelid closed for at least 80 ms for the movement can be considered as a blink (Faure, Lobjois, & Benguigui, 2016).
- *Glance duration* is the average time in seconds spent in the windshield area within one glance, which is positively correlated with situation awareness (Zhang, et al., 2023).
- *Monitoring frequency* is defined as the number of glances on AOIs / duration section [1/s] and can be considered as an indicator for attentional shifts (Kunze, Summerskill, Marshall, & Filtness, 2018).
- *Saccade frequency* describes the number of rapid eye movements between several fixations, in times per minute (Law et al., 2019), which acts as a potential indicator for attention shifts during visual search and scanning (Eriksson & Stanton, 2017).
- *Heart rate variability* is measured using standard deviation of normal-to-normal RR intervals (SDNN) in ms, which is negatively correlated with situation awareness (Sun, Wanyan, Wu, & Zhuang, 2017).
- *Yaw rate* is defined as the mean side rotation rate of the head [degree/s]), which can potentially indicate whether a driver is more situationally aware or unaware (Schewe, Cheng, Hafner, Sester, & Vollrath, 2019).
- *Hands-on detection* can measure drivers' attention, as people tend to position their hands differently or vary their grip force depending on how attentive they are (Morando, Gershon, & Mehler, 2021).

These metrics are associated with the perception level and interpretation level of SA underlying the psychological process. Based on these, a theoretical concept of situational awareness in the context of automated driving on SAE L2 and L3 has been created and defined.

4 Data collection and validation study

To validate the models created in DySAM, data sets are required that not only contain the sensor data for the models, but also annotations about the driver's current situational awareness. For this purpose, validation studies were carried out in the project. The general technical structure of the DySAM system is described below, as it was also used for the validation studies. This is followed by a description of the study implementation and data recording, as well as an explanation of the validation approach.

4.1 The DySAM system

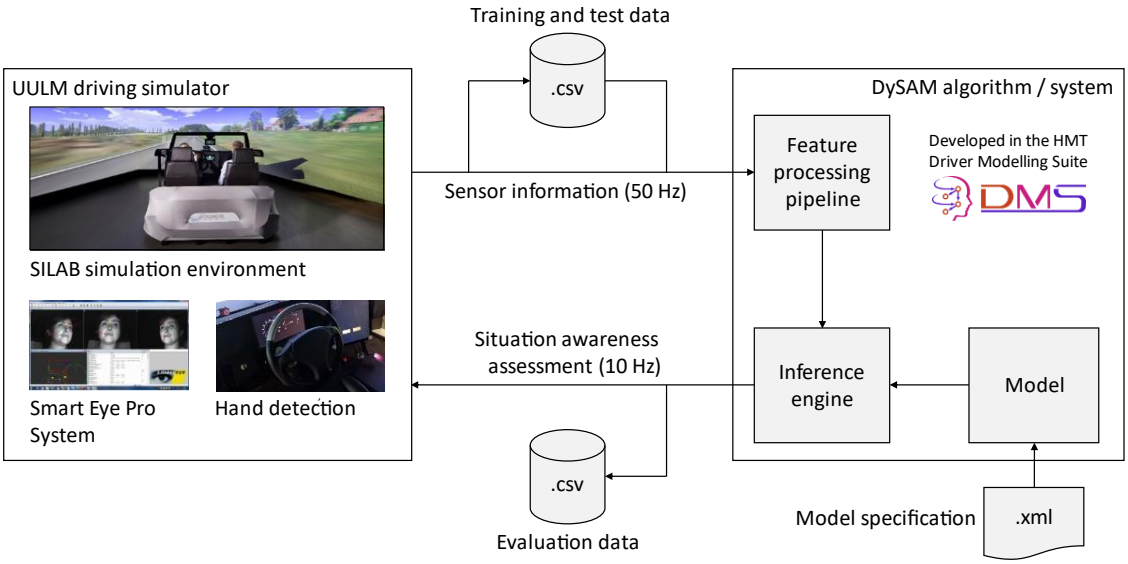

Figure 4: Overview of the DySAM system.

The DySAM system is conceptualized as a driver monitoring system that continuously provides assessments about the driver's situation awareness derived from sensor information about the driver. An overview of the system as implemented in the project is shown in Figure 4. The system is comprised of three major components: a feature processing pipeline, an inference engine, and a model. The feature processing pipeline collects the high-frequency sensor information provided by a driving simulator and processes them into a set of indicators or features to be used for assessing the situation awareness. The static driving simulator has a 190° viewing area and is equipped with a two-seater mock-up with a flexible interior. Three projectors (1920 px x 1080 px each, 5760 px x 1080 px in total) fill three screens (3.3 m x 2.1 m) for the front and side view. The rear view is generated by three screens at the positions of the rear-view mirror and the two side mirrors (each 7" with 800 x 400 px; 16:9). To simulate the traffic environment, the simulation software SILAB simulation software is used to simulate the traffic environment. The remote eye tracking system SmartEyePro, which uses four cameras to record the head and eye movements of test subjects at up to 120 fps, is integrated into the simulator and allows the exact recording of gaze behavior with high temporal resolution without affecting the test subject. In addition, 14 sensors implemented in SILAB via MQTT server are placed evenly inside the steering wheel enables the measurement of hand detection. The model is a probabilistic (graphical) model, whose structure and parameters can be configured via specification files. Every 100ms, the inference engine uses the model to infer probability distributions over the current situation awareness given the current evidence of the indicators provided by the feature processing pipeline. The output of the inference engine can then be provided to any consumer, e.g., to trigger interaction strategies or HMI output.

4.2 Data Collection

The data required for the parametrization and validation of the DySAM system, were collected in a validation experiment that was conducted in the driving simulator at Ulm University. A total of 37 valid samples (27 female, 10 male), with an average age of 23 years (SD = 4.95), passed the quality criteria and could be further processed.

4.2.1 Design

As a dependent variable, situation awareness was assessed in terms of gaze behavior including monitoring frequency, saccades frequency, mean pupil diameter, blink frequency and glance duration, head movement, as well as hand position. We manipulated the level of Automation (L2, L3) as a within-subjects-factor and non-driving related task (NDRT; none, auditory, visual) as a between-subjects-factor in a 2 x 3 mixed design. The participants were randomly assigned to the conditions. In Level 2 automated driving, the subject had to constantly monitor the situation and take control or reactivate the automation at their own discretion. Furthermore, they were not allowed to take their hands off the steering wheel for more than 15 seconds.

4.2.2 Driving Scenario

A three-lane highway scenario was considered for the evaluation study. For the driving scenario at SAE Level 3, the ego vehicle first drove in the right lane automatically at a speed of 130 km/h. After two minutes of driving, the ego vehicle changed to the middle lane due to the slow lead vehicle. After four minutes of driving in the middle lane, the scenario was frozen, and SAGAT questions were given. After the SAGAT questionnaire, the scenario continued until a traffic crash occurred in the front, where the SAE Level 3 system reached its limit and issued a TOR, the driver needed to take over control. The difference of the driving scenario at SAE Level 2 to SAE Level 3 is that, the duration of driving on the middle lane is seven minutes and that no TOR was given.

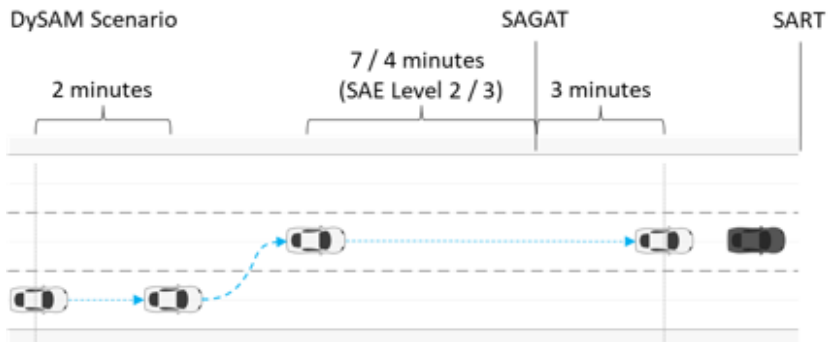

Figure 5:The driving scenarios at SAE Level 2 and SAE Level 3 for the validation study.

4.2.3 Material / Stimuli

The simulation was implemented using the SILAB Version 6.5 software environment and a touchscreen was placed in the center console to enable or disable the automation function. Three NDRT (Non-driving-related Tasks) were used to trigger different levels of situation awareness. As a visual NDRT, Surrogate Reference Task (SuRT) could be displayed in the center console. The participants had to identify a larger circle among several slightly smaller distractors. As an auditory NDRT, a 2-back task was used, where subjects heard a series of numbers, and they had to say it out when they heard the same number as two steps before. In the third condition, without NDRT, the subjects were theoretically able to concentrate exclusively on the driving task.

4.2.4 Procedure

In the beginning, participants were welcomed and brought to the driving simulator, where the eye tracker was calibrated, and they drove manually to familiarize themselves with the driving simulator. Each participant had two drives, starting from the right lane (see section 4.2.2). After the takeover

situation at the warning triangle, the participant was asked to drive to the right-hand side and stop. They were given the SART questionnaire on the tablet. After finishing it, they began the second drive after the instructor gave them the corresponding instructions.

4.3 Validation systematics for modeling situation awareness

A validation systematics is needed to, on the one hand, enable reliable recording of situational awareness but is independent of the measured variables that are included in the modeling. On the other hand, the measurement of the modeling parameters must not be influenced by the recording of this "ground truth". A combination of subjective and objective behavioral parameters could be the most promising solution.

4.3.1 SAGAT

One objective measure to assess the subjects' SA is the Situation Awareness Global Assessment Technique (SAGAT) (Endsley, 1995). It is a Freeze Technique, meaning that the simulation is frozen, and the displays are blanked at randomly selected times (Endsley, 1988). The subjects are then asked about their perception of the situation at that time. The SAGAT is a global measure tool that consists of items about all SA requirements, including the level components: Perception of elements in the current situation, comprehension of the current situation and projection of the future status (Endsley, 1988; 2019). To evaluate the subjects' SA, their answers are compared to the data from the simulation computer representing the actual situation. Based on these results, a composite SAGAT score is calculated (Endsley, 1988) .

4.3.2 SART

One subjective self-rating technique for SA is the Situation Awareness Rating Technique (SART; Liu et al., 2014). It is a ten-dimensional rating scale, which could be grouped into the three dimensions: Demand on attentional resources, supply of attentional resources and understanding. The calculation of the SART score is based on a subtraction of the results of each of these three major groupings: SA=Understanding-(Demand-Supply) (Liu, Wanyan, & Zhuang, 2014).

4.3.3 Results of Validation Systematics

In the validation study (see section 4), SAGAT and SART questionnaires are used to provide the "Ground Truth" of situation awareness. The mean and standard deviation of SAGAT scores and SART scores are shown in Table 1.

Table 1: Mean and standard deviation of the participants' answers in the SAGAT and SART.

Condition	SAGAT		SART	
	Mean	Sd	Mean	Sd
Level 2, no NDRT	55.00	15.08	11.25	4.79
Level 2, auditory NDRT	28.33	21.67	7.17	4.20
Level 2, visual NDRT	47.69	31.13	5.23	8.03
Level 3, no NDRT	67.69	23.86	11.38	6.38
Level 3, auditory NDRT	38.33	26.23	7.83	5.95
Level 3, visual NDRT	30.00	27.63	6.25	5.55

At SAE Level 2, The subjects' SA measured by the *SAGAT* differed significantly depending on the NDRT ($F_{(2,34)} = 4.03, p = .027; \eta^2 = 0.19$) (see Figure 6). The participants were possibly more aware of the situation when they did not have to complete any NDRT than when they had to focus on the auditory task (Bonferroni-test p= .029). At SAE Level 3, the subjects' SA measured by the *SAGAT* was also significantly different depending on the assigned condition ($F_{(2,34)} = 7.38, p = .002; \eta^2 = 0.30$). The visual (Bonferroni-test p= .003) as well as the auditory (Bonferroni-test p= .02) NDRT were apparently more distracting from the situation than the condition without any additional task. Neither SAE Level 2 driving ($F_{(2,34)} = 3.25, p = .051$) nor SAE Level 3 driving ($F_{(2,34)} = 2.43, p = .103$) evoked significant differences in the participants' self-assessments (*SART*) regarding SA (see Figure 7).

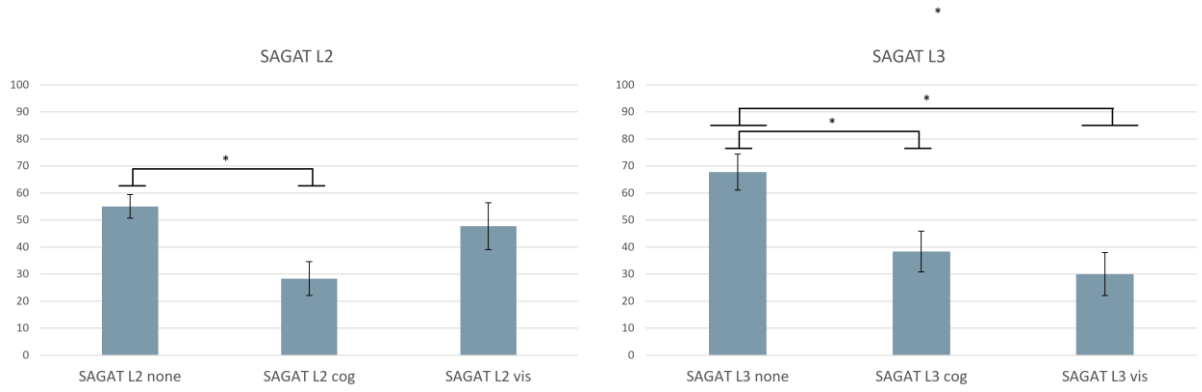

Figure 6: SAGAT scores at SAE Level2 and Level 3 (none: no NDRT; cog: auditory NDRT; vis: visual NDRT).

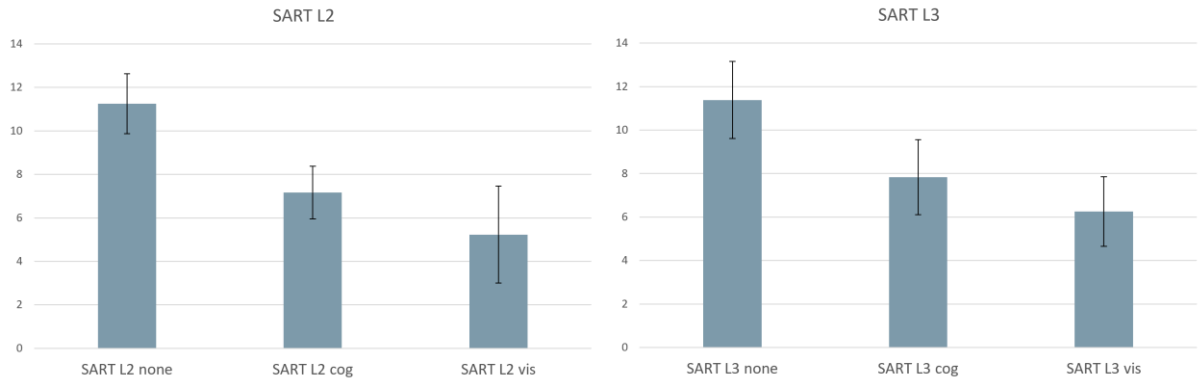

Figure 7: SART scores at SAE Level2 and Level 3 (none: no NDRT; cog: auditory NDRT; vis: visual NDRT).

5 Online assessment of driver situation awareness via Dynamic Bayesian Networks

The project's central objective was the development and validation of algorithms for online assessment of a driver's current SA at SAE Level 2 or SAE Level 3. To achieve this objective, we conceptualized a driver monitoring system that continuously provides assessments about the driver's SA derived from sensor information about the driver, referred to as the DySAM system.

An overview of the system as implemented in the project has been shown above in Section 4.1 (see Figure 4). The system is comprised of three major components: a feature processing pipeline, an inference engine, and a model. The feature processing pipeline collects the high-frequency sensor information provided by a driving simulator and processes them into a set of indicators or features to be used for assessing the SA. Every 100ms, the inference engine uses the model to infer probability distributions over the current SA given the current evidence of the indicators provided by the feature processing pipeline. The output of the inference engine can then be provided to any consumer, e.g., to trigger interaction strategies or HMI output.

The remainder of this section is structured as follows: Section 5.1 describes the feature processing pipeline of the DySAM system, detailing what input data is used, how it is processed, what kind of situation awareness indicators are considered and how they are obtained. Section 5.2 introduces the three different kinds of probabilistic models, we considered for the online assessment of SA in DySAM. Section 5.3 provides an overview of how the data collected during the validation study was transformed into training datasets for parameter estimation and structure learning and test datasets for validation of these models. Section 5.4 provides an analysis of the characteristics and utility of the situation awareness indicators considered in DySAM, given the training data. Section 5.5 provides the results of the structure learning process used to fully specify the three different kinds of probabilistic models, conceptualized in Section 5.2. Lastly, Section 5.6 focusses on the evaluation procedure and results of the trained models. We note that this section assumes some familiarity with probabilistic modelling, mathematical background material including definitions of DBNs and the distributions, and primers on probabilistic inference, Bayesian parameter estimation, and structure learning is provided in Appendix 1. For a more thorough foundation, we refer to (Koller & Friedman, 2009) and especially (Murphy, 2012).

5.1 Feature processing pipeline

The feature processing pipeline (FCP) serves as an interface between the driving simulator and the inference engine of the DySAM system. The purpose of the FCP is to collect the high-frequency sensor information provided by the driving simulator and process them into a set of assignments for *SA indicators* that can be used for assessing the driver's SA.

The FCP is implemented as a ring buffer that holds the last 20 seconds of raw sensor information provided and SA indicator assignments processed thereof. In the following, we will introduce the raw sensor input required by the DySAM FCP, the pre-processing applied to them, the different SA indicators considered for DySAM and how they are processed from the raw sensor information.

5.1.1 Sensor information provided by the UULM simulator

With a frequency of 60Hz, the UULM simulator provides the following information as input to the DySAM FCP. We note that the UULM simulator and its sensors provide more information than used by the DySAM system. In the following, we restrict the explanation to information that is actually required for the DySAM system to function properly.

5.1.1.1 Timestamp

The timestamp of the current measurements in milliseconds, measured by the SILAB simulation environment. We assume the timestamp measurement to always be valid.

5.1.1.2 Eyelid opening

The current height of the eyelid opening in meters, measured by the Smart Eye Pro eye-tracking system. We assume the eyelid opening measurement to always be valid.

5.1.1.3 Pupil diameter

The current diameter of the pupil in meters, measured by the Smart Eye Pro eye-tracking system. In case that no valid pupil diameter could be measured, the eye-tracker provides a default value of 0.004.

5.1.1.4 Gaze direction

The current direction of the driver's gaze, measured by the Smart Eye Pro eye-tracking system and reported as a three-dimensional (direction-)vector $(x, y, z)^T$ in the Smart Eye Pro's local coordinate system (c.f., Section 5.1.2.3). In case that no valid gaze direction could be measured, the Smart Eye Pro eye-tracking system reports a zero-vector, i.e., $(0,0,0)^T$.

5.1.1.5 Gaze origin

The current origin of the driver's gaze, measured by the Smart Eye Pro eye-tracking system and reported as a three-dimensional (position-)vector $(x, y, z)^T$ in the Smart Eye Pro's local coordinate system (c.f., Section 5.1.2.3). In case that no valid gaze origin could be measured, the Smart Eye Pro eye-tracking system reports a zero-vector, i.e., $(0,0,0)^T$.

5.1.1.6 Head rotation

The current rotation of the driver's head, measured by the Smart Eye Pro eye-tracking system and reported as a three-dimensional rotation-vector $(x, y, z)^T$ in the Smart Eye Pro's local coordinate system (c.f., Section 5.1.2.3). In case that no valid head rotation could be measured, the Smart Eye Pro eye-tracking system reports a zero-vector, i.e., $(0,0,0)^T$.

5.1.1.7 Current area of interest (AOI)

The Smart Eye Pro eye-tracking system allows the specification of static areas of interest (AOIs) in the form of two-dimensional rectangles in the system's three-dimensional coordinate system. For DySAM, we distinguish seven different AOIs (Figure 8): the left mirror, right mirror, rear mirror, a front area that includes the windshield and side windows, the tachometer area, the infotainment system, and an implicitly defined "other" AOI. During runtime, the Smart Eye Pro eye-tracking system automatically checks whether the current gaze vector intersects with an AOI and reports the AOI with the shortest distance between gaze origin and intersection point in terms of a string:

- Left Mirror: "LeftMirror"
- Right Mirror: "RightMirror"

- Rear Mirror: “RearMirror”
- Tachometer area: “Tacho”
- Infotainment system: “Infotainment”
- Front area: “Front”

If the gaze vector does not intersect with any of the AOI specified, the system reports an empty string, which the FCP interprets as an “other” AOI.

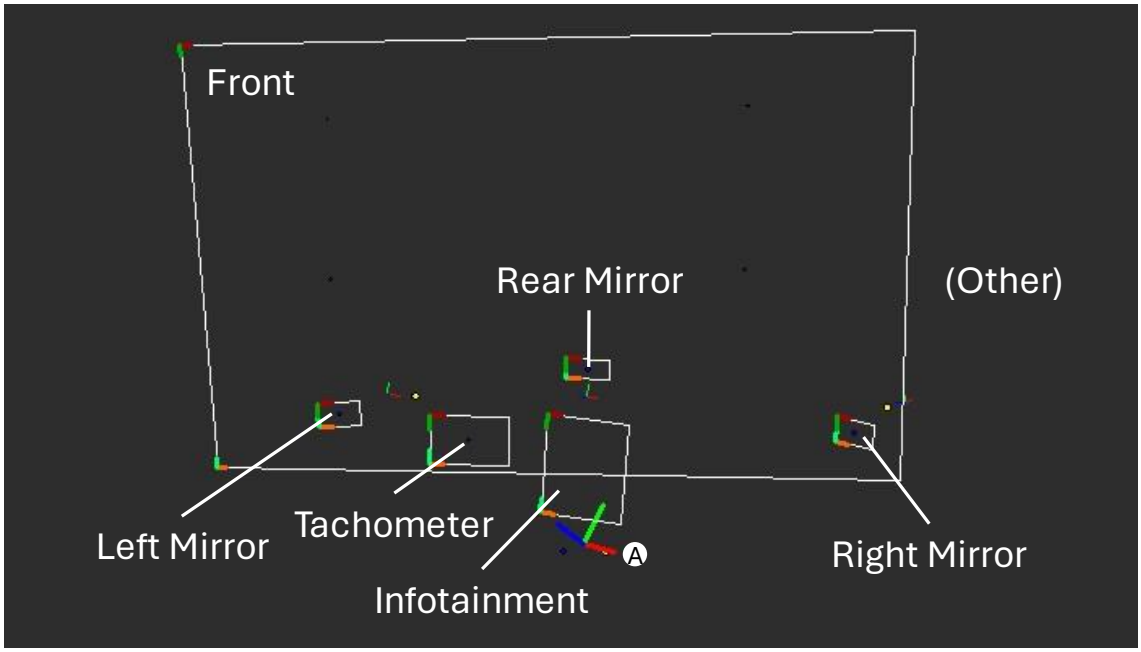

Figure 8: Overview of AOIs defined in the UULM driving simulator. The “Other” AOI is only implicitly defined, in that we deem the driver to look at the other AOI if the gaze does not intersect with any of the explicitly defined AOIs. The origin and axes of local coordinate system used by the Smart Eye Pro eye-tracking system is denoted by (A).

5.1.1.8 Hands-on detection

Within DySAM, UULM developed its own hands-on / hand placement detection system by covering the steering wheel of the UULM simulator with 16 pressure sensors. The resulting sensor provided information concerning the hand placement in terms of a 16-Bit vector, representing which of the 16 pressure sensors measured pressure and binary a hands-on detection, set to one if at least one of the pressure sensors measured pressure, and zero otherwise. For the DySAM system, only the hands-on detection was considered.

5.1.2 Data preprocessing

While the eyelid opening, pupil diameter, current AOI, and hands-on detection measurements can be used as provided, the timestamp and especially eye- and head-tracking information provided by the Smart Eye Pro eye-tracking system require additional pre-processing for better interpretation and derivation of additional information, to be explained in the following.

5.1.2.1 Timestamps

For the FCP, all timestamps are transformed to use seconds instead of milliseconds.

5.1.2.2 DySAM coordinate system

Unless specified otherwise, the DySAM system uses a vehicle-centric right-handed coordinate systems according to the ISO standard 8855-2011, in which the positive z-axis points upwards, angles are defined in radians and use a right-hand rule (Figure 9).

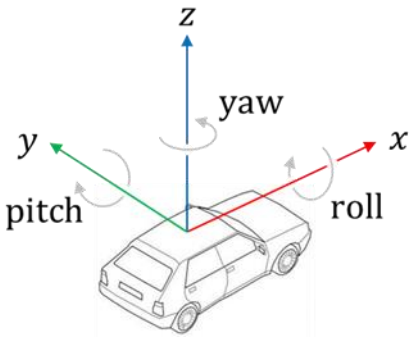

Figure 9: The coordinate system used by the DySAM system.

5.1.2.3 Gaze direction

The Smart Eye Pro eye-tracking system uses a local coordinate system, centered on and axis-aligned with its main camera (c.f.,Figure 8). To allow for a better interpretation of the gaze direction vector and derive additional measurements, a preprocessing step is employed to transform the gaze direction vector into the coordinate system used by DySAM (c.f., Section 5.1.2.1).

Let $\vec{m}_{\mathrm{GD}} = \begin{bmatrix} x \\ y \\ z \end{bmatrix}$ denote the current gaze direction reported by the Smart Eye Pro eye-tracking system, we derive the transformed gaze direction $\vec{m}'_{\mathrm{GD}}$ as

$$\begin{bmatrix} x' \\ y' \\ z' \end{bmatrix} = \begin{bmatrix} 0.7604214 & 0.3949404 & -0.5155399 \\ 0.1414529 & 0.7682356 & 0.6243438 \\ 0.6452007 & -0.5498759 & 0.5304268 \end{bmatrix} \vec{m}_{\mathrm{GD}},$$

$$\vec{m}'_{\mathrm{GD}} = \begin{bmatrix} -z' \\ -x' \\ y' \end{bmatrix}.$$

5.1.2.4 Gaze heading and pitch

The (transformed) gaze direction is used to derive the current gaze heading and pitch, as illustrated in Figure 10. Given a (transformed) gaze direction $\vec{m}'_{\mathrm{GD}}$, we define the gaze heading $\theta_{\mathrm{Heading}}$ as the angle between the x-axis and the projection of $\vec{m}'_{\mathrm{GD}}$ on the x-y-plane (blue) and the gaze pitch θ_{Pitch} as the angle between the y-axis and the projection of $\vec{m}'_{\mathrm{GD}}$ on the y-z-plane (red).

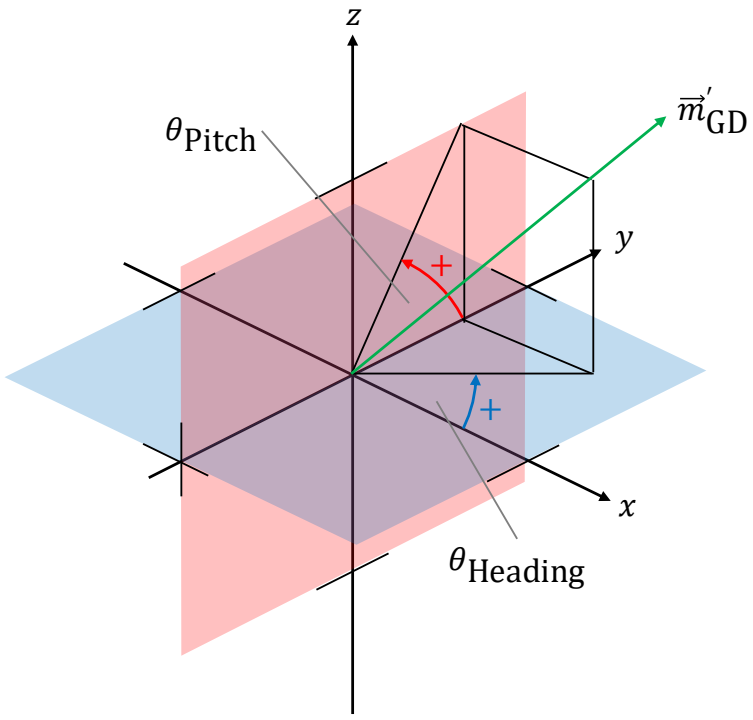

Figure 10: Illustration of the gaze heading and pitch angle, derived from the (transformed) gaze direction.

5.1.2.5 Gaze movement classification

The Smart Eye Pro System functions as a sensor to capture the eye movements of drivers. In the initial stage of data processing, a preprocessing step is employed to categorize the recorded eye movements into distinct higher-level gaze movement classes. Commonly, eye tracking applications employ either a region-based classification algorithm or a velocity/dispersion-based classification algorithm. DySAM, in particular, integrates algorithms from both these categories.

Velocity or dispersion-based algorithms discern gaze movement classes based solely on the temporal and spatial characteristics inherent in the eye tracking data (Stuart et al. 2019). Predominantly, eye tracking applications, including DySAM, concentrate on the most prevalent eye movement classes: fixations and saccades. Fixations denote prolonged periods during which the eyes remain relatively stationary and focused on a specific location, allowing the driver to process visual information. Saccades, on the other hand, are rapid and abrupt eye movements from one point to another.

For the identification of fixations and saccades, in DySAM we implemented a real-time version of the I-DT (Dispersion Threshold Fixation Identification) algorithm, presented by Salvucci and Goldberg (2000). Pseudocode for the classification is shown in Figure 11. The concept is based on the idea that new eye tracking samples are collected in a sample set G. The set is marked as a fixation if all samples are not farther away from the center of G as a dispersion threshold τ_d and samples in G span over a minimum duration of τ_t. Otherwise, it is a fixation and G is emptied.

```
function real_time_gaze_classification(g)
    // Dispersion threshold
    τ_d = 0.08 rad (≈ 4.58°)
    // Minimum fixation duration
    τ_t = 100 ms

    // calculate center of G
    c = Σ G / |G|
    // add g to G
    G = G ∪ g
    // Test if the duration of G is long enough to be a fixation
    if (now – time(first(G)) < τ_t
        return saccade
    // Test if any gaze location is too far away from G's center
    if ∃g ∈ G: distance(g, c) > τ_d:
        G = ∅ ∪ g
        return saccade
    // There are enough gaze locations that are close enough to form a fixation
    return fixation
```

```
// Set of gaze locations
G = ∅
// 2D current gaze location given as horizontal and vertical angle
g

do
        g = Wait for new eyetracker data
        print(real_time_gaze_classification(g))
while true
```

Figure 11. Pseudo code of the fixation classification. Top: the classification method. Bottom: the main loop.

In contrast to velocity or dispersion-based algorithms, region-based algorithms incorporate information about the driver's environment. This is achieved by defining Areas of Interest (AOIs) within the visual field, relevant to the ongoing driving task. Examples of AOIs for drivers include the rear-view mirror, the road ahead, the dashboard, or the infotainment system. Region-based algorithms diverge from physiological considerations and instead focus more on task-specific characteristics, such as the time elapsed since the last gaze at an AOI, or the dwell time associated with an AOI. The dwell time is defined as the duration for which the eyes remain located on a particular AOI. The dwell time might encompass multiple fixations and saccades as long as they occur within the defined AOI.

Internally, the FCP keeps track of all fixations and saccades detected within the last 10 seconds (or the last $n = 600$ measurements). For each fixation and saccade, we store a unique ID, the associated AOI (c.f., Section 5.1.1.7), the starting timestamp t^{start}, and the ending timestamp t^{end}. For this, the FCP

maintains a first-in-first-out queue each for fixations and saccades. Let t^t be the current timestamp and $t^{t-(n-1)}$ be the starting timestamp of the last $n = 600$ measurements. If a new fixation or saccade is detected, it is added to the end of the queue with the current timestamp t^t as starting timestamp t^{start} and ending timestamp t^{end}. While the fixation or saccade is continued, its ending timestamp t^{end} is updated using the current timestamp. To remove fixations or saccades that are older than 10 seconds, at each timestep t^t , the FCP checks the front of each queue and removes the fixation or saccade if $t^{\text{end}} < t^{t-(n-1)}$.

5.1.2.6 Head rotation

The untransformed nose direction $\vec{m}_{\text{ND}}$ is then transformed into the DySAM coordinate system analogous to the transformation of the gaze direction (c.f., Section 5.1.2.3). Given the (transformed) nose direction $\vec{m}'_{\text{ND}}$, we then derive the head heading and pitch analogues to the gaze heading and pitch (c.f., Figure 10) and define the head heading θ_{HHeading} as the angle between the x-axis and the projection of $\vec{m}'_{\text{ND}}$ on the x-y-plane (blue) and the head pitch θ_{HPitch} as the angle between the y-axis and the projection of $\vec{m}'_{\text{ND}}$ on the y-z-plane (red).

5.1.3 Situation awareness indicators

The (pre-processed) input data is then used to derive assignments for a set of indicators for assessing situation awareness (SA indicators). Literature research conducted in WP1 (c.f., Section 3.3) resulted in a set of eight important indicators for assessing SA. The practical implementation of these indicators in the FCP was complicated by the fact that not every indicator was defined in such detail that it allowed a straightforward implementation. Where necessary, we therefore relied on definitions provided by the ISO standard 15007 (2020), which also provided additional related indicators to be considered for the project.

We note that naming conventions for similar and approx. identical indicators vary across the literature and changed over time and we contribute to this confusion by occasionally having chosen new names for similar pre-existing indicators. Although we stick by these names for historical reasons, we will state alternative names, where possible. In total, we considered a set of 71 SA indicators[2], to be explained in the following. The complete list of all indicators is provided in Table 2.

Table 2: List of SA indicators

Index	Symbol	Name
1	F_1	Pupil diameter valid
2	F_2	Head rotation valid
3	F_3	Gaze origin valid
4	F_4	Gaze direction valid
5	F_5	Pupil diameter
6	F_6	Mean pupil diameter
7	F_7	Pupil diameter variability
8	F_8	Blink frequency

[2] During modelling, it showed that two indicators, the pupil diameter and the mean pupil diameter were not suited for DySAM and were excluded from modelling.

9	F_9	Mean blink frequency
10	F_{10}	Blink frequency variability
11	F_{11}	Yaw angle of the head
12	F_{12}	Mean yaw angle of the head
13	F_{13}	Yaw angle of the head variability
14	F_{14}	Yaw rate of the head
15	F_{15}	Mean yaw rate of the head
16	F_{16}	Yaw rate of the head variability
17	F_{17}	Gaze heading
18	F_{18}	Mean gaze heading
19	F_{19}	Gaze heading variability
20	F_{20}	Gaze pitch
21	F_{21}	Mean gaze pitch
22	F_{22}	Gaze pitch variability
23	F_{23}	Hands-on steering wheel
24	F_{24}	Current AOI
25	F_{25}	Glance duration
26	F_{26}	Mean glance duration
27	F_{27}	Glance duration variability
28	F_{28}	Monitoring frequency
29	F_{29}	Mean monitoring frequency
30	F_{30}	Monitoring frequency variability
31	F_{31}	Saccade frequency
32	F_{32}	Mean saccade frequency
33	F_{33}	Saccade frequency variability
34	F_{34}	Dwell percentage
35	F_{35}	Mean dwell percentage
36	F_{36}	Dwell percentage variability
37	F_{37}	Time since last looked at left mirror AOI
38	F_{38}	Mean time since last looked at left mirror AOI
39	F_{39}	Time since last looked at left mirror AOI variability
40	F_{40}	Left mirror AOI dwell percentage
41	F_{41}	Left mirror AOI frequency
42	F_{42}	Time since last looked at right mirror AOI
43	F_{43}	Mean time since last looked at right mirror AOI
44	F_{44}	Time since last looked at right mirror AOI variability
45	F_{45}	Right mirror AOI dwell percentage
46	F_{46}	Right mirror AOI frequency
47	F_{47}	Time since last looked at rear mirror AOI
48	F_{48}	Mean time since last looked at rear mirror AOI
49	F_{49}	Time since last looked at rear mirror AOI variability
50	F_{50}	Rear mirror AOI dwell percentage
51	F_{51}	Rear mirror AOI frequency

52	F_{52}	Time since last looked at tachometer AOI
53	F_{53}	Mean time since last looked at tachometer AOI
54	F_{54}	Time since last looked at tachometer AOI variability
55	F_{55}	Tachometer AOI dwell percentage
56	F_{56}	Tachometer AOI frequency
57	F_{57}	Time since last looked at infotainment AOI
58	F_{58}	Mean time since last looked at infotainment AOI
59	F_{59}	Time since last looked at infotainment AOI variability
60	F_{60}	Infotainment AOI dwell percentage
61	F_{61}	Infotainment AOI frequency
62	F_{62}	Time since last looked at front AOI
63	F_{63}	Mean time since last looked at front AOI
64	F_{64}	Time since last looked at front AOI variability
65	F_{65}	Front AOI dwell percentage
66	F_{66}	Front AOI frequency
67	F_{67}	Time since last looked at other AOI
68	F_{68}	Mean time since last looked at other AOI
69	F_{69}	Time since last looked at other AOI variability
70	F_{70}	Other AOI dwell percentage
71	F_{71}	Other AOI frequency

5.1.3.1 Mean and variability indicators

For continuous indicators, we commonly derive additional indicators by calculating their moving averages and standard deviations (as a measure of variability) over the last 10 seconds or, given an input frequency of 60Hz, the last 600 measurements. In the following, let t denote the current time step (of the FCP, not the model) and $x^t, x^{t-1}, \dots, x^{t-(n-1)}$ denote the sequence of the last $n = 600$ measurements of an indicator. Assuming the measurements to always be valid, we calculate the moving average $\bar{x}^t$ as

$$\bar{x}^t = \frac{\sum_{i=t-(n-1)}^{t} x^i}{n},$$

and the moving standard deviation σ_x^t as

$$\sigma_x^t = \sqrt[2]{\frac{\sum_{i=t-(n-1)}^{t} (x^i)^2}{n} - (\bar{x}^t)^2}.$$

For some indicators, sensor failures or insufficient measurement quality can result in invalid measurements. In such cases, the simulator will usually report a default or error value, such that invalid measurements can be detected. To not bias the moving averages and standard deviations with invalid measurements, we exclude them from the calculation of the moving average and standard deviation. For each measurement $x^i, i = t - (n-1), \dots, t$, let v_x^i denote the whether the measurement x^i, with $v_x^i = 1$, if x^i valid and 0 otherwise. The moving average $\bar{x}^t$ then calculated as

$$\bar{x}^t = \frac{\sum_{i=t-(n-1)}^{t} v_x^i x^i}{\sum_{i=t-(n-1)}^{t} v_x^i},$$

and the moving standard deviation σ_x^t is calculated as

$$\sigma_x^t = \sqrt[2]{\frac{\sum_{i=t-(n-1)}^{t} v_x^i (x^i)^2}{\sum_{i=t-(n-1)}^{t} v_x^i} - (\bar{x}^t)^2}.$$

5.1.3.2 Sensor failure indicators

The Smart Eye Pro eye-tracking system provides the FCP with measurements concerning the pupil diameter, eyelid opening, head rotation, and gaze direction. While these measurements are mostly trustworthy when the driver looks towards the front area, "extreme" head rotations or gaze directions can make render the eye-tracking system unable to provide valid measurements. To address this issue, we define a set of sensor failure indicators, representing, whether a measurement should be considered valid or invalid. The sensor failure indicators are mainly used as auxiliary variables to allow the model to distinguish between measurements resulting from sensor failures, which should be ignored, and valid measurements, which should be taken into account when assessing the driver's SA. That said, given that invalid measurements mostly occur when the driver is looking to an unusual location, knowledge about a sensor failure is itself a potential valuable indicator that should be taken into consideration by DySAM.

5.1.3.2.1 Pupil diameter valid

The pupil diameter valid indicator indicates whether the current measurement of the pupil diameter is valid. In case that no valid pupil diameter could be obtained, the eye-tracking system provides a default value of 0.004.

Let d_{Pupil}^t denote the current pupil diameter and v_{Pupil}^t denote whether the pupil diameter measurement is valid, with $v_{\text{Pupil}}^t = 1$, if valid and 0 otherwise, we define the pupil diameter valid indicator v_{Pupil}^t as

$$v_{\text{Pupil}}^t = \mathbb{I}\left(d_{\text{Pupil}}^t \neq 0.004\right).$$

5.1.3.2.2 Head rotation valid

The head rotation valid indicator indicates whether the current measurement of the head rotation is valid. In case that no valid head rotation could be obtained, the eye-tracking system reports a zero vector.

Let $\vec{m}_{\text{HR}}^t$ denote the current (untransformed) head rotation reported by the eye-tracking system and v_{Head}^t denote whether the head rotation measurement is valid, with $v_{\text{HR}}^t = 1$, if valid and 0 otherwise, we define the head rotation valid indicator v_{HR}^t as

$$v_{\text{HR}}^t = \mathbb{I}(\vec{m}_{\text{HR}}^t \neq (0,0,0)^T).$$

5.1.3.2.3 Gaze origin valid

The gaze origin valid indicator indicates whether the current measurement of the gaze origin is valid. In case that no valid gaze origin could be obtained, the eye-tracking system reports a zero vector.

Let $\vec{m}_{\mathrm{GO}}^{t}$ denote the current (untransformed) gaze origin reported by the eye-tracking system and v_{GO}^{t} denote whether said measurement is valid, with $v_{\mathrm{GO}}^{t} = 1$, if valid and 0 otherwise, we define the gaze origin valid indicator v_{GO}^{t} as

$$v_{\mathrm{GO}}^{t} = \mathbb{1}(\vec{m}_{\mathrm{GO}}^{t} \neq (0,0,0)^{T}).$$

5.1.3.2.4 Gaze direction valid

The gaze direction valid indicator indicates whether the current measurement of the gaze direction is valid. In case that no valid gaze direction could be obtained, the eye-tracking system reports a zero vector.

Let $\vec{m}_{\mathrm{GD}}^{t}$ denote the current (untransformed) gaze direction reported by the eye-tracking system and v_{GD}^{t} denote whether said measurement is valid, with $v_{\mathrm{GD}}^{t} = 1$, if valid and 0 otherwise, we define the gaze origin valid indicator v_{GD}^{t} as

$$v_{\mathrm{GD}}^{t} = \mathbb{1}(\vec{m}_{\mathrm{GD}}^{t} \neq (0,0,0)^{T}).$$

5.1.3.3 Pupil diameter indicators

The first set of indicators are based on the (mean) pupil diameter, selected as one of the original SA indicators in WP1 (c.f., Section 3.3). The mean pupil diameter is used e.g., by Liu et al. (2014) and Niezgoda et al. (2015), albeit, in slightly different forms. Liu et al. (2014) directly used the mean pupil diameter as an indicator for SA. A problem with this approach for DySAM is that due to a general pupil size variability among participants, the mean and raw pupil diameter sizes provide information that allows the identification of participants and consequently their NDRT condition and SAGAT score without providing actual information about SA. Similar consideration led Niezgoda et al. (2015) to use the percentual difference of the mean pupil diameter instead. To quote, "[c]hange in the pupil size was calculated as the average pupil size (given in millimetres) in each condition in relation to the average pupil size during the entire experimental run."

Unfortunately, the mean pupil diameter (and the same is true for the raw pupil diameter) as used by Niezgoda et al. (2015) poses problems for the DySAM system in that the general average pupil size is unknown during utilization with arbitrary participants. As such, we've decided to exclude both the pupil diameter and the mean pupil diameter indicators for DySAM during the course of the project.

5.1.3.3.1 Pupil diameter

The pupil diameter indicator represents the current diameter of the pupil in meters. The pupil diameter is provided directly from the Smart Eye Pro eye-tracking system (c.f., Section 5.1.3.1) and does not require any further processing.

5.1.3.3.2 Mean pupil diameter

The mean pupil diameter indicator represents the moving average of the pupil diameter over the last 10 seconds and is calculated as described in Section 5.1.3.1, using the pupil diameter and pupil diameter valid indictors.

5.1.3.3.3 Pupil diameter variability

The pupil diameter variability indicator represents the moving standard deviation of the pupil diameter over the last 10 seconds and is calculated as described in Section 5.1.3.1, using the pupil diameter and pupil diameter valid indictors.

5.1.3.4 Blink frequency indicators

5.1.3.4.1 Blink frequency

The blink frequency is one of the original SA indicators obtained in WP1 (c.f., Section 3.3) and used e.g., by Niezgoda et al. (2015) and Faure et al. (2016). Faure et al. (2016) define the blink frequency as the number of blinks per minute, where a blink is assumed if the pupil is occluded for at least 50ms and up to 500ms.

For DySAM, we use a slightly different definition for blinks and blink frequency: The blink frequency represents the *number of blinks per second* and is derived from number of blinks occurring during the last 10 seconds. The occurrence of blinks is derived from the eyelid opening provided by the Smart Eye Pro eye-tracking system (c.f., Section 5.1.1.2). Let e^t and e^{t-1} denote the current and previous eyelid opening measurements, and let b^t represents whether we have a blink, with $b^t = 1$, if true and 0 otherwise, we define the presence or absence of a blink as

$$b^t = \mathbb{I}(e^t < 0.005)\mathbb{I}(e^{t-1} \geq 0.005).$$

The blink frequency is then derived as follows: Let $b^t, b^{t-1}, \dots, b^{t-(n-1)}$ denote the sequence of the last $n = 600$ blink measurements and Δt denote the duration of the sequence (in seconds), the blink frequency ν^t_{Blink} is calculated as

$$\nu^t_{\text{Blink}} = \frac{\sum_{i=t-(n-1)}^{t} b^i}{\Delta t}.$$

5.1.3.4.2 Mean blink frequency

The mean blink frequency indicator represents the moving average of the blink frequency over the last 10 seconds and is calculated as described in Section 5.1.3.1, assuming the blink frequency measurements to always be valid.

5.1.3.4.3 Blink frequency variability

The blink frequency variability indicator represents the moving standard deviation of the blink frequency over the last 10 seconds and is calculated as described in Section 5.1.3.1, assuming the blink frequency measurements to always be valid.

5.1.3.5 Yaw angle of the head indicators

5.1.3.5.1 Yaw angle of the head

The yaw angle of the head indicator represents the angle (in radians) between the forward-direction of the driver's head, projected on the x-y-plane and the x-axis of the DySAM coordinate system (representing the forward-direction of the vehicle, or the driver's body, assuming that the driver is sitting normally). The yaw angle from the head is given by the head heading measurement $\theta^t_{\text{HHeading}}$, derived during pre-processing of the head rotation vector (c.f., Section 5.1.2.6) and does not require any further processing.

5.1.3.5.2 Mean yaw angle of the head

The mean yaw angle of the head indicator represents the moving average of the yaw angle of the head over the last 10 seconds and is calculated as described in Section 5.1.3.1, using the yaw angle of the head and head rotation valid indictors.

5.1.3.5.3 Yaw angle of the head variability

The yaw angle of the head variability indicator represents the moving standard deviation of the yaw angle of the head over the last 10 seconds and is calculated as described in Section 5.1.3.1, using the yaw angle of the head and head rotation valid indictors.

5.1.3.6 Yaw rate of the head indicators

5.1.3.6.1 Yaw rate of the head

The yaw rate of the head is one of the original SA indicators obtained in WP1 (c.f., Section 3.3) and used e.g., by Schewe et al. (2019). Schewe et al. (2019) define the yaw-rate of the head as the side-rotation rate in degrees per second, which we understand as the rotational velocity (in radians per seconds) of the driver's yaw angle of the head. Let $\theta^{t}_{\text{HHeading}}$ denote the current, $\theta^{t-1}_{\text{HHeading}}$ denote the previous yaw angle measurements, and Δt denote the duration (in seconds) between these measurements, the yaw rate of the head $\dot{\theta}^{t}_{\text{HHeading}}$ is calculated as

$$\dot{\theta}^{t}_{\text{HHeading}} = \frac{\theta^{t}_{\text{HHeading}} - \theta^{t-1}_{\text{HHeading}}}{\Delta t}.$$

5.1.3.6.2 Mean yaw rate of the head

The mean yaw rate of the head indicator represents the moving average of the yaw rate of the head over the last 10 seconds and is calculated as described in Section 5.1.3.1, using the yaw rate of the head and head rotation valid indictors.

5.1.3.6.3 Yaw rate of the head variability

The yaw rate of the head variability indicator represents the moving standard deviation of the yaw rate of the head over the last 10 seconds and is calculated as described in Section 5.1.3.1, using the yaw rate of the head and head rotation valid indictors.

5.1.3.7 Gaze heading indicators

5.1.3.7.1 Gaze heading

The gaze heading indicator represents the angle (in radians) between the driver's gaze, projected on the x-y-plane and the x-axis of the DySAM coordinate system. The gaze heading $\theta^{t}_{\text{Heading}}$ is derived during pre-processing of the gaze direction vector (c.f., Section 5.1.2.4) and does not require any further processing.

5.1.3.7.2 Mean gaze heading

The mean gaze heading indicator represents the moving average of the gaze heading over the last 10 seconds and is calculated as described in Section 5.1.3.1, using the gaze heading and gaze direction valid indictors.

5.1.3.7.3 Gaze heading variability

The gaze heading variability indicator represents the moving standard deviation of the gaze heading over the last 10 seconds and is calculated as described in Section 5.1.3.1, using the gaze heading and gaze direction valid indictors.

5.1.3.8 Gaze pitch indicators

5.1.3.8.1 Gaze pitch

The gaze pitch indicator represents the angle (in radians) between the driver's gaze, projected on the y-z-plane and the y-axis of the DySAM coordinate system. The gaze pitch $\theta^{t}_{\text{Pitch}}$ is derived during pre-processing of the gaze direction vector (c.f., Section 5.1.2.4) and does not require any further processing.

5.1.3.8.2 Mean gaze pitch

The mean gaze pitch indicator represents the moving average of the gaze pitch over the last 10 seconds and is calculated as described in Section 5.1.3.1, using the gaze pitch and gaze direction valid indictors.

5.1.3.8.3 Gaze pitch variability

The gaze pitch variability indicator represents the moving standard deviation of the gaze pitch over the last 10 seconds and is calculated as described in Section 5.1.3.1, using the gaze pitch and gaze direction valid indictors.

5.1.3.9 Hands-on steering wheel indicator

The hands-on steering wheel indicator represents whether the driver currently touches the steering wheel with at least one hand and is provided directly by the hands-on detection sensor developed by UULM. We define the hands-on steering wheel indicator to be 1 if the driver touches the steering wheel and 0 otherwise.

5.1.3.10 Current AOI indicator

The current AOI indictor represents which of the seven different AOIs the driver is currently looking at, as reported by the Smart Eye Pro eye-tracking system, for which we distinguish between the left mirror, right mirror, rear mirror, the front area, the tachometer area, the infotainment system, and an "other" AOI (Figure 8). While the Smart Eye Pro eye-tracking system reports the current AOI in terms of a string (c.f., Section 5.1.1.7), for the current AOI indicator, we encode the current AOI as an integer, for which we rely on the following mapping:

0. Left mirror AOI
1. Tachometer AOI
2. Infotainment AOI
3. Rear mirror AOI
4. Right mirror AOI
5. Front area AOI
6. Other AOI

We note that, as used within the DySAM probabilistic models, the current AOI indicator is strongly related to what the ISO standard 15007 (2020) calls the glance location probability metric, which it defines as the "probability that the eyes are fixated at an AOI (or set of related AOIs) during a condition, task, subtask or sub-subtask".

5.1.3.11 Glance duration indicators

5.1.3.11.1 Glance duration

The glance duration is one of the original SA indicators obtained in WP1 (c.f., Section 3.3) and used e.g., by Yang et al. (2018). Yang et al. (2018) define the glance duration as "[t]he average time spend

in the windshield area within on (sic) glance", measured over a duration of 37 mins. The authors do however not provide a definition for what they consider a glance. The ISO standard 15007 (2020) defines glances and glance duration as “temporal maintaining of visual gaze within an AOI, bounded by the perimeter of the AOI which can be comprise of more than one fixation and saccades within the AOI and its duration is measured as glance duration”. We note that the glance duration as used by Yang et al. (2018) therefore differs from the glance duration defined by the ISO standard 15007 (2020) in that the former is an average, while the latter refers to the duration of a single glance. The ISO standard 15007 (2020) provides its own definition for such averages, referred to as the mean glance duration, defined as “mean duration of all glance durations to an AOI (or set of related AOIs) during a condition, task, subtask or sub-subtask”.

For DySAM, we define the glance duration as the *average duration of glances over the last 10 seconds towards driving-related AOIs*, for which we consider the left, right, and rear mirror, the tachometer, and the front area AOI. Let t^t be the current timestamp and $t^{t-(n-1)}$ be the starting timestamp of the last $n = 600$ measurements, and let there be m glances towards driving-related AOIs, each beginning at time stamp t_i^{start} and ending at time stamp t_i^{end}, $i = 1, \dots, m$, the glance duration τ_{Glance}^t is calculated as

$$\tau_{\text{Glance}}^t = \frac{\sum_{i=1}^{m}\left[\max\left(t^{t-(n-1)}, t_i^{\text{start}}\right) - \min\left(t^t, t_i^{\text{end}}\right)\right]}{m}.$$

5.1.3.11.2 Mean glance duration

The mean glance duration indicator represents the moving average of the glance duration over the last 10 seconds and is calculated as described in Section 5.1.3.1, assuming the glance duration measurements to always be valid.

We note that the mean glance duration indicator is not to be confused with the mean glance duration defined in the ISO standard 15007 (2020) (c.f., Section 5.1.3.11.1) in that the former represents the moving average of the latter.

5.1.3.11.3 Glance duration variability

The glance duration variability indicator represents the moving standard deviation of the glance duration over the last 10 seconds and is calculated as described in Section 5.1.3.1, assuming the glance duration measurements to always be valid.

5.1.3.12 Monitoring frequency indicators

5.1.3.12.1 Monitoring frequency

The monitoring frequency is one of the original SA indicators obtained in WP1 (c.f., Section 3.3) and used e.g., by Kunze et al. (2018). Kunze et al. (2018) defined the monitoring frequency as the number of monitoring glances per second, where a monitoring glance was defined as glances on driving-related AOIs, including the field relevant for driving, instruments, and an uncertainty display. The ISO standard 15007 (2020) provides a similar definition for what it calls the *glance rate* or *number of glances per unit of time*, defined as the number of task-related glances divided by the task duration.

Adapting these definitions, we define the monitoring frequency as the *number of glances over the last 10 seconds towards driving-related AOIs*, for which we consider the left, right, and rear mirror, the tachometer, and the front area AOI. Let t^t be the current timestamp and $t^{t-(n-1)}$ be the starting

timestamp of the last $n = 600$ measurements, and let there be m glances towards driving-related AOIs, with the first glance starting at time step t^{start}, the monitoring frequency $v^t_{\text{Monitoring}}$ is calculated as

$$v^t_{\text{Monitoring}} = \frac{m}{t^t - \min(t^{t-(n-1)}, t^{\text{start}})}.$$

5.1.3.12.2 Mean monitoring frequency

The mean monitoring frequency indicator represents the moving average of the monitoring frequency over the last 10 seconds and is calculated as described in Section 5.1.3.1, assuming the monitoring frequency measurements to always be valid.

5.1.3.12.3 Monitoring frequency variability

The monitoring frequency variability indicator represents the moving standard deviation of the monitoring frequency over the last 10 seconds and is calculated as described in Section 5.1.3.1, assuming the monitoring frequency measurements to always be valid.

5.1.3.13 Saccade frequency indicators

5.1.3.13.1 Saccade frequency

The saccade frequency is one of the original SA indicators obtained in WP1 (c.f., Section 3.3) and used e.g., by Wu et al. (2018). Wu et al. (2018) did not explicitly define the saccade frequency but seem to refer to the general number of saccades per minute, unrelated to any specific AOI. We follow this general proposal but define the saccade frequency as the *number of saccades per second* occurred during the last 10 seconds, unrelated to any specific AOI.

Let t^t be the current timestamp and $t^{t-(n-1)}$ be the starting timestamp of the last $n = 600$ measurements, and let there be m saccades, with the first saccade starting at time step t^{start}, the saccade frequency v^t_{Saccade} is calculated as

$$v^t_{\text{Saccade}} = \frac{m}{t^t - \min(t^{t-(n-1)}, t^{\text{start}})}.$$

5.1.3.13.2 Mean saccade frequency

The mean saccade frequency indicator represents the moving average of the saccade frequency over the last 10 seconds and is calculated as described in Section 5.1.3.1, assuming the saccade frequency measurements to always be valid.

5.1.3.13.3 Saccade frequency variability

The saccade frequency variability indicator represents the moving standard deviation of the saccade frequency over the last 10 seconds and is calculated as described in Section 5.1.3.1, assuming the saccade frequency measurements to always be valid.

5.1.3.14 Dwell percentage indicators

5.1.3.14.1 Dwell percentage

Related to the glance duration and monitoring frequency indicators, older revisions of the ISO standard 15007 (2020) proposed the total or percentage of glance time to a target as a measure of visual demand posed by that location. The current revision of the ISO standard 15007 (2020) proposes the *percentage time on AOI* metric, defined as the "ratio representing the percentage of time glances are

within an AOI (or set of related AOIs) during a condition, task, subtask or sub-subtask. With the glance duration and monitoring frequency indicators focusing on driving-related AOIs, we considered the percentage time on driving-related AOIs as a meaningful addition to the set of SA indicators, which we refer to as *dwell percentage*.

Within DySAM, the dwell percentage indicator therefore represents the percentage of glances over the last 10 seconds that have been targeted driving-related AOIs, for which we consider the left, right, and rear mirror, the tachometer, and the front area AOI. Let t^t be the current timestamp and $t^{t-(n-1)}$ be the starting timestamp of the last $n = 600$ measurements, and let there be m glances, each beginning at time stamp t_i^{start} and ending at time stamp t_i^{end}, $i = 1, \dots, m$, the dwell percentage d_{Dwell}^t is calculated as

$$d_{\text{Dwell}}^t = \frac{\sum_{i=1}^{m}\left[\max\left(t^{t-(n-1)}, t_i^{\text{start}}\right) - \min\left(t^t, t_i^{\text{end}}\right)\right]}{t^t - t^{t-(n-1)}}.$$

5.1.3.14.2 Mean dwell percentage

The mean dwell percentage indicator represents the moving average of the dwell percentage over the last 10 seconds and is calculated as described in Section 5.1.3.1, assuming the dwell percentage measurements to always be valid.

5.1.3.14.3 Dwell percentage variability

The dwell percentage variability indicator represents the moving standard deviation of the dwell percentage over the last 10 seconds and is calculated as described in Section 5.1.3.1, assuming the dwell percentage measurements to always be valid.

5.1.3.15 Single AOI indicators

The glance duration, monitoring frequency, and dwell percentage indicators each consider a driving-related set of AOIs, comprised of the left, right, and rear mirror, tachometer, and front area. Similar indicators can also be defined for each single AOI. For each of the seven AOIs (left mirror, right mirror, rear mirror, tachometer, infotainment, front, and other), we define a set of five indicators.

5.1.3.15.1 Time since last looked at AOI

Kirchner and Ahlström (2013) proposed a computational model for detecting driver distraction, called AttenD, which uses a buffer that fills up as the driver looks through the windshield and drains as the driver looks away. Once the buffer is completely drained, it is assumed that the driver is distracted. Ahlström et al. (2022) introduced AttenD2.0, which extends the former approach by the introduction of multiple buffers for different AOIs and non-linear fill and decay rates, providing an easy to implement and understand way to detect whether a driver has lost SA in respect to a specific AOI.

Adapting the idea of AOI-specific buffers towards indicators that are more suitable for probabilistic models, we added the time since last looked at a specific AOI indicators, which, as the name suggest, represent the time since the driver last looked at a specific AOI. For this, we rely on the current AOI provided by the eye-tracking system: Let $a \in \{0, \dots, 6\}$ denote the AOI the driver is looking at, τ_{a_i} denote the time since the driver last looked at AOI $i, i \in \{0, \dots, 6\}$, and Δt denote the delta in timestamps between the sensor measurements at time steps t and $t-1$, we calculate $\tau_{a_i}^t$ as

$$\tau_{a_i}^t = \begin{cases} \tau_{a_i}^{t-1} + \Delta t, & i \neq a \\ 0, & \text{else} \end{cases}.$$

5.1.3.15.2 Mean time since last looked at AOI

The mean time since last looked at a specific AOI indicator represents the moving average of the time since last looked at the AOI over the last 10 seconds and is calculated as described in Section 5.1.3.1, using the time since last looked at the AOI indictor, assuming the measurements to always be valid.

5.1.3.15.3 Time since last looked at AOI variability

The time since last looked at a specific AOI variability indicator represents the moving standard deviation of the time since last looked at the AOI over the last 10 seconds and is calculated as described in Section 5.1.3.1, using the time since last looked at the AOI indictor, assuming the measurements to always be valid.

5.1.3.15.4 AOI dwell percentage

The AOI dwell percentage represents the percentage of time the driver looked into a specific AOI over the course of the last 10 seconds. Let $a^t, a^{t-1}, \dots, a^{t-(n-1)}$ denote the sequence of the last $n = 600$ current AOI measurements and $d_{a_j}^t$ denote the current dwell percentage for AOI $j, j \in \{0, \dots, 6\}$, $d_{a_j}^t$ is calculated as

$$d_{a_j}^t = \frac{\sum_{i=t-(n-1)}^{t} \mathbb{I}(j = a^i)}{n}.$$

We note that the AOI dwell percentage indicator is strongly related to the "percentage time on AOI" metric proposed by the ISO standard 15007 (2020), defined as the "ratio representing the percentage of time glances are within an AOI (or a set of related AOIs) during a condition, task, subtask, or sub-subtask", but differs in using the current AOI assessment provided by the Smart Eye Pro eye-tracking system instead of glances.

5.1.3.15.5 AOI frequency

The AOI frequency indicator represents the number of gazes into a specific AOI per second, as occurred during the last 10 seconds. $a^t, a^{t-1}, \dots, a^{t-(n-1)}$ denote the sequence of the last $n = 600$ current AOI measurements, Δt denote the duration of the sequence in seconds, and $\nu_{a_j}^t$ denote the current frequency for AOI $j, j \in \{0, \dots, 6\}$, $\nu_{a_j}^t$ is calculated as

$$\nu_{a_j}^t = \frac{\sum_{i=t-(n-1)}^{t} \mathbb{I}(j = a^i)}{\Delta t}.$$

We note that the AOI frequency indicator is strongly related to the "glance rate" or "number of glances per unit of time" metric proposed by the ISO standard 15007 (2020), defined as the "number of glances divided by the duration of condition, task, subtask, or sub-subtask", but differs in using the current AOI assessment provided by the Smart Eye Pro eye-tracking system instead of glances.

5.2 Conceptional framework for modelling situation awareness via Dynamic Bayesian Networks

For vehicle-based systems tasked with predicting a driver's situation awareness, a significant hurdle arises: the inherent challenge that neither Situation Awareness (SA) nor certain influencing or dependent aspects can be directly measured or accessed by the vehicle. This issue is depicted in Figure 12, outlining the relevant facets of a driver's SA within the DySAM context.

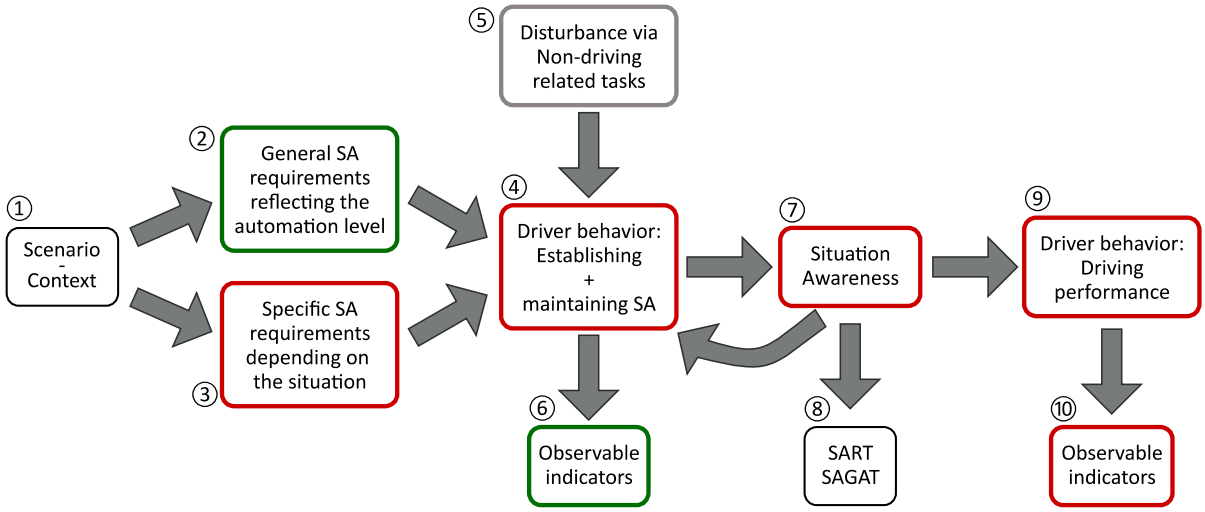

Figure 12. DySAM relevant aspects of drivers' situation awareness process. Some relationships between these aspects are considered accessible within the context of the DySAM system (green arrows), while other are not (red arrows).

Figure 12 showcases various aspects influencing a driver's SA. The accessibilities of these aspects within the DySAM system are indicated by the color of the surrounding boxes. Aspects in green boxes are directly accessible for the DySAM system, aspects in red boxes are inaccessible and the ones in grey boxes are only accessible during the design time of the system.

For a meticulous evaluation of a driver's SA, a driver monitoring system must discern the SA requirements the driver should be aware of (SA requirements ② + ③) and identify which aspects the driver is currently aware of ⑦. This information is crucial for determining whether the driver meets all SA requirements for the present situation.

Accurately gauging SA requirements for each potential situation is a challenge in itself. DySAM pragmatically assumes that situation-specific SA requirements③, such as awareness of a neighboring vehicle initiating a lane change, remain unknown to the monitoring system. Consequently, the system lacks knowledge of how these specific requirements influence the driver's behavior concerning the establishment and maintenance of an adequate level of SA ④.

Nevertheless, DySAM does factor in more generic SA requirements ② applicable to diverse driving scenarios. These include for example staying alert to traffic, being aware of surroundings, and maintaining attention with sufficient frequency and continuity. The system endeavors to model the impact of these generic requirements on the driver's behavior regarding establishing and maintain SA. However, the intricate cognitive processes within the driver's mind remain beyond direct reach, with the monitoring system relying solely on observable measurements ⑥ as indicators for the maintenance process.

Complicating matters further, driver behavior is not solely dictated by SA requirements; it can be significantly disrupted by a plethora of non-driving tasks ⑤, such as phone conversations, interaction with devices, or distractions. Acknowledging this, DySAM assumes that the monitoring system lacks real-time access to such information. The project, however, conducted experiments during the design phase, employing various non-driving related tasks to explore their impact.

Moreover, the system faces the challenge of limited direct access to the driver's SA state ⑦. Conclusions about SA can be drawn through two main avenues: direct questioning using SA

questionnaires like SART and SAGAT ⑧, employed in DySAM experiments during design, and indirect inference through its impact on the driver's behavior and performance ④, ⑨. The latter, however, relies on observable indicators ⑥+⑩ due to the unavailability of questionnaires in non-laboratory settings. The complexity of these interconnected challenges underscores the objectives of the DySAM project, including the identification of suitable indicators and the modeling of relationships between these indicators and the SA maintenance process.

5.2.1 Modelling approach

For modelling the uncertain relationship between SA and observable SA indicators, we used DBNs (c.f., Appendix 1, Section 1.3). DBNs are probabilistic graphical models that use directed acyclic graphs to factorize the joint probability / density distribution (JPD) of time series of set of variables into products of simpler (conditional) probability / density distributions (CPDs). They generalize well-known probabilistic models for dynamic systems like Hidden Markov Models and Kalman Filters.

Model development and validation requires ground truth data for both indicators and SA. While the indicators can be derived from the available sensor information, SA cannot be observed directly. As such, we rely on two surrogate measures, we assume to correlate with SA, the SAGAT score and the NDRT, and focus on different types of models, either focusing on the NDRT or the SAGAT score, which we refer to as the "NDRT", the "SAGAT Score", and the "extended SAGAT Score" models.

The SAGAT is the gold standard for assessing SA and the SAGAT Score and extended SAGAT Score models directly model the relationship between a driver's SAGAT score and the observable indicators. However, as the SAGAT queries drivers about their knowledge about the situation at a specific point in time, the resulting assessment is only representative for a short period of time prior to the test, limiting the amount of data available for model training and validation. To make use of all data available, we rely on the NDRT as a surrogate measure for SA. Assuming that attentive drivers are able to maintain *sufficient* SA, a distraction via NDRTs will, on average, result in diminished or *insufficient* SA. The NDRT models therefore aim to model the relationship between the different NDRT conditions and the observable indicators to reason about whether the driver's current SA is sufficient.

In the following subsections, we will provide the conceptual foundation for each of these models.

5.2.2 NDRT Models

The NDRT models are based on the assumption that an attentive driver is able to establish and maintain *sufficient* SA and that a disturbance of this process via the introduction of an NDRT will, on average, result in a diminished or *insufficient* SA. While the actual SA cannot be observed directly, the normal and disturbed process for establishing and maintaining SA is assumed to result in distinguishable behavioral processes that can be observed via the SA indicators, like e.g., the gaze and monitoring behavior of the driver. As such, for the NDRT models, observing these indicators allows to detect whether the SA process is disturbed or undisturbed, which allows to reason about whether the driver's current SA is sufficient or insufficient.

Let

$$S_1, \mathrm{Val}(S_1) = \{s_{1_0}, s_{1_1}\}$$

represent a binary assessment of SA, with s_{1_0} representing insufficient and s_{1_1} representing sufficient SA. Let

$$B, \mathrm{Val}(B) = \{b_0, b_1, b_2\}$$

represent three behavioral patterns for establishing and maintaining SA, with b_0 representing undisturbed driver behavior, and b_1 and b_2 representing driver behavior when disturbed by a cognitive and visual non-driving related task respectively. Lastly, let

$$\boldsymbol{F} = \{F_1, \dots F_{69}\}$$

denote the set of SA indicators. Conceptionally, the NDRT models are defined as DBNs, that, for any number of time slices T, define a JPD $p(S_1^{1:T}, B^{1:t}, \boldsymbol{F}^{1:T})$ as:

$$p(S_1^{1:T}, B^{1:t}, \boldsymbol{F}^{1:T}) = p(S_1^1|B^1)p(B^1)p(\boldsymbol{F}^1|B^1)\prod_{t=2}^{T} p(S_1^t|B^t)p(B^t|B^{t-1})p(\boldsymbol{F}^t|B^t).$$

Here, $p(S_1^t|B^t)$ is a conditional probability distribution (CPD) that describes the level of SA to expect for each behavioral pattern, while $p(B^t|B^{t-1})$ describes how the behavioral patterns change over time. Lastly, $p(\boldsymbol{F}^t|B^t)$ can be understood as an observation model that describes what indicators we expect to observe given the behavioral patterns. A graphical representation of the structure is shown in Figure 13.

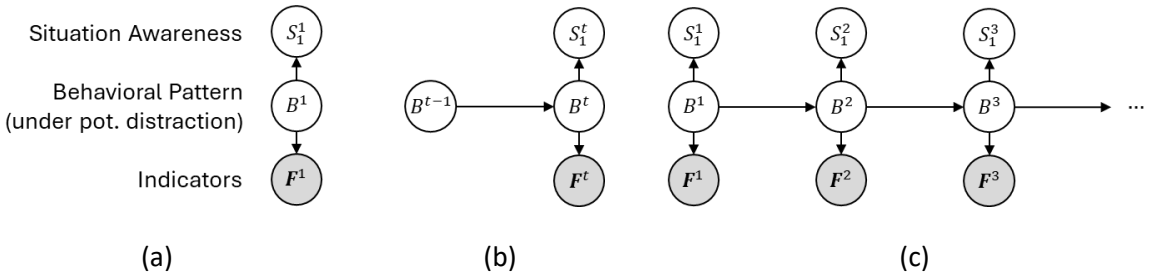

Figure 13: Conceptional structure of the NDRT models. (a) BN for the first times slice. (b) 2TBN for subsequent time slices. (c) Unrolled network over multiple time slices.

Within the DySAM system, the NDRT models shall be utilized as follows: With a constant frequency of 10Hz, the NDRT models are used to infer the belief state $p(S_1^t, B^t|\boldsymbol{f}^{1:t})$, i.e., the joint probability distribution over the binary situation awareness S_1^t and the behavioral patterns B^t at the current time step t, given the sequence $\boldsymbol{f}^{1:t}$ of all observed evidence of the SA indicators from the activation of the system until t, which is given by:

$$p(S_1^t, B^t|\boldsymbol{f}^{1:t}) \propto p(S_1^t|B^t)p(\boldsymbol{f}^t|B^t)\sum_{b^{t-1}\in \mathrm{Val}(B^{t-1})} p(B^t|b^{t-1})p(b^{t-1}|\boldsymbol{f}^{1:t-1}).$$

From this belief state, the belief state over the binary situation awareness

$$p(S_1^t|\boldsymbol{f}^{1:t}) = \sum_{b^t\in \mathrm{Val}(B^t)} p(S_1^t, b^t|\boldsymbol{f}^{1:t})$$

is considered as the primary model output, while the belief state over the behavioral patterns

$$p(B^t|\boldsymbol{f}^{1:t}) = \sum_{s_1^t \in \mathrm{Val}(S_1^t)} p(s_1^t, B^t|\boldsymbol{f}^{1:t})$$

is required to obtain the belief state $p(S_1^{t+1}, B^{t+1}|\boldsymbol{f}^{1:t+1})$ at time step $t+1$.

5.2.3 SAGAT Score Models

The SAGAT models aim at a finer resolution of SA by directly modelling the relationship between a driver's SAGAT score and the observable indicators.

Let

$$S_2, \mathrm{Val}(S_2) = \{s_{2_0}, s_{2_1} \dots, s_{2_5}\}$$

represent the SAGAT score, with the assignments $s_{2_0}, s_{2_1} \dots, s_{2_5}$ corresponding to a SAGAT score of 0%, 20%, …, 100%, and let

$$\boldsymbol{F} = \{F_1, \dots F_{69}\}$$

denote the set of SA indicators. The SAGAT Score models are conceptualized as state-observation DBNs, in this case, Hidden Markov Models, with dynamic model $p(S_2^t|S_2^{t-1})$ and observation model $p(\boldsymbol{F}^t|S_2^t)$. For any number of time slices T, the SAGAT Score models define a JPD $p(S_2^{1:T}, \boldsymbol{F}^{1:T})$ as:

$$p(S_2^{1:T}, \boldsymbol{F}^{1:T}) = p(S_2^1)p(\boldsymbol{F}^1|S_2^1)\prod_{t=2}^{T} p(S_2^t|S_2^{t-1})p(\boldsymbol{F}^t|S_2^t).$$

A graphical representation of the structure is shown in Figure 14.

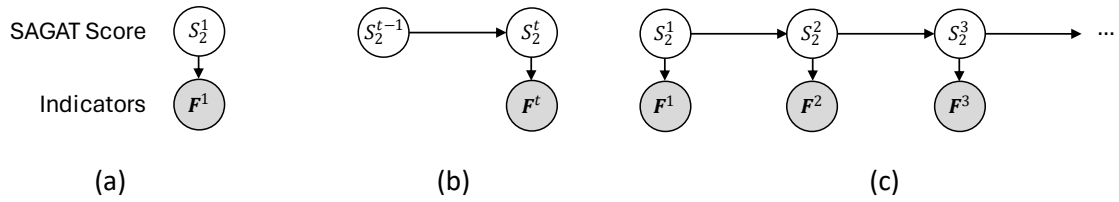

Figure 14: Conceptional structure of the SAGAT Score models. (a) BN for the first times slice. (b) 2TBN for subsequent time slices. (c) Unrolled network over multiple time slices.

Similar to the NDRT models, the aim of the SAGAT Score models is to, with a constant frequency of 10Hz, infer the belief state $p(S_2^t|\boldsymbol{f}^{1:t})$, i.e., the probability distribution over the SAGAT score S_2^t at the current time step t, given the sequence $\boldsymbol{f}^{1:t}$ of all observed evidence of the SA indicators from the activation of the system until t, given by:

$$p(S_2^t|\boldsymbol{f}^{1:t}) \propto p(\boldsymbol{f}^t|S_2^t) \sum_{s_2^{t-1} \in \mathrm{Val}(S_2^{t-1})} p(S_2^t|s_2^{t-1})p(s_2^{t-1}|\boldsymbol{f}^{1:t-1}).$$

5.2.4 Extended SAGAT Score Models

The SAGAT Score models abstract from whether the process for establishing and maintaining SA is disturbed by an NDRT. Information whether the process is disturbed by an NDRT could help in predicting the SAGAT score. As such, let S_2, B, and $\boldsymbol{F}$ denote the SAGAT score, the behavioral patterns, and the set of indicators, as defined previously. The extended SAGAT Score models extend the SAGAT Score models by conditioning both the SAGAT score and the indicators with the behavioral patterns.

As such, for any number of time slices T, the extended SAGAT Score models define a JPD $p(S_2^{1:T}, \boldsymbol{F}^{1:T}, B^{1:T})$ as:

$$p(S_2^{1:T}, \boldsymbol{F}^{1:T}, B^{1:T}) = p(B^1)p(S_2^1|B^1)p(\boldsymbol{F}^1|S_2^1, B^1)\prod_{t=2}^{T} p(B^t)p(S_2^t|S_2^{t-1}, B^t)p(\boldsymbol{F}^t|S_2^t, B^t).$$

A graphical representation of the structure is shown in Figure 15.

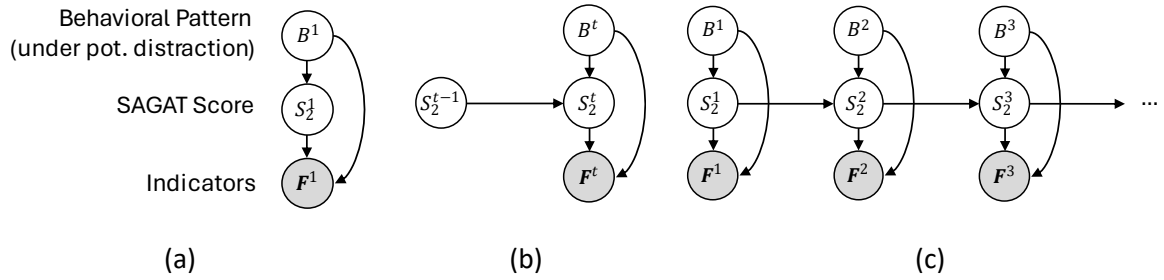

Figure 15: Conceptional structure of the extended SAGAT Score models. (a) BN for the first times slice. (b) 2TBN for subsequent time slices. (c) Unrolled network over multiple time slices.

Analogues to the SAGAT Score models, the extended SAGAT Score models are used to, with a constant frequency of 10Hz, infer the belief state $p(S_2^t|b^{1:t}, \boldsymbol{f}^{1:t})$, i.e., the probability distribution over the SAGAT score S_2^t at the current time step t, given the sequence of the behavioral patterns $b^{1:t}$ and the evidence of the SA indicators $\boldsymbol{f}^{1:t}$, from the activation of the system until t, given by:

$$p(S_2^t|b^{1:t}, \boldsymbol{f}^{1:t}) \propto p(\boldsymbol{f}^t|S_2^t, b^t) \sum_{s_2^{t-1} \in \mathrm{Val}(S_2^{t-1})} p(S_2^t|s_2^{t-1}, b^t)p(s_2^{t-1}|\boldsymbol{f}^{1:t-1}, b^{1:t-1}).$$

5.3 Datasets and annotations

The experiments conducted (c.f., Section 4.2) resulted in each 37 trials for SAE level 2 and 3 with approx. uniform distribution of trials without non-driving related task (SAE Level 2: 12 trials, SAE Level 3: 13 trials), cognitive non-driving related task (12, 12), and visual driving related task (13, 12). For training and validation of the DySAM models, the data was split into training data, used for parameter estimation and model selection, and test data, reserved exclusively for validation. The overall process is depicted in Figure 16. Each trial is composed of a two minute section where the vehicle drove on the right lane until changing to the middle lane, were it drove for seven (SAE Level 2) or four minutes (SAE Level 3), before the SAGAT was conducted, following by a three minute section on the middle lane until encountering a situation that required the driver to take over control.

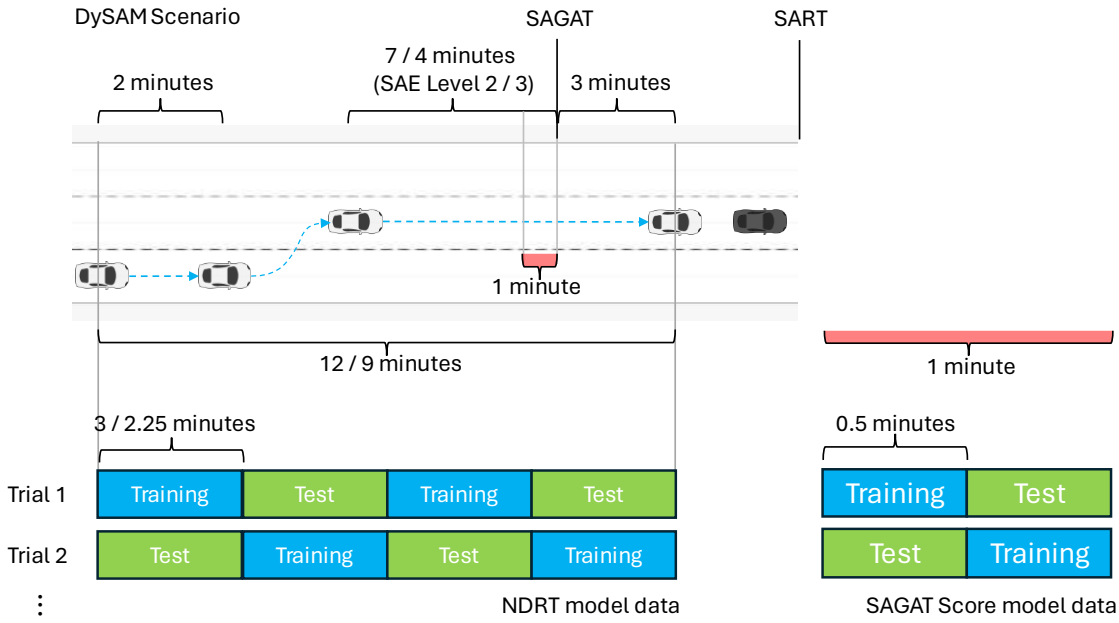

Figure 16: Illustration of splitting the DySAM data in training and test datasets for the NDRT and SAGAT models.

For the NDRT model, the data of each trial from start until the take-over situation was split into four equal-length sections of three (SAE Level 2) or 2.25 minutes (SAE Level 3) length that were alternately assigned to the training and test data. The order of assignment was changed for each trial, i.e., for half of the trials, the first and third sequence was assigned to the training data, the second and fourth sequence to the test data, and vice versa for the other half of the trials. To provide a ground truth situation awareness for training and evaluation, trials without NDRT $(B = b_0)$ were labelled as sufficient $(S_1 = s_{1_0})$, trials with cognitive $(B = b_1)$ or visual $(B = b_2)$ NDRT were labelled as insufficient $(S_1 = s_{1_1})$ SA. The result were two training datasets,

$$\mathcal{D}_{\text{Training}}^{\text{NDRT:L2}} = \left\{\left(b^{j,i}, s_1^{j,i}, \boldsymbol{f}^{j,i}\right)_{i=1}^{n_j}\right\}_{j=1}^{74}, \sum_{j=1}^{74} n_j = 148280$$

and

$$\mathcal{D}_{\text{Training}}^{\text{NDRT:L3}} = \left\{\left(b^{j,i}, s_1^{j,i}, \boldsymbol{f}^{j,i}\right)_{i=1}^{n_j}\right\}_{j=1}^{74}, \sum_{j=1}^{74} n_j = 101460,$$

and two test datasets

$$\mathcal{D}_{\text{Test}}^{\text{NDRT:L2}} = \left\{\left(b^{j,i}, s_1^{j,i}, \boldsymbol{f}^{j,i}\right)_{i=1}^{n_j}\right\}_{j=1}^{74}, \sum_{j=1}^{74} n_j = 148275$$

and

$$\mathcal{D}_{\text{Test}}^{\text{NDRT:L3}} = \left\{\left(b^{j,i}, s_1^{j,i}, \boldsymbol{f}^{j,i}\right)_{i=1}^{n_j}\right\}_{j=1}^{74}, \sum_{j=1}^{74} n_j = 101462,$$

each consisting of 74 approx. equal-sized sequences of approx. three / 2.25 minutes length.

For the "SAGAT Score" models, for each trial, a one-minute section before the SAGAT freeze was split into two equal length sections and allocated to training and test data in a similar fashion, using the SAGAT Score as a ground truth for S_2. The result were two training datasets,

$$\mathcal{D}_{\text{Training}}^{\text{SAG:L2}} = \left\{\left(b^{j,i}, s_2^{j,i}, \boldsymbol{f}^{j,i}\right)_{i=1}^{n_j}\right\}_{j=1}^{37}, \sum_{j=1}^{37} n_j = 11100$$

and

$$\mathcal{D}_{\text{Training}}^{\text{SAG:L3}} = \left\{\left(b^{j,i}, s_2^{j,i}, \boldsymbol{f}^{j,i}\right)_{i=1}^{n_j}\right\}_{j=1}^{37}, \sum_{j=1}^{37} n_j = 11100,$$

and two test datasets

$$\mathcal{D}_{\text{Test}}^{\text{SAG:L2}} = \left\{\left(b^{j,i}, s_2^{j,i}, \boldsymbol{f}^{j,i}\right)_{i=1}^{n_j}\right\}_{j=1}^{37}, \sum_{j=1}^{37} n_j = 11101$$

and

$$\mathcal{D}_{\text{Test}}^{\text{SAG:L3}} = \left\{\left(b^{j,i}, s_2^{j,i}, \boldsymbol{f}^{j,i}\right)_{i=1}^{n_j}\right\}_{j=1}^{37}, \sum_{j=1}^{37} n_j = 11100,$$

each consisting of 37 equal-sized sequences of 30 seconds length.

5.4 Indicator analysis

Section 5.1.3 provides an overview of how each of the selected SA indicators is obtained from the sensor information provided by the UULM simulator platform. This section provides a more detailed overview of the indicator measurements derived from the SAE Level 2 and SAE Level 3 training data and their discriminative power for discriminating between the three different behavioral patterns / NDRT conditions.

5.4.1 Indicator overview

This section provides histograms for each indicator derived from the SAE Level 2 and SAE Level 3 training data. In general, we have that driver behavior when distracted by a visual NDRT clearly differs from driver behavior without NDRT and when distracted by a cognitive NDRT, while distinction between the latter is much more difficult. Furthermore, there are only subtle differences between driver behavior under SAE Level 2 and SAE Level 3 conditions.

5.4.1.1 Sensor failure indicators

Figure 17 shows histograms of the four sensor failure indicators in the SAE Level 2 and SAE Level 3 training data. As a reminder, for sensor failure indicators, a value of 0 indicates an invalid, while a value of 1 indicates a valid measurement. As should be apparent, invalid measurements of the pupil diameter and the head rotation are quite rare, while invalid measurements concerning the gaze origin and especially the gaze direction are much more common. In all cases, sensor failures are more common during the visual NDRT, potentially caused by the tendency of the drivers to look at the infotainment system, where the Smart Eye Pro eye-tracking system is more likely to lose track of the gaze.

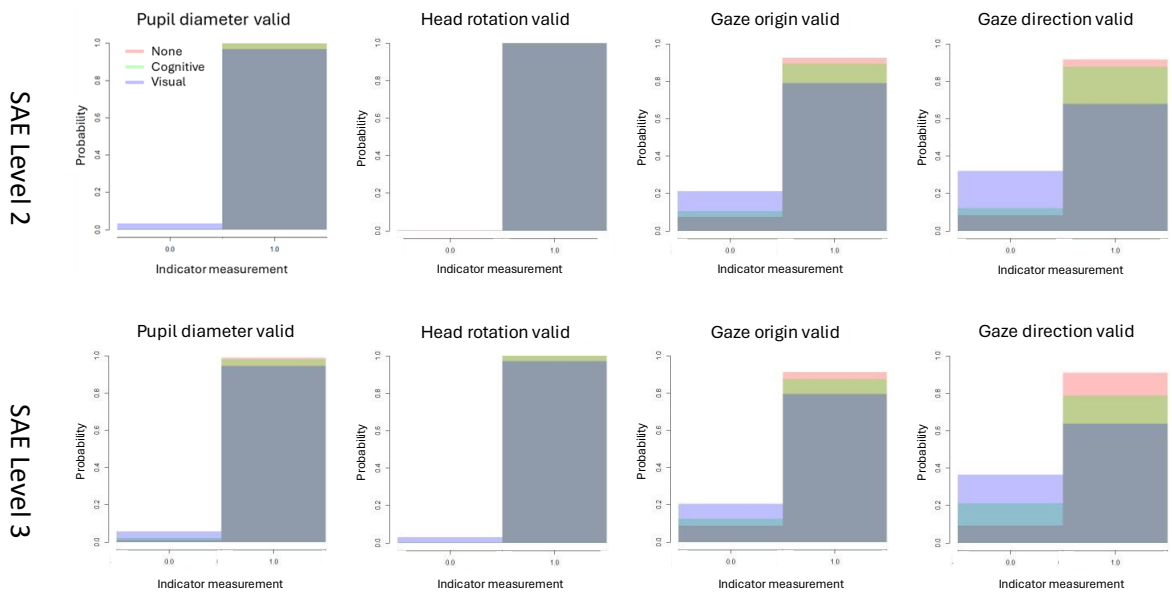

Figure 17: Histograms of the sensor failure indicators in the SAE Level 2 (top row) and SAE Level 3 (bottom row) training data.

5.4.1.2 Pupil diameter indicators

Figure 18 shows histograms of the three pupil diameter indicators in the SAE Level 2 and SAE Level 3 training data. Concerning the mean pupil diameter, there are some differences between the no NDRT and cognitive NDRT condition, although much more pronounced in SAE Level 2 than SAE Level 3. Unfortunately, we were unable to conclude whether these changes are an effect of the different NDRT conditions or an artifact of the natural variability in the participants average pupil diameters, resulting in the exclusion of the pupil diameter and mean pupil diameter indicators from modelling. The pupil diameter variability should be more robust to the natural variability in the participants average pupil diameters and provides some discrimination between the visual NDRT and the no / cognitive NDRT condition.

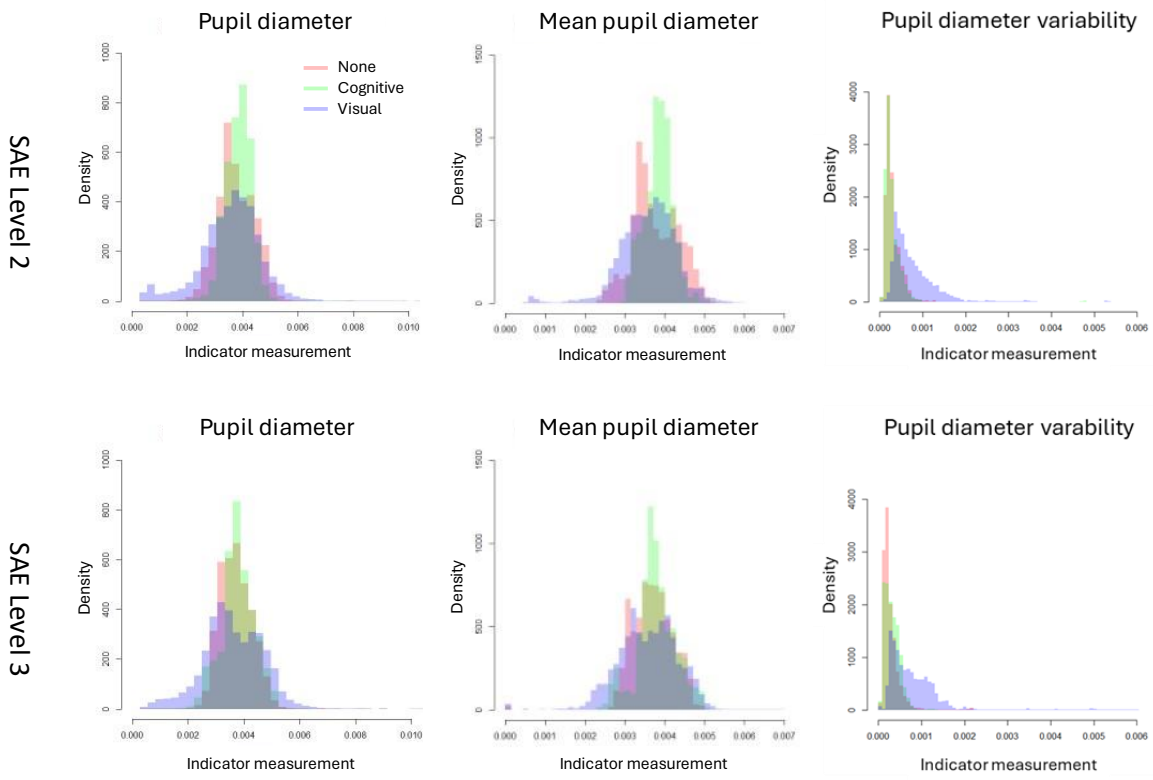

Figure 18: Histograms of the pupil diameter indicators in the SAE Level 2 (top row) and SAE Level 3 (bottom row) training data.

5.4.1.3 Blink frequency indicators

Figure 19 shows histograms of the three blink frequency indicators in the SAE Level 2 and SAE Level 3 training data. Participants without NDRT show normal and mean blink frequencies up to approx. 1.5 blinks per second, peaking at around 0.4 blinks per second. Participants tasked with the cognitive NDRT show higher frequences up to approx. 3 blinks per second, with a peak around 0.5 blinks per second. Participants tasked with the visual NDRT show even higher frequencies up to 4 blinks per second, but peak at the lowest frequency of around 0.1 blinks per second. Comparing SAE Level 2 and SAE Level 3, most noticeable, there is a peak for the normal and mean blink frequency in the region of 0.5 – 1.5 blinks per seconds for participants tasked with the cognitive NDRT and an opposite "dent" for participants tasked with the visual NDRT. More research is needed to conclude whether these changes are an effect of the different NDRT conditions or an artifact of a potential natural variability in the participants average blink frequency.

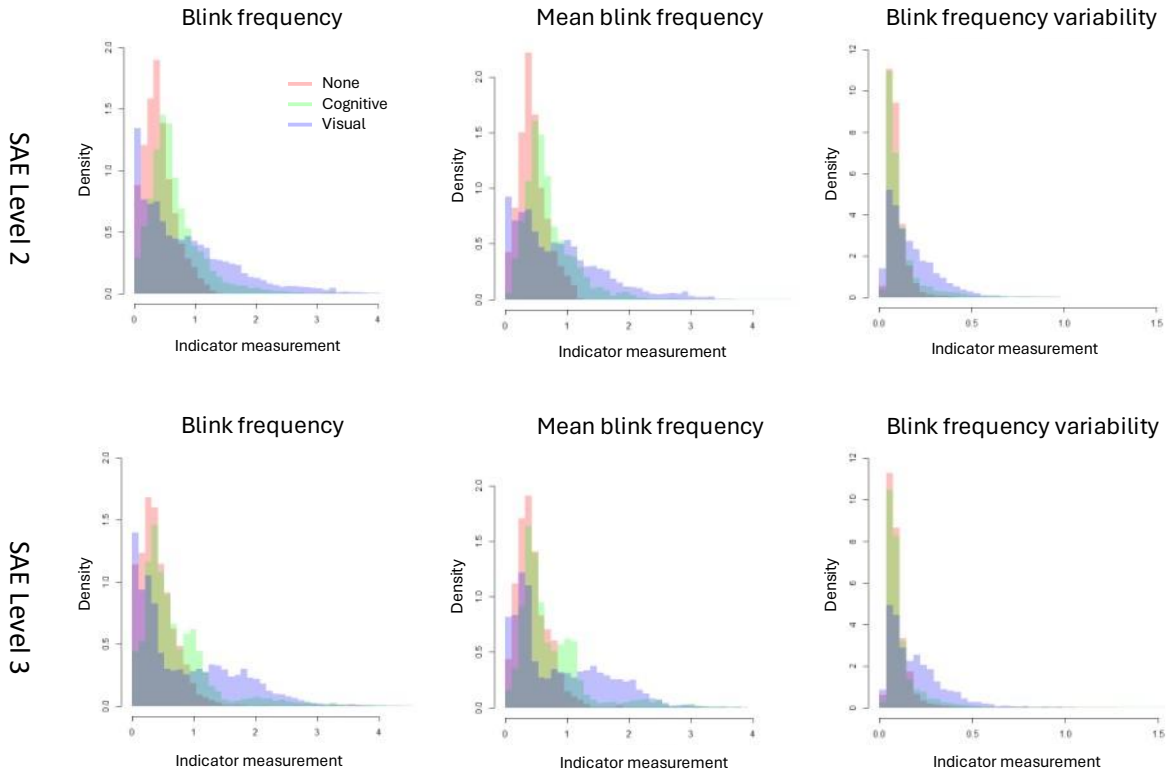

Figure 19: Histograms of the blink frequency indicators in the SAE Level 2 (top row) and SAE Level 3 (bottom row) training data.

5.4.1.4 Yaw angle of the head indicators

Figure 20 shows histograms of the three yaw angles of the head indicators in the SAE Level 2 and SAE Level 3 training data. As expected by the nature of the visual NDRT, participants tasked with the visual NDRT are much more likely to have their head rotated to the right (towards the infotainment AOI) allowing for a clear discrimination between the visual NDRT and the no / cognitive NDRT conditions, and show a slightly higher variability in the yaw angle of the head, Participants tasked with the cognitive NDRT keep their heads rotated slightly more to the right and center than participants without NDRT and show a lower variability. Comparing SAE Level 2 and SAE Level 3, the differences in variability reduce for SAE Level 3, while the (slight) differences between the (mean) yaw angle of the head between participants tasked with the cognitive vs. no NDRT strengthen.

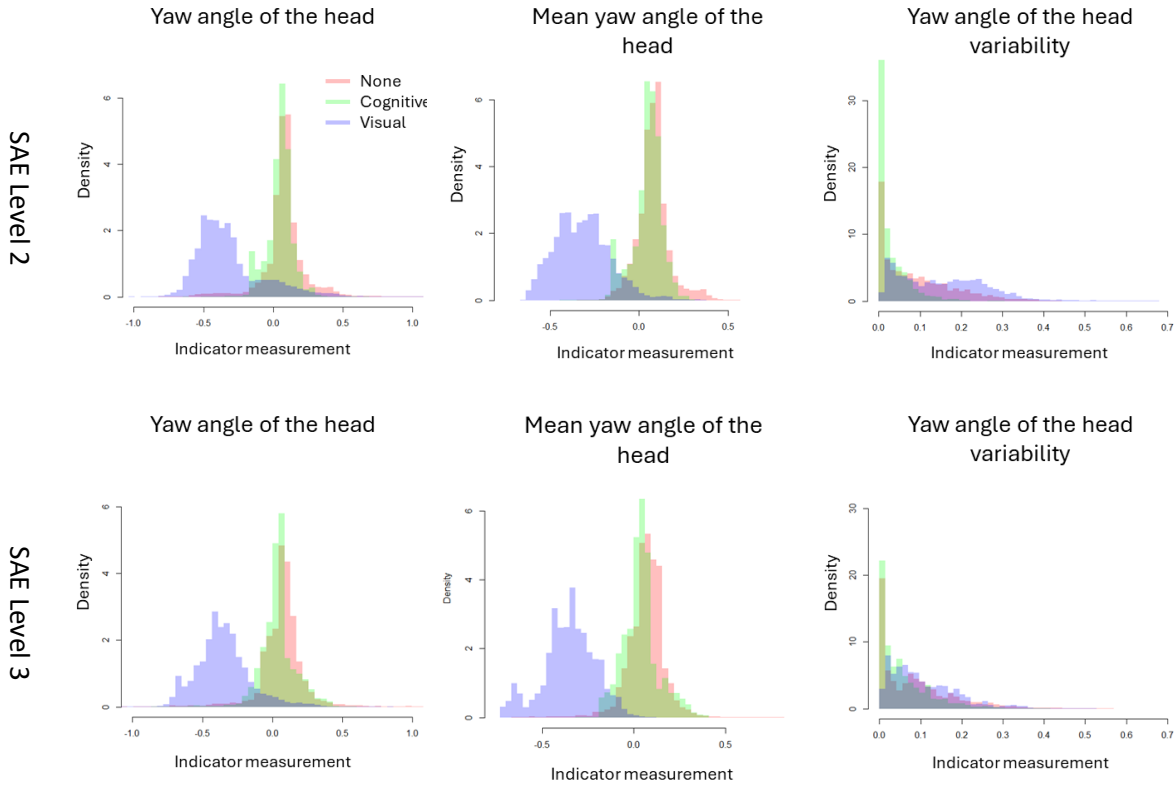

Figure 20: Histograms of the yaw angle of the head indicators in the SAE Level 2 (top row) and SAE Level 3 (bottom row) training data.

5.4.1.5 Yaw rate of the head indicators

Figure 22 shows histograms of the three yaw rates of the head indicators in the SAE Level 2 and SAE Level 3 training data. Visually, the yaw rate of the head and mean yaw rate of the head indicators do not provide a clear discrimination between the different NDRT conditions, although, within SAE Level 2, the mean yaw rate of the head indicator indicates that participants are more likely to keep their head rotation stable when tasked with the cognitive NDRT than when tasked with no or the visual NDRT. This difference is much less pronounced for SAE Level 3, which is consistent with the yaw angle of the head indicators. As with previous indicators, the yaw rate of the head variability is higher for the visual NDRT than for the no / cognitive NDRT conditions.

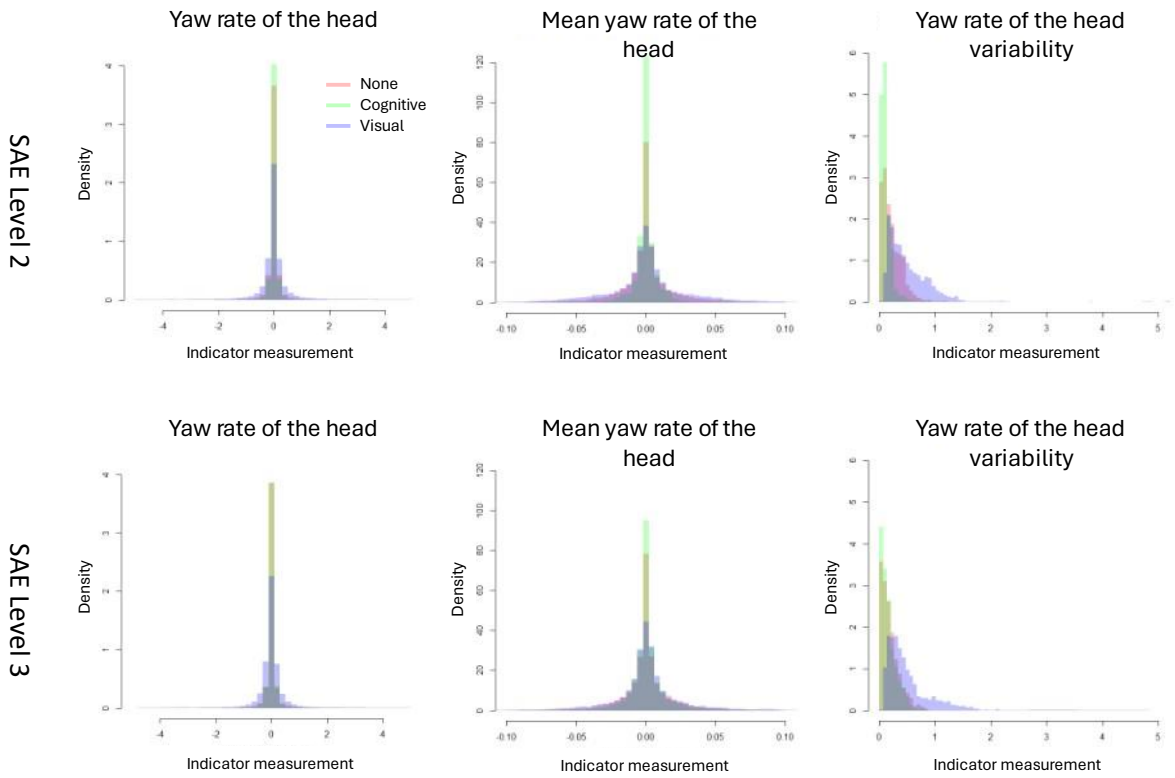

Figure 21: Histograms of the yaw rate of the head indicators in the SAE Level 2 (top row) and SAE Level 3 (bottom row) training data.

5.4.1.6 Gaze heading and pitch indicators

In contrast to the other indicators, Figure 22 shows scatter plots of the (inverted) gaze heading versus the gaze pitch angle, with the density color-encoded in a way that darker colors represent higher densities. The gaze heading has been inverted to allow for a more intuitive mapping of the scatter plot to the layout of the cockpit of the UULM driving simulator.

The gazes of participants without NDRT are primarily focused on the windshield, with a noticeable concentration of gazes towards the road center ahead, and otherwise distributed between the left, rear, and right mirror, the tachometer, and occasionally the infotainment system. As such, participants without NDRT seem to regularly monitor each of the driving-related AOIs. The gazes of participants tasked with the cognitive NDRT are more concentrated on a single region, representing the road center, with less gazes towards the mirrors and the tachometer, which is consistent with literature suggesting an increase of gaze concentration towards the road center under cognitive load (Victor, Harbluk, & Engström, 2005) (Wilkie, et al., 2019). Lastly, as confirmed by the current AOI indicator (c.f., Section 5.4.1.8), the majority of gazes of participants tasked with the visual NDRT are guided towards the infotainment system, with the remaining gazes focusing on the road ahead, the mirrors, and the tachometer.

Comparing SAE Level 2 and SAE Level 3, the overall distribution of gazes stays mostly identical for the participants without and tasked with the cognitive NDRT. For participants tasked with the visual NDRT, there seems to be an increase of gazes towards the infotainment system for SAE Level 3, which is confirmed by the current AOI indicator (c.f., Section 5.4.1.8).

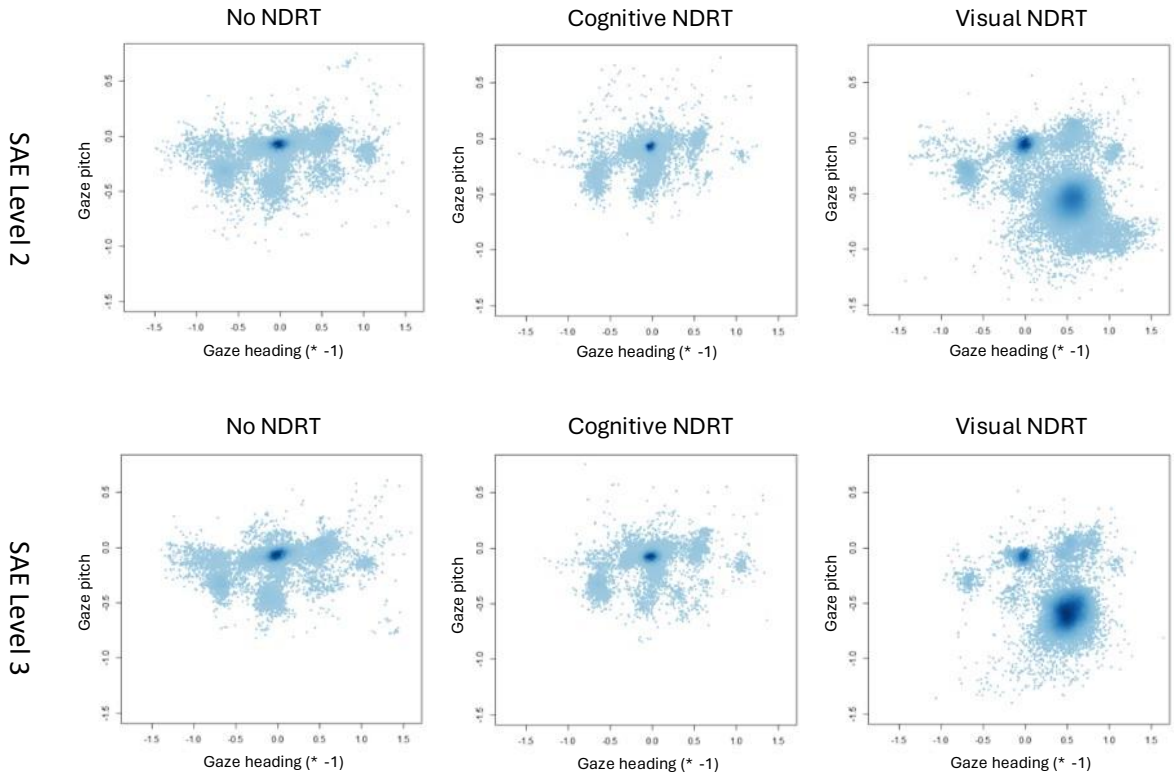

Figure 22: Scatter plots of the (inverted) gaze heading vs. gaze pitch in the SAE Level 2 (top row) and SAE Level 3 (bottom row) training data.

Figure 23 shows scatter plots of the (inverted) mean gaze heading versus the mean gaze pitch angle. As a reminder, the mean gaze heading and gaze pitch are calculated as the average gaze heading and pitch over the last ten seconds (c.f., Section 5.1). For participants without NDRT, the mean gazes show a high concentration on the road center ahead, but with a reasonable spread along the windshield area and towards, but not on, the left and rear mirror, which implies that glances towards the mirrors and tachometer last less than a few seconds. The distribution of mean gazes for participants tasked with the cognitive NDRT are similar but with a much higher concentration on a smaller region around the road center ahead, which implies a kind of “starring” behavior, in which the participants keep looking straight ahead without shifting attention to other regions of the visual field. For participants tasked with the visual NDRT, the mean gazes are mostly located on the infotainment system, which gets more prominent for SAE Level 3.

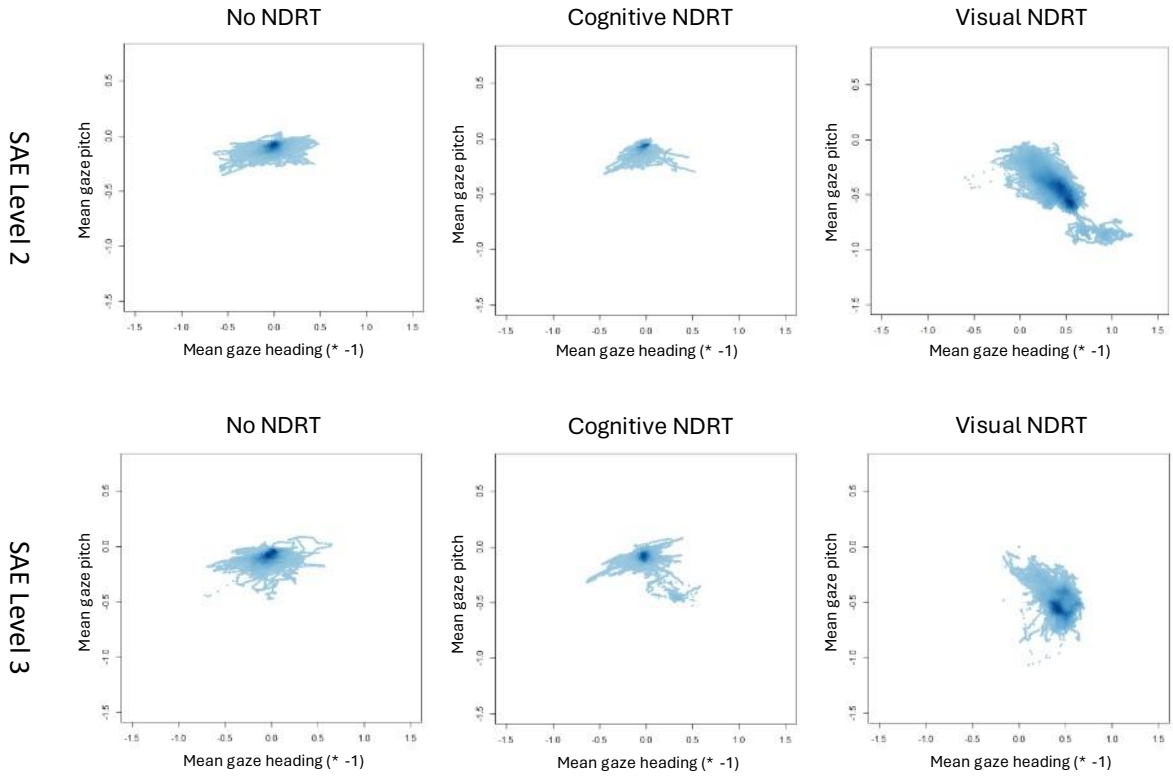

Figure 23: Scatter plots of the (inverted) mean gaze heading vs. mean gaze pitch in the SAE Level 2 (top row) and SAE Level 3 (bottom row) training data.

The assumption that participants tasked with the cognitive NDRT show some sort of "starring" behavior is also confirmed by the gaze heading and gaze pitch variability, whose scatter plots are shown in Figure 24. As apparent, under the cognitive NDRT condition, participants show a clearly reduced variability in gaze heading and pitch, when compared to the no / visual NDRT conditions. Participants without NDRT show a medium variability for the gaze pitch but a high variability for the gaze heading, participants tasked with the visual NDRT show high variability for both gaze heading and pitch. Noticeable, participants tasked with the visual NDRT have a much higher minimum heading and pitch variability compared to the no / cognitive NDRT conditions. Overall, the gaze heading and gaze pitch variability seem to promise a meaningful discrimination between the different NDRT conditions, especially, when taking into account the correlation between the indicators.

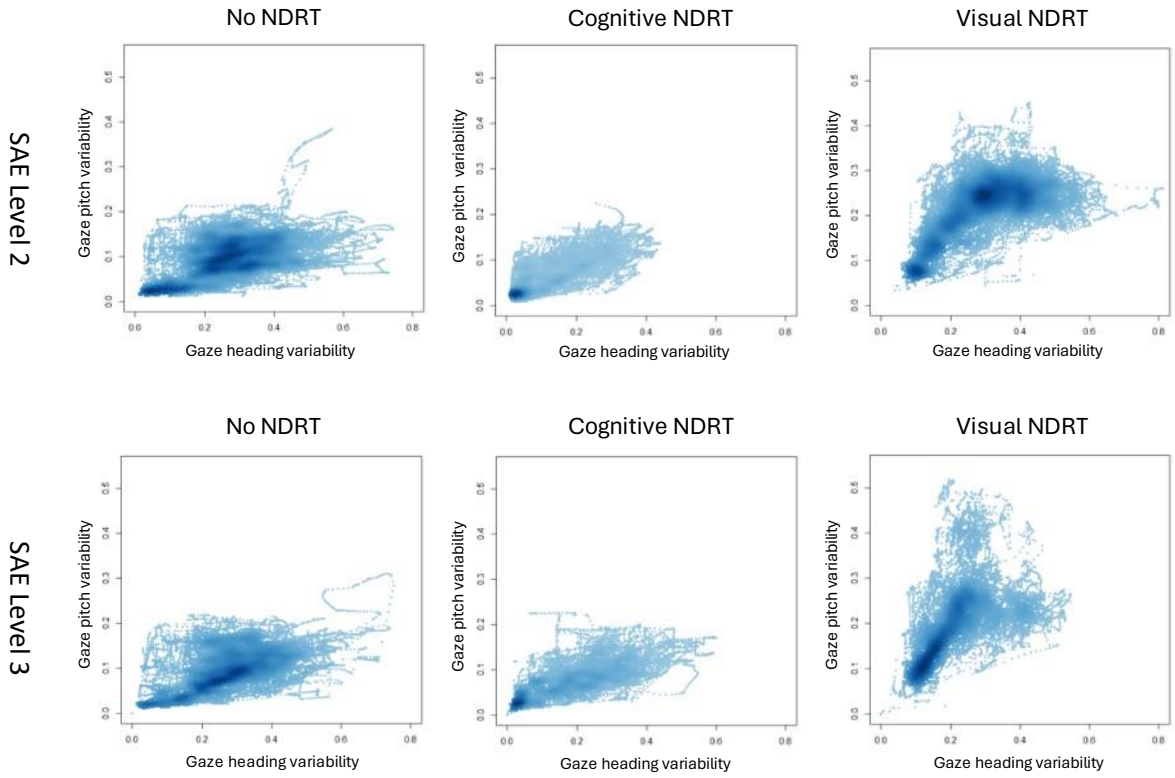

Figure 24: Scatter plots of the gaze heading vs. gaze pitch variability in the SAE Level 2 (top row) and SAE Level 3 (bottom row) training data.

5.4.1.7 Hands-on steering wheel indicator

Figure 25 shows histograms of the hands-on steering wheel indicator in the SAE Level 2 and SAE Level 3 training data. For SAE Level 2, participants without NDRT kept their hands on the steering wheel for 99.95% of the time, participants tasked with the cognitive NDRT still for 94.21% of the time, but participants tasked with the visual NDRT only for 86.44% of the time. Surprisingly, this somewhat reverses for SAE Level 3: Participants without and tasked with the cognitive NDRT kept their hands on the steering wheel for 86.07% and 86.71% respectively, while participants tasked with the visual NDRT kept their hands on the steering wheel for 97.12% of the time. However, more research is needed to determine, whether this is a consequence of the SAE level or just an artifact of participants prior preferences.

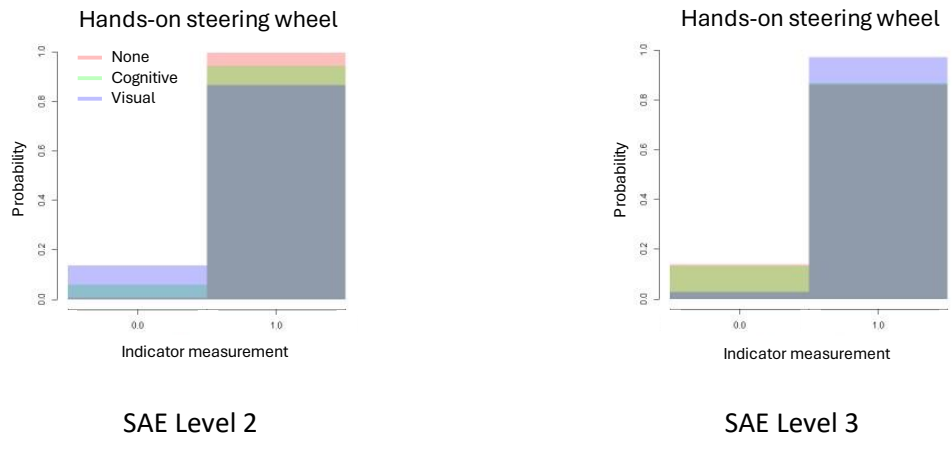

Figure 25: Histograms of the hands-on steering wheel indicator in the SAE Level 2 (left) and SAE Level 3 training data (right).

5.4.1.8 Current AOI indicator

Figure 26 shows histograms of the current AOI indicator in the SAE Level 2 and SAE Level 3 training data. Focusing on SAE Level 2, participants without NDRT primarily gazed at the front area (76.08%), followed by the "other" AOI (9.03%), the rear mirror (6.82%), left mirror (3.72%), tachometer (3.51%), and right mirror (0.16%)[3]. Participants tasked with the cognitive NDRT almost exclusively gazed at the front AOI (91.90%), followed by the "other" AOI (3.34%), the tachometer (2.17%), the left mirror (1.38%), the rear mirror (0.89%), the infotainment system (0.25%), and almost no gazes towards the right mirror (0.06%). In contrast, participants tasked with the visual NDRT primarily gazed at the infotainment system (57.86%), followed by the front area (19.58%), the "other" AOI (17.76%), the rear mirror (2.49%), the left mirror (1.45%), the tachometer (0.70%), and the right mirror (0.16%). For SAE Level 3, percentages change slightly, but the overall trend stays mostly the same: Participants without NDRT still primarily gazed at the front area (75.17%), followed by the "other" AOI (10.28%), the rear mirror (5.91%), tachometer (4.28%), left mirror (3.41%), and the right mirror (0.27%). Participants tasked with the cognitive NDRT focused a little less on the front AOI (86.93%), followed by the "other" AOI (6.16%), the rear mirror (3.54%), the left mirror (1.78%), the tachometer (1.11%), slightly more gazes towards the right mirror (0.12%), but almost no gazes towards the infotainment system (0.12%). Lastly, participants tasked with the visual NDRT increasingly gazed at the infotainment system (72.06%), followed by the "other" AOI (12.74%), the front area (12.46%), the rear mirror (1.58%), the tachometer (0.56%), the left mirror (0.53%), and the right mirror (0.49%).

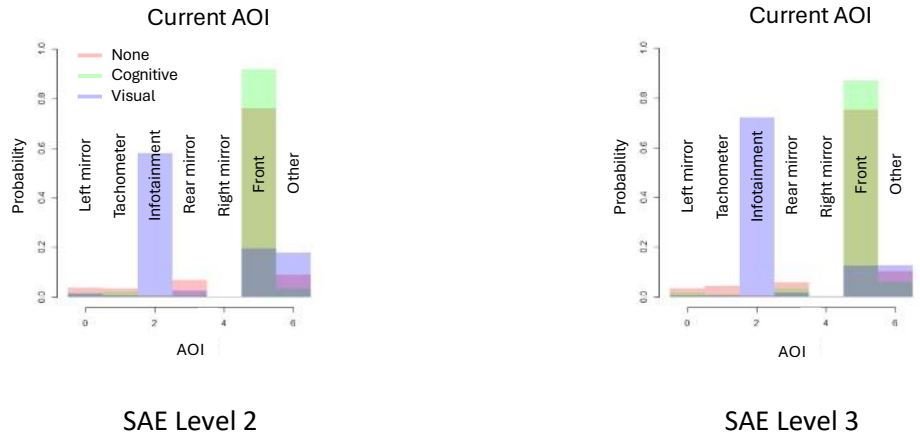

SAE Level 2 SAE Level 3

Figure 26: Histograms of the current AOI indicator in the SAE Level 2 (left) and SAE Level 3 training data (right).

5.4.1.9 Glance duration indicators

Figure 27 shows histograms of the three glance duration indicators in the SAE Level 2 and SAE Level 3 training data. Participants tasked with the visual NDRT have the shortest normal and mean glance duration (in the range of 1-3 seconds) and the lowest variability. Participants without and tasked with the cognitive NDRT have longer glance duration (mostly in the range of 1-20 seconds), with the latter showing longer tails (up to over 100 seconds), which fits the assumption of starring behavior.

[3] Considering the scatter plot of the gazes (c.f., Figure 22), it is likely that gazes towards the right mirror are not correctly detected by the Smart Eye Pro eye-tracking system and will be incorrectly labelled as an "other" AOI. Similarly, gazes towards the bottom of the infotainment system may not be correctly detected and will be incorrectly labelled as an "other" AOI in the same way.

Comparing SAE Level 2 and SAE Level 3, the histograms are mostly identical, with the (mean) glance duration and variability for participants without NDRT becoming slightly longer.

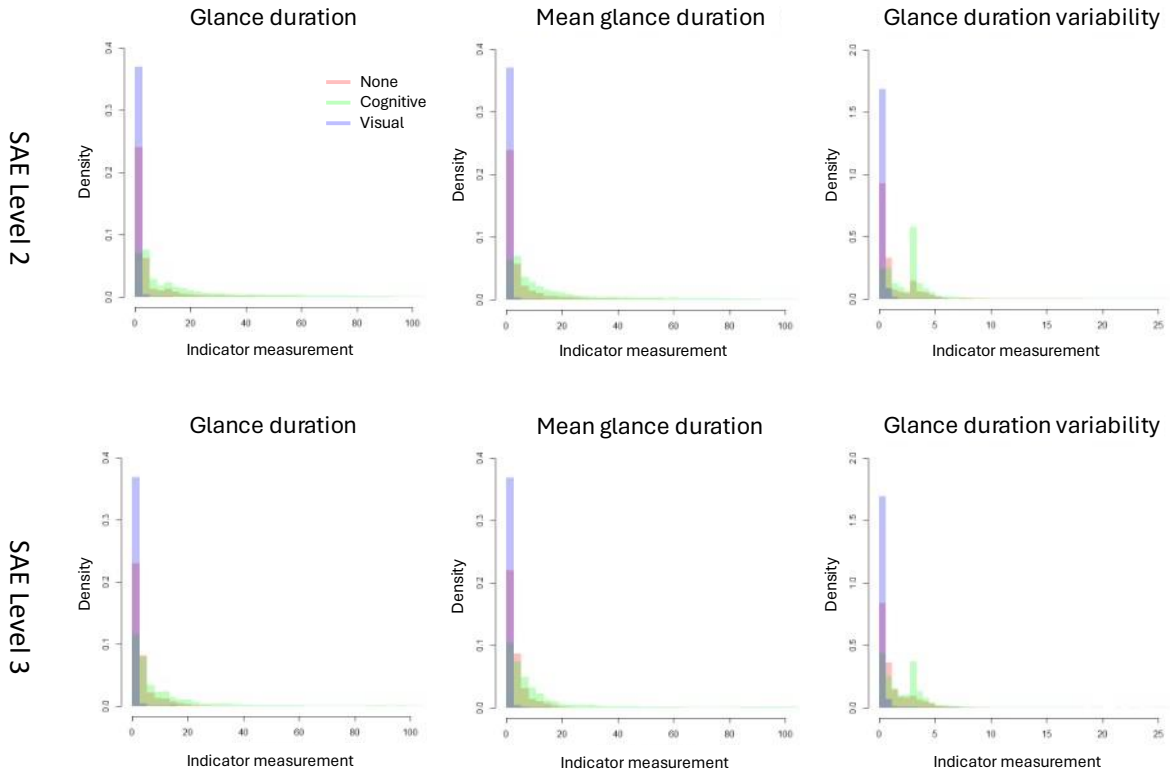

Figure 27: Histograms of the glance duration indicators in the SAE Level 2 (top row) and SAE Level 3 (bottom row) training data.

5.4.1.10 Monitoring frequency indicators

Figure 28 shows histograms of the three monitoring frequency indicators in the SAE Level 2 and SAE Level 3 training data. For participants without NDRT, the normal and mean monitoring frequency is well distributed over a region of approx. 0 – 1 glances per second, with a maximum at 0.5 glances per second. Compared to that, the distribution of glances per second for participants tasked with the cognitive NDRT is shifted and skewed towards lower frequencies, with a maximum of 0 glances per second. Once again, this hints at a kind of "starring" behavior of participants tasked with the cognitive NDRT, and consequently, the normal and mean monitoring frequency could provide some discrimination between the no and cognitive NDRT conditions. For participants tasked with the visual NDRT, the distribution over the monitoring frequency is similar to that of participants tasked with the cognitive NDRT, but with more density mass in the region of 0 – 0.5 glances per second. For SAE Level 3, most noticeable the normal and mean monitoring frequency increases for participants tasked with the cognitive but decreases for participants tasked with the visual NDRT. This is consistent with the current AOI indicator (c.f., Section 5.4.1.8), showing that for SAE Level 3, participants tasked with the cognitive NDRT focus less on the front AOI, while participants tasked with the visual NDRT focus more on the infotainment AOI.

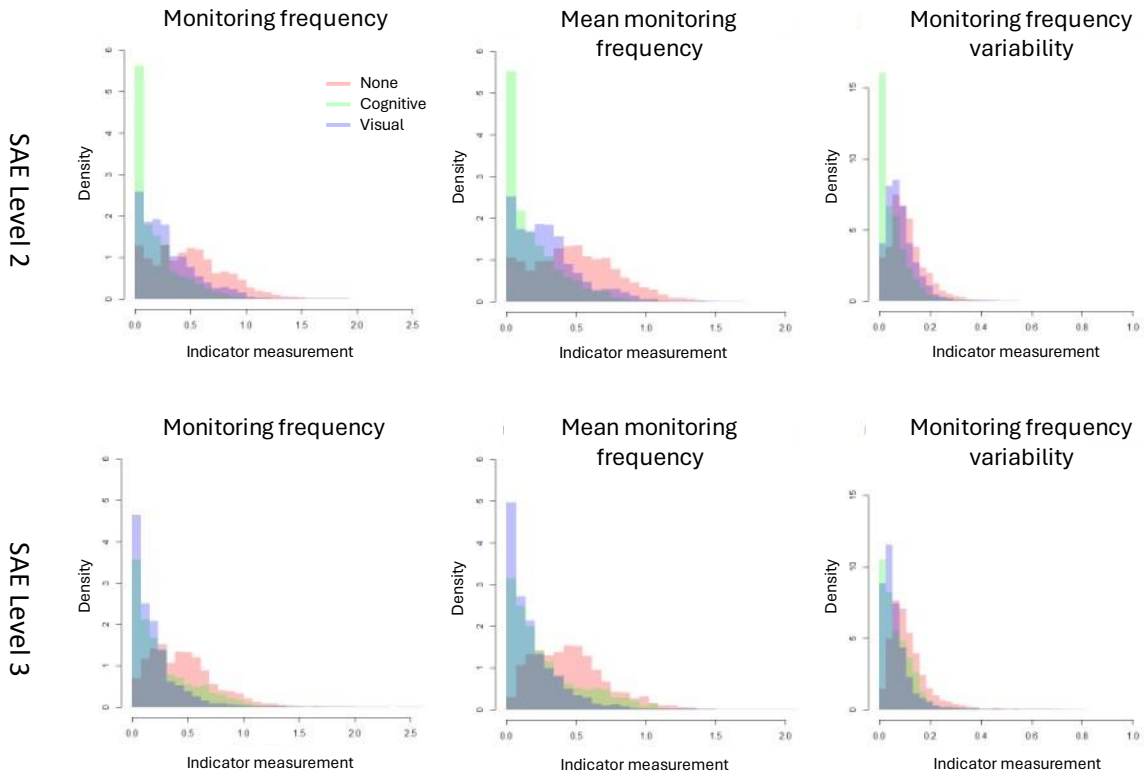

Figure 28: Histograms of the monitoring frequency indicators in the SAE Level 2 (top row) and SAE Level 3 (bottom row) training data.

5.4.1.11 Saccade frequency indicators

Figure 29 shows histograms of the three saccade frequency indicators in the SAE Level 2 and SAE Level 3 training data. To start, there are no noteworthy differences between SAE Level 2 and SAE Level 3 and the saccade frequency variability is almost identical for all three NDRT conditions. There are, however, some differences in the normal and mean saccade frequencies among the NDRT conditions. While participants without NDRT have average normal and mean saccade frequencies of approx. 1.4 saccades per second, the average normal and mean saccade frequencies is reduced to approx. 1.3 saccades per second for participants tasked with the cognitive NDRT, and enlarged to approx. 2.1 saccades per second for participants tasked with the visual NDRT.

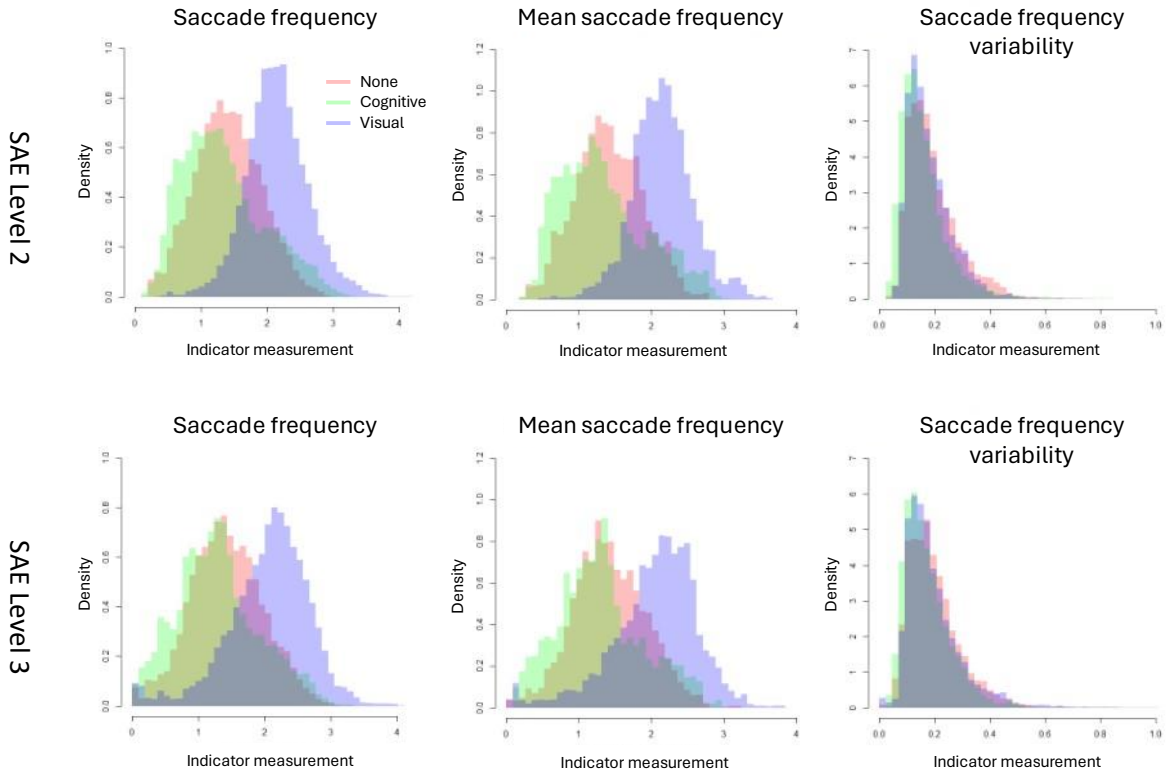

Figure 29: Histograms of the saccade frequency indicators in the SAE Level 2 (top row) and SAE Level 3 (bottom row) training data.

5.4.1.12 Dwell percentage indicators

Figure 30 shows histograms of the three dwell percentage indicators in the SAE Level 2 and SAE Level 3 training data. As apparent from the normal and mean dwell percentage, participants tasked with the visual NDRT almost spend approx. less than 60%, participants without NDRT approx. more than 50%, and participants tasked with the cognitive NDRT approx. more than 75% of the last ten seconds focusing on driving-related AOIs, allowing for a clear discrimination between participants tasked with the visual NDRT and the rest. Maybe even more importantly, the normal and mean dwell percentage indicators allows allow for some discrimination between participants tasked with no and the cognitive NDRT, in that the latter are much more likely to spend 100% of the last ten seconds focusing on driving-related AOIs.

When comparing SAE Level 2 and SAE Level 3, the histograms imply a decline in both mean and normal dwell percentage of participants tasked with the cognitive NDRT to focus 100% and a rise of participants tasked with the visual NDRT to focus 0% of the last ten seconds on driving-related AOIs. However, these differences are more likely an artifact of the comparably shorter duration of SAE Level 3 trials, rather than a change in behavior between SAE levels.

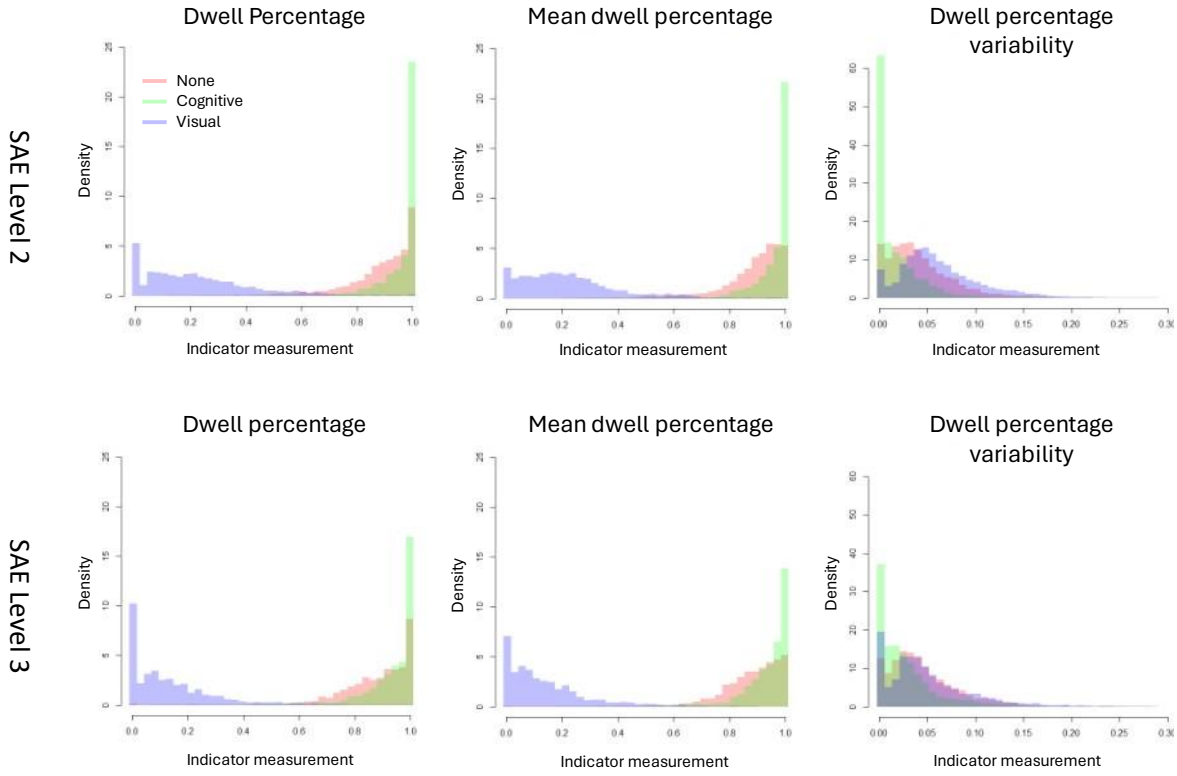

Figure 30: Histograms of the dwell percentage indicators in the SAE Level 2 (top row) and SAE Level 3 (bottom row) training data.

5.4.1.13 Left mirror AOI indicators

Figure 31 and Figure 32 show histograms of the five left mirror AOI indicators in the SAE Level 2 and SAE Level 3 training data. Starting with SAE Level 2, we have that participants without NDRT look at the left mirror with the highest frequency, accumulate the minimum (mean) time between looks to the left mirror and spend the most time looking into the left mirror, followed by participants tasks with the visual NDRT, and participants tasked with the cognitive NDRT. For the latter two, we notice frequent long tails in the (mean) time since the last look at the left mirror, implying that participants tasked with the visual and especially cognitive NDRT occasionally ignore the left mirror for several minutes.

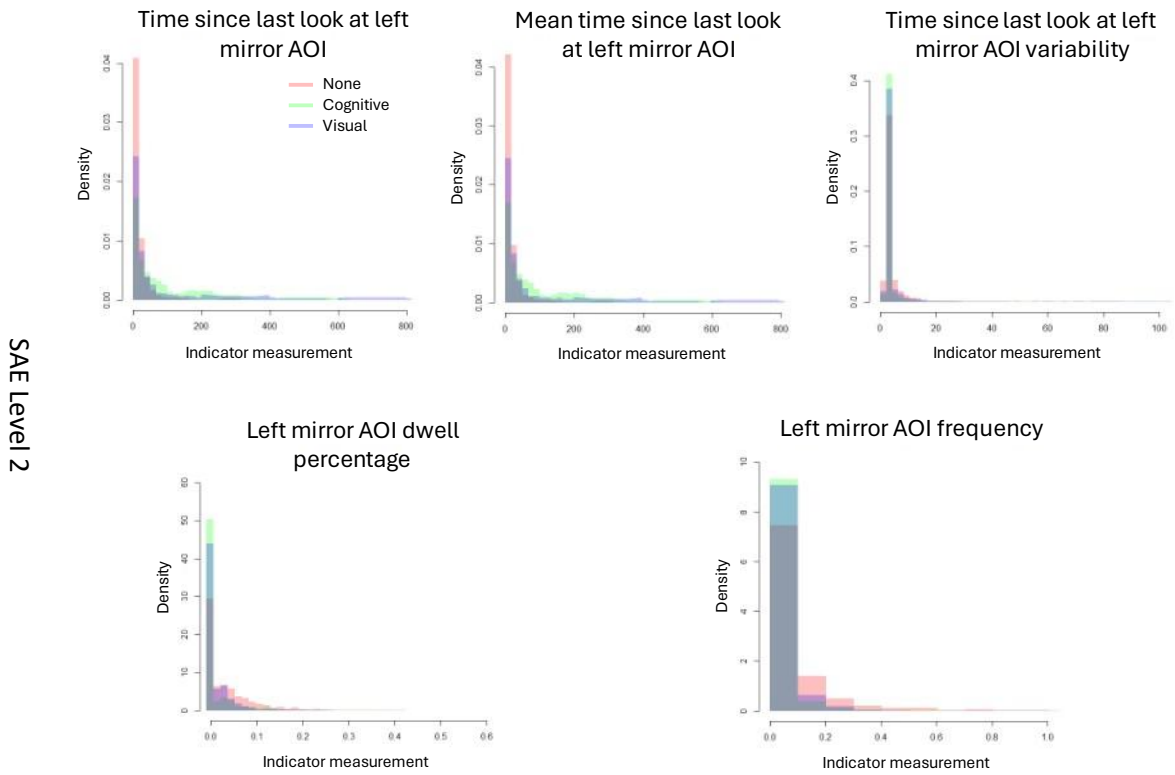

Figure 31: Histograms of the left mirror AOI indicators in the SAE Level 2 training data.

Comparing SAE Level 2 and SAE Level 3, the behavior of participants without NDRT stays mostly identical, while participants tasked with the cognitive NDRT become slightly more likely, while participants tasked with the visual NDRT become less likely to focus on the left mirror.

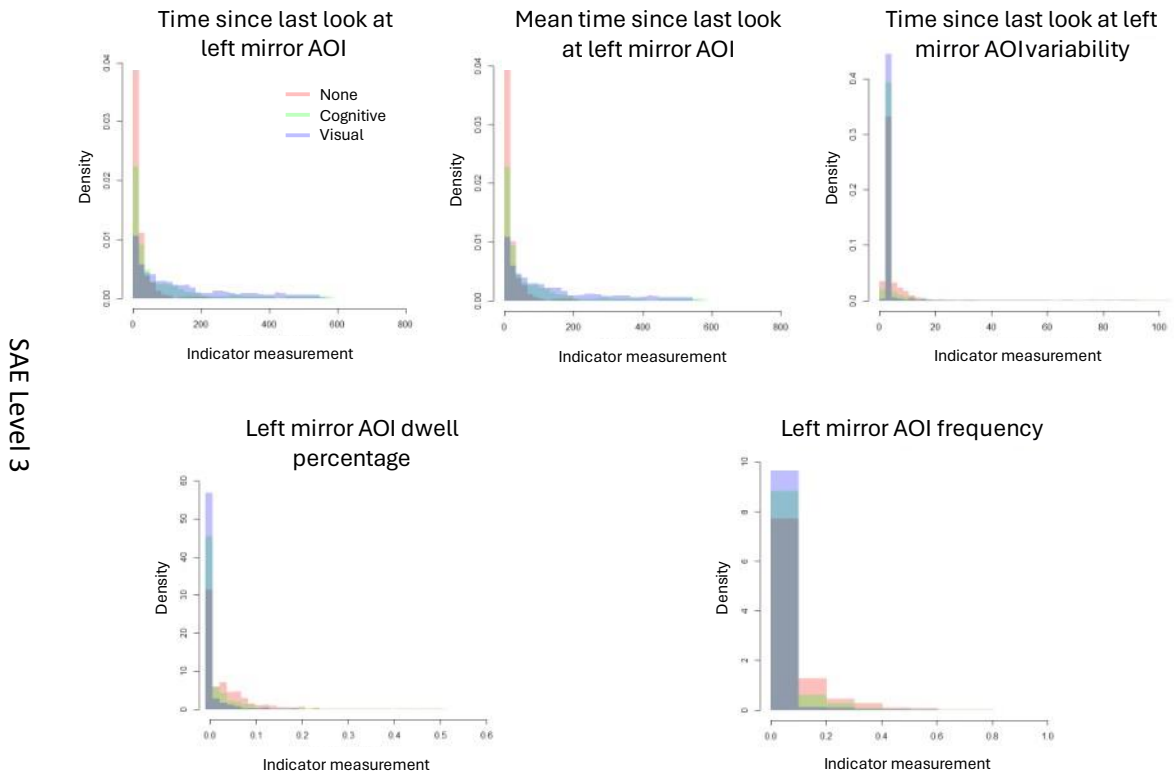

Figure 32: Histograms of the left mirror AOI indicators in the SAE Level 3 training data.

5.4.1.14 Right mirror AOI indicators

Figure 33 and Figure 34 show histograms of the five right mirror AOI indicators in the SAE Level 2 and SAE Level 3 training data. Unfortunately, the right mirror AOI indicators are limited by the ability of the Smart Eye Pro eye-tracking system to consistently detect glances to the right mirror, resulting in very long time and mean times and very low dwell percentages and frequencies for all NDRT conditions. As a consequence, the right mirror AOI indicators provide very little discrimination between the different NDRT conditions.

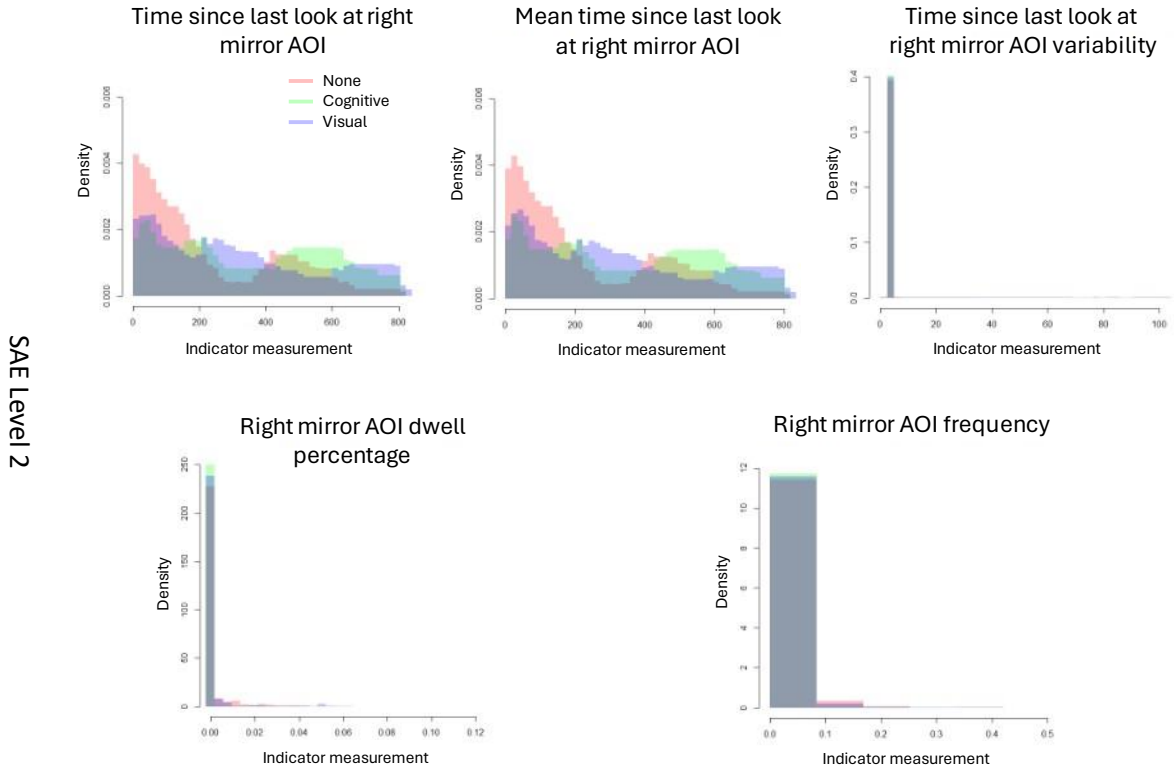

Figure 33: Histograms of the right mirror AOI indicators in the SAE Level 2 training data.

Comparing SAE Level 2 and SAE Level 3, we have a slightly higher likelihood of participants without NDRT to look at the right mirror within SAE Level 2 but a slightly higher likelihood of participants tasked with the cognitive NDRT to look at the right mirror within SAE Level 3.

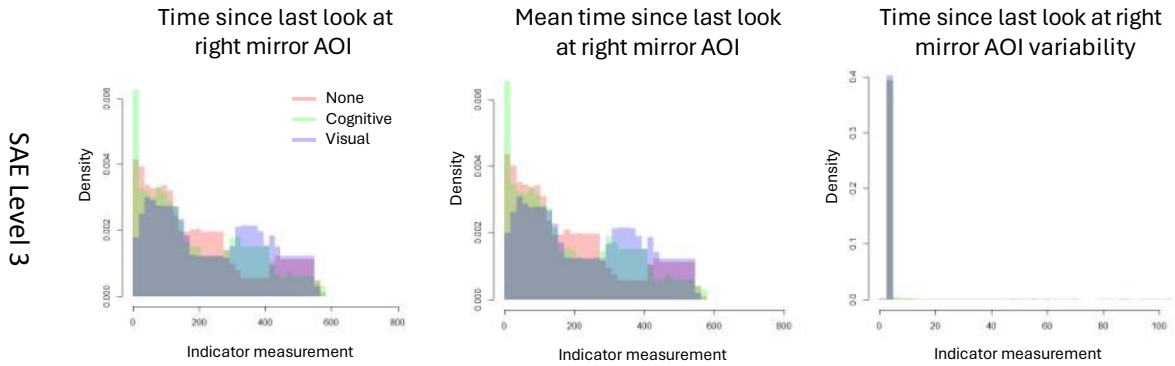

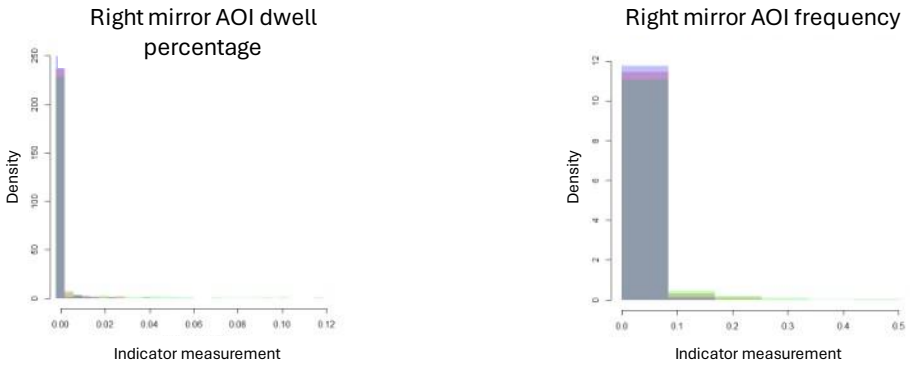

Figure 34: Histograms of the right mirror AOI indicators in the SAE Level 3 training data.

5.4.1.15 Rear mirror AOI indicators

Figure 35 and Figure 36 show histograms of the five rear mirror AOI indicators in the SAE Level 2 and SAE Level 3 training data. The rear mirror AOI indicators tell a very similar story to the left mirror AOI indicators (c.f., Section 5.4.1.13). Starting with SAE Level 2, we have that participants without NDRT look at the rear mirror with the highest frequency, accumulate the minimum (mean) time between looks to the rear mirror and spend the most time looking into the rear mirror, followed by participants tasks with the visual NDRT, and participants tasked with the cognitive NDRT. For the latter two, we, once again, notice frequent long tails in the (mean) time since the last look at the rear mirror, implying that participants tasked with the visual and especially cognitive NDRT occasionally ignore the rear mirror for several minutes.

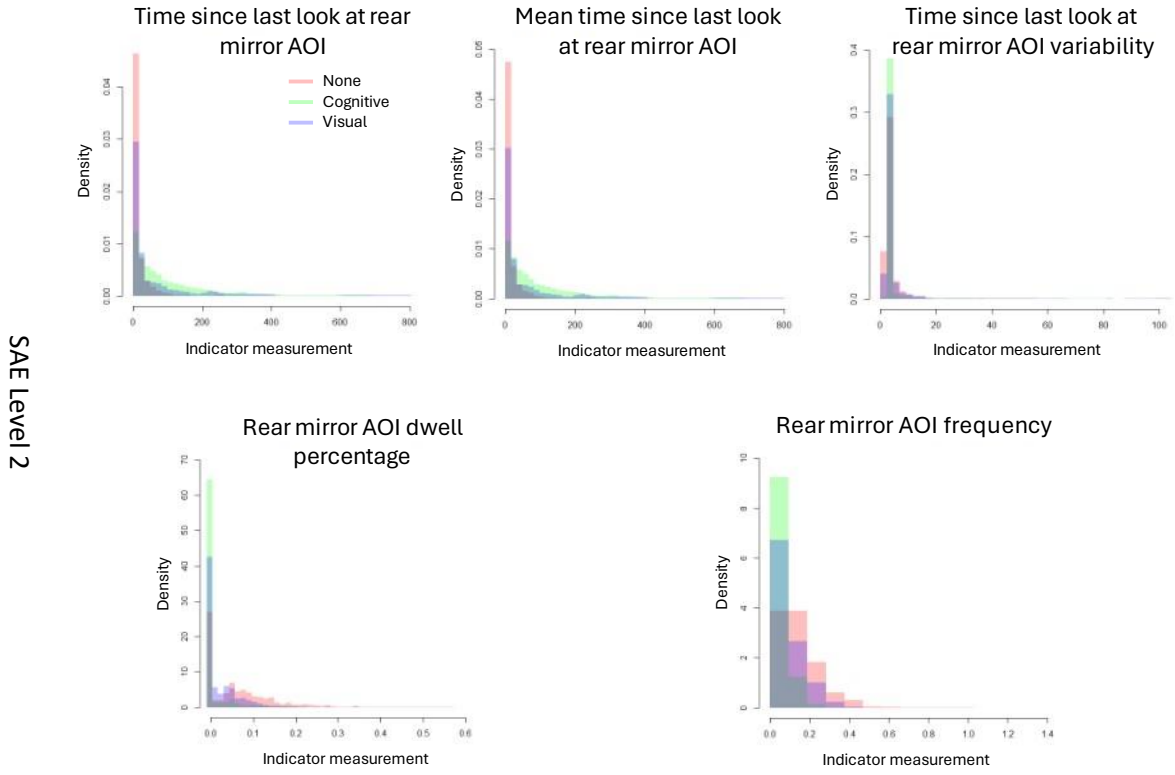

Figure 35: Histograms of the rear mirror AOI indicators in the SAE Level 2 training data.

Focusing on SAE Level 3, the behavior of participants without NDRT mostly stays identical. In contrast, participants tasked with the cognitive NDRT become more likely, while participants tasked with the visual NDRT become less likely to look at the rear mirror.

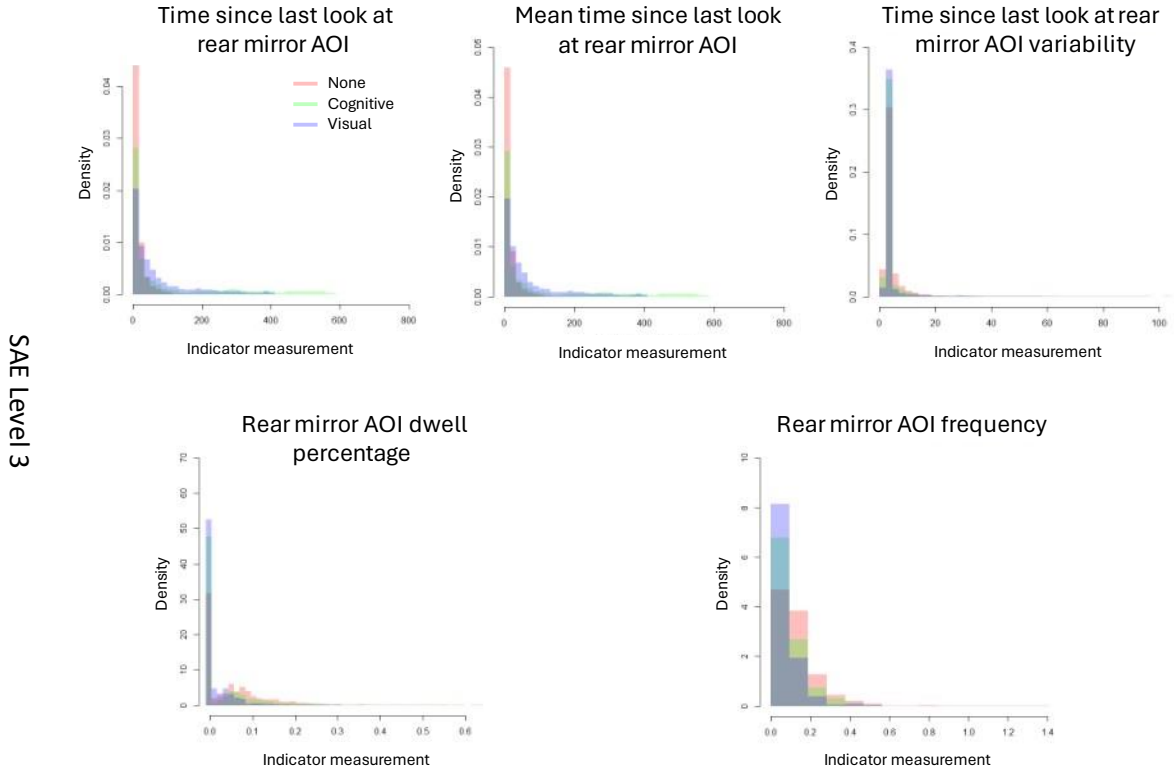

Figure 36: Histograms of the rear mirror AOI indicators in the SAE Level 3 training data.

5.4.1.16 Front AOI indicators

Figure 37 and Figure 38 show histograms of the five front area AOI indicators in the SAE Level 2 and SAE Level 3 training data. Comparing the no NDRT and cognitive NDRT conditions, we have that in both conditions, participants only look away from the front AOI for a short time. However, as implied by the front AOI dwell percentage and frequency, participants in the cognitive NDRT condition are more likely to keep their gaze at the front AOI, while participants in the no NDRT condition avert their gaze from the front AOI for a short while until returning. In the visual NDRT condition, participants only spend between 0% and approx. 40% focusing on the front AOI and are likely to look away for longer durations.

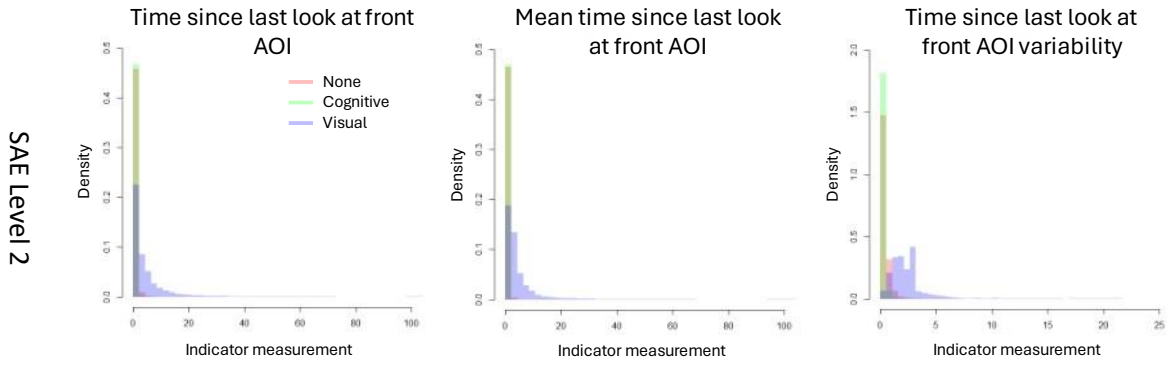

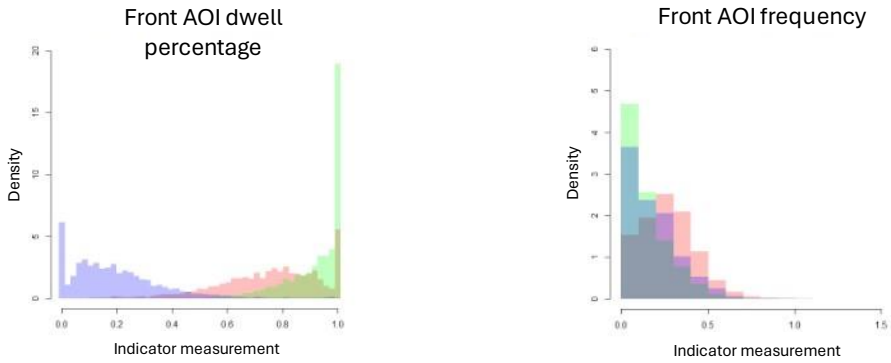

Figure 37: Histograms of the front AOI indicators in the SAE Level 2 training data.

Comparing SAE Level 2 and SAE Level 3, participants tasked with the cognitive NDRT become a little less likely to spend all their time focusing on the front AOI under SAE Level 3, while participants tasked with the visual NDRT become more likely to stay away from the front AOI.

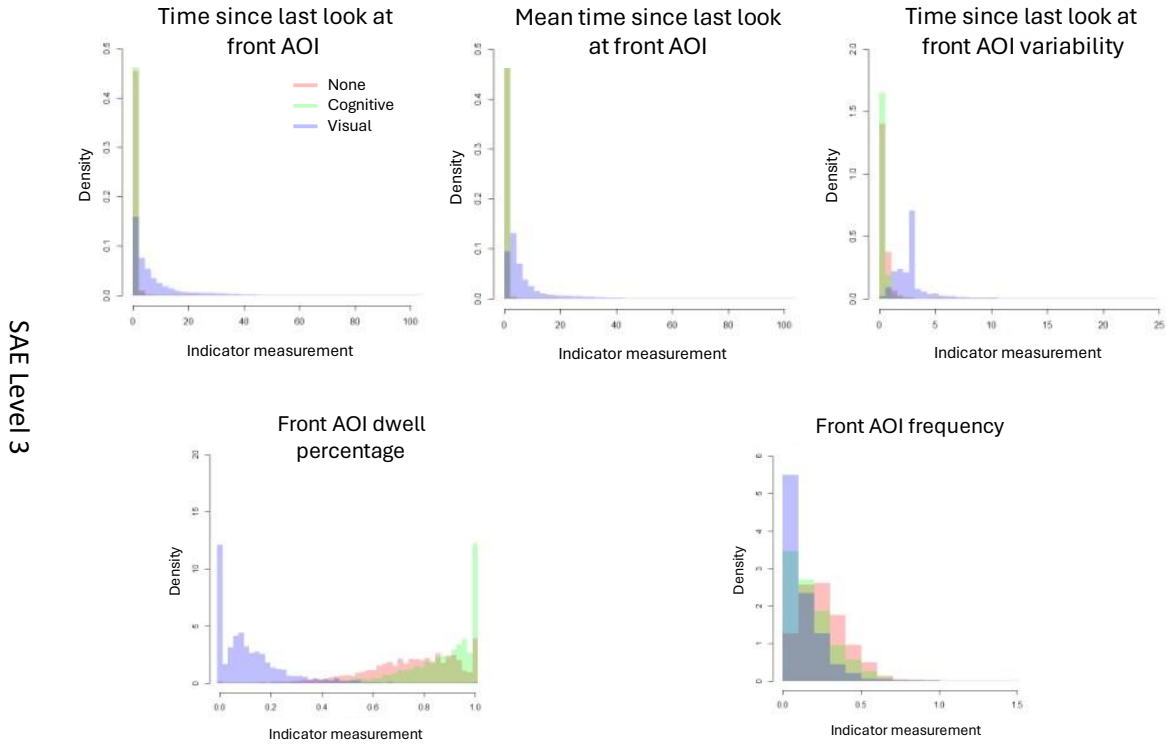

Figure 38: Histograms of the front AOI indicators in the SAE Level 3 training data.

5.4.1.17 Tachometer AOI indicators

Figure 39 and Figure 40 show histograms of the five tachometer AOI indicators in the SAE Level 2 and SAE Level 3 training data. Starting with SAE Level 2, participants without NDRT look at the tachometer with the highest frequency, accumulate the minimum (mean) time between looks to the rear mirror and spend the most time looking into the rear mirror, closely followed by participants tasks with the cognitive NDRT, and, lastly, participants tasked with the visual NDRT. For the latter two, we, once again, notice frequent long tails in the (mean) time since the last look at the tachometer, implying that participants tasked with NDRTs occasionally ignore the tachometer for several minutes.

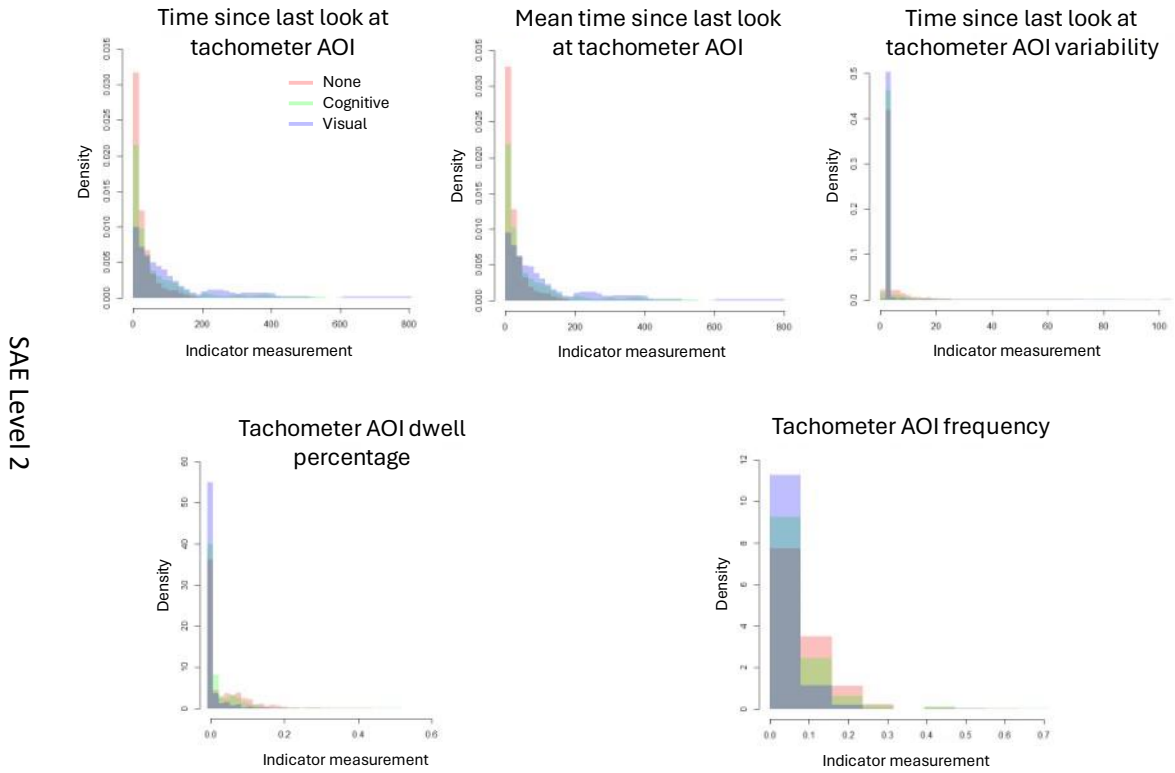

Figure 39: Histograms of the tachometer AOI indicators in the SAE Level 2 training data.

Comparing SAE Level 2 and SAE Level 3, the most noticeable difference concerns participants tasked with the cognitive NDRT, which become less likely to look at the tachometer under SAE Level 3. The same is true for participants tasked with the visual NDRT, although to a lesser degree. For participants without NDRT, the behavior remains approx. identical.

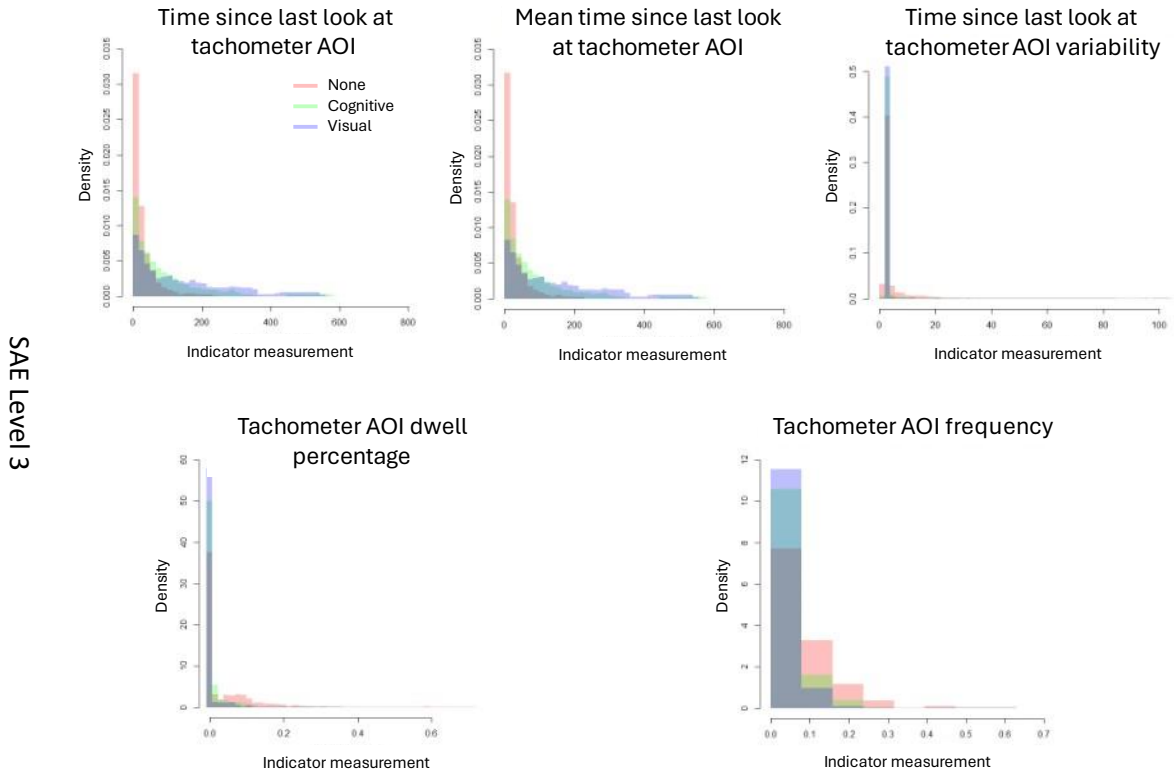

Figure 40: Histograms of the tachometer AOI indicators in the SAE Level 3 training data.

5.4.1.18 Infotainment AOI indicators

Figure 41 and Figure 42 show histograms of the five infotainment AOI indicators in the SAE Level 2 and SAE Level 3 training data. Immediately noticeable, participants tasked with the visual NDRT show very low normal and mean times since last looking at the infotainment system, and very high dwell percentages and frequencies. In combination with the front AOI indicators (c.f., Section 5.4.1.16), this implies that participants tasked with the visual NDRT tend to switch between the front and the infotainment AOI, while focusing on the latter. Overall, the infotainment AOI indicators seem to provide a very good discrimination between participants tasked with the visual NDRT and participants without or tasked with the cognitive NDRT.

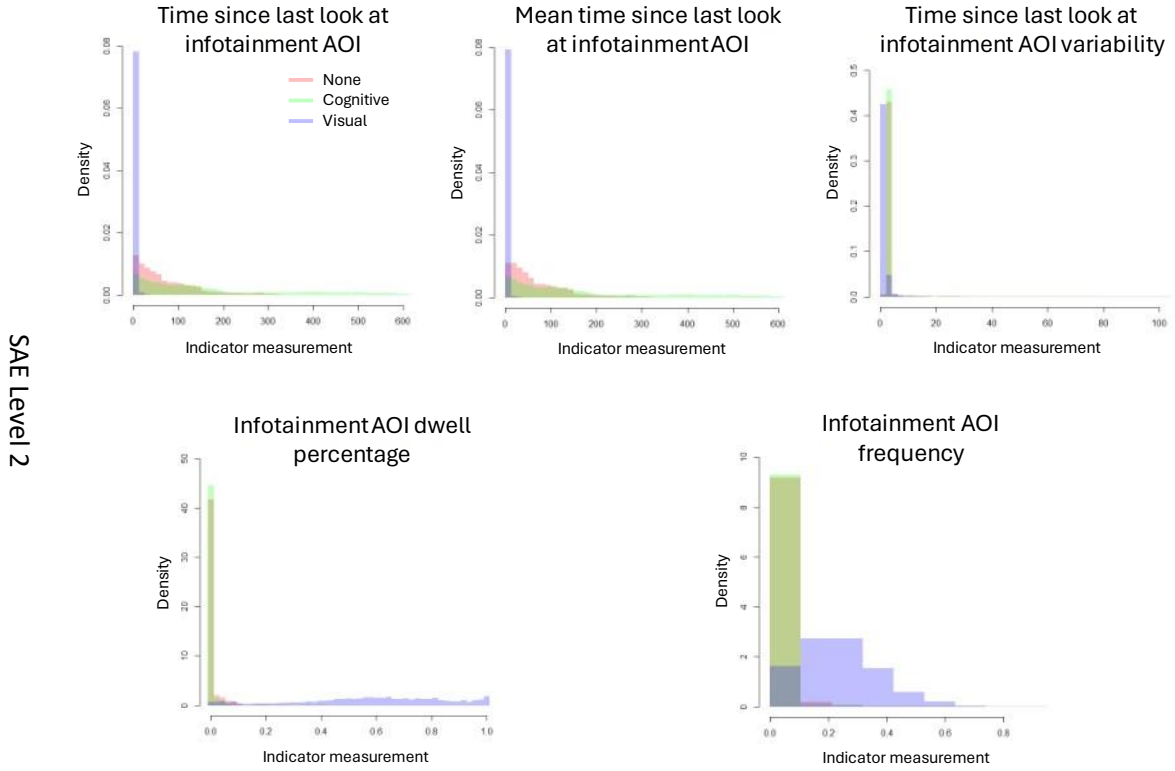

Figure 41: Histograms of the infotainment AOI indicators in the SAE Level 2 training data.

Although subtle, participants under the no NDRT condition are more likely to look at the infotainment AOI, at least a few times during a trial, while participants tasked with the cognitive NDRT rarely look at the infotainment system at all, as implied by the time and mean time and the dwell percentage indicator, especially for SAE Level 3. Otherwise, there are no noticeable differences between SAE Level 2 and SAE Level 3.

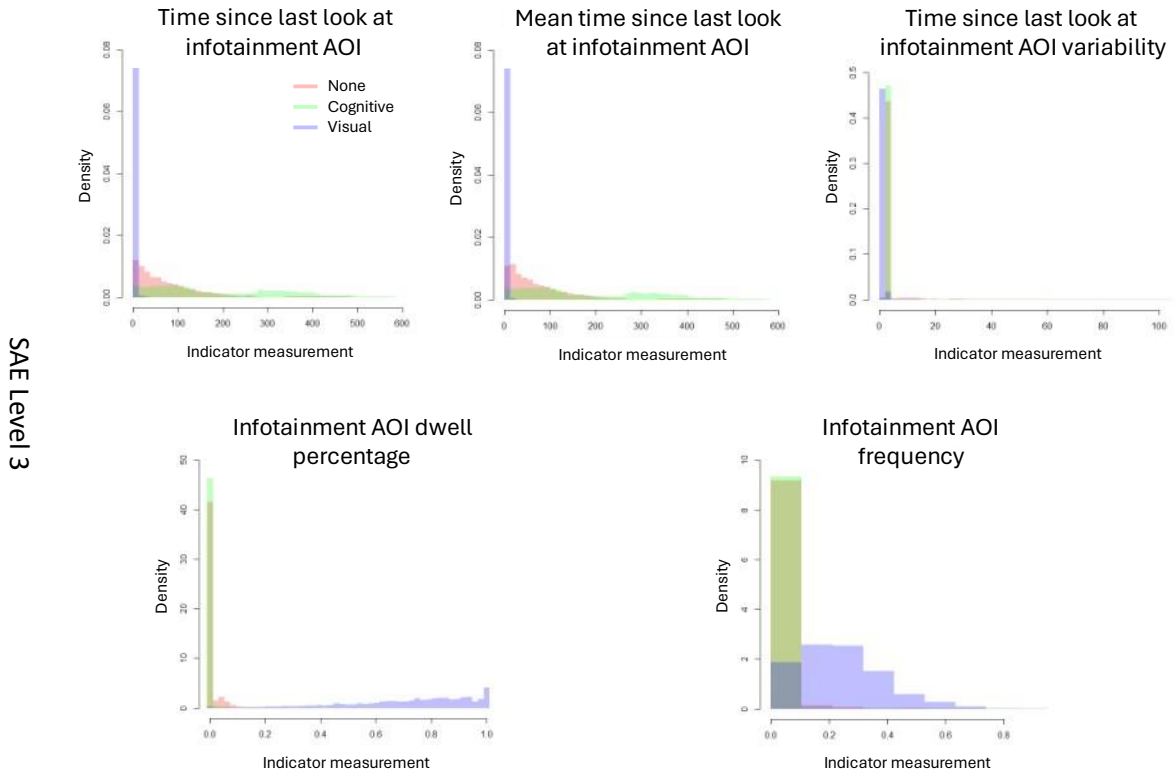

Figure 42: Histograms of the infotainment AOI indicators in the SAE Level 3 training data.

5.4.1.19 Other AOI indicators

Lastly, Figure 43 and Figure 44 show histograms of the five other AOI indicators in the SAE Level 2 and SAE Level 3 training data. As a reminder, the "other" AOI represents a situation, in which the driver's gaze could not be detected as looking into the left mirror, rear mirror, right mirror, tachometer, infotainment system, or the front area AOI, and, as such, includes miss-classifications of the Smart Eye Pro eye-tracking system (e.g., in the case of the right mirror and infotainment system). Participants without NDRT and participants tasked with the visual NDRT have a very similar normal and mean times since last looking at the other AOI, with the latter having a slightly higher dwell percentage, potentially caused by the Smart Eye Pro eye-tracking system's inability to correctly classify looks towards the bottom part of the infotainment system. In contrast, participants tasked with the cognitive NDRT, show much higher and long-tailed (mean) times, lower dwell percentages, and frequencies, likely caused by the tendency of these participants to look at the road center.

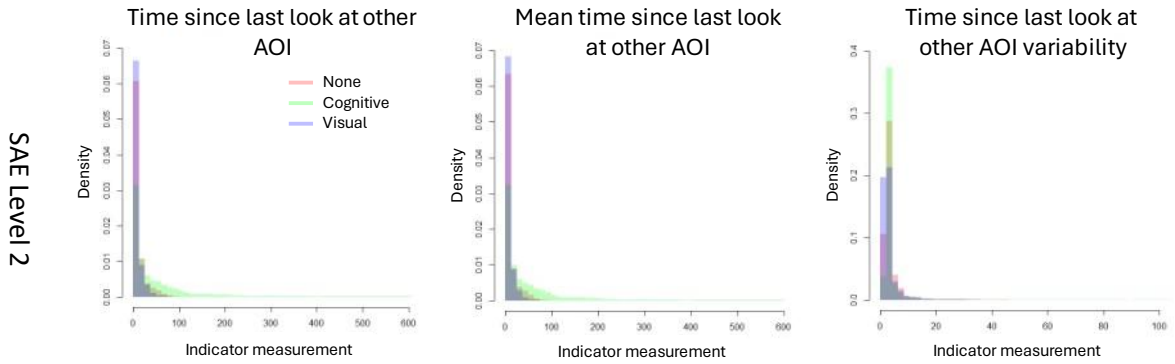

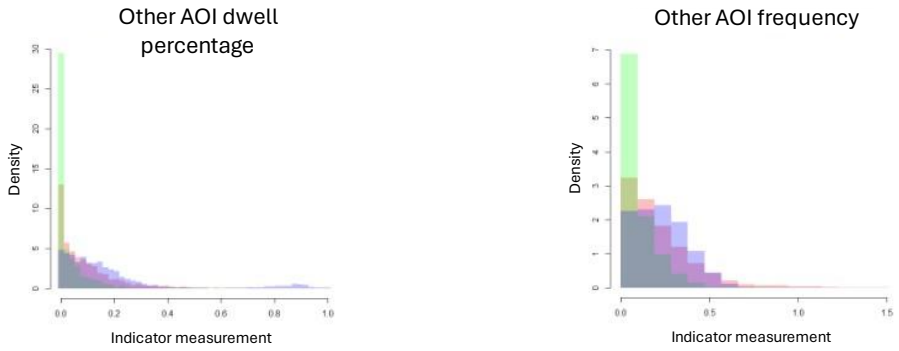

Figure 43: Histograms of the other AOI indicators in the SAE Level 2 training data.

Comparing SAE Level 2 and SAE Level 3, the behavior of participants without and tasked with the visual NDRT stays mostly identical, while the behavior of participants tasked with the cognitive NDRT becomes more similar.

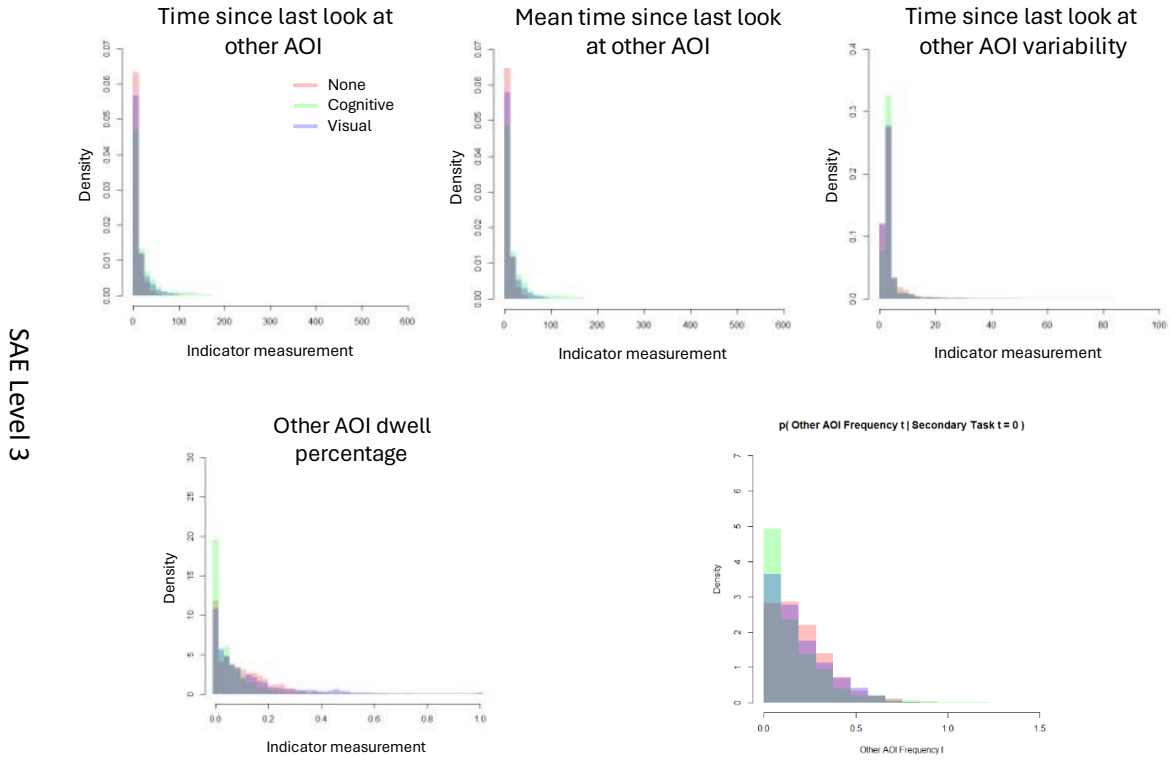

Figure 44: Histograms of the other AOI indicators in the SAE Level 3 training data.

5.4.2 SA indicator performance for discriminating between behavioral patterns (NDRT conditions)

The visual inspection of the histograms provided in Section 5.4.1 provides some idea concerning the potential performance of an SA indicator for discriminating between the different behavioral patterns / NDRT conditions. We can gain a better understanding by evaluating and comparing the isolated discriminative power of each individual indicator using an objective scoring criterion that measures how well the utilization of a single indicator helps in predicting the ground truth behavioral pattern in the training data.

Let $\mathcal{D} = \{(b^i, \boldsymbol{f}^i)\}_{i=1}^n$ denote a dataset, comprised of n samples $(b^i, \boldsymbol{f}^i)$ providing ground truth (training) data for the behavioral pattern B and the set of n_f SA indicators $\boldsymbol{F} = \{F_1, \dots, F_{n_f}\}$. Formally, we're interested in evaluating $p(b^i | f_j^i), i = 1, \dots, n$, the ability of a single indicator $F_j \in \boldsymbol{F}$ to predict the correct behavioral pattern for each sample, without the use of any extra information, like e.g., temporal dynamics. For this, we create a set of simple (non-dynamic) BNs: To establish a baseline, we create $\mathcal{B}_{\text{Baseline}}$, consisting of a single distribution $p(B : \boldsymbol{\theta}_B)$. For each indicator $F_j \in \boldsymbol{F}$, we create a BN $\mathcal{B}_{F_j}$ that defines a JPD

$$p\left(B, F_j : \boldsymbol{\theta}_{\mathcal{B}_{F_j}}\right) = p(B : \boldsymbol{\theta}_B) p\left(F_j | B : \boldsymbol{\theta}_{F_j|B}\right).$$

The parameters of the models are learnt from the dataset $\mathcal{D}$, distributions over discrete variables are realized as categorical distributions (c.f., Section X), distributions over continuous variables are realized as GMMs (c.f., Section Y). As a measure of performance, we use the log-likelihood

$$\log p(b^{1:n} : \boldsymbol{\theta}_B) = \log \prod_{i=1}^n p(b^i : \boldsymbol{\theta}_B) = \sum_{i=1}^n \log p(b^i : \boldsymbol{\theta}_B),$$

for the baseline, and the conditional log-likelihood

$$\log p\left(b^{1:n} | f_j^{1:n} : \boldsymbol{\theta}_{\mathcal{B}_{F_j}}\right) = \sum_{i=1}^n \log p\left(b^i | f_j^i : \boldsymbol{\theta}_{\mathcal{B}_{F_j}}\right) = \sum_{i=1}^n \log \frac{p(b^i : \boldsymbol{\theta}_B) p\left(f_j^i | b^i : \boldsymbol{\theta}_{F_j|B}\right)}{\sum_{b \in \text{Val}(B)} p(b : \boldsymbol{\theta}_B) p\left(f_j^i | b : \boldsymbol{\theta}_{F_j|B}\right)}$$

for each model $\mathcal{B}_{F_j}, j = 1, \dots, n_f$. In general, we have that more complex models have an (unfair) advantage over simpler models, so we use a penalty term that penalizes the number of parameters $\lfloor \boldsymbol{\theta} \rfloor$ in the model:

$$\frac{\lfloor \boldsymbol{\theta} \rfloor}{2} \log n.$$

The full score for the baseline in then defined as

$$\text{Score}(\mathcal{B}_{\text{Baseline}} : \mathcal{D}) \triangleq \sum_{i=1}^n \log p(b^i : \boldsymbol{\theta}_B) - \frac{\lfloor \boldsymbol{\theta}_B \rfloor}{2} \log n,$$

which, in this case, is equivalent to the Bayesian Information Criterion (BIC), a common scoring criterion for generative structure learning of (dynamic) BNs (Schwarz, 1976) (Murphy, 2012). The full score for the models $\mathcal{B}_{F_j}, j = 1, \dots, n_f$ is given by

$$\text{Score}\left(\mathcal{B}_{F_j} : \mathcal{D}\right) \triangleq \sum_{i=1}^n \log p\left(b^i | f_j^i : \boldsymbol{\theta}_{\mathcal{B}_{F_j}}\right) - \frac{\left\lfloor \boldsymbol{\theta}_{\mathcal{B}_{F_j}} \right\rfloor}{2} \log n,$$

which is known as the Discriminative Bayesian Information Criterion (DBIC), a discriminative variant of the BIC, used for discriminative structure learning of (dynamic) BNs (Guo & Greiner, 2005) (Santafe, Lozano, & Larranaga, 2007). For arbitrary models, the DBIC differs from the BIC in that it uses a discriminative log-likelihood instead of the joint log-likelihood, therefore favoring models that perform

well on an inference task instead of models that perform well on representing the complete data (Murphy, 2012).

We conducted the process described for the SAE Level 2 training data $\mathcal{D}_{\text{Training}}^{\text{L2}}$, consisting of $n_{\text{L2}} = 148280$ samples, and the SAE Level 3 training data $\mathcal{D}_{\text{Training}}^{\text{L3}}$, consisting of $n_{\text{L3}} = 101460$ samples. A visual overview of SA indicator performances is shown in Figure 45, the numerical scores are provided in Table 3.

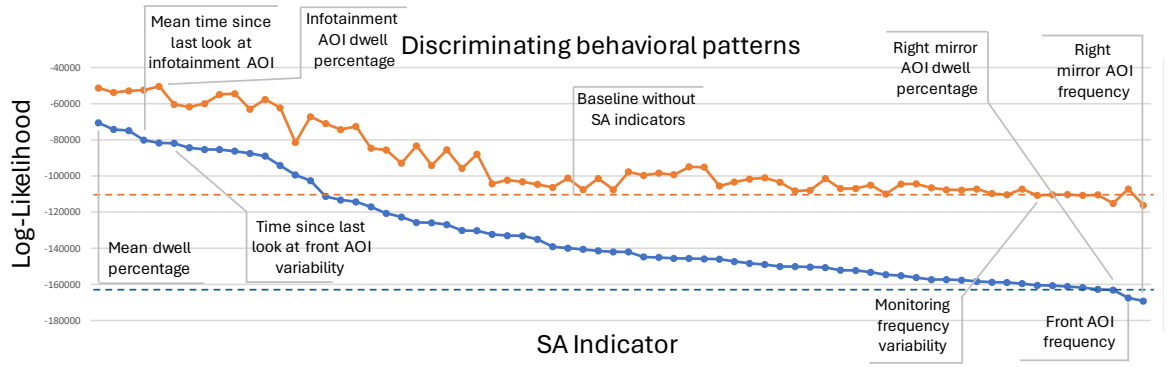

Figure 45: Overview of SA indicator performance for discriminating between behavioral patterns (NDRT conditions) on SAE Level 2 training data (blue) and SAE Level 3 training data (orange). The baselines for the SAE Level 2 and 3 training data are depicted by the blue and orange dashed line.

The top-scoring indicators are mostly related to the attention towards the front or the combination of driving-related AOIs (including e.g. the mean dwell percentage on driving related AOIs, the front AOI dwell percentage, the dwell percentage on driving related AOIs, the time since last look at front AOI variability, and the mean time since last look at front AOI indicators), or the infotainment AOIs (including e.g., the mean time since last look at infotainment AOI, infotainment AOI dwell percentage, and the time since last look at infotainment AOI variability, time since last look at infotainment AOI, and the infotainment AOI frequency indicators). The bottom-scoring indicators are mostly related to the right mirror AOI (namely, the right mirror AOI frequency, right mirror AOI dwell percentage, and time since last look at right mirror AOI variability indicators), which is most probably explained by the difficulties of the Smart Eye Pro eye-tracking system to consistently detect gazes towards the right mirror, and sensor failure indicators (namely, the head rotation valid, pupil diameter valid, and gaze origin valid indicators). Comparing the difference between SAE Level 2 and SAE Level 3 scores, we see on average, indicators that perform well or bad on the former, also perform well or bad on the latter. Potentially surprising is the bad performance of the front AOI frequency indicator, which is most probably explained by difficulties to accurately model distributions over frequencies using GMMs.

Table 3: Overview of indicator performance for discriminating between behavioral patterns (NDRT conditions) on SAE Level 2 and SAE Level 3 training data, sorted from best to worst performance for the SAE Level 2 training data. Baseline score for SAE Level 2 training data: $\text{Score}\left(\mathcal{B}_{\text{Baseline}} : \mathcal{D}_{\text{Training}}^{\text{L2}}\right) = -162803.04659$. *Baseline score for SAE Level 3 training data:* $\text{Score}\left(\mathcal{B}_{\text{Baseline}} : \mathcal{D}_{\text{Training}}^{\text{L3}}\right) = -111399.30478$.

SA Indicator	Score SAE Level 2	Score SAE Level 3
Mean dwell percentage	-70565.42044	-51229.39628
Front AOI dwell percentage	-74233.42019	-53757.61417
Dwell percentage	-74837.42041	-52865.30134
Mean time since last look at infotainment AOI	-80169.55428	-52471.09278

Infotainment AOI dwell percentage	-81634.00932	-50383.12086
Time since last look at front AOI variability	-81886.65875	-60336.13228
Mean time since last look at front AOI	-84338.06562	-61760.12565
Mean gaze pitch	-85257.50094	-59943.19518
Time since last look at infotainment AOI variability	-85353.01527	-54904.42562
Mean yaw angle of the head	-86210.68046	-54449.29351
Mean gaze heading	-87452.27336	-62956.28166
Time since last look at infotainment AOI	-89016.35137	-57631.07075
Infotainment AOI frequency	-94198.03887	-62218.65359
Gaze pitch variability	-99447.31527	-81448.39173
Yaw angle of the head	-102563.03082	-67178.26860
Mean glance duration	-111331.21141	-71006.53727
Glance duration	-113221.70654	-74271.30769
Current AOI	-114278.31911	-72566.37586
Glance duration variability	-117080.38658	-84669.95821
Pupil diameter variability	-120673.90807	-85551.31451
Yaw rate of the head variability	-122666.56511	-92933.91976
Time since last look at front AOI	-125706.28462	-83246.95036
Mean saccade frequency	-125904.89214	-94130.56973
Gaze pitch	-126903.26488	-85489.35845
Saccade frequency	-130130.66291	-95779.47792
Gaze heading	-130291.10815	-87891.24440
Yaw angle of the head variability	-132292.84730	-104316.38887
Gaze heading variability	-132960.78711	-102211.31021
Mean time since last look at other AOI	-133098.84186	-103192.71952
Time since last look at other AOI variability	-135072.07053	-104642.88926
Dwell percentage variability	-139113.67581	-106293.91696
Mean time since last look at rear mirror AOI	-139961.10715	-101140.51882
Time since last look at other AOI	-140569.38815	-107514.72708
Time since last look at rear mirror AOI	-141417.55012	-101394.30118
Other AOI dwell percentage	-141919.16474	-107575.87485
Mean blink frequency	-142016.97648	-97707.11700
Blink frequency	-144784.36355	-99646.67688
Mean monitoring frequency	-145036.69443	-98405.66095
Monitoring frequency	-145583.18534	-99276.45669
Mean time since last look at left mirror AOI	-145653.27401	-94921.93095
Time since last look at left mirror AOI	-145871.20880	-95100.80495
Rear mirror AOI dwell percentage	-146032.74630	-105498.11235
Mean pupil diameter	-147305.61236	-103337.93194
Blink frequency variability	-148303.51509	-101704.72807
Mean time since last look at tachometer AOI	-148968.71222	-101024.23075
Pupil diameter	-150070.20517	-103415.57512
Mean yaw rate of the head	-150147.27211	-108271.40320

Rear mirror AOI frequency	-150338.69316	-107910.58132
Time since last look at tachometer AOI	-150604.84949	-101456.56369
Other AOI frequency	-150915.44594	-110403.43499
Time since last look at right mirror AOI	-152186.94257	-106942.93357
Mean time since last look at right mirror AOI	-152265.16706	-106919.52369
Yaw rate of the head	-153221.47511	-105025.46612
Time since last look at rear mirror AOI variability	-154626.01374	-109948.37080
Tachometer AOI dwell percentage	-155170.98280	-104402.17884
Left mirror AOI dwell percentage	-156251.23312	-104365.69613
Left mirror AOI frequency	-157308.79068	-106495.86602
Gaze direction valid	-157311.80849	-107569.97333
Time since last look at tachometer AOI variability	-157624.12969	-107760.74792
Tachometer AOI frequency	-158289.72110	-107213.97755
Hands-on steering wheel	-158744.99130	-109700.84600
Saccade frequency variability	-158891.86577	-110328.35514
Time since last look at left mirror AOI variability	-159536.23891	-107204.93728
Monitoring frequency variability	-160477.99222	-110722.79247
Gaze origin valid	-160617.30665	-110376.06743
Time since last look at right mirror AOI variability	-161122.95699	-110281.22895
Pupil diameter valid	-161757.11223	-110712.05394
Head rotation valid	-162745.67443	-110412.63910
Right mirror AOI dwell percentage	-163138.13828	-115159.95153
Front AOI frequency	-167413.92060	-107168.38483
Right mirror AOI frequency	-169219.54469	-116239.45856

5.4.3 SA indicator performance for discriminating between cognitive NDRT and no NDRT

As apparent from the visual inspection in Section 5.4.1, many indicators provide information to easily detect the driver behavior during the visual NDRT condition. A discrimination between the cognitive and no NDRT condition seems to be much harder. As such, we repeated the SA indicator assessment in regards to their ability to only discriminate between the no NDRT and the cognitive NDRT condition.

For this, we derived each a reduced data set $\mathcal{R}^{\mathrm{L2}}_{\mathrm{Training}} \subset \mathcal{D}^{\mathrm{L2}}_{\mathrm{Training}}$, consisting of $n_{\mathrm{L2}} = 96208$ samples, and $\mathcal{R}^{\mathrm{L3}}_{\mathrm{Training}} \subset \mathcal{D}^{\mathrm{L3}}_{\mathrm{Training}}$, consisting of $n_{\mathrm{L3}} = 68652$ samples, comprised only of samples for which $B^t = b_0$ or $B^t = b_1$ and repeated the procedure described in Section 5.4.2 using the reduced datasets, replacing the variable B with a reduced binary variable B_*, $\mathrm{Val}(B_*) = \{b_{*_0}, b_{*_1}\}$ to reduce the number of parameters to the correct necessary amount.

A visual overview of SA indicator performances on the reduced SAE Level 2 and SAE Level 3 training data is shown in Figure 46, the numerical scores are provided in Table 4.

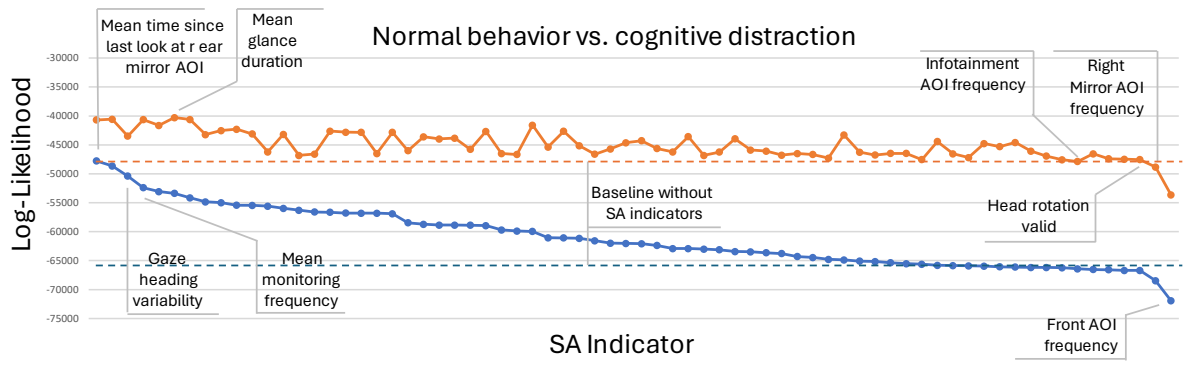

Figure 46: Overview of SA indicator performance for discriminating between normal behavior (no NDRT) and behavior under cognitive distraction (cognitive NDRT) on SAE Level 2 training data (blue) and SAE Level 3 training data (orange). The baselines for the SAE Level 2 and 3 training data are depicted by the blue and orange dashed line.

Table 4: Overview of indicator performance for discriminating between normal behavior (no NDRT) and behavior under cognitive distraction (cognitive NDRT) on the reduced SAE Level 2 and SAE Level 3 training data, sorted from best to worst performance for the SAE Level 2 training data. Baseline score for the reduced SAE Level 2 training data: $\mathrm{Score}\left(\mathcal{B}_{\mathrm{Baseline}} : \mathcal{R}^{\mathrm{L2}}_{\mathrm{Training}}\right) = -66689.14988$. *Baseline score for the reduced SAE Level 3 training data:* $\mathrm{Score}\left(\mathcal{B}_{\mathrm{Baseline}} : \mathcal{R}^{\mathrm{L3}}_{\mathrm{Training}}\right) = -47539.55465$.

SA Indicator	Score SAE Level 2	Score SAE Level 3
Mean time since last looked at rear mirror AOI	-47767.93871	-40677.86051
Time since last looked at rear mirror AOI	-48647.05945	-40576.99529
Gaze heading variability	-50381.52399	-43493.58182
Mean monitoring frequency	-52394.40053	-40633.31027
Monitoring frequency	-53075.31098	-41633.81123
Mean glance duration	-53379.48942	-40292.74972
Glance duration	-54135.08063	-40607.66652
Mean time since last look at front AOI	-54843.40909	-43238.45512
Front AOI dwell percentage	-54991.85860	-42539.72437
Time since last look at front AOI variability	-55421.77210	-42305.32561
Mean time since last look at left mirror AOI	-55439.11334	-43108.91861
Rear mirror AOI dwell percentage	-55592.98474	-46200.83945
Time since last look at left mirror AOI	-55963.07941	-43169.63270
Rear mirror AOI frequency	-56282.51764	-46819.30670
Mean time since last look at right mirror AOI	-56587.44854	-46579.20822
Mean dwell percentage	-56646.10537	-42615.45332
Mean time since last look at infotainment AOI	-56775.52726	-42803.71894
Dwell percentage variability	-56794.09140	-42826.63999
Time since last look at right mirror AOI	-56800.73993	-46496.08137
Time since last look at infotainment AOI	-56899.87915	-42841.42599
Yaw angle head variability	-58452.56286	-45999.16824
Mean pupil diameter	-58707.35511	-43600.19258
Gaze pitch variability	-58845.14815	-43981.14605
Dwell percentage	-58855.53710	-43842.11130
Mean time since last look at other AOI	-58876.17259	-45773.50519
Glance duration variability	-58944.27869	-42673.69648

Other AOI dwell percentage	-59684.06491	-46502.99472
Time since last look at right mirror AOI variability	-59873.81323	-46659.95370
Mean blink frequency	-59946.54390	-41593.61171
Other AOI dwell percentage	-61058.59375	-45376.39210
Blink frequency	-61060.19790	-42638.59637
Left mirror AOI dwell percentage	-61126.43538	-45133.97608
Yaw rate of the head variability	-61567.77672	-46603.99166
Left mirror AOI frequency	-61986.46296	-45698.46240
Mean gaze heading	-62034.47763	-44623.26778
Yaw angle of the head	-62063.68148	-44281.64963
Mean saccade frequency	-62368.65258	-45637.03035
Time since last look at left mirror AOI variability	-62907.57347	-46207.15586
Mean yaw angle of the head	-62923.04477	-43569.62156
Mean yaw rate of the head	-63017.18790	-46825.29247
Pupil diameter	-63119.48372	-46240.41332
Mean gaze pitch	-63419.49043	-43957.05067
Gaze heading	-63459.79879	-45892.13747
Saccade frequency	-63640.50411	-46060.86904
Saccade frequency variability	-63780.05395	-46763.15102
Current AOI	-64285.75402	-46488.64947
Time since last look at front AOI	-64453.47757	-46652.61198
Time since last look at other AOI variability	-64785.00868	-47289.36122
Tachometer AOI dwell percentage	-64870.02001	-43279.46197
Blink frequency variability	-65084.52771	-46255.11968
Time since last look at right mirror AOI variability	-65156.13999	-46752.49323
Right mirror AOI dwell percentage	-65351.59465	-46463.47702
Gaze pitch	-65533.60072	-46475.75166
Hands-on steering wheel	-65618.02872	-47534.82586
Mean time since last look at tachometer AOI	-65806.88483	-44423.98474
Time since last look at infotainment AOI variability	-65838.12071	-46534.3752
Monitoring frequency variability	-65905.29974	-47199.95420
Tachometer AOI frequency	-65954.75571	-44768.73543
Pupil diameter variability	-66068.74745	-45309.37477
Time since last look at the tachometer AOI	-66103.55749	-44571.99149
Infotainment AOI dwell percentage	-66172.39502	-46067.29686
Time since last look at tachometer AOI variability	-66182.65123	-46930.17895
Yaw rate of the head	-66220.74022	-47574.93009
Infotainment AOI frequency	-66419.00268	-47872.57873
Gaze direction valid	-66525.25147	-46535.33984
Gaze origin valid	-66578.26427	-47396.28140
Pupil diameter valid	-66686.70613	-47467.23922
Head rotation valid	-66693.78895	-47542.98262
Right mirror AOI frequency	-68450.12849	-48832.96670

Front AOI frequency	-71937.76201	-53651.57467

5.4.4 Latent patterns discovery

As implied from the visual comparison of the SA indicators and as became apparent during modelling, in isolation, the indicators provide sufficient information to discriminate between participants tasked with the visual NDRT and the rest, but lack in discrimination between participants without NDRT and tasked with the cognitive NDRT. As a side-analysis, we wanted to test whether we could detect finer-grained prototypical behavioral patterns in the interaction and relationship of selected groups of SA indicators that summarize typical and recurring behavior characteristically for participants without NDRT or tasked with the cognitive or visual NDRT.

The general idea is as follows: Let B denote the behavioral patterns / NDRT condition and $\boldsymbol{F}_{\subset} \subset \boldsymbol{F}$ denote a subset of SA indicators for which we want to find these prototypical patterns. Instead of modelling the relationship between B and $\boldsymbol{F}_{\subset}$ via an observation model $p(\boldsymbol{F}_{\subset}^{t}|B^{t})$ (as is the case for the NDRT models) we mediate the information between B and $\boldsymbol{F}_{\subset}$ via a discrete (latent) variable Z that can take one of n_Z different values, $\mathrm{Val}(Z) = \{z_1, \dots, z_{n_Z}\}$ and use an observation model $p(\boldsymbol{F}_{\subset}^{t}|Z^{t})p(Z^{t}|B^{t})$, i.e., we force the SA indicators $\boldsymbol{F}_{\subset}$ to be conditionally independent of the behavioral patterns B given Z. As Z can only take n_Z different values, Z acts as a kind of bottleneck, where each different $z_i, i = 1, \dots, n_Z$ summarizes information about $\boldsymbol{F}_{\subset}$ that provides information about B. By learning the parameters of $p(\boldsymbol{F}_{\subset}^{t}|Z^{t})p(Z^{t}|B^{t})$ from data, we can think of Z as an automatically created feature that condenses the information provided by $\boldsymbol{F}_{\subset}$.

We conducted the analysis with different subsets of indicators and will focus on two notable results in the following. We note that the results of this analysis were not yet included in the final models developed in DySAM, for which we relied on structure learning methods to derive the set of important indicators and used GMMs to directly model their correlations (c.f., Section 5.5). That said, we believe that the approach described in this section is a promising direction towards an improvement of the models developed in DySAM (c.f. Section 5.4.4.4).

5.4.4.1 Approach

The conceptual structure of the model used for the analysis is as follows: Let B denote the behavioral patterns / NDRT condition, Z, $\mathrm{Val}(Z) = \{z_1, \dots, z_{n_Z}\}$ denote a discrete latent variable to represent n_Z possible prototypical patterns and $\boldsymbol{F}_{\subset} \subset \boldsymbol{F}$ denote a subset of indicators of interest. We define a DBN where, for any number of time slices T, the JPD $p(B^{1:T}, Z^{1:T}, \boldsymbol{F}_{\subset}^{1:T} : \boldsymbol{\theta})$ is factorized as:

$$p\left(Z^1|B^1 : \boldsymbol{\theta}_{Z^1|B^1}\right)\prod_{i=2}^{T} p\left(Z^i|Z^{i-1}, B^i : \boldsymbol{\theta}_{Z^i|Z^{i-1},B^i}\right)\prod_{i=1}^{T} p\left(B^i : \boldsymbol{\theta}_{B^i}\right)p\left(\boldsymbol{F}_{\subset}^{i}|Z^i : \boldsymbol{\theta}_{\boldsymbol{F}_{\subset}^{i}|Z^i}\right),$$

with $p\left(\boldsymbol{F}_{\subset}^{i}|Z^i : \boldsymbol{\theta}_{\boldsymbol{F}_{\subset}^{i}|Z^i}\right)$ factorizing as

$$p\left(\boldsymbol{F}_{\subset}^{i}|Z^i : \boldsymbol{\theta}_{\boldsymbol{F}_{\subset}^{i}|Z^i}\right) = \prod_{F_j^i \in \boldsymbol{F}_{\subset}} p\left(F_j^i|Z^i : \boldsymbol{\theta}_{F_j^i|Z^i}\right),$$

i.e., we consider both the features $\boldsymbol{F}_{\subset}$ to be conditionally independent of the behavioral patterns B and the indicators in $\boldsymbol{F}_{\subset}$ to be conditionally independent from each other given the latent variable Z.

Distributions over discrete variables are encoded as categorical distributions, distributions over continuous variables are either encoded as Gaussian or exponential distributions (c.f., Appendix, Section 1.2).

Let $\mathcal{D} = \left\{\left(b^i, \boldsymbol{f}_{\subset}^i\right)\right\}_{i=1}^n$ denote a dataset, providing ground truth data for both the behavioral patterns / NDRT conditions and the selected subset of indicators (for ease of explanation, we assume the dataset to be comprised of a single sequence). We want to use the model to infer the sequence of filtered belief states

$$p\left(B^i, Z^i | \boldsymbol{f}_{\subset}^{1:i}\right), i = 1, \dots, n,$$

from we can derive $p\left(Z^i | \boldsymbol{f}_{\subset}^{1:i}\right)$ and $p\left(B^i | \boldsymbol{f}_{\subset}^{1:i}\right)$. The former provides a sequence of filtered belief states about the latent variable Z, given all the evidence observed so far. As Z summarizes our information about $\boldsymbol{F}_{\subset}$, we can think of this belief state as our belief about the current prototypical pattern. The latter provides a sequence of filtered belief states about the behavioral patterns B, given all the evidence obtained so far. As $\boldsymbol{F}_{\subset}$ is only accessible via Z, when comparing $p\left(B^i | \boldsymbol{f}_{\subset}^{1:i}\right)$ with ground truth data b^i, this provides us with an estimate of whether Z did manage to summarize $\boldsymbol{F}_{\subset}$ in a way that provides meaningful information about B.

As a general problem, we cannot readily estimate parameters involving Z, i.e., $\boldsymbol{\theta}_{Z^1|B^1}$, $\boldsymbol{\theta}_{Z^i|Z^{i-1},B^i}$, and $\boldsymbol{\theta}_{\boldsymbol{F}_{\subset}^i|Z^i}$, as the assignments $z^{1:n}$ are not provided in the data $\mathcal{D}$. With respect to our model, the dataset is *incomplete*. To perform parameter estimation with incomplete data, we use a variant of the Expectation-Maximization (EM-)algorithm, called hard-EM: We start by preparing a complete dataset $\mathcal{D}^0 = \left\{\left\{b^i, \boldsymbol{f}_{\subset}^i, z^i\right\}_{i=1}^n\right\}$ where the unknown assignments $z^{1:n}$ are randomly selected, $z^i \sim \mathrm{Cat}\left(\boldsymbol{\theta}_Z = \left\{\frac{1}{n_Z}, \dots, \frac{1}{n_Z}\right\}\right)$. We then repeat the following Expectation (E-) and Maximization (M-)steps, starting with the M-step:

During the M-step, we use the current version of the complete dataset $\mathcal{D}^k$ to update the parameters in the model via Bayesian parameter estimation, i.e., we infer $\boldsymbol{\theta}_{\mathrm{MAP}}^{k+1} = \arg\max_{\boldsymbol{\theta}} p\left(\boldsymbol{\theta} | \mathcal{D}^k\right)$. During the E-step, we use the parameterize the model with $\boldsymbol{\theta}_{\mathrm{MAP}}^{k+1}$ and use it to estimate an updated sequence of assignments $z^{1:n}$ and create an updated complete dataset $\mathcal{D}^{k+1}$, where each assignment z^i in the sequence $z^{1:n}$ is derived as

$$z^i = \arg\max_z p\left(z^i | b^{1:n}, \boldsymbol{f}^{1:n} : \boldsymbol{\theta}_{\mathrm{MAP}}^{k+1}\right).$$

Here, $p\left(Z^i | b^{1:n}, \boldsymbol{f}^{1:n} : \boldsymbol{\theta}_{\mathrm{MAP}}^{k+1}\right)$ is the probability distribution over Z^i having observed all other available data $b^{1:n}, \boldsymbol{f}^{1:n}$, obtained via smoothing (c.f. Section 1.4). Ideally, the process would be repeated until convergence, however, due to the large amount of data and therefore high computational effort required for each iteration, we stop the process after ten iterations.

5.4.4.2 Time since last look at AOI indicators

In DySAM, we consider seven different AOIs, the left, right, and rear mirror, the tachometer, the infotainment system, the front area, and an "other" AOI, capturing gaze targets that do not belong to either of the former AOIs (c.f., Section 5.1.3.10). Among others, each of these AOIs is associated with an "Time since last look at AOI" indicator that represents the time passed since the last look at the

associated AOI (c.f., Section 5.1.3.15.1). While each of these indicators provides some discrimination (most notably, the time since last look at the infotainment AOI for recognizing the behavior of participants tasked with the visual NDRT), we are interested in whether their combination and sequence provides additional discriminative power that can be represented by prototypical patterns.

As such, we used $\boldsymbol{F}_{\subset} = \{F_{37}, F_{42}, F_{47}, F_{52}, F_{57}, F_{62}, F_{67}\}$ and to tried to summarize the temporal and inter-relationships between the time since last looking at the different AOI indicators via five prototypical patterns, $Z, \mathrm{Val}(Z) = \{z_1, \dots, z_5\}$, with the hope to find at least one pattern each that is typical for participants without NDRT and tasked with the cognitive NDRT. After estimating the parameters using the hard-EM process described above on the SAE Level 2 training data,

$$\mathcal{D}_{\text{Training}}^{\text{NDRT:L2}} = \left\{\left(b^{j,i}, s_1^{j,i}, \boldsymbol{f}^{j,i}\right)_{i=1}^{n_j}\right\}_{j=1}^{74}, \sum_{j=1}^{74} n_j = 148280,$$

we used the model on the SAE Level 2 test data,

$$\mathcal{D}_{\text{Test}}^{\text{NDRT:L2}} = \left\{\left(b^{j,i}, s_1^{j,i}, \boldsymbol{f}^{j,i}\right)_{i=1}^{n_j}\right\}_{j=1}^{74}, \sum_{j=1}^{74} n_j = 148275,$$

to infer a sequence of filtered joint belief states

$$p\left(B^{j,i}, Z^{j,i} | \boldsymbol{f}_{\subset}^{j,1:i}\right), j = 1, \dots, 74, i = 1, \dots, n_j,$$

from which we derived a sequence $\hat{b}^{1,1:n_1}, \hat{b}^{2,1:n_2}, \dots, \hat{b}^{74,1:n_{74}}$, where each $\hat{b}^{j,i} = \mathbb{E}\left[B^{j,i} | \boldsymbol{f}_{\subset}^{j,1:i}\right]$ and a sequence $\hat{z}^{1,1:n_1}, \hat{z}^{2,1:n_2}, \dots, \hat{z}^{74,1:n_{74}}$, where each $\hat{z}^{j,i} = \arg\max_{z \in \mathrm{Val}(Z)} p\left(Z^{j,i} | \boldsymbol{f}_{\subset}^{j,1:i}\right)$. Figure 47 (bottom) shows the ground truth behavioral patterns $b^{1,1:n_1}, b^{2,1:n_2}, \dots, b^{74,1:n_{74}}$ as solid red line and the sequence $\hat{b}^{1,1:n_1}, \hat{b}^{2,1:n_2}, \dots, \hat{b}^{74,1:n_{74}}$ as solid blue line, Figure 47 (top) shows the sequence of latent states $\hat{z}^{1,1:n_1}, \hat{z}^{2,1:n_2}, \dots, \hat{z}^{74,1:n_{74}}$ as solid purple line. In both cases, the 74 different sequences in the test dataset are separated by vertical dotted lines.

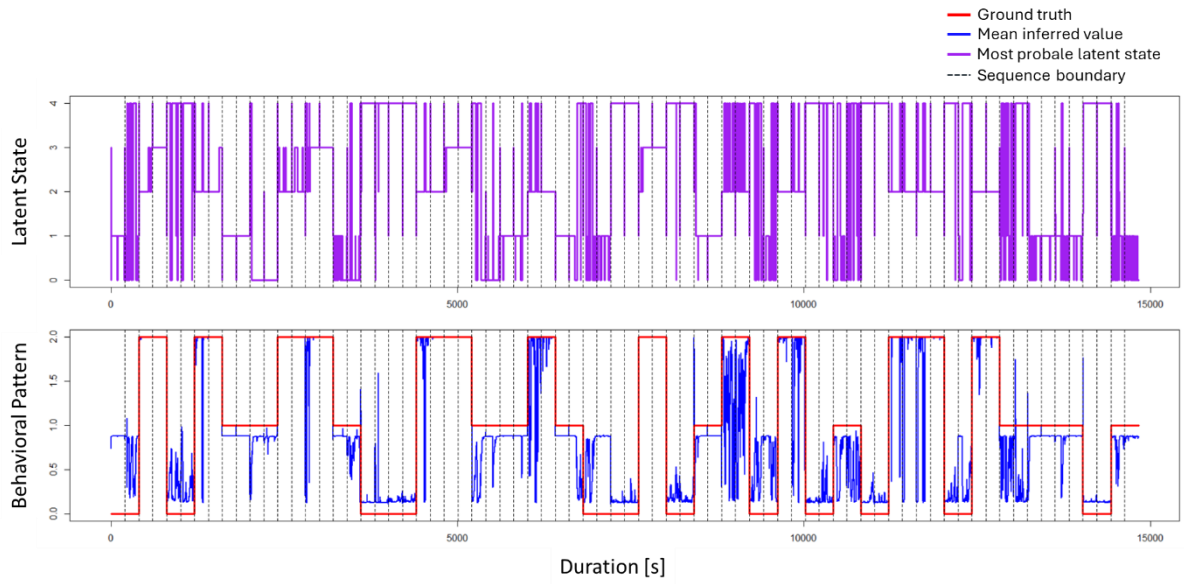

Figure 47: Comparison of ground truth and model predictions when using a latent variable Z summarizing $\boldsymbol{F}_{\subset} = \{F_{37}, F_{42}, F_{47}, F_{52}, F_{57}, F_{62}, F_{67}\}$ on test data $\mathcal{D}_{Test}^{NDRT:L2}$.

Comparing the mean inferred behavioral patterns $\hat{b}^{1,1:n_1}, \hat{b}^{2,1:n_2}, \dots, \hat{b}^{74,1:n_{74}}$ with the most probable latent states $\hat{z}^{1,1:n_1}, \hat{z}^{2,1:n_2}, \dots, \hat{z}^{74,1:n_{74}}$, we see that the states z_0 and z_1 summarize behavior that is most prototypical for participants tasked with the cognitive NDRT, the states z_2 and z_3 summarize behavior that is highly prototypical for participants tasked with the visual NDRT, while the state z_4 summarizes behavior that is most prototypical for participants without NDRT. Overall, just using the latent variable Z as the only relevant indicator, the model achieves a surprisingly high accuracy of 0.8425 on the test data.

5.4.4.3 Gaze behavior indicators

Given the characteristics and potential high discrimination of the gaze behavior indicators (c.f., Section 5.4.1.6), we used $\boldsymbol{F}_{\subset} = \{F_{18}, F_{19}, F_{21}, F_{22}\}$ and $Z, \mathrm{Val}(Z) = \{z_1, \dots, z_5\}$ to test whether we could detect prototypical gaze patterns that are typical for the different NDRT conditions. As before, we used the hard-EM process on the SAE Level 2 training data to estimate the parameters of the model, and used the model to infer the sequence of joint belief states on the SAE Level 2 test data, from which we derived two sequences $\hat{b}^{1,1:n_1}, \hat{b}^{2,1:n_2}, \dots, \hat{b}^{74,1:n_{74}}$ and $\hat{z}^{1,1:n_1}, \hat{z}^{2,1:n_2}, \dots, \hat{z}^{74,1:n_{74}}$, in the same way as described in Section 5.4.4.2. Figure 48 shows (bottom) shows the ground truth behavioral patterns $b^{1,1:n_1}, b^{2,1:n_2}, \dots, b^{74,1:n_{74}}$ as solid red line and the sequence $\hat{b}^{1,1:n_1}, \hat{b}^{2,1:n_2}, \dots, \hat{b}^{74,1:n_{74}}$ as solid blue line, Figure 48 (top) shows the sequence of latent states $\hat{z}^{1,1:n_1}, \hat{z}^{2,1:n_2}, \dots, \hat{z}^{74,1:n_{74}}$ as solid purple line, different sequences in the test dataset are separated by vertical dotted lines.

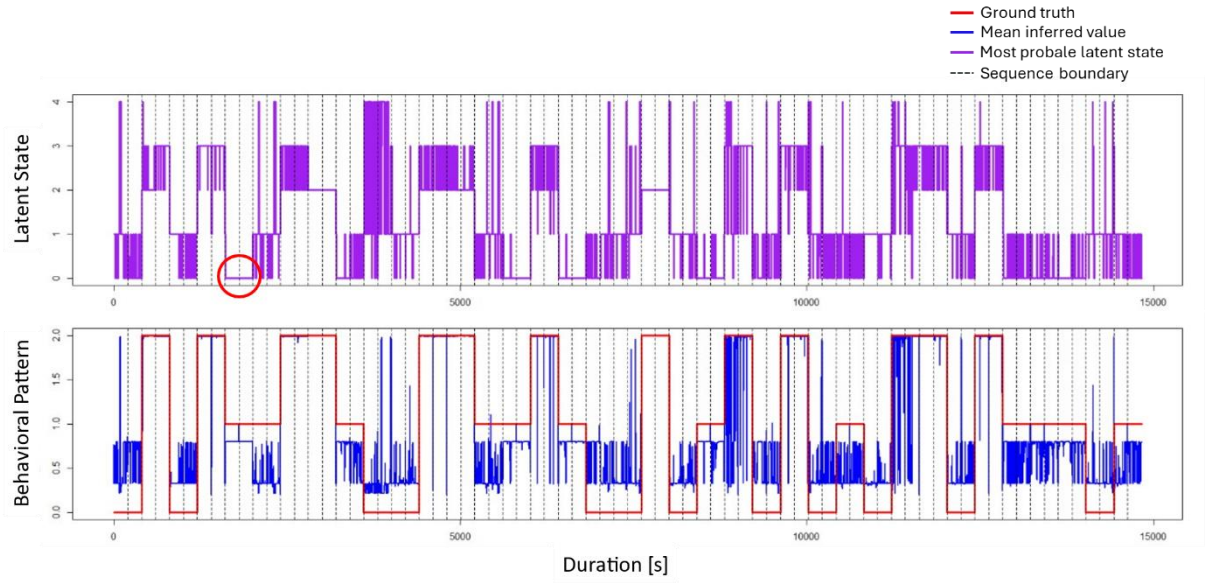

Figure 48: Comparison of ground truth and model predictions when using a latent variable Z summarizing $\boldsymbol{F}_{\subset} = \{F_{18}, F_{19}, F_{21}, F_{22}\}$ on test data $\mathcal{D}_{Test}^{NDRT:L2}$.

Comparing the mean inferred behavioral patterns $\hat{b}^{1,1:n_1}, \hat{b}^{2,1:n_2}, \dots, \hat{b}^{74,1:n_{74}}$ with the most probable latent states $\hat{z}^{1,1:n_1}, \hat{z}^{2,1:n_2}, \dots, \hat{z}^{74,1:n_{74}}$, we see that the state z_0 summarizes behavior that is most prototypical for participants tasked with the cognitive NDRT, the states z_1 and z_4 summarize behavior that is most prototypical for participants without NDRT, while the states z_2 and z_3 summarize behavior that is highly prototypical for participants tasked with the visual NDRT. Overall, just using the latent variable Z as the only relevant indicator, the model achieves an accuracy of 0.7926 on the test data. To provide some additional insight, Figure 49 shows the mean gaze heading and pitch (left) and the gaze heading and pitch variability (right) for the region marked by the red circle in Figure 48. As

apparent, the pattern represented by the latent state z_0 is characterized by a strong gaze concentration on the road ahead, characterized by a mean gaze heading around 0 rad, a near constant mean gaze pitch of approx. -0.1 rad combined with very low variabilities. We can interpret this gaze pattern as the "starring" behavior, hypothesized in Section 5.4.1.6.

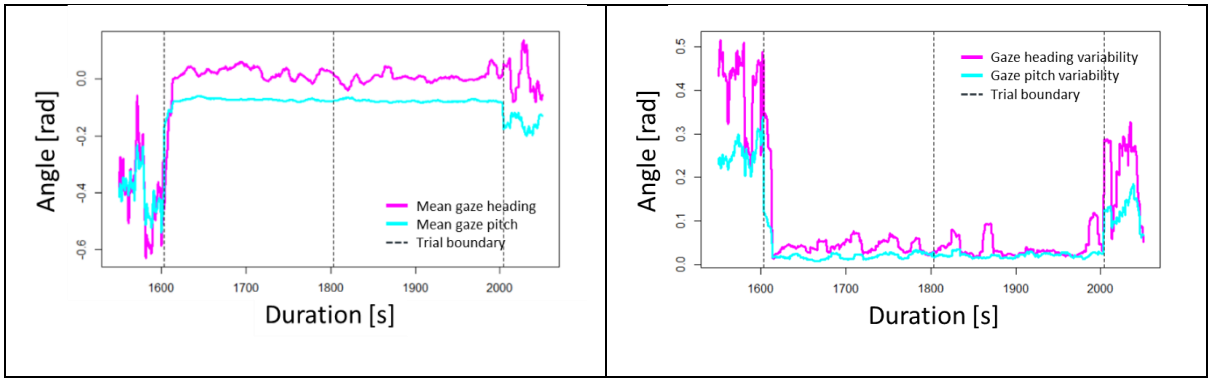

Figure 49: Mean gaze heading and pitch (left) and gaze heading and pitch variability (right) for the region marked by the red circle in Figure 48.

5.4.4.4 Potential for future model improvements

We believe that the approach described in this section is a promising direction towards an improvement of the models developed in DySAM.

Despite the strong modelling assumptions, enforcing the SA indicators $\boldsymbol{F}_{\subset}$ to be conditionally independent given the latent variable Z, akin to a naïve Bayesian classifier,

$$p(\boldsymbol{F}_{\subset}^{i}|Z^{i}) = \prod_{F_j \in \boldsymbol{F}_{\subset}} p(F_j^{i}|Z^{i}),$$

and using univariate Gaussian and exponential distribution that require few parameters, the analysis successfully discovered patterns that in isolation, help in discriminating between behavior of participants without NDRT, tasked with the cognitive NDRT, and tasked with the visual NDRT. Surprisingly, applied to the set of time since last look at AOI indicators, the resulting patterns achieved an accuracy of 0.8245 on the SAE Level 2 test data, which is close to the best-scoring SAE Level 2 NDRT model. This is a very promising result, when considering that the simplicity of the model should result in very robust estimation of the parameters, while preventing overfitting to the training data.

As already stated, the results of this analysis were not yet included in the final models developed in DySAM, for which we relied on structure learning methods to derive the set of important indicators and used GMMs to directly model their correlations (c.f., Section 5.4.2). Foreshadowing the results of the evaluation of the SAE Level 2 NDRT model (c.f., Section 5.6.2.1), the models obtained in this analysis and the SAE Level 2 NDRT model show very similar strengths and weaknesses, concerning the successful recognition of the behavioral pattern B in the test data, implying that both models utilize similar information from the SA indicators.

The main difference between the approach discussed in this section and the NDRT model's approach to directly model the correlation between indicators via GMMs is that the discovered prototypical patterns allow for a more dedicated interpretation. E.g., considering the gaze behavior indicators, the analysis discovered a prototypical pattern that represents a strong gaze concentration on the road center, typical, though not exclusive, for participants tasked with the cognitive NDRT.

To make use of prototypical patterns for a future improvements of the DySAM models, we believe that it would helpful to include experts on situation awareness to interpret potentially detected prototypical patterns and assess their potential relationship with the driver's SA. E.g., if a long-term gaze concentration implies a lack of SA (at least concerning regions outside of the road center), the detection of such a pattern could in itself provide valuable information about the driver's current SA. Given a sufficient amount of detectable and interpreted patterns, it should be able to construct models that provide valuable and robust online-assessments of the driver's SA.

5.5 Model selection

Section 5.2 provided the conceptional structures of three different kind of models we consider for DySAM, the NDRT, the SAGAT Score, and the extended SAGAT Score models. For a full specification of these models, we still require parameters and a potential factorization of their observation models, $p(\boldsymbol{F}^t|B^t)$, $p(\boldsymbol{F}^t|S_2^t)$, and $p(\boldsymbol{F}^t|S_2^t, B^t)$ respectively. For parameter estimation, we relied on Bayesian parameter estimation, as described in Section 1.5 of the appendix, for learning the structure of the observation models, we relied on the discriminative structure learning process, described in Section 1.6 of the appendix.

Discriminative structure learning in DySAM can also be interpreted as a kind of feature selection, in that the goal of the structure learning process is to find both a subset of relevant indicators $\boldsymbol{F}_{\text{Rel}} \subseteq \boldsymbol{F}$ and a factorization of an observation model over the relevant indicators, $\left(\boldsymbol{F}_{\text{Rel}}^t|B^t\right)$, $p\left(\boldsymbol{F}_{\text{Rel}}^t|S_2^t\right)$, and $p\left(\boldsymbol{F}_{\text{Rel}}^t|S_2^t, B^t\right)$. We'll use the NDRT model as an example for the explanation.

As a reminder, the NDRT models are defined as DBNs, that, for any number of time slices T, define a JPD $p(S_1^{1:T}, B^{1:t}, \boldsymbol{F}^{1:T})$ as:

$$p(S_1^{1:T}, B^{1:t}, \boldsymbol{F}^{1:T}) = p(S_1^1|B^1)p(B^1)p(\boldsymbol{F}^1|B^1)\prod_{t=2}^{T} p(S_1^t|B^t)p(B^t|B^{t-1})p(\boldsymbol{F}^t|B^t),$$

and shall be utilized exclusively to recursively infer filtered the belief state

$$p(S_1^t, B^t|\boldsymbol{f}^{1:t}) \propto p(S_1^t|B^t)p(\boldsymbol{f}^t|B^t)\sum_{b\in\text{Val}(B)} p(B^t|b^{t-1})\sum_{s_1\in\text{Val}(S_1)} p(s^{t-1}, b^{t-1}|\boldsymbol{f}^{1:t-1}).$$

As such, in DySAM, we rely on *discriminative* structure learning using the DBIC scoring criterion (c.f., Appendix, Section 1.6), with the aim to learn a factorization for $p(\boldsymbol{F}^t|B^t)$ that helps in solving $p(S_1^t, B^t|\boldsymbol{f}^{1:t})$.

Without loss of generalization, we can assume the set of indicators $\boldsymbol{F}$ to be comprised of two mutually exclusive sets, $\boldsymbol{F} = \boldsymbol{F}_{\text{Irrel}} \cup \boldsymbol{F}_{\text{Rel}}, \boldsymbol{F}_{\text{Irrel}} \cap \boldsymbol{F}_{\text{Rel}} = \emptyset$, where $\boldsymbol{F}_{\text{Rel}}$ shall contain all indicators relevant, while $\boldsymbol{F}_{\text{Irrel}}$ shall contains indicators that are irrelevant for predicting S_1 and B, such that the observation model $p(\boldsymbol{F}^t|B^t)$ can be factorized as

$$p(\boldsymbol{F}^t|B^t) = p\left(\boldsymbol{F}_{\text{Rel}}^t|B^t\right)p\left(\boldsymbol{F}_{\text{Irrel}}^t\right).$$

Regardless of the actual factorization of $p\left(\boldsymbol{F}_{\text{Rel}}^t|B^t\right)$ or $p\left(\boldsymbol{F}_{\text{Irrel}}^t\right)$, when it comes to inferring $p(S_1^t, B^t|\boldsymbol{f}^{1:t})$, we have that $p\left(\boldsymbol{f}_{\text{Irrel}}^t\right)$ cancels during inference and such provides no information about B^t and consequently, S_1^t:

$$
\begin{aligned}
p(S_1^t, B^t | \boldsymbol{f}^{1:t}) &= \frac{p(S_1^t, B^t, \boldsymbol{f}^t | \boldsymbol{f}^{1:t-1})}{\sum_{s_1 \in \mathrm{Val}(S_1)} \sum_{b \in \mathrm{Val}(B)} p(s_1^t, b^t, \boldsymbol{f}^t | \boldsymbol{f}^{1:t-1})} \\
&= \frac{p(S_1^t | B^t) p(\boldsymbol{f}^t | B^t) p(B^t | \boldsymbol{f}^{1:t-1})}{\sum_{s_1 \in \mathrm{Val}(S_1)} \sum_{b \in \mathrm{Val}(B)} p(s_1^t | b^t) p(\boldsymbol{f}^t | b^t) p(b^t | \boldsymbol{f}^{1:t-1})} \\
&= \frac{p(\boldsymbol{f}_{\mathrm{Irrel}}^t) p(S_1^t | B^t) p(\boldsymbol{f}_{\mathrm{Rel}}^t | B^t) p(B^t | \boldsymbol{f}^{1:t-1})}{p(\boldsymbol{f}_{\mathrm{Irrel}}^t) \sum_{b \in \mathrm{Val}(B)} p(\boldsymbol{f}_{\mathrm{Rel}}^t | b^t) p(b^t | \boldsymbol{f}^{1:t-1})} \\
&= p(S_1^t | B^t) \frac{p(\boldsymbol{f}_{\mathrm{Rel}}^t | B^t) p(B^t | \boldsymbol{f}^{1:t-1})}{\sum_{b \in \mathrm{Val}(B)} p(\boldsymbol{f}_{\mathrm{Rel}}^t | b^t) p(b^t | \boldsymbol{f}^{1:t-1})},
\end{aligned}
$$

where $p(B^t | \boldsymbol{f}^{1:t-1}) = \sum_{b \in \mathrm{Val}(B)} p(B^t | b^{t-1}) \sum_{s_1 \in \mathrm{Val}(S_1)} p(s_1^{t-1}, b^{t-1} | \boldsymbol{f}^{1:t-1})$. Formally, we have that any $F^t \in \boldsymbol{F}_{\mathrm{Irrel}}^t$ is *d-separated* from B^t given $\boldsymbol{F}_{\mathrm{Rel}}^t$ (Koller). As $p(\boldsymbol{F}_{\mathrm{Irrel}}^t)$ cancels during inference, we can simply omit $\boldsymbol{F}_{\mathrm{Irrel}}$ and reduce the model to only define a JPD over $p(S_1^{1:T}, B^{1:t}, \boldsymbol{F}_{\mathrm{Rel}}^{1:T})$ instead of $p(S_1^{1:T}, B^{1:t}, \boldsymbol{F}^{1:T})$, improving the computational efficiency of the inference without affecting the results.

As such, discriminative structure learning in DySAM can be understood as both finding a suitable set of relevant features $\boldsymbol{F}_{\mathrm{Rel}} \subseteq \boldsymbol{F}$ and the factorization of the relevant part of the observation models $p(\boldsymbol{F}_{\mathrm{Rel}}^t | B^t)$, $p(\boldsymbol{F}_{\mathrm{Rel}}^t | S_2^t)$, and $p(\boldsymbol{F}_{\mathrm{Rel}}^t | S_2^t, B^t)$ of the NDRT, SAGAT Score, and extended SAGAT Score models respectively. In the following sections, we'll provide an overview of the best-scoring structures to be used for evaluation (Section 5.6). The parameters for each model are provided in Section Appendix 2 of the appendix.

5.5.1 SAE Level 2 and SAE Level 3 NDRT models

The NDRT models rely on an observation model

$$p(\boldsymbol{F}^t | B^t) = p(\boldsymbol{F}_{\mathrm{Eff}}^t | B^t) p(\boldsymbol{F}_{\mathrm{Ineff}}^t).$$

Let $\mathcal{D} = \left\{ \left(b^{j,i}, s_1^{j,i}, \boldsymbol{f}^{j,i} \right)_{i=1}^{n_j} \right\}_{j=1}^{m}$ denote a set of training data, the goal of structure learning is to find the set of relevant features $\boldsymbol{F}_{\mathrm{Eff}} \subseteq \boldsymbol{F}$ and a graph structure $\mathcal{G}$ for $p(\boldsymbol{F}_{\mathrm{Eff}}^t | B^t)$ that maximizes a discriminate scoring criterion, which, for the NDRT models, we define as

$$\mathrm{DBIC}(\mathcal{G} : \mathcal{D}) = \left[\sum_{j=1}^{m} \sum_{i=1}^{n_j} \log p(b^{j,i} | \boldsymbol{f}^{j,i} : \boldsymbol{\theta}_{\mathrm{MAP}}) \right] - \frac{\lfloor \boldsymbol{\theta}_{\mathrm{MAP}} \rfloor}{2} \log \left(\sum_{j}^{m} n_j \right),$$

with $\boldsymbol{\theta}_{\mathrm{MAP}} = \max_{\boldsymbol{\theta}} p(\boldsymbol{\theta} | \mathcal{D})$ denoting the MAP parameters of the model.

We used the $\mathcal{D}_{\mathrm{Training}}^{\mathrm{NDRT:L2}}$ training data to learn the parameters and structure of the SAE Level 2 NDRT model and $\mathcal{D}_{\mathrm{Training}}^{\mathrm{NDRT:L3}}$ for the SAE Level 3 NDRT model. A graphical representation of the best-scoring factorizations of $p(\boldsymbol{F}_{\mathrm{Rel}}^t | B^t)$ for the NDRT models is shown in Figure 50.

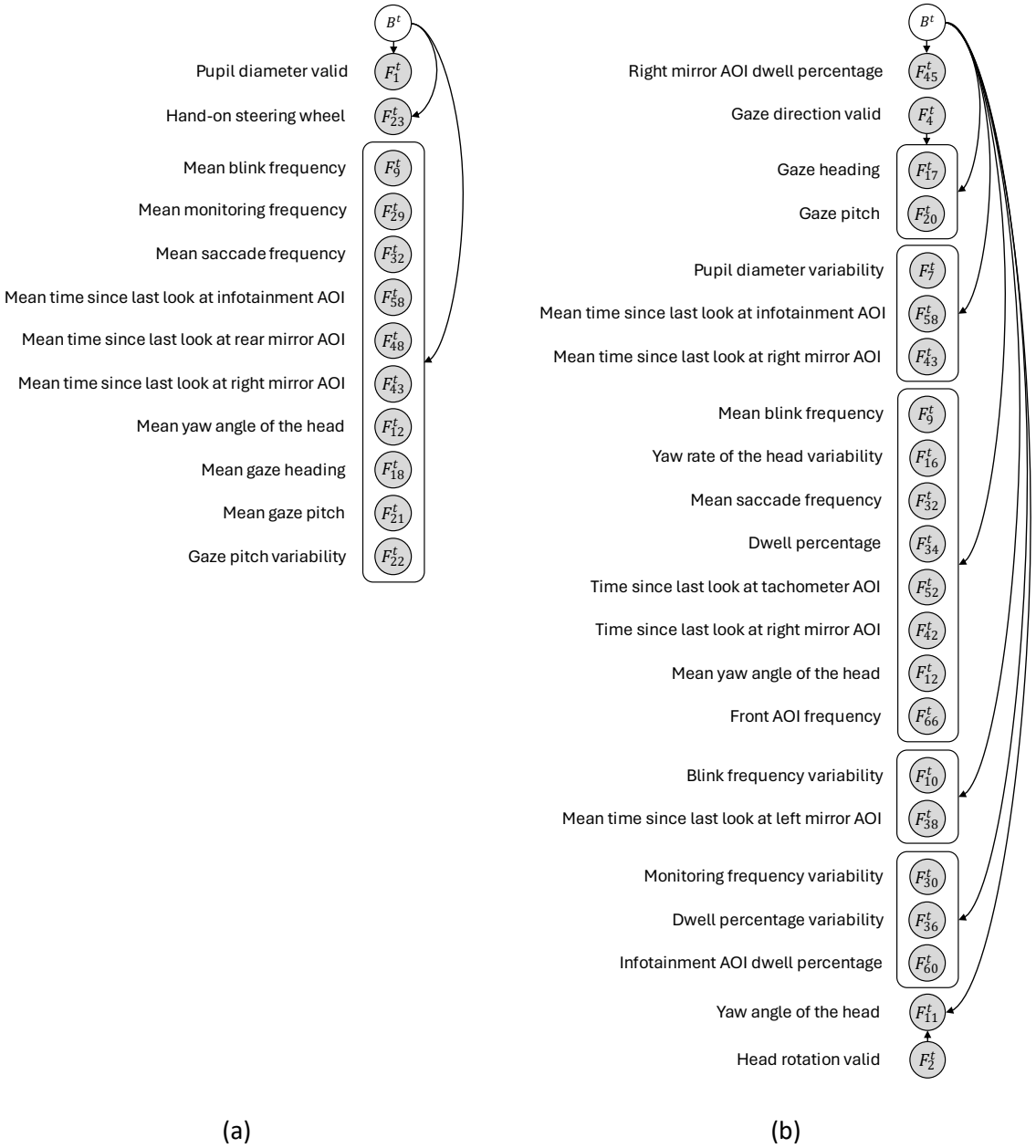

Figure 50: DAGs of the factorization of $p(\boldsymbol{F}_{\mathrm{Rel}}^t|B^t)$ for the SAE Level 2 NDRT model (a) and the SAE Level 3 NDRT model (b). White nodes indicate query variables, shaded nodes indicate observed variables. Boxed variables indicate multivariate distributions. Irrelevant indicators $\boldsymbol{F}_{\mathrm{Irrel}}$ are omitted.

During structure learning, CPDs over discrete variables were encoded as categorical distributions, CPDs over continuous variables as GMMs (c.f., Appendix 1, Section 1.2). To consider correlations between indicators, we allowed multiple continuous variables to be combined into multivariate GMMs.

The best-scoring SAE Level 2 NDRT model includes twelve indicators (5) and uses the factorization

$$p(\boldsymbol{F}_{\mathrm{Rel}}^t|B^t) = p(F_1^t|B^t)p(F_{23}^t|B^t)p(F_9^t, F_{29}^t, F_{32}^t, F_{58}^t, F_{48}^t, F_{43}^t, F_{12}^t, F_{18}^t, F_{21}^t, F_{22}^t|B^t),$$

where, for each $b \in \mathrm{Val}(B)$, $p(F_1^t|b^t)$ and $p(F_{23}^t|b^t)$ are categorical distributions, and $p(F_9^t, F_{29}^t, F_{32}^t, F_{58}^t, F_{48}^t, F_{43}^t, F_{12}^t, F_{18}^t, F_{21}^t, F_{22}^t|b^t)$ is a multivariate GMM. The MAP parameters of the distributions are provided in Section 2.1 of the appendix.

Table 5: The set of relevant indicators for the SAE Level 2 NDRT model, $\boldsymbol{F}_{\mathrm{Rel}} = \{F_1, F_9, F_{12}, F_{18}, F_{21}, F_{22}, F_{23}, F_{29}, F_{32}, F_{43}, F_{48}, F_{58}\}$.

Symbol	Name
F_1	Pupil diameter valid
F_9	Mean blink frequency
F_{12}	Mean yaw angle of the head
F_{18}	Mean gaze heading
F_{21}	Mean gaze pitch
F_{22}	Gaze pitch variability
F_{23}	Hands-on steering wheel
F_{29}	Mean monitoring frequency
F_{32}	Mean saccade frequency
F_{43}	Mean time since last look at right mirror AOI
F_{48}	Mean time since last look at rear mirror AOI
F_{58}	Mean time since last look at infotainment AOI

The best-scoring SAE Level 3 NDRT model includes 22 indicators (Table 6) and uses the factorization

$$\begin{aligned} p\left(\boldsymbol{F}_{\mathrm{Rel}}^t | B^t\right) \;=\; & p(F_{45}^t|B^t)\,p(F_{17}^t, F_{20}^t|B^t, F_4^t)\,p(F_7^t, F_{58}^t, F_{43}^t|B^t) \\ & p(F_9^t, F_{16}^t, F_{32}^t, F_{34}^t, F_{52}^t, F_{42}^t, F_{12}^t, F_{66}^t|B^t)\,p(F_{10}^t, F_{38}^t|B^t) \\ & p(F_{30}^t, F_{36}^t, F_{60}^t|B^t)\,p(F_{11}^t|B^t, F_2^t), \end{aligned}$$

where, for each configuration of the discrete parents, $\{b\} \in \mathrm{Val}(B)$, $\{b, f_2\} \in \mathrm{Val}(B) \times \mathrm{Val}(F_2)$, or $\{b, f_4\} \in \mathrm{Val}(B) \times \mathrm{Val}(F_4)$, each distribution is a (multivariate) GMM. The MAP parameters of the distributions are provided in Section 2.2 of the appendix.

Table 6: The set of relevant indicators for the SAE Level 3 NDRT model, $\boldsymbol{F}_{\mathrm{Rel}} = \{F_2, F_4, F_7, F_9, F_{10}, F_{11}, F_{12}, F_{16}, F_{17}, F_{20}, F_{30}, F_{32}, F_{34}, F_{36}, F_{38}, F_{42}, F_{43}, F_{45}, F_{52}, F_{58}, F_{60}, F_{66}\}$.

Symbol	Name
F_2	Head rotation valid
F_4	Gaze direction valid
F_7	Pupil diameter variability
F_9	Mean blink frequency
F_{10}	Blink frequency variability
F_{11}	Yaw angle of the head
F_{12}	Mean yaw angle of the head
F_{16}	Yaw rate of the head variability
F_{17}	Gaze heading
F_{20}	Gaze pitch
F_{30}	Monitoring frequency variability
F_{32}	Mean saccade frequency
F_{34}	Dwell percentage
F_{36}	Dwell percentage variability

F_{38}	Mean time since last look at left mirror AOI
F_{42}	Time since last look at right mirror AOI
F_{43}	Mean time since last look at right mirror AOI
F_{45}	Right mirror AOI dwell percentage
F_{52}	Time since last look at tachometer AOI
F_{58}	Mean time since last look at infotainment AOI
F_{60}	Infotainment AOI dwell percentage
F_{66}	Front AOI frequency

5.5.2 SAE Level 2 and SAE Level 3 SAGAT Score models

The SAGAT Score models rely on an observation model

$$p(\boldsymbol{F}^t|S_2^t) = p\left(\boldsymbol{F}_{\text{Rel}}^t|S_2^t\right)p\left(\boldsymbol{F}_{\text{Irrel}}^t\right).$$

Let $\mathcal{D} = \left\{\left(b^{j,i}, s_2^{j,i}, \boldsymbol{f}^{j,i}\right)_{i=1}^{n_j}\right\}_{j=1}^{m}$ denote a set of training data, the goal of structure learning is to find the set of relevant features $\boldsymbol{F}_{\text{Eff}} \subseteq \boldsymbol{F}$ and a graph structure $\mathcal{G}$ for $p\left(\boldsymbol{F}_{\text{Eff}}^t|S_2^t\right)$ that maximizes the discriminate scoring criterion

$$\text{DBIC}(\mathcal{G}:\mathcal{D}) = \left[\sum_{j=1}^{m}\sum_{i=1}^{n_j}\log p\left(s_2^{j,i}|\boldsymbol{f}^{j,i}:\boldsymbol{\theta}_{\text{MAP}}\right)\right] - \frac{\lfloor\boldsymbol{\theta}_{\text{MAP}}\rfloor}{2}\log\left(\sum_{j}^{m} n_j\right),$$

with $\boldsymbol{\theta}_{\text{MAP}} = \max_{\boldsymbol{\theta}} p(\boldsymbol{\theta}|\mathcal{D})$ denoting the MAP parameters of the model.

We used the $\mathcal{D}_{\text{Training}}^{\text{SAG:L2}}$ training data to learn the parameters and structure of the SAE Level 2 SAGAT Score model and $\mathcal{D}_{\text{Training}}^{\text{SAG:L3}}$ for the SAE Level 3 SAGAT Score model. A graphical representation of the best-scoring factorizations of $p\left(\boldsymbol{F}_{\text{Rel}}^t|B^t\right)$ for the SAGAT Score models is shown in Figure 51.

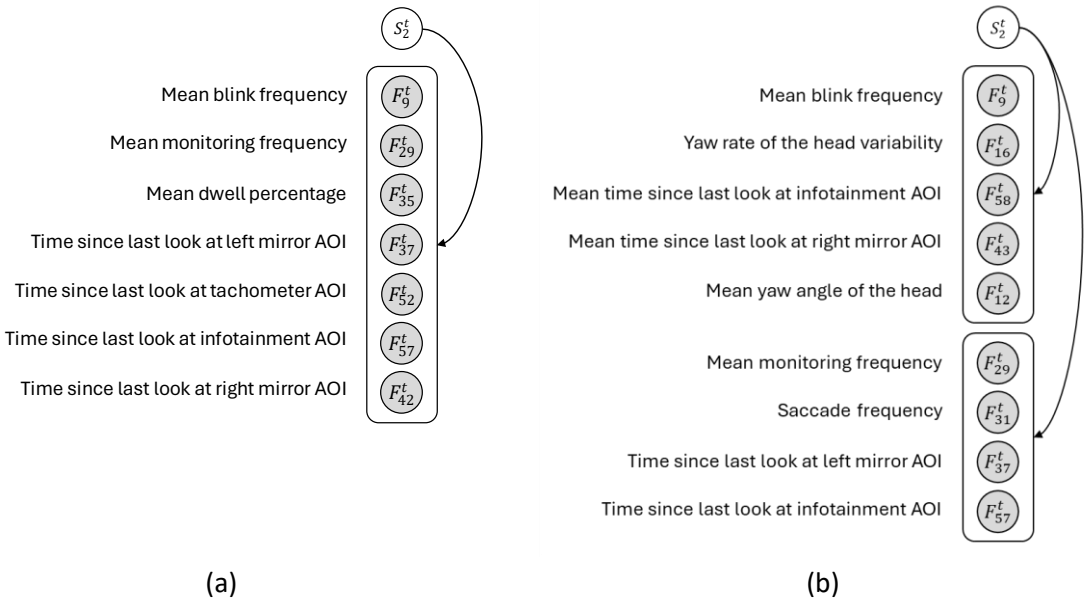

Figure 51: DAGs of the factorization of $p\left(\boldsymbol{F}_{\text{Rel}}^t|S_2^t\right)$ for the SAE Level 2 SAGAT Score model (a) and the SAE Level 3 SAGAT Score model (b). White nodes indicate query variables, shaded nodes indicate observed variables. Boxed variables indicate multivariate distributions. Irrelevant indicators $\boldsymbol{F}_{\text{Irrel}}$ are omitted.

During structure learning, CPDs over discrete variables were encoded as categorical distributions CPDs over continuous variables as GMMs (c.f., Appendix 1, Section 1.2). To consider correlations between indicators, we allowed multiple continuous variables to be combined into multivariate GMMs.

The best-scoring SAE Level 2 SAGAT Score model includes seven indicators (Table 7) and uses the factorization

$$p\left(\boldsymbol{F}_{\mathrm{Rel}}^{t}|S_2^t\right) = p(F_9^t, F_{29}^t, F_{35}^t, F_{37}^t, F_{52}^t, F_{57}^t, F_{42}^t|S_2^t),$$

where, for each $s_2 \in \mathrm{Val}(S_2)$, $p(F_9^t, F_{29}^t, F_{35}^t, F_{37}^t, F_{52}^t, F_{57}^t, F_{42}^t|s_2^t)$ is a multivariate GMM. The MAP parameters of the distributions are provided in Section 2.3 of the appendix.

Table 7: The set of relevant indicators for the SAE Level 2 SAGAT Score model, $\boldsymbol{F}_{\mathrm{Rel}} = \{F_9, F_{29}, F_{35}, F_{37}, F_{42}, F_{52}, F_{57}\}$.

Symbol	Name
F_9	Mean blink frequency
F_{29}	Mean monitoring frequency
F_{35}	Mean dwell percentage
F_{37}	Time since last look at left mirror AOI
F_{42}	Time since last look at right mirror AOI
F_{52}	Time since last look at tachometer AOI
F_{57}	Time since last look at infotainment AOI

The best-scoring SAE Level 3 SAGAT Score model includes nine indicators (Table 8) and uses the factorization

$$p\left(\boldsymbol{F}_{\mathrm{Rel}}^{t}|S_2^t\right) = p(F_9^t, F_{16}^t, F_{58}^t, F_{43}^t, F_{12}^t|S_2^t)p(F_{29}^t, F_{31}^t, F_{37}^t, F_{57}^t|S_2^t),$$

where, for each $s_2 \in \mathrm{Val}(S_2)$, $p(F_9^t, F_{16}^t, F_{58}^t, F_{43}^t, F_{12}^t|s_2^t)$ and $p(F_{29}^t, F_{31}^t, F_{37}^t, F_{57}^t|s_2^t)$ are multivariate GMM. The MAP parameters of the distributions are provided in Section 2.4 of the appendix.

Table 8: The set of relevant indicators for the SAE Level 3 SAGAT Score model, $\boldsymbol{F}_{\mathrm{Rel}} = \{F_9, F_{12}, F_{16}, F_{29}, F_{31}, F_{37}, F_{43}, F_{57}, F_{58}\}$.

Symbol	Name
F_9	Mean blink frequency
F_{12}	Mean yaw angle of the head
F_{16}	Yaw rate of the head variability
F_{29}	Mean monitoring frequency
F_{31}	Saccade frequency
F_{37}	Time since last look at left mirror AOI
F_{43}	Mean time since last look at right mirror AOI
F_{57}	Time since last look at infotainment AOI
F_{58}	Mean time since last look at infotainment AOI

5.5.3 Extended SAE Level 2 and SAE Level 3 SAGAT Score models

The extended SAGAT Score models rely on an observation model

$$p(\boldsymbol{F}^t|S_2^t, B^t) = p\left(\boldsymbol{F}_{\text{Rel}}^t|S_2^t, B^t\right)p\left(\boldsymbol{F}_{\text{Irrel}}^t\right).$$

Let $\mathcal{D} = \left\{\left(b^{j,i}, s_2^{j,i}, \boldsymbol{f}^{j,i}\right)_{i=1}^{n_j}\right\}_{j=1}^{m}$ denote the training data, the goal of structure learning is adapted to find the set of relevant features $\boldsymbol{F}_{\text{Rel}} \subseteq \boldsymbol{F}$ and a graph structure $\mathcal{G}$ for $p(\boldsymbol{F}_{\text{Re.}}^t|S_2^t, B^t)$ that maximizes the discriminate scoring criterion

$$\text{DBIC}(\mathcal{G}:\mathcal{D}) = \left[\sum_{j=1}^{m}\sum_{i=1}^{n_j}\log p\left(s_2^{j,i}|b^{j,i}, \boldsymbol{f}^{j,i}:\boldsymbol{\theta}_{\text{MAP}}\right)\right] - \frac{|\boldsymbol{\theta}_{\text{MAP}}|}{2}\log\left(\sum_{j}^{m} n_j\right),$$

with $\boldsymbol{\theta}_{\text{MAP}} = \max_{\boldsymbol{\theta}} p(\boldsymbol{\theta}|\mathcal{D})$ denoting the MAP parameters of the model.

We used the $\mathcal{D}_{\text{Training}}^{\text{SAG:L2}}$ training data to learn the parameters and structure of the extended SAE Level 2 SAGAT Score model and $\mathcal{D}_{\text{Training}}^{\text{SAG:L3}}$ for the extended SAE Level 3 SAGAT Score model. A graphical representation of the best-scoring factorizations of $p\left(\boldsymbol{F}_{\text{Rel}}^t|B^t\right)$ for the extended SAGAT Score models is shown in Figure 52.

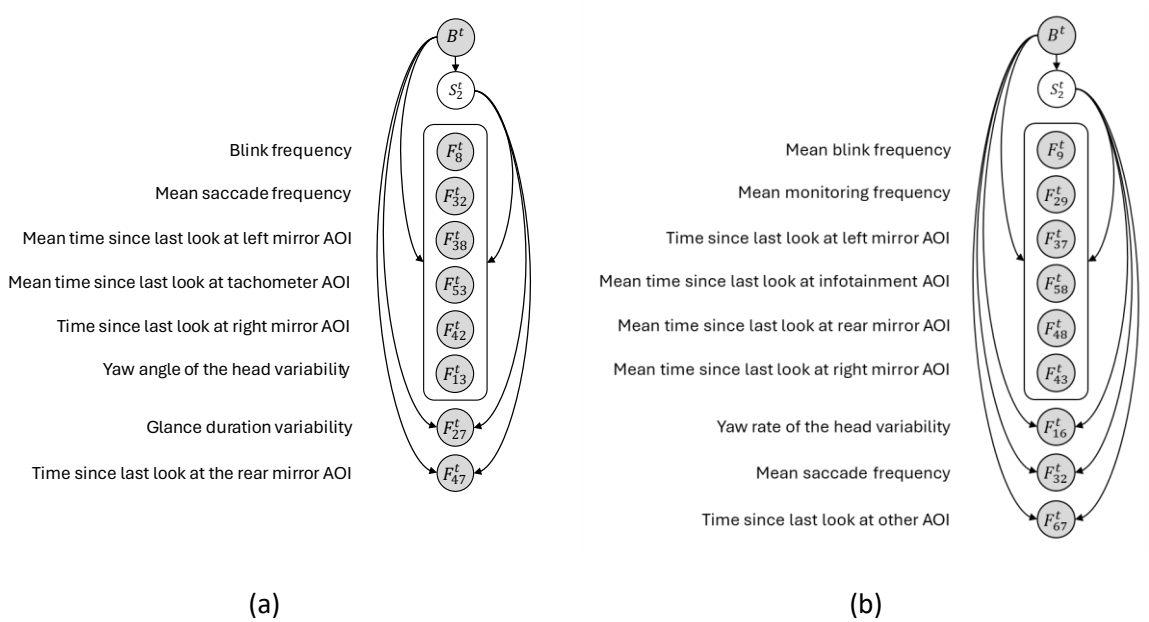

Figure 52: DAGs of the factorization of $p\left(\boldsymbol{F}_{Eff}^t|S_2^t\right)$ for the extended SAE Level 2 SAGAT Score model (a) and the extended SAE Level 3 SAGAT Score model (b). White nodes indicate query variables, shaded nodes indicate observed variables. Boxed variables indicate multivariate distributions. Irrelevant indicators $\boldsymbol{F}_{\text{Irrel}}$ are omitted.

During structure learning, CPDs over discrete variables were once again encoded as categorical distributions. However, due to the limited amount of training data when conditioning on the behavioral patterns, CPDs over continuous variables were encoded as either exponential or Gaussian distributions (c.f., Appendix 1, Section 1.2). To consider correlations between indicators, we allowed multiple continuous variables to be combined into multivariate Gaussian distributions.

The best-scoring extended SAE Level 2 SAGAT Score model includes 8 indicators (Table 9) and uses the factorization

$$p\left(\boldsymbol{F}_{\text{Rel}}^{t}|S_2^t, B^t\right) = p(F_8^t, F_{32}^t, F_{38}^t, F_{53}^t, F_{42}^t, F_{13}^t|S_2^t, B^t)p(F_{27}^t|S_2^t, B^t)p(F_{47}^t|S_2^t, B^t),$$

where, for each $\{s_2, b\} \in \text{Val}(S_2) \times \text{Val}(B)$, $p(F_8^t, F_{32}^t, F_{38}^t, F_{53}^t, F_{42}^t, F_{13}^t|S_2^t, B^t)$ is a multivariate Gaussian, while $p(F_{27}^t|s_2^t, b^t)$ and $p(F_{47}^t|s_2^t, b^t)$ are exponential distributions. The MAP parameters of the distributions are provided in Section 2.5 of the appendix.

Table 9: The set of relevant indicators for the extended SAE Level 2 SAGAT Score model, $\boldsymbol{F}_{\text{Rel}} = \{F_8, F_{13}, F_{27}, F_{32}, F_{38}, F_{42}, F_{47}, F_{53}\}$.

Symbol	Name
F_8	Blink frequency
F_{13}	Yaw angle of the head variability
F_{27}	Glance duration variability
F_{32}	Mean saccade frequency
F_{38}	Mean time since last look at left mirror AOI
F_{42}	Time since last look at right mirror AOI
F_{47}	Time since last look at the rear mirror AOI
F_{53}	Mean time since last look at tachometer AOI

The best-scoring extended SAE Level 3 SAGAT Score model includes nine indicators (Table 10) and uses the factorization

$$p\left(\boldsymbol{F}_{\text{Eff}}^{t}|S_2^t, B^t\right) = p(F_9^t, F_{29}^t, F_{37}^t, F_{58}^t, F_{48}^t, F_{43}^t|S_2^t, B^t)p(F_{16}^t|S_2^t, B^t)p(F_{32}^t|S_2^t, B^t)p(F_{67}^t|S_2^t, B^t),$$

where, for each $\{s_2, b\} \in \text{Val}(S_2) \times \text{Val}(B)$, $p(F_9^t, F_{29}^t, F_{37}^t, F_{58}^t, F_{48}^t, F_{43}^t|s_2^t, b^t)$ is a multivariate Gaussian, $p(F_{32}^t|s_2^t, b^t)$ is a univariate Gaussian, and $p(F_{16}^t|s_2^t, b^t)$ and $p(F_{67}^t|s_2^t, b^t)$ are exponential distributions. The MAP parameters of the distributions are provided in Section 2.6 of the appendix.

Table 10: The set of relevant indicators for the extended SAE Level 3 SAGAT Score model, $\boldsymbol{F}_{\text{Rel}} = \{F_9, F_{16}, F_{29}, F_{32}, F_{37}, F_{43}, F_{48}, F_{58}, F_{67}\}$.

Symbol	Name
F_9	Mean blink frequency
F_{16}	Yaw rate of the head variability
F_{29}	Mean monitoring frequency
F_{32}	Mean saccade frequency
F_{37}	Time since last look at left mirror AOI
F_{43}	Mean time since last look at right mirror AOI
F_{48}	Mean time since last look at rear mirror AOI
F_{58}	Mean time since last look at infotainment AOI
F_{67}	Time since last look at other AOI

5.6 Evaluation results

5.6.1 Evaluation procedure and metrics

We will explain the evaluation procedure using the example of the SAE Level 2 NDRT model. Evaluation of other models follow the same overall procedure but may require an adaptation of the probability query and classification rules to account for changes in the overall model structure.

As a reminder, the test set

$$\mathcal{D}_{\text{Test}}^{\text{NDRT:L2}} = \left\{\left(b^{j,i}, s_1^{j,i}, \boldsymbol{f}^{j,i}\right)_{i=1}^{n_j}\right\}_{j=1}^{74}, \sum_{j=1}^{74} n_j = 148275$$

for the SAE Level 2 NDRT model consists of $m = 74$ unseen sequences of approx. 2.5 minutes length (c.f. Section 5.3), each comprised of n_j samples $\left(s_1^{j,i}, b^{j,i}, \boldsymbol{f}^{j,i}\right)$, denoting the ground truth annotation for the binary situation awareness $s_1^{j,i}$, the behavioral pattern / NDRT condition $b^{j,i}$, and the indicators $\boldsymbol{f}^{j,i}$. For each sequence $j = 1, \dots, m$, we use the model to answer a probability query, in the case of the NDRT models, to infer the conditional probability distribution

$$p\left(S_1^{j,i}, B^{j,i} | \boldsymbol{f}^{j,1:j,i}\right),$$

i.e., the probability distribution over the binary situation awareness and the behavioral patterns / NDRT conditions given the observable indicators from the start of the sequence until the current sample. From this distribution, we then derive concrete assignments as model predictions by using the following classification function:

$$\hat{s}_1^{j,i} = \arg\max_{s_1^{j,i}} p\left(s_1^{j,i} | \boldsymbol{f}^{j,1:j,i}\right) = \arg\max_{s_1^{j,i}} \sum_{b \in \text{Val}(B)} p\left(s_1^{j,i}, b^{j,i} | \boldsymbol{f}^{j,1:j,i}\right),$$

$$\hat{b}^{j,i} = \arg\max_{b^{j,i}} p\left(b^{j,i} | \boldsymbol{f}^{j,1:j,i}\right) = \arg\max_{b^{j,i}} \sum_{s_1 \in \text{Val}(S_1)} p\left(s_1^{j,i}, b^{j,i} | \boldsymbol{f}^{j,1:j,i}\right).$$

5.6.1.1 Confusion matrices

For comparison of the ground truth and the model predictions, we then prepare confusion matrices. For the binary situation awareness, the confusion matrix is a 2×2 matrix, constructed as shown in Figure 53.

		Predicted situation awareness		
		$\hat{s}_{1_1}$ (sufficient)	$\hat{s}_{1_0}$ (insufficient)	Total
Ground truth situation awareness	s_{1_1}	$\text{TP} \triangleq \sum_{j=1}^{m}\sum_{i=1}^{n_j} \mathbb{I}\left(s_{1_1}^{j,i}\right)\mathbb{I}\left(\hat{s}_{1_1}^{j,i}\right)$	$\text{FN} \triangleq \sum_{j=1}^{m}\sum_{i=1}^{n_j} \mathbb{I}\left(s_{1_1}^{j,i}\right)\mathbb{I}\left(\hat{s}_{1_0}^{j,i}\right)$	$\sum_{j=1}^{m}\sum_{i=1}^{n_j} \mathbb{I}\left(s_{1_1}^{j,i}\right)$
	s_{1_0}	$\text{FP} \triangleq \sum_{j=1}^{m}\sum_{i=1}^{n_j} \mathbb{I}\left(s_{1_0}^{j,i}\right)\mathbb{I}\left(\hat{s}_{1_1}^{j,i}\right)$	$\text{TN} \triangleq \sum_{j=1}^{m}\sum_{i=1}^{n_j} \mathbb{I}\left(s_{1_0}^{j,i}\right)\mathbb{I}\left(\hat{s}_{1_0}^{j,i}\right)$	$\sum_{j=1}^{m}\sum_{i=1}^{n_j} \mathbb{I}\left(s_{1_0}^{j,i}\right)$
	Total	$\sum_{j=1}^{m}\sum_{i=1}^{n_j} \mathbb{I}\left(\hat{s}_{1_1}^{j,i}\right)$	$\sum_{j=1}^{m}\sum_{i=1}^{n_j} \mathbb{I}\left(\hat{s}_{1_0}^{j,i}\right)$	$\sum_{j=1}^{m} n_j$

Figure 53: Preparation of a 2×2 confusion matrix for recognizing the binary situation awareness from ground truth data and model answers.

Analogous, for the ternary behavioral patterns / NDRT conditions, the confusion matrix is a 3×3 matrix, constructed as shown in Figure 54.

		Predicted behavioral pattern			
		$\hat{b}_0$ (no NDRT)	$\hat{b}_1$ (cognitive NDRT)	$\hat{b}_2$ (visual NDRT)	Total
Ground truth behavioral pattern	b_0	$\sum_{j=1}^{m}\sum_{i=1}^{n_j} \mathbb{I}(b_0^{j,i})\,\mathbb{I}(\hat{b}_0^{j,i})$	$\sum_{j=1}^{m}\sum_{i=1}^{n_j} \mathbb{I}(b_0^{j,i})\,\mathbb{I}(\hat{b}_1^{j,i})$	$\sum_{j=1}^{m}\sum_{i=1}^{n_j} \mathbb{I}(b_0^{j,i})\,\mathbb{I}(\hat{b}_2^{j,i})$	$\sum_{j=1}^{m}\sum_{i=1}^{n_j} \mathbb{I}(b_0^{j,i})$
	b_1	$\sum_{j=1}^{m}\sum_{i=1}^{n_j} \mathbb{I}(b_1^{j,i})\,\mathbb{I}(\hat{b}_0^{j,i})$	$\sum_{j=1}^{m}\sum_{i=1}^{n_j} \mathbb{I}(b_1^{j,i})\,\mathbb{I}(\hat{b}_1^{j,i})$	$\sum_{j=1}^{m}\sum_{i=1}^{n_j} \mathbb{I}(b_1^{j,i})\,\mathbb{I}(\hat{b}_2^{j,i})$	$\sum_{j=1}^{m}\sum_{i=1}^{n_j} \mathbb{I}(b_1^{j,i})$
	b_2	$\sum_{j=1}^{m}\sum_{i=1}^{n_j} \mathbb{I}(b_2^{j,i})\,\mathbb{I}(\hat{b}_0^{j,i})$	$\sum_{j=1}^{m}\sum_{i=1}^{n_j} \mathbb{I}(b_2^{j,i})\,\mathbb{I}(\hat{b}_1^{j,i})$	$\sum_{j=1}^{m}\sum_{i=1}^{n_j} \mathbb{I}(b_2^{j,i})\,\mathbb{I}(\hat{b}_2^{j,i})$	$\sum_{j=1}^{m}\sum_{i=1}^{n_j} \mathbb{I}(b_2^{j,i})$
	Total	$\sum_{j=1}^{m}\sum_{i=1}^{n_j} \mathbb{I}(\hat{b}_0^{j,i})$	$\sum_{j=1}^{m}\sum_{i=1}^{n_j} \mathbb{I}(\hat{b}_1^{j,i})$	$\sum_{j=1}^{m}\sum_{i=1}^{n_j} \mathbb{I}(\hat{b}_2^{j,i})$	$\sum_{j=1}^{m} n_j$

Figure 54: Preparation of a 3×3 confusion matrix for recognizing the ternary behavioral patterns from ground truth data and model answers.

5.6.1.2 Evaluation metrics

We use the confusion matrices to derive a set of evaluation metrics. In the case of a 2×2 confusion matrix, we use the following metrics:

- Accuracy / 0-1-Loss: Defined as the proportion of test samples correctly classified as sufficient and insufficient situation awareness, among the total number of samples examined:

$$0 \text{ (worst)} \leq \text{Accuracy} \triangleq \frac{\text{TP} + \text{TN}}{\text{TP} + \text{FP} + \text{FN} + \text{TN}} \leq 1 \text{ (best)}.$$

  The accuracy is a standard measure for the performance of binary (and non-binary) classifiers but may provide a biased appearance in the case of non-uniformly distributed samples. E.g., if 99% of test samples were insufficient, a trivial classifier that simply predicts each case as insufficient would still achieve an accuracy of 0.99.

- Precision: Defined as the proportion of test samples classified as sufficient situation awareness that were correctly identified:

$$0 \text{ (worst)} \leq \text{Precision} \triangleq \frac{\text{TP}}{\text{TP} + \text{FP}} \leq 1 \text{ (best)}.$$

  A high precision indicates that samples that were classified as sufficient situation awareness are likely to be classified correctly, disregarding samples that were correctly or incorrectly classified as insufficient situation awareness. As such, precision can be interpreted as a measure of quality, meaning that given a high precision, we can trust the model that a sample classified as sufficient situation awareness truly represents sufficient situation awareness. A short-coming of the precision metric is that it is possible to improve the precision by minimizing the chance of false positives, e.g., by using a classification function

$$\hat{s}_1^{j,i} = \begin{cases} 1, & p\left(S_1^{j,i} = s_{1_1} | \boldsymbol{f}^{j,1:j,i}\right) > 0.99 \\ 0, & \text{otherwise} \end{cases},$$

which would decrease the number of false positives at the cost of an increase of false negatives. As such, the precision metric is usually not used in isolation but discussed in combination with the true positive rate / recall metric.

- True positive rate (TPR) / Recall: Defined as the proportion of test samples labelled as sufficient situation awareness in the ground truth test data that were correctly identified:

$$0 \text{ (worst)} \leq \text{TPR} \triangleq \frac{\text{TP}}{\text{TP} + \text{FN}} \leq 1 \text{ (best)}.$$

  The TPR measures the model's ability to correctly classify samples that were labelled as sufficient situation awareness, while disregarding the model's ability to correctly identify samples labelled as insufficient situation awareness. A short-coming of the TPR is that it is possible to improve the TPR by minimizing the chance of false negatives, e.g., it is possible to achieve a perfect TPR by using the trivial classification function $\hat{s}_1^{j,i} = 1$, which would ensure that there are no false negatives, at the cost of misclassifying all samples labelled as insufficient situation awareness. As such, the TPR is usually not used in isolation but should be discussed in combination with the precision or false positive rate.

- False positive rate (FPR): Defined as the proportion of test samples labelled as insufficient situation awareness in the ground truth test data that were incorrectly classified as sufficient situation awareness:

$$0 \text{ (best)} \leq \text{FPR} \triangleq \frac{\text{FP}}{\text{FP} + \text{TN}} \leq 1 \text{ (worst)}.$$

  The FPR can be seen as the equivalent of the FPR for insufficient situation awareness, in that the FPR measures the model's ability to correctly classify samples that were labelled as insufficient situation awareness, while disregarding the model's ability to correctly identify samples labelled as sufficient situation awareness. As such, a short-coming of the FPR is that it is possible to improve the FPR by minimizing the chance of false positives, e.g., it is possible to achieve a perfect FPR by using the trivial classification function $\hat{s}_1^{j,i} = 0$, which would ensure that there are no false positives, at the cost of misclassifying all samples labelled as sufficient situation awareness. As such, the TPR is usually not used in isolation but should be discussed in combination with the TPR, commonly in the form of Receiver Operating Characteristic curves.

- F_1 score: Defined as the harmonic mean of precision and recall:

$$0 \text{ (worst)} \leq F_1 \triangleq \frac{2 \cdot \text{TP}}{2 \cdot \text{TP} + \text{FP} + \text{FN}} \leq 1 \text{ (best)}.$$

  The F_1 score is a common measure of predictive performance and combines both precision and recall in a single metric. A short-coming of the F_1 score is its disregard of true negatives, which makes it less suitable for the assessment of (binary) classifiers, but we include it as an evaluation metric for the sake of completion and its common use as a summary metric for the predictive performance.

In the case of higher-dimensional confusion matrices, we use the following metrics:

- Accuracy / 0-1-Loss: Defined as the proportion of test samples correctly classified among the total number of samples examined, e.g., in the case of the behavioral patterns:

$$0 \text{ (worst)} \leq \text{Accuracy} \triangleq \frac{\sum_{j=1}^{m}\sum_{i=1}^{n_j}\mathbb{I}\left(b^{j,i}=\hat{b}^{j,i}\right)}{\sum_{j=1}^{m}n_j} \leq 1 \text{ (best)}.$$

  The accuracy is a standard measure for the performance of non-binary classifiers and measures the ability of the model to correctly classify the different behavioral patterns in the test data.

- Classification-rate: We define the classification-rate as the average probability of correctly classifying the ground truth:

$$0 \text{ (worst)} \leq CR \triangleq \frac{\sum_{j=1}^{m}\sum_{i=1}^{n_j}p\left(B^{j,i}=b^{j,i}|\boldsymbol{f}^{j,1:j,i}\right)}{\sum_{j=1}^{m}n_j} \leq 1 \text{ (best)}.$$

  As the accuracy only considers whether $\mathbb{I}\left(b^{j,i}=\hat{b}^{j,i}\right)$, $\hat{b}^{j,i}=\arg\max_{b^{j,i}} p\left(b^{j,i}|\boldsymbol{f}^{j,1:j,i}\right)$, it is insensitive to whether the probability $p\left(B^{j,i}=b^{j,i}|\boldsymbol{f}^{j,1:j,i}\right)$ of correctly predicting the ground truth is high or low. In contrast, the classification-rate represents the average probability with which the model was able to correctly predict the ground truth. A comparison of the accuracy with the classification-rate therefore allows an assessment of how certain the model is in its predictions.

5.6.1.2.1 Receiver Operating Characteristic Curve and Area under Curve

Fir binary classification problems, due to the inverse relationship between TPR and FPR, it is common to plot the TPR as a function of the FPR, obtained by deriving the TPR and FPR under different classification thresholds δ, resulting in a so-called Receiver Operating Characteristic (ROC) curve. The ROC curve visualizes the sensitivity of the model performance to the somewhat arbitrary classification thresholds[4] used for deriving concrete model answers from the probability distributions inferred by the models. An example is shown in Figure 55. For DySAM, the ROC curve of a model that has no ability to discriminate between sufficient and insufficient situation awareness would result in the dashed red ROC curve / line. A perfect model would achieve a TPR of 1 for a FPR of 0, resulting in a rectangular ROC curve.

[4] We note that, with the exception of preparing ROC curves, we use a single classification function for evaluation of the DySAM model for the derivation of evaluation metrics (c.f., Section 5.6.1), which in the case of the binary situation awareness S_1, corresponds to a classification threshold $\delta = 0.5$.

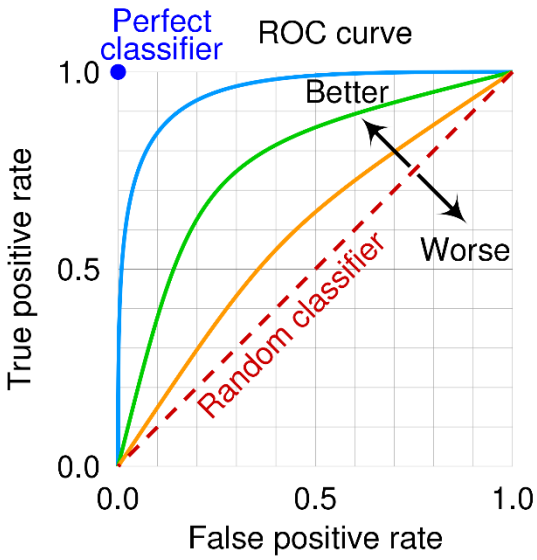

Figure 55: Exemplary ROC curves for three different hypothetical classifiers. Picture taken from "https://en.wikipedia.org/wiki/Receiver_operating_characteristic#/media/File:Roc_curve.svg", last visited 25.02.2024. Picture created by "cmglee, MartinThoma" under the CC BY-SA 4.0 DEED license (https://creativecommons.org/licenses/by-sa/4.0/).

The ROC curve is commonly summarized by the "area under curve" (AUC) statistic, integrating the area under the ROC. The AUC summarizes the model's ability to correctly discriminate between sufficient and insufficient situation awareness. An AUC of 1 represents perfect discrimination, an AUC of 0.5 means that a model has no ability to discriminate between classes. Although higher AUC are, in general, better than lower AUC scores, what constitutes a "good" AUC score naturally depends on the task and the available data. For a generic rule of thumb, Hosmer et al. (2013) provide the following guidelines, where we reinterpret "excellent" as good and "outstanding" as very good:

- $\mathrm{AUC} = 0.5$: No discrimination
- $0.5 < \mathrm{AUC} \leq 0.7$: Poor discrimination
- $0.7 < \mathrm{AUC} \leq 0.8$: Acceptable discrimination
- $0.8 < \mathrm{AUC} \leq 0.9$: Good (originally "Excellent") discrimination
- $\mathrm{AUC} \geq 0.9$: Very good (originally "Outstanding") discrimination.

For the preparation of ROC curves, applicable for the binary situation awareness S_1, we prepare the model answers parameterized by a classification threshold $\delta = \frac{0}{100}, \frac{1}{100}, \ldots, \frac{100}{100}$ and derive

$$\hat{s}_{1_\delta}^{j,i} = \begin{cases} 1, & p\left(S_1^{j,i} = s_{1_1} | \boldsymbol{f}^{j,1:j,i}\right) > \delta \\ 0, & \text{otherwise} \end{cases}$$

for each threshold δ, from which we can derive the threshold-dependent FPR and TPR as depicted in Section 5.6.1.2.

5.6.2 Evaluation of the NDRT models

The NDRT models use the evaluation procedure as explained in Section 5.6.1.

5.6.2.1 SAE Level 2 NDRT model

After being trained on the $\mathcal{D}_{\text{Ttaining}}^{\text{NDRT:L2}}$ training dataset, the best-scoring SAE Level 2 NDRT model (c.f., Section 5.2.2) was evaluated on the $\mathcal{D}_{\text{Test}}^{\text{NDRT:L2}}$ test dataset, following the evaluation procedure explained in Section 5.6.1. The resulting confusion matrix for recognizing the ternary behavioral patterns is shown in Figure 56. As apparent, the SAE Level 2 NDRT model is able to correctly recognize a majority of the ground truth behavioral patterns. The primary problem is a confusion between samples belonging to participants without NDRT and participants tasked with the cognitive NDRT. In contrast, the model is very capable to correctly recognize samples belonging to participants tasked with the visual NDRT, with only minor confusion between the no and visual NDRT condition, and minimal confusion between the cognitive and visual NDRT condition.

		Predicted behavioral pattern			
		$\hat{b}_0$ (no NDRT)	$\hat{b}_1$ (cognitive NDRT)	$\hat{b}_2$ (visual NDRT)	Total
Ground truth behavioral pattern	b_0	41244	6451	441	48136
	b_1	8507	39169	393	48069
	b_2	1401	114	50555	52070
	Total	51152	45734	51389	148275

Figure 56: 3 × 3 confusion matrix for recognizing behavioral patterns of the SAE Level 2 NDRT model on test data $\mathcal{D}_{Test}^{NDRT:L2}$.

The confusion matrix for recognizing the binary situation awareness follows directly from the confusion matrix for recognizing the behavioral patterns and is shown in Figure 57. As to be expected, the problems of the SAE Level 2 NDRT model to discriminate between the behavior of participants without NDRT and tasked with the cognitive NDRT results in a non-neglectable amount of false negatives and esp. false positives.

		Predicted situation awareness		
		$\hat{s}_{1_1}$ (sufficient)	$\hat{s}_{1_0}$ (insufficient)	Total
Ground truth situation awareness	s_{1_1}	TP ≙ 41244	FN ≙ 6892	48136
	s_{1_0}	FP ≙ 9908	TN ≙ 90231	100139
	Total	51152	97123	148275

Figure 57: 2 × 2 confusion matrix for recognizing situation awareness of the SAE Level 2 NDRT model on test data $\mathcal{D}_{Test}^{NDRT:L2}$.

To provide more insight into the performance and characteristics of the SAE Level 2 NDRT model, Figure 58 overlays the ground truth behavioral pattern and situation awareness annotations in the test data with the predictions of the model for each sample. As a reminder, the test set

$$\mathcal{D}_{\text{Test}}^{\text{NDRT:L2}} = \left\{\left(b^{j,i}, s_1^{j,i}, \boldsymbol{f}^{j,i}\right)_{i=1}^{n_j}\right\}_{j=1}^{74}, \sum_{j=1}^{74} n_j = 148275$$

for the SAE Level 2 NDRT model consists of $m = 74$ unseen sequences of approx. 2.5 minutes length (c.f. Section 5.3), each comprised of n_j samples $\left(b^{j,i}, s_1^{j,i}, \boldsymbol{f}^{j,i}\right)$, denoting the ground truth annotation for the ternary behavioral pattern / NDRT condition $b^{j,i}$, the binary situation awareness $s_1^{j,i}$, and the indicators $\boldsymbol{f}^{j,i}$. Figure 58 shows the sequences $b^{1,1:n_1}, b^{2,1:n_2}, \dots, b^{74,1:n_{74}}$ of ground truth behavioral patterns (top) and the sequences $s_1^{1,1:n_1}, s_1^{2,1:n_2}, \dots, s_1^{74,1:n_{74}}$ of ground truth binary situation awareness (bottom) as solid red lines. The sequences of model predictions $\hat{b}^{1,1:n_1}, \hat{b}^{2,1:n_2}, \dots, \hat{b}^{74,1:n_{74}}$ and $\hat{s}_1^{1,1:n_1}, \hat{s}_1^{2,1:n_2}, \dots, \hat{s}_1^{74,1:n_{74}}$ are shown as solid blue lines. The 74 different sequences are separated by vertical dotted lines. As already shown by Figure 56, the SAE Level 2 NDRT model is able to

consistently recognize visual NDRT behavior but has problems in discriminating between behavior without NDRT and cognitive NDRT behavior. Noticeable, the model occasionally rapidly changes its answer, especially in the case of participants without NDRT and participants tasked with the cognitive NDRT. These changes happen primarily, when participants show (short-term) gaze behavior that is characteristic for a different NDRT condition, e.g., when participants without NDRT show a high gaze concentration on the road center, or when participants tasked with the cognitive NDRT show a more balanced monitoring behavior.

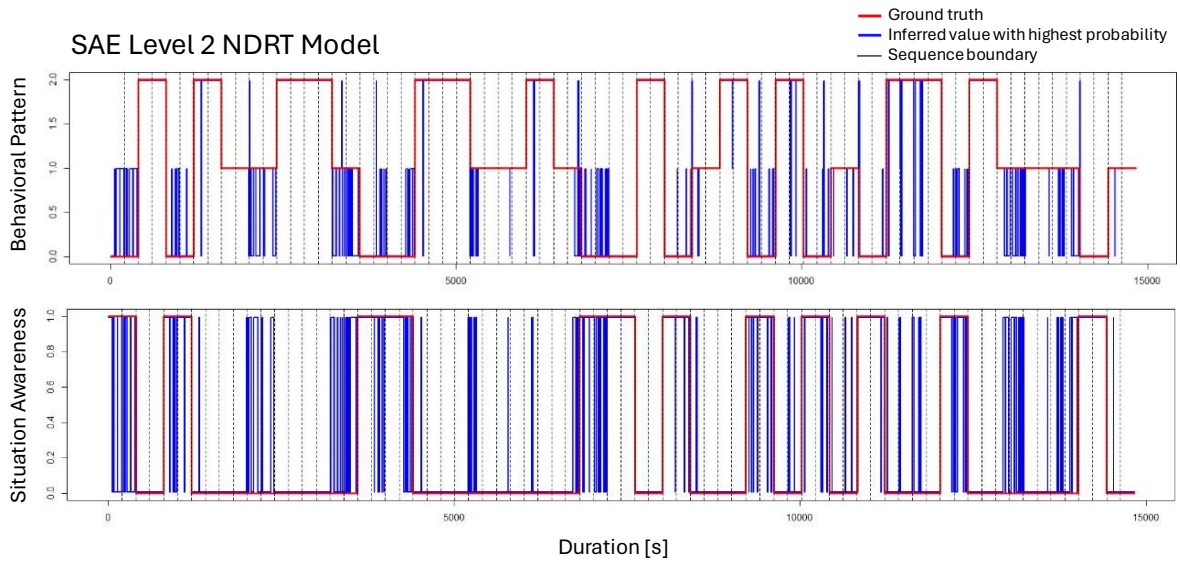

Figure 58: Comparison of ground truth and SAE Level 2 NDRT model predictions on test data $\mathcal{D}_{Test}^{NDRT:L2}$.

Concerning evaluation metrics, when tasked with the recognition of behavioral patterns, the SAE Level 2 NDRT model achieves an accuracy of 0.8833 and a classification rate of 0.8834 (Table 11). The accuracy and classification-rate are nearly identical, which implies that the model achieves very high probabilities for its predictions (regardless of whether these predictions are correct or incorrect). To put this numbers into some perspective, we can compare them to the expected metrics of an hypothetical baseline model that simply samples labels according to the statistical prior distribution over the behavioral patterns in the test data (which gives the baseline model a small advantage), here $p\left(B^{j,i} = b_0\right) = 0.3246$, $p\left(B^{j,i} = b_1\right) = 0.3242$, and $p\left(B^{j,i} = b_2\right) = 0.3512$. We would expect such a baseline model to achieve both an accuracy and a classification rate of 0.3338. As such, the indicators used by the SAE Level 2 NDRT model improve the accuracy over the baseline by 54.95%.

Table 11: Evaluation metrics of the SAE Level 2 NDRT model for recognizing behavioral patterns on test data $\mathcal{D}_{Test}^{NDRT:L2}$.

Metric	Value	Baseline
Accuracy	0.8833	0.3338
Classification rate	0.8834	0.3338

When tasked with the recognition of the binary situation awareness, the SAE Level 2 NDRT model achieves an accuracy of 0.8867, a precision of 0.8063, a TPR of 0.8568, an FPR of 0.0989, and an F_1 score of 0.8308 (Table 12). The accuracy is slightly better than for recognizing the behavioral patterns, which is explained by the fact that any confusion between the behavior of participants tasked with the

cognitive and visual NDRT will still result in a correct classification of insufficient situation awareness. Given these metrics, the biggest problem of the SAE Level 2 NDRT model is a lack in precision, resulting from the problems to discriminate between the behavior of participants without NDRT and tasked with the cognitive NDRT, which is also reflected in the comparably low F_1 score. To put this numbers into some perspective, we once again compare them to the expected metrics of an hypothetical baseline model that randomly samples labels according to the statistical prior distribution over the situation awareness in the test data, here $p\left(S_1^{j,i} = s_{1_1}\right) = 0.3246$ and $p\left(S_1^{j,i} = s_{1_0}\right) = 0.6754$. We would expect such a model to produce 15626.87 true positives, each 32509.13 false positives and false negatives, and 67629.87 true negatives, resulting in an accuracy of 0.5614, and an identical precision, TPR, FPR, and F_1 score of 0.3246. Due to the imbalance of sufficient and insufficient situation awareness in the ground truth data, the SAE Level 2 NDRT model only improves the accuracy over the baseline by 32.53%, however precision, TPR, FPR, and F_1 score are improved by 48.17%, 53.22%, 22.57%, and 50.62% respectively.

Table 12: Evaluation metrics of the SAE Level 2 NDRT model for recognizing binary situation awareness on test data $\mathcal{D}_{Test}^{NDRT:L2}$.

Metric	Value	Baseline
Accuracy	0.8867	0.5614
Precision	0.8063	0.3246
TPR	0.8568	0.3246
FPR	0.0989	0.3246
F_1 score	0.8308	0.3246

The ROC curve for the different classification thresholds $\delta = \frac{0}{100}, \frac{1}{100}, \dots, \frac{100}{100}$ is shown in Figure 59, where the TPR and FPR for each decision threshold is denoted by a black dot. As apparent, all classification thresholds result in a similar TPR and FPR, meaning that the model predicts its answers with very high probabilities (regardless of whether the answer correct or incorrect). The AUC is given by 0.8888, which, by Hosmer et al. (2013), would be considered a good discrimination.

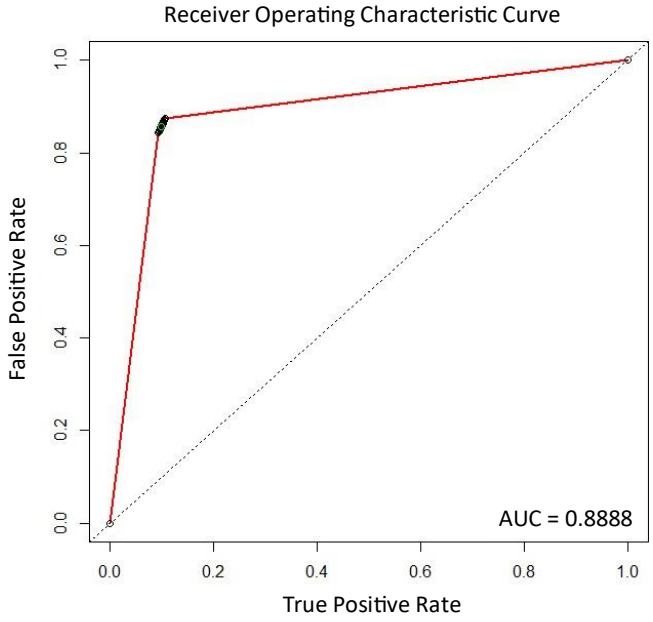

Figure 59: ROC curve for the SAE Level 2 NDRT model on test data $\mathcal{D}_{Test}^{NDRT:L2}$. The black dots denote the decision thresholds $\delta = \frac{0}{100}, \frac{1}{100}, \ldots, \frac{100}{100}$. The primary decision threshold used for evaluation, is denoted by a green circle.

5.6.2.2 SAE Level 3 NDRT model

After being trained on the $\mathcal{D}_{\text{Ttaining}}^{\text{NDRT:L3}}$ training dataset, the best-scoring SAE Level 3 NDRT model (c.f., Section 5.2.2) was evaluated on the test dataset

$$\mathcal{D}_{\text{Test}}^{\text{NDRT:L3}} = \left\{\left(b^{j,i}, s_1^{j,i}, \boldsymbol{f}^{j,i}\right)_{i=1}^{n_j}\right\}_{j=1}^{74}, \sum_{j=1}^{74} n_j = 101462,$$

using the evaluation procedure introduced in Section 5.6.1. The resulting confusion matrix for recognizing the ternary behavioral patterns is shown in Figure 60. As was the case for SAE Level 2, the SAE Level 3 NDRT model is able to correctly recognize the majority of the ground truth behavioral patterns but has problems to correctly discriminate between the behavior of participants without NDRT and participants tasked with the cognitive NDRT. Especially, behavior of participants tasked with the cognitive NDRT is misclassified as no NDRT behavior in 23.73% of the cases. In contrast, the model is very capable to correctly recognize samples belonging to participants tasked with the visual NDRT, with only minor confusion between the no and visual NDRT condition, and minimal confusion between the cognitive and visual NDRT condition.

		Predicted behavioral pattern			
		$\hat{b}_0$ (no NDRT)	$\hat{b}_1$ (cognitive NDRT)	$\hat{b}_2$ (visual NDRT)	Total
Ground truth behavioral pattern	b_0	29323	5983	318	35624
	b_1	7836	25127	63	33026
	b_2	50	69	32692	32811
	Total	37209	31179	33073	101461

Figure 60: 3×3 confusion matrix for recognizing behavioral patterns of the SAE Level 3 NDRT model on test data $\mathcal{D}_{Test}^{NDRT:L3}$.

The confusion matrix for recognizing the binary situation awareness is shown in Figure 61. As was the case for the SAE Level 2 NDRT model, the problems of the SAE Level 3 NDRT model to discriminate

between the behavior of participants without NDRT and the behavior of participants tasked with the cognitive NDRT result in a non-neglectable amount of false negatives and false positives.

		Predicted situation awareness		
		$\hat{s}_{1_1}$ (sufficient)	$\hat{s}_{1_0}$ (insufficient)	Total
Ground truth situation awareness	s_{1_1}	TP ≙ 29323	FN ≙ 6301	35624
	s_{1_0}	FP ≙ 7886	TN ≙ 57951	65837
	Total	37209	64252	101461

Figure 61: 2×2 confusion matrix for recognizing situation awareness of the SAE Level 3 NDRT model on test data $\mathcal{D}_{Test}^{NDRT:L3}$.

A visual comparison of the ground truth behavioral pattern / situation awareness annotations in the test data and the model predictions is shown in Figure 62. As was the case for the SAE Level 2 NDRT model, we have regions in which the model answer changes rapidly and frequently between no NDRT and cognitive NDRT behavior. However, we also notice an increase in longer durations of behavior being confused, with some sequences being misclassified completely.

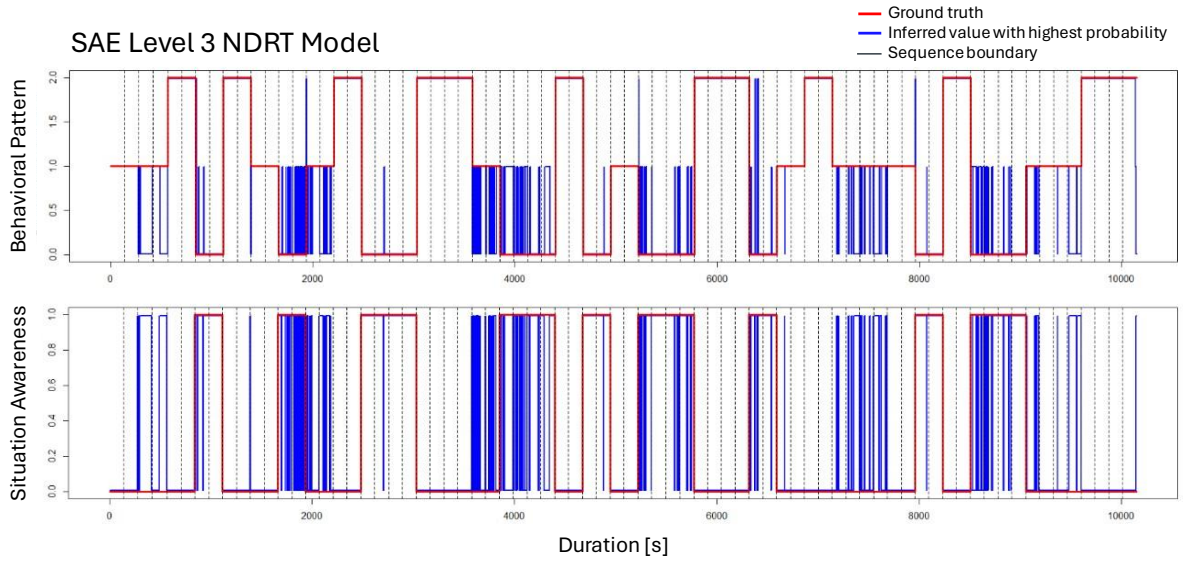

Figure 62: Comparison of ground truth and SAE Level 3 NDRT model predictions on test data $\mathcal{D}_{Test}^{NDRT:L3}$.

Concerning evaluation metrics, when tasked with the recognition of the behavioral patterns, the SAE Level 3 NDRT model achieves an accuracy of 0.8589, and a classification rate 0.8587 (Table 13), which is slightly worse than for the SAE Level 2 NDRT model. For comparison, we would expect a hypothetical baseline model that randomly samples labels according to the statistical prior distribution over the behavioral patterns in the test data, here $p\left(B^{j,i} = b_0\right) = 0.3511$, $p\left(B^{j,i} = b_1\right) = 0.3255$ and $p\left(B^{j,i} = b_2\right) = 0.3234$, to achieve an accuracy and classification rate of 0.3338. As such, the SAE Level 3 NDRT model improves the accuracy over the baseline by 52.51%, which is slightly worse than for the SAE Level 2 NDRT model.

Table 13: Evaluation metrics of the SAE Level 3 NDRT model for recognizing behavioral patterns on test data $\mathcal{D}_{Test}^{NDRT:L3}$.

Metric	Value	Baseline
Accuracy	0.8589	0.3338
Classification rate	0.8587	0.3338

When tasked with the recognition of the binary situation awareness, the SAE Level 3 NDRT model achieves an accuracy of 0.8602, a precision of 0.7881, a TPR of 0.8231, an FPR of 0.1198, and an F_1 score of 0.8052 (Table 14). For comparison, we would expect a hypothetical baseline model that randomly samples labels according to the statistical prior distribution over the situation awareness in the test data, here $p\left(S_1^{j,i} = s_{1_1}\right) = 0.3511$ and $p\left(S_1^{j,i} = s_{1_0}\right) = 0.6489$, to achieve an accuracy of 0.5443, and an identical precision, TPR, FPR, and F_1 score of 0.3511. Due to the imbalance of sufficient and insufficient situation awareness in the ground truth data, the SAE Level 3 NDRT model only improves the accuracy over the baseline by 31.59%, while precision, TPR, FPR, and F_1 score are improved by 43.7%, 47.2%, 23.13%, and 45.41% respectively. As to be expected from the confusion matrix (Figure 61), the primary problem of the SAE Level 3 NDRT model is a lack in precision, resulting from the problems to discriminate between the behavior of participants without NDRT and tasked with the cognitive NDRT.

Table 14: Evaluation metrics of the SAE Level 3 NDRT model for recognizing binary situation awareness on test data $\mathcal{D}_{Test}^{NDRT:L3}$.

Metric	Value	Baseline
Accuracy	0.8602	0.5443
Precision	0.7881	0.3511
TPR	0.8231	0.3511
FPR	0.1198	0.3511
F_1 score	0.8052	0.3511

The ROC curve for the different classification thresholds $\delta = \frac{0}{100}, \frac{1}{100}, \dots, \frac{100}{100}$ is shown in Figure 63. As was the case for the SAE Level 2 NDRT model (c.f., Figure 59), all decision thresholds result in a similar TPR and FPR, meaning that the model predicts its answers with very high probabilities (regardless of whether the answer correct or incorrect). The AUC is given by 0.862, which, by Hosmer et al. (2013), would still be considered a good discrimination.

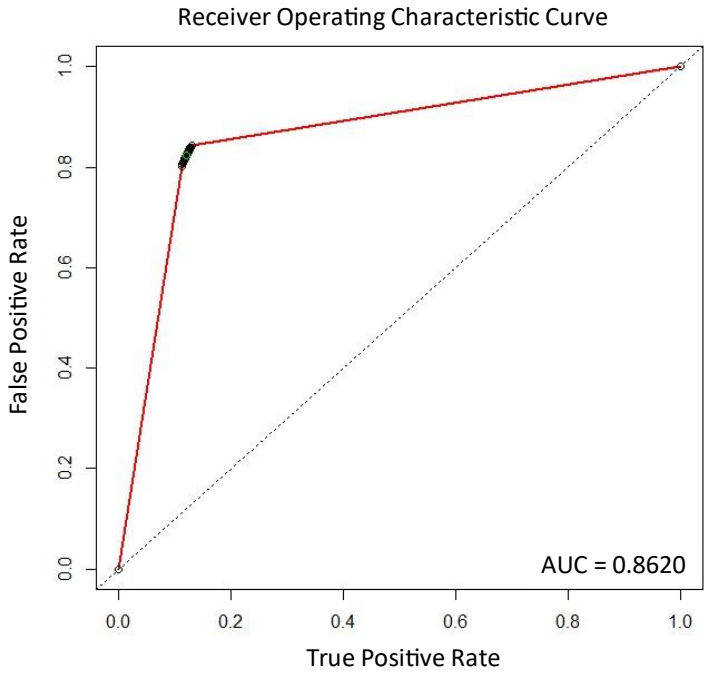

Figure 63: ROC curve for the SAE Level 3 NDRT model on test data $\mathcal{D}_{Test}^{NDRT:L3}$. The black dots denote the decision thresholds $\delta = \frac{0}{100}, \frac{1}{100}, \ldots, \frac{100}{100}$. The primary decision threshold used for evaluation, is denoted by a green circle.

5.6.2.3 Reinterpretation as maximum entropy Markov models

As a reminder, the NDRT models are conceptualized as DBNs that involve a state-observation model (c.f., Appendix 1, Section 1.3) with dynamic model $p(B^t|B^{t-1})$ and observation model $p(\boldsymbol{F}^t|B^t)$ (c.f., Section 5.2.2). As apparent from Figure 58 and Figure 62, the NDRTs model are very sensitive to short-term behavioral changes. which implies that the likelihood $p(\boldsymbol{f}^t|B^t)$ of the observed indicators $\boldsymbol{f}^t$ in the observation model dominates the behavioral inertia encoded by $p(B^t|B^{t-1})$. For a practical utilization of the NDRT models within the DySAM system, where a recognition of insufficient situation awareness may trigger warnings and/or interventions, we may prefer a more consistent behavior.

To obtain such behavior of the model, we could adjust the dynamic inertia of the NDRT models by adjusting the parameters of $p(B^t|B^{t-1})$, such that the probability $p\left(b_i^t|b_j^{t-1}\right), i \neq j$ of transitioning from a state b_j^{t-1} to a different state b_i^t are (much) smaller. An alternative solution that does not require the adaptation of any parameters is a reversal of the edge direction from the behavioral patterns to the SA indicators (Figure 64), such that the state-observation sub-structure is changed from $p(B^t|B^{t-1})p(\boldsymbol{F}^t|B^t)$ to $p(B^t|B^{t-1}, \boldsymbol{F}^t)$.

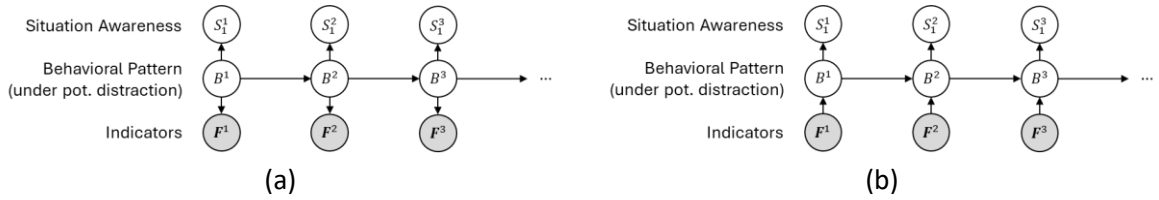

Figure 64: Unrolled network structure of the NDRT models. (a) NDRT models using a state-observation model. (b) Reformulation as a MEMM.

Such a DBN is referred to as a *maximum entropy Markov model* (MEMM) (Murphy, 2012). We can reuse the observation model $p(\boldsymbol{F}^t|B^t)$ of the NDRT models by defining a so-called *embedded Bayesian classifier* (Heckerman & Meek, 1997):

$$p(B^t|B^{t-1},\boldsymbol{F}^t) \triangleq \frac{p(B^t|B^{t-1})p(\boldsymbol{F}^t|B^t)}{\sum_{b\in \mathrm{Val}(B)} p(b|B^{t-1})p(\boldsymbol{F}^t|b)},$$

i.e., we define the distribution $p(B^t|B^{t-1},\boldsymbol{F}^t)$ as a probability query using the original state-observation model $p(B^t|B^{t-1})p(\boldsymbol{F}^t|B^t)$. Reformulating the NDRT models as MEMMs, we obtain the model structure

$$p(S_1^{1:T},B^{1:t},\boldsymbol{F}^{1:T}) = p(S_1^1|B^1)p(B^1|\boldsymbol{F}^1)\prod_{t=2}^{T} p(S_1^t|B^t)p(B^t|B^{t-1},\boldsymbol{F}^t)\prod_{t=1}^{T} p(\boldsymbol{F}^t),$$

where

$$p(B^1|\boldsymbol{F}^1) \triangleq \frac{p(B^1)p(\boldsymbol{F}^1|B^1)}{\sum_{b\in \mathrm{Val}(B)} p(b)p(\boldsymbol{F}^1|b)},$$

and

$$p(B^t|B^{t-1},\boldsymbol{F}^t) \triangleq \frac{p(B^t|B^{t-1})p(\boldsymbol{F}^t|B^t)}{\sum_{b\in \mathrm{Val}(B)} p(b|B^{t-1})p(\boldsymbol{F}^t|b)}.$$

Limited to the intended utilization of the NDRT models, this is equivalent to

$$p(S_1^{1:T},B^{1:t}|\boldsymbol{F}^{1:T}:\boldsymbol{\theta}) = p(S_1^1|B^1)p(B^1|\boldsymbol{F}^1)\prod_{t=2}^{T} p(S_1^t|B^t)p(B^t|B^{t-1},\boldsymbol{F}^t),$$

reusing the same parameters $\boldsymbol{\theta}$ and observation-model factorization $p(\boldsymbol{F}^t|B^t)$ of the original NDRT models. Although the state-observation and the MEMM formulation use the same model parameters and the same factorization for $p(\boldsymbol{F}^t|B^t)$, they differ in how they apply normalizations when inferring $p(S_1^t,B^t|\boldsymbol{f}^{1:t})$. For the original formulation, we have that

$$p(S_1^t,B^t|\boldsymbol{f}^{1:t}) = \frac{1}{Z}p(S_1^t|B^t)p(\boldsymbol{f}^t|B^t)\sum_{b^{t-1}\in \mathrm{Val}(B^{t-1})} p(B^t|b^{t-1})p(b^{t-1}|\boldsymbol{f}^{1:t-1}),$$

with Z denoting a "global" normalization constant

$$Z = \sum_{b^t\in \mathrm{Val}(B^t)} p(\boldsymbol{f}^t|b^t)\sum_{b^{t-1}\in \mathrm{Val}(B^{t-1})} p(b^t|b^{t-1})p(b^{t-1}|\boldsymbol{f}^{1:t-1}).$$

For the MEMM, we have that

$$p(S_1^t,B^t|\boldsymbol{f}^{1:t}) = p(S_1^t|B^t)\sum_{b^{t-1}\in \mathrm{Val}(B^{t-1})} \frac{1}{Z_{b^{t-1}}}p(\boldsymbol{f}^t|B^t)p(B^t|b^{t-1})p(b^{t-1}|\boldsymbol{f}^{1:t-1}),$$

with each $Z_{b^{t-1}}$ denoting a "local" normalization constant

$$Z_{b^{t-1}} = \sum_{b^t \in \mathrm{Val}(B^t)} p(b|b^{t-1}) p(\boldsymbol{f}^t|b).$$

By locally normalizing for each $b^{t-1} \in \mathrm{Val}(B^{t-1})$, the MEMM prevents the likelihood $p(\boldsymbol{f}^t|B^t)$ from dominating $p(B^t|B^{t-1})$, resulting in much smoother transitions from one state to another.

5.6.2.3.1 SAE Level 2 NDRT MEMM

Reinterpreting the SAE Level 2 NDRT model as a MEMM and repeating the evaluation on the $\mathcal{D}_{\mathrm{Test}}^{\mathrm{NDRT:L2}}$ test dataset, we obtain the 3×3 confusion matrix for recognizing the ternary behavioral patterns shown in Figure 65 and the 2×2 confusion matrix for recognizing the binary situation awareness shown in Figure 66.

		Predicted behavioral pattern			
		$\hat{b}_0$ (no NDRT)	$\hat{b}_1$ (cognitive NDRT)	$\hat{b}_2$ (visual NDRT)	Total
Ground truth behavioral pattern	b_0	43443	4283	410	48136
	b_1	6873	40649	547	48069
	b_2	1232	0	50838	52070
	Total	51548	44932	51795	148275

Figure 65: 3×3 confusion matrix for recognizing behavioral patterns of the SAE Level 2 NDRT MEMM model on test data $\mathcal{D}_{Test}^{NDRT:L2}$.

Comparing these confusion matrices with the results of the original SAE Level 2 NDRT model (Figure 56 and Figure 57), we have that misclassification of the behavior of participants without NDRT and tasked with the cognitive NDRT could be reduced, which results in an increase of true positives and negatives / a reduction of false positives and negatives.

		Predicted situation awareness		
		$\hat{s}_{1_1}$ (sufficient)	$\hat{s}_{1_0}$ (insufficient)	Total
Ground truth situation awareness	s_{1_1}	TP ≙ 43443	FN ≙ 4693	48136
	s_{1_0}	FP ≙ 8062	TN ≙ 92077	100139
	Total	51505	96770	148275

Figure 66: 2×2 confusion matrix for recognizing situation awareness of the SAE Level 2 NDRT MEMM model on test data $\mathcal{D}_{Test}^{NDRT:L2}$.

Figure 67 shows the comparison of the ground truth behavioral pattern / situation awareness annotations in the test data and the model predictions, where, in addition to the model predictions $\hat{b}^{1,1:n_1}, \hat{b}^{2,1:n_2}, \dots, \hat{b}^{74,1:n_{74}}$ and $\hat{s}_1^{1,1:n_1}, \hat{s}_1^{2,1:n_2}, \dots, \hat{s}_1^{74,1:n_{74}}$,shown as solid blue lines, we show the mean inferred values $\mathbb{E}\left[B^{j,i}|\boldsymbol{f}^{j,1:i}\right]$ and $\mathbb{E}\left[S_0^{j,i}|\boldsymbol{f}^{j,1:i}\right]$ as dashed blue lines. Comparing Figure 67 to the original SAE Level 2 NDRT model (Figure 58) As apparent, the use of MEMM-like structure successfully filters short-term fluctuations, while still being sensitive to long-term changes.

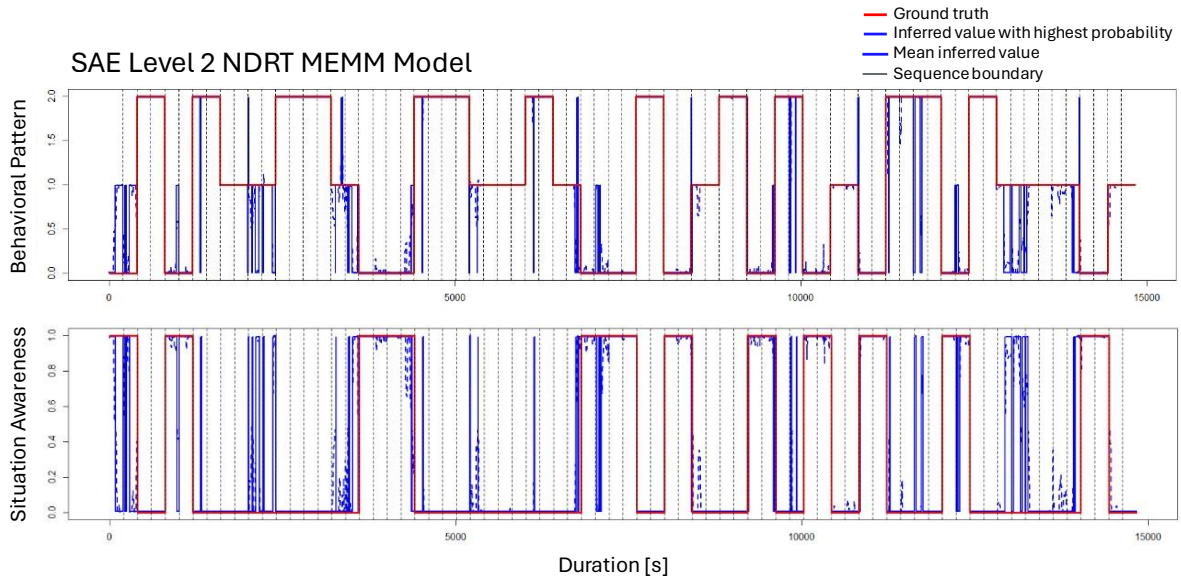

Figure 67: Comparison of ground truth and SAE Level 2 NDRT MEMM model predictions on test data $\mathcal{D}_{Test}^{NDRT:L2}$.

When tasked with the recognition of behavioral patterns, the reinterpretation of the SAE Level 2 NDRT model as a MEMM improves the accuracy by 2.67%.to 0.91 and the classification rate by 2.07% to 0.9041 (Table 15). Compared to the hypothetical baseline of the SAE Level 2 NDRT model, the MEMM interpretation improves the accuracy by 57.12%.

Table 15: Evaluation metrics of the SAE Level 2 NDRT MEMM model for recognizing behavioral patterns on test data $\mathcal{D}_{Test}^{NDRT:L2}$.

Metric	Value	Baseline
Accuracy	$0.8833 \rightarrow 0.9100$	0.3338
Classification rate	$0.8834 \rightarrow 0.9041$	0.3338

When tasked with the recognition of the binary situation awareness, the reinterpretation as a MEMM improves all metrics (Table 16), more specifically, the accuracy is improved by 2.73% to 0.9140, the precision is improved by 3.72% to 0.8435, the TPR is improved by 4.57% to 0.9025, the FPR is improved by 1.84% down to 0.0805, and the F_1 score is improved by 4.12% to 0.8720. Compared to the baseline, the MEMM interpretation improves accuracy, precision, TPR, FPR, and F_1 score by 35.26%, 51.89%, 57.79%, 24.41%, and 54.74%.

Table 16: Evaluation metrics of the SAE Level 2 NDRT model for recognizing binary situation awareness on test data $\mathcal{D}_{Test}^{NDRT:L2}$.

Metric	Value	Baseline
Accuracy	$0.8867 \rightarrow 0.9140$	0.5614
Precision	$0.8063 \rightarrow 0.8435$	0.3246
TPR	$0.8568 \rightarrow 0.9025$	0.3246
FPR	$0.0989 \rightarrow 0.0805$	0.3246
F_1 score	$0.8308 \rightarrow 0.8720$	0.3246

The ROC curve for the different classification thresholds $\delta = \frac{0}{100}, \frac{1}{100}, \ldots, \frac{100}{100}$ is shown in Figure 68. Compared to the original SAE Level 2 NDRT model (Figure 59), the reinterpretation as a MEMM enables the classification thresholds to have a much stronger effect on the TPR and FPR, resulting in a more curve-like impression, more characteristic for an ROC. The AUC is improved to 0.9491, which, by Hosmer et al. (2013), would be considered a very good discrimination.

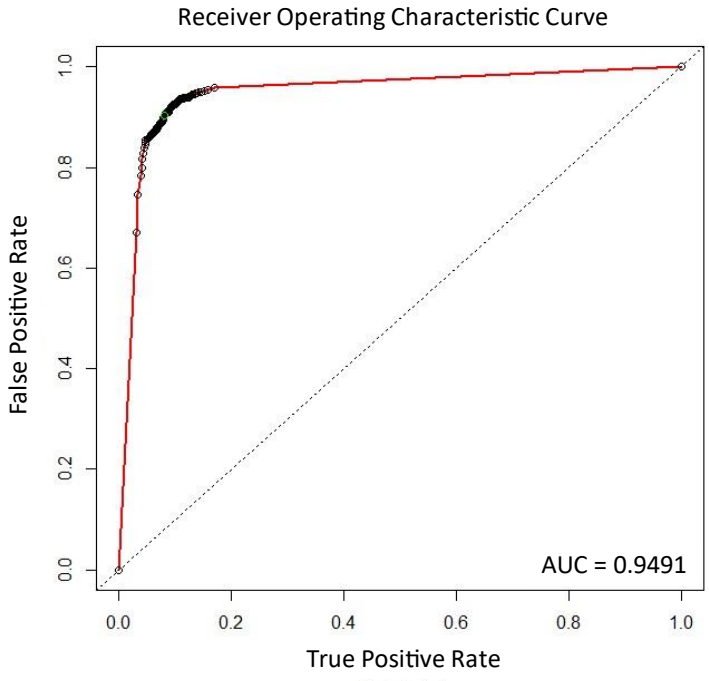

Figure 68: ROC curve for the SAE Level 2 NDRT MEMM model on test data $\mathcal{D}_{Test}^{NDRT:L2}$. The black dots denote the decision thresholds $\delta = \frac{0}{100}, \frac{1}{100}, \ldots, \frac{100}{100}$. The primary decision threshold used for evaluation, is denoted by a green circle.

5.6.2.3.2 SAE Level 3 NDRT MEMM

As was the case with the SAE Level 2 NDRT model, we can strengthen the inertia of the model by using a MEMM-like model structure. Reinterpreting the SAE Level 3 NDRT model as a MEMM and repeating the evaluation on the $\mathcal{D}_{\text{Test}}^{\text{NDRT:L3}}$ test dataset, we obtain the 3×3 confusion matrix for recognizing the ternary behavioral patterns shown in Figure 69 and the 2×2 confusion matrix for recognizing the binary situation awareness shown in Figure 70.

		Predicted behavioral pattern			
		$\hat{b}_0$ (no NDRT)	$\hat{b}_1$ (cognitive NDRT)	$\hat{b}_2$ (visual NDRT)	Total
Ground truth behavioral pattern	b_0	30624	4661	339	35624
	b_1	8311	24650	65	33026
	b_2	50	63	32698	32811
	Total	38985	29374	33102	101461

Figure 69: 3×3 confusion matrix for recognizing behavioral patterns of the SAE Level 3 NDRT MEMM model on test data $\mathcal{D}_{Test}^{NDRT:L3}$.

Comparing these confusion matrices with the results of the original SAE Level 3 NDRT model (Figure 60 and Figure 61), we have that the misclassification of the behavior of participants without NDRT as behavior of participants tasked with the cognitive NDRT could be reduced, which however comes at the cost of an increase of the reverse. In contrast to the SAE Level 2 NDRT model. The interpretation of the SAE Level 3 NDRT model as a MEMM only reduces the number of false negatives, while increasing the number of false positives, albeit by a smaller amount.

		Predicted situation awareness		
		$\hat{s}_{1_1}$ (sufficient)	$\hat{s}_{1_0}$ (insufficient)	Total
Ground truth situation awareness	s_{1_1}	TP ≙ 30612	FN ≙ 5012	35624
	s_{1_0}	FP ≙ 8259	TN ≙ 57478	65837
	Total	38971	62490	101461

Figure 70: 2×2 confusion matrix for recognizing situation awareness of the alternative SAE Level 3 NDRT MEMM model on test data $\mathcal{D}_{Test}^{NDRT:L3}$.

Figure 71 shows the comparison of the ground truth behavioral pattern / situation awareness annotations in the test data and the model predictions. As was the case for the SAE Level 2 NDRT model, a comparison of Figure 71 and the results of the original SAE Level 3 NDRT model (Figure 62), the use of MEMM-like structure successfully filters most of the short-term fluctuations, while still being sensitive to long-term changes, resulting in an overall smoother model output.

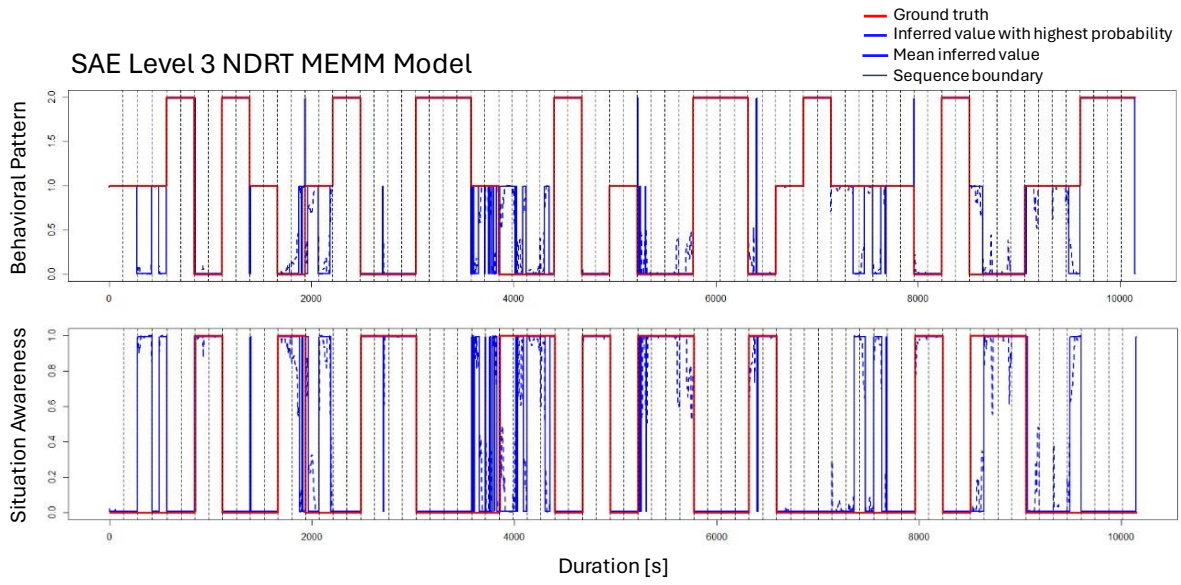

Figure 71: Comparison of ground truth and SAE Level 3 NDRT model predictions on test data $\mathcal{D}_{Test}^{NDRT:L3}$.

Although the benefits are much less pronounced than for the SAE Level 2 NDRT model, a reinterpretation of the SAE Level 3 NDRT model is still able to slightly improve its performance. When tasked with the recognition of behavioral patterns, the reinterpretation as a MEMM improves the accuracy by 0.82%.to 0.8671 and the classification rate by 0.3% to 0.8617 (Table 17). Compared to the hypothetical baseline of the SAE Level 3 NDRT model, the MEMM interpretation improves the accuracy by 53.33%.

Table 17: Evaluation metrics of the SAE Level 3 NDRT MEMM model for recognizing behavioral patterns on test data $\mathcal{D}_{Test}^{NDRT:L3}$.

Metric	Value	Baseline
Accuracy	$0.8589 \rightarrow 0.8671$	0.3338
Classification rate	$0.8587 \rightarrow 0.8617$	0.3338

When tasked with the recognition of the binary situation awareness, the reinterpretation as a MEMM improves the accuracy by 0.8% to 0.8682, the TPR by 3.62% to 0.8593, and the F_1 score by 1.56% to 0.8208, however the already weak precision is further decreased by 0.26% to 0.7855 and the FPR is increased by 0.72% up to 0.1270 (Table 18). Compared to the baseline, the MEMM interpretation improves accuracy, precision, TPR, FPR, and F_1 score by 32.39%, 43.44%, 50.82%, 22.41%, and 46.97%.

Table 18: Evaluation metrics of the SAE Level 3 NDRT model for recognizing binary situation awareness on test data $\mathcal{D}_{Test}^{NDRT:L3}$.

Metric	Value	Baseline
Accuracy	$0.8602 \rightarrow 0.8682$	0.5443
Precision	$0.7881 \rightarrow 0.7855$	0.3511
TPR	$0.8231 \rightarrow 0.8593$	0.3511
FPR	$0.1198 \rightarrow 0.1270$	0.3511
F_1 score	$0.8052 \rightarrow 0.8208$	0.3511

The ROC curve for the different classification thresholds $\delta = \frac{0}{100}, \frac{1}{100}, \dots, \frac{100}{100}$ is shown in Figure 72. Similar to the SAE Level 2 case, the reinterpretation as a MEMM enables the classification thresholds to have a much stronger effect on the TPR and FPR, when compared to the original SAE Level 3 NDRT model (c.f., Figure 63). The AUC is improved to 0.9121, which, by Hosmer et al. (2013), would still be considered a very good discrimination.

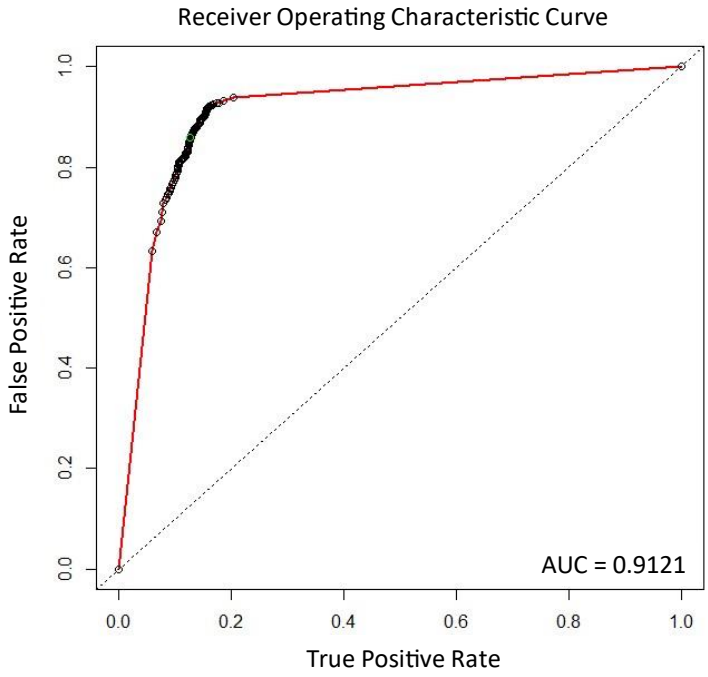

Figure 72: ROC curve for the SAE Level 3 NDRT MEMM model on test data $\mathcal{D}_{Test}^{NDRT:L3}$. The black dots denote the decision thresholds $\delta = \frac{0}{100}, \frac{1}{100}, \ldots, \frac{100}{100}$. The primary decision threshold used for evaluation, is denoted by a green circle.

5.6.2.4 Discussion

The primary goal of the NDRT models is the correct discrimination of the behavior of participants without, tasked with the cognitive, and the visual NDRT, from which the classification of binary situation awareness follows by design. Concerning this task, the SAE Level 2 and SAE Level 3 NDRT models achieve accuracies of 0.8833 (or 0.9100 when reinterpreted as a MEMM) and 0.8589 (or 0.8671), which we consider a promising result. This is especially true when considering that the structural assumptions and comparably low number of parameters should prevent overfitting of the models to the data, when compared to approaches like e.g., deep neural networks. The SAE Level 2 NDRT model achieves a slightly better performance than the SAE Level 3 NDRT model, which is potentially explained by the fact that the former is trained on approx. 46% more data, which should result in more robust estimations of both parameters and structure of the model.

In our opinion, the two main problems of the NDRT models are the remaining confusion between the behavior of participants without NDRT and tasked with the cognitive NDRT and, to a lesser extent, the sensibility of the model output to short-term changes in the SA indicators. As shown, the latter can be addressed e.g., by a reinterpretation of the NDRT models as MEMMs. However, whether the increased smoothness of the model output is important and beneficial to an assistance system, will naturally depend on the details of the system and the utilization, a problem that has not been addressed in the project. Concerning the former, although it is possible that additional data could help in further improving the accuracy of the models, esp. the SAE Level 3 NDRT model, we believe that the nature of the ground truth training and test data suggests some upper limit on the accuracy that cannot be exceeded without the risk of overfitting. If we compare the comparison of the ground truth and model predictions of the SAE Level 2 NDRT model (Figure 58) with the comparison of the ground truth and model predictions of the latent patterns analysis of the time since last look at AOI indicators, we see

that both approaches misclassify very similar regions of the test data. As such, we assume that an improvement of the performance of the NDRT models require a more detailed annotation of the ground truth data for training and evaluation.

Using the NDRT condition as a surrogate measure of situation awareness, we treated behavior of participants without NDRT as sufficient and behavior of participants tasked with a cognitive or visual NDRT as insufficient situation awareness. By design, this approximate method of labelling is prone to introduce uncertainties and errors to the ground truth, generalizing both situations in which participants without NDRT had sufficient and insufficient situation awareness as sufficient and analogous for participants tasked with the cognitive and visual NDRT. Given the accuracies of the NDRT models, it is safe to assume that the NDRT models capture behavior that is, on average, characteristic for the different NDRT conditions. Whenever participants deviate from this average behavior by showing behavior that is more characteristic for a different, it is to some extent desirable for the models to misclassify such situations, as a correct classification would imply that the models overfit the training data.

5.6.3 Evaluation of the SAGAT Score models

For the evaluation of the SAGAT Score models, we adapt the evaluation procedure introduced in Section 5.6.1 to the utilization of SAGAT Score models and their test datasets. Using the SAE Level 2 SAGAT Score model as an example for the explanation, the test set

$$\mathcal{D}_{\text{Test}}^{\text{SAG:L2}} = \left\{\left(b^{j,i}, s_2^{j,i}, \boldsymbol{f}^{j,i}\right)_{i=1}^{n_j}\right\}_{j=1}^{37}, \sum_{j=1}^{37} n_j = 11101$$

for the SAE Level 2 SAGAT Score model consists of $m = 37$ unseen sequences of approx. 30 seconds length (c.f. Section 5.3), each comprised of n_j samples $\left(b^{j,i}, s_2^{j,i}, \boldsymbol{f}^{j,i}\right)$, denoting the ground truth annotation for the ternary behavioral pattern / NDRT task $b^{j,i}$, the SAGAT scores $s_2^{j,i}$ and the indicators $\boldsymbol{f}^{j,i}$. For each sequence $j = 1, \dots, m$, we use the SAE Level 2 SAGAT Score model to infer the conditional probability distribution $p\left(S_2^{j,i} | \boldsymbol{f}^{j,1:j,i}\right)$, i.e., the probability distribution over the SAGAT score given the observable indicators from the start of the sequence until the current sample. Given this distribution, we use the classification function

$$\hat{s}_2^{j,i} = \arg\max_{s_2^{j,i}} p\left(s_2^{j,i} | \boldsymbol{f}^{j,1:j,i}\right)$$

to derive concrete assignments as model answers. The ground truth SAGAT scores $s_2^{j,i}$ and model answers $\hat{s}_2^{j,i}, j = 1, \dots, 37, i = 1, \dots, n_j$ are then summarized in a 6×6 confusion matrix for recognizing the correct SAGAT score.

5.6.3.1 SAE Level 2 SAGAT Score model

After being trained on the $\mathcal{D}_{\text{Training}}^{\text{SAG:L2}}$ training dataset, the best-scoring SAE Level 2 SAGAT Score model (c.f., Section 5.2.3) was evaluated on the $\mathcal{D}_{\text{Test}}^{\text{SAG:L2}}$ test data. The resulting confusion matrix is shown in Figure 73. The SAE Level 2 SAGAT Score model is able to correctly recognize the majority of the ground truth SAGAT scores, especially the comparably rare low and high scores, More specifically, the low SAGAT scores s_{2_0} (0% correct answers) and s_{2_1} (20% correct answers) are correctly recognized in 100% of the cases, the high SAGAT scores s_{2_4} (80% correct answers) and s_{2_5} (100% correct answers) are

correctly recognized in 100% and 88.17% of the cases. In contrast, the comparable frequent medium SAGAT scores s_{2_2} (40% correct answers) and s_{2_3} (60% correct answers) are correctly classified in only 67.31% and 76.23% of the cases, often confused with higher SAGAT scores.

		Predicted SAGAT score						
		$\hat{s}_{2_0}$ (0%)	$\hat{s}_{2_1}$ (20%)	$\hat{s}_{2_2}$ (40%)	$\hat{s}_{2_3}$ (60%)	$\hat{s}_{2_4}$ (80%)	$\hat{s}_{2_5}$ (100%)	Total
Ground truth SAGAT score	s_{2_0}	1500	0	0	0	0	0	1500
	s_{2_1}	0	1200	0	0	0	0	1200
	s_{2_2}	65	0	3029	432	809	165	4500
	s_{2_3}	0	0	178	2059	162	302	2701
	s_{2_4}	0	0	0	0	600	0	600
	s_{2_5}	0	0	71	0	0	529	600
	Total	1565	1200	3728	2491	1571	996	11101

Figure 73: 6 × 6 confusion matrix of the SAE Level 2 SAGAT Score model on test data $\mathcal{D}_{Test}^{SAG:L2}$.

The visual comparison of the ground truth SAGAT scores in the test data and the model predictions, shown in Figure 74, provides additional details. As implied by the confusion matrix, the model has problems in correctly recognizing medium SAGAT scores corresponding to 40% and 60% of correct answers. With two exceptions, sequences are only partially misclassified. Furthermore, within each sequence, misclassifications show some temporal stability and consistency, meaning that the model does not rapidly change its answers and does not switch between more than three answers.

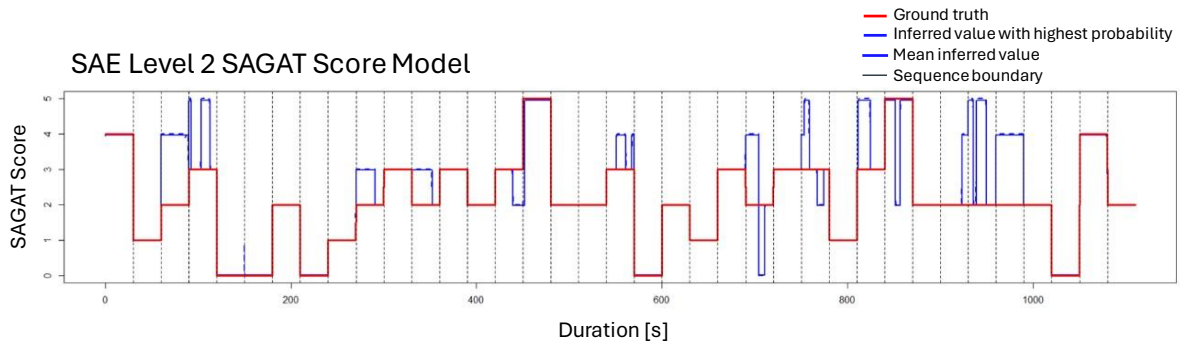

Figure 74: Comparison of ground truth and SAE Level 2 SAGAT Score model predictions on test data $\mathcal{D}_{Test}^{SAG:L2}$.

Overall, the SAE Level 2 SAGAT Score model achieves an identical accuracy and classification rate of 0.8033 (Table 19). As was the case for the NDRT models, we use a hypothetical baseline model that randomly samples SAGAT scores according to their statistical prior distribution in the test data for comparison . We would expect such a model to achieve an accuracy and classification rate of 0.2594. As such, the SAE Level 2 SAGAT Score model is able to improve the accuracy over the baseline by 54.39%, which is comparable to the improvements of the NDRT models.

Table 19: Evaluation metrics of the SAE Level 2 SAGAT Score model for on test data $\mathcal{D}_{Test}^{SAG:L2}$.

Metric	Value	Baseline
Accuracy	0.8033	0.2594
Classification rate	0.8033	0.2594

5.6.3.2 SAE Level 3 SAGAT Score model

After being trained on the $\mathcal{D}_{\text{Training}}^{\text{SAG:L3}}$ training dataset, the best-scoring SAE Level 3 SAGAT Score model (c.f., Section 5.2.3) was evaluated on the test dataset

$$\mathcal{D}_{\text{Test}}^{\text{SAG:L3}} = \left\{\left(b^{j,i}, s_2^{j,i}, \boldsymbol{f}^{j,i}\right)_{i=1}^{n_j}\right\}_{j=1}^{37}, \sum_{j=1}^{37} n_j = 11100.$$

The resulting 6×6 confusion matrix is shown in Figure 75. As was the case for the SAE Level 2 SAGAT Score model, the SAE Level 3 SAGAT Score model able to correctly recognize the majority of the ground truth SAGAT scores, albeit less consistently. The low SAGAT scores s_{2_0} (0% correct answers) and s_{2_1} (20% correct answers) are correctly recognized in 78.48% and 73.14% of the cases respectively. The SAGAT score s_{2_2} (40% correct answers) is correctly recognized in 73.06% of the cases. The biggest problem for the SAE Level 3 SAGAT Score model is the correct recognition of the medium to high SAGAT scores s_{2_3} (60% correct answers) and s_{2_4} (80% correct answers), which are only correctly recognized in 64.11% and 62.11% of the cases. Lastly, the rare highest SAGAT score s_{2_5} (100% correct answers) is correctly recognized in 84.67% of the case.

		Predicted SAGAT score						
		$\hat{s}_{2_0}$ (0%)	$\hat{s}_{2_1}$ (20%)	$\hat{s}_{2_2}$ (40%)	$\hat{s}_{2_3}$ (60%)	$\hat{s}_{2_4}$ (80%)	$\hat{s}_{2_5}$ (100%)	Total
Ground truth SAGAT score	s_{2_0}	2119	0	483	0	98	0	2700
	s_{2_1}	64	1536	158	135	108	99	2100
	s_{2_2}	192	23	1315	0	134	136	1800
	s_{2_3}	0	0	63	1154	583	0	1800
	s_{2_4}	112	134	220	324	1509	101	2400
	s_{2_5}	0	0	0	0	46	254	300
	Total	2487	1693	2239	1613	2478	590	11100

Figure 75: 6×6 confusion matrix of the SAE Level 3 SAGAT Score model on test data $\mathcal{D}_{Test}^{SAG:L3}$.

A visual comparison of the ground truth SAGAT scores in the test data and the model predictions is shown in Figure 76. Although the SAE Level 3 SAGAT Score model is capable of predicting multiple sequences correctly, when misclassifications occur, they often occur erratically, with the model switching between different answers in a very short time.

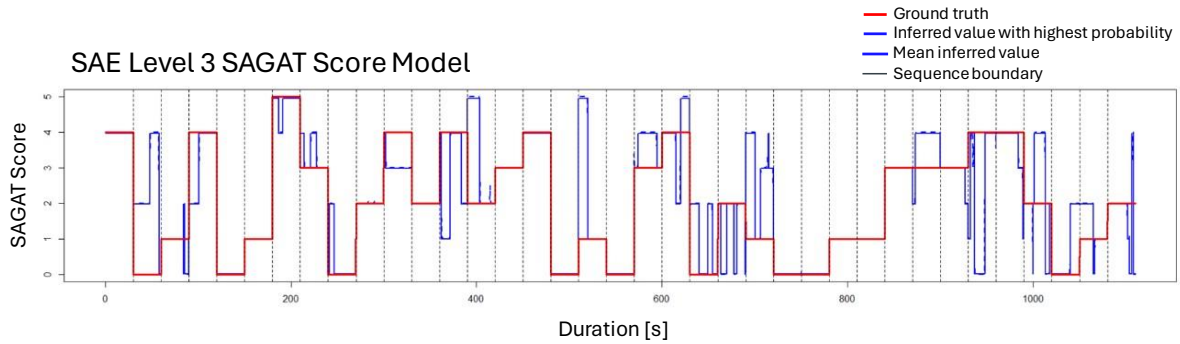

Figure 76: Comparison of ground truth and SAE Level 3 SAGAT Score model predictions on test data $\mathcal{D}_{Test}^{SAG:L3}$.

Overall, the SAE Level 3 SAGAT Score model achieves an accuracy of 0.7105 and a classification rate of 0.7098 (Table 20). As a comparison, a hypothetical baseline model that randomly samples SAGAT

scores according to their statistical prior distribution in the test data would achieve an accuracy and classification rate of 0.1950. As such, the SAE Level 3 SAGAT Score model is able to improve the accuracy over the baseline by 51.48%, which is slightly lower than for the NDRT models.

Table 20: Evaluation metrics of the SAE Level 3 SAGAT Score model for on test data $\mathcal{D}_{Test}^{SAG:L3}$.

Metric	Value	Baseline
Accuracy	0.7105	0.1950
Classification rate	0.7098	0.1950

5.6.3.3 Discussion

The SAE Level 2 and SAE Level 3 SAGAT Score models only achieve somewhat mediocre accuracies of 0.8033 and 0.7105. As was the case for the NDRT models, the SAE Level 2 SAGAT Score model achieves better results than the SAE Level 3 SAGAT Score model. Unlike for the NDRT models however, the amount of training data available was the same for both the SAE Level 2 and the SAE Level 3 SAGAT Score models, which could imply that a recognition of situation awareness is more difficult for SAE Level 3 than SAE Level 2.

We believe that the main problem responsible for the mediocre performance of the SAGAT Score models is a severe lack of training data for parameter estimation and structure learning. As the SAGAT queries the participants concerning their knowledge about the driving situation, the resulting score can only be considered valid for a short period of time. As a trade-off between ensuring some validity of the SAGAT score and maximizing the amount of data for training and validation, we considered a period of one minute length (c.f., Section 5.3) before the SAGAT was conducted. Despite these efforts, the amount of training data available to robustly estimate the parameters and structure of the models remained too sparse, esp. when considering the high variability of the behavior of the participants before the SAGAT. As such, we believe that the accuracies of the model could be improved significantly by providing more training (and test) data.

5.6.4 Evaluation of the extended SAGAT Score models

The extended SAGAT Score models extend the SAGAT Score models by incorporating information about whether the participant is currently tasked with the cognitive or visual NDRT or is not performing any NDRT. Accordingly, for the extended SAGAT Score models, we adapt the evaluation procedure by using the probability query $p\left(S_2^{j,i} | b^{j,1:j,i}, \boldsymbol{f}^{j,1:j,i}\right)$, i.e., the conditional probability distribution over the SAGAT score given both the observable indicators and the behavioral patterns, from the start of the sequence until the current sample, and the classification function

$$\hat{s}_2^{j,i} = \arg\max_{s_2^{j,i}} p\left(s_2^{j,i} | b^{j,1:j,i}, \boldsymbol{f}^{j,1:j,i}\right).$$

5.6.4.1 Extended SAE Level 2 SAGAT Score model

After being trained on the $\mathcal{D}_{\text{Training}}^{\text{SAG:L3}}$ training dataset, the best-scoring extended SAE Level 2 SAGAT Score model (c.f., Section 5.2.4) was evaluated on the test dataset

$$\mathcal{D}_{\text{Test}}^{\text{SAG:L2}} = \left\{\left(b^{j,i}, s_2^{j,i}, \boldsymbol{f}^{j,i}\right)_{i=1}^{n_j}\right\}_{j=1}^{37}, \sum_{j=1}^{37} n_j = 11101.$$

The resulting 6×6 confusion matrix is shown in Figure 77. Compared to the SAE Level 2 SAGAT Score model, the extended variant keeps the 100% correct classification for the low SAGAT scores s_{2_0} (0% correct answers) and s_{2_1} (20% correct answers) but has problems in correctly recognizing the comparably rare high SAGAT scores s_{2_4} (80% correct answers) and s_{2_5} (100% correct answers), which are correctly recognized in only 59.5% and 76% of all cases. However, the extended SAE Level 2 SAGAT Score model is noticeably better in correctly recognizing the more frequent medium SAGAT scores scores s_{2_2} (40% correct answers) and s_{2_3} (60% correct answers), which are correctly recognized in 88.16% and 88.12% of all cases.

		Predicted SAGAT score						
		$\hat{s}_{2_0}$ (0%)	$\hat{s}_{2_1}$ (20%)	$\hat{s}_{2_2}$ (40%)	$\hat{s}_{2_3}$ (60%)	$\hat{s}_{2_4}$ (80%)	$\hat{s}_{2_5}$ (100%)	Total
Ground truth SAGAT score	s_{2_0}	1500	0	0	0	0	0	1500
	s_{2_1}	0	1200	0	0	0	0	1200
	s_{2_2}	0	0	3967	282	174	77	4500
	s_{2_3}	12	0	139	2380	105	65	2701
	s_{2_4}	0	0	125	118	357	0	600
	s_{2_5}	0	0	144	0	0	456	600
	Total	1512	1200	4375	2780	636	598	11101

Figure 77: 6×6 confusion matrix of the extended SAE Level 2 SAGAT Score model on test data $\mathcal{D}_{Test}^{SAG:L2}$.

A visual comparison of the ground truth SAGAT scores in the test data and the model predictions of the extended SAE Level 2 SAGAT Score model is shown in Figure 78. Compared to the SAE Level 2 SAGAT Score model (Figure 74), we have a slightly more consistent prediction, with mostly short-term misclassifications. As already shown by the confusion matrix, the most noticeable problem of the extended SAE Level 2 SAGAT Score model is a confusion concerning the high SAGAT scores s_{2_4} (80% correct answers) and s_{2_5} (100% correct answers), which lack both accuracy and precision, i.e., the ground truth SAGAT scores s_{2_4} and s_{2_5} are often misclassified and other ground truth SAGAT scores are often misclassified as $\hat{s}_{2_4}$ and $\hat{s}_{2_5}$.

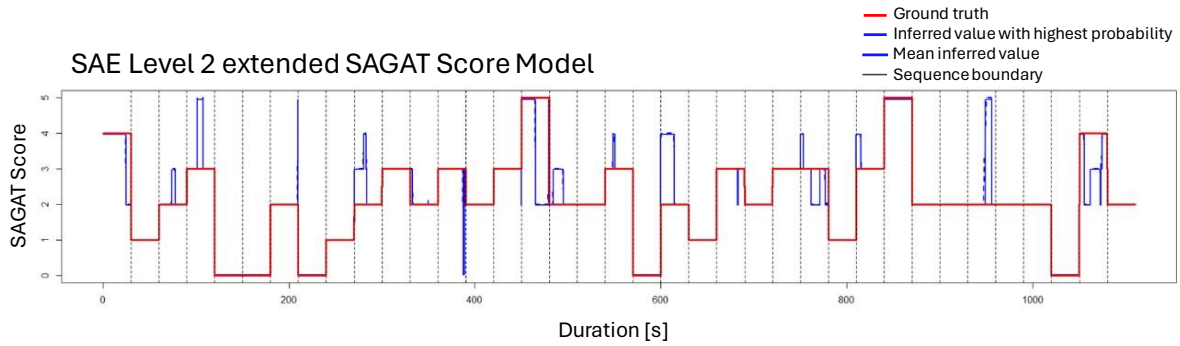

Figure 78: Comparison of ground truth and extended SAE Level 2 SAGAT Score model predictions on test data $\mathcal{D}_{Test}^{SAG:L2}$.

Overall, the extended SAE Level 2 SAGAT Score model achieves an improved accuracy of 0.8882 and an improved classification rate of 0.8883 (Table 21), representing an improvement of 62.88% and 62.89% over the hypothetical baseline model used for the SAE Level 2 SAGAT Score model (c.f., Section 5.6.3.1).

Table 21: Evaluation metrics of the extended SAE Level 2 SAGAT Score model for on test data $\mathcal{D}_{Test}^{SAG:L2}$.

Metric	Value	Baseline
Accuracy	$0.8033 \rightarrow 0.8882$	0.2594
Classification rate	$0.8033 \rightarrow 0.8883$	0.2594

5.6.4.2 Extended SAE Level 3 SAGAT Score model

After being trained on the $\mathcal{D}_{\text{Training}}^{\text{SAG:L3}}$ training dataset, the best-scoring extended SAE Level 3 SAGAT Score model (c.f., Section 5.2.4) was evaluated on the test dataset

$$\mathcal{D}_{\text{Test}}^{\text{NDRT:L3}} = \left\{\left(b^{j,i}, s_1^{j,i}, \boldsymbol{f}^{j,i}\right)_{i=1}^{n_j}\right\}_{j=1}^{74}, \sum_{j=1}^{74} n_j = 101462.$$

The resulting 6×6 confusion matrix is shown in Figure 79. Compared to the SAE Level 3 SAGAT Score model, the extended variant can improve all classifications, except the SAGAT score s_{2_4} (80% correct answers). More specifically, the low SAGAT scores s_{2_0} (0% correct answers) and s_{2_1} (20% correct answers) are correctly recognized in 85.57% and 89.2% of all cases, the medium SAGAT scores s_{2_2} (40% correct answers) and s_{2_3} (60% correct answers) are correctly recognized in 74.17% and 89.2% of all cases, while the highest SAGAT score s_{2_5} (100% correct answers) is correctly recognized in 81.33% of all cases. In contrast, the high SAGAT score s_{2_4} (80% correct answers) is correctly recognized in only 56.33% of all cases.

		Predicted SAGAT score						
		$\hat{s}_{2_0}$ (0%)	$\hat{s}_{2_1}$ (20%)	$\hat{s}_{2_2}$ (40%)	$\hat{s}_{2_3}$ (60%)	$\hat{s}_{2_4}$ (80%)	$\hat{s}_{2_5}$ (100%)	Total
Ground truth SAGAT score	s_{2_0}	2622	0	78	0	0	0	2700
	s_{2_1}	0	1875	17	200	8	0	2100
	s_{2_2}	0	0	1335	0	465	0	1800
	s_{2_3}	0	280	0	1413	107	0	1800
	s_{2_4}	0	465	56	372	1352	155	2400
	s_{2_5}	0	0	0	56	0	244	300
	Total	2622	2620	1486	2041	1932	399	11100

Figure 79: 6×6 confusion matrix of the extended SAE Level 3 SAGAT Score model on test data $\mathcal{D}_{Test}^{SAG:L3}$.

A visual comparison of the ground truth SAGAT scores in the test data and the model predictions of the extended SAE Level 3 SAGAT Score model is shown in Figure 80. Compared to the SAE Level 3 SAGAT Score model (Figure 76), the extended SAE Level 3 SAGAT Score model provides a more stable output. Once again, and as already shown by the confusion matrix, the most noticeable problem of the model is the confusion concerning the SAGAT score s_{2_4} (80% correct answers), which lacks both accuracy and precision, the ground truth SAGAT score s_{2_4} is often misclassified and other SAGAT scores are often misclassified as $\hat{s}_{2_5}$.

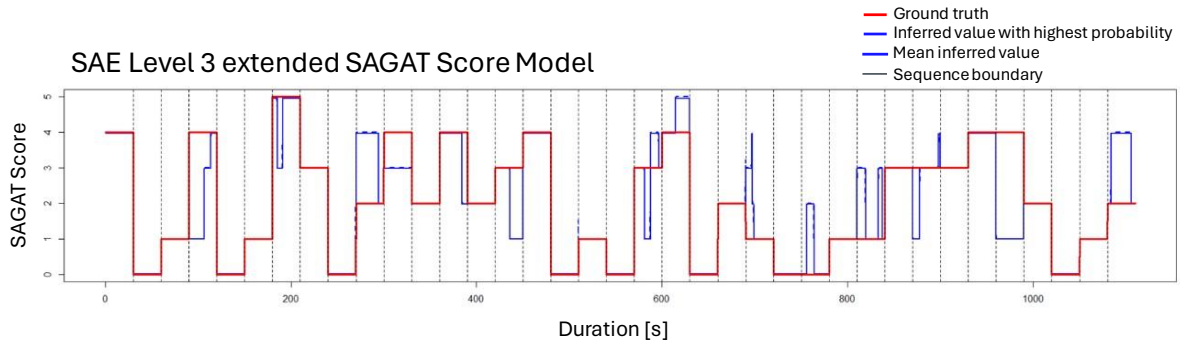

Figure 80: Comparison of ground truth and extended SAE Level 3 SAGAT Score model predictions on test data $\mathcal{D}_{Test}^{SAG:L3}$.

Compared to the SAE Level 3 SAGAT Score model, the extended SAE Level 3 SAGAT Score model achieves an improved accuracy of 0.7965 and an improved classification rate of 0.7967 (Table 22), representing an improvement of 60.15% and 60.17% over the hypothetical baseline model used for the SAE Level 3 SAGAT Score model (c.f., Section 5.6.3.2).

Table 22: Evaluation metrics of the extended SAE Level 3 SAGAT Score model for on test data $\mathcal{D}_{Test}^{SAG:L3}$.

Metric	Value	Baseline
Accuracy	$0.7105 \rightarrow 0.7965$	0.1950
Classification rate	$0.7098 \rightarrow 0.7967$	0.1950

5.6.4.3 Discussion

By incorporating information about whether the participant is currently tasked with the cognitive or visual NDRT or is not performing any NDRT, the extended SAE Level 2 and SAE Level 3 SAGAT Score models can significantly improve the accuracy of the (non-extended) SAE Level 2 and SAE Level by 8.49% and 8.6% towards a more promising accuracy of 0.8882 and 0.7965 respectively. This improvement is however a trade-off, the extended SAGAT Score models provide better results where the (non-extended) SAGAT Score models had problems, but vice versa, have problems, where the SAGAT Score models worked better.

Overall, the extended SAGAT Score models suffer from the same lack of data as the SAGAT Score models and we believe that the performance could be improved significantly, if additional data would become available.

6 Conclusion

The DySAM project has yielded significant insights into the assessment of situational awareness (SA). Below, we delineate several conclusions drawn from our work.

6.1 Utilization of literature results

Initially, our efforts were directed towards extracting indicators from scientific literature known to correlate with SA. We also tried to extract the distribution parameters for these indicators from the literature. However, this endeavor proved less fruitful than anticipated due to several challenges. The selection of potential indicators revealed that many literature results can only partially or not at all be incorporated into a real-time model for SA assessment. Some indicators lacked precise operational

descriptions, while others were confined to simulated environments. Other were not accessible in real-time, but could only be calculated during post-hoc analysis. Additionally, some indicators had high inter-driver variability, such that it was hard to generalize the indicator. Other indicators showed a strong dependence on the scenario investigated in the respective study. Furthermore, some indicators for which the literature identified a significant relationship to SA are not discriminative enough to provide a benefit for a dynamic real time model. This happened when the literature study showed the significant relationship on a large number of measurements, but the predictive power of each individual measurement was very low.

Even when utilized, the distribution parameters of an indicator derived from literature often failed to align with those observed in DySAM experiments, rendering purely literature-based models impractical. However, the literature review did provide us with a list of potential indicators, for which we then estimated the distribution parameters from the experiment data. We collected these potential indicators and extended the list with additional ones, resulting in a total of 71 indicators, which were evaluated during the modelling process.

6.2 Suitability and performance of Dynamic Bayesian Networks

A deliberate choice was made to model SA in a generic, context-independent manner, acknowledging that achieving high accuracy levels for such abstract representations would be challenging. Despite this, our analysis found that Dynamic Bayesian Networks (DBNs) demonstrated good validity in capturing training data information, with model accuracies consistently ranging from 0.71 to 0.89. This indicates that DBNs are nonetheless expressive enough for this abstract model of SA. Based on the training results, our assessment is that the generalization performance of the models on the test data can still be increased if more data is available.

6.3 SAGAT assessments for abstract SA modelling approach

The DySAM project consciously decided to create models that predict a generic level of situational awareness (sufficient/insufficient level of situational awareness). Other approaches, such as those pursued by the Situware project (Osterloh, Suchan, & Weber, 2023), attempt to specifically predict situation awareness by determining whether the driver is aware of each piece of information that is relevant to the current situation. The advantages of the DySAM approach are that the situation-relevant information does not have to be determined at runtime for every possible situation. In addition, the sensors required to determine the situation-specific indicators can be dispensed with. All that is needed are sensors for the indicators that abstract from the surrounding context.

The disadvantage, however, is that the level of detail of the predictions with the DySAM approach is lower. The SAGAT questionnaire, which was used to validate the models, asks questions about specific information in the respective driving situation. The DySAM modeling approach was unable to create models that were able to predict the answer to individual SAGAT questions well. However, the percentage of correct answers could be predicted well with an accuracy of 0.888 at SAE level 2 and an accuracy of 0.797 at SAE level 3.

6.4 Unsupervised learning of latent behavioral patterns

The process of establishing and maintaining a suitable level of SA is susceptible to various disturbances, each eliciting distinct behavioral responses within this SA maintenance process. In the validation study described in Section 4 disturbances were introduced via a cognitive NDRT and a visual NDRT, which

resulted in different behavioral changes. Learning fine grained behavioral patterns that are associated with a good process of maintaining a suitable level of SA, respectively with a bad process of maintaining a suitable level of SA seems like a promising approach. In Section 5.4.4 we described how the DySAM modelling approach can be used to uncover such behavioral patterns. If any improvements are to be made to the models, we believe it makes sense to focus on identifying and evaluating these latent behavioral patterns. Understanding the behavioral patterns and their consequences for situation awareness can be beneficial for any interaction or intervention strategy pursued by the vehicle.

7 References

Alhström, C., Georgoulas, G., & Kircher, K. (2022, May). Towards a Context-Dependent Multi-Buffer Driver Distraction Detection Algorithm. *IEEE Transactions on Intelligent Transportation Systems, 23*(5), 4778-4790.

Bishop, C. M. (2006). *Pattern Recognition and Machine Learning.* Springer Science+Business Media, LLC.

Endsley, M. R. (1988). Situation awareness global assessment technique (SAGAT). *Proceedings of the IEEE 1988 National Aerospace and Electronics Conference*, *3*, pp. 789-795. doi:https://doi.org/10.1109/naecon.1988.195097

Endsley, M. R. (1995). Toward a theory of situation awareness in dynamic systems. *Human Factors, 37*(1), 32-64.

Endsley, M. R. (2019). A Systematic Review and Meta-Analysis of Direct Objective Measures of Situation Awareness: A comparison of SAGAT and SPAM. *Human Factors, 63*(1), 124-150. doi:https://doi.org/10.1177/0018720819875376

Eriksson, A., & Stanton, N. A. (2017). akeover time in highly automated vehicles: Noncritical transitions to and from manual control. *Human Factors: The Journal of the Human Factors and Ergonomics Society*(59), 689–705. doi:https://doi.org/10.1177/ 0018720816685832

Faure, V., Lobjois, R., & Benguigui, N. (2016). The effects of driving environment complexity and dual tasking on driver's mental workload and eye blink behavior. *Transportation Research Part F 40*, 78-90.

Guo, Y., & Greiner, R. (2005). Discriminative model selection for belief net structures. *Proceedings of the 20th National Conference on Artificial Intelligence*, (pp. 770-776).

Heckerman, D., & Meek, C. (1997). *Embedded Bayesian Network Classifiers.* Redmond, WA: Microsoft Research.

Hosmer Jr., D. W., Lemeshow, S., & Sturdivant, R. X. (2013). *Applied Logistic Regression.* John Wiley & Sons, Inc.

International Organization for Standardization. (2020). *Road vehicles - Measurement and analysis of driver visual behaviour with respect to transport information and control systems, ISO 15006.* ISO.

Kircher, K., & Ahlström, C. (2013). The driver distraction detection algorithm AttenD. *Driver Distraction and Inattention: Advances in Research and Countermeasures*, (pp. 327-348). Surrey, U.K.

Klingner, J., Kumar, R., & Hanrahan, P. (2008). Measuring the task-evoked pupillary response with a remote eye tracker. *Proceedings of the 2008 symposium on Eye tracking research & applications (ETRA '08).* doi:https://doi.org/10.1145/1344471.1344489

Koller, D., & Friedman, N. (2009). *Probabilistic Graphical Models: Principles and Technique.* Cambridge, Massachusetts, London, England: The MIT Press.

Kunze, A., Summerskill, S. J., Marshall, R., & Filtness, A. J. (2018). Automation Transparency: Implications of Uncertainty Communication for Human-Automation Interaction and Interfaces. *Ergonomics*.

Liu, S., Wanyan, X., & Zhuang, D. (2014). Modeling the situation awareness by the analysis of cognitive process. *Bio-Medical Materials and Engineering 24*, 2311-2318.

Morando, A., Gershon, P., & Mehler, B. (2021). A model for naturalistic glance behavior around Tesla autopilot disengagements. *Accident Analysis & Prevention*. doi:https://doi.org/10.1016/j.aap.2021.106348

Murphy, K. P. (2012). *Machine Learning: A Probabilistic Perspective.* Cambridge, Massachusetts, London, England: The MIT Press.

Natarajan, S., Wong, W.-K., & Tadepalli, P. (2006). Structure refinement in first order conditional influence language. *Proceedings of the Workshop on Open Problems in Statistical Relational Learning (SRL)*, (p. 8 pages).

National Highway Traffic Safety Administration. (2017). *Automated driving system 2.0: A vision for safety.* U.S. Department of Transportation.

Naujoks, F., Wiedemann, K., Schömig, N., Hergeth, S., & Keinath, A. (2019). Towards guidelines and verification methods for automated vehicle HMIs. *Transportation Research Part F: Traffic Psychology and Behaviour, 60*, 121-136.

Niezgoda, M., Tarnowski, A., Kruszewski, M., & Kaminski, T. (2015). Towards testing auditory-vocal interfaces and detecting distraction while driving: A comparison of eye-movement measures in the assessment of cognitive workload. *Transportation Research Part F*, 23-34.

Osterloh, J.-P., Suchan, J., & Weber, L. (2023). *Erfassung des Fahrersituationsbewusstseins für adaptive kooperative Übergabestrategien beim hochautomatisierten Fahren : Abschlussbericht SituWare.* Oldenburg: TIB-online. doi:10.2314/KXP:1881698068

Pernkopf, F., & Bilmes, J. (2005). Discriminative versus generative parameter and structure learning of Bayesian network classifiers. *Proceedings of the 22nd International Conference on Machine Learning*, (pp. 657-664).

SAE International. (2021). *Taxonomy and Definitions for Terms Related to Driving Automation Systems for On-Road Motor Vehicles (J3016).* Retrieved from https://www.sae.org/standards/content/j3016_202104/

Santafe, G., Lozano, J., & Larranaga, P. (2007). Discriminative vs. generative learning of Bayesian network classifiers. *LNAI 4724*, pp. 453-464.

Schewe, F., Cheng, H., Hafner, A., Sester, M., & Vollrath, M. (2019). Occupant Monitoring in Automated Vehicles: Classification of Situation Awareness Based on Head Movements While Cornering. *Proceedings of the Human Factors and Ergonomics Society 2019 Annual Meeting.*

Schwarz, G. (1976). Estimating the dimension of a model. *Annals of statistics, 6*, 461-464.

Sun, G., Wanyan, X., Wu, X., & Zhuang, D. (2017). The Influence of HUD Information Visual Coding on Pilot's Situational Awareness. *9th International Conference on Intelligent Human-Machine Systems and Cybernetics (IHMSC).* doi:https://doi.org/10.1109/ihmsc.2017.38

Teoh, E. R. (2020). What's in a name? Drivers' perceptions of the use of five SAE Level 2 driving automation systems. *Journal of safety research, 72*, 145-141.

Victor, T. W., Harbluk, J. L., & Engström, J. A. (2005). Sensitivity of eye-movement measures to in-vehicle task difficulty. *Transportation Research Part F, 8*(2), 167-190.

Wilkie, R., Mole, C., Giles, O., Merat, N., Romano, R., & Markkula, G. (2019). Cognitive load during automation affects gaze behaviour and transitions to manual steering control. *Proceedings of the 10th International Driving Symposium on Human Factors in Driver Assessment, Training and Vehicle Design*, (pp. 426-432).

Wu, X., Feng, C., Wanyan, X., Liu, S., Ding, L., Miao, C., & He, X. (2018). How shared screen affected team collaboration task, a case study of ergonomics experiment on team situation awareness. *Engineering Psychology and Cognitive Ergonomics: 15th International Conference (EPCE 2018)* (pp. 241-249). Springer International Publishing.

Yang, Y., Karakaya, B., Dominioni, G. C., Kawabe, K., & Bengler, K. (2018). An HMI Concept to Improve Driver's Visual Behavior and Situation Awareness in Automated Vehicle. *Proceedings of the 21st International Conference on Intelligent Transportation Systems (ITSC)*, (pp. 650-655). Maui, Hawayii, USA.

Zhang, T., Yang, J., Liang, N., Pitts, B. J., Prakah-Asante, K., Curry, R., & Yu, D. (2023). Physiological measurements of situation awareness: a systematic review. *Human Factors, 65*(5), 737-758.

Zhou, F., Yang, X. J., & De Winter, J. C. (2021). Using eye-tracking data to predict situation awareness in real time during takeover transitions in conditionally automated driving. *IEEE transactions on intelligent transportation systems, 23*(3), 2284-2295.

Appendix

Appendix 1 Mathematical background

Most of the content of this section is condensed from (Murphy, 2012), to which we refer for additional information. We assume the reader to be familiar with the basic rules of probability and probabilistic inference and will refrain from providing a definition for basic concepts, which can be found e.g., in (Murphy, 2012) and (Koller & Friedman, 2009).

1.1 Notation

Notation-wise, we will mostly follow (Murphy, 2012) and (Koller & Friedman, 2009). In general, we will use capital letters, like X, Y, Z, for random variables and bold capital letters, like $\boldsymbol{X}$, $\boldsymbol{Y}$, $\boldsymbol{Z}$, for sets of variables. Specific assignments to (sets of) variables will be denoted by lowercase letters, like $X = x$ and $\boldsymbol{X} = \boldsymbol{x}$, or just x and $\boldsymbol{x}$. An exception to the capital / lowercase rule are special symbols like θ and $\mathcal{D}$, where we assume the meaning of variable vs. assignment to be clear from the context.

Throughout this report, we will be concerned with probability distributions over discrete and density functions over continuous random variables and we will use a lowercase p for both and mixtures thereof, with the exact meaning to be given by the context, unless we want to emphasize that we speak of probabilities and not densities, in which case we will use a capital P instead.

Occasionally, we will use $p(\cdot)$ to indicate distributions over arbitrary (sets of) variables. We denote that a distribution p is parameterized a parameter θ (or set of parameters $\boldsymbol{\theta}$) by $p(\cdot : \theta)$ (or $p(\cdot : \boldsymbol{\theta})$). If the notion of parameters is not important, we may omit them and just write $p(\cdot)$.

For time series, we assume that the timeline is discretized into time-slices with a constant granularity of 100ms. We will index these time-slices by non-negative integers and will use X_i^t to represent the instantiation of a variable X_i at time t. A sequences of variables $X_i^j, X_i^{j+1}, \dots, X_i^k$ (or sets of variables $\boldsymbol{X}_i^j, \boldsymbol{X}_i^{j+1}, \dots, \boldsymbol{X}_i^k$) will be denoted by $X_i^{j:k}$ (or $\boldsymbol{X}_i^{j:k}$) and we will use $X_i^{j:k} = x_i^{j:k}$ ($\boldsymbol{X}_i^{j:k} = \boldsymbol{x}_i^{j:k}$) or just $x_i^{j:k}$ ($\boldsymbol{x}_i^{j:k}$) for an assignment of values to such sequences.

To keep the notation in equations and figures short, we will denote the set of considered SA indicators as $\boldsymbol{F}$ and single indicators by a generic F, using subscripts, like F_1, F_2, F_3 to distinguish different indicators. We note that indicators F_i with the same subscript i from different models will in general not refer to the same variable and will define their concrete meaning in auxiliary tables.

1.2 Distributions

The DySAM models utilize a number of discrete probability distributions and continuous density functions that shall be introduced in the following, with all definitions taken from (Murphy, 2012).

Throughout this section, let A denote a discrete random variable that can take one of n_A different values, i.e., $\text{Val}(A) = \{a_1, \dots, a_{n_A}\}$, X denote a continuous random variable, and $\boldsymbol{X} = \{X_1, \dots, X_{n_{\boldsymbol{X}}}\}$ denote a set of $n_{\boldsymbol{X}} > 1$ continuous variables. Lastly, let $\boldsymbol{B}$ denote an arbitrary non-empty set of discrete variables. For DySAM, we consider unconditioned distributions of the form $p(A : \boldsymbol{\theta}_A)$, $p(X : \boldsymbol{\theta}_X)$, and $p(\boldsymbol{X} : \boldsymbol{\theta}_{\boldsymbol{X}})$, and conditional distributions of the form $p(A|\boldsymbol{B} : \boldsymbol{\theta}_{A|\boldsymbol{B}})$, $p(X|\boldsymbol{B} : \boldsymbol{\theta}_{X|\boldsymbol{B}})$, and $p(\boldsymbol{X}|\boldsymbol{B} : \boldsymbol{\theta}_{\boldsymbol{X}|\boldsymbol{B}})$, each governed by their own set of parameters.

In the case of a discrete variable A, $p(A)$ is a probability mass function (PMF) that has to satisfy the properties, $0 < p(a) < 1$, for each $a \in \mathrm{Val}(A)$ and $\sum_{a \in \mathrm{Val}(A)} p(a) = 1$. In the case of a continuous variable X, $p(X)$ is a probability density functions (PDF), defined as the derivative of the cumulative distribution function of X. Given a PDF, the probability of a continuous variable being in a finite interval is given by

$$P(l < X < u) = \int_l^u p(x)dx.$$

It is required that $p(x) \geq 0$ but unlike for PMFs, it is possible that $p(x) > 1$, as long as $\int_{-\infty}^{\infty} p(x)dx = 1$. Both PMFs and PDFs generalize to multivariate sets of variables as well as joint distributions over discrete and continuous variables.

For CPDs, in general, if we have a non-empty set of discrete parents $\boldsymbol{B}$, we can simply think of a distribution $p(\cdot \mid \boldsymbol{B} : \boldsymbol{\theta}_{\cdot \mid \boldsymbol{B}})$ as a collection of PMFs or PDFs with each a PMF or PDF $p(\cdot \mid \boldsymbol{b} : \boldsymbol{\theta}_{\cdot \mid \boldsymbol{b}})$ and a distinct set of parameters $\boldsymbol{\theta}_{\cdot \mid \boldsymbol{b}}$ for each possible assignment $\boldsymbol{b} \in \mathrm{Val}(\boldsymbol{B})$. To keep the notation short, in the following, we assume the absence of any parents.

Categorical distribution

Categorical distributions are the most straightforward method to encode a distribution over a discrete random variable A that can take one of n_A different values and can be understood as modeling the outcome of a single n_A-sided dice toss. A categorical distribution over A, denoted $\mathrm{Cat}(A : \boldsymbol{\theta}_A)$, is governed by a set of parameters $\boldsymbol{\theta}_A = \{\theta_{a_1}, \ldots, \theta_{a_{n_A}}\}$ that directly encode the probability that $A = a$, for each $a \in \mathrm{Val}(A)$, such that if $A \sim \mathrm{Cat}(\boldsymbol{\theta}_A)$, then $p(A = a_i : \boldsymbol{\theta}_A) = \theta_{a_i}$. More formally, the PMF is given by

$$p(a_i : \boldsymbol{\theta}_A) = \mathrm{Cat}(A : \boldsymbol{\theta}_A) \triangleq \prod_{j=1}^{n_A} \theta_{a_j}^{\mathbb{I}(i=j)},$$

where $\mathbb{I}(e)$ is the indicator function, which returns 1, if e is true, and 0 otherwise. If A is a binary variable, i.e., $n_A = 2$, the categorical distribution reduces to the Bernoulli distribution.

Exponential distribution

Exponential distributions are special cases of Gamma distributions used to model the duration between events in memoryless continuous processes, i.e., processes in which events occur continuously and independently at a constant average rate. Within DySAM, they are used to model distributions over single non-negative continuous variables, such as frequencies or durations. We define the exponential distribution over a continuous variable X, denoted $\mathrm{Expon}(X : \lambda_X)$, in terms of a single rate factor $\boldsymbol{\theta}_X = \{\lambda_X\}$ with $\lambda_x > 0$, as such, if X is exponentially distributed, i.e., $X \sim \mathrm{Expon}(\lambda_X)$, then

$$p(x : \boldsymbol{\theta}_X) = \begin{cases} \lambda_X \exp[-\lambda_X x], & x \geq 0 \\ 0, & x < 0 \end{cases}.$$

(Multivariate) Gaussian distribution

The Gaussian or normal distribution is the most widely used distribution in statistics and machine learning (Murphy, 2012). In the univariate case, a Gaussian distribution over a continuous variable X,

denoted $\mathrm{N}(X : \mu_X, \sigma_X^2)$, is parameterized via mean $\mu_X = \mathbb{E}[X]$ and variance $\sigma_X^2 = \mathrm{var}[X]$. If X is normally distributed, $X \sim \mathrm{N}(\mu_X, \sigma_X^2)$, its PDF is given by

$$p(x : \boldsymbol{\theta}_X) = \mathrm{N}(X : \mu_X, \sigma_X^2) \triangleq \frac{1}{\sqrt{2\pi\sigma_X^2}} \exp\left[-\frac{(x-\mu_X)^2}{2\sigma_X^2}\right].$$

Gaussian distributions generalize to sets of continuous variables $\boldsymbol{X}$, in which case we assume $\boldsymbol{X}$ to be treated as a vector of variables, such that the order of variables is fixed. In the multivariate case, a Gaussian distribution over $\boldsymbol{X}$, denoted $\mathrm{N}(\boldsymbol{X} : \boldsymbol{\mu_X}, \Sigma_{\boldsymbol{X}})$, is parameterized via a mean vector $\boldsymbol{\mu_X} = \mathbb{E}[\boldsymbol{X}]$ and a $n_{\boldsymbol{X}} \times n_{\boldsymbol{X}}$ covariance matrix $\Sigma_{\boldsymbol{X}} = \mathrm{cov}[\boldsymbol{X}]$ and the PDF is given by

$$p(\boldsymbol{x} : \boldsymbol{\theta_X}) = \mathrm{N}(\boldsymbol{X} : \boldsymbol{\mu_X}, \Sigma_{\boldsymbol{X}}) \triangleq \frac{1}{(2\pi)^{n/2}|\Sigma_{\boldsymbol{X}}|^{1/2}} \exp\left[-\frac{1}{2}(\boldsymbol{x}-\boldsymbol{\mu_X})^T \Sigma_{\boldsymbol{X}}^{-1}(\boldsymbol{x}-\boldsymbol{\mu_X})\right].$$

(Multivariate) Gaussian mixture models

A Gaussian mixture model (GMM) assumes is a probabilistic model / distribution in which the probability density is a mixture of a finite number of Gaussian distribution. Given a sufficient number of mixture components, a GMM can approximate any PDF (Murphy, 2012).

Let n_k dente the number of components in the mixture model, in the univariate case, a GMM over X is parameterized by $\boldsymbol{\theta}_X = \left\{\left\{\pi_{X_i}, \mu_{X_i}, \sigma_{X_i}^2\right\}_{i=1}^{n_k}\right\}$, comprised of a mixture weight π_{X_i}, and the mean μ_{X_i} and variance $\sigma_{X_i}^2$ for each of the n_k Gaussian components. To ensure a valid PDF, we require that $0 < \pi_{X_i} < 1$ and $\sum_{1i}^{n_k} \pi_{X_i} = 1$. The PDF is given by

$$p(x : \boldsymbol{\theta}_X) \triangleq \sum_{i=1}^{n_k} \pi_{X_i} \mathcal{N}\left(\mu_{X_i}, \sigma_{X_i}^2\right).$$

Likewise, a multivariate GMM over $\boldsymbol{X}$ is parameterized by $\boldsymbol{\theta_X} = \left\{\left\{\pi_{\boldsymbol{X}_i}, \boldsymbol{\mu}_{\boldsymbol{X}_i}, \Sigma_{\boldsymbol{X}_i}\right\}_{i=1}^{n_k}\right\}$, comprised of a mixture weight $\pi_{\boldsymbol{X}_i}$, and the mean vector $\boldsymbol{\mu}_{\boldsymbol{X}_i}$ and covariance matrix $\Sigma_{\boldsymbol{X}_i}$ for each multivariate Gaussian component, and the PDF is given by

$$p(\boldsymbol{x} : \boldsymbol{\theta_X}) = \sum_{i=1}^{n_k} \pi_{\boldsymbol{X}_i} \mathcal{N}\left(\boldsymbol{\mu}_{\boldsymbol{X}_i}, \Sigma_{\boldsymbol{X}_i}\right).$$

1.3 Dynamic Bayesian Networks

A Bayesian Network (BN) is an annotated directed acyclic graph (DAG) that encodes a joint probability / density distribution (JPD) over a set of variables $\boldsymbol{X} = \{X_1, \ldots, X_n\}$ (Koller & Friedman, 2009) (Murphy, 2012). Formally, a BN $\mathcal{B}$ is defined as a pair $\mathcal{B} = \langle \mathcal{G}, \boldsymbol{\theta} \rangle$. The component $\mathcal{G}$ is a DAG whose vertices correspond to the random variables $X_1, \ldots, X_n$ and whose arcs define the (in)dependencies between these variables, in that each variable $X_i \in \boldsymbol{X}$ is independent of its non-descendants given its (possible empty) set of parents $\mathrm{Pa}(X_i)$ in $\mathcal{G}$. The component $\boldsymbol{\theta} = \left\{\boldsymbol{\theta}_{X_1|\mathrm{Pa}(X_1)}, \ldots, \boldsymbol{\theta}_{X_n|\mathrm{Pa}(X_n)}\right\}$ represents a set of parameters that quantify the probabilities / densities of the network. Given $\mathcal{G}$ and $\boldsymbol{\theta}$, a BN $\mathcal{B}$ defines a unique JPD over $\boldsymbol{X}$ as

$$p(\boldsymbol{X} : \boldsymbol{\theta}) = \prod_{i=1}^{n} p\left(X_i | \mathrm{Pa}(X_i) : \boldsymbol{\theta}_{X_i|\mathrm{Pa}(X_i)}\right).$$

Dynamic Bayesian Networks (DBNs) extend BNs to model the stochastic evolution of $\boldsymbol{X}$ over time. A DBN $\mathcal{D}$ is defined as a pair $\mathcal{D} = \langle \mathcal{B}^1, \mathcal{B}^{\rightarrow} \rangle$, where $\mathcal{B}^1 = \langle \mathcal{G}^1, \boldsymbol{\theta}^1 = \left\{ \boldsymbol{\theta}^1_{X_1^1|\mathrm{Pa}(X_1^1)}, \dots, \boldsymbol{\theta}^1_{X_n^1|\mathrm{Pa}(X_n^1)} \right\} \rangle$ is a BN that defines the JPD $p(\boldsymbol{X}^1 : \boldsymbol{\theta}^1)$ for the first time slice, and, under the assumption of first-order Markov and stationary processes, $\mathcal{B}^{\rightarrow} = \langle \mathcal{G}^{\rightarrow}, \boldsymbol{\theta}^{\rightarrow} = \left\{ \boldsymbol{\theta}^{\rightarrow}_{X_1^t|\mathrm{Pa}(X_1^t)}, \dots, \boldsymbol{\theta}^{\rightarrow}_{X_n^t|\mathrm{Pa}(X_n^t)} \right\} \rangle$ is a so-called two time-slice Bayesian Network (2TBN), a conditional BN over two time slices, that defines the conditional probability / density distribution (CPD) $p(\boldsymbol{X}^t | \boldsymbol{X}^{t-1} : \boldsymbol{\theta}^{\rightarrow})$ for all $t > 1$ as

$$p(\boldsymbol{X}^t | \boldsymbol{X}^{t-1} : \boldsymbol{\theta}^{\rightarrow}) = \prod_{i=1}^{n} p\left(X_i^t | \mathrm{Pa}(X_i^t) : \boldsymbol{\theta}^{\rightarrow}_{X_i^t|\mathrm{Pa}(X_i^t)} \right),$$

where the parents of X_i^t may be comprised of both variables from time slice t and $t-1$, $\mathrm{Pa}(X_i^t) \subset \{\boldsymbol{X}^t, \boldsymbol{X}^{t-1}\}$. The 2TBN is a conditional BN in that it only defines distributions over $\boldsymbol{X}^t$, not $\boldsymbol{X}^{t-1}$, and accordingly, $\boldsymbol{\theta}^{\rightarrow}$ is only comprised of parameters for distributions over $\boldsymbol{X}^t$. For any number of time slices $T \geq 1$, a DBN then defines the JPD $p(\boldsymbol{X}^{1:T} : \boldsymbol{\theta}^1, \boldsymbol{\theta}^{\rightarrow})$ over the time series $\boldsymbol{X}^1, \boldsymbol{X}^2, \dots, \boldsymbol{X}^T$ as

$$\begin{aligned} p(\boldsymbol{X}^{1:T} : \boldsymbol{\theta}^1, \boldsymbol{\theta}^{\rightarrow}) &= p(\boldsymbol{X}^1 : \boldsymbol{\theta}^1) \prod_{t=2}^{T} p(\boldsymbol{X}^t | \boldsymbol{X}^{t-1} : \boldsymbol{\theta}^{\rightarrow}) \\ &= \prod_{i=1}^{n} p\left(X_i^1 | \mathrm{Pa}(X_i^1) : \boldsymbol{\theta}^1_{X_i^1|\mathrm{Pa}(X_i^1)} \right) \prod_{t=2}^{T} \prod_{i=1}^{n} p\left(X_i^t | \mathrm{Pa}(X_i^t) : \boldsymbol{\theta}^{\rightarrow}_{X_i^t|\mathrm{Pa}(X_i^t)} \right). \end{aligned}$$

State-observation models

A common sub-class of DBNs and the one we use in DySAM are *state-observation* models (Koller & Friedman, 2009), which incl. e.g., Hidden Markov Models and Kalman-Filters, where $\boldsymbol{X} = \{\boldsymbol{Z}, \boldsymbol{Y}\}$ is comprised of a set of unobservable state variables $\boldsymbol{Z}$ with Markov dynamics, that we like to reason about, and a set of observable variables $\boldsymbol{Y}$ that can be used to reason about $\boldsymbol{Z}$. In this case, the 2TBN $p(\boldsymbol{X}^t | \boldsymbol{X}^{t-1})$ is commonly factorized as

$$p(\boldsymbol{X}^t | \boldsymbol{X}^{t-1}) = p(\boldsymbol{Z}^t | \boldsymbol{Z}^{t-1}) p(\boldsymbol{Y}^t | \boldsymbol{Z}^t),$$

where $p(\boldsymbol{Z}^t | \boldsymbol{Z}^{t-1})$ is called a dynamic model, as it models the temporal dynamics of the state, and $p(\boldsymbol{Y}^t | \boldsymbol{Z}^t)$ is called an observation model, as it describes how the state generates observable measurements.

1.4 Probabilistic inference

If we have access to a state-observation model that defines a JPD $p(\boldsymbol{Z}^{1:T}, \boldsymbol{Y}^{1:T})$, we usually want to utilize it to infer probability queries over $\boldsymbol{Z}$ given some observed evidence over $\boldsymbol{Y}$. The most common inference task in DBNs include (Koller & Friedman, 2009):

- Filtering: At any point in time $t \geq 1$, we want to infer the most informed distribution over the system state $\boldsymbol{Z}^t$ given *all* the evidence $\boldsymbol{Y}^{1:t} = \boldsymbol{y}^{1:t}$ obtained to far, $p(\boldsymbol{Z}^t | \boldsymbol{y}^{1:t})$.
- Prediction: At any point in time $t \geq 1$, given the available evidence $\boldsymbol{y}^{1:t}$, predict a distribution over state and/or observable variable $\boldsymbol{X}_{\subseteq} \subseteq \boldsymbol{X}$ over the next n time-slices, $p\left(\boldsymbol{X}_{\subseteq}{}^{t+1:t+n} | \boldsymbol{y}^{1:t} \right)$

- Smoothing: At any point in time $t \geq 1$, infer the posterior distribution over the system state $\boldsymbol{Z}^t$ given the evidence of some longer trajectory $\boldsymbol{y}^{1:T}$, $p(\boldsymbol{Z}^t|\boldsymbol{y}^{1:T})$.

For the DySAM system, we require a solution for filtering, i.e., we're interested in inferring $p(\boldsymbol{Z}^t|\boldsymbol{y}^{1:t})$ at each time step t. A straightforward solution is the standard recursively defined filtering algorithm (Koller & Friedman, 2009), which allows us to infer $p(\boldsymbol{Z}^{t+1}|\boldsymbol{y}^{1:t+1})$ from a previously inferred $p(\boldsymbol{Z}^t|\boldsymbol{y}^{1:t})$ and the new evidence $\boldsymbol{y}^{t+1}$, using constant memory and computational effort. For the first time slice $t = 1$, we can infer $p(\boldsymbol{Z}^1|\boldsymbol{y}^1)$ as

$$p(\boldsymbol{Z}^1|\boldsymbol{y}^1) = \frac{p(\boldsymbol{Z}^1, \boldsymbol{y}^1)}{p(\boldsymbol{y}^1)} \propto p(\boldsymbol{Z}^1)p(\boldsymbol{y}^1|\boldsymbol{Z}^1).$$

Given $p(\boldsymbol{Z}^t|\boldsymbol{y}^{1:t})$, we can infer $p(\boldsymbol{Z}^{t+1}|\boldsymbol{y}^{1:t+1})$ as

$$\begin{aligned} p(\boldsymbol{Z}^{t+1}|\boldsymbol{y}^{1:t+1}) &= \frac{1}{p(\boldsymbol{y}^{t+1}|\boldsymbol{y}^{1:t})} \sum_{\boldsymbol{z}^t \in \mathrm{Val}(\boldsymbol{Z})} p(\boldsymbol{z}^t, \boldsymbol{Z}^{t+1}, \boldsymbol{y}^{t+1}|\boldsymbol{y}^{1:t}) \\ &= \frac{1}{p(\boldsymbol{y}^{t+1}|\boldsymbol{y}^{1:t})} \sum_{\boldsymbol{z}^t \in \mathrm{Val}(\boldsymbol{Z})} p(\boldsymbol{z}^t|\boldsymbol{y}^{1:t}) p(\boldsymbol{Z}^{t+1}|\boldsymbol{z}^t, \boldsymbol{y}^{1:t}) p(\boldsymbol{y}^{t+1}|\boldsymbol{z}^t, \boldsymbol{Z}^{t+1}, \boldsymbol{y}^{1:t}). \end{aligned}$$

Here, $\frac{1}{p(\boldsymbol{y}^{t+1}|\boldsymbol{y}^{1:t})}$ is a normalization factor that ensures that $\sum_{\boldsymbol{z}^{t+1} \in \mathrm{Val}(\boldsymbol{Z})} p(\boldsymbol{Z}^{t+1}|\boldsymbol{y}^{1:t+1}) = 1$. Furthermore, given the overall assumption of a state-observation model (e.g., the Markov assumption), we have that $p(\boldsymbol{Z}^{t+1}|\boldsymbol{Z}^t, \boldsymbol{Y}^{1:t}) = p(\boldsymbol{Z}^{t+1}|\boldsymbol{Z}^t)$ and $p(\boldsymbol{y}^{t+1}|\boldsymbol{z}^t, \boldsymbol{Z}^{t+1}, \boldsymbol{y}^{1:t}) = p(\boldsymbol{y}^{t+1}|\boldsymbol{Z}^{t+1})$, such that

$$p(\boldsymbol{Z}^{t+1}|\boldsymbol{y}^{1:t+1}) \propto p(\boldsymbol{y}^{t+1}|\boldsymbol{Z}^{t+1}) \sum_{\boldsymbol{z}^t \in \mathrm{Val}(\boldsymbol{Z})} p(\boldsymbol{z}^t|\boldsymbol{y}^{1:t}) p(\boldsymbol{Z}^{t+1}|\boldsymbol{z}^t).$$

1.5 Bayesian parameter estimation

Distributions and DBNs (which are composed of distributions) require specific parameters to be fully specified. Ideally, we want to be able to estimate these parameters from prior knowledge and/or data, if available. In DySAM, we rely on Bayesian parameter estimation, which provides a common framework for both use cases.

In the following, let $\boldsymbol{\theta}$ denote some set of parameters for some arbitrary distribution $p(\cdot : \boldsymbol{\theta})$ and let $\mathcal{D}$ denote some dataset, consisting of n training samples that can be used to estimate $\boldsymbol{\theta}$. In Bayesian parameter estimation, we treat the parameters $\boldsymbol{\theta}$ as random variables and use probabilistic inference to update our beliefs given the data $\mathcal{D}$, i.e., we want to infer $p(\boldsymbol{\theta}|\mathcal{D})$. Using the Bayes rule, we have that

$$p(\boldsymbol{\theta}|\mathcal{D}) \propto p(\boldsymbol{\theta})p(\mathcal{D}|\boldsymbol{\theta}).$$

Here, $p(\boldsymbol{\theta})$ is called the prior distribution over the parameters, to be used to incorporate any prior knowledge we may have available, $p(\mathcal{D}|\boldsymbol{\theta})$ is the likelihood of the data given the parameters, and $p(\boldsymbol{\theta}|\mathcal{D})$ is called the posterior distribution over the parameters, given the data. Bayesian parameter

estimation allows for incremental parameter estimation, in that given $p(\boldsymbol{\theta}|\mathcal{D})$ and a new dataset $\mathcal{D}'$, we can infer an updated posterior

$$p(\boldsymbol{\theta}|\mathcal{D},\mathcal{D}') \propto p(\boldsymbol{\theta}|\mathcal{D})p(\mathcal{D}'|\boldsymbol{\theta},\mathcal{D}) = p(\boldsymbol{\theta}|\mathcal{D})p(\mathcal{D}'|\boldsymbol{\theta}),$$

using $p(\boldsymbol{\theta}|\mathcal{D})$ as a new prior.

For Bayesian parameter estimation to be computationally efficient, we require the parametric form of the distribution to be conjugate, meaning that if $p(\boldsymbol{\theta})$ is of a specific parametric form, the posterior distribution $p(\boldsymbol{\theta}|\mathcal{D})$ will be of the same parametric form. Fortunately, there are conjugate priors available for all distributions considered in DySAM. E.g., a conjugate prior for categorical distributions of the form $p(A : \boldsymbol{\theta}_A) = \mathrm{Cat}(A : \boldsymbol{\theta}_A), \mathrm{Val}(A) = \{a_1, \dots, a_{n_A}\}, \boldsymbol{\theta}_A = \{\theta_{a_1}, \dots, \theta_{a_{n_A}}\}$ is the Dirichlet distribution

$$p(\boldsymbol{\theta}_A : \boldsymbol{\alpha}) = \mathrm{Dir}(\boldsymbol{\theta}_A : \boldsymbol{\alpha}),$$

itself governed by a set of (hyper-)parameters $\boldsymbol{\alpha} = \{\alpha_1, \dots, \alpha_n\}$. With the Dirichlet distribution being a conjugate prior for the categorical distribution, the posterior distribution $p(\boldsymbol{\theta}_A|\boldsymbol{\mathcal{D}} : \boldsymbol{\alpha}')$ is itself a Dirichlet distribution with updated (hyper-)parameters $\boldsymbol{\alpha}' = \{\alpha_1', \dots, \alpha_n'\}$,

$$p(\boldsymbol{\theta}_A|\boldsymbol{\mathcal{D}} : \boldsymbol{\alpha}') = \mathrm{Dir}(\boldsymbol{\theta}_A : \boldsymbol{\alpha}').$$

Bayesian parameter estimation is completed with the inference of the posterior distribution $p(\boldsymbol{\theta}|\mathcal{D})$, capturing all available knowledge about the parameters given the data. There are several method to utilize such a distribution for inference. The most Bayesian approach would to integrate our uncertainty concerning the parameters into the inference process itself. E.g., given an arbitrary distribution $p(\cdot : \boldsymbol{\theta})$ parameterized by $\boldsymbol{\theta}$ and a posterior distribution $p(\boldsymbol{\theta}|\mathcal{D})$ over the parameters given the data, we can integrate over all possible parameters according to our posterior beliefs to obtain

$$p(\cdot : \mathcal{D}) = \int p(\cdot : \boldsymbol{\theta})p(\boldsymbol{\theta}|\mathcal{D})d\boldsymbol{\theta}.$$

Here, $p(\cdot : \mathcal{D})$ is known as the posterior predictive, representing our best guess about $\cdot$ after having seen the data $\mathcal{D}$. There are however some potential disadvantages discouraging the use of the posterior predictive. A computationally viable utilization of the posterior predictive requires the integral to be solvable in closed form, which depends on the parametric form of $p(\cdot : \mathcal{D})$ and $p(\boldsymbol{\theta}|\mathcal{D})$. More importantly however, we may not solely be interested in inferring $p(\cdot : \mathcal{D})$ but may also be interested in the parameters $\boldsymbol{\theta}$ for knowledge discovery.

An alternative for utilizing the posterior distribution and the one we use for DySAM is to select a single point estimate $\widehat{\boldsymbol{\theta}} = f\big(p(\boldsymbol{\theta}|\mathcal{D})\big)$ from the posterior distribution and use it for inference, sometimes called a plug-in approximation (Murphy, 2012). The most common point estimates are the mean and the mode of the posterior distribution. Within DySAM, we will use the mode of the posterior distribution as plug-in approximation parameters, which is identical to the maximum a posteriori (MAP) estimate,

$$\widehat{\boldsymbol{\theta}}_{\mathrm{MAP}} = \arg\max_{\boldsymbol{\theta}} p(\boldsymbol{\theta})p(\mathcal{D}|\boldsymbol{\theta}).$$

In contrast, the maximum likelihood estimate (MLE) would be given by

$$\widehat{\boldsymbol{\theta}}_{\mathrm{MLE}} = \arg\max_{\boldsymbol{\theta}} p(\mathcal{D}|\boldsymbol{\theta}).$$

However, although we only need a single point estimate $\widehat{\boldsymbol{\theta}}$ for inference, it is always preferable to have access to the posterior $p(\boldsymbol{\theta}|\mathcal{D})$, e.g., to obtain confidence measures about our parameters, perform incremental parameter estimation, etc.

Example: Bayesian parameter estimation for (multivariate) Gaussians

To provide an in-depth example for Bayesian parameter estimation, we choose the case of (multivariate) Gaussians as provided by (Murphy, 2012). As a reminder, a Gaussian distribution over $\boldsymbol{X} = \{X_1, \dots, X_{n_{\boldsymbol{X}}}\}$, is parameterized by a set of parameters $\boldsymbol{\theta}_{\boldsymbol{X}} = \{\boldsymbol{\mu}_{\boldsymbol{X}}, \Sigma_{\boldsymbol{X}}\}$, comprised of a mean vector $\boldsymbol{\mu}_{\boldsymbol{X}} = \mathbb{E}[\boldsymbol{X}]$ and a $n_{\boldsymbol{X}} \times n_{\boldsymbol{X}}$ covariance matrix $\Sigma_{\boldsymbol{X}} = \mathrm{cov}[\boldsymbol{X}]$. In the univariate case, the parameters reduce to the mean μ_X and variance σ_X^2, $\boldsymbol{\theta}_X = \{\mu_X, \sigma_X^2\}$. To simplify the notion, we will drop the suffices $\boldsymbol{X}$ and X for the remainder of the example.

Prior distribution

Bayesian parameter estimation treats the parameters as random variables, and therefore these parameters themselves have a distribution. For the case of (multivariate) Gaussian distributions, it is common to use the normal inverse Wishart distribution (NIW) as a distribution over the parameters $\boldsymbol{\theta} = \{\boldsymbol{\mu}, \Sigma\}$, defined as:

$$p(\boldsymbol{\mu}, \Sigma) = p(\boldsymbol{\mu}|\Sigma)p(\Sigma) = \mathcal{N}\left(\boldsymbol{\mu} : \mathbf{m}_0, \frac{1}{k_0}\Sigma\right) \times \mathrm{IW}(\Sigma : \mathrm{S}_0, v_0) \triangleq \mathrm{NIW}(\boldsymbol{\mu}, \Sigma : \mathbf{m}_0, k_0, \mathrm{S}_0, v_0).$$

The NIW distribution itself is parametrized by a set of four parameters $\{\mathbf{m}_0, k_0, \mathrm{S}_0, v_0\}$, referred to as hyperparameters to distinguish them from the parameters $\boldsymbol{\theta} = \{\boldsymbol{\mu}, \Sigma\}$ of the Gaussian. The hyperparameters can be interpreted as follows (Murphy, 2012): $\mathbf{m}_0$ is the prior mean vector for $\boldsymbol{\mu}$, and k_0 is the strength of this prior; S_0 is a scatter matrix that is proportional to the prior mean for Σ, and v_0 is the strength of this prior.

To provide some additional insight into a (prior) NIW distribution, Figure 81 shows the density plot for an exemplary NIW distribution $\mathrm{NIW}(\mu, \sigma^2 : m_0 = 0, k_0 = 1, S_0 = 1, v_0 = 1)$[5] over the parameters $\boldsymbol{\theta} = \{\mu, \sigma^2\}$ of an univariate Gaussian, $p(X : \mu, \sigma^2)$. The solid red lines cross at the mode of the distribution $p\left(\hat{\mu}_{\mathrm{Mode}}, \hat{\sigma}^2_{\mathrm{Mode}}\right)$[6] and indicate $p(\hat{\mu}_{\mathrm{Mode}}, \sigma^2)$ and $p\left(\mu, \hat{\sigma}^2_{\mathrm{Mode}}\right)$. Although the mode is the most likely point estimate for the parameters, the distribution assigns high densities for a variety of point estimates, reflecting our prior uncertainty over which parameters to choose. The black projections show the marginal distributions $p(\sigma^2)$ and $p(\mu)$. The marginal $p(\sigma^2)$ is an inverse Wishart distribution, $p(\sigma^2) = \mathrm{IW}(\sigma^2 : S_0, v_0)$[7]. As apparent, the marginal has a slightly different mode (dotted black line) than the joint distribution (dotted red line). Due to the dependency of μ on σ^2, the

[5] In the univariate case, the vector $\mathbf{m}$ and matrix S are reduced to scalars.
[6] The mode of the distribution would represent the MAP estimate of the parameters.
[7] The univariate inverse Wishart reduces to an inverse Gamma distribution.

marginal $p(\mu)$ is no Gaussian, but a Student T distribution[8], $p(\mu) = \mathcal{T}\left(\mu : m, \frac{S}{k_0 v_0}, v_0\right)$, however with the same mode as the joint.

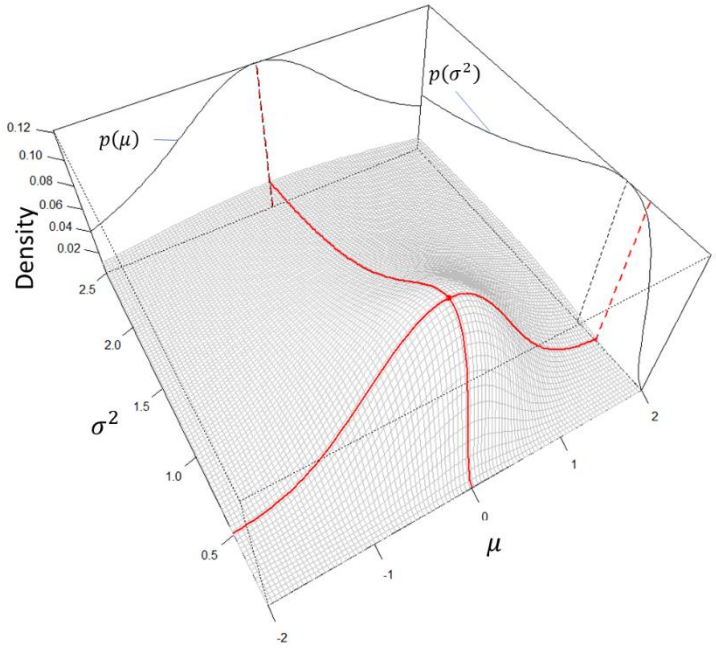

Figure 81: Example visualization of a (univariate) prior distribution $p(\mu, \sigma^2) = \mathrm{NIW}(\mu, \sigma^2 : m_0 = 0, k_0 = 1, S_0 = 1, v_0 = 1)$ over the parameters of a univariate Gaussian.

Posterior distribution

The choice of a NIW distribution for $\boldsymbol{\theta}$ is important in that the NIW distribution is conjugate to the Gaussian distribution, meaning that if we specify the prior distribution $p(\boldsymbol{\mu}, \Sigma)$ to be a NIW distribution, the posterior distribution

$$p(\boldsymbol{\mu}, \Sigma|\mathcal{D}) \propto p(\mathcal{D}|\boldsymbol{\mu}, \Sigma)\, p(\boldsymbol{\mu}, \Sigma)$$

will also be a NIW distribution. More specifically, $p(\boldsymbol{\mu}, \Sigma|\mathcal{D})$ is a NIW distribution with updated hyperparameters $\{\mathbf{m}_n, k_n, \mathrm{S}_n, v_n\}$:

$$p(\boldsymbol{\mu}, \Sigma|\mathcal{D}) = \mathrm{NIW}(\boldsymbol{\mu}, \Sigma : \mathbf{m}_n, k_n, \mathrm{S}_n, v_n).$$

Fortunately, there is a closed form solution to define the posterior hyperparameters $\{\mathbf{m}_n, k_n, \mathrm{S}_n, v_n\}$ of this posterior distribution, using the prior hyperparameters $\{\mathbf{m}_0, k_0, \mathrm{S}_0, v_0\}$ and a set of sufficient statistics $\{\overline{\mathbf{x}}, \mathrm{S}_{\mathbf{x}}\}$ to be derived from the dataset $\mathcal{D} = (\mathbf{x}^1, \ldots, \mathbf{x}^n)$, where $\overline{\mathbf{x}}$ denotes the empirical mean,

$$\overline{\mathbf{x}} = \frac{1}{n}\sum_{i=1}^{n} \mathbf{x}^i,$$

and $\mathrm{S}_{\mathbf{x}}$ denotes the empirical scatter matrix centered on $\overline{\mathbf{x}}$,

[8] The Student T distribution can be seen as an infinite mixture of Gaussians with different variances, $p(\mu_X) = \int \mathcal{N}\left(\mu_X \middle| m, \frac{1}{k}\sigma_X^2\right) \cdot \mathrm{IW}(\sigma_X^2 | S, v)\, \mathrm{d}\sigma = \mathcal{T}\left(\mu_X | m, \frac{S}{k(v - \mathrm{Dim} + 1)}, v - \mathrm{Dim} + 1\right)$.

$$\mathrm{S}_{\mathbf{x}} = \sum_{i=1}^{n} (\mathbf{x}^i - \overline{\mathbf{x}})(\mathbf{x}^i - \overline{\mathbf{x}})^T.$$

Given the prior hyperparameters $\{\mathbf{m}_0, k_0, \mathrm{S}_0, v_0\}$ and sufficient statistics $\{\overline{\mathbf{x}}, \mathrm{S}_{\mathbf{x}}\}$, we can calculate the hyperparameters of the posterior distribution $p(\boldsymbol{\mu}, \Sigma|\mathcal{D}) = \mathrm{NIW}(\boldsymbol{\mu}, \Sigma : \mathbf{m}_n, k_n, \mathrm{S}_n, v_n)$ using the following closed-form solution (Murphy, 2012):

$$\mathbf{m}_n = \frac{k_0}{k_0 + n}\mathbf{m}_0 + \frac{n}{k_0 + n}\overline{\mathbf{x}},$$

$$k_n = k_0 + n,$$

$$v_n = v_0 + n,$$

$$\mathrm{S}_n = \mathrm{S}_0 + \mathrm{S}_{\mathbf{x}} + \frac{k_0 n}{k_0 + n}(\overline{\mathbf{x}} - \mathbf{m}_0)(\overline{\mathbf{x}} - \mathbf{m}_0)^T.$$

To illustrate the difference between the prior and a hypothetical posterior distribution, Figure 82 shows the density plot of an exemplary posterior NIW distribution $p(\mu, \sigma^2|\mathcal{D}) = \mathrm{NIW}(\mu, \sigma^2 : m_n = 1, k_n = 100, \mathrm{S}_n = 50, v_n = 100)$ updated (using some hypothetical dataset $\mathcal{D}$ of size $n = 99$) from the prior NIW distribution $p(\mu, \sigma^2) = \mathrm{NIW}(\mu, \sigma^2 : m_0 = 0, k_0 = 1, \mathrm{S}_0 = 1, v_0 = 1)$ shown in Figure 81. Compared with the somehow vague prior distribution, the posterior distribution focusses most of the density mass on the mode, which consequently dominates all other point estimates.

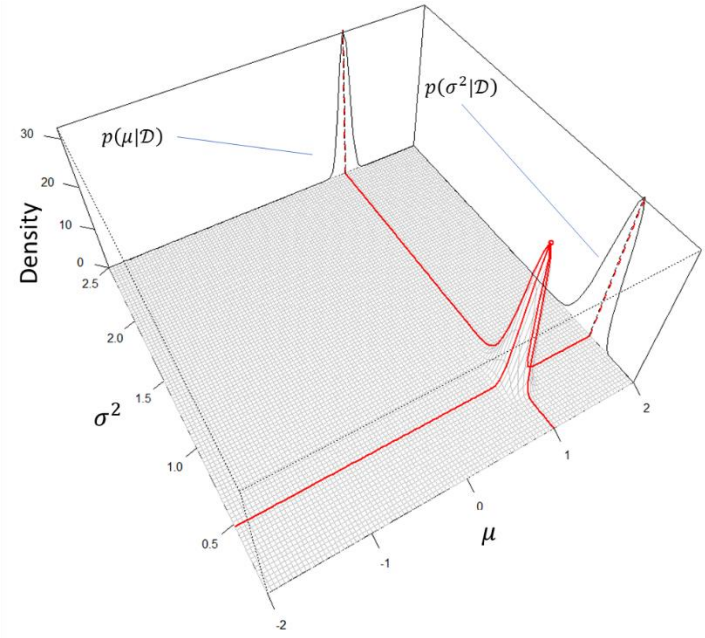

Figure 82: Example visualization of a (univariate) posterior distribution $p(\mu, \sigma^2|\mathcal{D}) = \mathrm{NIW}(\mu, \sigma^2 : m_n = 1, k_n = 100, S_n = 50, v_n = 100)$ over the parameters of a univariate Gaussian.

Point parameter estimates

Bayesian parameter estimation is completed with the inference of the posterior distribution over the parameters given the data, $p(\boldsymbol{\mu}, \Sigma|\mathcal{D})$. There are several method to utilize such a distribution for inference. The common approach is to select a single point estimate from the posterior distribution, e.g., the mean or the mode. The mode of the posterior distribution is also known as the Maximum a posteriori (MAP) parameter estimate.

In the case of a multivariate Gaussian distribution with NIW posterior distribution,

$$p(\boldsymbol{\mu}, \Sigma|\mathcal{D}) = \mathrm{NIW}(\boldsymbol{\mu}, \Sigma : \mathbf{m}_n, k_n, \mathrm{S}_n, v_n),$$

the MAP parameters are given by the mode of the distribution, defined as:

$$\boldsymbol{\theta}_{\boldsymbol{X}} = \{\widehat{\boldsymbol{\mu}}_{\mathrm{MAP}}, \widehat{\Sigma}_{\mathrm{MAP}}\} = \left\{\mathbf{m}_n, \frac{\mathrm{S}_n}{v_n + n_{\boldsymbol{X}} + 2}\right\}.$$

In the absence of data, the prior (MAP) parameters would be simply given by the mode of the prior distribution:

$$\{\widehat{\boldsymbol{\mu}}_{\mathrm{Prior}}, \widehat{\Sigma}_{\mathrm{Prior}}\} = \left\{\mathbf{m}_0, \frac{\mathrm{S}_0}{v_0 + n_{\boldsymbol{X}} + 2}\right\}.$$

We note that a more "Bayesian" approach would be to use the not decide on any singular parameter point estimate but instead to use the posterior predictive distribution:

$$p(\boldsymbol{X}|\mathcal{D}) = \int p(\boldsymbol{X}|\boldsymbol{\theta}_{\boldsymbol{X}}) p(\boldsymbol{\theta}|\mathcal{D}) d\boldsymbol{\theta}.$$

Given sufficient amount of data, the posterior predictive will rapidly approach the MAP estimate, which we use for DySAM in favor of the posterior predictive.

Bayesian parameter estimation of GMMs

Let $\boldsymbol{X} = \{X_1, \dots, X_{n_{\boldsymbol{X}}}\}$ be a set of continuous variables and $\mathcal{D} = \{\boldsymbol{x}^i\}_{i=1}^n$ be a dataset to be used to estimate the parameters $\boldsymbol{\theta}_{\boldsymbol{X}}$ of a GMM comprised of n_k Gaussian components,

$$p(\boldsymbol{x} : \boldsymbol{\theta}_{\boldsymbol{X}}) = \sum_{i=1}^{n_k} \pi_{\boldsymbol{X}_i} \mathcal{N}(\boldsymbol{\mu}_{\boldsymbol{X}_i}, \Sigma_{\boldsymbol{X}_i}),$$

i.e., we want to perform Bayesian parameter estimation to infer $p(\boldsymbol{\theta}_{\boldsymbol{X}} \mid \mathcal{D})$. Interpreting $p(\boldsymbol{x} : \boldsymbol{\theta}_{\boldsymbol{X}})$ as a generative model for $\mathcal{D}$, we can think each sample $\boldsymbol{x}^i$ to be generated by one of the n_k Gaussian components. Formally, we can encode the association of a sample $\boldsymbol{x}^i$ with one of the mixture components by using an assignment to a latent variable Z^i, $\mathrm{Val}(Z^i) = \{z_1^i, \dots, z_{n_k}^i\}$, such that $Z^i = z_j^i$ if $\boldsymbol{x}^i$ is generated by the j-th mixture components. Now consider a *complete* dataset $\mathcal{D}' = \{\boldsymbol{x}^i, z^i\}_{i=1}^n$ that provides both the samples and their association with one of the mixture components. Given $\mathcal{D}'$, the posterior $p(\boldsymbol{\theta}_{\boldsymbol{X}} \mid \mathcal{D}')$ would factorize into a product of independent factors that could be inferred independently,

$$p(\boldsymbol{\theta}_{\boldsymbol{X}} \mid \mathcal{D}') = p(\boldsymbol{\pi}_{\boldsymbol{X}} \mid \mathcal{D}') \prod_{i=1}^{n_k} p(\boldsymbol{\mu}_{\boldsymbol{X}_i}, \Sigma_{\boldsymbol{X}_i} \mid \mathcal{D}'),$$

where $p(\boldsymbol{\pi}_{\boldsymbol{X}} \mid \mathcal{D}')$ corresponds to Bayesian parameter estimation for categorical distributions and $p(\boldsymbol{\mu}_{\boldsymbol{X}_i}, \Sigma_{\boldsymbol{X}_i} \mid \mathcal{D}')$ corresponds to Bayesian parameter estimation for multivariate Gaussians. Unfortunately, we do not have access to the complete dataset $\mathcal{D}'$ but only to the incomplete dataset $\mathcal{D}$. We can think of the missing annotations $z^{1:n}$ as the unknown assignments of a set of additional hidden variables $Z^{1:n}$, that have to be estimated.

As such, the true goal is to infer $p(\boldsymbol{\theta}_{\boldsymbol{X}}, Z^{1:n}|\mathcal{D})$. For this, we rely on a technique called variational Bayes Expectation Maximization (VBEM). The details of VBEM would go beyond the scope of this report, so

we refer to (Murphy, 2012) and (Bishop, 2006) for additional information and only provide the general idea. We will once again drop the subscript $\boldsymbol{X}$ in the following.

For VBEM of GMMs, we use a factored prior of the form

$$p(\boldsymbol{\theta}) = \mathrm{Dir}(\boldsymbol{\pi}|\alpha_0)\prod_{i=1}^{n_X}\mathcal{N}\left(\boldsymbol{\mu}_i : \mathbf{m}_0, \frac{1}{k_0}\Sigma\right)\mathrm{Wi}\left(\Sigma_i^{-1}|\mathrm{L}_0, v_0\right),$$

where $\mathrm{Wi}(\cdot)$ denotes the (non-inverse) Wishart distribution, as an alternative to the NIW prior used for the multivariate Gaussian. Unfortunately, the exact posterior

$$p(\boldsymbol{\theta}|\mathcal{D}) = \sum_{z^1\in\mathrm{Val}(Z^1)}\sum_{z^2\in\mathrm{Val}(Z^2)}\dots\sum_{z^n\in\mathrm{Val}(Z^n)}p(\boldsymbol{\theta}, z^{1:n}|\mathcal{D})$$

is an highly complex mixture distribution that cannot be reasonably solved analytically. VBEM makes the problem tractable by applying a mean field approximating to $p(\boldsymbol{\theta}, Z^{1:n}|\mathcal{D})$, resulting in:

$$p(\boldsymbol{\theta}, Z^{1:n}|\mathcal{D}) \approx q(\boldsymbol{\pi}|\mathcal{D})\prod_{i=1}^{n_k}q\left(\boldsymbol{\mu}_i, \Sigma_i^{-1}|\mathcal{D}\right)\prod_{i=1}^{n}q\left(Z^i|\mathcal{D}\right).$$

The idea is then to apply the Expectation-Maximization (EM)-algorithm by alternating between a (variational) Expectation (E)-step and a (variational) Maximization (M)-step.

In essence, during the variational E-step, we will derive the posterior mean parameters from $q(\boldsymbol{\pi}|\mathcal{D})\prod_{i=1}^{n}q\left(\boldsymbol{\mu}_i, \Sigma_i^{-1}|\mathcal{D}\right)$ and use them to infer an updated estimate for the unknown labels, $z^{1:n}$. During the variational M-step, we then use these estimates to derive a new estimate for the parameters $\boldsymbol{\theta}$. The process is repeated until convergence.

An advantage of VBEM for GMMs is that it is sparsity-inducing: We can start with a maximum number of components we're willing to accept and the VBEM will automatically remove unnecessary components. For the DySAM models, we use a maximum number of components of $n_k = 10$.

1.6 Generative and discriminative structure learning

Let $\mathcal{B} = \langle\mathcal{G}, \boldsymbol{\theta}\rangle$ be a BN over a set of n variables $\boldsymbol{X} = \{X_1, \dots, X_n\}$ and let $\mathcal{D} = \left\{\boldsymbol{x}^i\right\}_{i=1}^{m}$ denote a set of m complete training samples (i.e. no missing values). Just as parameter estimation can be used to estimate the parameters $\boldsymbol{\theta}$ of a BN from data, the goal of structure learning is to estimate a suitable graph structure $\mathcal{G}$ from data. As the space of possible graph structures $\boldsymbol{\mathcal{G}}$ grows super-exponentially with the number of variables n, it is common to follow a local score and search paradigm, where a local heuristic search in the space of possible graph structures $\boldsymbol{\mathcal{G}}$ is guided by a scoring function $\mathrm{Score}(\mathcal{G} : \mathcal{D})$ that evaluates the degree of fitness between the structure $\mathcal{G}$ and training data $\mathcal{D}$ (Koller, Murphy). From a Bayesian perspective, the most natural scoring criterion is the so-called *Bayesian score* (Koller), the probability of a structure $\mathcal{G}$ given the available data $\mathcal{D}$:

$$p(\mathcal{G}|\mathcal{D}) = \frac{p(\mathcal{G}, \mathcal{D})}{p(\mathcal{D})} \propto p(\mathcal{G})p(\mathcal{D}|\mathcal{G}).$$

Here, $p(\mathcal{G})$ is the prior probability for $\mathcal{G}$, usually chosen to be non-informative, $p(\mathcal{G}) \propto 1$, and therefore ignored, while $p(\mathcal{D}|\mathcal{G})$ is the *marginal* likelihood of the data given the graph structure, as it involves an integration over all possible parameters $\boldsymbol{\theta}$:

$$p(\mathcal{D}|\mathcal{G}) = \int p(\mathcal{D}|\boldsymbol{\theta}, \mathcal{G}) p(\boldsymbol{\theta}|\mathcal{G})\, d\boldsymbol{\theta},$$

where the term $p(\boldsymbol{\theta}|\mathcal{G})$ is the prior over the parameters given the graph structure and $p(\mathcal{D}|\boldsymbol{\theta}, \mathcal{G})$ is the likelihood of the data given the parameters and graph structure:

$$p(\mathcal{D}|\boldsymbol{\theta}, \mathcal{G}) = \prod_{i=1}^{m} p\left(x_1^i, \dots, x_n^i : \boldsymbol{\theta}\right),$$

with $p\left(x_1^i, \dots, x_n^i : \boldsymbol{\theta}\right)$ factorizing according to $\mathcal{G}$. As, depending on the underlying model, no closed form solution for $p(\mathcal{D}|\mathcal{G})$ may be available, it is common to use an approximation known as the *Bayesian Information Criterion* (BIC) (Koller, Schwartz, Murphy). Let $\widehat{\boldsymbol{\theta}}$ denote the MLE of the model parameters and $\left|\widehat{\boldsymbol{\theta}}\right|$ denote the number of independent parameters of the model, the BIC score for a structure $\mathcal{G}$ is commonly defined as

$$\mathrm{BIC}(\mathcal{G} : \mathcal{D}) = \log p\left(\mathcal{D} : \widehat{\boldsymbol{\theta}}\right) - \frac{\left|\widehat{\boldsymbol{\theta}}\right|}{2} \log m,$$

where $\log p\left(\mathcal{D} : \widehat{\boldsymbol{\theta}}\right) = \sum_{i=1}^{m} \log p\left(x_1^i, \dots, x_n^i : \widehat{\boldsymbol{\theta}}\right)$, factorizing according to $\mathcal{G}$, is the *joint* log-likelihood of the data, and $\frac{\left|\widehat{\theta}\right|}{2} \log m$ is a penalty term that grows with the complexity of the model. Structure learning with the BIC then equates to finding a structure $\mathcal{G}$ that maximizes the joint log-likelihood while minimizing the number of independent parameters.

Structure learning aimed at maximizing the joint (log-)likelihood is commonly referred to as *generative* training (Koller, Murphy). Generative training has many advantages, most notably the fact that the joint (log-)likelihood is decomposable into independently maximizable factors, which dramatically reduces the computational overhead of evaluating different graph structure (Koller). However, for models indicated for specific classification purpose, as in DySAM, generative training can lead to sub-optimal performance, since it aims at finding an optimal structure over all variables instead of trying to find a structure that allows for optimal classification (Pernkopf & Bilmes, 2005).

An alternative reported to yield better results for structure learning of models with a dedicated purpose is *discriminative* training, which aims at finding a structure and/or parameters that maximize a conditional (log-)likelihood corresponding to the intended utilization of the model (Koller, Murphy, Pernkopf). E.g., assume that the BN $\mathcal{B}$ shall be utilized to infer $p(X_1|x_2, \dots, x_n)$, i.e., the probability distribution over X_1 given the evidence over all other variables in the network. In discriminative training, we would choose a scoring criterion that maximizes the conditional log-likelihood $\sum_{i=1}^{m} \log p\left(x_1^i | x_2^i, \dots, x_n^i\right)$ instead of the joint log-likelihood $\sum_{i=1}^{m} \log p\left(x_1^i, \dots, x_n^i\right)$. Replacing the joint log-likelihood in the BIC results in a discriminative variant of the BIC (Guo) (Natarajan, Wong, & Tadepalli, 2006), we refer to as the *discriminative BIC* (DBIC). For the current example, the DBIC would be given by

$$\mathrm{DBIC}(\mathcal{G}:\mathcal{D}) = \sum_{i=1}^{m} \log p\left(x_1^i | x_2^i, \dots, x_n^i : \widehat{\boldsymbol{\theta}}\right) - \frac{|\widehat{\boldsymbol{\theta}}|}{2} \log m.$$

In addition to a score to assess the goodness of fit between a graph structure $\mathcal{G}$ and the training data $\mathcal{D}$, structure learning requires a *search procedure* to traverse the search space of all possible graph structures $\boldsymbol{\mathcal{G}}$. A search procedure is a procedure that, starting from one graph structure, explores the search space in attempt to find a high-scoring graph structure. Given a "current" graph structure, the search procedure derives a set of graph structures that are similar or "neighbors" to the current one. These structures are generated by a set of *search operators*, each of which takes a structure and makes a small modification to it. The search procedure selects one of these neighbors and makes it the current structure. As such, the search procedure can be thought of as moving around in the search space by taking small steps. We can visualize the search space as a directed (but not necessarily acyclic graph), whose nodes are the potential graph structures and whose edges are the search operators that the search procedure can perform to move between the different graph structures (c.f. Figure 83).

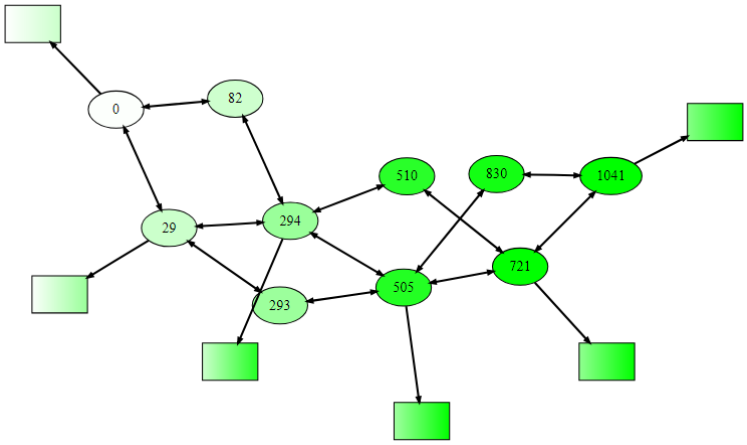

Figure 83: Exemplary visualization of the currently explored search space with elliptical nodes representing graph structures and edges representing graph manipulations. The number indicate the ID of the candidate graph structure, whose scores are color-coded (white = worse score, green = best score). To avoid clutter, rectangular nodes summarize "dead end" solutions that could not improve the score and have not been explored further.

A crucial design choice that has large impact on the success of the heuristic search is the interconnectivity of the search space: "If each state has few neighbours, then the search procedure has to consider only a few options at each point of the search. Thus, it can afford to evaluate each of these options. However, this comes at a price. Paths from the initial solution to a good one might be long and complex. On the other hand, if each state has many neighbours, we may be able to move quickly from the initial state to a good state, but it may be difficult to determine which step to take at each point in the search." (Koller & Friedman, 2009, p. 812). Koller and Friedman (2009) propose to define the connectivity of the search space in terms of atomic *edge additions*, *deletions*, and *reversals*, such that the neighborhood of a graph structure is given by the set of structures in which we changed exactly one edge, either by adding one, deleting one, or reversing the orientation of one. This is a very natural set of search operators for generative structure learning, where each (valid) edge manipulation results in a usually new factorization of $p(X_1, \dots, X_n)$, with an usually new score.

In contrast, for discriminative structure learning of BNs, we only need to consider edge manipulations that result in changes to the structure that actually affect the inference result, in the current example

$p(X_1|x_2 \ldots, x_n)$. This greatly reduces the interconnectivity of the search space, with the advantages and disadvantages mentioned above. For DySAM, we therefore currently use a slightly different set of search operators, better fitted for discriminative learning, in that we allow each search operator to be comprised of multiple edge additions and removals. The increase in search operators counterbalances the reduced interconnectivity allowing for a more meaningful traversal of the search space.

The actual search procedure used for structure learning in DySAM is a beam-search variant of the common *greedy hill-climbing* procedure (Koller), in which we perform K (called the beam width) searches simultaneously (the pseudo-code is provided in Table 23): We initialize the search with some initial solution $\mathcal{G}_0$. We then repeatedly consider all the solutions that are neighbors of the current K highest-scoring structures, compute their score, and select the K structures with the highest improvement for the next iteration. The process is repeated until the score cannot be improved any longer and the highest-scoring of the current K highest-scoring structures is returned.

Table 23: Pseudo-code implementation of the beam search learning procedure.

Procedure Learn-Structure-via-Beam-Search (
$\mathcal{G}_0$, // Initial graph structure
Score, // Scoring function
$\mathcal{D}$, // Fully observed dataset
K // Beam width
)
1: $\boldsymbol{\mathcal{G}}_{\text{Beam}} \leftarrow \{\mathcal{G}_0\}$ // Use the initial graph structure to initialize the beam set
2: $\mathcal{G}_{\text{best}} \leftarrow \mathcal{G}_0$ // Initialize the best graph structure with $\mathcal{G}_0$
3: $improved \leftarrow true$
4: **while**($improved$) **{** // Repeat the learning process until the score can't be improved any longer
5: $\boldsymbol{\mathcal{G}}_{\text{hyp}} \leftarrow \boldsymbol{\mathcal{G}}_{\text{Beam}}$ // Initialize the set of hypothetical graph structures with the beam set
6: **for each** $\mathcal{G} \in \boldsymbol{\mathcal{G}}_{\text{Beam}}$ **do {** // Go through all structures in the beam set
7: $\boldsymbol{\mathcal{G}}_{\text{hyp}} \leftarrow \boldsymbol{\mathcal{G}}_{\text{hyp}} \cup \text{neighbours}(\mathcal{G})$ // Derive a set of adjacent graph structures of $\mathcal{G}$ in the search space
8: **}**
9: $\boldsymbol{\mathcal{G}}_{\text{Beam}} \leftarrow \text{K-Best}(\text{Score}, \boldsymbol{\mathcal{G}}_{hyp}, K, \mathcal{D})$ // Score all graph structures in $\boldsymbol{G}_{hyp}$ on D and return the K individual structures with the highest scores
10: **if** $\exists \mathcal{G} \in \boldsymbol{\mathcal{G}}_{\text{Beam}} : \text{Score}(\mathcal{G}:\mathcal{D}) > \text{Score}(\mathcal{G}_{\text{best}} : \mathcal{D})$ **{** // Evaluate, whether any hypothetical graph structure $\mathcal{G}$ in the beam improves the score compared to the score of $\mathcal{G}_{\text{best}}$
11: $\mathcal{G}_{\text{best}} \leftarrow \max_{\mathcal{G} \in \boldsymbol{\mathcal{G}}_{\text{Beam}}} \text{Score}(\mathcal{G} : \mathcal{D})$ // Use the graph with the highest score as the new best graph-structure
12: $improved \leftarrow true$ // We have an overall improvement of the score
13: **}**
14: **else {**
15: $improved \leftarrow$ false // We have no overall improvement of the score
16: **}**
17: **}**
18: **return** $\mathcal{G}_{\text{best}}$ // Return the best graph structure

Appendix 2 Model parameterization

The following sections will provide the MAP parameters used for each distribution of each model.

2.1 Parameters of the SAE Level 2 NDRT Model

For any number of time slices $T \geq 1$, the SAE Level 2 NDRT model defines the JPD

$$p\left(S_1^{1:T}, B^{1:T}, \boldsymbol{F}_{\text{Rel}}^{1:T} : \boldsymbol{\theta}\right) = p(B^1 : \boldsymbol{\theta}_{B^1}) \prod_{t=2}^{T} p\left(B^t | B^{t-1} : \boldsymbol{\theta}_{B^t|B^{t-1}}\right) \prod_{t=1}^{T} p\left(S_1^t | B^t : \boldsymbol{\theta}_{S_1^t|B^t}\right) p\left(\boldsymbol{F}_{\text{Rel}}^t | B^t : \boldsymbol{\theta}\right),$$

with $p\left(\boldsymbol{F}_{\text{Rel}}^t \mid B^t : \boldsymbol{\theta}\right)$ factorizing as

$$p\left(F_1^t | B^t : \boldsymbol{\theta}_{F_1^t|B^t}\right) p\left(F_{23}^t | B^t : \boldsymbol{\theta}_{F_{23}^t|B^t}\right)$$

$$p\left(F_9^t, F_{29}^t, F_{32}^t, F_{58}^t, F_{48}^t, F_{43}^t, F_{12}^t, F_{18}^t, F_{21}^t, F_{22}^t | B^t : \boldsymbol{\theta}_{F_9^t,\ldots,F_{22}^t|B^t}\right).$$

As such, the model is defined by six probability /density distribution to be detailed in the following. The names of the relevant indicators $\boldsymbol{F}_{\text{Rel}} = \{F_1, F_9, F_{12}, F_{18}, F_{21}, F_{22}, F_{23}, F_{29}, F_{32}, F_{43}, F_{48}, F_{58}\}$ are provided in Table 24.

Table 24: The set of relevant indicators for the SAE Level 2 NDRT model, $\boldsymbol{F}_{\text{Rel}} = \{F_1, F_9, F_{12}, F_{18}, F_{21}, F_{22}, F_{23}, F_{29}, F_{32}, F_{43}, F_{48}, F_{58}\}$.

Symbol	Name
F_1	Pupil diameter valid
F_9	Mean blink frequency
F_{12}	Mean yaw angle of the head
F_{18}	Mean gaze heading
F_{21}	Mean gaze pitch
F_{22}	Gaze pitch variability
F_{23}	Hands-on steering wheel
F_{29}	Mean monitoring frequency
F_{32}	Mean saccade frequency
F_{43}	Mean time since last look at right mirror AOI
F_{48}	Mean time since last look at rear mirror AOI
F_{58}	Mean time since last look at infotainment AOI

Distribution $p(B^1 : \boldsymbol{\theta}_{B^1})$

The distribution $p(B^1 : \boldsymbol{\theta}_{B^1})$ is a categorical distribution

$$p(B^1 : \boldsymbol{\theta}_{B^1}) = \text{Cat}(B^1 : \boldsymbol{\theta}_{B^1})$$

over the discrete variable B, $\text{Val}(B) = \{b_0, b_1, b_2\}$ at time slice $t = 1$, with MAP parameters

$$\boldsymbol{\theta}_{B^1} = \left\{\theta_{b_0^1}, \theta_{b_1^1}, \theta_{b_2^1}\right\} = \{0.324644, 0.324213, 0.351143\}.$$

Distribution $p\left(B^t | B^{t-1} : \boldsymbol{\theta}_{B^t|B^{t-1}}\right)$

The distribution $p\left(B^t|B^{t-1}:\boldsymbol{\theta}_{B^t|B^{t-1}}\right)$ over the discrete variable B, $\mathrm{Val}(B)=\{b_0,b_1,b_2\}$ at time slice $t>1$ is a collection of categorical distributions with a categorical distribution

$$p\left(B^t|b^{t-1}:\boldsymbol{\theta}_{B^t|b^{t-1}}\right)=\mathrm{Cat}\left(B^t:\boldsymbol{\theta}_{B^t|b^{t-1}}\right)$$

for each $b^{t-1}\in\mathrm{Val}(B)$, parameterized with MAP parameters $\boldsymbol{\theta}_{B^t|B^{t-1}}=\left\{\boldsymbol{\theta}_{B^t|b_0^{t-1}},\boldsymbol{\theta}_{B^t|b_1^{t-1}},\boldsymbol{\theta}_{B^t|b_2^{t-1}}\right\}$, where

$$\boldsymbol{\theta}_{B^t|b_0^{t-1}}=\left\{\theta_{b_0^t|b_0^{t-1}},\theta_{b_1^t|b_0^{t-1}},\theta_{b_2^t|b_0^{t-1}}\right\}=\{0.999358,0.000321,0.000321\},$$

$$\boldsymbol{\theta}_{B^t|b_1^{t-1}}=\left\{\theta_{b_0^t|b_1^{t-1}},\theta_{b_1^t|b_1^{t-1}},\theta_{b_2^t|b_1^{t-1}}\right\}=\{0.000321,0.999357,0.000321\},$$

$$\boldsymbol{\theta}_{B^t|b_2^{t-1}}=\left\{\theta_{b_0^t|b_2^{t-1}},\theta_{b_1^t|b_2^{t-1}},\theta_{b_2^t|b_2^{t-1}}\right\}=\{0.000297,0.000297,0.999406\}.$$

Distribution $p\left(S_1^t|B^t:\boldsymbol{\theta}_{S_1^t|B^t}\right)$

The distribution $p\left(S_1^t|B^t:\boldsymbol{\theta}_{S_1^t|B^t}\right)$ over the binary variable S_1, $\mathrm{Val}(S_1)=\{s_{1_0},s_{1_1}\}$ at time slice $t\geq 1$ is a collection of categorical distributions with a categorical distribution

$$p\left(S_1^t:b^t,\boldsymbol{\theta}_{S_1^t|b^t}\right)=\mathrm{Cat}\left(S_1^t:\boldsymbol{\theta}_{S_1^t|b^t}\right)$$

for each $b^t\in\mathrm{Val}(B)$, parameterized with MAP parameters $\boldsymbol{\theta}_{S_1^t|B^t}=\left\{\boldsymbol{\theta}_{S_1^t|b_0^t},\boldsymbol{\theta}_{S_1^t|b_1^t},\boldsymbol{\theta}_{S_1^t|b_2^t}\right\}$, where

$$\boldsymbol{\theta}_{S_1^t|b_0^t}=\left\{\theta_{s_{1_0}^t|b_0^t},\theta_{s_{1_1}^t|b_0^t}\right\}=\{0.000492,0.999508\},$$

$$\boldsymbol{\theta}_{S_1^t|b_1^t}=\left\{\theta_{s_{1_0}^t|b_1^t},\theta_{s_{1_1}^t|b_1^t}\right\}=\{0.999507,0.000493\},$$

$$\boldsymbol{\theta}_{S_1^t|b_2^t}=\left\{\theta_{s_{1_0}^t|b_2^t},\theta_{s_{1_1}^t|b_2^t}\right\}=\{0.999545,0.000455\}.$$

Distribution $p\left(F_1^t|B^t,\boldsymbol{\theta}_{F_1^t|B^t}\right)$

The distribution $p\left(F_1^t|B^t,\boldsymbol{\theta}_{F_1^t|B^t}\right)$ over the binary variable F_1, $\mathrm{Val}(F_1)=\{f_{1_0},f_{1_1}\}$ at time slice $t\geq 1$ is a collection of categorical distributions with a categorical distribution

$$p\left(F_1^t|b^t:\boldsymbol{\theta}_{F_1^t|b^t}\right)=\mathrm{Cat}\left(F_1^t:\boldsymbol{\theta}_{F_1^t|b^t}\right)$$

for each $b^t\in\mathrm{Val}(B)$, parameterized with MAP parameters $\boldsymbol{\theta}_{F_1^t|B^t}=\left\{\boldsymbol{\theta}_{F_1^t|b_0^t},\boldsymbol{\theta}_{F_1^t|b_1^t},\boldsymbol{\theta}_{F_1^t|b_2^t}\right\}$, where

$$\boldsymbol{\theta}_{F_1^t|b_0^t}=\left\{\theta_{f_{1_0}^t|b_0^t},\theta_{f_{1_1}^t|b_0^t}\right\}=\{0.002754,0.997246\},$$

$$\boldsymbol{\theta}_{F_1^t|b_1^t}=\left\{\theta_{f_{1_0}^t|b_1^t},\theta_{f_{1_1}^t|b_1^t}\right\}=\{0.004587,0.995413\},$$

$$\boldsymbol{\theta}_{F_1^t|b_2^t}=\left\{\theta_{f_{1_0}^t|b_2^t},\theta_{f_{1_1}^t|b_2^t}\right\}=\{0.032536,0.967464\}.$$

Distribution $p\left(F_{23}^t|B^t:\boldsymbol{\theta}_{F_1^t|B^t}\right)$

The distribution $p\left(F_{23}^t|B^t : \boldsymbol{\theta}_{F_1^t|B^t}\right)$ over the binary variable F_{23}, $\mathrm{Val}(F_{23}) = \{f_{23_0}, f_{23_1}\}$ at time slice $t \geq 1$ is a collection of categorical distributions with a categorical distribution

$$p\left(F_{23}^t|b^t : \boldsymbol{\theta}_{F_{23}^t|b^t}\right) = \mathrm{Cat}\left(F_{23}^t : \boldsymbol{\theta}_{F_{23}^t|b^t}\right)$$

for each $b^t \in \mathrm{Val}(B)$, parameterized with MAP parameters $\boldsymbol{\theta}_{F_{23}^t|B^t} = \left\{\boldsymbol{\theta}_{F_{23}^t|b_0^t}, \boldsymbol{\theta}_{F_{23}^t|b_1^t}, \boldsymbol{\theta}_{F_{23}^t|b_2^t}\right\}$, where

$$\boldsymbol{\theta}_{F_{23}^t|b_0^t} = \left\{\theta_{f_{23_0}^t|b_0^t}, \theta_{f_{23_1}^t|b_0^t}\right\} = \{0.005203, 0.994797\},$$

$$\boldsymbol{\theta}_{F_{23}^t|b_1^t} = \left\{\theta_{f_{23_0}^t|b_1^t}, \theta_{f_{23_1}^t|b_1^t}\right\} = \{0.058368, 0.941632\},$$

$$\boldsymbol{\theta}_{F_{23}^t|b_2^t} = \left\{\theta_{f_{23_0}^t|b_2^t}, \theta_{f_{23_1}^t|b_2^t}\right\} = \{0.135976, 0.864024\}.$$

Distribution $p\left(F_9^t, F_{29}^t, F_{32}^t, F_{58}^t, F_{48}^t, F_{43}^t, F_{12}^t, F_{18}^t, F_{21}^t, F_{22}^t|B^t : \boldsymbol{\theta}_{F_9^t,\ldots,F_{22}^t|B^t}\right)$

The distribution $p\left(F_9^t, F_{29}^t, F_{32}^t, F_{58}^t, F_{48}^t, F_{43}^t, F_{12}^t, F_{18}^t, F_{21}^t, F_{22}^t|B^t : \boldsymbol{\theta}_{F_9^t,\ldots,F_{22}^t|B^t}\right)$ over a ten-dimensional vector of continuous variables $(F_9, F_{29}, F_{32}, F_{58}, F_{48}, F_{43}, F_{12}, F_{18}, F_{21}, F_{22})$ at time slice $t \geq 1$ is a collection of multivariate Gaussian mixture distributions with a multivariate GMM

$$p\left(F_9^t, F_{29}^t, F_{32}^t, F_{58}^t, F_{48}^t, F_{43}^t, F_{12}^t, F_{18}^t, F_{21}^t, F_{22}^t|b^t : \boldsymbol{\theta}_{F_9^t,\ldots,F_{22}^t|b^t}\right) = \sum_{i=1}^{n_b} \pi_{b^t{}_i} \mathcal{N}\left(\boldsymbol{\mu}_{b^t{}_i}, \Sigma_{b^t{}_i}\right)$$

composed of n_b components for each $b^t \in \mathrm{Val}(B)$, parameterized with MAP parameters $\boldsymbol{\theta}_{F_9^t,\ldots,F_{22}^t|B^t} = \left\{\boldsymbol{\theta}_{F_9^t,\ldots,F_{22}^t|b_0^t}, \boldsymbol{\theta}_{F_9^t,\ldots,F_{22}^t|b_1^t}, \boldsymbol{\theta}_{F_9^t,\ldots,F_{22}^t|b_2^t}\right\}$.

The distribution

$$p\left(F_9^t, F_{29}^t, F_{32}^t, F_{58}^t, F_{48}^t, F_{43}^t, F_{12}^t, F_{18}^t, F_{21}^t, F_{22}^t|b_0^t : \boldsymbol{\theta}_{F_9^t,\ldots,F_{22}^t|b_0^t} = \left\{\left\{\pi_{b_0^t{}_i}, \boldsymbol{\mu}_{b_0^t{}_i}, \Sigma_{b_0^t{}_i}\right\}_{i=1}^{6}\right\}\right)$$

consists of six components, where

$$\pi_{b_0^t{}_1} = 0.010657, \pi_{b_0^t{}_2} = 0.075461, \pi_{b_0^t{}_3} = 0.095207,$$

$$\pi_{b_0^t{}_4} = 0.532933, \pi_{b_0^t{}_5} = 0.284807, \pi_{b_0^t{}_6} = 0.000935,$$

$$\boldsymbol{\mu}_{b_0^t{}_1} = \begin{pmatrix} 0.464910 \\ 0.452272 \\ 1.716468 \\ 88.416617 \\ 105.170067 \\ 212.806472 \\ 0.050879 \\ -0.036855 \\ -0.112307 \\ 0.148282 \end{pmatrix}, \boldsymbol{\mu}_{b_0^t{}_2} = \begin{pmatrix} 0.493630 \\ 0.588150 \\ 1.841275 \\ 80.715528 \\ 10.748530 \\ 521.325653 \\ 0.188972 \\ 0.196200 \\ -0.139233 \\ 0.107972 \end{pmatrix}, \boldsymbol{\mu}_{b_0^t{}_3} = \begin{pmatrix} 0.665674 \\ 0.155297 \\ 1.646815 \\ 156.488420 \\ 50.457821 \\ 382.635128 \\ 0.105790 \\ 0.037464 \\ -0.083028 \\ 0.058732 \end{pmatrix},$$

$$\boldsymbol{\mu}_{b_{0_4}^t} = \begin{pmatrix} 0.407820 \\ 0.623915 \\ 1.411906 \\ 73.540547 \\ 6.228482 \\ 88.029871 \\ 0.062682 \\ 0.013080 \\ -0.120141 \\ 0.107307 \end{pmatrix}, \boldsymbol{\mu}_{b_{0_5}^t} = \begin{pmatrix} 0.434232 \\ 0.343784 \\ 1.230431 \\ 35.664319 \\ 18.570101 \\ 381.476372 \\ 0.080316 \\ -0.000810 \\ -0.101096 \\ 0.084889 \end{pmatrix}, \boldsymbol{\mu}_{b_{0_6}^t} = \begin{pmatrix} 0.243788 \\ 13.348888 \\ 1.685575 \\ 17.725819 \\ 17.725819 \\ 65.831887 \\ -0.095144 \\ -0.177381 \\ -0.211792 \\ 0.140121 \end{pmatrix},$$

$$\Sigma_{b_{0_1}^t} = \begin{bmatrix} 0.101395 & -0.030582 & -0.030420 & 12.065302 & 12.874710 & 18.012518 & -0.003221 & 0.001787 & -0.003407 & -0.012685 \\ -0.030582 & 0.146514 & 0.102074 & -21.332288 & -24.888897 & -42.851187 & -0.007503 & -0.031016 & -0.008857 & 0.018785 \\ -0.030420 & 0.102074 & 0.320866 & -32.007662 & -40.035101 & -52.551519 & -0.027915 & -0.069619 & -0.005712 & 0.019409 \\ 12.065302 & -21.332288 & -32.007662 & 12988.213871 & 10015.235072 & 15283.205922 & 0.936175 & 5.193772 & 1.774361 & -7.367564 \\ 12.874710 & -24.888897 & -40.035101 & 10015.235072 & 15127.973878 & 16097.544722 & 2.423651 & 8.457445 & 1.427744 & -8.062354 \\ 18.012518 & -42.851187 & -52.551519 & 15283.205922 & 16097.544722 & 40323.148654 & 0.719644 & 8.056554 & 4.684907 & -12.551466 \\ -0.003221 & -0.007503 & -0.027915 & 0.936175 & 2.423651 & 0.719644 & 0.019813 & 0.015350 & 0.000918 & 0.002001 \\ 0.001787 & -0.031016 & -0.069619 & 5.193772 & 8.457445 & 8.056554 & 0.015350 & 0.051533 & 0.001030 & 0.000167 \\ -0.003407 & -0.008857 & -0.005712 & 1.774361 & 1.427744 & 4.68491 & 0.000918 & 0.001030 & 0.016176 & 0.002779 \\ -0.012685 & 0.018785 & 0.019409 & -7.367564 & -8.062354 & -12.551466 & 0.002001 & 0.000167 & 0.002779 & 0.013681 \end{bmatrix},$$

$$\Sigma_{b_{0_2}^t} = \begin{bmatrix} 0.07483 & 0.000843 & 0.026974 & 1.675446 & -0.595647 & 4.973664 & -0.011556 & -0.027065 & 0.005905 & 0.003274 \\ 0.000843 & 0.093515 & -0.003583 & -2.815946 & -1.225973 & -16.242744 & 0.002215 & 0.008085 & -0.009796 & 0.004741 \\ 0.026974 & -0.003583 & 0.102362 & -1.073699 & -0.591993 & 2.264475 & -0.015296 & -0.026557 & 0.007235 & -0.001781 \\ 1.675446 & -2.815946 & -1.073699 & 2675.06846 & -18.630811 & 19.289762 & -1.776246 & -2.879728 & 0.352 & 0.120931 \\ -0.595647 & -1.225973 & -0.591993 & -18.630811 & 624.219828 & 278.653954 & 0.394386 & 0.618953 & -0.092046 & -0.11357 \\ 4.973664 & -16.242744 & 2.264475 & 19.289762 & 278.653954 & 10760.37288 & 0.90811 & -0.802583 & 2.948077 & -1.216016 \\ -0.011556 & 0.002215 & -0.015296 & -1.776246 & 0.394386 & 0.90811 & 0.018682 & 0.023655 & -0.00493 & -0.000252 \\ -0.027065 & 0.008085 & -0.026557 & -2.879728 & 0.618953 & -0.802583 & 0.023655 & 0.044954 & -0.008893 & -0.001363 \\ 0.005905 & -0.009796 & 0.007235 & 0.352 & -0.092046 & 2.94807 & -0.00493 & -0.008893 & 0.006098 & -0.001025 \\ 0.003274 & 0.004741 & -0.001781 & 0.120931 & -0.11357 & -1.216016 & -0.000252 & -0.001363 & -0.001025 & 0.001733 \end{bmatrix},$$

$$\Sigma_{b_{0_3}^t} = \begin{bmatrix} 0.069074 & -0.003071 & 0.065782 & -2.995375 & -0.592999 & -6.581665 & 0.001541 & -0.000289 & 0.001055 & -0.001102 \\ -0.003071 & 0.025238 & 0.016835 & 2.814376 & -3.13268 & 1.201293 & -0.0003 & 0.000152 & 0.000006 & 0.002174 \\ 0.065782 & 0.016835 & 0.229415 & 1.2853 & -4.320678 & -18.966361 & 0.002197 & 0.008692 & 0.000719 & -0.000395 \\ -2.995375 & 2.814376 & 1.2853 & 5790.685986 & -1715.435199 & -1963.042308 & 0.413263 & -0.984919 & 0.462782 & -0.105158 \\ -0.592999 & -3.13268 & -4.320678 & -1715.435199 & 2208.928506 & 1996.598122 & -0.235655 & -0.019688 & -0.208172 & -0.232314 \\ -6.581665 & 1.201293 & -18.966361 & -1963.042308 & 1996.598122 & 20257.89338 & -2.565929 & -2.041014 & -0.034683 & -0.469695 \\ 0.001541 & -0.0003 & 0.002197 & 0.413263 & -0.235655 & -2.565929 & 0.002402 & 0.00123 & 0.000082 & 0.000042 \\ -0.000289 & 0.000152 & 0.008692 & -0.984919 & -0.019688 & -2.041014 & 0.00123 & 0.008884 & -0.000628 & 0.000133 \\ 0.001055 & 0.000006 & 0.000719 & 0.462782 & -0.208172 & -0.034683 & 0.000082 & -0.000628 & 0.001744 & -0.00078 \\ -0.001102 & 0.002174 & -0.000395 & -0.105158 & -0.232314 & -0.469695 & 0.000042 & 0.000133 & -0.00078 & 0.001761 \end{bmatrix},$$

$$\Sigma_{b_{0_4}^t} = \begin{bmatrix} 0.038707 & 0.019189 & 0.025302 & 0.335548 & -0.225187 & 0.236951 & 0.002339 & -0.000356 & 0.00054 & 0.001568 \\ 0.019189 & 0.066373 & 0.038793 & -1.567437 & -0.483736 & -3.212564 & 0.002804 & 0.00155 & -0.00284 & 0.003214 \\ 0.025302 & 0.038793 & 0.17853 & -6.136782 & -0.16404 & -6.501844 & 0.004837 & 0.002272 & -0.005964 & 0.004875 \\ 0.335548 & -1.567437 & -6.136782 & 4020.929878 & 24.419003 & 204.536914 & -0.597608 & 0.306417 & 0.241617 & -0.427123 \\ -0.225187 & -0.483736 & -0.16404 & 24.419003 & 101.213713 & 18.143468 & 0.120999 & 0.193153 & -0.051457 & 0.003621 \\ 0.236951 & -3.212564 & -6.501844 & 204.536914 & 18.143468 & 3999.009842 & 0.257917 & 0.237757 & 0.61827 & -0.537067 \\ 0.002339 & 0.002804 & 0.004837 & -0.597608 & 0.120999 & 0.257917 & 0.009235 & 0.009178 & -0.001207 & 0.000861 \\ -0.000356 & 0.00155 & 0.002272 & 0.306417 & 0.193153 & 0.237757 & 0.009178 & 0.015813 & -0.002545 & 0.001095 \\ 0.00054 & -0.00284 & -0.005964 & 0.241617 & -0.051457 & 0.61827 & -0.001207 & -0.002545 & 0.002208 & -0.001221 \\ 0.001568 & 0.003214 & 0.004875 & -0.427123 & 0.003621 & -0.537067 & 0.000861 & 0.001095 & -0.001221 & 0.001587 \end{bmatrix},$$

$$\Sigma_{b_{0_5}^t} = \begin{bmatrix} 0.058247 & 0.013987 & 0.07152 & -1.009222 & -1.231935 & -11.654191 & 0.00051 & -0.00089 & 0.000939 & 0.001094 \\ 0.013987 & 0.051407 & 0.045299 & -2.345656 & -2.546025 & 6.831527 & -0.002709 & -0.005278 & -0.001337 & 0.00425 \\ 0.07152 & 0.045299 & 0.214784 & -3.771325 & -3.453472 & 1.376192 & 0.001601 & -0.001786 & 0.000339 & 0.00489 \\ -1.009222 & -2.345656 & -3.771325 & 776.743408 & 139.172258 & -366.982381 & 0.148611 & 0.057755 & 0.223786 & -0.327497 \\ -1.231935 & -2.546025 & -3.453472 & 139.172258 & 488.939075 & -50.18754 & 0.169093 & 0.410336 & 0.032671 & -0.200399 \\ -11.654191 & 6.831527 & 1.376192 & -366.982381 & -50.18754 & 42393.77187 & 0.398829 & 0.714668 & -0.863061 & 1.098365 \\ 0.00051 & -0.002709 & 0.001601 & 0.148611 & 0.169093 & 0.398829 & 0.003689 & 0.002184 & 0.000627 & -0.000563 \\ -0.00089 & -0.005278 & -0.001786 & 0.057755 & 0.410336 & 0.714668 & 0.002184 & 0.006576 & -0.000619 & -0.000256 \\ 0.000939 & -0.001337 & 0.000339 & 0.223786 & 0.032671 & -0.863061 & 0.000627 & -0.000619 & 0.001708 & -0.001129 \\ 0.001094 & 0.00425 & 0.00489 & -0.327497 & -0.200399 & 1.098365 & -0.000563 & -0.000256 & -0.001129 & 0.002017 \end{bmatrix},$$

$$\Sigma_{b_{0_6}^t} = \begin{bmatrix} 0.785405 & -1.863581 & -0.005365 & 8.842449 & 7.606601 & 33.285154 & 0.003941 & 0.008045 & -0.001791 & -0.001906 \\ -1.863581 & 63.539933 & 0.278321 & -265.183084 & -229.263417 & -997.995293 & -0.185079 & -0.322426 & 0.034173 & 0.07184 \\ -0.005365 & 0.278321 & 0.983374 & -0.692613 & -0.616743 & -2.601981 & -0.001531 & -0.002118 & -0.00021 & 0.000413 \\ 8.842449 & -265.183084 & -0.692613 & 40367.78293 & 1103.182698 & 4831.239417 & 0.523301 & 1.108202 & -0.273644 & -0.266247 \\ 7.606601 & -229.263417 & -0.616743 & 1103.182698 & 42852.48628 & 4152.7494 & 0.462049 & 0.967613 & -0.231674 & -0.231596 \\ 33.285154 & -997.995293 & -2.601981 & 4831.239417 & 4152.7494 & 156076.2918 & 1.967542 & 4.168712 & -1.029957 & -1.002499 \\ 0.003941 & -0.185079 & -0.001531 & 0.523301 & 0.462049 & 1.967542 & 0.119846 & 0.001325 & 0.0001 & -0.00027 \\ 0.008045 & -0.322426 & -0.002118 & 1.108202 & 0.967613 & 4.168712 & 0.001325 & 0.170476 & 0.000026 & -0.000434 \\ -0.001791 & 0.034173 & -0.00021 & -0.273644 & -0.231674 & -1.029957 & 0.0001 & 0.000026 & 0.09991 & -0.000004 \\ -0.001906 & 0.07184 & 0.000413 & -0.266247 & -0.231596 & -1.002499 & -0.00027 & -0.000434 & -0.000004 & 0.017904 \end{bmatrix},$$

The distribution

$$p\left(F_9^t, F_{29}^t, F_{32}^t, F_{58}^t, F_{48}^t, F_{43}^t, F_{12}^t, F_{18}^t, F_{21}^t, F_{22}^t | b_1^t : \boldsymbol{\theta}_{F_9^t,\dots,F_{22}^t|b_1^t} = \left\{\left\{\pi_{b_{1i}^t}, \boldsymbol{\mu}_{b_{1i}^t}, \Sigma_{b_{1i}^t}\right\}_{i=1}^{9}\right\}\right)$$

consists of nine components, where

$$\pi_{b_{11}^t} = 0.223168, \pi_{b_{12}^t} = 0.029221, \pi_{b_{13}^t} = 0.073630,$$

$$\pi_{b_{14}^t} = 0.109578, \pi_{b_{15}^t} = 0.209613, \pi_{b_{16}^t} = 0.128705,$$

$$\pi_{b_{17}^t} = 0.170325, \pi_{b_{18}^t} = 0.019290, \pi_{b_{19}^t} = 0.036471,$$

$$\boldsymbol{\mu}_{b_{11}^t} = \begin{pmatrix} 0.663347 \\ 0.061683 \\ 1.16527 \\ 196.552966 \\ 208.090248 \\ 235.573518 \\ -0.003843 \\ 0.03015 \\ -0.076019 \\ 0.039065 \end{pmatrix}, \boldsymbol{\mu}_{b_{12}^t} = \begin{pmatrix} 1.446787 \\ 0.681982 \\ 2.288055 \\ 13.363604 \\ 32.287283 \\ 358.398518 \\ 0.09489 \\ 0.013928 \\ -0.185204 \\ 0.123967 \end{pmatrix}, \boldsymbol{\mu}_{b_{13}^t} = \begin{pmatrix} 1.087966 \\ 0.231743 \\ 1.843896 \\ 134.888543 \\ 133.047491 \\ 457.884303 \\ 0.09537 \\ 0.065131 \\ -0.094216 \\ 0.09204 \end{pmatrix},$$

$$\boldsymbol{\mu}_{b_{14}^t} = \begin{pmatrix} 0.468387 \\ 0.500928 \\ 1.667181 \\ 39.488754 \\ 69.852672 \\ 489.481186 \\ 0.110748 \\ 0.070525 \\ -0.157324 \\ 0.113811 \end{pmatrix}, \boldsymbol{\mu}_{b_{15}^t} = \begin{pmatrix} 0.72706 \\ 0.050834 \\ 0.867885 \\ 317.85026 \\ 129.35088 \\ 371.636113 \\ 0.064577 \\ 0.009258 \\ -0.06785 \\ 0.037092 \end{pmatrix}, \boldsymbol{\mu}_{b_{16}^t} = \begin{pmatrix} 0.45828 \\ 0.133534 \\ 1.078625 \\ 92.659968 \\ 62.330735 \\ 590.276959 \\ 0.007412 \\ 0.055159 \\ -0.080502 \\ 0.051522 \end{pmatrix},$$

$$\boldsymbol{\mu}_{b_{17}^t} = \begin{pmatrix} 0.787458 \\ 0.266171 \\ 1.723765 \\ 128.292341 \\ 19.77285 \\ 93.438727 \\ 0.046382 \\ 0.017164 \\ -0.108915 \\ 0.082044 \end{pmatrix}, \boldsymbol{\mu}_{b_{18}^t} = \begin{pmatrix} 0.560234 \\ 0.158464 \\ 1.348824 \\ 90.325392 \\ 628.509886 \\ 644.262152 \\ 0.090483 \\ 0.077412 \\ -0.100144 \\ 0.062364 \end{pmatrix}, \boldsymbol{\mu}_{b_{19}^t} = \begin{pmatrix} 0.55669 \\ 0.316724 \\ 1.593132 \\ 436.170891 \\ 56.057906 \\ 495.047958 \\ 0.029142 \\ 0.022736 \\ -0.121456 \\ 0.085111 \end{pmatrix},$$

$$\Sigma_{b_{11}^t} = \begin{bmatrix} 0.054632 & -0.004805 & 0.066309 & 11.374726 & 11.131535 & 12.42698 & -0.003868 & -0.000437 & 0.000824 & 0.000078 \\ -0.004805 & 0.007116 & -0.003114 & -2.141256 & -1.824987 & -2.548025 & 0.003781 & 0.000599 & -0.000691 & 0.000704 \\ 0.066309 & -0.003114 & 0.151171 & 23.382926 & 22.374701 & 25.29254 & -0.005857 & 0.002336 & -0.001044 & 0.001059 \\ 11.374726 & -2.141256 & 23.382926 & 30154.68679 & 29185.84922 & 31571.36403 & -7.749559 & -0.604642 & -1.074281 & -0.464655 \\ 11.131535 & -1.824987 & 22.374701 & 29185.84922 & 28742.31739 & 30806.19372 & -7.05596 & -0.633193 & -1.047501 & -0.409613 \\ 12.42698 & -2.548025 & 25.29254 & 31571.36403 & 30806.19372 & 34805.56944 & -9.906637 & -1.014412 & -1.181613 & -0.784359 \\ -0.003868 & 0.003781 & -0.005857 & -7.749559 & -7.05596 & -9.906637 & 0.012446 & 0.001505 & -0.000262 & 0.001626 \\ -0.000437 & 0.000599 & 0.002336 & -0.604642 & -0.633193 & -1.014412 & 0.001505 & 0.001684 & -0.000284 & 0.000338 \\ 0.000824 & -0.000691 & -0.001044 & -1.074281 & -1.047501 & -1.181613 & -0.000262 & -0.000284 & 0.000856 & -0.000197 \\ 0.000078 & 0.000704 & 0.001059 & -0.464655 & -0.409613 & -0.784359 & 0.001626 & 0.000338 & -0.000197 & 0.00068 \end{bmatrix},$$

$$\Sigma_{b_{i_2}^t} = \begin{bmatrix} 0.696411 & -0.040519 & 0.06684 & -3.261698 & -3.841105 & -22.44343 & -0.014446 & -0.042677 & 0.002474 & -0.001524 \\ -0.040519 & 0.062345 & 0.027847 & 0.608008 & -1.439974 & -19.854787 & -0.003043 & -0.010934 & 0.002083 & 0.000157 \\ 0.06684 & 0.027847 & 0.160706 & -0.592033 & -0.44346 & -5.038179 & 0.00003 & -0.012665 & 0.006084 & -0.003039 \\ -3.261698 & 0.608008 & -0.592033 & 1559.406205 & 31.611186 & 300.926184 & 0.145964 & -0.026015 & -0.044951 & 0.005046 \\ -3.841105 & -1.439974 & -0.44346 & 31.611186 & 2103.621364 & 4129.795683 & 0.850817 & 1.984054 & -0.17609 & -0.015263 \\ -22.44343 & -19.854787 & -5.038179 & 300.926184 & 4129.795683 & 62218.07413 & 16.074939 & 20.971692 & -0.020195 & -1.90134 \\ -0.014446 & -0.003043 & 0.00003 & 0.145964 & 0.850817 & 16.074939 & 0.013837 & 0.008864 & -0.000008 & -0.001513 \\ -0.042677 & -0.010934 & -0.012665 & -0.026015 & 1.984054 & 20.971692 & 0.008864 & 0.028355 & -0.003046 & 0.000206 \\ 0.002474 & 0.002083 & 0.006084 & -0.044951 & -0.17609 & -0.020195 & -0.000008 & -0.003046 & 0.005257 & -0.000638 \\ -0.001524 & 0.000157 & -0.003039 & 0.005046 & -0.015263 & -1.90134 & -0.001513 & 0.000206 & -0.000638 & 0.001368 \end{bmatrix},$$

$$\Sigma_{b_{i_3}^t} = \begin{bmatrix} 0.373379 & -0.004707 & 0.193077 & -27.125826 & -45.026173 & 46.67971 & -0.021025 & -0.023641 & 0.029011 & -0.004118 \\ -0.004707 & 0.029606 & -0.01512 & 4.093806 & 5.069115 & -2.783874 & 0.002041 & 0.004693 & -0.004378 & 0.00182 \\ 0.193077 & -0.01512 & 0.231001 & -19.615695 & -33.147143 & 41.449103 & -0.016747 & -0.0205 & 0.022687 & -0.004642 \\ -27.125826 & 4.093806 & -19.615695 & 5590.806747 & 6507.908577 & -4684.679096 & 2.699086 & 3.812564 & -3.52859 & 0.800613 \\ -45.026173 & 5.069115 & -33.147143 & 6507.908577 & 10774.1451 & -7998.227739 & 4.074345 & 5.381831 & -5.673047 & 1.31061 \\ 46.67971 & -2.783874 & 41.449103 & -4684.679096 & -7998.227739 & 15793.44959 & -2.862684 & -4.156328 & 5.494859 & -1.616469 \\ -0.021025 & 0.002041 & -0.016747 & 2.699086 & 4.074345 & -2.862684 & 0.005608 & 0.003383 & -0.002847 & 0.000445 \\ -0.023641 & 0.004693 & -0.0205 & 3.812564 & 5.381831 & -4.156328 & 0.003383 & 0.007332 & -0.003659 & 0.00085 \\ 0.029011 & -0.004378 & 0.022687 & -3.52859 & -5.673047 & 5.494859 & -0.002847 & -0.003659 & 0.005474 & -0.001061 \\ -0.004118 & 0.00182 & -0.004642 & 0.800613 & 1.31061 & -1.616469 & 0.000445 & 0.00085 & -0.001061 & 0.000951 \end{bmatrix},$$

$$\Sigma_{b_{i_4}^t} = \begin{bmatrix} 0.036127 & -0.002412 & 0.035215 & -0.691473 & 2.313606 & 10.427043 & 0.000817 & -0.00196 & -0.000515 & 0.000509 \\ -0.002412 & 0.027074 & -0.002446 & 0.21471 & -1.447622 & -17.681614 & -0.002057 & -0.000098 & -0.000363 & 0.000401 \\ 0.035215 & -0.002446 & 0.226279 & -7.395927 & -5.941562 & -17.827937 & -0.006439 & -0.019508 & 0.001612 & -0.000486 \\ -0.691473 & 0.21471 & -7.395927 & 1476.844234 & 727.259425 & -1050.429939 & 0.222899 & 1.26243 & 0.006808 & -0.066471 \\ 2.313606 & -1.447622 & -5.941562 & 727.259425 & 2607.94643 & 3213.71474 & 0.558579 & 1.005641 & 0.028806 & 0.072397 \\ 10.427043 & -17.681614 & -17.827937 & -1050.429939 & 3213.71474 & 69725.0709 & 6.477808 & 2.789972 & -0.769522 & 0.540034 \\ 0.000817 & -0.002057 & -0.006439 & 0.222899 & 0.558579 & 6.477808 & 0.003575 & 0.002292 & -0.000529 & -0.000032 \\ -0.00196 & -0.000098 & -0.019508 & 1.26243 & 1.005641 & 2.789972 & 0.002292 & 0.011228 & -0.002042 & 0.000908 \\ -0.000515 & -0.000363 & 0.001612 & 0.006808 & 0.028806 & -0.769522 & -0.000529 & -0.002042 & 0.002448 & -0.000802 \\ 0.000509 & 0.000401 & -0.000486 & -0.066471 & 0.072397 & 0.540034 & -0.000032 & 0.000908 & -0.000802 & 0.001008 \end{bmatrix},$$

$$\Sigma_{b_{i_5}^t} = \begin{bmatrix} 0.249082 & 0.002238 & 0.058105 & 4.798814 & 0.572099 & 0.848097 & 0.003706 & -0.001687 & 0.003051 & 0.002406 \\ 0.002238 & 0.004332 & 0.005366 & -0.304577 & -1.571955 & 0.019541 & 0.000133 & -0.000161 & -0.00014 & 0.000271 \\ 0.058105 & 0.005366 & 0.083829 & 2.111065 & -2.280324 & -1.848045 & -0.001241 & 0.001359 & -0.000737 & 0.001487 \\ 4.798814 & -0.304577 & 2.111065 & 26205.40566 & -1642.570651 & 24631.93851 & -2.414454 & -0.805903 & -0.384329 & -0.302109 \\ 0.572099 & -1.571955 & -2.280324 & -1642.570651 & 8793.2044 & -3268.315483 & -0.569421 & 0.773203 & -0.076177 & -0.163847 \\ 0.848097 & 0.019541 & -1.848045 & 24631.93851 & -3268.315483 & 27044.36484 & -1.127679 & -1.420953 & -0.204031 & -0.316876 \\ 0.003706 & 0.000133 & -0.001241 & -2.414454 & -0.569421 & -1.127679 & 0.002508 & -0.000247 & 0.000322 & 0.000037 \\ -0.001687 & -0.000161 & 0.001359 & -0.805903 & 0.773203 & -1.420953 & -0.000247 & 0.001678 & -0.000242 & 0.000095 \\ 0.003051 & -0.00014 & -0.000737 & -0.384329 & -0.076177 & -0.204031 & 0.000322 & -0.000242 & 0.000755 & -0.000072 \\ 0.002406 & 0.000271 & 0.001487 & -0.302109 & -0.163847 & -0.316876 & 0.000037 & 0.000095 & -0.000072 & 0.000358 \end{bmatrix},$$

$$\Sigma_{b_{i_6}^t} = \begin{bmatrix} 0.043714 & 0.006665 & 0.063325 & 0.874534 & -4.226873 & -10.49096 & 0.005582 & -0.002722 & 0.002737 & 0.002458 \\ 0.006665 & 0.011696 & 0.013633 & 0.051057 & -2.677924 & -3.246141 & 0.002247 & -0.000927 & -0.000134 & 0.001035 \\ 0.063325 & 0.013633 & 0.171703 & 2.66021 & -5.722564 & -13.546072 & 0.011647 & -0.005199 & 0.00457 & 0.004586 \\ 0.874534 & 0.051057 & 2.66021 & 2603.819029 & -435.002379 & 2379.266821 & 0.844026 & -0.436978 & -0.093078 & 0.052762 \\ -4.226873 & -2.677924 & -5.722564 & -435.002379 & 4810.714505 & 2174.313511 & -2.369814 & 1.608755 & -0.259936 & -0.519166 \\ -10.49096 & -3.246141 & -13.546072 & 2379.266821 & 2174.313511 & 15710.75077 & -1.110439 & 1.491353 & -1.255741 & -1.184228 \\ 0.005582 & 0.002247 & 0.011647 & 0.844026 & -2.369814 & -1.110439 & 0.004551 & -0.000265 & 0.00015 & 0.000858 \\ -0.002722 & -0.000927 & -0.005199 & -0.436978 & 1.608755 & 1.491353 & -0.000265 & 0.004626 & -0.00076 & 0.000129 \\ 0.002737 & -0.000134 & 0.00457 & -0.093078 & -0.259936 & -1.255741 & 0.00015 & -0.00076 & 0.001518 & -0.000123 \\ 0.002458 & 0.001035 & 0.004586 & 0.052762 & -0.519166 & -1.184228 & 0.000858 & 0.000129 & -0.000123 & 0.00085 \end{bmatrix},$$

$$\Sigma_{b_{i_7}^t} = \begin{bmatrix} 0.119197 & 0.012277 & 0.226702 & -0.005214 & -1.548405 & -7.080485 & -0.001672 & -0.011838 & -0.002817 & 0.003692 \\ 0.012277 & 0.022657 & 0.038929 & -7.829902 & -0.52217 & -4.171293 & -0.0005 & -0.000981 & -0.001442 & 0.001925 \\ 0.226702 & 0.038929 & 0.520798 & -8.252749 & -3.896937 & -19.692779 & -0.007973 & -0.023786 & -0.008056 & 0.010591 \\ -0.005214 & -7.829902 & -8.252749 & 11846.86021 & 166.375999 & 4620.516846 & 0.322548 & 0.032754 & 0.992769 & -1.000653 \\ -1.548405 & -0.52217 & -3.896937 & 166.375999 & 526.487229 & 100.497083 & 0.284734 & 0.278766 & 0.023263 & -0.043289 \\ -7.080485 & -4.171293 & -19.692779 & 4620.516846 & 100.497083 & 6063.662441 & 0.369492 & 0.314248 & 0.615462 & -0.777827 \\ -0.001672 & -0.0005 & -0.007973 & 0.322548 & 0.284734 & 0.369492 & 0.005046 & 0.002844 & -0.000216 & 0.000063 \\ -0.011838 & -0.000981 & -0.023786 & 0.032754 & 0.278766 & 0.314248 & 0.002844 & 0.007181 & -0.000631 & 0.000329 \\ -0.002817 & -0.001442 & -0.008056 & 0.992769 & 0.023263 & 0.615462 & -0.000216 & -0.000631 & 0.001506 & -0.000765 \\ 0.003692 & 0.001925 & 0.010591 & -1.000653 & -0.043289 & -0.777827 & 0.000063 & 0.000329 & -0.000765 & 0.001246 \end{bmatrix},$$

$$\Sigma_{b_{i_8}^t} = \begin{bmatrix} 0.039549 & 0.003297 & 0.007625 & 0.193597 & -0.750314 & -0.319725 & 0.000042 & 0.000225 & -0.000095 & 0.000148 \\ 0.003297 & 0.030892 & 0.020008 & 1.49527 & -0.925801 & 0.746772 & 0.000316 & -0.000181 & 0.000121 & 0.000055 \\ 0.007625 & 0.020008 & 0.114819 & 4.032855 & 2.144406 & 2.718993 & 0.002273 & 0.000665 & -0.000379 & 0.001309 \\ 0.193597 & 1.49527 & 4.032855 & 2695.398686 & 210.212331 & 759.302045 & 0.133824 & 0.084663 & 0.130186 & -0.063927 \\ -0.750314 & -0.925801 & 2.144406 & 210.212331 & 9101.264523 & 2621.076838 & 1.484959 & 1.531855 & 0.871644 & -0.37593 \\ -0.319725 & 0.746772 & 2.718993 & 759.302045 & 2621.076838 & 9211.265641 & 0.827884 & 0.953995 & 0.672697 & -0.344342 \\ 0.000042 & 0.000316 & 0.002273 & 0.133824 & 1.484959 & 0.827884 & 0.006768 & 0.000883 & 0.000002 & 0.000272 \\ 0.000225 & -0.000181 & 0.000665 & 0.084663 & 1.531855 & 0.953995 & 0.000883 & 0.010011 & -0.000036 & 0.000305 \\ -0.000095 & 0.000121 & -0.000379 & 0.130186 & 0.871644 & 0.672697 & 0.000002 & -0.000036 & 0.005585 & -0.000621 \\ 0.000148 & 0.000055 & 0.001309 & -0.063927 & -0.37593 & -0.344342 & 0.000272 & 0.000305 & -0.000621 & 0.001916 \end{bmatrix},$$

$$\Sigma_{b_{1_9}^t} = \begin{bmatrix} 0.070417 & -0.007546 & 0.045241 & 8.999374 & -2.640496 & 4.820088 & 0.003291 & 0.005093 & 0.00289 & -0.002195 \\ -0.007546 & 0.038942 & 0.000095 & -8.125502 & -2.323164 & -3.987021 & -0.003221 & -0.006026 & -0.003314 & 0.002788 \\ 0.045241 & 0.000095 & 0.166734 & 5.745456 & -2.287217 & -1.528077 & -0.003033 & -0.000535 & 0.000659 & -0.001707 \\ 8.999374 & -8.125502 & 5.745456 & 23156.56927 & 1861.50279 & 19670.22713 & 9.628247 & 12.841797 & 2.580321 & -0.882839 \\ -2.640496 & -2.323164 & -2.287217 & 1861.50279 & 2674.568029 & 2745.279062 & 1.004296 & 1.87681 & -0.200758 & -0.03283 \\ 4.820088 & -3.987021 & -1.528077 & 19670.22713 & 2745.279062 & 27032.7099 & 8.622141 & 11.140946 & 0.930869 & 0.081672 \\ 0.003291 & -0.003221 & -0.003033 & 9.628247 & 1.004296 & 8.622141 & 0.010005 & 0.007359 & 0.001094 & -0.000513 \\ 0.005093 & -0.006026 & -0.000535 & 12.841797 & 1.87681 & 11.140946 & 0.007359 & 0.017081 & 0.00184 & -0.000889 \\ 0.00289 & -0.003314 & 0.000659 & 2.580321 & -0.200758 & 0.930869 & 0.001094 & 0.00184 & 0.004587 & -0.001162 \\ -0.002195 & 0.002788 & -0.001707 & -0.882839 & -0.03283 & 0.081672 & -0.000513 & -0.000889 & -0.001162 & 0.00173 \end{bmatrix}.$$

The distribution

$$p\left(F_9^t, F_{29}^t, F_{32}^t, F_{58}^t, F_{48}^t, F_{43}^t, F_{12}^t, F_{18}^t, F_{21}^t, F_{22}^t | b_2^t : \boldsymbol{\theta}_{F_9^t,\dots,F_{22}^t | b_2^t} = \left\{\left\{\pi_{b_{1_i}^t}, \boldsymbol{\mu}_{b_{1_i}^t}, \Sigma_{b_{1_i}^t}\right\}_{i=1}^{8}\right\}\right)$$

consists of eight components, where

$$\pi_{b_{2_1}^t} = 0.056343, \pi_{b_{2_2}^t} = 0.000267, \pi_{b_{2_3}^t} = 0.076837, \pi_{b_{2_4}^t} = 0.148932,$$

$$\pi_{b_{2_5}^t} = 0.123758, \pi_{b_{2_6}^t} = 0.082786, \pi_{b_{2_7}^t} = 0.099131, \pi_{b_{2_8}^t} = 0.411947,$$

$$\boldsymbol{\mu}_{b_{2_1}^t} = \begin{pmatrix} 0.733691 \\ 0.29301 \\ 1.88611 \\ 1.112354 \\ 14.047579 \\ 621.857109 \\ -0.356668 \\ -0.396104 \\ -0.416862 \\ 0.289352 \end{pmatrix}, \boldsymbol{\mu}_{b_{2_2}^t} = \begin{pmatrix} 0.658679 \\ 0.297305 \\ 1.16976 \\ 36.439988 \\ 35.246384 \\ 178.198473 \\ -0.17901 \\ 0.223589 \\ -0.317743 \\ 0.116319 \end{pmatrix}, \boldsymbol{\mu}_{b_{2_3}^t} = \begin{pmatrix} 1.14575 \\ 0.097793 \\ 2.403694 \\ 5.423863 \\ 231.264715 \\ 509.156315 \\ -0.463582 \\ -0.841279 \\ -0.848576 \\ 0.151481 \end{pmatrix},$$

$$\boldsymbol{\mu}_{b_{2_4}^t} = \begin{pmatrix} 0.110421 \\ 0.275511 \\ 2.147294 \\ 0.51767 \\ 40.546161 \\ 523.416807 \\ -0.249328 \\ -0.412486 \\ -0.418133 \\ 0.209638 \end{pmatrix}, \boldsymbol{\mu}_{b_{2_5}^t} = \begin{pmatrix} 0.36995 \\ 0.11252 \\ 2.1912 \\ 0.40132 \\ 98.571018 \\ 327.115464 \\ -0.469845 \\ -0.490396 \\ -0.534467 \\ 0.188484 \end{pmatrix}, \boldsymbol{\mu}_{b_{2_6}^t} = \begin{pmatrix} 0.994044 \\ 0.023652 \\ 2.827477 \\ 0.247914 \\ 464.542372 \\ 466.548347 \\ -0.413291 \\ -0.537447 \\ -0.573209 \\ 0.091406 \end{pmatrix},$$

$$\boldsymbol{\mu}_{b_{2_7}^t} = \begin{pmatrix} 1.841332 \\ 0.718022 \\ 1.755981 \\ 3.439172 \\ 8.360183 \\ 289.869351 \\ -0.056309 \\ -0.113392 \\ -0.174895 \\ 0.228243 \end{pmatrix}, \boldsymbol{\mu}_{b_{2_8}^t} = \begin{pmatrix} 1.014852 \\ 0.341248 \\ 2.091396 \\ 0.851472 \\ 16.334651 \\ 155.818807 \\ -0.303952 \\ -0.34017 \\ -0.404918 \\ 0.243492 \end{pmatrix},$$

$$\Sigma_{b_{z1}^t} = \begin{bmatrix} 0.06014 & -0.008076 & -0.032672 & -0.036257 & 0.417475 & -7.945657 & 0.007564 & 0.003529 & -0.004552 & -0.001471 \\ -0.008076 & 0.020469 & 0.014596 & 0.024653 & -0.539754 & 3.542173 & -0.002046 & -0.000626 & 0.001745 & 0.000343 \\ -0.032672 & 0.014596 & 0.103658 & -0.086046 & -1.644286 & 12.673608 & -0.011025 & -0.004935 & 0.002029 & 0.001425 \\ -0.036257 & 0.024653 & -0.086046 & 652.200359 & 19.654641 & -91.429786 & 0.103612 & 0.106533 & 0.087648 & -0.045256 \\ 0.417475 & -0.539754 & -1.644286 & 19.654641 & 929.215915 & -659.408123 & 0.398534 & 0.355719 & 0.018227 & -0.112266 \\ -7.945657 & 3.542173 & 12.673608 & -91.429786 & -659.408123 & 16223.78192 & -3.401455 & 0.725311 & 3.560455 & 0.630206 \\ 0.007564 & -0.002046 & -0.011025 & 0.103612 & 0.398534 & -3.401455 & 0.008011 & 0.004454 & 0.001853 & -0.000575 \\ 0.003529 & -0.000626 & -0.004935 & 0.106533 & 0.355719 & 0.725311 & 0.004454 & 0.012261 & 0.003664 & -0.000334 \\ -0.004552 & 0.001745 & 0.002029 & 0.087648 & 0.018227 & 3.560455 & 0.001853 & 0.003664 & 0.009259 & 0.000634 \\ -0.001471 & 0.000343 & 0.001425 & -0.045256 & -0.112266 & 0.630206 & -0.000575 & -0.000334 & 0.000634 & 0.001941 \end{bmatrix},$$

$$\Sigma_{b_{z2}^t} = \begin{bmatrix} 2.140717 & 0.000823 & 0.012886 & 1.210607 & 1.01017 & 3.420715 & 0.003122 & -0.008988 & 0.002698 & 0.000407 \\ 0.000823 & 1.225803 & 0.022758 & 2.046487 & 1.699472 & 5.775353 & 0.004755 & -0.016521 & 0.003751 & 0.000154 \\ 0.012886 & 0.022758 & 3.215861 & 29.16242 & 24.274572 & 82.285341 & 0.07109 & -0.229018 & 0.059371 & 0.006182 \\ 1.210607 & 2.046487 & 29.16242 & 118167.434 & 2237.343826 & 7579.728393 & 6.616869 & -20.969874 & 5.595759 & 0.653995 \\ 1.01017 & 1.699472 & 24.274572 & 2237.343826 & 125674.8695 & 6312.023714 & 5.516517 & -17.450816 & 4.669721 & 0.551923 \\ 3.420715 & 5.775353 & 82.285341 & 7579.728393 & 6312.023714 & 428800.8841 & 18.67139 & -59.162848 & 15.783878 & 1.846876 \\ 0.003122 & 0.004755 & 0.07109 & 6.616869 & 5.516517 & 18.67139 & 0.368086 & -0.050999 & 0.014598 & 0.002188 \\ -0.008988 & -0.016521 & -0.229018 & -20.969874 & -17.450816 & -59.162848 & -0.050999 & 0.666671 & -0.043454 & -0.005263 \\ 0.002698 & 0.003751 & 0.059371 & 5.595759 & 4.669721 & 15.783878 & 0.014598 & -0.043454 & 0.308636 & 0.003114 \\ 0.000407 & 0.000154 & 0.006182 & 0.653995 & 0.551923 & 1.846876 & 0.002188 & -0.005263 & 0.003114 & 0.054308 \end{bmatrix}$$

$$\Sigma_{b_{z3}^t} = \begin{bmatrix} 0.114443 & 0.002095 & 0.006511 & -0.305635 & 5.168836 & -14.844807 & -0.002834 & -0.01721 & -0.00207 & -0.000285 \\ 0.002095 & 0.008685 & -0.003426 & 0.076777 & -1.541674 & 0.677386 & 0.000644 & 0.002869 & 0.000936 & 0.000789 \\ 0.006511 & -0.003426 & 0.07796 & -0.159071 & -6.784884 & 27.104764 & 0.002563 & 0.01676 & -0.001972 & 0.000486 \\ -0.305635 & 0.076777 & -0.159071 & 482.830351 & -16.003606 & 96.135845 & 0.097323 & 0.270774 & 0.121965 & 0.006534 \\ 5.168836 & -1.541674 & -6.784884 & -16.003606 & 9997.579779 & -12181.19459 & -2.143999 & -6.403374 & -1.249745 & 0.315873 \\ -14.844807 & 0.677386 & 27.104764 & 96.135845 & -12181.19459 & 45079.92933 & 4.969365 & 23.457062 & 1.041791 & 0.175346 \\ -0.002834 & 0.000644 & 0.002563 & 0.097323 & -2.143999 & 4.969365 & 0.003648 & 0.00427 & 0.001591 & 0.000523 \\ -0.01721 & 0.002869 & 0.01676 & 0.270774 & -6.403374 & 23.457062 & 0.00427 & 0.029598 & 0.002919 & 0.00268 \\ -0.00207 & 0.000936 & -0.001972 & 0.121965 & -1.249745 & 1.041791 & 0.001591 & 0.002919 & 0.004756 & 0.001437 \\ -0.000285 & 0.000789 & 0.000486 & 0.006534 & 0.315873 & 0.175346 & 0.000523 & 0.00268 & 0.001437 & 0.002466 \end{bmatrix}$$

$$\Sigma_{b_{z4}^t} = \begin{bmatrix} 0.010315 & 0.003558 & -0.000663 & 0.081303 & 0.564006 & 0.405984 & 0.001825 & 0.002237 & 0.001782 & 0.000784 \\ 0.003558 & 0.022492 & 0.000342 & 0.023268 & -1.361118 & 1.68292 & 0.002983 & 0.006544 & 0.002971 & 0.001055 \\ -0.000663 & 0.000342 & 0.086243 & -0.087566 & 1.518579 & -14.689145 & -0.003887 & -0.002742 & -0.004931 & -0.000632 \\ 0.081303 & 0.023268 & -0.087566 & 247.000547 & 4.090684 & -12.974617 & 0.038593 & 0.063091 & 0.045512 & -0.002078 \\ 0.564006 & -1.361118 & 1.518579 & 4.090684 & 1945.53733 & -1173.434002 & 0.087778 & -1.409679 & -0.249561 & 0.064401 \\ 0.405984 & 1.68292 & -14.689145 & -12.974617 & -1173.434002 & 45300.98992 & 1.679133 & 2.595185 & 2.000222 & 1.798773 \\ 0.001825 & 0.002983 & -0.003887 & 0.038593 & 0.087778 & 1.679133 & 0.004333 & 0.004821 & 0.003378 & 0.001543 \\ 0.002237 & 0.006544 & -0.002742 & 0.063091 & -1.409679 & 2.595185 & 0.004821 & 0.014179 & 0.006977 & 0.002446 \\ 0.001782 & 0.002971 & -0.004931 & 0.045512 & -0.249561 & 2.000222 & 0.003378 & 0.006977 & 0.006505 & 0.002025 \\ 0.000784 & 0.001055 & -0.000632 & -0.002078 & 0.064401 & 1.798773 & 0.001543 & 0.002446 & 0.002025 & 0.001932 \end{bmatrix}$$

$$\Sigma_{b_{z5}^t} = \begin{bmatrix} 0.035532 & 0.004383 & 0.000461 & 0.063558 & 4.015366 & -3.816191 & 0.009644 & 0.01122 & 0.00133 & 0.00192 \\ 0.004383 & 0.012182 & -0.00345 & 0.046536 & -1.234491 & -5.642179 & 0.007415 & 0.006831 & 0.001971 & 0.001806 \\ 0.000461 & -0.00345 & 0.147067 & -0.120239 & 4.523266 & -42.359306 & -0.000503 & -0.004915 & -0.006552 & -0.005438 \\ 0.063558 & 0.046536 & -0.120239 & 297.204168 & -3.286785 & 0.452213 & 0.084751 & 0.082462 & 0.062133 & 0.000427 \\ 4.015366 & -1.234491 & 4.523266 & -3.286785 & 4382.126213 & -732.471572 & -0.437392 & -0.018407 & 0.065854 & -0.180156 \\ -3.816191 & -5.642179 & -42.359306 & 0.452213 & -732.471572 & 31813.78435 & -9.868748 & -7.074935 & 1.255976 & 0.906287 \\ 0.009644 & 0.007415 & -0.000503 & 0.084751 & -0.437392 & -9.868748 & 0.019315 & 0.016406 & 0.004107 & 0.003073 \\ 0.01122 & 0.006831 & -0.004915 & 0.082462 & -0.018407 & -7.074935 & 0.016406 & 0.0211 & 0.006124 & 0.00408 \\ 0.00133 & 0.001971 & -0.006552 & 0.062133 & 0.065854 & 1.255976 & 0.004107 & 0.006124 & 0.008235 & 0.003431 \\ 0.00192 & 0.001806 & -0.005438 & 0.000427 & -0.180156 & 0.906287 & 0.003073 & 0.00408 & 0.003431 & 0.003157 \end{bmatrix}$$

$$\Sigma_{b_{z6}^t} = \begin{bmatrix} 0.260152 & -0.000759 & -0.07807 & -0.071349 & -74.517392 & -74.548034 & 0.000568 & -0.007383 & 0.002285 & -0.002711 \\ -0.000759 & 0.005694 & -0.003277 & 0.069601 & 0.006431 & 0.279731 & 0.000276 & 0.000299 & 0.000637 & 0.00042 \\ -0.07807 & -0.003277 & 0.163365 & -0.266907 & 50.350178 & 48.476528 & 0.000908 & 0.002219 & -0.005132 & -0.000536 \\ -0.071349 & 0.069601 & -0.266907 & 444.164393 & -87.907423 & -36.135977 & 0.077848 & 0.093787 & 0.078571 & 0.008917 \\ -74.517392 & 0.006431 & 50.350178 & -87.907423 & 56283.73209 & 54998.84085 & 1.030493 & 4.385472 & -1.619441 & 1.55398 \\ -74.548034 & 0.279731 & 48.476528 & -36.135977 & 54998.84085 & 55925.68443 & 1.248181 & 4.606288 & -1.336685 & 1.617551 \\ 0.000568 & 0.000276 & 0.000908 & 0.077848 & 1.030493 & 1.248181 & 0.003248 & 0.001294 & 0.000463 & 0.000327 \\ -0.007383 & 0.000299 & 0.002219 & 0.093787 & 4.385472 & 4.606288 & 0.001294 & 0.004592 & 0.000047 & 0.000589 \\ 0.002285 & 0.000637 & -0.005132 & 0.078571 & -1.619441 & -1.336685 & 0.000463 & 0.000047 & 0.002383 & 0.000301 \\ -0.002711 & 0.00042 & -0.000536 & 0.008917 & 1.55398 & 1.617551 & 0.000327 & 0.000589 & 0.000301 & 0.001147 \end{bmatrix}$$

$$\Sigma_{b_{z7}^t} = \begin{bmatrix} 0.664992 & 0.064582 & 0.044836 & -0.740218 & -4.80114 & 58.369125 & -0.011792 & -0.037875 & -0.001233 & 0.028489 \\ 0.064582 & 0.073847 & 0.047572 & -0.381734 & -1.907918 & -3.98616 & -0.000768 & 0.004088 & -0.002518 & 0.006428 \\ 0.044836 & 0.047572 & 0.135309 & -0.987556 & -0.938017 & 14.097774 & -0.010419 & -0.003655 & -0.011878 & 0.012202 \\ -0.740218 & -0.381734 & -0.987556 & 390.527618 & 24.472053 & -253.63455 & 0.298702 & 0.106712 & 0.095716 & -0.202949 \\ -4.80114 & -1.907918 & -0.938017 & 24.472053 & 612.380687 & -405.159002 & 0.472932 & 0.284248 & 0.073249 & -0.420891 \\ 58.369125 & -3.98616 & 14.097774 & -253.63455 & -405.159002 & 43202.52485 & -7.498365 & -16.248078 & -3.574697 & 7.873121 \\ -0.011792 & -0.000768 & -0.010419 & 0.298702 & 0.472932 & -7.498365 & 0.016606 & 0.008903 & 0.002473 & -0.003567 \\ -0.037875 & 0.004088 & -0.003655 & 0.106712 & 0.284248 & -16.248078 & 0.008903 & 0.019725 & 0.001675 & -0.004679 \\ -0.001233 & -0.002518 & -0.011878 & 0.095716 & 0.073249 & -3.574697 & 0.002473 & 0.001675 & 0.005796 & -0.002676 \\ 0.028489 & 0.006428 & 0.012202 & -0.202949 & -0.420891 & 7.873121 & -0.003567 & -0.004679 & -0.002676 & 0.005017 \end{bmatrix}$$

$$\Sigma_{b_{28}^t} = \begin{bmatrix} 0.419793 & -0.00464 & 0.006104 & -0.063121 & 1.532001 & 26.322499 & -0.000716 & -0.005122 & 0.015477 & 0.003489 \\ -0.00464 & 0.027888 & 0.002442 & 0.04575 & -0.608392 & 0.874365 & 0.008064 & 0.008209 & 0.004769 & 0.00115 \\ 0.006104 & 0.002442 & 0.124974 & -0.094322 & 0.327492 & 1.591006 & -0.004556 & -0.007818 & -0.005713 & -0.00231 \\ -0.063121 & 0.04575 & -0.094322 & 90.338091 & 2.479707 & -9.204134 & 0.066078 & 0.065373 & 0.054813 & 0.003732 \\ 1.532001 & -0.608392 & 0.327492 & 2.479707 & 378.048846 & 631.525289 & 0.036195 & -0.018803 & 0.004193 & 0.032235 \\ 26.322499 & 0.874365 & 1.591006 & -9.204134 & 631.525289 & 17191.97124 & 1.363858 & 2.56628 & 0.379649 & 0.648953 \\ -0.000716 & 0.008064 & -0.004556 & 0.066078 & 0.036195 & 1.363858 & 0.015201 & 0.015065 & 0.007225 & 0.001366 \\ -0.005122 & 0.008209 & -0.007818 & 0.065373 & -0.018803 & 2.56628 & 0.015065 & 0.021197 & 0.007344 & 0.001525 \\ 0.015477 & 0.004769 & -0.005713 & 0.054813 & 0.004193 & 0.379649 & 0.007225 & 0.007344 & 0.010115 & 0.001062 \\ 0.003489 & 0.00115 & -0.00231 & 0.003732 & 0.032235 & 0.648953 & 0.001366 & 0.001525 & 0.001062 & 0.002081 \end{bmatrix}.$$

2.2 Parameters of the SAE Level 3 NDRT Model

For any number of time slices $T \geq 1$, the SAE Level 3 NDRT model defines the JPD

$$p\left(S_1^{1:T}, B^{1:T}, \boldsymbol{F}_{\text{Rel}}^{1:T} : \boldsymbol{\theta}\right) = p(B^1 : \boldsymbol{\theta}_{B^1}) \prod_{t=2}^{T} p\left(B^t | B^{t-1} : \boldsymbol{\theta}_{B^t|B^{t-1}}\right) \prod_{t=1}^{T} p\left(S_1^t | B^t : \boldsymbol{\theta}_{S_1^t|B^t}\right) p\left(\boldsymbol{F}_{\text{Rel}}^t | B^t : \boldsymbol{\theta}\right),$$

with $p\left(\boldsymbol{F}_{\text{Rel}}^t \mid B^t : \boldsymbol{\theta}\right)$ factorizing as

$$p\left(F_{45}^t | B^t : \boldsymbol{\theta}_{F_{45}^t|B^t}\right) p\left(F_{17}^t, F_{20}^t | B^t, F_4^t : \boldsymbol{\theta}_{F_{17}^t,F_{20}^t|B^t,F_4^t}\right) p\left(F_7^t, F_{58}^t, F_{43}^t | B^t : \boldsymbol{\theta}_{F_7^t,\ldots,F_{43}^t|B^t}\right)$$

$$p\left(F_9^t, F_{16}^t, F_{32}^t, F_{34}^t, F_{52}^t, F_{42}^t, F_{12}^t, F_{66}^t | B^t : \boldsymbol{\theta}_{F_9^t,\ldots,F_{66}^t|B^t}\right) p\left(F_{10}^t, F_{38}^t | B^t : \boldsymbol{\theta}_{F_{10}^t,F_{38}^t|B^t}\right)$$

$$p\left(F_{30}^t, F_{36}^t, F_{60}^t | B^t : \boldsymbol{\theta}_{F_{30}^t,\ldots,F_{60}^t|B^t}\right) p\left(F_{11}^t | B^t, F_2^t : \boldsymbol{\theta}_{F_{11}^t|B^t,F_2^t}\right).$$

As such, the model is defined by ten probability /density distribution to be detailed in the following. The names of the relevant indicators $\boldsymbol{F}_{\text{Rel}} = \{F_2, F_4, F_7, F_9, F_{10}, F_{11}, F_{12}, F_{16}, F_{17}, F_{20}, F_{30}, F_{32}, F_{34}, F_{36}, F_{38}, F_{42}, F_{43}, F_{45}, F_{52}, F_{58}, F_{60}, F_{66}\}$ are provided in Table 6.

Table 25: The set of relevant indicators for the SAE Level 3 NDRT model, $\boldsymbol{F}_{\text{Rel}} = \{F_2, F_4, F_7, F_9, F_{10}, F_{11}, F_{12}, F_{16}, F_{17}, F_{20}, F_{30}, F_{32}, F_{34}, F_{36}, F_{38}, F_{42}, F_{43}, F_{45}, F_{52}, F_{58}, F_{60}, F_{66}\}$.

Symbol	Name
F_2	Head rotation valid
F_4	Gaze direction valid
F_7	Pupil diameter variability
F_9	Mean blink frequency
F_{10}	Blink frequency variability
F_{11}	Yaw angle of the head
F_{12}	Mean yaw angle of the head
F_{16}	Yaw rate of the head variability
F_{17}	Gaze heading
F_{20}	Gaze pitch
F_{30}	Monitoring frequency variability
F_{32}	Mean saccade frequency
F_{34}	Dwell percentage
F_{36}	Dwell percentage variability
F_{38}	Mean time since last look at left mirror AOI
F_{42}	Time since last look at right mirror AOI

F_{43}	Mean time since last look at right mirror AOI
F_{45}	Right mirror AOI dwell percentage
F_{52}	Time since last look at tachometer AOI
F_{58}	Mean time since last look at infotainment AOI
F_{60}	Infotainment AOI dwell percentage
F_{66}	Front AOI frequency

Distribution $p(B^1 : \boldsymbol{\theta}_{B^1})$

The distribution $p(B^1 : \boldsymbol{\theta}_{B^1})$ is a categorical distribution

$$p(B^1 : \boldsymbol{\theta}_{B^1}) = \mathrm{Cat}(B^1 : \boldsymbol{\theta}_{B^1})$$

over the discrete variable B, $\mathrm{Val}(B) = \{b_0, b_1, b_2\}$ at time slice $t = 1$, with MAP parameters

$$\boldsymbol{\theta}_{B^1} = \left\{\theta_{b_0^1}, \theta_{b_1^1}, \theta_{b_2^1}\right\} = \{0.351067, 0.325515, 0.323418\}.$$

Distribution $p\left(B^t|B^{t-1} : \boldsymbol{\theta}_{B^t|B^{t-1}}\right)$

The distribution $p\left(B^t|B^{t-1} : \boldsymbol{\theta}_{B^t|B^{t-1}}\right)$ over the discrete variable B, $\mathrm{Val}(B) = \{b_0, b_1, b_2\}$ at time slice $t > 1$ is a collection of categorical distributions with a categorical distribution

$$p\left(B^t|b^{t-1} : \boldsymbol{\theta}_{B^t|b^{t-1}}\right) = \mathrm{Cat}\left(B^t : \boldsymbol{\theta}_{B^t|b^{t-1}}\right)$$

for each $b^{t-1} \in \mathrm{Val}(B)$, parameterized with MAP parameters $\boldsymbol{\theta}_{B^t|B^{t-1}} = \left\{\boldsymbol{\theta}_{B^t|b_0^{t-1}}, \boldsymbol{\theta}_{B^t|b_1^{t-1}}, \boldsymbol{\theta}_{B^t|b_2^{t-1}}\right\}$, where

$$\boldsymbol{\theta}_{B^t|b_0^{t-1}} = \left\{\theta_{b_0^t|b_0^{t-1}}, \theta_{b_1^t|b_0^{t-1}}, \theta_{b_2^t|b_0^{t-1}}\right\} = \{0.999424, 0.000288, 0.000288\},$$

$$\boldsymbol{\theta}_{B^t|b_1^{t-1}} = \left\{\theta_{b_0^t|b_1^{t-1}}, \theta_{b_1^t|b_1^{t-1}}, \theta_{b_2^t|b_1^{t-1}}\right\} = \{0.000311, 0.999378, 0.000311\},$$

$$\boldsymbol{\theta}_{B^t|b_2^{t-1}} = \left\{\theta_{b_0^t|b_2^{t-1}}, \theta_{b_1^t|b_2^{t-1}}, \theta_{b_2^t|b_2^{t-1}}\right\} = \{0.000313, 0.000313, 0.999374\}.$$

Distribution $p\left(S_1^t|B^t : \boldsymbol{\theta}_{S_1^t|B^t}\right)$

The distribution $p\left(S_1^t|B^t : \boldsymbol{\theta}_{S_1^t|B^t}\right)$ over the binary variable S_1, $\mathrm{Val}(S_1) = \{s_{1_0}, s_{1_1}\}$ at time slice $t \geq 1$ is a collection of categorical distributions with a categorical distribution

$$p\left(S_1^t : b^t, \boldsymbol{\theta}_{S_1^t|b^t}\right) = \mathrm{Cat}\left(S_1^t : \boldsymbol{\theta}_{S_1^t|b^t}\right)$$

for each $b^t \in \mathrm{Val}(B)$, parameterized with MAP parameters $\boldsymbol{\theta}_{S_1^t|B^t} = \left\{\boldsymbol{\theta}_{S_1^t|b_0^t}, \boldsymbol{\theta}_{S_1^t|b_1^t}, \boldsymbol{\theta}_{S_1^t|b_2^t}\right\}$, where

$$\boldsymbol{\theta}_{S_1^t|b_0^t} = \left\{\theta_{s_{1_0}^t|b_0^t}, \theta_{s_{1_1}^t|b_0^t}\right\} = \{0.000446, 0.999554\},$$

$$\boldsymbol{\theta}_{S_1^t|b_1^t} = \left\{\theta_{s_{1_0}^t|b_1^t}, \theta_{s_{1_1}^t|b_1^t}\right\} = \{0.999519, 0.000481\},$$

$$\boldsymbol{\theta}_{S_1^t|b_2^t} = \left\{\theta_{s_{1_0}^t|b_2^t}, \theta_{s_{1_1}^t|b_2^t}\right\} = \{0.999516, 0.000484\}.$$

Distribution $p\left(F_{45}^t|B^t : \boldsymbol{\theta}_{F_{45}^t|B^t}\right)$

The distribution $p\left(F_{45}^t|B^t : \boldsymbol{\theta}_{F_{45}^t|B^t}\right)$ over the continuous variable F_{45} at time slice $t \geq 1$ is a collection of Gaussian mixture distributions with a GMM

$$p\left(F_{45}^t|b^t : \boldsymbol{\theta}_{F_{45}^t|b^t}\right) = \sum_{i=1}^{n_b} \pi_{b^t{}_i} \mathcal{N}\left(\mu_{b^t{}_i}, \sigma^2_{b^t{}_i}\right)$$

composed of n_b components for each $b^t \in \mathrm{Val}(B)$, parameterized with MAP parameters $\boldsymbol{\theta}_{F_{45}^t|B^t} = \left\{\boldsymbol{\theta}_{F_{45}^t|b_0^t}, \boldsymbol{\theta}_{F_{45}^t|b_1^t}, \boldsymbol{\theta}_{F_{45}^t|b_2^t}\right\}$.

The distribution

$$p\left(F_{45}^t|b_0^t : \boldsymbol{\theta}_{F_{45}^t|b_0^t} = \left\{\left\{\pi_{b_{0i}^t}, \mu_{b_{0i}^t}, \sigma^2_{b_{0i}^t}\right\}_{i=1}^4\right\}\right)$$

consists of four components, where

$$\pi_{b_{01}^t} = 0.0041, \pi_{b_{02}^t} = 0.926419, \pi_{b_{03}^t} = 0.02003, \pi_{b_{04}^t} = 0.049452,$$

$$\mu_{b_{01}^t} = 0.375621, \mu_{b_{02}^t} = 0.000018, \mu_{b_{03}^t} = 0.022852, \mu_{b_{04}^t} = 0.007424,$$

$$\sigma^2_{b_{01}^t} = 0.033238, \sigma^2_{b_{02}^t} = 3.7154\text{e-}7, \sigma^2_{b_{03}^t} = 0.00012, \sigma^2_{b_{04}^t} = 0.000029.$$

The distribution

$$p\left(F_{45}^t|b_1^t : \boldsymbol{\theta}_{F_{45}^t|b_1^t} = \left\{\left\{\pi_{b_{1i}^t}, \mu_{b_{1i}^t}, \sigma^2_{b_{1i}^t}\right\}_{i=1}^4\right\}\right)$$

consists of four components, where

$$\pi_{b_{11}^t} = 0.012508, \pi_{b_{12}^t} = 0.043687, \pi_{b_{13}^t} = 0.048598, \pi_{b_{14}^t} = 0.895207,$$

$$\mu_{b_{11}^t} = 0.093504, \mu_{b_{12}^t} = 0.008892, \mu_{b_{13}^t} = 0.040133, \mu_{b_{14}^t} = 0.000016,$$

$$\sigma^2_{b_{11}^t} = 0.000358, \sigma^2_{b_{12}^t} = 0.000045, \sigma^2_{b_{13}^t} = 0.000178, \sigma^2_{b_{14}^t} = 4.0639\text{e-}7.$$

The distribution

$$p\left(F_{45}^t|b_2^t : \boldsymbol{\theta}_{F_{45}^t|b_2^t} = \left\{\left\{\pi_{b_{2i}^t}, \mu_{b_{2i}^t}, \sigma^2_{b_{2i}^t}\right\}_{i=1}^5\right\}\right)$$

consists of five components, where

$$\pi_{b_{21}^t} = 0.243136, \pi_{b_{22}^t} = 0.243136, \pi_{b_{23}^t} = 0.243136, \pi_{b_{24}^t} = 0.243136, \pi_{b_{25}^t} = 0.027455,$$

$$\mu_{b_{21}^t} = 9.8394\text{e-}6, \mu_{b_{22}^t} = 9.8394\text{e-}6, \mu_{b_{23}^t} = 9.8394\text{e-}6, \mu_{b_{24}^t} = 9.8394\text{e-}6, \mu_{b_{25}^t} = 0.010093$$

$$\sigma^2_{b_{21}^t} = 1.4213\text{e-}6, \sigma^2_{b_{22}^t} = 1.4213\text{e-}6, \sigma^2_{b_{23}^t} = 1.4213\text{e-}6, \sigma^2_{b_{24}^t} = 1.4213\text{e-}6, \sigma^2_{b_{25}^t} = 0.000041.$$

Distribution $p\left(F_{17}^t, F_{20}^t|B^t, F_4^t : \boldsymbol{\theta}_{F_{17}^t, F_{20}^t|B^t, F_4^t}\right)$

The distribution $p\left(F_{17}^t, F_{20}^t | B^t, F_4^t : \boldsymbol{\theta}_{F_{17}^t, F_{20}^t | B^t, F_4^t}\right)$ over the two-dimensional vector of continuous variables (F_{17}, F_{20}) at time slice $t \geq 1$ is a collection of bivariate Gaussian mixture distributions with a bivariate GMM

$$p\left(F_{17}^t, F_{20}^t | b^t, f_2^t : \boldsymbol{\theta}_{F_{17}^t, F_{20}^t | b^t, f_4^t}\right) = \sum_{i=1}^{n_{b,f}} \pi_{b^t{}_i} \mathcal{N}\left(\boldsymbol{\mu}_{b^t, f^t{}_i}, \Sigma_{b^t, f^t{}_i}\right)$$

composed of $n_{b,f}$ components for each $\{b^t, f_4^t\} \in \mathrm{Val}(B) \times \mathrm{Val}(F_4)$, parameterized with MAP parameters

$$\boldsymbol{\theta}_{F_{17}^t, F_{20}^t | B^t, F_4^t} = \left\{\boldsymbol{\theta}_{F_{17}^t, F_{20}^t | b_0^t, f_0^t}, \boldsymbol{\theta}_{F_{17}^t, F_{20}^t | b_1^t, f_0^t}, \boldsymbol{\theta}_{F_{17}^t, F_{20}^t | b_2^t, f_0^t}, \boldsymbol{\theta}_{F_{17}^t, F_{20}^t | b_0^t, f_1^t}, \boldsymbol{\theta}_{F_{17}^t, F_{20}^t | b_1^t, f_1^t}, \boldsymbol{\theta}_{F_{17}^t, F_{20}^t | b_2^t, f_1^t}\right\}.$$

The distribution

$$p\left(F_{17}^t, F_{20}^t | b_0^t, f_4^t{}_0 : \boldsymbol{\theta}_{F_{17}^t, F_{20}^t | b_0^t, f_0^t} = \left\{\left\{\pi_{b_0^t, f_0^t{}_i}, \boldsymbol{\mu}_{b_0^t, f_0^t{}_i}, \Sigma_{b_0^t, f_0^t{}_i}\right\}_{i=1}^{1}\right\}\right)$$

consists of one component, where

$$\pi_{b_0^t, f_0^t{}_1} = 1, \boldsymbol{\mu}_{b_0^t, f_0^t{}_1} = \begin{pmatrix} -0.086255 \\ -0.207994 \end{pmatrix}, \Sigma_{b_0^t, f_0^t{}_1} = \begin{bmatrix} 4.989933 & 0 \\ 0 & 2.217657 \end{bmatrix}.$$

The distribution

$$p\left(F_{17}^t, F_{20}^t | b_1^t, f_4^t{}_0 : \boldsymbol{\theta}_{F_{17}^t, F_{20}^t | b_1^t, f_0^t} = \left\{\left\{\pi_{b_1^t, f_0^t{}_i}, \boldsymbol{\mu}_{b_1^t, f_0^t{}_i}, \Sigma_{b_1^t, f_0^t{}_i}\right\}_{i=1}^{1}\right\}\right)$$

consists of one component, where

$$\pi_{b_1^t, f_0^t{}_1} = 1, \boldsymbol{\mu}_{b_1^t, f_0^t{}_1} = \begin{pmatrix} -0.086255 \\ -0.207994 \end{pmatrix}, \Sigma_{b_1^t, f_0^t{}_1} = \begin{bmatrix} 4.989933 & 0 \\ 0 & 2.217657 \end{bmatrix}.$$

The distribution

$$p\left(F_{17}^t, F_{20}^t | b_2^t, f_4^t{}_0 : \boldsymbol{\theta}_{F_{17}^t, F_{20}^t | b_2^t, f_0^t} = \left\{\left\{\pi_{b_2^t, f_0^t{}_i}, \boldsymbol{\mu}_{b_2^t, f_0^t{}_i}, \Sigma_{b_2^t, f_0^t{}_i}\right\}_{i=1}^{1}\right\}\right)$$

consists of one component, where

$$\pi_{b_2^t, f_0^t{}_1} = 1, \boldsymbol{\mu}_{b_2^t, f_0^t{}_1} = \begin{pmatrix} -0.086255 \\ -0.207994 \end{pmatrix}, \Sigma_{b_2^t, f_0^t{}_1} = \begin{bmatrix} 4.989933 & 0 \\ 0 & 2.217657 \end{bmatrix}.$$

The distribution

$$p\left(F_{17}^t, F_{20}^t | b_0^t, f_4^t{}_1 : \boldsymbol{\theta}_{F_{17}^t, F_{20}^t | b_0^t, f_1^t} = \left\{\left\{\pi_{b_0^t, f_1^t{}_i}, \boldsymbol{\mu}_{b_0^t, f_1^t{}_i}, \Sigma_{b_0^t, f_1^t{}_i}\right\}_{i=1}^{7}\right\}\right)$$

consists of seven components, where

$$\pi_{b_0^t, f_1^t{}_1} = 0.060685, \pi_{b_0^t, f_1^t{}_2} = 0.077781, \pi_{b_0^t, f_1^t{}_3} = 0.565049, \pi_{b_0^t, f_1^t{}_4} = 0.146582,$$

$$\pi_{b_0^t, f_1^t{}_5} = 0.083988, \pi_{b_0^t, f_1^t{}_6} = 0.016744, \pi_{b_0^t, f_1^t{}_7} = 0.04917,$$

$$\boldsymbol{\mu}_{b_0^t, f_1^t{}_1} = \begin{pmatrix} -0.541597 \\ 0.009207 \end{pmatrix}, \boldsymbol{\mu}_{b_0^t, f_1^t{}_2} = \begin{pmatrix} 0.682617 \\ -0.321907 \end{pmatrix}, \boldsymbol{\mu}_{b_0^t, f_1^t{}_3} = \begin{pmatrix} 0.00675 \\ -0.065621 \end{pmatrix},$$

$$\boldsymbol{\mu}_{b_0^t,f_1^t{}_4} = \begin{pmatrix} 0.087835 \\ -0.078207 \end{pmatrix}, \boldsymbol{\mu}_{b_0^t,f_1^t{}_5} = \begin{pmatrix} 0.073547 \\ -0.115864 \end{pmatrix}, \boldsymbol{\mu}_{b_0^t,f_1^t{}_6} = \begin{pmatrix} -0.409551 \\ -0.151175 \end{pmatrix},$$

$$\boldsymbol{\mu}_{b_0^t,f_1^t{}_7} = \begin{pmatrix} 0.097175 \\ -0.443795 \end{pmatrix},$$

$$\Sigma_{b_0^t,f_1^t{}_1} = \begin{bmatrix} 0.009947 & -0.001771 \\ -0.001771 & 0.004572 \end{bmatrix}, \Sigma_{b_0^t,f_1^t{}_2} = \begin{bmatrix} 0.007001 & 0.000381 \\ 0.000381 & 0.004523 \end{bmatrix},$$

$$\Sigma_{b_0^t,f_1^t{}_3} = \begin{bmatrix} 0.002536 & -0.000671 \\ -0.000671 & 0.000941 \end{bmatrix}, \Sigma_{b_0^t,f_1^t{}_4} = \begin{bmatrix} 0.049745 & -0.004773 \\ -0.004773 & 0.002749 \end{bmatrix},$$

$$\Sigma_{b_0^t,f_1^t{}_5} = \begin{bmatrix} 0.414968 & 0.008459 \\ 0.008459 & 0.013105 \end{bmatrix}, \Sigma_{b_0^t,f_1^t{}_6} = \begin{bmatrix} 0.285366 & 0.006683 \\ 0.006683 & 0.085211 \end{bmatrix},$$

$$\Sigma_{b_0^t,f_1^t{}_7} = \begin{bmatrix} 0.010575 & -0.000727 \\ -0.000727 & 0.007919 \end{bmatrix}.$$

The distribution

$$p\left(F_{17}^t, F_{20}^t | b_1^t, f_4^t{}_1 : \boldsymbol{\theta}_{F_{17}^t,F_{20}^t|b_1^t,f_1^t} = \left\{\left\{\pi_{b_1^t,f_1^t{}_i}, \boldsymbol{\mu}_{b_1^t,f_1^t{}_i}, \Sigma_{b_1^t,f_1^t{}_i}\right\}_{i=1}^{8}\right\}\right)$$

consists of eight components, where

$$\pi_{b_1^t,f_1^t{}_1} = 0.705296, \pi_{b_1^t,f_1^t{}_2} = 0.04684, \pi_{b_1^t,f_1^t{}_3} = 0.010643,$$

$$\pi_{b_1^t,f_1^t{}_4} = 0.00922, \pi_{b_1^t,f_1^t{}_5} = 0.053758, \pi_{b_1^t,f_1^t{}_6} = 0.003761,$$

$$\pi_{b_1^t,f_1^t{}_7} = 0.070669, \pi_{b_1^t,f_1^t{}_8} = 0.099812,$$

$$\boldsymbol{\mu}_{b_1^t,f_1^t{}_1} = \begin{pmatrix} 0.015512 \\ -0.07703 \end{pmatrix}, \boldsymbol{\mu}_{b_1^t,f_1^t{}_2} = \begin{pmatrix} -0.546049 \\ 0.002305 \end{pmatrix}, \boldsymbol{\mu}_{b_1^t,f_1^t{}_3} = \begin{pmatrix} -0.269904 \\ -0.41516 \end{pmatrix},$$

$$\boldsymbol{\mu}_{b_1^t,f_1^t{}_4} = \begin{pmatrix} -1.002795 \\ -0.153243 \end{pmatrix}, \boldsymbol{\mu}_{b_1^t,f_1^t{}_5} = \begin{pmatrix} -0.029412 \\ -0.196255 \end{pmatrix}, \boldsymbol{\mu}_{b_1^t,f_1^t{}_6} = \begin{pmatrix} 0.245931 \\ 0.037466 \end{pmatrix},$$

$$\boldsymbol{\mu}_{b_1^t,f_1^t{}_7} = \begin{pmatrix} 0.635173 \\ -0.326585 \end{pmatrix}, \boldsymbol{\mu}_{b_1^t,f_1^t{}_8} = \begin{pmatrix} 0.099579 \\ -0.055232 \end{pmatrix},$$

$$\Sigma_{b_1^t,f_1^t{}_1} = \begin{bmatrix} 0.001415 & -0.000075 \\ -0.000075 & 0.00092 \end{bmatrix}, \Sigma_{b_1^t,f_1^t{}_2} = \begin{bmatrix} 0.009258 & -0.002274 \\ -0.002274 & 0.007474 \end{bmatrix},$$

$$\Sigma_{b_1^t,f_1^t{}_3} = \begin{bmatrix} 0.081442 & 0.002338 \\ 0.002338 & 0.026413 \end{bmatrix}, \Sigma_{b_1^t,f_1^t{}_4} = \begin{bmatrix} 0.054998 & -0.002912 \\ -0.002912 & 0.015058 \end{bmatrix},$$

$$\Sigma_{b_1^t,f_1^t{}_5} = \begin{bmatrix} 0.01493 & -0.009576 \\ -0.009576 & 0.034119 \end{bmatrix}, \Sigma_{b_1^t,f_1^t{}_6} = \begin{bmatrix} 0.428541 & -0.037214 \\ -0.037214 & 0.101003 \end{bmatrix},$$

$$\Sigma_{b_1^t,f_1^t{}_7} = \begin{bmatrix} 0.007759 & 0.000152 \\ 0.000152 & 0.006165 \end{bmatrix}, \Sigma_{b_1^t,f_1^t{}_8} = \begin{bmatrix} 0.048551 & -0.003522 \\ -0.003522 & 0.006642 \end{bmatrix}.$$

The distribution

$$p\left(F_{17}^t, F_{20}^t | b_2^t, f_4^t{}_1 : \boldsymbol{\theta}_{F_{17}^t,F_{20}^t|b_2^t,f_1^t} = \left\{\left\{\pi_{b_2^t,f_1^t{}_i}, \boldsymbol{\mu}_{b_2^t,f_1^t{}_i}, \Sigma_{b_2^t,f_1^t{}_i}\right\}_{i=1}^{5}\right\}\right)$$

consists of five components, where

$$\pi_{b_2^t,f_1^t{}_1} = 0.055343, \pi_{b_2^t,f_1^t{}_2} = 0.101241, \pi_{b_2^t,f_1^t{}_3} = 0.741498,$$

$$\pi_{b_2^t,f_1^t{}_4} = 0.00309, \pi_{b_2^t,f_1^t{}_5} = 0.098829,$$

$$\boldsymbol{\mu}_{b_2^t,f_1^t{}_1} = \begin{pmatrix}-0.413927\\-0.772137\end{pmatrix}, \boldsymbol{\mu}_{b_2^t,f_1^t{}_2} = \begin{pmatrix}-0.244466\\-0.10883\end{pmatrix}, \boldsymbol{\mu}_{b_2^t,f_1^t{}_3} = \begin{pmatrix}-0.513355\\-0.589431\end{pmatrix},$$

$$\boldsymbol{\mu}_{b_2^t,f_1^t{}_4} = \begin{pmatrix}0.131744\\-0.570139\end{pmatrix}, \boldsymbol{\mu}_{b_2^t,f_1^t{}_5} = \begin{pmatrix}0.02788\\-0.075629\end{pmatrix},$$

$$\Sigma_{b_2^t,f_1^t{}_1} = \begin{bmatrix}0.099779 & -0.014832\\-0.014832 & 0.054602\end{bmatrix}, \Sigma_{b_2^t,f_1^t{}_2} = \begin{bmatrix}0.253046 & -0.051573\\-0.051573 & 0.027301\end{bmatrix},$$

$$\Sigma_{b_2^t,f_1^t{}_3} = \begin{bmatrix}0.016979 & -0.002544\\-0.002544 & 0.011119\end{bmatrix}, \Sigma_{b_2^t,f_1^t{}_4} = \begin{bmatrix}0.310457 & -0.095383\\-0.095383 & 0.292944\end{bmatrix},$$

$$\Sigma_{b_2^t,f_1^t{}_5} = \begin{bmatrix}0.006297 & 0.000138\\0.000138 & 0.002303\end{bmatrix}.$$

Distribution $p\left(F_7^t, F_{58}^t, F_{43}^t | B^t : \boldsymbol{\theta}_{F_7^t,\dots,F_{43}^t|B^t}\right)$

The distribution $p\left(F_7^t, F_{58}^t, F_{43}^t | B^t : \boldsymbol{\theta}_{F_7^t,\dots,F_{43}^t|B^t}\right)$ over a three-dimensional vector of continuous variables (F_7, F_{58}, F_{43}) at time slice $t \geq 1$ is a collection of multivariate Gaussian mixture distributions with a multivariate GMM

$$p\left(F_7^t, F_{58}^t, F_{43}^t | b^t : \boldsymbol{\theta}_{F_7^t,\dots,F_{43}^t|b^t}\right) = \sum_{i=1}^{n_b} \pi_{b^t{}_i} \mathcal{N}\left(\boldsymbol{\mu}_{b^t{}_i}, \Sigma_{b^t{}_i}\right)$$

composed of n_b components for each $b^t \in \mathrm{Val}(B)$, parameterized with MAP parameters $\boldsymbol{\theta}_{F_7^t,\dots,F_{43}^t|B^t} = \left\{\boldsymbol{\theta}_{F_7^t,\dots,F_{43}^t|b_0^t}, \boldsymbol{\theta}_{F_7^t,\dots,F_{43}^t|b_1^t}, \boldsymbol{\theta}_{F_7^t,\dots,F_{43}^t|b_2^t}\right\}$.

The distribution

$$p\left(F_7^t, F_{58}^t, F_{43}^t | b_0^t : \boldsymbol{\theta}_{F_7^t,\dots,F_{43}^t|b_0^t} = \left\{\left\{\pi_{b_0^t{}_i}, \boldsymbol{\mu}_{b_0^t{}_i}, \Sigma_{b_0^t{}_i}\right\}_{i=1}^{9}\right\}\right)$$

consists of nine components, where

$$\pi_{b_0^t{}_1} = 0.116926, \pi_{b_0^t{}_2} = 0.132012, \pi_{b_0^t{}_3} = 0093628,$$

$$\pi_{b_0^t{}_4} = 0.236375, \pi_{b_0^t{}_5} = 0.038621, \pi_{b_0^t{}_6} = 0.005913,$$

$$\pi_{b_0^t{}_7} = 0.262419, \pi_{b_0^t{}_8} = 0.10419, \pi_{b_0^t{}_9} = 0.009918,$$

$$\boldsymbol{\mu}_{b_0^t{}_1} = \begin{pmatrix}0.000357\\60.445776\\465.063784\end{pmatrix}, \boldsymbol{\mu}_{b_0^t{}_2} = \begin{pmatrix}0.000263\\126.246888\\53.262756\end{pmatrix}, \boldsymbol{\mu}_{b_0^t{}_3} = \begin{pmatrix}0.000478\\31.457492\\56.395437\end{pmatrix},$$

$$\boldsymbol{\mu}_{b_0^t{}_4} = \begin{pmatrix}0.000173\\59.26661\\92.537564\end{pmatrix}, \boldsymbol{\mu}_{b_0^t{}_5} = \begin{pmatrix}0.000204\\407.372676\\479.222643\end{pmatrix}, \boldsymbol{\mu}_{b_0^t{}_6} = \begin{pmatrix}0.001446\\69.229103\\397.991361\end{pmatrix},$$

$$\boldsymbol{\mu}_{b_0^t{}_7} = \begin{pmatrix}0.000223\\24.020484\\232.480424\end{pmatrix}, \boldsymbol{\mu}_{b_0^t{}_8} = \begin{pmatrix}0.00028\\163.432617\\230.398624\end{pmatrix}, \boldsymbol{\mu}_{b_0^t{}_9} = \begin{pmatrix}0.001169\\92.827234\\53.103306\end{pmatrix},$$

$$\Sigma_{b_0^t{}_1} = \begin{bmatrix}2.4509\text{e-}8 & -0.001049 & -0.00199\\-0.001049 & 1454.470942 & 511.185861\\-0.00199 & 511.185861 & 4564.496159\end{bmatrix}, \Sigma_{b_0^t{}_2} = \begin{bmatrix}1.3082\text{e-}8 & -0.000482 & 0.001798\\-0.000482 & 2273.545082 & -273.916668\\0.001798 & -273.916668 & 1773.062508\end{bmatrix},$$

$$\Sigma_{b_{0}^{t}{}_{3}} = \begin{bmatrix} 4.1325\text{e-}8 & -0.0014 & -0.002496 \\ -0.0014 & 800.497342 & 595.092411 \\ -0.002496 & 595.092411 & 1979.139837 \end{bmatrix}, \Sigma_{b_{0}^{t}{}_{4}} = \begin{bmatrix} 4.5022\text{e-}9 & -0.000185 & -0.000557 \\ -0.000185 & 1118.421241 & 880.482994 \\ -0.000557 & 880.482994 & 3099.338621 \end{bmatrix},$$

$$\Sigma_{b_{0}^{t}{}_{5}} = \begin{bmatrix} 3.0394\text{e-}8 & 0.001587 & 0.001626 \\ 0.001587 & 2509.285491 & 1896.834595 \\ 0.001626 & 1896.834595 & 2764.966613 \end{bmatrix}, \Sigma_{b_{0}^{t}{}_{6}} = \begin{bmatrix} 5.1470\text{e-}7 & 0.01643 & 0.036807 \\ 0.01643 & 4513.635891 & 1152.850965 \\ 0.036807 & 1152.850965 & 9632.065782 \end{bmatrix},$$

$$\Sigma_{b_{0}^{t}{}_{7}} = \begin{bmatrix} 7.2935e-9 & -0.000059 & 0.000587 \\ -0.000059 & 341.060922 & 340.458268 \\ 0.000587 & 340.458268 & 13252.27354 \end{bmatrix}, \Sigma_{b_{0}^{t}{}_{8}} = \begin{bmatrix} 1.4413e-8 & 0.003262 & -0.000914 \\ 0.003262 & 3290.294604 & -93.205655 \\ -0.000914 & -93.205655 & 2903.398131 \end{bmatrix},$$

$$\Sigma_{b_{0}^{t}{}_{9}} = \begin{bmatrix} 3.8649e-7 & -0.042143 & -0.020577 \\ -0.042143 & 9274.476445 & 3041.157569 \\ -0.020577 & 3041.157569 & 5873.543773 \end{bmatrix}.$$

The distribution

$$p\left(F_7^t, F_{58}^t, F_{43}^t | b_1^t : \boldsymbol{\theta}_{F_7^t,\dots,F_{43}^t | b_1^t} = \left\{\left\{\pi_{b_{1}^{t}{}_{i}}, \boldsymbol{\mu}_{b_{1}^{t}{}_{i}}, \Sigma_{b_{1}^{t}{}_{i}}\right\}_{i=1}^{7}\right\}\right)$$

consists of seven components, where

$$\pi_{b_{1}^{t}{}_{1}} = 0.046635, \pi_{b_{1}^{t}{}_{2}} = 0.008009, \pi_{b_{1}^{t}{}_{3}} = 0.099755,$$

$$\pi_{b_{1}^{t}{}_{4}} = 0.56357, \pi_{b_{1}^{t}{}_{5}} = 0.124829, \pi_{b_{1}^{t}{}_{6}} = 0.124162,$$

$$\pi_{b_{1}^{t}{}_{7}} = 0.03304,$$

$$\boldsymbol{\mu}_{b_{1}^{t}{}_{1}} = \begin{pmatrix} 0.000194 \\ 142.914008 \\ 77.743366 \end{pmatrix}, \boldsymbol{\mu}_{b_{1}^{t}{}_{2}} = \begin{pmatrix} 0.000808 \\ 192.505648 \\ 335.65919 \end{pmatrix}, \boldsymbol{\mu}_{b_{1}^{t}{}_{3}} = \begin{pmatrix} 0.000413 \\ 52.732736 \\ 40.155825 \end{pmatrix},$$

$$\boldsymbol{\mu}_{b_{1}^{t}{}_{4}} = \begin{pmatrix} 0.000274 \\ 214.889271 \\ 228.417813 \end{pmatrix}, \boldsymbol{\mu}_{b_{1}^{t}{}_{5}} = \begin{pmatrix} 0.000361 \\ 114.940917 \\ 260.457261 \end{pmatrix}, \boldsymbol{\mu}_{b_{1}^{t}{}_{6}} = \begin{pmatrix} 0.000414 \\ 338.31525 \\ 32.338659 \end{pmatrix},$$

$$\boldsymbol{\mu}_{b_{1}^{t}{}_{7}} = \begin{pmatrix} 0.000214 \\ 36.960203 \\ 443.747062 \end{pmatrix},$$

$$\Sigma_{b_{1}^{t}{}_{1}} = \begin{bmatrix} 1.2802\text{e-}8 & -0.000772 & -0.000106 \\ -0.000772 & 3124.963561 & 1162.741171 \\ -0.000106 & 1162.741171 & 2463.244067 \end{bmatrix}, \Sigma_{b_{1}^{t}{}_{2}} = \begin{bmatrix} 1.8658\text{e-}7 & -0.005624 & -0.014598 \\ -0.005624 & 15181.02221 & 11203.76446 \\ -0.014598 & 11203.76446 & 18371.87139 \end{bmatrix},$$

$$\Sigma_{b_{1}^{t}{}_{3}} = \begin{bmatrix} 2.8183\text{e-}8 & -0.002127 & -0.000753 \\ -0.002127 & 1122.241348 & 170.570597 \\ -0.000753 & 170.570597 & 1528.277141 \end{bmatrix}, \Sigma_{b_{1}^{t}{}_{4}} = \begin{bmatrix} 2.2098\text{e-}8 & -0.005135 & -0.004638 \\ -0.005135 & 23027.09138 & 22735.01559 \\ -0.004638 & 22735.01559 & 22660.68877 \end{bmatrix},$$

$$\Sigma_{b_{1}^{t}{}_{5}} = \begin{bmatrix} 3.1902\text{e-}8 & 0.008007 & 0.005982 \\ 0.008007 & 6230.531822 & 5243.110329 \\ 0.005982 & 5243.110329 & 5292.376553 \end{bmatrix}, \Sigma_{b_{1}^{t}{}_{6}} = \begin{bmatrix} 1.3462\text{e-}8 & 0.00154 & 0.000429 \\ 0.00154 & 3190.224345 & 273.331221 \\ 0.000429 & 273.331221 & 1191.494545 \end{bmatrix},$$

$$\Sigma_{b_{1}^{t}{}_{7}} = \begin{bmatrix} 1.6363\text{e-}8 & 0.000198 & -0.002807 \\ 0.000198 & 1392.377827 & -288.214407 \\ -0.002807 & -288.214407 & 6847.526558 \end{bmatrix}.$$

The distribution

$$p\left(F_7^t, F_{58}^t, F_{43}^t | b_2^t : \boldsymbol{\theta}_{F_7^t,\dots,F_{43}^t | b_2^t} = \left\{\left\{\pi_{b_{2}^{t}{}_{i}}, \boldsymbol{\mu}_{b_{2}^{t}{}_{i}}, \Sigma_{b_{2}^{t}{}_{i}}\right\}_{i=1}^{2}\right\}\right)$$

consists of two components, where

$$\pi_{b_2^t{}_1} = 0.023254, \pi_{b_2^t{}_2} = 0.976746,$$

$$\boldsymbol{\mu}_{b_2^t{}_1} = \begin{pmatrix} 0.003461 \\ 4.731391 \\ 403.234708 \end{pmatrix}, \boldsymbol{\mu}_{b_2^t{}_2} = \begin{pmatrix} 0.000722 \\ 0.480384 \\ 234.366398 \end{pmatrix},$$

$$\Sigma_{b_2^t{}_1} = \begin{bmatrix} 1.5702\text{e-}6 & -0.006964 & -0.004462 \\ -0.006964 & 1109.863582 & 62.763171 \\ -0.004462 & 62.763171 & 17833.41172 \end{bmatrix}, \Sigma_{b_2^t{}_2} = \begin{bmatrix} 1.5775\text{e-}7 & 0.000053 & -0.008444 \\ 0.000053 & 26.636652 & 7.611175 \\ -0.008444 & 7.611175 & 24802.69987 \end{bmatrix}.$$

Distribution $p\left(F_9^t, F_{16}^t, F_{32}^t, F_{34}^t, F_{52}^t, F_{42}^t, F_{12}^t, F_{66}^t | B^t : \boldsymbol{\theta}_{F_9^t,\dots,F_{66}^t|B^t}\right)$

The distribution $p\left(F_9^t, F_{16}^t, F_{32}^t, F_{34}^t, F_{52}^t, F_{42}^t, F_{12}^t, F_{66}^t | B^t : \boldsymbol{\theta}_{F_9^t,\dots,F_{66}^t|B^t}\right)$ over a eight-dimensional vector of continuous variables $(F_9, F_{16}, F_{32}, F_{34}, F_{52}, F_{42}, F_{12}, F_{66})$ at time slice $t \geq 1$ is a collection of multivariate Gaussian mixture distributions with a multivariate GMM

$$p\left(F_9^t, F_{16}^t, F_{32}^t, F_{34}^t, F_{52}^t, F_{42}^t, F_{12}^t, F_{66}^t | b^t : \boldsymbol{\theta}_{F_9^t,\dots,F_{66}^t|b^t}\right) = \sum_{i=1}^{n_b} \pi_{b^t{}_i} \mathcal{N}\left(\boldsymbol{\mu}_{b^t{}_i}, \Sigma_{b^t{}_i}\right)$$

composed of n_b components for each $b^t \in \mathrm{Val}(B)$, parameterized with MAP parameters $\boldsymbol{\theta}_{F_9^t,\dots,F_{66}^t|B^t} = \left\{\boldsymbol{\theta}_{F_9^t,\dots,F_{66}^t|b_0^t}, \boldsymbol{\theta}_{F_9^t,\dots,F_{66}^t|b_1^t}, \boldsymbol{\theta}_{F_9^t,\dots,F_{66}^t|b_2^t}\right\}$.

The distribution

$$p\left(F_9^t, F_{16}^t, F_{32}^t, F_{34}^t, F_{52}^t, F_{42}^t, F_{12}^t, F_{66}^t | b_0^t : \boldsymbol{\theta}_{F_9^t,\dots,F_{66}^t|b_0^t} = \left\{\left\{\pi_{b_0^t{}_i}, \boldsymbol{\mu}_{b_0^t{}_i}, \Sigma_{b_0^t{}_i}\right\}_{i=1}^{8}\right\}\right)$$

consists of eight components, where

$$\pi_{b_0^t{}_1} = 0.002053, \pi_{b_0^t{}_2} = 0.040003, \pi_{b_0^t{}_3} = 0.284031,$$

$$\pi_{b_0^t{}_4} = 0.00322, \pi_{b_0^t{}_5} = 0.04463, \pi_{b_0^t{}_6} = 0.048237,$$

$$\pi_{b_0^t{}_7} = 0.17114, \pi_{b_0^t{}_8} = 0.406686,$$

$$\boldsymbol{\mu}_{b_0^t{}_1} = \begin{pmatrix} 0.81975 \\ 2.623162 \\ 1.944301 \\ 0.459535 \\ 15.790784 \\ 34.066807 \\ -0.375772 \\ 0.46986 \end{pmatrix}, \boldsymbol{\mu}_{b_0^t{}_2} = \begin{pmatrix} 0.297115 \\ 0.341997 \\ 1.135936 \\ 0.725991 \\ 139.367746 \\ 72.582847 \\ 0.080933 \\ 0.290121 \end{pmatrix}, \boldsymbol{\mu}_{b_0^t{}_3} = \begin{pmatrix} 0.379798 \\ 0.098594 \\ 1.294088 \\ 0.933292 \\ 27.583977 \\ 106.842192 \\ 0.087405 \\ 0.308929 \end{pmatrix},$$

$$\boldsymbol{\mu}_{b_0^t{}_4} = \begin{pmatrix} 2.48979 \\ 0.211666 \\ 1.087206 \\ 0.942484 \\ 92.813902 \\ 443.931027 \\ -0.01615 \\ 0.260306 \end{pmatrix}, \boldsymbol{\mu}_{b_0^t{}_5} = \begin{pmatrix} 0.749833 \\ 0.305987 \\ 1.902421 \\ 0.787972 \\ 97.59248 \\ 444.517175 \\ 0.13999 \\ 0.26187 \end{pmatrix}, \boldsymbol{\mu}_{b_0^t{}_6} = \begin{pmatrix} 0.492039 \\ 0.459523 \\ 2.092578 \\ 0.637556 \\ 11.988973 \\ 129.40794 \\ -0.060228 \\ 0.516885 \end{pmatrix},$$

$$\boldsymbol{\mu}_{b_0^t 7} = \begin{pmatrix} 0.724578 \\ 0.11964 \\ 1.769563 \\ 0.890491 \\ 26.874672 \\ 375.19107 \\ 0.087744 \\ 0.308943 \end{pmatrix}, \boldsymbol{\mu}_{b_0^t 8} = \begin{pmatrix} 0.351352 \\ 0.232743 \\ 1.269895 \\ 0.880714 \\ 13.440228 \\ 180.251622 \\ 0.058416 \\ 0.301927 \end{pmatrix},$$

$$\Sigma_{b_0^t 1} = \begin{bmatrix} 0.470077 & 0.030326 & 0.01538 & -0.000839 & -1.788715 & -3.362306 & 0.004137 & 0.006542 \\ 0.030326 & 1.024495 & 0.10691 & -0.080508 & -26.1847 & -63.15604 & -0.133632 & 0.08717 \\ 0.01538 & 0.10691 & 0.591652 & -0.007423 & -4.373796 & -9.378982 & -0.005658 & 0.013132 \\ -0.000839 & -0.080508 & -0.007423 & 0.201564 & 2.168471 & 5.362986 & 0.014656 & -0.007334 \\ -1.788715 & -26.1847 & -4.373796 & 2.168471 & 19637.83385 & 2012.296147 & 3.13024 & -2.735192 \\ -3.362306 & -63.15604 & -9.378982 & 5.362986 & 2012.296147 & 38632.9553 & 8.299236 & -6.23692 \\ 0.004137 & -0.133632 & -0.005658 & 0.014656 & 3.13024 & 8.299236 & 0.095552 & -0.009852 \\ 0.006542 & 0.08717 & 0.013132 & -0.007334 & -2.735192 & -6.23692 & -0.009852 & 0.04876 \end{bmatrix},$$

$$\Sigma_{b_0^t 2} = \begin{bmatrix} 0.072263 & 0.006937 & 0.07365 & 0.013591 & -2.354338 & 4.170623 & 0.002615 & 0.016104 \\ 0.006937 & 0.045188 & 0.047527 & 0.020529 & -7.288126 & -1.587453 & -0.009705 & 0.001171 \\ 0.07365 & 0.047527 & 0.335974 & 0.075867 & -10.775862 & -1.971751 & -0.015717 & 0.034226 \\ 0.013591 & 0.020529 & 0.075867 & 0.085162 & -1.180576 & -3.060765 & 0.001064 & 0.020272 \\ -2.354338 & -7.288126 & -10.775862 & -1.180576 & 5467.129188 & -246.039303 & 3.306684 & 0.779184 \\ 4.170623 & -1.587453 & -1.971751 & -3.060765 & -246.039303 & 4300.388471 & 2.505662 & 1.583032 \\ 0.002615 & -0.009705 & -0.015717 & 0.001064 & 3.306684 & 2.505662 & 0.021071 & 0.005633 \\ 0.016104 & 0.001171 & 0.034226 & 0.020272 & 0.779184 & 1.583032 & 0.005633 & 0.022648 \end{bmatrix},$$

$$\Sigma_{b_0^t 3} = \begin{bmatrix} 0.037383 & 0.003005 & 0.051061 & -0.004332 & -1.358167 & 3.34181 & -0.000601 & 0.008141 \\ 0.003005 & 0.004866 & 0.003408 & -0.000921 & -0.457757 & 0.361845 & 0.000576 & 0.002651 \\ 0.051061 & 0.003408 & 0.225259 & -0.011444 & -2.611116 & 10.304998 & -0.000948 & 0.030167 \\ -0.004332 & -0.000921 & -0.011444 & 0.005737 & 0.098032 & -0.949549 & -0.000254 & -0.004976 \\ -1.358167 & -0.457757 & -2.611116 & 0.098032 & 827.37626 & 424.425209 & 0.004262 & -0.795169 \\ 3.34181 & 0.361845 & 10.304998 & -0.949549 & 424.425209 & 4584.148371 & -0.115933 & 4.005952 \\ -0.000601 & 0.000576 & -0.000948 & -0.000254 & 0.004262 & -0.115933 & 0.002392 & 0.000536 \\ 0.008141 & 0.002651 & 0.030167 & -0.004976 & -0.795169 & 4.005952 & 0.000536 & 0.022459 \end{bmatrix},$$

$$\Sigma_{b_0^t 4} = \begin{bmatrix} 0.788242 & -0.004324 & -0.108718 & 0.045225 & 0.339893 & 39.711336 & 0.010881 & 0.026428 \\ -0.004324 & 0.089064 & 0.002751 & -0.002454 & -0.040236 & -1.780798 & -0.000271 & 0.00161 \\ -0.108718 & 0.002751 & 0.390896 & -0.013224 & -0.217046 & -11.185861 & -0.002584 & -0.003293 \\ 0.045225 & -0.002454 & -0.013224 & 0.131988 & 0.068407 & 6.287739 & 0.001532 & -0.000059 \\ 0.339893 & -0.040236 & -0.217046 & 0.068407 & 12099.13118 & 61.199138 & -0.031422 & -0.075383 \\ 39.711336 & -1.780798 & -11.185861 & 6.287739 & 61.199138 & 26993.77585 & 1.241066 & 0.412877 \\ 0.010881 & -0.000271 & -0.002584 & 0.001532 & -0.031422 & 1.241066 & 0.043307 & 0.000524 \\ 0.026428 & 0.00161 & -0.003293 & -0.000059 & -0.075383 & 0.412877 & 0.000524 & 0.027357 \end{bmatrix},$$

$$\Sigma_{b_0^t 5} = \begin{bmatrix} 0.05015 & -0.000254 & 0.054005 & 0.000911 & 2.696649 & 4.024001 & 0.006787 & -0.002595 \\ -0.000254 & 0.018934 & 0.001101 & -0.012099 & 0.347071 & -0.348715 & -0.000789 & 0.003111 \\ 0.054005 & 0.001101 & 0.214719 & -0.004808 & 2.010092 & -2.175236 & 0.023097 & -0.002001 \\ 0.000911 & -0.012099 & -0.004808 & 0.033486 & 0.011421 & 2.948939 & -0.002454 & -0.001247 \\ 2.696649 & 0.347071 & 2.010092 & 0.011421 & 2903.066467 & 3176.992931 & -2.520256 & 0.536655 \\ 4.024001 & -0.348715 & -2.175236 & 2.948939 & 3176.992931 & 9730.161628 & -5.606222 & 1.484464 \\ 0.006787 & -0.000789 & 0.023097 & -0.002454 & -2.520256 & -5.606222 & 0.026368 & -0.006301 \\ -0.002595 & 0.003111 & -0.002001 & -0.001247 & 0.536655 & 1.484464 & -0.006301 & 0.011628 \end{bmatrix},$$

$$\Sigma_{b_0^t 6} = \begin{bmatrix} 0.08749 & 0.011906 & -0.000811 & -0.00329 & -0.076986 & -10.444863 & -0.007667 & -0.017203 \\ 0.011906 & 0.046796 & 0.001682 & -0.020556 & 0.345341 & -3.085258 & -0.009818 & -0.024684 \\ -0.000811 & 0.001682 & 0.228313 & -0.002183 & -2.660756 & -48.869224 & -0.031301 & -0.041057 \\ -0.00329 & -0.020556 & -0.002183 & 0.045324 & -0.866336 & -2.096832 & 0.003934 & 0.028717 \\ -0.076986 & 0.345341 & -2.660756 & -0.866336 & 1042.016766 & 895.389527 & 0.912228 & -1.182972 \\ -10.444863 & -3.085258 & -48.869224 & -2.096832 & 895.389527 & 22533.41507 & 16.079122 & 11.030961 \\ -0.007667 & -0.009818 & -0.031301 & 0.003934 & 0.912228 & 16.079122 & 0.063271 & -0.00428 \\ -0.017203 & -0.024684 & -0.041057 & 0.028717 & -1.182972 & 11.030961 & -0.00428 & 0.089437 \end{bmatrix},$$

$$\Sigma_{b_0^t 7} = \begin{bmatrix} 0.103643 & 0.000575 & 0.03882 & 0.003576 & 0.522412 & -2.641135 & -0.004543 & -0.008206 \\ 0.000575 & 0.006058 & -0.000963 & -0.001929 & 0.080666 & 1.286855 & -0.000994 & 0.002964 \\ 0.03882 & -0.000963 & 0.144435 & -0.004067 & -2.386337 & -5.945531 & -0.001664 & -0.002959 \\ 0.003576 & -0.001929 & -0.004067 & 0.010841 & 0.711684 & -2.735277 & 0.000582 & -0.00952 \\ 0.522412 & 0.080666 & -2.386337 & 0.711684 & 813.171912 & 182.810906 & -0.165175 & -1.132824 \\ -2.641135 & 1.286855 & -5.945531 & -2.735277 & 182.810906 & 15814.14312 & -2.929442 & 6.698459 \\ -0.004543 & -0.000994 & -0.001664 & 0.000582 & -0.165175 & -2.929442 & 0.004732 & -0.000613 \\ -0.008206 & 0.002964 & -0.002959 & -0.00952 & -1.132824 & 6.698459 & -0.000613 & 0.022201 \end{bmatrix},$$

$$\Sigma_{b_{68}^t} = \begin{bmatrix} 0.029698 & 0.006583 & 0.028265 & -0.004902 & -0.233809 & -6.42322 & -0.000149 & 0.005482 \\ 0.006583 & 0.024496 & 0.026048 & -0.006826 & -0.349284 & -10.572607 & 0.00027 & 0.0104 \\ 0.028265 & 0.026048 & 0.162523 & -0.016115 & -1.295099 & -25.574682 & 0.004545 & 0.023557 \\ -0.004902 & -0.006826 & -0.016115 & 0.010818 & 0.204306 & 6.125879 & -0.001879 & -0.005342 \\ -0.233809 & -0.349284 & -1.295099 & 0.204306 & 234.158726 & 376.139257 & -0.081351 & -0.589591 \\ -6.42322 & -10.572607 & -25.574682 & 6.125879 & 376.139257 & 20345.07366 & -1.511536 & -6.428036 \\ -0.000149 & 0.00027 & 0.004545 & -0.001879 & -0.081351 & -1.511536 & 0.007433 & 0.001053 \\ 0.005482 & 0.0104 & 0.023557 & -0.005342 & -0.589591 & -6.428036 & 0.001053 & 0.018897 \end{bmatrix}.$$

The distribution

$$p\left(F_9^t, F_{16}^t, F_{32}^t, F_{34}^t, F_{52}^t, F_{42}^t, F_{12}^t, F_{66}^t | b_1^t : \boldsymbol{\theta}_{F_9^t,\dots,F_{66}^t | b_1^t} = \left\{\left\{\pi_{b_{1i}^t}, \boldsymbol{\mu}_{b_{1i}^t}, \Sigma_{b_{1i}^t}\right\}_{i=1}^{9}\right\}\right)$$

consists of nine components, where

$$\pi_{b_{11}^t} = 0.156672, \pi_{b_{12}^t} = 0.019726, \pi_{b_{13}^t} = 0.072743,$$

$$\pi_{b_{14}^t} = 0.135269, \pi_{b_{15}^t} = 0.099846, \pi_{b_{16}^t} = 0.058998,$$

$$\pi_{b_{17}^t} = 0.190388, \pi_{b_{18}^t} = 0.128558, \pi_{b_{19}^t} = 0.137801,$$

$$\boldsymbol{\mu}_{b_{11}^t} = \begin{pmatrix} 0.531349 \\ 0.062987 \\ 0.96035 \\ 0.997117 \\ 149.733387 \\ 212.696934 \\ 0.037172 \\ 0.108445 \end{pmatrix}, \boldsymbol{\mu}_{b_{12}^t} = \begin{pmatrix} 1.175641 \\ 0.244669 \\ 2.065949 \\ 0.790987 \\ 102.338776 \\ 121.092573 \\ -0.119136 \\ 0.327292 \end{pmatrix}, \boldsymbol{\mu}_{b_{13}^t} = \begin{pmatrix} 1.035485 \\ 0.052906 \\ 1.092769 \\ 0.848391 \\ 403.358153 \\ 403.85568 \\ -0.111523 \\ 0.200388 \end{pmatrix},$$

$$\boldsymbol{\mu}_{b_{14}^t} = \begin{pmatrix} 0.4545 \\ 0.26997 \\ 1.397835 \\ 0.887294 \\ 19.009587 \\ 32.039094 \\ -0.01854 \\ 0.373948 \end{pmatrix}, \boldsymbol{\mu}_{b_{15}^t} = \begin{pmatrix} 1.991799 \\ 0.320799 \\ 0.919077 \\ 0.957298 \\ 93.340093 \\ 258.118119 \\ 0.141691 \\ 0.23637 \end{pmatrix}, \boldsymbol{\mu}_{b_{16}^t} = \begin{pmatrix} 0.341263 \\ 0.213457 \\ 1.495354 \\ 0.72658 \\ 136.29799 \\ 110.440643 \\ 0.237027 \\ 0.370619 \end{pmatrix},$$

$$\boldsymbol{\mu}_{b_{17}^t} = \begin{pmatrix} 0.812829 \\ 0.129887 \\ 1.738544 \\ 0.957306 \\ 61.578686 \\ 67.420578 \\ 0.044165 \\ 0.208093 \end{pmatrix}, \boldsymbol{\mu}_{b_{18}^t} = \begin{pmatrix} 0.524626 \\ 0.240273 \\ 1.520805 \\ 0.962604 \\ 30.538918 \\ 235.221127 \\ 0.029893 \\ 0.206634 \end{pmatrix}, \boldsymbol{\mu}_{b_{19}^t} = \begin{pmatrix} 0.392986 \\ 0.115946 \\ 0.965133 \\ 0.951238 \\ 53.741029 \\ 354.763044 \\ 0.040946 \\ 0.269591 \end{pmatrix},$$

$$\Sigma_{b_{11}^t} = \begin{bmatrix} 0.056819 & 0.001339 & 0.056484 & -0.00006 & 3.295203 & 6.097452 & 0.00226 & 0.001064 \\ 0.001339 & 0.00397 & 0.000166 & -0.000213 & 0.882965 & 1.171459 & -0.000133 & 0.000239 \\ 0.056484 & 0.000166 & 0.136244 & -0.000676 & 14.506152 & 18.095003 & 0.001689 & 0.001791 \\ -0.00006 & -0.000213 & -0.000676 & 0.003096 & -0.211893 & -0.217394 & 0.000104 & -0.000257 \\ 3.295203 & 0.882965 & 14.506152 & -0.211893 & 10421.76125 & 11033.66395 & 0.048368 & 0.715592 \\ 6.097452 & 1.171459 & 18.095003 & -0.217394 & 11033.66395 & 17548.93695 & 1.217911 & 0.907724 \\ 0.00226 & -0.000133 & 0.001689 & 0.000104 & 0.048368 & 1.217911 & 0.001771 & -0.000029 \\ 0.001064 & 0.000239 & 0.001791 & -0.000257 & 0.715592 & 0.907724 & -0.000029 & 0.001286 \end{bmatrix},$$

$$\Sigma_{b_{i_2}^t} = \begin{bmatrix} 0.102164 & -0.009119 & -0.010391 & 0.004278 & 5.364341 & 3.196266 & -0.004757 & -0.008608 \\ -0.009119 & 0.05058 & 0.023993 & -0.013739 & -13.413692 & -11.826747 & 0.006105 & 0.011531 \\ -0.010391 & 0.023993 & 0.187543 & -0.028823 & -17.468287 & -21.43878 & 0.005016 & 0.000595 \\ 0.004278 & -0.013739 & -0.028823 & 0.043608 & 6.21774 & 7.349136 & 0.002618 & -0.000466 \\ 5.364341 & -13.413692 & -17.468287 & 6.21774 & 9767.605996 & 5924.610676 & -4.732457 & -5.688414 \\ 3.196266 & -11.826747 & -21.43878 & 7.349136 & 5924.610676 & 10778.11817 & -2.399922 & -0.205467 \\ -0.004757 & 0.006105 & 0.005016 & 0.002618 & -4.732457 & -2.399922 & 0.015423 & 0.006985 \\ -0.008608 & 0.011531 & 0.000595 & -0.000466 & -5.688414 & -0.205467 & 0.006985 & 0.033455 \end{bmatrix},$$

$$\Sigma_{b_{i_3}^t} = \begin{bmatrix} 0.025078 & -0.000713 & 0.011014 & -0.00129 & 6.33088 & 6.157416 & 0.000949 & 0.002792 \\ -0.000713 & 0.004548 & -0.000863 & -0.000443 & -0.789698 & -0.670821 & -0.000018 & -0.000073 \\ 0.011014 & -0.000863 & 0.130063 & 0.023702 & 35.146217 & 35.392805 & 0.005348 & 0.004087 \\ -0.00129 & -0.000443 & 0.023702 & 0.037493 & 12.170697 & 12.074992 & 0.002237 & -0.007381 \\ 6.33088 & -0.789698 & 35.146217 & 12.170697 & 18431.43148 & 17689.44823 & 2.904921 & -0.12403 \\ 6.157416 & -0.670821 & 35.392805 & 12.074992 & 17689.44823 & 18651.29928 & 2.922306 & -0.105606 \\ 0.000949 & -0.000018 & 0.005348 & 0.002237 & 2.904921 & 2.922306 & 0.002942 & -0.000291 \\ 0.002792 & -0.000073 & 0.004087 & -0.007381 & -0.12403 & -0.105606 & -0.000291 & 0.009009 \end{bmatrix},$$

$$\Sigma_{b_{i_4}^t} = \begin{bmatrix} 0.027856 & 0.002011 & 0.016428 & 0.002737 & -0.00266 & 2.503709 & 0.000441 & -0.005378 \\ 0.002011 & 0.018646 & 0.008452 & -0.005646 & -0.063569 & -1.892322 & -0.001545 & 0.003105 \\ 0.016428 & 0.008452 & 0.138537 & -0.001788 & -2.278508 & 2.114264 & -0.000563 & -0.001006 \\ 0.002737 & -0.005646 & -0.001788 & 0.010203 & -0.104676 & 1.373413 & -0.000648 & -0.004474 \\ -0.00266 & -0.063569 & -2.278508 & -0.104676 & 660.529546 & -57.757822 & 0.121573 & 0.091787 \\ 2.503709 & -1.892322 & 2.114264 & 1.373413 & -57.757822 & 2025.991935 & 0.110432 & -1.879999 \\ 0.000441 & -0.001545 & -0.000563 & -0.000648 & 0.121573 & 0.110432 & 0.004799 & 0.002917 \\ -0.005378 & 0.003105 & -0.001006 & -0.004474 & 0.091787 & -1.879999 & 0.002917 & 0.023277 \end{bmatrix},$$

$$\Sigma_{b_{i_5}^t} = \begin{bmatrix} 0.576236 & 0.041006 & -0.017818 & -0.00066 & 7.162318 & -12.984813 & 0.017195 & 0.016215 \\ 0.041006 & 0.023827 & -0.00289 & -0.002692 & 2.613603 & 4.141043 & -0.000902 & 0.011211 \\ -0.017818 & -0.00289 & 0.372494 & -0.006267 & -8.581798 & 35.104199 & -0.026309 & 0.008586 \\ -0.00066 & -0.002692 & -0.006267 & 0.007444 & -0.200978 & -0.875167 & 0.000467 & -0.00449 \\ 7.162318 & 2.613603 & -8.581798 & -0.200978 & 2353.622944 & 1410.881601 & 0.544352 & 1.272265 \\ -12.984813 & 4.141043 & 35.104199 & -0.875167 & 1410.881601 & 22043.57451 & -5.086068 & 0.373846 \\ 0.017195 & -0.000902 & -0.026309 & 0.000467 & 0.544352 & -5.086068 & 0.006411 & -0.000196 \\ 0.016215 & 0.011211 & 0.008586 & -0.00449 & 1.272265 & 0.373846 & -0.000196 & 0.016707 \end{bmatrix},$$

$$\Sigma_{b_{i_6}^t} = \begin{bmatrix} 0.031894 & -0.001529 & 0.000367 & 0.003743 & -3.075993 & 0.335594 & 0.000759 & -0.001343 \\ -0.001529 & 0.028139 & 0.004414 & -0.002899 & 1.664341 & -1.231822 & -0.007447 & 0.001472 \\ 0.000367 & 0.004414 & 0.106469 & -0.015663 & 3.330759 & 4.885737 & 0.003319 & -0.017893 \\ 0.003743 & -0.002899 & -0.015663 & 0.039741 & -2.495571 & -3.166351 & -0.006042 & 0.002957 \\ -3.075993 & 1.664341 & 3.330759 & -2.495571 & 7036.114195 & 1002.593893 & -0.50677 & -3.987955 \\ 0.335594 & -1.231822 & 4.885737 & -3.166351 & 1002.593893 & 4646.507489 & 0.487152 & -0.059002 \\ 0.000759 & -0.007447 & 0.003319 & -0.006042 & -0.50677 & 0.487152 & 0.010499 & -0.002454 \\ -0.001343 & 0.001472 & -0.017893 & 0.002957 & -3.987955 & -0.059002 & -0.002454 & 0.033084 \end{bmatrix},$$

$$\Sigma_{b_{i_7}^t} = \begin{bmatrix} 0.1136 & 0.006478 & 0.153739 & -0.001063 & -5.029185 & -2.620495 & -0.013922 & 0.000213 \\ 0.006478 & 0.004869 & 0.014678 & -0.00127 & -0.700464 & -0.31756 & -0.001127 & 0.001202 \\ 0.153739 & 0.014678 & 0.364424 & -0.003764 & -12.267554 & -4.997879 & -0.023084 & 0.003291 \\ -0.001063 & -0.00127 & -0.003764 & 0.004919 & 0.243105 & 0.541861 & 0.000334 & -0.002951 \\ -5.029185 & -0.700464 & -12.267554 & 0.243105 & 2014.061267 & 1141.233045 & 0.053791 & -0.006733 \\ -2.620495 & -0.31756 & -4.997879 & 0.541861 & 1141.233045 & 2010.213379 & 0.019545 & -0.868379 \\ -0.013922 & -0.001127 & -0.023084 & 0.000334 & 0.053791 & 0.019545 & 0.007096 & 0.000449 \\ 0.000213 & 0.001202 & 0.003291 & -0.002951 & -0.006733 & -0.868379 & 0.000449 & 0.01016 \end{bmatrix},$$

$$\Sigma_{b_{i_8}^t} = \begin{bmatrix} 0.083004 & -0.014074 & 0.140211 & 0.003067 & -2.193768 & 14.028347 & 0.001395 & -0.000511 \\ -0.014074 & 0.034435 & -0.04819 & -0.004345 & 1.751637 & 1.409391 & -0.003278 & 0.007243 \\ 0.140211 & -0.04819 & 0.530963 & 0.005108 & -4.657572 & 24.087814 & 0.004415 & -0.006635 \\ 0.003067 & -0.004345 & 0.005108 & 0.005294 & -0.469579 & 1.054758 & 0.000821 & -0.00165 \\ -2.193768 & 1.751637 & -4.657572 & -0.469579 & 1048.74472 & -622.800981 & -0.421949 & 0.192006 \\ 14.028347 & 1.409391 & 24.087814 & 1.054758 & -622.800981 & 7800.779093 & 0.71566 & 0.89297 \\ 0.001395 & -0.003278 & 0.004415 & 0.000821 & -0.421949 & 0.71566 & 0.004044 & -0.001062 \\ -0.000511 & 0.007243 & -0.006635 & -0.00165 & 0.192006 & 0.89297 & -0.001062 & 0.006358 \end{bmatrix},$$

$$\Sigma_{b_{i_9}^t} = \begin{bmatrix} 0.024252 & 0.001969 & 0.034616 & -0.001227 & -4.789066 & -8.251884 & -0.000093 & 0.007008 \\ 0.001969 & 0.007547 & 0.005232 & -0.002424 & -0.578334 & -2.046382 & 0.000561 & 0.004941 \\ 0.034616 & 0.005232 & 0.131013 & -0.006996 & -10.82109 & -24.309198 & 0.00016 & 0.027881 \\ -0.001227 & -0.002424 & -0.006996 & 0.006598 & 0.328813 & 1.912666 & -0.000525 & -0.006272 \\ -4.789066 & -0.578334 & -10.82109 & 0.328813 & 3102.52963 & 4344.375089 & -0.129613 & -3.034024 \\ -8.251884 & -2.046382 & -24.309198 & 1.912666 & 4344.375089 & 11735.66909 & -0.546143 & -10.419821 \\ -0.000093 & 0.000561 & 0.00016 & -0.000525 & -0.129613 & -0.546143 & 0.002941 & 0.001402 \\ 0.007008 & 0.004941 & 0.027881 & -0.006272 & -3.034024 & -10.419821 & 0.001402 & 0.024758 \end{bmatrix}.$$

The distribution

$$p\left(F_9^t, F_{16}^t, F_{32}^t, F_{34}^t, F_{52}^t, F_{42}^t, F_{12}^t, F_{66}^t | b_2^t : \boldsymbol{\theta}_{F_9^t,\ldots,F_{66}^t|b_2^t} = \left\{\left\{\pi_{b_2^t i}, \boldsymbol{\mu}_{b_2^t i}, \Sigma_{b_2^t i}\right\}_{i=1}^{9}\right\}\right)$$

consists of nine components, where

$$\pi_{b_2^t 1} = 0.067276, \pi_{b_2^t 2} = 0.007735, \pi_{b_2^t 3} = 0.307573,$$

$$\pi_{b_2^t 4} = 0.203191, \pi_{b_2^t 5} = 0.074633, \pi_{b_2^t 6} = 0.036256,$$

$$\pi_{b_2^t 7} = 0.22387, \pi_{b_2^t 8} = 0.019627, \pi_{b_2^t 9} = 0.05984,$$

$$\boldsymbol{\mu}_{b_2^t 1} = \begin{pmatrix} 1.143574 \\ 1.126899 \\ 1.92779 \\ 0.066001 \\ 72.512257 \\ 172.925427 \\ -0.300664 \\ 0.064414 \end{pmatrix}, \boldsymbol{\mu}_{b_2^t 2} = \begin{pmatrix} 1.080309 \\ 1.459061 \\ 1.409659 \\ 0.334308 \\ 315.550838 \\ 353.250564 \\ -0.183936 \\ 0.207741 \end{pmatrix}, \boldsymbol{\mu}_{b_2^t 3} = \begin{pmatrix} 1.311743 \\ 0.570771 \\ 1.701795 \\ 0.073878 \\ 240.312532 \\ 250.997408 \\ -0.366386 \\ 0.102953 \end{pmatrix},$$

$$\boldsymbol{\mu}_{b_2^t 4} = \begin{pmatrix} 0.30508 \\ 0.348043 \\ 2.307847 \\ 0.243704 \\ 20.424459 \\ 184.685731 \\ -0.282841 \\ 0.243462 \end{pmatrix}, \boldsymbol{\mu}_{b_2^t 5} = \begin{pmatrix} 2.040673 \\ 0.356006 \\ 2.154744 \\ 0.061102 \\ 169.494996 \\ 355.969087 \\ -0.648605 \\ 0.091486 \end{pmatrix}, \boldsymbol{\mu}_{b_2^t 6} = \begin{pmatrix} 0.966862 \\ 0.522019 \\ 1.750517 \\ 0.401631 \\ 201.574732 \\ 193.721281 \\ -0.244567 \\ 0.346173 \end{pmatrix},$$

$$\boldsymbol{\mu}_{b_2^t 7} = \begin{pmatrix} 0.235882 \\ 0.256663 \\ 2.509579 \\ 0.095554 \\ 181.430424 \\ 199.345761 \\ -0.371175 \\ 0.134331 \end{pmatrix}, \boldsymbol{\mu}_{b_2^t 8} = \begin{pmatrix} 1.711117 \\ 1.269749 \\ 1.023775 \\ 0.315406 \\ 179.520729 \\ 455.256728 \\ -0.134568 \\ 0.125366 \end{pmatrix}, \boldsymbol{\mu}_{b_2^t 9} = \begin{pmatrix} 1.102161 \\ 0.832099 \\ 1.910687 \\ 0.309344 \\ 37.187408 \\ 421.684837 \\ -0.287136 \\ 0.262421 \end{pmatrix},$$

$$\Sigma_{b_2^t 1} = \begin{bmatrix} 0.244974 & 0.076746 & -0.083684 & -0.004575 & 9.564033 & 3.939812 & 0.010596 & -0.001025 \\ 0.076746 & 0.524549 & -0.218686 & -0.019823 & 4.428636 & -12.205394 & -0.012368 & -0.006504 \\ -0.083684 & -0.218686 & 0.22657 & -0.000092 & -5.944544 & 1.673146 & 0.002963 & -0.003271 \\ -0.004575 & -0.019823 & -0.000092 & 0.015938 & -1.685704 & -4.485135 & -0.00363 & 0.006374 \\ 9.564033 & 4.428636 & -5.944544 & -1.685704 & 2744.339081 & 3442.092339 & 3.558765 & -1.543902 \\ 3.939812 & -12.205394 & 1.673146 & -4.485135 & 3442.092339 & 12161.96809 & 8.968906 & -4.267216 \\ 0.010596 & -0.012368 & 0.002963 & -0.00363 & 3.558765 & 8.968906 & 0.014835 & -0.003615 \\ -0.001025 & -0.006504 & -0.003271 & 0.006374 & -1.543902 & -4.267216 & -0.003615 & 0.00732 \end{bmatrix},$$

$$\Sigma_{b_2^t 2} = \begin{bmatrix} 0.263752 & 0.069767 & 0.058764 & -0.052578 & -1.586263 & 9.251698 & -0.022871 & 0.011718 \\ 0.069767 & 0.221997 & 0.059279 & -0.037071 & 9.639574 & 1.887854 & -0.009474 & 0.023304 \\ 0.058764 & 0.059279 & 0.296728 & -0.025647 & -9.109592 & -0.507487 & -0.021634 & 0.016959 \\ -0.052578 & -0.037071 & -0.025647 & 0.085578 & -1.603196 & -4.026954 & 0.009384 & -0.002153 \\ -1.586263 & 9.639574 & -9.109592 & -1.603196 & 8784.225478 & 541.516799 & 1.570068 & -0.910588 \\ 9.251698 & 1.887854 & -0.507487 & -4.026954 & 541.516799 & 12927.7837 & -3.927667 & -2.105253 \\ -0.022871 & -0.009474 & -0.021634 & 0.009384 & 1.570068 & -3.927667 & 0.033562 & -0.000511 \\ 0.011718 & 0.023304 & 0.016959 & -0.002153 & -0.910588 & -2.105253 & -0.000511 & 0.02185 \end{bmatrix},$$

$$\Sigma_{b_{23}^t} = \begin{bmatrix} 0.418361 & 0.033713 & 0.080007 & 0.012587 & -3.648415 & -2.718459 & 0.011842 & 0.020342 \\ 0.033713 & 0.141008 & -0.09814 & 0.009378 & -17.262276 & -15.104953 & 0.01056 & 0.01312 \\ 0.080007 & -0.09814 & 0.313055 & 0.005183 & 3.824454 & 1.458809 & -0.001805 & 0.008165 \\ 0.012587 & 0.009378 & 0.005183 & 0.009222 & -4.358401 & -4.001148 & 0.005358 & 0.008849 \\ -3.648415 & -17.262276 & 3.824454 & -4.358401 & 24885.53578 & 24150.97254 & -2.03519 & -5.987549 \\ -2.718459 & -15.104953 & 1.458809 & -4.001148 & 24150.97254 & 23928.64268 & -1.850234 & -5.548977 \\ 0.011842 & 0.01056 & -0.001805 & 0.005358 & -2.03519 & -1.850234 & 0.013869 & 0.006724 \\ 0.020342 & 0.01312 & 0.008165 & 0.008849 & -5.987549 & -5.548977 & 0.006724 & 0.01351 \end{bmatrix},$$

$$\Sigma_{b_{24}^t} = \begin{bmatrix} 0.039018 & 0.010394 & 0.00457 & 0.007233 & -0.326393 & -0.890157 & -0.003492 & 0.005941 \\ 0.010394 & 0.022933 & -0.003439 & 0.006715 & -0.796399 & -3.325187 & 0.001621 & 0.006654 \\ 0.00457 & -0.003439 & 0.096919 & -0.006412 & 0.181232 & -19.438853 & -0.01129 & 0.003816 \\ 0.007233 & 0.006715 & -0.006412 & 0.037144 & -1.625664 & -0.649556 & 0.013483 & 0.025403 \\ -0.326393 & -0.796399 & 0.181232 & -1.625664 & 500.200481 & 587.718471 & -0.781269 & -1.29371 \\ -0.890157 & -3.325187 & -19.438853 & -0.649556 & 587.718471 & 20687.13873 & 2.569042 & -4.207991 \\ -0.003492 & 0.001621 & -0.01129 & 0.013483 & -0.781269 & 2.569042 & 0.01453 & 0.010261 \\ 0.005941 & 0.006654 & 0.003816 & 0.025403 & -1.29371 & -4.207991 & 0.010261 & 0.025499 \end{bmatrix},$$

$$\Sigma_{b_{25}^t} = \begin{bmatrix} 0.164318 & 0.014037 & 0.014715 & -0.003483 & -6.364108 & -8.42431 & -0.003966 & -0.000033 \\ 0.014037 & 0.017615 & 0.005771 & 0.003085 & -2.467651 & 0.113384 & 0.001146 & 0.003544 \\ 0.014715 & 0.005771 & 0.087544 & 0.002581 & -5.492691 & 19.842419 & 0.001343 & -0.000722 \\ -0.003483 & 0.003085 & 0.002581 & 0.010905 & -0.745483 & 1.723394 & 0.002281 & 0.003208 \\ -6.364108 & -2.467651 & -5.492691 & -0.745483 & 2731.017297 & -2042.386627 & -0.603838 & -0.116231 \\ -8.42431 & 0.113384 & 19.842419 & 1.723394 & -2042.386627 & 22301.62858 & 3.431961 & 0.07429 \\ -0.003966 & 0.001146 & 0.001343 & 0.002281 & -0.603838 & 3.431961 & 0.004566 & 0.000949 \\ -0.000033 & 0.003544 & -0.000722 & 0.003208 & -0.116231 & 0.07429 & 0.000949 & 0.005436 \end{bmatrix},$$

$$\Sigma_{b_{26}^t} = \begin{bmatrix} 0.20265 & 0.067243 & 0.084273 & 0.033893 & -18.023192 & -4.411517 & 0.026644 & 0.026694 \\ 0.067243 & 0.061532 & -0.002548 & 0.019617 & -18.553826 & -13.553926 & 0.009614 & 0.010794 \\ 0.084273 & -0.002548 & 0.252122 & 0.002979 & 25.075645 & 33.311025 & 0.023981 & 0.024499 \\ 0.033893 & 0.019617 & 0.002979 & 0.035867 & -5.651925 & -3.190402 & 0.009016 & 0.004185 \\ -18.023192 & -18.553826 & 25.075645 & -5.651925 & 30229.8615 & 30431.62136 & 2.668364 & -4.10872 \\ -4.411517 & -13.553926 & 33.311025 & -3.190402 & 30431.62136 & 36381.18446 & 5.415853 & -2.190039 \\ 0.026644 & 0.009614 & 0.023981 & 0.009016 & 2.668364 & 5.415853 & 0.015934 & 0.004168 \\ 0.026694 & 0.010794 & 0.024499 & 0.004185 & -4.10872 & -2.190039 & 0.004168 & 0.016814 \end{bmatrix},$$

$$\Sigma_{b_{27}^t} = \begin{bmatrix} 0.024672 & 0.002294 & -0.012302 & 0.001199 & -2.088621 & -4.571956 & -0.001988 & 0.000989 \\ 0.002294 & 0.012939 & 0.005313 & 0.004626 & -2.813629 & -3.470453 & 0.000189 & 0.005569 \\ -0.012302 & 0.005313 & 0.19192 & 0.002976 & -23.208619 & -19.773205 & -0.002349 & 0.009155 \\ 0.001199 & 0.004626 & 0.002976 & 0.008665 & -1.120167 & -0.47307 & 0.001998 & 0.006088 \\ -2.088621 & -2.813629 & -23.208619 & -1.120167 & 15400.38456 & 16372.04883 & 4.624858 & -2.796614 \\ -4.571956 & -3.470453 & -19.773205 & -0.47307 & 16372.04883 & 21762.74189 & 6.267205 & -1.000399 \\ -0.001988 & 0.000189 & -0.002349 & 0.001998 & 4.624858 & 6.267205 & 0.005925 & 0.002111 \\ 0.000989 & 0.005569 & 0.009155 & 0.006088 & -2.796614 & -1.000399 & 0.002111 & 0.011035 \end{bmatrix},$$

$$\Sigma_{b_{28}^t} = \begin{bmatrix} 0.712361 & 0.117471 & 0.549562 & 0.014822 & -9.850269 & -7.108881 & 0.004807 & 0.035335 \\ 0.117471 & 0.334022 & 0.007695 & 0.057106 & 3.216467 & 5.575115 & 0.013442 & 0.001615 \\ 0.549562 & 0.007695 & 0.828977 & 0.00265 & -19.365231 & -20.495042 & 0.002329 & 0.044243 \\ 0.014822 & 0.057106 & 0.00265 & 0.119627 & -0.739126 & -1.525965 & 0.011726 & 0.006201 \\ -9.850269 & 3.216467 & -19.365231 & -0.739126 & 2911.463402 & 851.047054 & 0.040331 & -0.921461 \\ -7.108881 & 5.575115 & -20.495042 & -1.525965 & 851.047054 & 5445.499242 & -0.093542 & -1.146658 \\ 0.004807 & 0.013442 & 0.002329 & 0.011726 & 0.040331 & -0.093542 & 0.010161 & 0.00183 \\ 0.035335 & 0.001615 & 0.044243 & 0.006201 & -0.921461 & -1.146658 & 0.00183 & 0.01074 \end{bmatrix},$$

$$\Sigma_{b_{29}^t} = \begin{bmatrix} 0.386256 & 0.120258 & -0.166508 & 0.005539 & -5.083699 & 33.628444 & 0.042788 & -0.040887 \\ 0.120258 & 0.180782 & -0.068075 & 0.033591 & -3.696982 & 12.271952 & 0.036015 & 0.026813 \\ -0.166508 & -0.068075 & 0.408102 & -0.006782 & 2.764152 & -32.179256 & -0.033967 & 0.03406 \\ 0.005539 & 0.033591 & -0.006782 & 0.042906 & 0.417015 & 2.921825 & 0.018238 & 0.023918 \\ -5.083699 & -3.696982 & 2.764152 & 0.417015 & 1425.08446 & -281.190456 & -0.57824 & 1.987535 \\ 33.628444 & 12.271952 & -32.179256 & 2.921825 & -281.190456 & 7076.258526 & 6.074098 & -2.594563 \\ 0.042788 & 0.036015 & -0.033967 & 0.018238 & -0.57824 & 6.074098 & 0.022253 & 0.011426 \\ -0.040887 & 0.026813 & 0.03406 & 0.023918 & 1.987535 & -2.594563 & 0.011426 & 0.044985 \end{bmatrix}.$$

Distribution $p\left(F_{10}^t, F_{38}^t | B^t : \boldsymbol{\theta}_{F_{10}^t, F_{38}^t | B^t}\right)$

The distribution $p\left(F_{10}^t, F_{38}^t | B^t : \boldsymbol{\theta}_{F_{10}^t, F_{38}^t | B^t}\right)$ over a two-dimensional vector of continuous variables (F_{10}, F_{38}) at time slice $t \geq 1$ is a collection of bivariate Gaussian mixture distributions with a bivariate GMM

$$p\left(F_{10}^t, F_{38}^t | b^t : \boldsymbol{\theta}_{F_{10}^t, F_{38}^t | b^t}\right) = \sum_{i=1}^{n_b} \pi_{b^t{}_i} \mathcal{N}\left(\boldsymbol{\mu}_{b^t{}_i}, \Sigma_{b^t{}_i}\right)$$

composed of n_b components for each $b^t \in \mathrm{Val}(B)$, parameterized with MAP parameters $\boldsymbol{\theta}_{F_{10}^t,F_{38}^t|B^t} = \left\{\boldsymbol{\theta}_{F_{10}^t,F_{38}^t|b_0^t}, \boldsymbol{\theta}_{F_{10}^t,F_{38}^t|b_1^t}, \boldsymbol{\theta}_{F_{10}^t,F_{38}^t|b_2^t}\right\}$.

The distribution

$$p\left(F_{10}^t, F_{38}^t | b_0^t : \boldsymbol{\theta}_{F_{10}^t,F_{38}^t|b_0^t} = \left\{\left\{\pi_{b_{0_i}^t}, \boldsymbol{\mu}_{b_{0_i}^t}, \Sigma_{b_{0_i}^t}\right\}_{i=1}^{5}\right\}\right)$$

consists of five components, where

$$\pi_{b_{0_1}^t} = 0.702216, \pi_{b_{0_2}^t} = 0.026314, \pi_{b_{0_3}^t} = 0.006789,$$

$$\pi_{b_{0_4}^t} = 0.167489, \pi_{b_{0_5}^t} = 0.097193,$$

$$\boldsymbol{\mu}_{b_{0_1}^t} = \begin{pmatrix}0.085547\\9.891586\end{pmatrix}, \boldsymbol{\mu}_{b_{0_2}^t} = \begin{pmatrix}0.069626\\161.415727\end{pmatrix}, \boldsymbol{\mu}_{b_{0_3}^t} = \begin{pmatrix}0.815368\\11.827344\end{pmatrix},$$

$$\boldsymbol{\mu}_{b_{0_4}^t} = \begin{pmatrix}0.06322\\44.903817\end{pmatrix}, \boldsymbol{\mu}_{b_{0_5}^t} = \begin{pmatrix}0.197613\\20.662485\end{pmatrix},$$

$$\Sigma_{b_{0_1}^t} = \begin{bmatrix}0.001142 & -0.024045\\-0.024045 & 68.371946\end{bmatrix}, \Sigma_{b_{0_2}^t} = \begin{bmatrix}0.001024 & -0.141281\\-0.141281 & 1977.990171\end{bmatrix},$$

$$\Sigma_{b_{0_3}^t} = \begin{bmatrix}0.093905 & -1.097098\\-1.097098 & 2560.323888\end{bmatrix}, \Sigma_{b_{0_4}^t} = \begin{bmatrix}0.000563 & 0.002292\\0.002292 & 665.55367\end{bmatrix},$$

$$\Sigma_{b_{0_5}^t} = \begin{bmatrix}0.007316 & -0.679912\\-0.679912 & 493.337061\end{bmatrix}.$$

The distribution

$$p\left(F_{10}^t, F_{38}^t | b_1^t : \boldsymbol{\theta}_{F_{10}^t,F_{38}^t|b_1^t} = \left\{\left\{\pi_{b_{1_i}^t}, \boldsymbol{\mu}_{b_{1_i}^t}, \Sigma_{b_{1_i}^t}\right\}_{i=1}^{8}\right\}\right)$$

consists of eight components, where

$$\pi_{b_{1_1}^t} = 0.196181, \pi_{b_{1_2}^t} = 0.089549, \pi_{b_{1_3}^t} = 0.473485,$$

$$\pi_{b_{1_4}^t} = 0.004462, \pi_{b_{1_5}^t} = 0.026928, \pi_{b_{1_6}^t} = 0.122865,$$

$$\pi_{b_{1_7}^t} = 0.057238, \pi_{b_{1_8}^t} = 0.02929,$$

$$\boldsymbol{\mu}_{b_{1_1}^t} = \begin{pmatrix}0.079769\\102.221613\end{pmatrix}, \boldsymbol{\mu}_{b_{1_2}^t} = \begin{pmatrix}0.069395\\372.770913\end{pmatrix}, \boldsymbol{\mu}_{b_{1_3}^t} = \begin{pmatrix}0.077586\\14.049404\end{pmatrix},$$

$$\boldsymbol{\mu}_{b_{1_4}^t} = \begin{pmatrix}0.339149\\311.250659\end{pmatrix}, \boldsymbol{\mu}_{b_{1_5}^t} = \begin{pmatrix}0.637417\\54.205471\end{pmatrix}, \boldsymbol{\mu}_{b_{1_6}^t} = \begin{pmatrix}0.244908\\41.0763\end{pmatrix},$$

$$\boldsymbol{\mu}_{b_{1_7}^t} = \begin{pmatrix}0.160345\\100.37751\end{pmatrix}, \boldsymbol{\mu}_{b_{1_8}^t} = \begin{pmatrix}0.139966\\311.404522\end{pmatrix},$$

$$\Sigma_{b_{1_1}^t} = \begin{bmatrix}0.000784 & 0.308564\\0.308564 & 2521.618852\end{bmatrix}, \Sigma_{b_{1_2}^t} = \begin{bmatrix}0.000628 & 0.247296\\0.247296 & 16717.13608\end{bmatrix},$$

$$\Sigma_{b_{1_3}^t} = \begin{bmatrix}0.000706 & -0.025232\\-0.025232 & 158.456696\end{bmatrix}, \Sigma_{b_{1_4}^t} = \begin{bmatrix}0.016983 & 5.681652\\5.681652 & 20271.07123\end{bmatrix},$$

$$\Sigma_{b_{1_5}^t} = \begin{bmatrix}0.070856 & -6.648618\\-6.648618 & 2768.591235\end{bmatrix}, \Sigma_{b_{1_6}^t} = \begin{bmatrix}0.010581 & -0.097943\\-0.097943 & 1053.011972\end{bmatrix},$$

$$\Sigma_{b_{1}^{t}7} = \begin{bmatrix} 0.003163 & -0.110589 \\ -0.110589 & 3505.922819 \end{bmatrix}, \Sigma_{b_{1}^{t}8} = \begin{bmatrix} 0.002741 & -0.351155 \\ -0.351155 & 18134.75103 \end{bmatrix}.$$

The distribution

$$p\left(F_{10}^{t}, F_{38}^{t} | b_{2}^{t} : \boldsymbol{\theta}_{F_{10}^{t}, F_{38}^{t} | b_{2}^{t}} = \left\{\left\{\pi_{b_{2}^{t}i}, \boldsymbol{\mu}_{b_{2}^{t}i}, \Sigma_{b_{2}^{t}i}\right\}_{i=1}^{9}\right\}\right)$$

consists of nine components, where

$$\pi_{b_{2}^{t}1} = 0.198117, \pi_{b_{2}^{t}2} = 0.063268, \pi_{b_{2}^{t}3} = 0.06613,$$

$$\pi_{b_{2}^{t}4} = 0.153222, \pi_{b_{2}^{t}5} = 0.129291, \pi_{b_{2}^{t}6} = 0.126657,$$

$$\pi_{b_{2}^{t}7} = 0.007314, \pi_{b_{2}^{t}8} = 0.113982, \pi_{b_{2}^{t}9} = 0.143019,$$

$$\boldsymbol{\mu}_{b_{2}^{t}1} = \begin{pmatrix} 0.088937 \\ 18.554789 \end{pmatrix}, \boldsymbol{\mu}_{b_{2}^{t}2} = \begin{pmatrix} 0.347218 \\ 316.04149 \end{pmatrix}, \boldsymbol{\mu}_{b_{2}^{t}3} = \begin{pmatrix} 0.481193 \\ 111.63058 \end{pmatrix},$$

$$\boldsymbol{\mu}_{b_{2}^{t}4} = \begin{pmatrix} 0.247392 \\ 112.678493 \end{pmatrix}, \boldsymbol{\mu}_{b_{2}^{t}5} = \begin{pmatrix} 0.060801 \\ 77.921397 \end{pmatrix}, \boldsymbol{\mu}_{b_{2}^{t}6} = \begin{pmatrix} 0.183969 \\ 440.732399 \end{pmatrix},$$

$$\boldsymbol{\mu}_{b_{2}^{t}7} = \begin{pmatrix} 0.614764 \\ 294.833974 \end{pmatrix}, \boldsymbol{\mu}_{b_{2}^{t}8} = \begin{pmatrix} 0.115587 \\ 232.69083 \end{pmatrix}, \boldsymbol{\mu}_{b_{2}^{t}9} = \begin{pmatrix} 0.251185 \\ 27.73391 \end{pmatrix},$$

$$\Sigma_{b_{2}^{t}1} = \begin{bmatrix} 0.001332 & -0.117595 \\ -0.117595 & 312.056363 \end{bmatrix}, \Sigma_{b_{2}^{t}2} = \begin{bmatrix} 0.017425 & 1.898672 \\ 1.898672 & 4469.572513 \end{bmatrix},$$

$$\Sigma_{b_{2}^{t}3} = \begin{bmatrix} 0.037758 & -1.441373 \\ -1.441373 & 2339.29167 \end{bmatrix}, \Sigma_{b_{2}^{t}4} = \begin{bmatrix} 0.008431 & 1.009807 \\ 1.009807 & 1839.110608 \end{bmatrix},$$

$$\Sigma_{b_{2}^{t}5} = \begin{bmatrix} 0.000596 & -0.13177 \\ -0.13177 & 1751.810429 \end{bmatrix}, \Sigma_{b_{2}^{t}6} = \begin{bmatrix} 0.006906 & 0.343896 \\ 0.343896 & 4421.182612 \end{bmatrix},$$

$$\Sigma_{b_{2}^{t}7} = \begin{bmatrix} 0.050555 & 8.340104 \\ 8.340104 & 7895.072264 \end{bmatrix}, \Sigma_{b_{2}^{t}8} = \begin{bmatrix} 0.003726 & 0.900001 \\ 0.900001 & 2810.288139 \end{bmatrix},$$

$$\Sigma_{b_{2}^{t}9} = \begin{bmatrix} 0.009619 & 0.340039 \\ 0.340039 & 522.947477 \end{bmatrix}.$$

Distribution $p\left(F_{30}^{t}, F_{36}^{t}, F_{60}^{t} | B^{t} : \boldsymbol{\theta}_{F_{30}^{t}, \ldots, F_{60}^{t} | B^{t}}\right)$

The distribution $p\left(F_{30}^{t}, F_{36}^{t}, F_{60}^{t} | B^{t} : \boldsymbol{\theta}_{F_{30}^{t}, \ldots, F_{60}^{t} | B^{t}}\right)$ over a three-dimensional vector of continuous variables (F_{30}, F_{36}, F_{60}) at time slice $t \geq 1$ is a collection of multivariate Gaussian mixture distributions with a multivariate GMM

$$p\left(F_{30}^{t}, F_{36}^{t}, F_{60}^{t} | b^{t} : \boldsymbol{\theta}_{F_{30}^{t}, \ldots, F_{60}^{t} | b^{t}}\right) = \sum_{i=1}^{n_b} \pi_{b^{t}i} \mathcal{N}\left(\boldsymbol{\mu}_{b^{t}i}, \Sigma_{b^{t}i}\right)$$

composed of n_b components for each $b^{t} \in \mathrm{Val}(B)$, parameterized with MAP parameters $\boldsymbol{\theta}_{F_{30}^{t}, \ldots, F_{60}^{t} | B^{t}} = \left\{\boldsymbol{\theta}_{F_{30}^{t}, \ldots, F_{60}^{t} | b_{0}^{t}}, \boldsymbol{\theta}_{F_{30}^{t}, \ldots, F_{60}^{t} | b_{1}^{t}}, \boldsymbol{\theta}_{F_{30}^{t}, \ldots, F_{60}^{t} | b_{2}^{t}}\right\}$.

The distribution

$$p\left(F_{30}^{t}, F_{36}^{t}, F_{60}^{t} | b_{0}^{t} : \boldsymbol{\theta}_{F_{30}^{t}, \ldots, F_{60}^{t} | b_{0}^{t}} = \left\{\left\{\pi_{b_{0}^{t}i}, \boldsymbol{\mu}_{b_{0}^{t}i}, \Sigma_{b_{0}^{t}i}\right\}_{i=1}^{2}\right\}\right)$$

consists of two components, where

$$\pi_{b_{0_1}^t} = 0.962171, \pi_{b_{0_2}^t} = 0.037829,$$

$$\boldsymbol{\mu}_{b_{0_1}^t} = \begin{pmatrix} 0.113466 \\ 0.043239 \\ 0.004567 \end{pmatrix}, \boldsymbol{\mu}_{b_{0_2}^t} = \begin{pmatrix} 0.182941 \\ 0.119592 \\ 0.089998 \end{pmatrix},$$

$$\Sigma_{b_{0_1}^t} = \begin{bmatrix} 0.11748 & 0.000582 & 0.000079 \\ 0.000582 & 0.001056 & 0.000006 \\ 0.000079 & 0.000006 & 0.000391 \end{bmatrix}, \Sigma_{b_{0_2}^t} = \begin{bmatrix} 2.833012 & 0.004207 & -0.001345 \\ 0.004207 & 0.004247 & -0.002107 \\ -0.001345 & -0.002107 & 0.009124 \end{bmatrix}.$$

The distribution

$$p\left(F_{30}^t, F_{36}^t, F_{60}^t | b_1^t : \boldsymbol{\theta}_{F_{30}^t,\dots,F_{60}^t | b_1^t} = \left\{\left\{\pi_{b_{1_i}^t}, \boldsymbol{\mu}_{b_{1_i}^t}, \Sigma_{b_{1_i}^t}\right\}_{i=1}^3\right\}\right)$$

consists of three components, where

$$\pi_{b_{1_1}^t} = 0.001726, \pi_{b_{1_2}^t} = 0.037256, \pi_{b_{1_3}^t} = 0.961018,$$

$$\boldsymbol{\mu}_{b_{1_1}^t} = \begin{pmatrix} 333.241715 \\ 0.132911 \\ 0.08516 \end{pmatrix}, \boldsymbol{\mu}_{b_{1_2}^t} = \begin{pmatrix} 0.095118 \\ 0.134383 \\ 0.075553 \end{pmatrix}, \boldsymbol{\mu}_{b_{1_3}^t} = \begin{pmatrix} 0.067324 \\ 0.024611 \\ 0.000756 \end{pmatrix},$$

$$\Sigma_{b_{1_1}^t} = \begin{bmatrix} 12306.19648 & 3.352828 & -4.678675 \\ 3.352828 & 0.002304 & -0.001277 \\ -4.678675 & -0.001277 & 0.111274 \end{bmatrix}, \Sigma_{b_{1_2}^t} = \begin{bmatrix} 3.094262 & 0.000311 & 0.000781 \\ 0.000311 & 0.002771 & -0.002759 \\ 0.000781 & -0.002759 & 0.016524 \end{bmatrix},$$

$$\Sigma_{b_{1_3}^t} = \begin{bmatrix} 0.123253 & 0.000681 & 0.000039 \\ 0.000681 & 0.000694 & 0.000008 \\ 0.000039 & 0.000008 & 0.000234 \end{bmatrix}.$$

The distribution

$$p\left(F_{30}^t, F_{36}^t, F_{60}^t | b_2^t : \boldsymbol{\theta}_{F_{30}^t,\dots,F_{60}^t | b_2^t} = \left\{\left\{\pi_{b_{2_i}^t}, \boldsymbol{\mu}_{b_{2_i}^t}, \Sigma_{b_{2_i}^t}\right\}_{i=1}^2\right\}\right)$$

consists of two components, where

$$\pi_{b_{2_1}^t} = 0.974088, \pi_{b_{2_2}^t} = 0.25912,$$

$$\boldsymbol{\mu}_{b_{2_1}^t} = \begin{pmatrix} 0.062702 \\ 0.046683 \\ 0.728183 \end{pmatrix}, \boldsymbol{\mu}_{b_{2_2}^t} = \begin{pmatrix} 0.156219 \\ 0.197705 \\ 0.461905 \end{pmatrix},$$

$$\Sigma_{b_{2_1}^t} = \begin{bmatrix} 0.122652 & 0.001465 & -0.00534 \\ 0.001465 & 0.001425 & -0.003937 \\ -0.00534 & -0.003937 & 0.046984 \end{bmatrix}, \Sigma_{b_{2_2}^t} = \begin{bmatrix} 4.483815 & -0.000912 & -0.004391 \\ -0.000912 & 0.001365 & -0.004217 \\ -0.004391 & -0.004217 & 0.126785 \end{bmatrix}.$$

Distribution $p\left(F_{11}^t | B^t, F_2^t : \boldsymbol{\theta}_{F_{11}^t | B^t, F_2^t}\right)$

The distribution $p\left(F_{11}^t | B^t, F_2^t : \boldsymbol{\theta}_{F_{11}^t | B^t, F_2^t}\right)$ over the continuous variable F_{11} at time slice $t \geq 1$ is a collection of Gaussian mixture distributions with a GMM

$$p\left(F_{11}^t | b^t, f_2^t : \boldsymbol{\theta}_{F_{45}^t | b^t, f_2^t}\right) = \sum_{i=1}^{n_{b,f}} \pi_{b^t{}_i} \mathcal{N}\left(\mu_{b^t, f^t{}_i}, \sigma^2_{b^t, f^t{}_i}\right)$$

composed of $n_{b,f}$ components for each $\{b^t, f_2^t\} \in \mathrm{Val}(B) \times \mathrm{Val}(F_2)$, parameterized with MAP parameters $\boldsymbol{\theta}_{F_{11}^t|B^t,F_2^t} = \left\{\boldsymbol{\theta}_{F_{11}^t|b_0^t,f_0^t}, \boldsymbol{\theta}_{F_{11}^t|b_1^t,f_0^t}, \boldsymbol{\theta}_{F_{11}^t|b_2^t,f_0^t}, \boldsymbol{\theta}_{F_{11}^t|b_0^t,f_1^t}, \boldsymbol{\theta}_{F_{11}^t|b_1^t,f_1^t}, \boldsymbol{\theta}_{F_{11}^t|b_2^t,f_1^t}\right\}$.

The distribution

$$p\left(F_{11}^t|b_0^t, f_{2\,0}^t : \boldsymbol{\theta}_{F_{11}^t|b_0^t,f_0^t} = \left\{\left\{\pi_{b_0^t,f_0^t\,i}, \mu_{b_0^t,f_0^t\,i}, \sigma^2_{b_0^t,f_0^t\,i}\right\}_{i=1}^{1}\right\}\right)$$

consists of a single component, where

$$\pi_{b_0^t,f_0^t\,1} = 1, \mu_{b_0^t,f_0^t\,1} = -0.07166, \sigma^2_{b_0^t,f_0^t\,1} = 1.531553.$$

The distribution

$$p\left(F_{11}^t|b_1^t, f_{2\,0}^t : \boldsymbol{\theta}_{F_{11}^t|b_1^t,f_0^t} = \left\{\left\{\pi_{b_1^t,f_0^t\,i}, \mu_{b_1^t,f_0^t\,i}, \sigma^2_{b_1^t,f_0^t\,i}\right\}_{i=1}^{1}\right\}\right)$$

consists of a single component, where

$$\pi_{b_1^t,f_0^t\,1} = 1, \mu_{b_1^t,f_0^t\,1} = -0.07166, \sigma^2_{b_1^t,f_0^t\,1} = 1.531553.$$

The distribution

$$p\left(F_{11}^t|b_2^t, f_{2\,0}^t : \boldsymbol{\theta}_{F_{11}^t|b_2^t,f_0^t} = \left\{\left\{\pi_{b_2^t,f_0^t\,i}, \mu_{b_2^t,f_0^t\,i}, \sigma^2_{b_2^t,f_0^t\,i}\right\}_{i=1}^{1}\right\}\right)$$

consists of a single component, where

$$\pi_{b_0^t,f_0^t\,1} = 1, \mu_{b_0^t,f_0^t\,1} = -0.07166, \sigma^2_{b_0^t,f_0^t\,1} = 1.531553.$$

The distribution

$$p\left(F_{11}^t|b_0^t, f_{2\,1}^t : \boldsymbol{\theta}_{F_{11}^t|b_0^t,f_1^t} = \left\{\left\{\pi_{b_0^t,f_1^t\,i}, \mu_{b_0^t,f_1^t\,i}, \sigma^2_{b_0^t,f_1^t\,i}\right\}_{i=1}^{3}\right\}\right)$$

consists of a three component, where

$$\pi_{b_0^t,f_1^t\,1} = 0.09059, \pi_{b_0^t,f_1^t\,2} = 0.81067, \pi_{b_0^t,f_1^t\,3} = 0.098712,$$

$$\mu_{b_0^t,f_1^t\,1} = 0.0188, \mu_{b_0^t,f_1^t\,2} = 0.076347, \mu_{b_0^t,f_1^t\,3} = 0.095784,$$

$$\sigma^2_{b_0^t,f_1^t\,1} = 0.172237, \sigma^2_{b_0^t,f_1^t\,2} = 0.006726, \sigma^2_{b_0^t,f_1^t\,3} = 0.046214.$$

The distribution

$$p\left(F_{11}^t|b_1^t, f_{2\,1}^t : \boldsymbol{\theta}_{F_{11}^t|b_1^t,f_1^t} = \left\{\left\{\pi_{b_1^t,f_1^t\,i}, \mu_{b_1^t,f_1^t\,i}, \sigma^2_{b_1^t,f_1^t\,i}\right\}_{i=1}^{4}\right\}\right)$$

consists of a four component, where

$$\pi_{b_1^t,f_1^t\,1} = 0.469497, \pi_{b_1^t,f_1^t\,2} = 0.021337, \pi_{b_1^t,f_1^t\,3} = 0.25414, \pi_{b_1^t,f_1^t\,4} = 0.255026,$$

$$\mu_{b_1^t,f_1^t\,1} = 0.042208, \mu_{b_1^t,f_1^t\,2} = -0.301057, \mu_{b_1^t,f_1^t\,3} = -0.060852, \mu_{b_1^t,f_1^t\,4} = 0.174713,$$

$$\sigma^2_{b_1^t,f_1^t{}_1} = 0.001427, \sigma^2_{b_1^t,f_1^t{}_2} = 0.052428, \sigma^2_{b_1^t,f_1^t{}_3} = 0.005467, \sigma^2_{b_1^t,f_1^t{}_4} = 0.013002.$$

The distribution

$$p\left(F_{11}^t | b_2^t, f_2^t{}_1 : \boldsymbol{\theta}_{F_{11}^t | b_2^t, f_1^t} = \left\{\left\{\pi_{b_2^t,f_1^t{}_i}, \mu_{b_2^t,f_1^t{}_i}, \sigma^2_{b_2^t,f_1^t{}_i}\right\}_{i=1}^4\right\}\right)$$

consists of a four component, where

$$\pi_{b_2^t,f_1^t{}_1} = 0.168888, \pi_{b_2^t,f_1^t{}_2} = 0.00431, \pi_{b_2^t,f_1^t{}_3} = 0.122409, \pi_{b_2^t,f_1^t{}_4} = 0.704394,$$

$$\mu_{b_2^t,f_1^t{}_1} = -0.117194, \mu_{b_2^t,f_1^t{}_2} = -0.13554, \mu_{b_2^t,f_1^t{}_3} = -0.612456, \mu_{b_2^t,f_1^t{}_4} = -0.362567,$$

$$\sigma^2_{b_2^t,f_1^t{}_1} = 0.048962, \sigma^2_{b_2^t,f_1^t{}_2} = 0.360318, \sigma^2_{b_2^t,f_1^t{}_3} = 0.007322, \sigma^2_{b_2^t,f_1^t{}_4} = 0.01292.$$

2.3 Parameters of the SAE Level 2 SAGAT Score Model

For any number of time slices $T \geq 1$, the SAE Level 2 SAGAT Score model defines the JPD

$$p\left(S_2^{1:T}, \boldsymbol{F}_{\text{Rel}}^{1:T} : \boldsymbol{\theta}\right) = p\left(S_2^1 : \boldsymbol{\theta}_{S_2^1}\right) \prod_{t=2}^{T} p\left(S_2^t \mid S_2^{t-1} : \boldsymbol{\theta}_{S_2^t | S_2^{t-1}}\right) \prod_{t=1}^{T} p\left(\boldsymbol{F}_{\text{Rel}}^t \mid S_2^t : \boldsymbol{\theta}\right),$$

with $p\left(\boldsymbol{F}_{\text{Rel}}^t \mid S_2^t : \boldsymbol{\theta}\right)$ given by

$$p\left(F_9^t, F_{29}^t, F_{35}^t, F_{37}^t, F_{52}^t, F_{57}^t, F_{42}^t \mid S_2^t : \boldsymbol{\theta}_{F_9^t,\ldots,F_{42}^t | S_2^t}\right).$$

As such, the model is defined by three probability /density distribution to be detailed in the following. The names of the relevant indicators $\boldsymbol{F}_{\text{Rel}} = \{F_9, F_{29}, F_{35}, F_{37}, F_{42}, F_{52}, F_{57}\}$ are provided in Table 7.

Table 26: The set of relevant indicators for the SAE Level 2 SAGAT Score model, $\boldsymbol{F}_{\text{Rel}} = \{F_9, F_{29}, F_{35}, F_{37}, F_{42}, F_{52}, F_{57}\}$.

Symbol	Name
F_9	Mean blink frequency
F_{29}	Mean monitoring frequency
F_{35}	Mean dwell percentage
F_{37}	Time since last look at left mirror AOI
F_{42}	Time since last look at right mirror AOI
F_{52}	Time since last look at tachometer AOI
F_{57}	Time since last look at infotainment AOI

Distribution $p\left(S_2^1 : \boldsymbol{\theta}_{S_2^1}\right)$

The distribution $p\left(S_2^1 : \boldsymbol{\theta}_{S_2^1}\right)$ is a categorical distribution

$$p\left(S_2^1 : \boldsymbol{\theta}_{S_2^1}\right) = \text{Cat}\left(S_2^1 : \boldsymbol{\theta}_{S_2^1}\right)$$

over the discrete variable $S_2, \text{Val}(S_2) = \{s_{2_0}, s_{2_1}, s_{2_2}, s_{2_3}, s_{2_4}, s_{2_5}\}$ at time slice $t = 1$, with MAP parameters

$$\boldsymbol{\theta}_{S_2^1} = \left\{\theta_{s_{2_0}^1}, \theta_{s_{2_1}^1}, \theta_{s_{2_2}^1}, \theta_{s_{2_3}^1}, \theta_{s_{2_4}^1}, \theta_{s_{2_5}^1}\right\} = \{0.135163, 0.10816, 0.405193, 0.243175, 0.054154, 0.054154\}.$$

Distribution $p\left(S_2^t \mid S_2^{t-1} : \boldsymbol{\theta}_{S_2^t|S_2^{t-1}}\right)$

The distribution $p\left(S_2^t \mid S_2^{t-1} : \boldsymbol{\theta}_{S_2^t|S_2^{t-1}}\right)$ over the discrete variable $S_2, \mathrm{Val}(S_2) = \{s_{2_0}, s_{2_1}, s_{2_2}, s_{2_3}, s_{2_4}, s_{2_5}\}$ at time slice $t > 1$ is a collection of categorical distributions with a categorical distribution

$$p\left(S_2^t | s_2^{t-1} : \boldsymbol{\theta}_{S_2^t|s_2^{t-1}}\right) = \mathrm{Cat}\left(S_2^t : \boldsymbol{\theta}_{S_2^t|s_2^{t-1}}\right)$$

for each $s_2^{t-1} \in \mathrm{Val}(S_2)$, parameterized with MAP parameters

$$\boldsymbol{\theta}_{S_2^t|S_2^{t-1}} = \left\{\boldsymbol{\theta}_{S_2^t|s_{2_0}^{t-1}}, \boldsymbol{\theta}_{S_2^t|s_{2_1}^{t-1}}, \boldsymbol{\theta}_{S_2^t|s_{2_2}^{t-1}}, \boldsymbol{\theta}_{S_2^t|s_{2_3}^{t-1}}, \boldsymbol{\theta}_{S_2^t|s_{2_4}^{t-1}}, \boldsymbol{\theta}_{S_2^t|s_{2_5}^{t-1}}\right\},$$

where

$$\boldsymbol{\theta}_{S_2^t|s_{2_0}^{t-1}} = \left\{\theta_{s_{2_0}^t|s_{2_0}^{t-1}}, \theta_{s_{2_1}^t|s_{2_0}^{t-1}}, \theta_{s_{2_2}^t|s_{2_0}^{t-1}}, \theta_{s_{2_3}^t|s_{2_0}^{t-1}}, \theta_{s_{2_4}^t|s_{2_0}^{t-1}}, \theta_{s_{2_5}^t|s_{2_0}^{t-1}}\right\} = \{0.999639, 0.000072, 0.000072, 0.000072, 0.000072, 0.000072\},$$

$$\boldsymbol{\theta}_{S_2^t|s_{2_1}^{t-1}} = \left\{\theta_{s_{2_0}^t|s_{2_1}^{t-1}}, \theta_{s_{2_1}^t|s_{2_1}^{t-1}}, \theta_{s_{2_2}^t|s_{2_1}^{t-1}}, \theta_{s_{2_3}^t|s_{2_1}^{t-1}}, \theta_{s_{2_4}^t|s_{2_1}^{t-1}}, \theta_{s_{2_5}^t|s_{2_1}^{t-1}}\right\} = \{0.00009, 0.999549, 0.00009, 0.00009, 0.00009, 0.00009\},$$

$$\boldsymbol{\theta}_{S_2^t|s_{2_2}^{t-1}} = \left\{\theta_{s_{2_0}^t|s_{2_2}^{t-1}}, \theta_{s_{2_1}^t|s_{2_2}^{t-1}}, \theta_{s_{2_2}^t|s_{2_2}^{t-1}}, \theta_{s_{2_3}^t|s_{2_2}^{t-1}}, \theta_{s_{2_4}^t|s_{2_2}^{t-1}}, \theta_{s_{2_5}^t|s_{2_2}^{t-1}}\right\} = \{0.000024, 0.000024, 0.99988, 0.000024, 0.000024, 0.000024\},$$

$$\boldsymbol{\theta}_{S_2^t|s_{2_3}^{t-1}} = \left\{\theta_{s_{2_0}^t|s_{2_3}^{t-1}}, \theta_{s_{2_1}^t|s_{2_3}^{t-1}}, \theta_{s_{2_2}^t|s_{2_3}^{t-1}}, \theta_{s_{2_3}^t|s_{2_3}^{t-1}}, \theta_{s_{2_4}^t|s_{2_3}^{t-1}}, \theta_{s_{2_5}^t|s_{2_3}^{t-1}}\right\} = \{0.00004, 0.00004, 0.00004, 0.999799, 0.00004, 0.00004\},$$

$$\boldsymbol{\theta}_{S_2^t|s_{2_4}^{t-1}} = \left\{\theta_{s_{2_0}^t|s_{2_4}^{t-1}}, \theta_{s_{2_1}^t|s_{2_4}^{t-1}}, \theta_{s_{2_2}^t|s_{2_4}^{t-1}}, \theta_{s_{2_3}^t|s_{2_4}^{t-1}}, \theta_{s_{2_4}^t|s_{2_4}^{t-1}}, \theta_{s_{2_5}^t|s_{2_4}^{t-1}}\right\} = \{0.00018, 0.00018, 0.00018, 0.00018, 0.999098, 0.00018\},$$

$$\boldsymbol{\theta}_{S_2^t|s_{2_5}^{t-1}} = \left\{\theta_{s_{2_0}^t|s_{2_5}^{t-1}}, \theta_{s_{2_1}^t|s_{2_5}^{t-1}}, \theta_{s_{2_2}^t|s_{2_5}^{t-1}}, \theta_{s_{2_3}^t|s_{2_5}^{t-1}}, \theta_{s_{2_4}^t|s_{2_5}^{t-1}}, \theta_{s_{2_5}^t|s_{2_5}^{t-1}}\right\} = \{0.00018, 0.00018, 0.00018, 0.00018, 0.00018, 0.999098\}.$$

Distribution $p\left(F_9^t, F_{29}^t, F_{35}^t, F_{37}^t, F_{52}^t, F_{57}^t, F_{42}^t \mid S_2^t : \boldsymbol{\theta}_{F_9^t,\ldots,F_{42}^t|S_2^t}\right)$

The distribution $p\left(F_9^t, F_{29}^t, F_{35}^t, F_{37}^t, F_{52}^t, F_{57}^t, F_{42}^t \mid S_2^t : \boldsymbol{\theta}_{F_9^t,\ldots,F_{42}^t|S_2^t}\right)$ over a seven-dimensional vector of continuous variables $(F_9, F_{29}, F_{35}, F_{37}, F_{52}, F_{57}, F_{42})$ at time slice $t \geq 1$ is a collection of multivariate Gaussian mixture distributions with a multivariate GMM

$$p\left(F_9^t, F_{29}^t, F_{35}^t, F_{37}^t, F_{52}^t, F_{57}^t, F_{42}^t \mid s_2^t : \boldsymbol{\theta}_{F_9^t,\ldots,F_{42}^t|s_2^t}\right) = \sum_{i=1}^{n_{s_2}} \pi_{s_{2_i}^t} \mathcal{N}\left(\boldsymbol{\mu}_{s_{2_i}^t}, \Sigma_{s_{2_i}^t}\right)$$

composed of n_{s_2} components for each $s_2^t \in \mathrm{Val}(S_2)$, parameterized with MAP parameters $\boldsymbol{\theta}_{F_9^t,\ldots,F_{42}^t|S_2^t} = \left\{\boldsymbol{\theta}_{F_9^t,\ldots,F_{42}^t|s_{2_0}^t}, \boldsymbol{\theta}_{F_9^t,\ldots,F_{42}^t|s_{2_1}^t}, \boldsymbol{\theta}_{F_9^t,\ldots,F_{42}^t|s_{2_2}^t}, \boldsymbol{\theta}_{F_9^t,\ldots,F_{42}^t|s_{2_3}^t}, \boldsymbol{\theta}_{F_9^t,\ldots,F_{42}^t|s_{2_4}^t}, \boldsymbol{\theta}_{F_9^t,\ldots,F_{42}^t|s_{2_5}^t}\right\}$.

The distribution $p\left(F_9^t, F_{29}^t, F_{35}^t, F_{37}^t, F_{52}^t, F_{57}^t, F_{42}^t \mid s_{2_0}^t : \boldsymbol{\theta}_{F_9^t,\ldots,F_{42}^t \mid s_{2_0}^t} = \left\{\left\{\pi_{s_{2_0}^t i}, \boldsymbol{\mu}_{s_{2_0}^t i}, \Sigma_{s_{2_0}^t i}\right\}_{i=1}^{3}\right\}\right)$ consists of three components, where

$$\pi_{s_{2_0}^t 1} = 0.199947, \pi_{s_{2_0}^t 2} = 0.400027, \pi_{s_{2_0}^t 3} = 0.400027$$

$$\boldsymbol{\mu}_{s_{2_0}^t 1} = \begin{pmatrix} 0.781966 \\ 0.004969 \\ 0.998037 \\ 501.492584 \\ 284.524865 \\ 486.863493 \\ 558.708556 \end{pmatrix}, \boldsymbol{\mu}_{s_{2_0}^t 2} = \begin{pmatrix} 0.694945 \\ 0.252155 \\ 0.913035 \\ 138.271519 \\ 18.975042 \\ 80.23718 \\ 514.293089 \end{pmatrix}, \boldsymbol{\mu}_{s_{2_0}^t 3} = \begin{pmatrix} 0.987175 \\ 0.040322 \\ 0.026824 \\ 527.712665 \\ 277.149587 \\ 1.659239 \\ 528.509907 \end{pmatrix}$$

$$\Sigma_{s_{2_0}^t 1} = \begin{bmatrix} 0.018071 & -0.000165 & 0.000227 & 0.445593 & 0.335516 & 0.446644 & 0.300411 \\ -0.000165 & 0.002755 & -0.000462 & -0.517602 & -0.293713 & -0.51974 & -0.222312 \\ 0.000227 & -0.000462 & 0.009059 & 0.722822 & 0.409588 & 0.725812 & 0.309694 \\ 0.445593 & -0.517602 & 0.722822 & 3116.83075 & 533.437328 & 887.415093 & 421.61793 \\ 0.335516 & -0.293713 & 0.409588 & 533.437328 & 977.923578 & 535.334102 & 271.389758 \\ 0.446644 & -0.51974 & 0.725812 & 887.415093 & 535.334102 & 2822.347208 & 423.052104 \\ 0.300411 & -0.222312 & 0.309694 & 421.61793 & 271.389758 & 423.052104 & 1923.052325 \end{bmatrix},$$

$$\Sigma_{s_{2_0}^t 1} = \begin{bmatrix} 0.019873 & 0.002894 & 0.001863 & 2.961732 & 0.070398 & -0.138681 & -0.739775 \\ 0.002894 & 0.038099 & -0.003656 & -7.873079 & -0.554688 & -0.285748 & 1.224512 \\ 0.001863 & -0.003656 & 0.007696 & 3.292939 & 0.084354 & -0.396062 & -1.010929 \\ 2.961732 & -7.873079 & 3.292939 & 6215.53858 & 369.024845 & -196.768645 & -1244.929336 \\ 0.070398 & -0.554688 & 0.084354 & 369.024845 & 431.383102 & 20.031784 & -77.004721 \\ -0.138681 & -0.285748 & -0.396062 & -196.768645 & 20.031784 & 1060.279783 & 133.173844 \\ -0.739775 & 1.224512 & -1.010929 & -1244.929336 & -77.004721 & 133.173844 & 1310.426599 \end{bmatrix},$$

$$\Sigma_{s_{2_0}^t 1} = \begin{bmatrix} 0.340792 & 0.022966 & 0.01198 & 2.300344 & -132.142596 & 0.670962 & 2.044395 \\ 0.022966 & 0.003035 & 0.001363 & -0.092989 & -9.951665 & 0.125715 & 0.065693 \\ 0.01198 & 0.001363 & 0.006155 & -0.603954 & -6.480759 & 0.257655 & -0.089141 \\ 2.300344 & -0.092989 & -0.603954 & 1679.253388 & -899.724587 & -134.575626 & 248.773121 \\ -132.142596 & -9.951665 & -6.480759 & -899.724587 & 61121.27295 & -394.692512 & -1059.725845 \\ 0.670962 & 0.125715 & 0.257655 & -134.575626 & -394.692512 & 1011.561018 & -40.697456 \\ 2.044395 & 0.065693 & -0.089141 & 248.773121 & -1059.725845 & -40.697456 & 997.545386 \end{bmatrix}.$$

The distribution $p\left(F_9^t, F_{29}^t, F_{35}^t, F_{37}^t, F_{52}^t, F_{57}^t, F_{42}^t \mid s_{2_1}^t : \boldsymbol{\theta}_{F_9^t,\ldots,F_{42}^t \mid s_{2_1}^t} = \left\{\left\{\pi_{s_{2_1}^t i}, \boldsymbol{\mu}_{s_{2_1}^t i}, \Sigma_{s_{2_1}^t i}\right\}_{i=1}^{3}\right\}\right)$ consists of three components, where

$$\pi_{s_{2_1}^t 1} = 0.022198, \pi_{s_{2_1}^t 2} = 0.500083, \pi_{s_{2_1}^t 1} = 0.477718$$

$$\boldsymbol{\mu}_{s_{2_1}^t 1} = \begin{pmatrix} 0.920254 \\ 0.103412 \\ 0.949427 \\ 30.831751 \\ 47.469392 \\ 346.396353 \\ 26.550465 \end{pmatrix}, \boldsymbol{\mu}_{s_{2_1}^t 2} = \begin{pmatrix} 1.259215 \\ 0.091513 \\ 0.507263 \\ 522.059599 \\ 121.421227 \\ 34.864517 \\ 522.856841 \end{pmatrix}, \boldsymbol{\mu}_{s_{2_1}^t 3} = \begin{pmatrix} 0.543961 \\ 0.063043 \\ 0.98916 \\ 297.357684 \\ 157.819812 \\ 435.888976 \\ 390.236057 \end{pmatrix}$$

$$\Sigma_{s_{2_1}^t 1} = \begin{bmatrix} 0.197788 & -0.002557 & 0.005102 & -1.882869 & -0.538495 & 4.084476 & -6.757668 \\ -0.002557 & 0.02843 & -0.002822 & 1.022743 & 0.293728 & -2.178122 & 3.630677 \\ 0.005102 & -0.002822 & 0.099081 & -2.07746 & -0.592039 & 4.492909 & -7.439099 \\ -1.882869 & 1.022743 & -2.07746 & 25605.003 & 216.045625 & -1689.829943 & 2815.921804 \\ -0.538495 & 0.293728 & -0.592039 & 216.045625 & 7207.652865 & -475.770656 & 782.999648 \\ 4.084476 & -2.178122 & 4.492909 & -1689.829943 & -475.770656 & 25129.73278 & -6066.347786 \\ -6.757668 & 3.630677 & -7.439099 & 2815.921804 & 782.999648 & -6066.347786 & 28936.75802 \end{bmatrix},$$

$$\Sigma_{s_{2_1}^t 2} = \begin{bmatrix} 0.643078 & 0.043139 & 0.364969 & 3.422743 & -84.113214 & 22.86346 & 2.949334 \\ 0.043139 & 0.00578 & 0.023959 & -0.034014 & -5.447369 & 0.429156 & 0.083747 \\ 0.364969 & 0.023959 & 0.225557 & 1.126472 & -50.7741 & 16.722845 & 1.257238 \\ 3.422743 & -0.034014 & 1.126472 & 1652.889308 & -247.142716 & -230.399385 & 226.927916 \\ -84.113214 & -5.447369 & -50.7741 & -247.142716 & 12003.82375 & -3867.036442 & -282.659745 \\ 22.86346 & 0.429156 & 16.722845 & -230.399385 & -3867.036442 & 4545.057267 & -163.064443 \\ 2.949334 & 0.083747 & 1.257238 & 226.927916 & -282.659745 & -163.064443 & 980.219061 \end{bmatrix},$$

$$\Sigma_{s_{2_1}^t} = \begin{bmatrix} 0.152952 & 0.015833 & -0.003944 & -89.057384 & -45.390401 & -32.116183 & -53.007634 \\ 0.015833 & 0.003488 & -0.000789 & -9.750997 & -5.30524 & -3.917498 & -6.123498 \\ -0.003944 & -0.000789 & 0.004939 & 2.256311 & 1.367311 & 1.236445 & 1.485071 \\ -89.057384 & -9.750997 & 2.256311 & 61393.12725 & 28970.62194 & 20579.65426 & 33797.01577 \\ -45.390401 & -5.30524 & 1.367311 & 28970.62194 & 15238.2956 & 10624.69598 & 17361.31248 \\ -32.116183 & -3.917498 & 1.236445 & 20579.65426 & 10624.69598 & 8804.310848 & 12288.71633 \\ -53.007634 & -6.123498 & 1.485071 & 33797.01577 & 17361.31248 & 12288.71633 & 21154.11305 \end{bmatrix}.$$

The distribution $p\left(F_9^t, F_{29}^t, F_{35}^t, F_{37}^t, F_{52}^t, F_{57}^t, F_{42}^t \mid s_{2_2}^t : \boldsymbol{\theta}_{F_9^t,\dots,F_{42}^t|s_{2_2}^t} = \left\{\left\{\pi_{s_{2_2}^t i}, \boldsymbol{\mu}_{s_{2_2}^t i}, \Sigma_{s_{2_2}^t i}\right\}_{i=1}^{4}\right\}\right)$ consists of four components, where

$$\pi_{s_{2_2}^t 1} = 0.250336, \pi_{s_{2_2}^t 2} = 0.149863, \pi_{s_{2_2}^t 3} = 0.162118, \pi_{s_{2_2}^t 4} = 0.437682,$$

$$\boldsymbol{\mu}_{s_{2_2}^t 1} = \begin{pmatrix} 0.279036 \\ 0.304791 \\ 0.485321 \\ 36.446345 \\ 34.962404 \\ 42.943766 \\ 258.488153 \end{pmatrix}, \boldsymbol{\mu}_{s_{2_2}^t 2} = \begin{pmatrix} 0.443577 \\ 0.204295 \\ 0.160487 \\ 12.109562 \\ 113.768241 \\ 0.486691 \\ 266.438129 \end{pmatrix},$$

$$\boldsymbol{\mu}_{s_{2_2}^t 3} = \begin{pmatrix} 0.783571 \\ 0.066575 \\ 0.981091 \\ 157.451287 \\ 74.197428 \\ 276.619425 \\ 517.311032 \end{pmatrix}, \boldsymbol{\mu}_{s_{2_2}^t 4} = \begin{pmatrix} 0.434456 \\ 0.276997 \\ 0.928227 \\ 9.461318 \\ 21.123373 \\ 208.52134 \\ 509.579516 \end{pmatrix},$$

$$\Sigma_{s_{2_2}^t 1} = \begin{bmatrix} 0.022495 & -0.000567 & 0.01393 & -1.332635 & -1.209682 & 2.270549 & -17.689437 \\ -0.000567 & 0.028228 & 0.051791 & -2.321017 & -1.430089 & 4.988003 & 3.210427 \\ 0.01393 & 0.051791 & 0.143657 & -7.592448 & -6.861933 & 14.227393 & -29.679145 \\ -1.332635 & -2.321017 & -7.592448 & 1438.763626 & 401.031725 & -914.370216 & 3015.786355 \\ -1.209682 & -1.430089 & -6.861933 & 401.031725 & 859.999775 & -628.957825 & 3936.440002 \\ 2.270549 & 4.988003 & 14.227393 & -914.370216 & -628.957825 & 2162.438739 & -3482.119296 \\ -17.689437 & 3.210427 & -29.679145 & 3015.786355 & 3936.440002 & -3482.119296 & 42577.50007 \end{bmatrix},$$

$$\Sigma_{s_{2_2}^t 2} = \begin{bmatrix} 0.073843 & -0.00032 & 0.001525 & -0.546721 & -11.246912 & 0.086574 & -34.41288 \\ -0.00032 & 0.004813 & 0.002464 & 0.08869 & -0.310381 & 0.000093 & -0.868886 \\ 0.001525 & 0.002464 & 0.007373 & 0.125207 & -0.568122 & 0.155132 & -1.57633 \\ -0.546721 & 0.08869 & 0.125207 & 1086.572194 & 96.555273 & 39.276996 & 401.502331 \\ -11.246912 & -0.310381 & -0.568122 & 96.555273 & 2659.867081 & -12.760122 & 7041.254581 \\ 0.086574 & 0.000093 & 0.155132 & 39.276996 & -12.760122 & 898.173608 & 41.166511 \\ -34.41288 & -0.868886 & -1.57633 & 401.502331 & 7041.254581 & 41.166511 & 22158.09931 \end{bmatrix},$$

$$\Sigma_{s_{2_2}^t 3} = \begin{bmatrix} 0.104678 & -0.001573 & 0.003502 & 1.216304 & -9.279259 & 37.391605 & -1.568406 \\ -0.001573 & 0.002353 & -0.000614 & -0.717112 & 1.121457 & -5.459019 & -0.263316 \\ 0.003502 & -0.000614 & 0.004643 & -0.081036 & -0.723704 & 4.580116 & 0.034051 \\ 1.216304 & -0.717112 & -0.081036 & 2057.714232 & -390.152006 & 201.67478 & 340.357262 \\ -9.279259 & 1.121457 & -0.723704 & -390.152006 & 2505.793166 & -10285.46465 & 97.274693 \\ 37.391605 & -5.459019 & 4.580116 & 201.67478 & -10285.46465 & 54944.52396 & -684.010724 \\ -1.568406 & -0.263316 & 0.034051 & 340.357262 & 97.274693 & -684.010724 & 880.537805 \end{bmatrix},$$

$$\Sigma_{s_{2_2}^t 4} = \begin{bmatrix} 0.045897 & -0.001059 & -0.001142 & 0.060292 & -0.740815 & -3.916704 & 1.568318 \\ -0.001059 & 0.023215 & -0.005794 & -0.152564 & -0.793892 & -10.146754 & -0.119185 \\ -0.001142 & -0.005794 & 0.005595 & 0.07765 & -0.021862 & 1.686484 & -0.348656 \\ 0.060292 & -0.152564 & 0.07765 & 407.484772 & -13.950146 & -317.771307 & -0.093255 \\ -0.740815 & -0.793892 & -0.021862 & -13.950146 & 351.640173 & 1319.118322 & -64.309529 \\ -3.916704 & -10.146754 & 1.686484 & -317.771307 & 1319.118322 & 46361.41783 & 1072.144068 \\ 1.568318 & -0.119185 & -0.348656 & -0.093255 & -64.309529 & 1072.144068 & 627.392451 \end{bmatrix}.$$

The distribution $p\left(F_9^t, F_{29}^t, F_{35}^t, F_{37}^t, F_{52}^t, F_{57}^t, F_{42}^t \mid s_{2_3}^t : \boldsymbol{\theta}_{F_9^t,\dots,F_{42}^t|s_{2_3}^t} = \left\{\left\{\pi_{s_{2_3}^t i}, \boldsymbol{\mu}_{s_{2_3}^t i}, \Sigma_{s_{2_3}^t i}\right\}_{i=1}^{3}\right\}\right)$ consists of three components, where

$$\pi_{s_{2_3}^t 1} = 0.444469, \pi_{s_{2_3}^t 2} = 0.333333, \pi_{s_{2_3}^t 3} = 0.222198,$$

$$\boldsymbol{\mu}_{s_{2_3}^t{}_1} = \begin{pmatrix} 0.501033 \\ 0.443337 \\ 0.859019 \\ 13.431129 \\ 24.077924 \\ 39.693507 \\ 287.970781 \end{pmatrix}, \boldsymbol{\mu}_{s_{2_3}^t{}_2} = \begin{pmatrix} 0.830328 \\ 0.125639 \\ 0.400015 \\ 272.236737 \\ 70.735764 \\ 121.661237 \\ 410.334385 \end{pmatrix}, \boldsymbol{\mu}_{s_{2_3}^t{}_3} = \begin{pmatrix} 1.626248 \\ 0.518032 \\ 0.408081 \\ 12.113145 \\ 89.352978 \\ 1.32464 \\ 498.151 \end{pmatrix},$$

$$\Sigma_{s_{2_3}^t{}_1} = \begin{bmatrix} 0.073826 & 0.022858 & 0.000636 & -0.751665 & -0.501334 & 0.101585 & 28.307815 \\ 0.022858 & 0.022259 & -0.001946 & -1.203065 & -1.330808 & 0.550683 & 1.837308 \\ 0.000636 & -0.001946 & 0.010094 & -0.336168 & -0.319491 & -0.34663 & 4.70314 \\ -0.751665 & -1.203065 & -0.336168 & 865.394807 & 86.775056 & -50.197512 & 1.213522 \\ -0.501334 & -1.330808 & -0.319491 & 86.775056 & 473.823775 & 11.787009 & 442.749316 \\ 0.101585 & 0.550683 & -0.34663 & -50.197512 & 11.787009 & 1059.012117 & -115.458208 \\ 28.307815 & 1.837308 & 4.70314 & 1.213522 & 442.749316 & -115.458208 & 19242.10361 \end{bmatrix},$$

$$\Sigma_{s_{2_3}^t{}_2} = \begin{bmatrix} 0.499934 & 0.054683 & -0.041993 & -85.689175 & 27.156393 & -39.588329 & -89.591083 \\ 0.054683 & 0.010894 & 0.011437 & -12.530175 & 2.931497 & 1.50962 & -9.488056 \\ -0.041993 & 0.011437 & 0.177237 & -20.537941 & -4.424114 & 69.503944 & 17.581943 \\ -85.689175 & -12.530175 & -20.537941 & 21445.73398 & -4506.069784 & -3146.128403 & 15333.04191 \\ 27.156393 & 2.931497 & -4.424114 & -4506.069784 & 1811.995913 & -3087.65452 & -5205.126827 \\ -39.588329 & 1.50962 & 69.503944 & -3146.128403 & -3087.65452 & 30081.54387 & 11967.86258 \\ -89.591083 & -9.488056 & 17.581943 & 15333.04191 & -5205.126827 & 11967.86258 & 19009.2892 \end{bmatrix},$$

$$\Sigma_{s_{2_3}^t{}_3} = \begin{bmatrix} 0.748676 & 0.224966 & 0.154853 & -4.192448 & 34.603741 & -0.148133 & 1.667625 \\ 0.224966 & 0.088439 & 0.056803 & -1.520401 & 12.383782 & -0.015677 & 0.237072 \\ 0.154853 & 0.056803 & 0.044138 & -0.686427 & 8.698238 & 0.148074 & 0.184355 \\ -4.192448 & -1.520401 & -0.686427 & 1227.70381 & -138.573351 & 42.296101 & -4.222391 \\ 34.603741 & 12.383782 & 8.698238 & -138.573351 & 2403.501417 & 8.99414 & 167.681348 \\ -0.148133 & -0.015677 & 0.148074 & 42.296101 & 8.99414 & 1009.479191 & -33.654143 \\ 1.667625 & 0.237072 & 0.184355 & -4.222391 & 167.681348 & -33.654143 & 956.934204 \end{bmatrix}.$$

The distribution $p\left(F_9^t, F_{29}^t, F_{35}^t, F_{37}^t, F_{52}^t, F_{57}^t, F_{42}^t \mid s_{2_4}^t : \boldsymbol{\theta}_{F_9^t,\dots,F_{42}^t|s_{2_4}^t} = \left\{\left\{\pi_{s_{2_4}^t{}_i}, \boldsymbol{\mu}_{s_{2_4}^t{}_i}, \Sigma_{s_{2_4}^t{}_i}\right\}_{i=1}^{2}\right\}\right)$ consists of two components, where

$$\pi_{s_{2_4}^t{}_1} = 0.5, \pi_{s_{2_4}^t{}_2} = 0.5,$$

$$\boldsymbol{\mu}_{s_{2_4}^t{}_1} = \begin{pmatrix} 0.298987 \\ 0.071915 \\ 0.994981 \\ 12.98663 \\ 51.443285 \\ 49.726247 \\ 491.650833 \end{pmatrix}, \boldsymbol{\mu}_{s_{2_4}^t{}_2} = \begin{pmatrix} 0.454703 \\ 0.443627 \\ 0.829744 \\ 9.465794 \\ 26.174894 \\ 33.225252 \\ 68.941687 \end{pmatrix},$$

$$\Sigma_{s_{2_4}^t{}_1} = \begin{bmatrix} 0.023878 & -0.000367 & -0.000713 & -0.021593 & -0.47538 & -0.378094 & -0.731559 \\ -0.000367 & 0.002903 & -0.000354 & 0.131265 & 0.036348 & 0.080474 & -0.079849 \\ -0.000713 & -0.000354 & 0.009055 & -0.226668 & -0.045642 & -0.13133 & 0.179999 \\ -0.021593 & 0.131265 & -0.226668 & 2396.960837 & 48.376016 & 80.6964 & -36.732527 \\ -0.47538 & 0.036348 & -0.045642 & 48.376016 & 722.057861 & 85.640164 & 61.102567 \\ -0.378094 & 0.080474 & -0.13133 & 80.6964 & 85.640164 & 2035.550908 & 37.346328 \\ -0.731559 & -0.079849 & 0.179999 & -36.732527 & 61.102567 & 37.346328 & 1823.231109 \end{bmatrix},$$

$$\Sigma_{s_{2_4}^t{}_1} = \begin{bmatrix} 0.028899 & 0.020337 & 0.002483 & 0.198073 & 0.738283 & 0.783177 & -3.178141 \\ 0.020337 & 0.046626 & 0.005406 & 0.098301 & 1.176524 & 1.133215 & -8.451297 \\ 0.002483 & 0.005406 & 0.009364 & -0.077569 & 0.06612 & 0.032517 & -1.204525 \\ 0.198073 & 0.098301 & -0.077569 & 2361.030022 & 32.236774 & 58.836188 & 192.605383 \\ 0.738283 & 1.176524 & 0.06612 & 32.236774 & 733.696795 & 101.271801 & -192.621693 \\ 0.783177 & 1.133215 & 0.032517 & 58.836188 & 101.271801 & 2051.003352 & -122.231639 \\ -3.178141 & -8.451297 & -1.204525 & 192.605383 & -192.621693 & -122.231639 & 4395.718723 \end{bmatrix}.$$

The distribution $p\left(F_9^t, F_{29}^t, F_{35}^t, F_{37}^t, F_{52}^t, F_{57}^t, F_{42}^t \mid s_{2_5}^t : \boldsymbol{\theta}_{F_9^t,\dots,F_{42}^t|s_{2_5}^t} = \left\{\left\{\pi_{s_{2_5}^t{}_i}, \boldsymbol{\mu}_{s_{2_5}^t{}_i}, \Sigma_{s_{2_5}^t{}_i}\right\}_{i=1}^{1}\right\}\right)$ consists of a single component, where

$$\pi_{s_{2_5}^t{}_1} = 1,$$

$$\boldsymbol{\mu}_{S_{2_{5_1}}^t} = \begin{pmatrix} 0.791217 \\ 0.325507 \\ 0.506691 \\ 13.458963 \\ 75.336068 \\ 3.821791 \\ 158.968508 \end{pmatrix},$$

$$\Sigma_{S_{2_{5_1}}^t} = \begin{bmatrix} 0.121724 & 0.004611 & 0.013229 & 2.365665 & -7.505928 & 0.447338 & 8.152855 \\ 0.004611 & 0.009165 & -0.001136 & -0.204106 & -1.195165 & 0.097213 & -0.250741 \\ 0.013229 & -0.001136 & 0.075913 & -0.169265 & -11.445818 & 0.849885 & 7.128616 \\ 2.365665 & -0.204106 & -0.169265 & 1289.740792 & -113.925517 & 38.400307 & 256.053358 \\ -7.505928 & -1.195165 & -11.445818 & -113.925517 & 2960.682017 & -139.948638 & -1463.086337 \\ 0.447338 & 0.097213 & 0.849885 & 38.400307 & -139.948638 & 1030.244676 & 189.364818 \\ 8.152855 & -0.250741 & 7.128616 & 256.053358 & -1463.086337 & 189.364818 & 2401.569986 \end{bmatrix}.$$

2.4 Parameters of the SAE Level 3 SAGAT Score Model

For any number of time slices $T \geq 1$, the SAE Level 3 SAGAT Score model defines the JPD

$$p\left(S_2^{1:T}, \boldsymbol{F}_{\text{Rel}}^{1:T} : \boldsymbol{\theta}\right) = p\left(S_2^1 : \boldsymbol{\theta}_{S_2^1}\right) \prod_{t=2}^{T} p\left(S_2^t \mid S_2^{t-1} : \boldsymbol{\theta}_{S_2^t | S_2^{t-1}}\right) \prod_{t=1}^{T} p\left(\boldsymbol{F}_{\text{Rel}}^t \mid S_2^t : \boldsymbol{\theta}\right),$$

with $p\left(\boldsymbol{F}_{\text{Rel}}^t \mid S_2^t : \boldsymbol{\theta}\right)$ given by

$$p\left(F_9^t, F_{16}^t, F_{58}^t, F_{43}^t, F_{12}^t \mid S_2^t : \boldsymbol{\theta}_{F_9^t,\ldots,F_{12}^t | S_2^t}\right) p\left(F_{29}^t, F_{31}^t, F_{37}^t, F_{57}^t \mid S_2^t : \boldsymbol{\theta}_{F_{29}^t,\ldots,F_{57}^t | S_2^t}\right).$$

As such, the model is defined by four probability /density distribution to be detailed in the following. The names of the relevant indicators $\boldsymbol{F}_{\text{Rel}} = \{F_9, F_{12}, F_{16}, F_{29}, F_{31}, F_{37}, F_{43}, F_{57}, F_{58}\}$ are provided in Table 8.

Table 27: The set of relevant indicators for the SAE Level 3 SAGAT Score model, $\boldsymbol{F}_{\text{Rel}} = \{F_9, F_{12}, F_{16}, F_{29}, F_{31}, F_{37}, F_{43}, F_{57}, F_{58}\}$.

Symbol	Name
F_9	Mean blink frequency
F_{12}	Mean yaw angle of the head
F_{16}	Yaw rate of the head variability
F_{29}	Mean monitoring frequency
F_{31}	Saccade frequency
F_{37}	Time since last look at left mirror AOI
F_{43}	Mean time since last look at right mirror AOI
F_{57}	Time since last look at infotainment AOI
F_{58}	Mean time since last look at infotainment AOI

Distribution $p\left(S_2^1 : \boldsymbol{\theta}_{S_2^1}\right)$

The distribution $p\left(S_2^1 : \boldsymbol{\theta}_{S_2^1}\right)$ is a categorical distribution

$$p\left(S_2^1 : \boldsymbol{\theta}_{S_2^1}\right) = \text{Cat}\left(S_2^1 : \boldsymbol{\theta}_{S_2^1}\right)$$

over the discrete variable S_2, $\text{Val}(S_2) = \left\{s_{2_0}, s_{2_1}, s_{2_2}, s_{2_3}, s_{2_4}, s_{2_5}\right\}$ at time slice $t = 1$, with MAP parameters

$$\boldsymbol{\theta}_{S_2^1} = \left\{\theta_{s_{2_0}^1}, \theta_{s_{2_1}^1}, \theta_{s_{2_2}^1}, \theta_{s_{2_3}^1}, \theta_{s_{2_4}^1}, \theta_{s_{2_5}^1}\right\}$$
$$= \{0.243175, 0.189169, 0.162166, 0.162184, 0.216154, 0.027151\}.$$

Distribution $p\left(S_2^t \mid S_2^{t-1} : \boldsymbol{\theta}_{S_2^t|S_2^{t-1}}\right)$

The distribution $p\left(S_2^t \mid S_2^{t-1} : \boldsymbol{\theta}_{S_2^t|S_2^{t-1}}\right)$ over the discrete variable $S_2, \mathrm{Val}(S_2) = \{s_{2_0}, s_{2_1}, s_{2_2}, s_{2_3}, s_{2_4}, s_{2_5}\}$ at time slice $t > 1$ is a collection of categorical distributions with a categorical distribution

$$p\left(S_2^t | s_2^{t-1} : \boldsymbol{\theta}_{S_2^t|s_2^{t-1}}\right) = \mathrm{Cat}\left(S_2^t : \boldsymbol{\theta}_{S_2^t|s_2^{t-1}}\right)$$

for each $s_2^{t-1} \in \mathrm{Val}(S_2)$, parameterized with MAP parameters $\boldsymbol{\theta}_{S_2^t|s_2^{t-1}} = \left\{\boldsymbol{\theta}_{S_2^t|s_{2_0}^{t-1}}, \boldsymbol{\theta}_{S_2^t|s_{2_1}^{t-1}}, \boldsymbol{\theta}_{S_2^t|s_{2_2}^{t-1}}, \boldsymbol{\theta}_{S_2^t|s_{2_3}^{t-1}}, \boldsymbol{\theta}_{S_2^t|s_{2_4}^{t-1}}, \boldsymbol{\theta}_{S_2^t|s_{2_5}^{t-1}}\right\}$, where

$$\boldsymbol{\theta}_{S_2^t|s_{2_0}^{t-1}} = \left\{\theta_{s_{2_0}^t|s_{2_0}^{t-1}}, \theta_{s_{2_1}^t|s_{2_0}^{t-1}}, \theta_{s_{2_2}^t|s_{2_0}^{t-1}}, \theta_{s_{2_3}^t|s_{2_0}^{t-1}}, \theta_{s_{2_4}^t|s_{2_0}^{t-1}}, \theta_{s_{2_5}^t|s_{2_0}^{t-1}}\right\}$$
$$= \{0.999799, 0.00004, 0.00004, 0.00004, 0.00004, 0.00004\},$$

$$\boldsymbol{\theta}_{S_2^t|s_{2_1}^{t-1}} = \left\{\theta_{s_{2_0}^t|s_{2_1}^{t-1}}, \theta_{s_{2_1}^t|s_{2_1}^{t-1}}, \theta_{s_{2_2}^t|s_{2_1}^{t-1}}, \theta_{s_{2_3}^t|s_{2_1}^{t-1}}, \theta_{s_{2_4}^t|s_{2_1}^{t-1}}, \theta_{s_{2_5}^t|s_{2_1}^{t-1}}\right\}$$
$$= \{0.000052, 0.999742, 0.000052, 0.000052, 0.000052, 0.000052\},$$

$$\boldsymbol{\theta}_{S_2^t|s_{2_2}^{t-1}} = \left\{\theta_{s_{2_0}^t|s_{2_2}^{t-1}}, \theta_{s_{2_1}^t|s_{2_2}^{t-1}}, \theta_{s_{2_2}^t|s_{2_2}^{t-1}}, \theta_{s_{2_3}^t|s_{2_2}^{t-1}}, \theta_{s_{2_4}^t|s_{2_2}^{t-1}}, \theta_{s_{2_5}^t|s_{2_2}^{t-1}}\right\}$$
$$= \{0.00006, 0.00006, 0.999699, 0.00006, 0.00006, 0.00006\},$$

$$\boldsymbol{\theta}_{S_2^t|s_{2_3}^{t-1}} = \left\{\theta_{s_{2_0}^t|s_{2_3}^{t-1}}, \theta_{s_{2_1}^t|s_{2_3}^{t-1}}, \theta_{s_{2_2}^t|s_{2_3}^{t-1}}, \theta_{s_{2_3}^t|s_{2_3}^{t-1}}, \theta_{s_{2_4}^t|s_{2_3}^{t-1}}, \theta_{s_{2_5}^t|s_{2_3}^{t-1}}\right\}$$
$$= \{0.00006, 0.00006, 0.00006, 0.999699, 0.00006, 0.00006\},$$

$$\boldsymbol{\theta}_{S_2^t|s_{2_4}^{t-1}} = \left\{\theta_{s_{2_0}^t|s_{2_4}^{t-1}}, \theta_{s_{2_1}^t|s_{2_4}^{t-1}}, \theta_{s_{2_2}^t|s_{2_4}^{t-1}}, \theta_{s_{2_3}^t|s_{2_4}^{t-1}}, \theta_{s_{2_4}^t|s_{2_4}^{t-1}}, \theta_{s_{2_5}^t|s_{2_4}^{t-1}}\right\}$$
$$= \{0.000045, 0.000045, 0.000045, 0.000045, 0.999774, 0.000045\},$$

$$\boldsymbol{\theta}_{S_2^t|s_{2_5}^{t-1}} = \left\{\theta_{s_{2_0}^t|s_{2_5}^{t-1}}, \theta_{s_{2_1}^t|s_{2_5}^{t-1}}, \theta_{s_{2_2}^t|s_{2_5}^{t-1}}, \theta_{s_{2_3}^t|s_{2_5}^{t-1}}, \theta_{s_{2_4}^t|s_{2_5}^{t-1}}, \theta_{s_{2_5}^t|s_{2_5}^{t-1}}\right\}$$
$$= \{0.00036, 0.00036, 0.00036, 0.00036, 0.00036, 0.998198\}.$$

Distribution $p\left(F_9^t, F_{16}^t, F_{58}^t, F_{43}^t, F_{12}^t \mid S_2^t : \boldsymbol{\theta}_{F_9^t,\ldots,F_{12}^t|S_2^t}\right)$

The distribution $p\left(F_9^t, F_{16}^t, F_{58}^t, F_{43}^t, F_{12}^t \mid S_2^t : \boldsymbol{\theta}_{F_9^t,\ldots,F_{12}^t|S_2^t}\right)$ over a five-dimensional vector of continuous variables $(F_9, F_{16}, F_{58}, F_{43}, F_{12})$ at time slice $t \geq 1$ is a collection of multivariate Gaussian mixture distributions with a multivariate GMM

$$p\left(F_9^t, F_{16}^t, F_{58}^t, F_{43}^t, F_{12}^t \mid s_2^t : \boldsymbol{\theta}_{F_9^t,\ldots,F_{12}^t|s_2^t}\right) = \sum_{i=1}^{n_{s_2}} \pi_{s_{2_i}^t} \mathcal{N}\left(\boldsymbol{\mu}_{s_{2_i}^t}, \Sigma_{s_{2_i}^t}\right)$$

composed of n_{s_2} components for each $s_2^t \in \mathrm{Val}(S_2)$, parameterized with MAP parameters $\boldsymbol{\theta}_{F_9^t,\ldots,F_{12}^t|S_2^t} = \left\{\boldsymbol{\theta}_{F_9^t,\ldots,F_{12}^t|s_{2_0}^t}, \boldsymbol{\theta}_{F_9^t,\ldots,F_{12}^t|s_{2_1}^t}, \boldsymbol{\theta}_{F_9^t,\ldots,F_{12}^t|s_{2_2}^t}, \boldsymbol{\theta}_{F_9^t,\ldots,F_{12}^t|s_{2_3}^t}, \boldsymbol{\theta}_{F_9^t,\ldots,F_{12}^t|s_{2_4}^t}, \boldsymbol{\theta}_{F_9^t,\ldots,F_{12}^t|s_{2_5}^t}\right\}$.

The distribution $p\left(F_9^t, F_{16}^t, F_{58}^t, F_{43}^t, F_{12}^t \mid s_{2_0}^t : \boldsymbol{\theta}_{F_9^t,\dots,F_{12}^t|s_{2_0}^t} = \left\{\left\{\pi_{s_{2_0}^t i}, \boldsymbol{\mu}_{s_{2_0}^t i}, \Sigma_{s_{2_0}^t i}\right\}_{i=1}^{5}\right\}\right)$ consists of five components, where

$$\pi_{s_{2_0}^t 1} = 0.354124, \pi_{s_{2_0}^t 2} = 0.111078, \pi_{s_{2_0}^t 3} = 0.105965, \pi_{s_{2_0}^t 4} = 0.408781, \pi_{s_{2_0}^t 5} = 0.020051,$$

$$\boldsymbol{\mu}_{s_{2_0}^t 1} = \begin{pmatrix} 0.998207 \\ 0.49185 \\ 4.884591 \\ 353.719197 \\ -0.355784 \end{pmatrix}, \boldsymbol{\mu}_{s_{2_0}^t 2} = \begin{pmatrix} 1.196385 \\ 0.184465 \\ 302.447637 \\ 334.218223 \\ 0.171572 \end{pmatrix}, \boldsymbol{\mu}_{s_{2_0}^t 3} = \begin{pmatrix} 1.063341 \\ 1.32041 \\ 1.45427 \\ 324.811379 \\ -0.261918 \end{pmatrix},$$

$$\boldsymbol{\mu}_{s_{2_0}^t 4} = \begin{pmatrix} 0.300914 \\ 0.150305 \\ 164.400883 \\ 316.764475 \\ -0.16165 \end{pmatrix}, \boldsymbol{\mu}_{s_{2_0}^t 5} = \begin{pmatrix} 0.19029 \\ 0.175349 \\ 97.657166 \\ 387.066817 \\ 0.053045 \end{pmatrix},$$

$$\Sigma_{s_{2_0}^t 1} = \begin{bmatrix} 0.280035 & 0.117991 & -2.815073 & -10.523058 & -0.124693 \\ 0.117991 & 0.085504 & -1.369285 & -5.223094 & -0.051323 \\ -2.815073 & -1.369285 & 343.10996 & 213.317739 & 1.925602 \\ -10.523058 & -5.223094 & 213.317739 & 1124.932199 & 7.439929 \\ -0.124693 & -0.051323 & 1.925602 & 7.439929 & 0.077321 \end{bmatrix},$$

$$\Sigma_{s_{2_0}^t 2} = \begin{bmatrix} 0.03718 & -0.000099 & 1.132272 & 0.725282 & -0.004189 \\ -0.000099 & 0.007055 & 0.203908 & 0.271313 & -0.001361 \\ 1.132272 & 0.203908 & 1040.728553 & 122.426056 & -0.0524 \\ 0.725282 & 0.271313 & 122.426056 & 636.808261 & -0.223932 \\ -0.004189 & -0.001361 & -0.0524 & -0.223932 & 0.004495 \end{bmatrix},$$

$$\Sigma_{s_{2_0}^t 3} = \begin{bmatrix} 0.168178 & 0.090548 & -0.062489 & 1.262115 & 0.029818 \\ 0.090548 & 0.233062 & -0.399029 & 2.136897 & 0.03706 \\ -0.062489 & -0.399029 & 879.480861 & -20.357836 & 0.141187 \\ 1.262115 & 2.136897 & -20.357836 & 657.571022 & 0.489549 \\ 0.029818 & 0.03706 & 0.141187 & 0.489549 & 0.013742 \end{bmatrix},$$

$$\Sigma_{s_{2_0}^t 4} = \begin{bmatrix} 0.032807 & -0.009147 & 20.530641 & 0.149889 & 0.02354 \\ -0.009147 & 0.011683 & -13.540046 & 0.640877 & -0.014827 \\ 20.530641 & -13.540046 & 22939.90675 & -739.759728 & 25.593922 \\ 0.149889 & 0.640877 & -739.759728 & 313.432971 & -0.802975 \\ 0.02354 & -0.014827 & 25.593922 & -0.802975 & 0.030211 \end{bmatrix},$$

$$\Sigma_{s_{2_0}^t 5} = \begin{bmatrix} 0.063411 & 0.001227 & -1.678308 & -0.775997 & -0.001261 \\ 0.001227 & 0.027619 & 0.132723 & -0.286207 & -0.000447 \\ -1.678308 & 0.132723 & 5843.547261 & -176.981391 & 0.038051 \\ -0.775997 & -0.286207 & -176.981391 & 3340.903637 & 0.393108 \\ -0.001261 & -0.000447 & 0.038051 & 0.393108 & 0.013739 \end{bmatrix}.$$

The distribution $p\left(F_9^t, F_{16}^t, F_{58}^t, F_{43}^t, F_{12}^t \mid s_{2_1}^t : \boldsymbol{\theta}_{F_9^t,\dots,F_{12}^t|s_{2_1}^t} = \left\{\left\{\pi_{s_{2_1}^t i}, \boldsymbol{\mu}_{s_{2_1}^t i}, \Sigma_{s_{2_1}^t i}\right\}_{i=1}^{4}\right\}\right)$ consists of four components, where

$$\pi_{s_{2_1}^t 1} = 0.172303, \pi_{s_{2_1}^t 2} = 0.256504, \pi_{s_{2_1}^t 3} = 0.142816, \pi_{s_{2_1}^t 4} = 0.428376,$$

$$\boldsymbol{\mu}_{s_{2_1}^t 1} = \begin{pmatrix} 0.432434 \\ 0.416753 \\ 83.648455 \\ 228.732384 \\ -0.036407 \end{pmatrix}, \boldsymbol{\mu}_{s_{2_1}^t 2} = \begin{pmatrix} 0.475514 \\ 0.161682 \\ 161.753187 \\ 334.385665 \\ -0.262146 \end{pmatrix}, \boldsymbol{\mu}_{s_{2_1}^t 3} = \begin{pmatrix} 0.23213 \\ 0.117963 \\ 18.803877 \\ 339.195005 \\ -0.01679 \end{pmatrix},$$

$$\boldsymbol{\mu}_{s_{2_1}^t 4} = \begin{pmatrix} 0.944837 \\ 0.467568 \\ 141.398794 \\ 303.399442 \\ 0.024308 \end{pmatrix},$$

$$\Sigma_{s_{2_1}^t{}_1} = \begin{bmatrix} 0.132036 & 0.032707 & 45.595531 & 23.944132 & -0.017231 \\ 0.032707 & 0.072584 & 4.637417 & 4.038668 & -0.009123 \\ 45.595531 & 4.637417 & 18837.0245 & 9212.613848 & -5.58693 \\ 23.944132 & 4.038668 & 9212.613848 & 5337.642897 & -3.365136 \\ -0.017231 & -0.009123 & -5.58693 & -3.365136 & 0.006508 \end{bmatrix},$$

$$\Sigma_{s_{2_1}^t{}_1} = \begin{bmatrix} 0.222257 & -0.042198 & 83.044766 & 13.572011 & 0.053211 \\ -0.042198 & 0.015965 & -16.881438 & -2.459491 & -0.010671 \\ 83.044766 & -16.881438 & 33385.20463 & 5259.760901 & 21.235768 \\ 13.572011 & -2.459491 & 5259.760901 & 1207.344169 & 3.311774 \\ 0.053211 & -0.010671 & 21.235768 & 3.311774 & 0.015259 \end{bmatrix},$$

$$\Sigma_{s_{2_1}^t{}_1} = \begin{bmatrix} 0.0342 & -0.008198 & 0.089153 & -1.28787 & 0.001801 \\ -0.008198 & 0.02747 & 0.514354 & 0.704414 & -0.002485 \\ 0.089153 & 0.514354 & 916.591919 & -39.990443 & 0.034747 \\ -1.28787 & 0.704414 & -39.990443 & 639.344288 & -0.141119 \\ 0.001801 & -0.002485 & 0.034747 & -0.141119 & 0.002878 \end{bmatrix},$$

$$\Sigma_{s_{2_1}^t{}_1} = \begin{bmatrix} 0.378955 & 0.234178 & -57.36198 & 18.068005 & -0.11325 \\ 0.234178 & 0.252858 & -48.599471 & 12.561779 & -0.083861 \\ -57.36198 & -48.599471 & 10958.04913 & -2851.036006 & 19.967604 \\ 18.068005 & 12.561779 & -2851.036006 & 1159.796937 & -5.568102 \\ -0.11325 & -0.083861 & 19.967604 & -5.568102 & 0.041493 \end{bmatrix}.$$

The distribution $p\left(F_9^t, F_{16}^t, F_{58}^t, F_{43}^t, F_{12}^t \mid s_{2_2}^t : \boldsymbol{\theta}_{F_9^t,\dots,F_{12}^t|s_{2_2}^t} = \left\{\left\{\pi_{s_{2_2}^t i}, \boldsymbol{\mu}_{s_{2_2}^t i}, \Sigma_{s_{2_2}^t i}\right\}_{i=1}^{4}\right\}\right)$ consists of four components, where

$$\pi_{s_{2_2}^t 1} = 0.500111, \pi_{s_{2_2}^t 2} = 0.066476, \pi_{s_{2_2}^t 3} = 0.266783, \pi_{s_{2_2}^t 4} = 0.16663,$$

$$\boldsymbol{\mu}_{s_{2_2}^t 1} = \begin{pmatrix} 1.103758 \\ 0.446624 \\ 0.547038 \\ 330.218985 \\ -0.362522 \end{pmatrix}, \boldsymbol{\mu}_{s_{2_2}^t 2} = \begin{pmatrix} 0.272084 \\ 0.711233 \\ 98.894977 \\ 198.055446 \\ 0.013296 \end{pmatrix}, \boldsymbol{\mu}_{s_{2_2}^t 3} = \begin{pmatrix} 0.233219 \\ 0.165228 \\ 90.547067 \\ 193.076166 \\ 0.029272 \end{pmatrix},$$

$$\boldsymbol{\mu}_{s_{2_2}^t 4} = \begin{pmatrix} 0.124485 \\ 0.126456 \\ 331.77072 \\ 342.021738 \\ 0.060199 \end{pmatrix},$$

$$\Sigma_{s_{2_2}^t{}_1} = \begin{bmatrix} 0.166964 & -0.031926 & -0.123631 & 2.111055 & -0.013615 \\ -0.031926 & 0.037319 & 0.003122 & -0.542773 & 0.013363 \\ -0.123631 & 0.003122 & 280.036624 & -9.397327 & 0.059029 \\ 2.111055 & -0.542773 & -9.397327 & 477.526746 & 0.174995 \\ -0.013615 & 0.013363 & 0.059029 & 0.174995 & 0.008992 \end{bmatrix},$$

$$\Sigma_{s_{2_2}^t{}_2} = \begin{bmatrix} 0.052272 & 0.014318 & 10.905991 & -30.368109 & -0.011072 \\ 0.014318 & 0.023889 & 6.462349 & -18.801035 & -0.006196 \\ 10.905991 & 6.462349 & 6503.689454 & -12703.03845 & -4.199779 \\ -30.368109 & -18.801035 & -12703.03845 & 37480.63917 & 11.932406 \\ -0.011072 & -0.006196 & -4.199779 & 11.932406 & 0.011527 \end{bmatrix},$$

$$\Sigma_{s_{2_2}^t{}_3} = \begin{bmatrix} 0.018119 & 0.010036 & 4.683567 & -15.494831 & -0.008132 \\ 0.010036 & 0.024193 & 8.353843 & -25.337262 & -0.011346 \\ 4.683567 & 8.353843 & 4186.427327 & -11194.2805 & -5.112736 \\ -15.494831 & -25.337262 & -11194.2805 & 34919.85229 & 16.298637 \\ -0.008132 & -0.011346 & -5.112736 & 16.298637 & 0.011451 \end{bmatrix},$$

$$\Sigma_{s_{2_2}^t{}_4} = \begin{bmatrix} 0.017687 & 0.001906 & -0.965245 & -0.603432 & -0.000066 \\ 0.001906 & 0.017402 & -0.018047 & 0.104355 & -0.000796 \\ -0.965245 & -0.018047 & 1098.482512 & 137.766958 & 0.06152 \\ -0.603432 & 0.104355 & 137.766958 & 640.883223 & -0.049487 \\ -0.000066 & -0.000796 & 0.06152 & -0.049487 & 0.002638 \end{bmatrix}.$$

The distribution $p\left(F_9^t, F_{16}^t, F_{58}^t, F_{43}^t, F_{12}^t \mid s_{2_3}^t : \boldsymbol{\theta}_{F_9^t,\dots,F_{12}^t|s_{2_3}^t} = \left\{\left\{\pi_{s_{2_3}^t i}, \boldsymbol{\mu}_{s_{2_3}^t i}, \Sigma_{s_{2_3}^t i}\right\}_{i=1}^{3}\right\}\right)$ consists of three components, where

$$\pi_{s_{2_3}^t 1} = 0.166704, \pi_{s_{2_3}^t 2} = 0.5, \pi_{s_{2_3}^t 3} = 0.333296,$$

$$\boldsymbol{\mu}_{s_{2_3}^t{}_1} = \begin{pmatrix} 0.336465 \\ 0.039687 \\ 31.313578 \\ 35.080789 \\ 0.07995 \end{pmatrix}, \boldsymbol{\mu}_{s_{2_3}^t{}_2} = \begin{pmatrix} 0.52301 \\ 0.189244 \\ 34.041718 \\ 337.787248 \\ 0.057523 \end{pmatrix}, \boldsymbol{\mu}_{s_{2_3}^t{}_3} = \begin{pmatrix} 0.720108 \\ 0.217793 \\ 151.889971 \\ 42.779146 \\ -0.256548 \end{pmatrix},$$

$$\Sigma_{s_{2_3}^t{}_1} = \begin{bmatrix} 0.012592 & 0.000738 & 0.375983 & 0.113605 & -0.000015 \\ 0.000738 & 0.005243 & -0.022174 & 0.287276 & -0.000116 \\ 0.375983 & -0.022174 & 2146.647732 & -70.495397 & -0.167242 \\ 0.113605 & 0.287276 & -70.495397 & 910.338116 & -0.182674 \\ -0.000015 & -0.000116 & -0.167242 & -0.182674 & 0.002545 \end{bmatrix},$$

$$\Sigma_{s_{2_3}^t{}_2} = \begin{bmatrix} 0.021095 & -0.001322 & -0.870028 & -0.141637 & -0.00201 \\ -0.001322 & 0.016611 & 1.112584 & 0.140606 & -0.002482 \\ -0.870028 & 1.112584 & 767.98048 & 0.383231 & -0.556985 \\ -0.141637 & 0.140606 & 0.383231 & 266.493081 & 0.187485 \\ -0.00201 & -0.002482 & -0.556985 & 0.187485 & 0.004991 \end{bmatrix},$$

$$\Sigma_{s_{2_3}^t{}_3} = \begin{bmatrix} 0.163826 & -0.023968 & 58.802882 & 5.521306 & 0.089901 \\ -0.023968 & 0.015941 & -9.273682 & -1.013223 & -0.01442 \\ 58.802882 & -9.273682 & 23412.19386 & 2138.362866 & 34.007893 \\ 5.521306 & -1.013223 & 2138.362866 & 680.434879 & 3.501795 \\ 0.089901 & -0.01442 & 34.007893 & 3.501795 & 0.053759 \end{bmatrix}.$$

The distribution $p\left(F_9^t, F_{16}^t, F_{58}^t, F_{43}^t, F_{12}^t \mid s_{2_4}^t : \boldsymbol{\theta}_{F_9^t,\dots,F_{12}^t|s_{2_4}^t} = \left\{\left\{\pi_{s_{2_4}^t{}_i}, \boldsymbol{\mu}_{s_{2_4}^t{}_i}, \Sigma_{s_{2_4}^t{}_i}\right\}_{i=1}^{4}\right\}\right)$ consists of four components, where

$$\pi_{s_{2_4}^t{}_1} = 0.475115, \pi_{s_{2_4}^t{}_2} = 0.37493, \pi_{s_{2_4}^t{}_3} = 0.125029, \pi_{s_{2_4}^t{}_4} = 0.024927,$$

$$\boldsymbol{\mu}_{s_{2_4}^t{}_1} = \begin{pmatrix} 0.296084 \\ 0.141028 \\ 23.309735 \\ 315.154563 \\ -0.034965 \end{pmatrix}, \boldsymbol{\mu}_{s_{2_4}^t{}_2} = \begin{pmatrix} 0.587321 \\ 0.084191 \\ 255.266304 \\ 248.424193 \\ 0.109114 \end{pmatrix}, \boldsymbol{\mu}_{s_{2_4}^t{}_3} = \begin{pmatrix} 0.284545 \\ 0.167614 \\ 267.771239 \\ 339.930298 \\ 0.023065 \end{pmatrix},$$

$$\boldsymbol{\mu}_{s_{2_4}^t{}_4} = \begin{pmatrix} 0.423869 \\ 1.242519 \\ 58.842895 \\ 350.022009 \\ 0.157961 \end{pmatrix},$$

$$\Sigma_{s_{2_4}^t{}_1} = \begin{bmatrix} 0.013383 & 0.002141 & 0.877331 & 0.406829 & 0.005782 \\ 0.002141 & 0.008695 & -0.40694 & 0.083467 & -0.005105 \\ 0.877331 & -0.40694 & 787.93504 & 255.822342 & 2.466053 \\ 0.406829 & 0.083467 & 255.822342 & 339.068153 & 0.465229 \\ 0.005782 & -0.005105 & 2.466053 & 0.465229 & 0.025793 \end{bmatrix},$$

$$\Sigma_{s_{2_4}^t{}_2} = \begin{bmatrix} 0.02586 & -0.002524 & 11.228084 & 16.730884 & -0.002862 \\ -0.002524 & 0.002961 & -2.11311 & -3.145352 & 0.000781 \\ 11.228084 & -2.11311 & 8389.851822 & 12114.80298 & -1.974341 \\ 16.730884 & -3.145352 & 12114.80298 & 18383.99034 & -3.121037 \\ -0.002862 & 0.000781 & -1.974341 & -3.121037 & 0.001876 \end{bmatrix},$$

$$\Sigma_{s_{2_4}^t{}_3} = \begin{bmatrix} 0.018046 & 0.005092 & -0.0461 & 0.0958 & -0.001134 \\ 0.005092 & 0.01344 & 0.528234 & 0.587164 & 0.001466 \\ -0.0461 & 0.528234 & 983.353347 & 118.236132 & 0.337758 \\ 0.0958 & 0.587164 & 118.236132 & 639.481883 & 0.284769 \\ -0.001134 & 0.001466 & 0.337758 & 0.284769 & 0.003811 \end{bmatrix},$$

$$\Sigma_{s_{2_4}^t{}_4} = \begin{bmatrix} 0.049989 & -0.003865 & 0.391383 & -0.297565 & -0.00101 \\ -0.003865 & 0.045893 & -1.164792 & 1.551202 & 0.005495 \\ 0.391383 & -1.164792 & 4138.029819 & -99.265509 & -0.31283 \\ -0.297565 & 1.551202 & -99.265509 & 2850.907579 & 0.393067 \\ -0.00101 & 0.005495 & -0.31283 & 0.393067 & 0.013386 \end{bmatrix}.$$

The distribution $p\left(F_9^t, F_{16}^t, F_{58}^t, F_{43}^t, F_{12}^t \mid s_{2_5}^t : \boldsymbol{\theta}_{F_9^t,\dots,F_{12}^t|s_{2_5}^t} = \left\{\left\{\pi_{s_{2_5}^t{}_i}, \boldsymbol{\mu}_{s_{2_5}^t{}_i}, \Sigma_{s_{2_5}^t{}_i}\right\}_{i=1}^{1}\right\}\right)$ consists of a single component, where

$$\pi_{s_{2_5}^t{}_1} = 1,$$

$$\boldsymbol{\mu}_{s_{2_5}^t{}_1} = \begin{pmatrix} 0.412788 \\ 0.351516 \\ 90.715442 \\ 110.160576 \\ 0.159405 \end{pmatrix},$$

$$\Sigma_{s_{2_5}^t{}_1} = \begin{bmatrix} 0.080801 & 0.008745 & 0.66874 & 1.725614 & 0.003627 \\ 0.008745 & 0.010819 & 0.102851 & 0.064256 & 0.007594 \\ 0.66874 & 0.102851 & 862.843003 & 41.754791 & -0.786508 \\ 1.725614 & 0.064256 & 41.754791 & 775.354803 & -0.323846 \\ 0.003627 & 0.007594 & -0.786508 & -0.323846 & 0.028863 \end{bmatrix}.$$

Distribution $p\left(F_{29}^t, F_{31}^t, F_{37}^t, F_{57}^t \mid S_2^t : \boldsymbol{\theta}_{F_{29}^t,\ldots,F_{57}^t|S_2^t}\right)$

The distribution $p\left(F_{29}^t, F_{31}^t, F_{37}^t, F_{57}^t \mid S_2^t : \boldsymbol{\theta}_{F_{29}^t,\ldots,F_{57}^t|S_2^t}\right)$ over a four-dimensional vector of continuous variables $(F_{29}, F_{31}, F_{37}, F_{57})$ at time slice $t \geq 1$ is a collection of multivariate Gaussian mixture distributions with a multivariate GMM

$$p\left(F_{29}^t, F_{31}^t, F_{37}^t, F_{57}^t \mid s_2^t : \boldsymbol{\theta}_{F_{29}^t,\ldots,F_{57}^t|s_2^t}\right) = \sum_{i=1}^{n_{s_2}} \pi_{s_2^t{}_i} \mathcal{N}\left(\boldsymbol{\mu}_{s_2^t{}_i}, \Sigma_{s_2^t{}_i}\right)$$

composed of n_{s_2} components for each $s_2^t \in \mathrm{Val}(S_2)$, parameterized with MAP parameters $\boldsymbol{\theta}_{F_{29}^t,\ldots,F_{57}^t|S_2^t} = \left\{\boldsymbol{\theta}_{F_{29}^t,\ldots,F_{57}^t|s_{2_0}^t}, \boldsymbol{\theta}_{F_{29}^t,\ldots,F_{57}^t|s_{2_1}^t}, \boldsymbol{\theta}_{F_{29}^t,\ldots,F_{57}^t|s_{2_2}^t}, \boldsymbol{\theta}_{F_{29}^t,\ldots,F_{57}^t|s_{2_3}^t}, \boldsymbol{\theta}_{F_{29}^t,\ldots,F_{57}^t|s_{2_4}^t}, \boldsymbol{\theta}_{F_{29}^t,\ldots,F_{57}^t|s_{2_5}^t}\right\}$.

The distribution $p\left(F_{29}^t, F_{31}^t, F_{37}^t, F_{57}^t \mid s_{2_0}^t : \boldsymbol{\theta}_{F_{29}^t,\ldots,F_{57}^t|s_{2_0}^t} = \left\{\left\{\pi_{s_{2_0}^t{}_i}, \boldsymbol{\mu}_{s_{2_0}^t{}_i}, \Sigma_{s_{2_0}^t{}_i}\right\}_{i=1}^4\right\}\right)$ consists of four components, where

$$\pi_{s_{2_0}^t{}_1} = 0.11107, \pi_{s_{2_0}^t{}_2} = 0.555646, \pi_{s_{2_0}^t{}_3} = 0.11107, \pi_{s_{2_0}^t{}_4} = 0.222214,$$

$$\boldsymbol{\mu}_{s_{2_0}^t{}_1} = \begin{pmatrix} 0.031913 \\ 1.130844 \\ 312.306102 \\ 307.052591 \end{pmatrix}, \boldsymbol{\mu}_{s_{2_0}^t{}_2} = \begin{pmatrix} 0.090008 \\ 1.961423 \\ 292.836935 \\ 0.458007 \end{pmatrix}, \boldsymbol{\mu}_{s_{2_0}^t{}_3} = \begin{pmatrix} 0.439662 \\ 1.391309 \\ 18.641658 \\ 17.530823 \end{pmatrix},$$

$$\boldsymbol{\mu}_{s_{2_0}^t{}_4} = \begin{pmatrix} 0.229065 \\ 0.800428 \\ 15.183225 \\ 307.290975 \end{pmatrix},$$

$$\Sigma_{s_{2_0}^t{}_1} = \begin{bmatrix} 0.002017 & 0.002253 & -0.077311 & -0.059524 \\ 0.002253 & 0.138032 & 1.572257 & 1.60459 \\ -0.077311 & 1.572257 & 880.23294 & 251.747417 \\ -0.059524 & 1.60459 & 251.747417 & 937.586233 \end{bmatrix}, \Sigma_{s_{2_0}^t{}_2} = \begin{bmatrix} 0.009731 & 0.017925 & -2.56754 & 0.036439 \\ 0.017925 & 0.484587 & -12.870633 & -0.083823 \\ -2.56754 & -12.870633 & 3404.88569 & -18.42454 \\ 0.036439 & -0.083823 & -18.42454 & 150.608576 \end{bmatrix},$$

$$\Sigma_{s_{2_0}^t{}_3} = \begin{bmatrix} 0.024695 & 0.057076 & -1.116055 & 0.959694 \\ 0.057076 & 0.184675 & -2.740089 & 2.305402 \\ -1.116055 & -2.740089 & 875.865756 & 7.557769 \\ 0.959694 & 2.305402 & 7.557769 & 810.720368 \end{bmatrix}, \Sigma_{s_{2_0}^t{}_4} = \begin{bmatrix} 0.013501 & 0.032706 & -0.368009 & 0.06507 \\ 0.032706 & 0.154674 & -2.20359 & 0.600055 \\ -0.368009 & -2.20359 & 407.853189 & -60.316354 \\ 0.06507 & 0.600055 & -60.316354 & 506.903852 \end{bmatrix}.$$

The distribution $p\left(F_{29}^t, F_{31}^t, F_{37}^t, F_{57}^t \mid s_{2_1}^t : \boldsymbol{\theta}_{F_{29}^t,\ldots,F_{57}^t|s_{2_1}^t} = \left\{\left\{\pi_{s_{2_1}^t{}_i}, \boldsymbol{\mu}_{s_{2_1}^t{}_i}, \Sigma_{s_{2_1}^t{}_i}\right\}_{i=1}^4\right\}\right)$ consists of four components, where

$$\pi_{s_{2_1}^t{}_1} = 0.142816, \pi_{s_{2_1}^t{}_2} = 0.142817, \pi_{s_{2_1}^t{}_3} = 0.57155, \pi_{s_{2_1}^t{}_4} = 0.142817,$$

$$\boldsymbol{\mu}_{s_{2_1}^t{}_1} = \begin{pmatrix} 0.27409 \\ 1.148377 \\ 373.720477 \\ 372.291667 \end{pmatrix}, \boldsymbol{\mu}_{s_{2_1}^t{}_2} = \begin{pmatrix} 0.101335 \\ 1.802608 \\ 128.977652 \\ 185.279463 \end{pmatrix}, \boldsymbol{\mu}_{s_{2_1}^t{}_3} = \begin{pmatrix} 0.157113 \\ 1.671719 \\ 28.65708 \\ 8.553599 \end{pmatrix}$$

$$, \boldsymbol{\mu}_{s_{2_1}^t{}_4} = \begin{pmatrix} 0.141415 \\ 1.114646 \\ 16.794366 \\ 248.047925 \end{pmatrix},$$

$$\Sigma_{s_{2_1}^t{}_1} = \begin{bmatrix} 0.00238 & 0.000495 & 0.185872 & 0.183215 \\ 0.000495 & 0.046293 & 0.602816 & 0.628178 \\ 0.185872 & 0.602816 & 1004.301203 & 374.820924 \\ 0.183215 & 0.628178 & 374.820924 & 1059.059895 \end{bmatrix}, \Sigma_{s_{2_1}^t{}_2} = \begin{bmatrix} 0.002491 & -0.005336 & -0.21556 & -0.237202 \\ -0.005336 & 0.33926 & 2.905767 & 2.951961 \\ -0.21556 & 2.905767 & 690.105181 & 86.679214 \\ -0.237202 & 2.951961 & 86.679214 & 802.422407 \end{bmatrix},$$

$$\Sigma_{s_{2_1}^t{}_3} = \begin{bmatrix} 0.010819 & -0.009186 & -1.413846 & 0.296284 \\ -0.009186 & 0.789851 & 5.989069 & -7.336144 \\ -1.413846 & 5.989069 & 821.090788 & -32.214805 \\ 0.296284 & -7.336144 & -32.214805 & 337.538865 \end{bmatrix}, \Sigma_{s_{2_1}^t{}_4} = \begin{bmatrix} 0.004196 & 0.004461 & 0.034534 & -0.277625 \\ 0.004461 & 0.18485 & -2.055146 & 1.880832 \\ 0.034534 & -2.055146 & 774.589555 & -59.9922 \\ -0.277625 & 1.880832 & -59.9922 & 857.218892 \end{bmatrix}.$$

The distribution $p\left(F_{29}^t, F_{31}^t, F_{37}^t, F_{57}^t \mid s_{2_2}^t : \boldsymbol{\theta}_{F_{29}^t,\dots,F_{57}^t|s_{2_2}^t} = \left\{\left\{\pi_{s_{2_2}^t{}_i}, \boldsymbol{\mu}_{s_{2_2}^t{}_i}, \Sigma_{s_{2_2}^t{}_i}\right\}_{i=1}^4\right\}\right)$ consists of four components, where

$$\pi_{s_{2_2}^t{}_1} = 0.449754, \pi_{s_{2_2}^t{}_2} = 0.16663, \pi_{s_{2_2}^t{}_3} = 0.050256, \pi_{s_{2_2}^t{}_4} = 0.33336,$$

$$\boldsymbol{\mu}_{s_{2_2}^t{}_1} = \begin{pmatrix} 0.248582 \\ 1.644591 \\ 11.931372 \\ 11.100367 \end{pmatrix}, \boldsymbol{\mu}_{s_{2_2}^t{}_2} = \begin{pmatrix} 0.551126 \\ 1.382762 \\ 10.138191 \\ 158.705752 \end{pmatrix}, \boldsymbol{\mu}_{s_{2_2}^t{}_3} = \begin{pmatrix} 0.003655 \\ 2.23618 \\ 228.028958 \\ 1.693283 \end{pmatrix},$$

$$\boldsymbol{\mu}_{s_{2_2}^t{}_4} = \begin{pmatrix} 0.206387 \\ 1.10487 \\ 180.017874 \\ 168.96736 \end{pmatrix},$$

$$\Sigma_{s_{2_2}^t{}_1} = \begin{bmatrix} 0.029752 & -0.097185 & -0.395654 & 2.055558 \\ -0.097185 & 0.78833 & 5.163235 & -10.412508 \\ -0.395654 & 5.163235 & 304.008681 & -34.010592 \\ 2.055558 & -10.412508 & -34.010592 & 539.404497 \end{bmatrix}, \Sigma_{s_{2_2}^t{}_2} = \begin{bmatrix} 0.086294 & 0.122809 & -1.900067 & 2.529234 \\ 0.122809 & 0.227738 & -3.338176 & 3.69441 \\ -1.900067 & -3.338176 & 727.199874 & -74.986333 \\ 2.529234 & 3.69441 & -74.986333 & 788.569272 \end{bmatrix},$$

$$\Sigma_{s_{2_2}^t{}_3} = \begin{bmatrix} 0.006145 & -0.002364 & -0.41985 & 0.331667 \\ -0.002364 & 0.096543 & 1.240592 & -1.083481 \\ -0.41985 & 1.240592 & 2273.640521 & -192.900723 \\ 0.331667 & -1.083481 & -192.900723 & 2474.979302 \end{bmatrix}, \Sigma_{s_{2_2}^t{}_4} = \begin{bmatrix} 0.013889 & 0.087534 & 18.143013 & -18.745276 \\ 0.087534 & 0.694511 & 130.912694 & -135.24096 \\ 18.143013 & 130.912694 & 27476.50247 & -27713.26551 \\ -18.745276 & -135.24096 & -27713.26551 & 28855.67759 \end{bmatrix}.$$

The distribution $p\left(F_{29}^t, F_{31}^t, F_{37}^t, F_{57}^t \mid s_{2_3}^t : \boldsymbol{\theta}_{F_{29}^t,\dots,F_{57}^t|s_{2_3}^t} = \left\{\left\{\pi_{s_{2_3}^t{}_i}, \boldsymbol{\mu}_{s_{2_3}^t{}_i}, \Sigma_{s_{2_3}^t{}_i}\right\}_{i=1}^3\right\}\right)$ consists of three components, where

$$\pi_{s_{2_3}^t{}_1} = 0.451453, \pi_{s_{2_3}^t{}_2} = 0.261208, \pi_{s_{2_3}^t{}_3} = 0.28734,$$

$$\boldsymbol{\mu}_{s_{2_3}^t{}_1} = \begin{pmatrix} 0.173674 \\ 1.549939 \\ 27.787112 \\ 36.831191 \end{pmatrix}, \boldsymbol{\mu}_{s_{2_3}^t{}_2} = \begin{pmatrix} 0.202541 \\ 2.479534 \\ 29.193879 \\ 196.810506 \end{pmatrix}, \boldsymbol{\mu}_{s_{2_3}^t{}_3} = \begin{pmatrix} 0.509982 \\ 1.100802 \\ 22.357792 \\ 13.658749 \end{pmatrix},$$

$$\Sigma_{s_{2_3}^t{}_1} = \begin{bmatrix} 0.007608 & 0.031755 & -0.725512 & 0.55021 \\ 0.031755 & 0.262668 & -4.297699 & 0.588278 \\ -0.725512 & -4.297699 & 571.007375 & -333.050523 \\ 0.55021 & 0.588278 & -333.050523 & 909.397638 \end{bmatrix}, \Sigma_{s_{2_3}^t{}_2} = \begin{bmatrix} 0.016145 & -0.042102 & -0.371132 & 15.998061 \\ -0.042102 & 0.213379 & -0.009726 & -49.960885 \\ -0.371132 & -0.009726 & 567.279507 & -370.425925 \\ 15.998061 & -49.960885 & -370.425925 & 22434.21068 \end{bmatrix},$$

$$\Sigma_{s_{2_3}^t{}_3} = \begin{bmatrix} 0.035461 & 0.00677 & -1.700938 & -0.276572 \\ 0.00677 & 0.043767 & -0.271145 & 0.188718 \\ -1.700938 & -0.271145 & 483.082712 & 9.198255 \\ -0.276572 & 0.188718 & 9.198255 & 508.410869 \end{bmatrix},$$

The distribution $p\left(F_{29}^t, F_{31}^t, F_{37}^t, F_{57}^t \mid s_{2_4}^t : \boldsymbol{\theta}_{F_{29}^t,\ldots,F_{57}^t|s_{2_4}^t} = \left\{\left\{\pi_{s_{2_4}^t i}, \boldsymbol{\mu}_{s_{2_4}^t i}, \Sigma_{s_{2_4}^t i}\right\}_{i=1}^{3}\right\}\right)$ consists of three components, where

$$\pi_{s_{2_4}^t 1} = 0.26277, \pi_{s_{2_4}^t 2} = 0.237164, \pi_{s_{2_4}^t 3} = 0.500068,$$

$$\boldsymbol{\mu}_{s_{2_4}^t 1} = \begin{pmatrix} 0.084999 \\ 1.122169 \\ 78.507624 \\ 223.315752 \end{pmatrix}, \boldsymbol{\mu}_{s_{2_4}^t 2} = \begin{pmatrix} 0.358232 \\ 1.195114 \\ 6.485601 \\ 307.854018 \end{pmatrix}, \boldsymbol{\mu}_{s_{2_4}^t 3} = \begin{pmatrix} 0.389875 \\ 1.587373 \\ 26.329552 \\ 23.214887 \end{pmatrix},$$

$$\Sigma_{s_{2_4}^t 1} = \begin{bmatrix} 0.007439 & 0.003735 & -3.331525 & -6.383244 \\ 0.003735 & 0.183437 & -0.464626 & -0.322744 \\ -3.331525 & -0.464626 & 2239.717655 & 3740.7714 \\ -6.383244 & -0.322744 & 3740.7714 & 7642.125286 \end{bmatrix}, \Sigma_{s_{2_4}^t 2} = \begin{bmatrix} 0.045994 & 0.112682 & 0.134118 & 6.55242 \\ 0.112682 & 0.380323 & 0.123483 & 17.318859 \\ 0.134118 & 0.123483 & 356.963625 & 4.915314 \\ 6.55242 & 17.318859 & 4.915314 & 1516.870146 \end{bmatrix},$$

$$\Sigma_{s_{2_4}^t 3} = \begin{bmatrix} 0.047958 & -0.031671 & -2.415569 & 3.529097 \\ -0.031671 & 0.354213 & -8.096071 & -9.084462 \\ -2.415569 & -8.096071 & 773.547235 & -119.627045 \\ 3.529097 & -9.084462 & -119.627045 & 876.734747 \end{bmatrix}.$$

The distribution $p\left(F_{29}^t, F_{31}^t, F_{37}^t, F_{57}^t \mid s_{2_5}^t : \boldsymbol{\theta}_{F_{29}^t,\ldots,F_{57}^t|s_{2_5}^t} = \left\{\left\{\pi_{s_{2_5}^t i}, \boldsymbol{\mu}_{s_{2_5}^t i}, \Sigma_{s_{2_5}^t i}\right\}_{i=1}^{2}\right\}\right)$ consists of two components, where

$$\pi_{s_{2_5}^t 1} = 0.074127, \pi_{s_{2_5}^t 2} = 0.925873,$$

$$\boldsymbol{\mu}_{s_{2_5}^t 1} = \begin{pmatrix} 0.106692 \\ 0.515378 \\ 5.845092 \\ 83.085749 \end{pmatrix}, \boldsymbol{\mu}_{s_{2_5}^t 2} = \begin{pmatrix} 0.551721 \\ 1.3502 \\ 6.150518 \\ 96.795931 \end{pmatrix},$$

$$\Sigma_{s_{2_5}^t 1} = \begin{bmatrix} 0.022973 & 0.008822 & 0.616934 & 0.191083 \\ 0.008822 & 0.35194 & 4.716452 & 1.415381 \\ 0.616934 & 4.716452 & 8516.85125 & 117.388605 \\ 0.191083 & 1.415381 & 117.388605 & 9370.889173 \end{bmatrix}, \Sigma_{s_{2_5}^t 2} = \begin{bmatrix} 0.023257 & -0.004155 & 0.23269 & 0.915808 \\ -0.004155 & 0.04612 & -0.141575 & -0.053543 \\ 0.23269 & -0.141575 & 704.874544 & 19.305685 \\ 0.915808 & -0.053543 & 19.305685 & 824.576939 \end{bmatrix}.$$

2.5 Parameters of the extended SAE Level 2 SAGAT Score Model

For any number of time slices $T \geq 1$, the extended SAE Level 2 SAGAT Score model defines the JPD

$$p\left(S_2^{1:T}, \boldsymbol{F}_{\text{Rel}}^{1:T}, B^{1:T} : \boldsymbol{\theta}\right)$$

$$= p\left(S_2^1 \mid B^1 : \boldsymbol{\theta}_{S_2^1|B^1}\right) \prod_{t=2}^{T} p\left(S_2^t \mid S_2^{t-1}, B^t : \boldsymbol{\theta}_{S_2^t|S_2^{t-1},B^t}\right) \prod_{t=1}^{T} p(B^t : \boldsymbol{\theta}_{B^t}) p\left(\boldsymbol{F}_{\text{Rel}}^t \mid S_2^t, B^t : \boldsymbol{\theta}\right),$$

with $p\left(\boldsymbol{F}_{\text{Rel}}^t \mid S_2^t, B^t : \boldsymbol{\theta}\right)$ given by

$$p\left(F_8^t, F_{32}^t, F_{38}^t, F_{53}^t, F_{42}^t, F_{13}^t | S_2^t, B^t : \boldsymbol{\theta}_{F_8^t,\ldots,F_{13}^t|S_2^t,B^t}\right)$$

$$p\left(F_{27}^t | S_2^t, B^t : \boldsymbol{\theta}_{F_{27}^t|S_2^t,B^t}\right) p\left(F_{47}^t | S_2^t, B^t : \boldsymbol{\theta}_{F_{47}^t|S_2^t,B^t}\right).$$

As such, the model is defined by six probability /density distribution to be detailed in the following. The names of the relevant indicators $\boldsymbol{F}_{\text{Rel}} = \{F_8, F_{13}, F_{27}, F_{32}, F_{38}, F_{42}, F_{47}, F_{53}\}$ are provided in Table 9.

Table 28: The set of relevant indicators for the extended SAE Level 2 SAGAT Score model, $\boldsymbol{F}_{\text{Rel}} = \{F_8, F_{13}, F_{27}, F_{32}, F_{38}, F_{42}, F_{47}, F_{53}\}$.

Symbol	Name
F_8	Blink frequency
F_{13}	Yaw angle of the head variability
F_{27}	Glance duration variability
F_{32}	Mean saccade frequency
F_{38}	Mean time since last look at left mirror AOI
F_{42}	Time since last look at right mirror AOI
F_{47}	Time since last look at the rear mirror AOI
F_{53}	Mean time since last look at tachometer AOI

Distribution $p(B^t : \boldsymbol{\theta}_{B^t})$

The distribution $p(B^t : \boldsymbol{\theta}_{B^t})$ is a categorical distribution

$$p(B^t : \boldsymbol{\theta}_{B^t}) = \text{Cat}(B^t : \boldsymbol{\theta}_{B^t})$$

over the discrete variable B, $\text{Val}(B) = \{b_0, b_1, b_2\}$ at time slice $t = 1$, with MAP parameters

$$\boldsymbol{\theta}_{B^t} = \left\{\theta_{b_0^t}, \theta_{b_1^t}, \theta_{b_2^t}\right\} = \{0.324333, 0.324333, 0.351334\}.$$

Distribution $p\left(S_2^1 \mid B^1 : \boldsymbol{\theta}_{S_2^1|B^1}\right)$

The distribution $p\left(S_2^1 \mid B^1 : \boldsymbol{\theta}_{S_2^1|B^1}\right)$ over the discrete variable S_2, $\text{Val}(S_2) = \left\{s_{2_0}, s_{2_1}, s_{2_2}, s_{2_3}, s_{2_4}, s_{2_5}\right\}$ at time slice $t = 1$ is a collection of categorical distributions with a categorical distribution

$$p\left(S_2^1 \mid b^1 : \boldsymbol{\theta}_{S_2^1|b^1}\right) = \text{Cat}\left(S_2^1 : \boldsymbol{\theta}_{S_2^1|b^1}\right)$$

for each $b^t \in \text{Val}(B)$, parameterized with MAP parameters $\boldsymbol{\theta}_{S_2^1|B^1} = \left\{\boldsymbol{\theta}_{S_2^1|b_0^1}, \boldsymbol{\theta}_{S_2^1|b_1^1}, \boldsymbol{\theta}_{S_2^1|b_2^1}\right\}$, where

$$\begin{aligned}\boldsymbol{\theta}_{S_2^1|b_0^1} &= \left\{\theta_{s_{2_0}^1|b_0^1}, \theta_{s_{2_1}^1|b_0^1}, \theta_{s_{2_2}^1|b_0^1}, \theta_{s_{2_3}^1|b_0^1}, \theta_{s_{2_4}^1|b_0^1}, \theta_{s_{2_5}^1|b_0^1}\right\} \\ &= \{0.000116, 0.000116, 0.499769, 0.333218, 0.166667, 0.000116\},\end{aligned}$$

$$\begin{aligned}\boldsymbol{\theta}_{S_2^1|b_1^1} &= \left\{\theta_{s_{2_0}^1|b_1^1}, \theta_{s_{2_1}^1|b_1^1}, \theta_{s_{2_2}^1|b_1^1}, \theta_{s_{2_3}^1|b_1^1}, \theta_{s_{2_4}^1|b_1^1}, \theta_{s_{2_5}^1|b_1^1}\right\} \\ &= \{0.249942, 0.249942, 0.416493, 0.083391, 0.000116, 0.000116\},\end{aligned}$$

$$\begin{aligned}\boldsymbol{\theta}_{S_2^1|b_2^1} &= \left\{\theta_{s_{2_0}^1|b_2^1}, \theta_{s_{2_1}^1|b_2^1}, \theta_{s_{2_2}^1|b_2^1}, \theta_{s_{2_3}^1|b_2^1}, \theta_{s_{2_4}^1|b_2^1}, \theta_{s_{2_5}^1|b_2^1}\right\} \\ &= \{0.153854, 0.076981, 0.307602, 0.307602, 0.000107, 0.153854\}.\end{aligned}$$

Distribution $p\left(S_2^t \mid S_2^{t-1}, B^t : \boldsymbol{\theta}_{S_2^t|S_2^{t-1},B^t}\right)$

The distribution $p\left(S_2^t \mid S_2^{t-1}, B^t : \boldsymbol{\theta}_{S_2^t|S_2^{t-1},B^t}\right)$ over the discrete variable S_2, $\text{Val}(S_2) = \left\{s_{2_0}, s_{2_1}, s_{2_2}, s_{2_3}, s_{2_4}, s_{2_5}\right\}$ at time slice $t > 1$ is a collection of categorical distributions with a categorical distribution

$$p\left(S_2^t | s_2^{t-1}, b^t : \boldsymbol{\theta}_{S_2^t|s_2^{t-1},b^t}\right) = \text{Cat}\left(S_2^t : \boldsymbol{\theta}_{S_2^t|s_2^{t-1},b^t}\right)$$

for each $\{s_2^{t-1}, b^t\} \in \mathrm{Val}(S_2) \times \mathrm{Val}(B)$, parameterized with MAP parameters

$$\boldsymbol{\theta}_{S_2^t|s_2^{t-1},B^t} = \begin{Bmatrix} \boldsymbol{\theta}_{S_2^t|s_{2_0}^{t-1},b_0^t}, \boldsymbol{\theta}_{S_2^t|s_{2_1}^{t-1},b_0^t}, \boldsymbol{\theta}_{S_2^t|s_{2_2}^{t-1},b_0^t}, \boldsymbol{\theta}_{S_2^t|s_{2_3}^{t-1},b_0^t}, \boldsymbol{\theta}_{S_2^t|s_{2_4}^{t-1},b_0^t}, \boldsymbol{\theta}_{S_2^t|s_{2_5}^{t-1},b_0^t}, \\ \boldsymbol{\theta}_{S_2^t|s_{2_0}^{t-1},b_1^t}, \boldsymbol{\theta}_{S_2^t|s_{2_1}^{t-1},b_1^t}, \boldsymbol{\theta}_{S_2^t|s_{2_2}^{t-1},b_1^t}, \boldsymbol{\theta}_{S_2^t|s_{2_3}^{t-1},b_1^t}, \boldsymbol{\theta}_{S_2^t|s_{2_4}^{t-1},b_1^t}, \boldsymbol{\theta}_{S_2^t|s_{2_5}^{t-1},b_1^t}, \\ \boldsymbol{\theta}_{S_2^t|s_{2_0}^{t-1},b_2^t}, \boldsymbol{\theta}_{S_2^t|s_{2_1}^{t-1},b_2^t}, \boldsymbol{\theta}_{S_2^t|s_{2_2}^{t-1},b_2^t}, \boldsymbol{\theta}_{S_2^t|s_{2_3}^{t-1},b_2^t}, \boldsymbol{\theta}_{S_2^t|s_{2_4}^{t-1},b_2^t}, \boldsymbol{\theta}_{S_2^t|s_{2_5}^{t-1},b_2^t} \end{Bmatrix},$$

where

$$\begin{aligned} \boldsymbol{\theta}_{S_2^t|s_{2_0}^{t-1},b_0^t} &= \left\{\theta_{s_{2_0}^t|s_{2_0}^{t-1},b_0^t}, \theta_{s_{2_1}^t|s_{2_0}^{t-1},b_0^t}, \theta_{s_{2_2}^t|s_{2_0}^{t-1},b_0^t}, \theta_{s_{2_3}^t|s_{2_0}^{t-1},b_0^t}, \theta_{s_{2_4}^t|s_{2_0}^{t-1},b_0^t}, \theta_{s_{2_5}^t|s_{2_0}^{t-1},b_0^t}\right\} \\ &= \{0.166667, 0.166667, 0.166667, 0.166667, 0.166667, 0.166667\}, \end{aligned}$$

$$\begin{aligned} \boldsymbol{\theta}_{S_2^t|s_{2_1}^{t-1},b_0^t} &= \left\{\theta_{s_{2_0}^t|s_{2_1}^{t-1},b_0^t}, \theta_{s_{2_1}^t|s_{2_1}^{t-1},b_0^t}, \theta_{s_{2_2}^t|s_{2_1}^{t-1},b_0^t}, \theta_{s_{2_3}^t|s_{2_1}^{t-1},b_0^t}, \theta_{s_{2_4}^t|s_{2_1}^{t-1},b_0^t}, \theta_{s_{2_5}^t|s_{2_1}^{t-1},b_0^t}\right\} \\ &= \{0.166667, 0.166667, 0.166667, 0.166667, 0.166667, 0.166667\}, \end{aligned}$$

$$\begin{aligned} \boldsymbol{\theta}_{S_2^t|s_{2_2}^{t-1},b_0^t} &= \left\{\theta_{s_{2_0}^t|s_{2_2}^{t-1},b_0^t}, \theta_{s_{2_1}^t|s_{2_2}^{t-1},b_0^t}, \theta_{s_{2_2}^t|s_{2_2}^{t-1},b_0^t}, \theta_{s_{2_3}^t|s_{2_2}^{t-1},b_0^t}, \theta_{s_{2_4}^t|s_{2_2}^{t-1},b_0^t}, \theta_{s_{2_5}^t|s_{2_2}^{t-1},b_0^t}\right\} \\ &= \{0.000019, 0.000019, 0.999907, 0.000019, 0.000019, 0.000019\}, \end{aligned}$$

$$\begin{aligned} \boldsymbol{\theta}_{S_2^t|s_{2_3}^{t-1},b_0^t} &= \left\{\theta_{s_{2_0}^t|s_{2_3}^{t-1},b_0^t}, \theta_{s_{2_1}^t|s_{2_3}^{t-1},b_0^t}, \theta_{s_{2_2}^t|s_{2_3}^{t-1},b_0^t}, \theta_{s_{2_3}^t|s_{2_3}^{t-1},b_0^t}, \theta_{s_{2_4}^t|s_{2_3}^{t-1},b_0^t}, \theta_{s_{2_5}^t|s_{2_3}^{t-1},b_0^t}\right\} \\ &= \{0.000028, 0.000028, 0.000028, 0.999861, 0.000028, 0.000028\}, \end{aligned}$$

$$\begin{aligned} \boldsymbol{\theta}_{S_2^t|s_{2_4}^{t-1},b_0^t} &= \left\{\theta_{s_{2_0}^t|s_{2_4}^{t-1},b_0^t}, \theta_{s_{2_1}^t|s_{2_4}^{t-1},b_0^t}, \theta_{s_{2_2}^t|s_{2_4}^{t-1},b_0^t}, \theta_{s_{2_3}^t|s_{2_4}^{t-1},b_0^t}, \theta_{s_{2_4}^t|s_{2_4}^{t-1},b_0^t}, \theta_{s_{2_5}^t|s_{2_4}^{t-1},b_0^t}\right\} \\ &= \{0.000056, 0.000056, 0.000056, 0.000056, 0.999722, 0.000056\}, \end{aligned}$$

$$\begin{aligned} \boldsymbol{\theta}_{S_2^t|s_{2_5}^{t-1},b_0^t} &= \left\{\theta_{s_{2_0}^t|s_{2_5}^{t-1},b_0^t}, \theta_{s_{2_1}^t|s_{2_5}^{t-1},b_0^t}, \theta_{s_{2_2}^t|s_{2_5}^{t-1},b_0^t}, \theta_{s_{2_3}^t|s_{2_5}^{t-1},b_0^t}, \theta_{s_{2_4}^t|s_{2_5}^{t-1},b_0^t}, \theta_{s_{2_5}^t|s_{2_5}^{t-1},b_0^t}\right\} \\ &= \{0.166667, 0.166667, 0.166667, 0.166667, 0.166667, 0.166667\}, \end{aligned}$$

$$\begin{aligned} \boldsymbol{\theta}_{S_2^t|s_{2_0}^{t-1},b_1^t} &= \left\{\theta_{s_{2_0}^t|s_{2_0}^{t-1},b_1^t}, \theta_{s_{2_1}^t|s_{2_0}^{t-1},b_1^t}, \theta_{s_{2_2}^t|s_{2_0}^{t-1},b_1^t}, \theta_{s_{2_3}^t|s_{2_0}^{t-1},b_1^t}, \theta_{s_{2_4}^t|s_{2_0}^{t-1},b_1^t}, \theta_{s_{2_5}^t|s_{2_0}^{t-1},b_1^t}\right\} \\ &= \{0.999815, 0.000037, 0.000037, 0.000037, 0.000037, 0.000037\}, \end{aligned}$$

$$\begin{aligned} \boldsymbol{\theta}_{S_2^t|s_{2_1}^{t-1},b_1^t} &= \left\{\theta_{s_{2_0}^t|s_{2_1}^{t-1},b_1^t}, \theta_{s_{2_1}^t|s_{2_1}^{t-1},b_1^t}, \theta_{s_{2_2}^t|s_{2_1}^{t-1},b_1^t}, \theta_{s_{2_3}^t|s_{2_1}^{t-1},b_1^t}, \theta_{s_{2_4}^t|s_{2_1}^{t-1},b_1^t}, \theta_{s_{2_5}^t|s_{2_1}^{t-1},b_1^t}\right\} \\ &= \{0.000037, 0.999815, 0.000037, 0.000037, 0.000037, 0.000037\}, \end{aligned}$$

$$\begin{aligned} \boldsymbol{\theta}_{S_2^t|s_{2_2}^{t-1},b_1^t} &= \left\{\theta_{s_{2_0}^t|s_{2_2}^{t-1},b_1^t}, \theta_{s_{2_1}^t|s_{2_2}^{t-1},b_1^t}, \theta_{s_{2_2}^t|s_{2_2}^{t-1},b_1^t}, \theta_{s_{2_3}^t|s_{2_2}^{t-1},b_1^t}, \theta_{s_{2_4}^t|s_{2_2}^{t-1},b_1^t}, \theta_{s_{2_5}^t|s_{2_2}^{t-1},b_1^t}\right\} \\ &= \{0.000022, 0.000022, 0.999889, 0.000022, 0.000022, 0.000022\}, \end{aligned}$$

$$\begin{aligned} \boldsymbol{\theta}_{S_2^t|s_{2_3}^{t-1},b_1^t} &= \left\{\theta_{s_{2_0}^t|s_{2_3}^{t-1},b_1^t}, \theta_{s_{2_1}^t|s_{2_3}^{t-1},b_1^t}, \theta_{s_{2_2}^t|s_{2_3}^{t-1},b_1^t}, \theta_{s_{2_3}^t|s_{2_3}^{t-1},b_1^t}, \theta_{s_{2_4}^t|s_{2_3}^{t-1},b_1^t}, \theta_{s_{2_5}^t|s_{2_3}^{t-1},b_1^t}\right\} \\ &= \{0.000111, 0.000111, 0.000111, 0.999445, 0.000111, 0.000111\}, \end{aligned}$$

$$\begin{aligned} \boldsymbol{\theta}_{S_2^t|s_{2_4}^{t-1},b_1^t} &= \left\{\theta_{s_{2_0}^t|s_{2_4}^{t-1},b_1^t}, \theta_{s_{2_1}^t|s_{2_4}^{t-1},b_1^t}, \theta_{s_{2_2}^t|s_{2_4}^{t-1},b_1^t}, \theta_{s_{2_3}^t|s_{2_4}^{t-1},b_1^t}, \theta_{s_{2_4}^t|s_{2_4}^{t-1},b_1^t}, \theta_{s_{2_5}^t|s_{2_4}^{t-1},b_1^t}\right\} \\ &= \{0.166667, 0.166667, 0.166667, 0.166667, 0.166667, 0.166667\}, \end{aligned}$$

$$\begin{aligned} \boldsymbol{\theta}_{S_2^t|s_{2_5}^{t-1},b_1^t} &= \left\{\theta_{s_{2_0}^t|s_{2_5}^{t-1},b_1^t}, \theta_{s_{2_1}^t|s_{2_5}^{t-1},b_1^t}, \theta_{s_{2_2}^t|s_{2_5}^{t-1},b_1^t}, \theta_{s_{2_3}^t|s_{2_5}^{t-1},b_1^t}, \theta_{s_{2_4}^t|s_{2_5}^{t-1},b_1^t}, \theta_{s_{2_5}^t|s_{2_5}^{t-1},b_1^t}\right\} \\ &= \{0.166667, 0.166667, 0.166667, 0.166667, 0.166667, 0.166667\}, \end{aligned}$$

$$\begin{aligned} \boldsymbol{\theta}_{S_2^t|s_{2_0}^{t-1},b_2^t} &= \left\{\theta_{s_{2_0}^t|s_{2_0}^{t-1},b_2^t}, \theta_{s_{2_1}^t|s_{2_0}^{t-1},b_2^t}, \theta_{s_{2_2}^t|s_{2_0}^{t-1},b_2^t}, \theta_{s_{2_3}^t|s_{2_0}^{t-1},b_2^t}, \theta_{s_{2_4}^t|s_{2_0}^{t-1},b_2^t}, \theta_{s_{2_5}^t|s_{2_0}^{t-1},b_2^t}\right\} \\ &= \{0.999722, 0.000056, 0.000056, 0.000056, 0.000056, 0.000056\}, \end{aligned}$$

$$\boldsymbol{\theta}_{S_2^t|s_{2_1}^{t-1},b_2^t} = \left\{\theta_{s_{2_0}^t|s_{2_1}^{t-1},b_2^t}, \theta_{s_{2_1}^t|s_{2_1}^{t-1},b_2^t}, \theta_{s_{2_2}^t|s_{2_1}^{t-1},b_2^t}, \theta_{s_{2_3}^t|s_{2_1}^{t-1},b_2^t}, \theta_{s_{2_4}^t|s_{2_1}^{t-1},b_2^t}, \theta_{s_{2_5}^t|s_{2_1}^{t-1},b_2^t}\right\}$$
$$= \{0.000111, 0.999445, 0.000111, 0.000111, 0.000111, 0.000111\},$$

$$\boldsymbol{\theta}_{S_2^t|s_{2_2}^{t-1},b_2^t} = \left\{\theta_{s_{2_0}^t|s_{2_2}^{t-1},b_2^t}, \theta_{s_{2_1}^t|s_{2_2}^{t-1},b_2^t}, \theta_{s_{2_2}^t|s_{2_2}^{t-1},b_2^t}, \theta_{s_{2_3}^t|s_{2_2}^{t-1},b_2^t}, \theta_{s_{2_4}^t|s_{2_2}^{t-1},b_2^t}, \theta_{s_{2_5}^t|s_{2_2}^{t-1},b_2^t}\right\}$$
$$= \{0.000028, 0.000028, 0.999861, 0.000028, 0.000028, 0.000028\},$$

$$\boldsymbol{\theta}_{S_2^t|s_{2_3}^{t-1},b_2^t} = \left\{\theta_{s_{2_0}^t|s_{2_3}^{t-1},b_2^t}, \theta_{s_{2_1}^t|s_{2_3}^{t-1},b_2^t}, \theta_{s_{2_2}^t|s_{2_3}^{t-1},b_2^t}, \theta_{s_{2_3}^t|s_{2_3}^{t-1},b_2^t}, \theta_{s_{2_4}^t|s_{2_3}^{t-1},b_2^t}, \theta_{s_{2_5}^t|s_{2_3}^{t-1},b_2^t}\right\}$$
$$= \{0.000028, 0.000028, 0.000028, 0.999861, 0.000028, 0.000028\},$$

$$\boldsymbol{\theta}_{S_2^t|s_{2_4}^{t-1},b_2^t} = \left\{\theta_{s_{2_0}^t|s_{2_4}^{t-1},b_2^t}, \theta_{s_{2_1}^t|s_{2_4}^{t-1},b_2^t}, \theta_{s_{2_2}^t|s_{2_4}^{t-1},b_2^t}, \theta_{s_{2_3}^t|s_{2_4}^{t-1},b_2^t}, \theta_{s_{2_4}^t|s_{2_4}^{t-1},b_2^t}, \theta_{s_{2_5}^t|s_{2_4}^{t-1},b_2^t}\right\}$$
$$= \{0.166667, 0.166667, 0.166667, 0.166667, 0.166667, 0.166667\},$$

$$\boldsymbol{\theta}_{S_2^t|s_{2_5}^{t-1},b_2^t} = \left\{\theta_{s_{2_0}^t|s_{2_5}^{t-1},b_2^t}, \theta_{s_{2_1}^t|s_{2_5}^{t-1},b_2^t}, \theta_{s_{2_2}^t|s_{2_5}^{t-1},b_2^t}, \theta_{s_{2_3}^t|s_{2_5}^{t-1},b_2^t}, \theta_{s_{2_4}^t|s_{2_5}^{t-1},b_2^t}, \theta_{s_{2_5}^t|s_{2_5}^{t-1},b_2^t}\right\}$$
$$= \{0.000056, 0.000056, 0.000056, 0.000056, 0.000056, 0.999722\}.$$

Distribution $p\left(F_8^t, F_{32}^t, F_{38}^t, F_{53}^t, F_{42}^t, F_{13}^t \mid S_2^t, B^t : \boldsymbol{\theta}_{F_8^t,\dots,F_{13}^t|S_2^t,B^t}\right)$

The distribution $p\left(F_8^t, F_{32}^t, F_{38}^t, F_{53}^t, F_{42}^t, F_{13}^t \mid S_2^t, B^t : \boldsymbol{\theta}_{F_8^t,\dots,F_{13}^t|S_2^t,B^t}\right)$ over a six-dimensional vector of continuous variables $(F_8, F_{32}, F_{38}, F_{53}, F_{42}, F_{13})$ at time slice $t \geq 1$ is a collection of multivariate Gaussian distributions with a multivariate Gaussian

$$p\left(F_8^t, F_{32}^t, F_{38}^t, F_{53}^t, F_{42}^t, F_{13}^t \mid s_2^t, b^t : \boldsymbol{\theta}_{F_8^t,\dots,F_{13}^t|s_2^t,b^t}\right) = \mathcal{N}\left(\boldsymbol{\mu}_{s_2^t|b^t{}_i}, \Sigma_{s_2^t|b^t{}_i}\right)$$

for each $\{s_2^{t-1}, b^t\} \in \mathrm{Val}(S_2) \times \mathrm{Val}(B)$, parameterized with MAP parameters

$$\boldsymbol{\theta}_{F_8^t,\dots,F_{13}^t|S_2^t,B^t} = \begin{Bmatrix} \boldsymbol{\theta}_{F_8^t,\dots,F_{13}^t|s_{2_0}^t,b_0^t}, \boldsymbol{\theta}_{F_8^t,\dots,F_{13}^t|s_{2_1}^t,b_0^t}, \boldsymbol{\theta}_{F_8^t,\dots,F_{13}^t|s_{2_2}^t,b_0^t}, \boldsymbol{\theta}_{F_8^t,\dots,F_{13}^t|s_{2_3}^t,b_0^t}, \boldsymbol{\theta}_{F_8^t,\dots,F_{13}^t|s_{2_4}^t,b_0^t}, \boldsymbol{\theta}_{F_8^t,\dots,F_{13}^t|s_{2_5}^t,b_0^t}, \\ \boldsymbol{\theta}_{F_8^t,\dots,F_{13}^t|s_{2_0}^t,b_1^t}, \boldsymbol{\theta}_{F_8^t,\dots,F_{13}^t|s_{2_1}^t,b_1^t}, \boldsymbol{\theta}_{F_8^t,\dots,F_{13}^t|s_{2_2}^t,b_1^t}, \boldsymbol{\theta}_{F_8^t,\dots,F_{13}^t|s_{2_3}^t,b_1^t}, \boldsymbol{\theta}_{F_8^t,\dots,F_{13}^t|s_{2_4}^t,b_1^t}, \boldsymbol{\theta}_{F_8^t,\dots,F_{13}^t|s_{2_5}^t,b_1^t}, \\ \boldsymbol{\theta}_{F_8^t,\dots,F_{13}^t|s_{2_0}^t,b_2^t}, \boldsymbol{\theta}_{F_8^t,\dots,F_{13}^t|s_{2_1}^t,b_2^t}, \boldsymbol{\theta}_{F_8^t,\dots,F_{13}^t|s_{2_2}^t,b_2^t}, \boldsymbol{\theta}_{F_8^t,\dots,F_{13}^t|s_{2_3}^t,b_2^t}, \boldsymbol{\theta}_{F_8^t,\dots,F_{13}^t|s_{2_4}^t,b_2^t}, \boldsymbol{\theta}_{F_8^t,\dots,F_{13}^t|s_{2_5}^t,b_2^t} \end{Bmatrix},$$

where

$$\boldsymbol{\theta}_{F_8^t,\dots,F_{13}^t|s_{2_0}^t,b_0^t} = \left\{\boldsymbol{\mu}_{s_{2_0}^t,b_0^t} = \mathbf{0}_6, \Sigma_{s_{2_0}^t,b_0^t} = \mathbf{I}_6\right\},$$

$$\boldsymbol{\theta}_{F_8^t,\dots,F_{13}^t|s_{2_1}^t,b_0^t} = \left\{\boldsymbol{\mu}_{s_{2_1}^t,b_0^t} = \mathbf{0}_6, \Sigma_{s_{2_1}^t,b_0^t} = \mathbf{I}_6\right\},$$

$$\boldsymbol{\theta}_{\left(F_8^t,\dots,F_{13}^t|s_{2_2}^t,b_0^t\right)} = \left\{\boldsymbol{\mu}_{s_{2_2}^t,b_0^t}, \Sigma_{s_{2_2}^t,b_0^t}\right\}, \boldsymbol{\mu}_{s_{2_2}^t,b_0^t} = \begin{pmatrix} 0.424419 \\ 1.305315 \\ 38.157631 \\ 33.973369 \\ 400.917517 \\ 0.085536 \end{pmatrix},$$

$$\Sigma_{s_{2_2}^t,b_0^t} = \begin{bmatrix} 0.08012 & 0.01353 & 4.773425 & 0.679966 & 7.767003 & -0.003165 \\ 0.01353 & 0.184326 & 6.413222 & 5.082756 & 32.257262 & 0.008817 \\ 4.773425 & 6.413222 & 3816.150503 & 1970.305249 & 3061.573432 & -2.157207 \\ 0.679966 & 5.082756 & 1970.305249 & 1465.422903 & 1650.50768 & -0.338575 \\ 7.767003 & 32.257262 & 3061.573432 & 1650.50768 & 29156.98913 & -3.28025 \\ -0.003165 & 0.008817 & -2.157207 & -0.338575 & -3.28025 & 0.008219 \end{bmatrix},$$

$$\boldsymbol{\theta}_{F_8^t,\dots,F_{13}^t|s_{2_3}^t,b_0^t} = \left\{\boldsymbol{\mu}_{s_{2_3}^t,b_0^t}, \Sigma_{s_{2_3}^t,b_0^t}\right\}, \boldsymbol{\mu}_{s_{2_3}^t,b_0^t} = \begin{pmatrix} 0.5212 \\ 1.508461 \\ 14.974388 \\ 21.456281 \\ 287.951837 \\ 0.102731 \end{pmatrix},$$

$$\Sigma_{s_{2_3}^t,b_0^t} = \begin{bmatrix} 0.083107 & 0.080643 & -1.568247 & 0.142766 & 24.665862 & -0.004086 \\ 0.080643 & 0.300815 & -1.701552 & 3.219238 & 51.618697 & -0.010963 \\ -1.568247 & -1.701552 & 770.829809 & 114.961942 & -162.191101 & 0.042093 \\ 0.142766 & 3.219238 & 114.961942 & 379.280575 & 232.028474 & 0.443666 \\ 24.665862 & 51.618697 & -162.191101 & 232.028474 & 19144.85645 & -8.552253 \\ -0.004086 & -0.010963 & 0.042093 & 0.443666 & -8.552253 & 0.007518 \end{bmatrix},$$

$$\boldsymbol{\theta}_{F_8^t,\dots,F_{13}^t|s_{2_4}^t,b_0^t} = \left\{\boldsymbol{\mu}_{s_{2_4}^t,b_0^t}, \Sigma_{s_{2_4}^t,b_0^t}\right\}, \boldsymbol{\mu}_{s_{2_4}^t,b_0^t} = \begin{pmatrix} 0.365028 \\ 0.880845 \\ 11.40316 \\ 33.699631 \\ 279.892362 \\ 0.098628 \end{pmatrix},$$

$$\Sigma_{s_{2_4}^t,b_0^t} = \begin{bmatrix} 0.031643 & 0.034275 & -0.138413 & -0.70557 & -16.328374 & 0.004836 \\ 0.034275 & 0.17404 & -0.956192 & -4.506297 & -76.926188 & 0.032139 \\ -0.138413 & -0.956192 & 1031.345374 & 50.835047 & 736.218898 & -0.27338 \\ -0.70557 & -4.506297 & 50.835047 & 517.842831 & 2592.088451 & -1.218731 \\ -16.328374 & -76.926188 & 736.218898 & 2592.088451 & 46806.49236 & -20.810504 \\ 0.004836 & 0.032139 & -0.27338 & -1.218731 & -20.810504 & 0.011021 \end{bmatrix},$$

$$\boldsymbol{\theta}_{F_8^t,\dots,F_{13}^t|s_{2_5}^t,b_0^t} = \left\{\boldsymbol{\mu}_{s_{2_5}^t,b_0^t} = \mathbf{0}_6, \Sigma_{s_{2_5}^t,b_0^t} = \mathbf{I}_6\right\},$$

$$\boldsymbol{\theta}_{F_8^t,\dots,F_{13}^t|s_{2_0}^t,b_1^t} = \left\{\boldsymbol{\mu}_{s_{2_0}^t,b_1^t}, \Sigma_{s_{2_0}^t,b_1^t}\right\}, \boldsymbol{\mu}_{s_{2_0}^t,b_1^t} = \begin{pmatrix} 0.712513 \\ 1.500095 \\ 254.881257 \\ 104.404561 \\ 529.41021 \\ 0.024596 \end{pmatrix},$$

$$\Sigma_{s_{2_0}^t,b_1^t} = \begin{bmatrix} 0.026269 & -0.015893 & 11.840772 & 7.126603 & 0.543942 & -0.000789 \\ -0.015893 & 0.151122 & -33.848399 & -18.750072 & -1.145235 & 0.002506 \\ 11.840772 & -33.848399 & 33645.92329 & 21580.28805 & 2866.7418 & -2.770175 \\ 7.126603 & -18.750072 & 21580.28805 & 15742.75464 & 2676.920757 & -1.785992 \\ 0.543942 & -1.145235 & 2866.7418 & 2676.920757 & 1285.355495 & -0.293091 \\ -0.000789 & 0.002506 & -2.770175 & -1.785992 & -0.293091 & 0.000696 \end{bmatrix},$$

$$\boldsymbol{\theta}_{F_8^t,\dots,F_{13}^t|s_{2_1}^t,b_1^t} = \left\{\boldsymbol{\mu}_{s_{2_1}^t,b_1^t}, \Sigma_{s_{2_1}^t,b_1^t}\right\}, \boldsymbol{\mu}_{s_{2_1}^t,b_1^t} = \begin{pmatrix} 1.077379 \\ 1.617362 \\ 372.978124 \\ 102.664786 \\ 424.021234 \\ 0.026269 \end{pmatrix},$$

$$\Sigma_{s_{2_1}^t,b_1^t} = \begin{bmatrix} 0.638548 & 0.60877 & 21.206215 & -73.954045 & 15.472882 & 0.006639 \\ 0.60877 & 0.802389 & -58.007328 & -102.485533 & -40.515444 & 0.0125 \\ 21.206215 & -58.007328 & 46622.50769 & 10973.58739 & 30379.16139 & -2.709657 \\ -73.954045 & -102.485533 & 10973.58739 & 14095.61031 & 7642.354956 & -1.868823 \\ 15.472882 & -40.515444 & 30379.16139 & 7642.354956 & 22916.32658 & -2.383629 \\ 0.006639 & 0.0125 & -2.709657 & -1.868823 & -2.383629 & 0.000745 \end{bmatrix},$$

$$\boldsymbol{\theta}_{F_8^t,\dots,F_{13}^t|s_{2_2}^t,b_1^t} = \left\{\boldsymbol{\mu}_{s_{2_2}^t,b_1^t}, \Sigma_{s_{2_2}^t,b_1^t}\right\}, \boldsymbol{\mu}_{s_{2_2}^t,b_1^t} = \begin{pmatrix} 0.524986 \\ 1.029317 \\ 52.447886 \\ 33.819258 \\ 512.444059 \\ 0.023705 \end{pmatrix},$$

$$\Sigma_{s_{2_2}^t,b_1^t} = \begin{bmatrix} 0.081357 & -0.024643 & 12.234926 & -1.586743 & -0.001848 & -0.000586 \\ -0.024643 & 0.084981 & -9.695691 & -1.846891 & 0.90378 & 0.003889 \\ 12.234926 & -9.695691 & 4336.306212 & -94.552372 & 59.842235 & -0.654056 \\ -1.586743 & -1.846891 & -94.552372 & 1242.348315 & -291.702711 & -0.055757 \\ -0.001848 & 0.90378 & 59.842235 & -291.702711 & 612.719735 & 0.11626 \\ -0.000586 & 0.003889 & -0.654056 & -0.055757 & 0.11626 & 0.000816 \end{bmatrix},$$

$$\boldsymbol{\theta}_{F_8^t,\dots,F_{13}^t|s_{2_3}^t,b_1^t} = \left\{\boldsymbol{\mu}_{s_{2_3}^t,b_1^t}, \Sigma_{s_{2_3}^t,b_1^t}\right\}, \boldsymbol{\mu}_{s_{2_3}^t,b_1^t} = \begin{pmatrix} 0.524065 \\ 0.848716 \\ 240.976701 \\ 40.204648 \\ 508.421396 \\ 0.007134 \end{pmatrix},$$

$$\Sigma_{s_{2_3}^t,b_1^t} = \begin{bmatrix} 0.033312 & 0.007131 & 0.217141 & 0.321921 & 0.216393 & 0.000071 \\ 0.007131 & 0.036288 & 0.24994 & 0.813203 & 0.24594 & 0.000289 \\ 0.217141 & 0.24994 & 2041.394889 & 54.815012 & 133.967896 & -0.047402 \\ 0.321921 & 0.813203 & 54.815012 & 633.744263 & 54.632127 & 0.009604 \\ 0.216393 & 0.24594 & 133.967896 & 54.632127 & 1630.313101 & -0.047807 \\ 0.000071 & 0.000289 & -0.047402 & 0.009604 & -0.047807 & 0.000519 \end{bmatrix},$$

$$\boldsymbol{\theta}_{F_8^t,\dots,F_{13}^t|s_{2_4}^t,b_1^t} = \left\{\boldsymbol{\mu}_{s_{2_4}^t,b_1^t} = \mathbf{0}_6, \Sigma_{s_{2_4}^t,b_1^t} = \mathbf{I}_6\right\},$$

$$\boldsymbol{\theta}_{F_8^t,\dots,F_{13}^t|s_{2_5}^t,b_1^t} = \left\{\boldsymbol{\mu}_{s_{2_5}^t,b_1^t} = \mathbf{0}_6, \Sigma_{s_{2_5}^t,b_1^t} = \mathbf{I}_6\right\},$$

$$\boldsymbol{\theta}_{F_8^t,\dots,F_{13}^t|s_{2_0}^t,b_2^t} = \left\{\boldsymbol{\mu}_{s_{2_0}^t,b_2^t}, \Sigma_{s_{2_0}^t,b_2^t}\right\}, \boldsymbol{\mu}_{s_{2_0}^t,b_2^t} = \begin{pmatrix} 0.915163 \\ 2.839784 \\ 522.866656 \\ 272.233593 \\ 528.552035 \\ 0.028492 \end{pmatrix},$$

$$\Sigma_{s_{2_0}^t,b_2^t} = \begin{bmatrix} 0.358406 & -0.125455 & 1.138115 & -123.491444 & 0.964548 & 0.006221 \\ -0.125455 & 0.234388 & -1.24156 & 90.802581 & -2.097379 & -0.001503 \\ 1.138115 & -1.24156 & 1457.144625 & -926.892732 & 229.330514 & -0.050268 \\ -123.491444 & 90.802581 & -926.892732 & 60759.00382 & -1063.812638 & -1.876293 \\ 0.964548 & -2.097379 & 229.330514 & -1063.812638 & 893.275635 & -0.011941 \\ 0.006221 & -0.001503 & -0.050268 & -1.876293 & -0.011941 & 0.000598 \end{bmatrix},$$

$$\boldsymbol{\theta}_{F_8^t,\dots,F_{13}^t|s_{2_1}^t,b_2^t} = \left\{\boldsymbol{\mu}_{s_{2_1}^t,b_2^t}, \Sigma_{s_{2_1}^t,b_2^t}\right\}, \boldsymbol{\mu}_{s_{2_1}^t,b_2^t} = \begin{pmatrix} 0.458416 \\ 1.885947 \\ 512.886418 \\ 223.546736 \\ 519.263473 \\ 0.036328 \end{pmatrix},$$

$$\Sigma_{s_{2_1}^t,b_2^t} = \begin{bmatrix} 0.040195 & 0.039047 & -1.259074 & -1.008431 & -0.974184 & 0.002422 \\ 0.039047 & 0.120922 & -1.743955 & -2.084043 & -2.130509 & 0.006721 \\ -1.259074 & -1.743955 & 2738.40527 & 372.124306 & 309.505577 & -0.236262 \\ -1.008431 & -2.084043 & 372.124306 & 744.758026 & 166.905586 & -0.178691 \\ -0.974184 & -2.130509 & 309.505577 & 166.905586 & 1643.204229 & -0.170825 \\ 0.002422 & 0.006721 & -0.236262 & -0.178691 & -0.170825 & 0.001543 \end{bmatrix},$$

$$\boldsymbol{\theta}_{F_8^t,\ldots,F_{13}^t|s_{2_2}^t,b_2^t} = \left\{\boldsymbol{\mu}_{s_{2_2}^t,b_2^t}, \Sigma_{s_{2_2}^t,b_2^t}\right\}, \boldsymbol{\mu}_{s_{2_2}^t,b_2^t} = \begin{pmatrix} 0.376102 \\ 2.338862 \\ 33.973608 \\ 80.780846 \\ 301.224215 \\ 0.12992 \end{pmatrix},$$

$$\Sigma_{s_{2_2}^t,b_2^t} = \begin{bmatrix} 0.08629 & -0.02481 & -3.26245 & -4.395125 & -36.946268 & 0.0232 \\ -0.02481 & 0.089806 & -3.356181 & 10.732843 & 14.077324 & -0.011763 \\ -3.26245 & -3.356181 & 1161.750949 & -672.03049 & 1878.467625 & -0.842032 \\ -4.395125 & 10.732843 & -672.03049 & 2632.146546 & 4546.092859 & -2.061812 \\ -36.946268 & 14.077324 & 1878.467625 & 4546.092859 & 40148.1453 & -13.455166 \\ 0.0232 & -0.011763 & -0.842032 & -2.061812 & -13.455166 & 0.014601 \end{bmatrix},$$

$$\boldsymbol{\theta}_{F_8^t,\ldots,F_{13}^t|s_{2_3}^t,b_2^t} = \left\{\boldsymbol{\mu}_{s_{2_3}^t,b_2^t}, \Sigma_{s_{2_3}^t,b_2^t}\right\}, \boldsymbol{\mu}_{s_{2_3}^t,b_2^t} = \begin{pmatrix} 1.366229 \\ 1.950829 \\ 145.771333 \\ 81.486465 \\ 429.698911 \\ 0.186115 \end{pmatrix},$$

$$\Sigma_{s_{2_3}^t,b_2^t} = \begin{bmatrix} 1.05745 & 0.016268 & -113.340742 & 41.067913 & -41.103432 & 0.069196 \\ 0.016268 & 0.07637 & -9.541527 & 2.424336 & -10.764504 & 0.004542 \\ -113.340742 & -9.541527 & 33787.49809 & -4087.866937 & 3187.316137 & -14.747715 \\ 41.067913 & 2.424336 & -4087.866937 & 2115.332941 & -2683.279154 & 3.257159 \\ -41.103432 & -10.764504 & 3187.316137 & -2683.279154 & 15265.48829 & -8.1969 \\ 0.069196 & 0.004542 & -14.747715 & 3.257159 & -8.1969 & 0.011902 \end{bmatrix},$$

$$\boldsymbol{\theta}_{F_8^t,\ldots,F_{13}^t|s_{2_4}^t,b_2^t} = \left\{\boldsymbol{\mu}_{s_{2_4}^t,b_2^t} = \mathbf{0}_6, \Sigma_{s_{2_4}^t,b_2^t} = \mathbf{I}_6\right\},$$

$$\boldsymbol{\theta}_{F_8^t,\ldots,F_{13}^t|s_{2_5}^t,b_2^t} = \left\{\boldsymbol{\mu}_{s_{2_5}^t,b_2^t}, \Sigma_{s_{2_5}^t,b_2^t}\right\}, \boldsymbol{\mu}_{s_{2_5}^t,b_2^t} = \begin{pmatrix} 0.731486 \\ 1.85648 \\ 14.172817 \\ 81.072865 \\ 158.887783 \\ 0.171135 \end{pmatrix},$$

$$\Sigma_{s_{2_5}^t,b_2^t} = \begin{bmatrix} 0.116967 & -0.022933 & 2.621197 & 0.115619 & 7.143726 & 0.003787 \\ -0.022933 & 0.195368 & -0.553685 & 14.544871 & -9.534996 & 0.007822 \\ 2.621197 & -0.553685 & 1088.978694 & -49.870141 & 286.530303 & 0.004979 \\ 0.115619 & 14.544871 & -49.870141 & 2168.699698 & -1128.126578 & 1.401465 \\ 7.143726 & -9.534996 & 286.530303 & -1128.126578 & 2276.087348 & -0.904149 \\ 0.003787 & 0.007822 & 0.004979 & 1.401465 & -0.904149 & 0.003502 \end{bmatrix}.$$

Distribution $p\left(F_{27}^t \mid S_2^t, B^t : \boldsymbol{\theta}_{F_{27}^t|S_2^t,B^t}\right)$

The distribution $p\left(F_{27}^t \mid S_2^t, B^t : \boldsymbol{\theta}_{F_{27}^t|S_2^t,B^t}\right)$ over the continuous variable F_{27} at time slice $t \geq 1$ is a collection of exponential distributions with an exponential distribution

$$p\left(F_{27}^t \mid s_2^t, b^t : \lambda_{F_{27}^t|s_2^t,b^t}\right) = \text{Expon}\left(F_{27}^t : \lambda_{F_{27}^t|s_2^t,b^t}\right)$$

for each $\{s_2^t, b^t\} \in \text{Val}(S_2) \times \text{Val}(B)$, parameterized with MAP parameters

$$\boldsymbol{\theta}_{F_{27}^t|S_2^{t-1},B^t} = \begin{Bmatrix} \lambda_{F_{27}^t|s_{2_0}^t,b_0^t}, \lambda_{F_{27}^t|s_{2_1}^t,b_0^t}, \lambda_{F_{27}^t|s_{2_2}^t,b_0^t}, \lambda_{F_{27}^t|s_{2_3}^t,b_0^t}, \lambda_{F_{27}^t|s_{2_4}^t,b_0^t}, \lambda_{F_{27}^t|s_{2_5}^t,b_0^t}, \\ \lambda_{F_{27}^t|s_{2_0}^t,b_1^t}, \lambda_{F_{27}^t|s_{2_1}^t,b_1^t}, \lambda_{F_{27}^t|s_{2_2}^t,b_1^t}, \lambda_{F_{27}^t|s_{2_3}^t,b_1^t}, \lambda_{F_{27}^t|s_{2_4}^t,b_1^t}, \lambda_{F_{27}^t|s_{2_5}^t,b_1^t}, \\ \lambda_{F_{27}^t|s_{2_0}^t,b_2^t}, \lambda_{F_{27}^t|s_{2_1}^t,b_2^t}, \lambda_{F_{27}^t|s_{2_2}^t,b_2^t}, \lambda_{F_{27}^t|s_{2_3}^t,b_2^t}, \lambda_{F_{27}^t|s_{2_4}^t,b_2^t}, \lambda_{F_{27}^t|s_{2_5}^t,b_2^t} \end{Bmatrix}$$
$$= \begin{Bmatrix} 0.583943, 0.583943, 0.83865, 1.206156, 0.376448, 0.583943, \\ 0.501114, 0.324152, 0.296224, 0.259526, 0.583943, 0.583943, \\ 9.790407, 5.825088, 5.291385, 5.497436, 0.583943, 1.141708 \end{Bmatrix}.$$

Distribution $p\left(F_{47}^t \mid S_2^t, B^t : \boldsymbol{\theta}_{F_{27}^t|S_2^t,B^t}\right)$

The distribution $p\left(F_{47}^t \mid S_2^t, B^t : \boldsymbol{\theta}_{F_{27}^t|S_2^t,B^t}\right)$ over the continuous variable F_{47} at time slice $t \geq 1$ is a collection of exponential distributions with an exponential distribution

$$p\left(F_{47}^t \mid s_2^t, b^t : \lambda_{F_{47}^t|s_2^t,b^t}\right) = \text{Expon}\left(F_{47}^t : \lambda_{F_{47}^t|s_2^t,b^t}\right)$$

for each $\{s_2^t, b^t\} \in \text{Val}(S_2) \times \text{Val}(B)$, parameterized with MAP parameters

$$\boldsymbol{\theta}_{F_{47}^t|S_2^{t-1},B^t} = \begin{Bmatrix} \lambda_{F_{47}^t|s_{2_0}^t,b_0^t}, \lambda_{F_{47}^t|s_{2_1}^t,b_0^t}, \lambda_{F_{47}^t|s_{2_2}^t,b_0^t}, \lambda_{F_{47}^t|s_{2_3}^t,b_0^t}, \lambda_{F_{47}^t|s_{2_4}^t,b_0^t}, \lambda_{F_{47}^t|s_{2_5}^t,b_0^t}, \\ \lambda_{F_{47}^t|s_{2_0}^t,b_1^t}, \lambda_{F_{47}^t|s_{2_1}^t,b_1^t}, \lambda_{F_{47}^t|s_{2_2}^t,b_1^t}, \lambda_{F_{47}^t|s_{2_3}^t,b_1^t}, \lambda_{F_{47}^t|s_{2_4}^t,b_1^t}, \lambda_{F_{47}^t|s_{2_5}^t,b_1^t}, \\ \lambda_{F_{47}^t|s_{2_0}^t,b_2^t}, \lambda_{F_{47}^t|s_{2_1}^t,b_2^t}, \lambda_{F_{47}^t|s_{2_2}^t,b_2^t}, \lambda_{F_{47}^t|s_{2_3}^t,b_2^t}, \lambda_{F_{47}^t|s_{2_4}^t,b_2^t}, \lambda_{F_{47}^t|s_{2_5}^t,b_2^t} \end{Bmatrix}$$
$$= \begin{Bmatrix} 0.011602, 0.011602, 0.048626, 0.133335, .035936, 0.011602, \\ 0.004304, 0.019260, 0.007216, 0.064874, 0.011602, 0.011602, \\ 0.001893, 0.007976, 0.078177, 0.04165, 0.011602, 0.024549 \end{Bmatrix}.$$

2.6 Parameters of the extended SAE Level 3 SAGAT Score Model

For any number of time slices $T \geq 1$, the extended SAE Level 3 SAGAT Score model defines the JPD

$$p\left(S_2^{1:T}, \boldsymbol{F}_{\text{Rel}}^{1:T}, B^{1:T} : \boldsymbol{\theta}\right)$$
$$= p\left(S_2^1 \mid B^1 : \boldsymbol{\theta}_{S_2^1|B^1}\right) \prod_{t=2}^{T} p\left(S_2^t \mid S_2^{t-1}, B^t : \boldsymbol{\theta}_{S_2^t|S_2^{t-1},B^t}\right) \prod_{t=1}^{T} p(B^t : \boldsymbol{\theta}_{B^t}) p\left(\boldsymbol{F}_{\text{Rel}}^t \mid S_2^t, B^t : \boldsymbol{\theta}\right),$$

with $p\left(\boldsymbol{F}_{\text{Rel}}^t \mid S_2^t, B^t : \boldsymbol{\theta}\right)$ given by

$$p\left(F_9^t, F_{29}^t, F_{37}^t, F_{58}^t, F_{48}^t, F_{43}^t | S_2^t, B^t : \boldsymbol{\theta}_{F_9^t,\ldots,F_{43}^t|S_2^t,B^t}\right) p\left(F_{16}^t | S_2^t, B^t : \boldsymbol{\theta}_{F_{16}^t|S_2^t,B^t}\right)$$
$$p\left(F_{32}^t | S_2^t, B^t : \boldsymbol{\theta}_{F_{32}^t|S_2^t,B^t}\right) p\left(F_{67}^t | S_2^t, B^t : \boldsymbol{\theta}_{F_{67}^t|S_2^t,B^t}\right).$$

As such, the model is defined by seven probability /density distribution to be detailed in the following. The names of the relevant indicators $\boldsymbol{F}_{\text{Rel}} = \{F_9, F_{16}, F_{29}, F_{32}, F_{37}, F_{43}, F_{48}, F_{58}, F_{67}\}$ are provided in Table 29.

Table 29: The set of relevant indicators for the SAE Level 2 NDRT model, $\boldsymbol{F}_{\text{Rel}} = \{F_9, F_{16}, F_{29}, F_{32}, F_{37}, F_{43}, F_{48}, F_{58}, F_{67}\}$.

Symbol	Name
F_9	Mean blink frequency
F_{16}	Yaw rate of the head variability
F_{29}	Mean monitoring frequency
F_{32}	Mean saccade frequency
F_{37}	Time since last look at left mirror AOI

F_{43}	Mean time since last look at right mirror AOI
F_{48}	Mean time since last look at rear mirror AOI
F_{58}	Mean time since last look at infotainment AOI
F_{67}	Time since last look at other AOI

Distribution $p(B^t : \boldsymbol{\theta}_{B^t})$

The distribution $p(B^t : \boldsymbol{\theta}_{B^t})$ is a categorical distribution

$$p(B^t : \boldsymbol{\theta}_{B^t}) = \mathrm{Cat}(B^t : \boldsymbol{\theta}_{B^t})$$

over the discrete variable B, $\mathrm{Val}(B) = \{b_0, b_1, b_2\}$ at time slice $t = 1$, with MAP parameters

$$\boldsymbol{\theta}_{B^t} = \left\{\theta_{b_0^t}, \theta_{b_1^t}, \theta_{b_2^t}\right\} = \{0.351334, 0.324333, 0.324333\}.$$

Distribution $p\left(S_2^1 \mid B^1 : \boldsymbol{\theta}_{S_2^1|B^1}\right)$

The distribution $p\left(S_2^1 \mid B^1 : \boldsymbol{\theta}_{S_2^1|B^1}\right)$ over the discrete variable S_2, $\mathrm{Val}(S_2) = \left\{s_{2_0}, s_{2_1}, s_{2_2}, s_{2_3}, s_{2_4}, s_{2_5}\right\}$ at time slice $t = 1$ is a collection of categorical distributions with a categorical distribution

$$p\left(S_2^1 \mid b^1 : \boldsymbol{\theta}_{S_2^1|b^1}\right) = \mathrm{Cat}\left(S_2^1 : \boldsymbol{\theta}_{S_2^1|b^1}\right)$$

for each $b^t \in \mathrm{Val}(B)$, parameterized with MAP parameters $\boldsymbol{\theta}_{S_2^1|B^1} = \left\{\boldsymbol{\theta}_{S_2^1|b_0^1}, \boldsymbol{\theta}_{S_2^1|b_1^1}, \boldsymbol{\theta}_{S_2^1|b_2^1}\right\}$, where

$$\begin{aligned}\boldsymbol{\theta}_{S_2^1|b_0^1} &= \left\{\theta_{s_{2_0}^1|b_0^1}, \theta_{s_{2_1}^1|b_0^1}, \theta_{s_{2_2}^1|b_0^1}, \theta_{s_{2_3}^1|b_0^1}, \theta_{s_{2_4}^1|b_0^1}, \theta_{s_{2_5}^1|b_0^1}\right\} \\ &= \{0.000107, 0.153854, 0.076981, 0.230779, 0.461298, 0.076981\},\end{aligned}$$

$$\begin{aligned}\boldsymbol{\theta}_{S_2^1|b_1^1} &= \left\{\theta_{s_{2_0}^1|b_1^1}, \theta_{s_{2_1}^1|b_1^1}, \theta_{s_{2_2}^1|b_1^1}, \theta_{s_{2_3}^1|b_1^1}, \theta_{s_{2_4}^1|b_1^1}, \theta_{s_{2_5}^1|b_1^1}\right\} \\ &= \{0.333218, 0.249942, 0.166667, 0.166667, 0.083391, 0.000116\},\end{aligned}$$

$$\begin{aligned}\boldsymbol{\theta}_{S_2^1|b_2^1} &= \left\{\theta_{s_{2_0}^1|b_2^1}, \theta_{s_{2_1}^1|b_2^1}, \theta_{s_{2_2}^1|b_2^1}, \theta_{s_{2_3}^1|b_2^1}, \theta_{s_{2_4}^1|b_2^1}, \theta_{s_{2_5}^1|b_2^1}\right\} \\ &= \{0.416493, 0.166667, 0.249942, 0.083391, 0.083391, 0.000116\}.\end{aligned}$$

Distribution $p\left(S_2^t \mid S_2^{t-1}, B^t : \boldsymbol{\theta}_{S_2^t|S_2^{t-1},B^t}\right)$

The distribution $p\left(S_2^t \mid S_2^{t-1}, B^t : \boldsymbol{\theta}_{S_2^t|S_2^{t-1},B^t}\right)$ over the discrete variable S_2, $\mathrm{Val}(S_2) = \left\{s_{2_0}, s_{2_1}, s_{2_2}, s_{2_3}, s_{2_4}, s_{2_5}\right\}$ at time slice $t > 1$ is a collection of categorical distributions with a categorical distribution

$$p\left(S_2^t | s_2^{t-1}, b^t : \boldsymbol{\theta}_{S_2^t|s_2^{t-1},b^t}\right) = \mathrm{Cat}\left(S_2^t : \boldsymbol{\theta}_{S_2^t|s_2^{t-1},b^t}\right)$$

for each $\{s_2^{t-1}, b^t\} \in \mathrm{Val}(S_2) \times \mathrm{Val}(B)$, parameterized with MAP parameters

$$\boldsymbol{\theta}_{S_2^t|S_2^{t-1},B^t} = \begin{Bmatrix}\boldsymbol{\theta}_{S_2^t|s_{2_0}^{t-1},b_0^t}, \boldsymbol{\theta}_{S_2^t|s_{2_1}^{t-1},b_0^t}, \boldsymbol{\theta}_{S_2^t|s_{2_2}^{t-1},b_0^t}, \boldsymbol{\theta}_{S_2^t|s_{2_3}^{t-1},b_0^t}, \boldsymbol{\theta}_{S_2^t|s_{2_4}^{t-1},b_0^t}, \boldsymbol{\theta}_{S_2^t|s_{2_5}^{t-1},b_0^t}, \\ \boldsymbol{\theta}_{S_2^t|s_{2_0}^{t-1},b_1^t}, \boldsymbol{\theta}_{S_2^t|s_{2_1}^{t-1},b_1^t}, \boldsymbol{\theta}_{S_2^t|s_{2_2}^{t-1},b_1^t}, \boldsymbol{\theta}_{S_2^t|s_{2_3}^{t-1},b_1^t}, \boldsymbol{\theta}_{S_2^t|s_{2_4}^{t-1},b_1^t}, \boldsymbol{\theta}_{S_2^t|s_{2_5}^{t-1},b_1^t}, \\ \boldsymbol{\theta}_{S_2^t|s_{2_0}^{t-1},b_2^t}, \boldsymbol{\theta}_{S_2^t|s_{2_1}^{t-1},b_2^t}, \boldsymbol{\theta}_{S_2^t|s_{2_2}^{t-1},b_2^t}, \boldsymbol{\theta}_{S_2^t|s_{2_3}^{t-1},b_2^t}, \boldsymbol{\theta}_{S_2^t|s_{2_4}^{t-1},b_2^t}, \boldsymbol{\theta}_{S_2^t|s_{2_5}^{t-1},b_2^t}\end{Bmatrix},$$

where

$$\boldsymbol{\theta}_{S_2^t|s_{2_0}^{t-1},b_0^t} = \left\{\theta_{s_{2_0}^t|s_{2_0}^{t-1},b_0^t}, \theta_{s_{2_1}^t|s_{2_0}^{t-1},b_0^t}, \theta_{s_{2_2}^t|s_{2_0}^{t-1},b_0^t}, \theta_{s_{2_3}^t|s_{2_0}^{t-1},b_0^t}, \theta_{s_{2_4}^t|s_{2_0}^{t-1},b_0^t}, \theta_{s_{2_5}^t|s_{2_0}^{t-1},b_0^t}\right\}$$
$$= \{0.166667, 0.166667, 0.166667, 0.166667, 0.166667, 0.166667\},$$

$$\boldsymbol{\theta}_{S_2^t|s_{2_1}^{t-1},b_0^t} = \left\{\theta_{s_{2_0}^t|s_{2_1}^{t-1},b_0^t}, \theta_{s_{2_1}^t|s_{2_1}^{t-1},b_0^t}, \theta_{s_{2_2}^t|s_{2_1}^{t-1},b_0^t}, \theta_{s_{2_3}^t|s_{2_1}^{t-1},b_0^t}, \theta_{s_{2_4}^t|s_{2_1}^{t-1},b_0^t}, \theta_{s_{2_5}^t|s_{2_1}^{t-1},b_0^t}\right\}$$
$$= \{0.000056, 0.999722, 0.000056, 0.000056, 0.000056, 0.000056\},$$

$$\boldsymbol{\theta}_{S_2^t|s_{2_2}^{t-1},b_0^t} = \left\{\theta_{s_{2_0}^t|s_{2_2}^{t-1},b_0^t}, \theta_{s_{2_1}^t|s_{2_2}^{t-1},b_0^t}, \theta_{s_{2_2}^t|s_{2_2}^{t-1},b_0^t}, \theta_{s_{2_3}^t|s_{2_2}^{t-1},b_0^t}, \theta_{s_{2_4}^t|s_{2_2}^{t-1},b_0^t}, \theta_{s_{2_5}^t|s_{2_2}^{t-1},b_0^t}\right\}$$
$$= \{0.000111, 0.000111, 0.999445, 0.000111, 0.000111, 0.000111\},$$

$$\boldsymbol{\theta}_{S_2^t|s_{2_3}^{t-1},b_0^t} = \left\{\theta_{s_{2_0}^t|s_{2_3}^{t-1},b_0^t}, \theta_{s_{2_1}^t|s_{2_3}^{t-1},b_0^t}, \theta_{s_{2_2}^t|s_{2_3}^{t-1},b_0^t}, \theta_{s_{2_3}^t|s_{2_3}^{t-1},b_0^t}, \theta_{s_{2_4}^t|s_{2_3}^{t-1},b_0^t}, \theta_{s_{2_5}^t|s_{2_3}^{t-1},b_0^t}\right\}$$
$$= \{0.000037, 0.000037, 0.000037, 0.999815, 0.000037, 0.000037\},$$

$$\boldsymbol{\theta}_{S_2^t|s_{2_4}^{t-1},b_0^t} = \left\{\theta_{s_{2_0}^t|s_{2_4}^{t-1},b_0^t}, \theta_{s_{2_1}^t|s_{2_4}^{t-1},b_0^t}, \theta_{s_{2_2}^t|s_{2_4}^{t-1},b_0^t}, \theta_{s_{2_3}^t|s_{2_4}^{t-1},b_0^t}, \theta_{s_{2_4}^t|s_{2_4}^{t-1},b_0^t}, \theta_{s_{2_5}^t|s_{2_4}^{t-1},b_0^t}\right\}$$
$$= \{0.000019, 0.000019, 0.000019, 0.000019, 0.999907, 0.000019\},$$

$$\boldsymbol{\theta}_{S_2^t|s_{2_5}^{t-1},b_0^t} = \left\{\theta_{s_{2_0}^t|s_{2_5}^{t-1},b_0^t}, \theta_{s_{2_1}^t|s_{2_5}^{t-1},b_0^t}, \theta_{s_{2_2}^t|s_{2_5}^{t-1},b_0^t}, \theta_{s_{2_3}^t|s_{2_5}^{t-1},b_0^t}, \theta_{s_{2_4}^t|s_{2_5}^{t-1},b_0^t}, \theta_{s_{2_5}^t|s_{2_5}^{t-1},b_0^t}\right\}$$
$$= \{0.000111, 0.000111, 0.000111, 0.000111, 0.000111, 0.999445\},$$

$$\boldsymbol{\theta}_{S_2^t|s_{2_0}^{t-1},b_1^t} = \left\{\theta_{s_{2_0}^t|s_{2_0}^{t-1},b_1^t}, \theta_{s_{2_1}^t|s_{2_0}^{t-1},b_1^t}, \theta_{s_{2_2}^t|s_{2_0}^{t-1},b_1^t}, \theta_{s_{2_3}^t|s_{2_0}^{t-1},b_1^t}, \theta_{s_{2_4}^t|s_{2_0}^{t-1},b_1^t}, \theta_{s_{2_5}^t|s_{2_0}^{t-1},b_1^t}\right\}$$
$$= \{0.999861, 0.000028, 0.000028, 0.000028, 0.000028, 0.000028\},$$

$$\boldsymbol{\theta}_{S_2^t|s_{2_1}^{t-1},b_1^t} = \left\{\theta_{s_{2_0}^t|s_{2_1}^{t-1},b_1^t}, \theta_{s_{2_1}^t|s_{2_1}^{t-1},b_1^t}, \theta_{s_{2_2}^t|s_{2_1}^{t-1},b_1^t}, \theta_{s_{2_3}^t|s_{2_1}^{t-1},b_1^t}, \theta_{s_{2_4}^t|s_{2_1}^{t-1},b_1^t}, \theta_{s_{2_5}^t|s_{2_1}^{t-1},b_1^t}\right\}$$
$$= \{0.000037, 0.999815, 0.000037, 0.000037, 0.000037, 0.000037\},$$

$$\boldsymbol{\theta}_{S_2^t|s_{2_2}^{t-1},b_1^t} = \left\{\theta_{s_{2_0}^t|s_{2_2}^{t-1},b_1^t}, \theta_{s_{2_1}^t|s_{2_2}^{t-1},b_1^t}, \theta_{s_{2_2}^t|s_{2_2}^{t-1},b_1^t}, \theta_{s_{2_3}^t|s_{2_2}^{t-1},b_1^t}, \theta_{s_{2_4}^t|s_{2_2}^{t-1},b_1^t}, \theta_{s_{2_5}^t|s_{2_2}^{t-1},b_1^t}\right\}$$
$$= \{0.000056, 0.000056, 0.999722, 0.000056, 0.000056, 0.000056\},$$

$$\boldsymbol{\theta}_{S_2^t|s_{2_3}^{t-1},b_1^t} = \left\{\theta_{s_{2_0}^t|s_{2_3}^{t-1},b_1^t}, \theta_{s_{2_1}^t|s_{2_3}^{t-1},b_1^t}, \theta_{s_{2_2}^t|s_{2_3}^{t-1},b_1^t}, \theta_{s_{2_3}^t|s_{2_3}^{t-1},b_1^t}, \theta_{s_{2_4}^t|s_{2_3}^{t-1},b_1^t}, \theta_{s_{2_5}^t|s_{2_3}^{t-1},b_1^t}\right\}$$
$$= \{0.000056, 0.000056, 0.000056, 0.999722, 0.000056, 0.000056\},$$

$$\boldsymbol{\theta}_{S_2^t|s_{2_4}^{t-1},b_1^t} = \left\{\theta_{s_{2_0}^t|s_{2_4}^{t-1},b_1^t}, \theta_{s_{2_1}^t|s_{2_4}^{t-1},b_1^t}, \theta_{s_{2_2}^t|s_{2_4}^{t-1},b_1^t}, \theta_{s_{2_3}^t|s_{2_4}^{t-1},b_1^t}, \theta_{s_{2_4}^t|s_{2_4}^{t-1},b_1^t}, \theta_{s_{2_5}^t|s_{2_4}^{t-1},b_1^t}\right\}$$
$$= \{0.000111, 0.000111, 0.000111, 0.000111, 0.999445, 0.000111\},$$

$$\boldsymbol{\theta}_{S_2^t|s_{2_5}^{t-1},b_1^t} = \left\{\theta_{s_{2_0}^t|s_{2_5}^{t-1},b_1^t}, \theta_{s_{2_1}^t|s_{2_5}^{t-1},b_1^t}, \theta_{s_{2_2}^t|s_{2_5}^{t-1},b_1^t}, \theta_{s_{2_3}^t|s_{2_5}^{t-1},b_1^t}, \theta_{s_{2_4}^t|s_{2_5}^{t-1},b_1^t}, \theta_{s_{2_5}^t|s_{2_5}^{t-1},b_1^t}\right\}$$
$$= \{0.166667, 0.166667, 0.166667, 0.166667, 0.166667, 0.166667\},$$

$$\boldsymbol{\theta}_{S_2^t|s_{2_0}^{t-1},b_2^t} = \left\{\theta_{s_{2_0}^t|s_{2_0}^{t-1},b_2^t}, \theta_{s_{2_1}^t|s_{2_0}^{t-1},b_2^t}, \theta_{s_{2_2}^t|s_{2_0}^{t-1},b_2^t}, \theta_{s_{2_3}^t|s_{2_0}^{t-1},b_2^t}, \theta_{s_{2_4}^t|s_{2_0}^{t-1},b_2^t}, \theta_{s_{2_5}^t|s_{2_0}^{t-1},b_2^t}\right\}$$
$$= \{0.999889, 0.000022, 0.000022, 0.000022, 0.000022, 0.000022\},$$

$$\boldsymbol{\theta}_{S_2^t|s_{2_1}^{t-1},b_2^t} = \left\{\theta_{s_{2_0}^t|s_{2_1}^{t-1},b_2^t}, \theta_{s_{2_1}^t|s_{2_1}^{t-1},b_2^t}, \theta_{s_{2_2}^t|s_{2_1}^{t-1},b_2^t}, \theta_{s_{2_3}^t|s_{2_1}^{t-1},b_2^t}, \theta_{s_{2_4}^t|s_{2_1}^{t-1},b_2^t}, \theta_{s_{2_5}^t|s_{2_1}^{t-1},b_2^t}\right\}$$
$$= \{0.000056, 0.999722, 0.000056, 0.000056, 0.000056, 0.000056\},$$

$$\boldsymbol{\theta}_{S_2^t|s_{2_2}^{t-1},b_2^t} = \left\{\theta_{s_{2_0}^t|s_{2_2}^{t-1},b_2^t}, \theta_{s_{2_1}^t|s_{2_2}^{t-1},b_2^t}, \theta_{s_{2_2}^t|s_{2_2}^{t-1},b_2^t}, \theta_{s_{2_3}^t|s_{2_2}^{t-1},b_2^t}, \theta_{s_{2_4}^t|s_{2_2}^{t-1},b_2^t}, \theta_{s_{2_5}^t|s_{2_2}^{t-1},b_2^t}\right\}$$
$$= \{0.000037, 0.000037, 0.999815, 0.000037, 0.000037, 0.000037\},$$

$$\boldsymbol{\theta}_{S_2^t|s_{23}^{t-1},b_2^t} = \left\{\theta_{s_{20}^t|s_{23}^{t-1},b_2^t}, \theta_{s_{21}^t|s_{23}^{t-1},b_2^t}, \theta_{s_{22}^t|s_{23}^{t-1},b_2^t}, \theta_{s_{23}^t|s_{23}^{t-1},b_2^t}, \theta_{s_{24}^t|s_{23}^{t-1},b_2^t}, \theta_{s_{25}^t|s_{23}^{t-1},b_2^t}\right\}$$
$$= \{0.000111, 0.000111, 0.000111, 0.999445, 0.000111, 0.000111\},$$

$$\boldsymbol{\theta}_{S_2^t|s_{24}^{t-1},b_2^t} = \left\{\theta_{s_{20}^t|s_{24}^{t-1},b_2^t}, \theta_{s_{21}^t|s_{24}^{t-1},b_2^t}, \theta_{s_{22}^t|s_{24}^{t-1},b_2^t}, \theta_{s_{23}^t|s_{24}^{t-1},b_2^t}, \theta_{s_{24}^t|s_{24}^{t-1},b_2^t}, \theta_{s_{25}^t|s_{24}^{t-1},b_2^t}\right\}$$
$$= \{0.000111, 0.000111, 0.000111, 0.000111, 0.999445, 0.000111\},$$

$$\boldsymbol{\theta}_{S_2^t|s_{25}^{t-1},b_2^t} = \left\{\theta_{s_{20}^t|s_{25}^{t-1},b_2^t}, \theta_{s_{21}^t|s_{25}^{t-1},b_2^t}, \theta_{s_{22}^t|s_{25}^{t-1},b_2^t}, \theta_{s_{23}^t|s_{25}^{t-1},b_2^t}, \theta_{s_{24}^t|s_{25}^{t-1},b_2^t}, \theta_{s_{25}^t|s_{25}^{t-1},b_2^t}\right\}$$
$$= \{0.166667, 0.166667, 0.166667, 0.166667, 0.166667, 0.166667\}.$$

Distribution $\mathrm{p}\left(\mathrm{F}_9^t, \mathrm{F}_{29}^t, \mathrm{F}_{37}^t, \mathrm{F}_{58}^t, \mathrm{F}_{48}^t, \mathrm{F}_{43}^t | \mathrm{S}_2^t, \mathrm{B}^t : \boldsymbol{\theta}_{\mathrm{F}_9^t,\ldots,\mathrm{F}_{43}^t|\mathrm{S}_2^t,\mathrm{B}^t}\right)$

The distribution $p\left(F_9^t, F_{29}^t, F_{37}^t, F_{58}^t, F_{48}^t, F_{43}^t | S_2^t, B^t : \boldsymbol{\theta}_{F_9^t,\ldots,F_{43}^t|S_2^t,B^t}\right)$ over a six-dimensional vector of continuous variables $(F_9, F_{29}, F_{37}, F_{58}, F_{48}, F_{43})$ at time slice $t \geq 1$ is a collection of multivariate Gaussian distributions with a multivariate Gaussian

$$p\left(F_9^t, F_{29}^t, F_{37}^t, F_{58}^t, F_{48}^t, F_{43}^t \mid s_2^t, b^t : \boldsymbol{\theta}_{F_9^t,\ldots,F_{43}^t|s_2^t,b^t}\right) = \mathcal{N}\left(\boldsymbol{\mu}_{s_2^t|b^t{}_i}, \Sigma_{s_2^t|b^t{}_i}\right)$$

for each $\{s_2^{t-1}, b^t\} \in \mathrm{Val}(S_2) \times \mathrm{Val}(B)$, parameterized with MAP parameters

$$\boldsymbol{\theta}_{F_9^t,\ldots,F_{43}^t|S_2^t,B^t}$$
$$= \begin{Bmatrix} \boldsymbol{\theta}_{F_9^t,\ldots,F_{43}^t|s_{20}^t,b_0^t}, \boldsymbol{\theta}_{F_9^t,\ldots,F_{43}^t|s_{21}^t,b_0^t}, \boldsymbol{\theta}_{F_9^t,\ldots,F_{43}^t|s_{22}^t,b_0^t}, \boldsymbol{\theta}_{F_9^t,\ldots,F_{43}^t|s_{23}^t,b_0^t}, \boldsymbol{\theta}_{F_9^t,\ldots,F_{43}^t|s_{24}^t,b_0^t}, \boldsymbol{\theta}_{F_9^t,\ldots,F_{43}^t|s_{25}^t,b_0^t}, \\ \boldsymbol{\theta}_{F_9^t,\ldots,F_{43}^t|s_{20}^t,b_1^t}, \boldsymbol{\theta}_{F_9^t,\ldots,F_{43}^t|s_{21}^t,b_1^t}, \boldsymbol{\theta}_{F_9^t,\ldots,F_{43}^t|s_{22}^t,b_1^t}, \boldsymbol{\theta}_{F_9^t,\ldots,F_{43}^t|s_{23}^t,b_1^t}, \boldsymbol{\theta}_{F_9^t,\ldots,F_{43}^t|s_{24}^t,b_1^t}, \boldsymbol{\theta}_{F_9^t,\ldots,F_{43}^t|s_{25}^t,b_1^t}, \\ \boldsymbol{\theta}_{F_9^t,\ldots,F_{43}^t|s_{20}^t,b_2^t}, \boldsymbol{\theta}_{F_9^t,\ldots,F_{43}^t|s_{21}^t,b_2^t}, \boldsymbol{\theta}_{F_9^t,\ldots,F_{43}^t|s_{22}^t,b_2^t}, \boldsymbol{\theta}_{F_9^t,\ldots,F_{43}^t|s_{23}^t,b_2^t}, \boldsymbol{\theta}_{F_9^t,\ldots,F_{43}^t|s_{24}^t,b_2^t}, \boldsymbol{\theta}_{F_9^t,\ldots,F_{43}^t|s_{25}^t,b_2^t} \end{Bmatrix},$$

where

$$\boldsymbol{\theta}_{F_9^t,\ldots,F_{43}^t|s_{20}^t,b_0^t} = \left\{\boldsymbol{\mu}_{s_{20}^t,b_0^t} = \mathbf{0}_6, \Sigma_{s_{20}^t,b_0^t} = \mathbf{I}_6\right\},$$

$$\boldsymbol{\theta}_{\left(F_9^t,\ldots,F_{43}^t|s_{21}^t,b_0^t\right)} = \left\{\boldsymbol{\mu}_{s_{21}^t,b_0^t}, \Sigma_{s_{21}^t,b_0^t}\right\}, \boldsymbol{\mu}_{s_{21}^t,b_0^t} = \begin{pmatrix} 0.25416 \\ 0.206493 \\ 19.739553 \\ 20.801873 \\ 33.146397 \\ 268.312292 \end{pmatrix},$$

$$\Sigma_{s_{21}^t,b_0^t} = \begin{bmatrix} 0.021664 & 0.011189 & -0.996966 & -0.153596 & -1.20389 & -2.108719 \\ 0.011189 & 0.014358 & -1.227966 & -0.506122 & -1.919624 & -4.918942 \\ -0.996966 & -1.227966 & 806.477585 & 189.908541 & 220.089933 & -95.177338 \\ -0.153596 & -0.506122 & 189.908541 & 644.533419 & 97.99755 & -204.852486 \\ -1.20389 & -1.919624 & 220.089933 & 97.99755 & 761.229456 & 976.268992 \\ -2.108719 & -4.918942 & -95.177338 & -204.852486 & 976.268992 & 5435.290231 \end{bmatrix}$$

$$\boldsymbol{\theta}_{\left(F_9^t,\ldots,F_{43}^t|s_{22}^t,b_0^t\right)} = \left\{\boldsymbol{\mu}_{s_{22}^t,b_0^t}, \Sigma_{s_{22}^t,b_0^t}\right\}, \boldsymbol{\mu}_{s_{22}^t,b_0^t} = \begin{pmatrix} 0.142942 \\ 0.418991 \\ 7.489884 \\ 30.799829 \\ 8.777225 \\ 379.772007 \end{pmatrix},$$

$$\Sigma_{s_{2_2}^t, b_0^t} = \begin{bmatrix} 0.015559 & -0.005773 & 0.172442 & -0.14071 & 0.31914 & -0.608281 \\ -0.005773 & 0.014966 & -0.032715 & 0.483853 & -0.48481 & 0.598988 \\ 0.172442 & -0.032715 & 861.858642 & 29.946693 & 34.521898 & -50.90591 \\ -0.14071 & 0.483853 & 29.946693 & 967.491978 & 13.723146 & 10.415277 \\ 0.31914 & -0.48481 & 34.521898 & 13.723146 & 831.88557 & -52.674455 \\ -0.608281 & 0.598988 & -50.90591 & 10.415277 & -52.674455 & 754.618703 \end{bmatrix},$$

$$\boldsymbol{\theta}\left(F_9^t, \dots, F_{43}^t \middle| s_{2_3}^t, b_0^t\right) = \left\{\boldsymbol{\mu}_{s_{2_3}^t, b_0^t}, \Sigma_{s_{2_3}^t, b_0^t}\right\}, \boldsymbol{\mu}_{s_{2_3}^t, b_0^t} = \begin{pmatrix} 0.473825 \\ 0.364269 \\ 28.809672 \\ 23.857914 \\ 10.557547 \\ 237.164465 \end{pmatrix},$$

$$\Sigma_{s_{2_3}^t, b_0^t} = \begin{bmatrix} 0.029737 & -0.008313 & -0.268651 & -0.550772 & -0.358145 & 13.953635 \\ -0.008313 & 0.050338 & -2.401457 & 0.718546 & -0.870473 & 11.155746 \\ -0.268651 & -2.401457 & 492.673413 & -25.412124 & 70.051296 & -1255.937296 \\ -0.550772 & 0.718546 & -25.412124 & 869.433086 & 0.733184 & -774.906122 \\ -0.358145 & -0.870473 & 70.051296 & 0.733184 & 315.744478 & -552.235336 \\ 13.953635 & 11.155746 & -1255.937296 & -774.906122 & -552.235336 & 20866.00079 \end{bmatrix},$$

$$\boldsymbol{\theta}\left(F_9^t, \dots, F_{43}^t \middle| s_{2_4}^t, b_0^t\right) = \left\{\boldsymbol{\mu}_{s_{2_4}^t, b_0^t}, \Sigma_{s_{2_4}^t, b_0^t}\right\}, \boldsymbol{\mu}_{s_{2_4}^t, b_0^t} = \begin{pmatrix} 0.39457 \\ 0.373188 \\ 24.148939 \\ 138.481251 \\ 19.114328 \\ 285.963803 \end{pmatrix},$$

$$\Sigma_{s_{2_4}^t, b_0^t} = \begin{bmatrix} 0.033501 & 0.01916 & -1.942912 & 12.317297 & -0.284933 & 1.353682 \\ 0.01916 & 0.04867 & -2.462218 & -2.719917 & -2.819569 & 10.177529 \\ -1.942912 & -2.462218 & 723.685007 & -1260.496957 & 95.313907 & -669.628314 \\ 12.317297 & -2.719917 & -1260.496957 & 15123.09615 & 189.483076 & 2359.948821 \\ -0.284933 & -2.819569 & 95.313907 & 189.483076 & 554.239458 & -1878.363915 \\ 1.353682 & 10.177529 & -669.628314 & 2359.948821 & -1878.363915 & 10797.43962 \end{bmatrix},$$

$$\boldsymbol{\theta}\left(F_9^t, \dots, F_{43}^t \middle| s_{2_5}^t, b_0^t\right) = \left\{\boldsymbol{\mu}_{s_{2_5}^t, b_0^t}, \Sigma_{s_{2_5}^t, b_0^t}\right\}, \boldsymbol{\mu}_{s_{2_5}^t, b_0^t} = \begin{pmatrix} 0.412906 \\ 0.517721 \\ 5.900671 \\ 90.72619 \\ 7.290656 \\ 110.274789 \end{pmatrix},$$

$$\Sigma_{s_{2_5}^t, b_0^t} = \begin{bmatrix} 0.081413 & 0.01742 & 0.349533 & 0.664036 & 0.24013 & 1.728873 \\ 0.01742 & 0.035951 & 0.332084 & 1.293921 & -0.390324 & 0.483444 \\ 0.349533 & 0.332084 & 859.482656 & 25.943369 & 35.392346 & 80.032522 \\ 0.664036 & 1.293921 & 25.943369 & 965.747175 & -10.019212 & 43.181929 \\ 0.24013 & -0.390324 & 35.392346 & -10.019212 & 827.129709 & 65.310913 \\ 1.728873 & 0.483444 & 80.032522 & 43.181929 & 65.310913 & 864.928902 \end{bmatrix},$$

$$\boldsymbol{\theta}\left(F_9^t, \dots, F_{43}^t \middle| s_{2_0}^t, b_1^t\right) = \left\{\boldsymbol{\mu}_{s_{2_0}^t, b_1^t}, \Sigma_{s_{2_0}^t, b_1^t}\right\}, \boldsymbol{\mu}_{s_{2_0}^t, b_1^t} = \begin{pmatrix} 0.595107 \\ 0.232422 \\ 90.401967 \\ 234.905145 \\ 87.606857 \\ 339.79358 \end{pmatrix},$$

$$\Sigma_{s_{2_0}^t, b_1^t} = \begin{bmatrix} 0.140894 & -0.012344 & -15.230819 & 17.587954 & -16.173299 & -1.803888 \\ -0.012344 & 0.033541 & -15.216234 & -15.092331 & -14.986473 & 4.72856 \\ -15.230819 & -15.216234 & 16831.0998 & 4985.349171 & 16348.97782 & -2297.710775 \\ 17.587954 & -15.092331 & 4985.349171 & 14328.5032 & 5004.030842 & -4095.468835 \\ -16.173299 & -14.986473 & 16348.97782 & 5004.030842 & 16441.93591 & -2335.837053 \\ -1.803888 & 4.72856 & -2297.710775 & -4095.468835 & -2335.837053 & 1565.743631 \end{bmatrix},$$

$$\boldsymbol{\theta}\left(F_9^t, \dots, F_{43}^t \middle| s_{2_1}^t, b_1^t\right) = \left\{\boldsymbol{\mu}_{s_{2_1}^t, b_1^t}, \Sigma_{s_{2_1}^t, b_1^t}\right\}, \boldsymbol{\mu}_{s_{2_1}^t, b_1^t} = \begin{pmatrix} 0.738945 \\ 0.172137 \\ 173.345836 \\ 263.914319 \\ 142.318901 \\ 313.910715 \end{pmatrix},$$

$$\Sigma_{s_{2_1}^t, b_1^t} = \begin{bmatrix} 0.159557 & 0.010595 & 43.944285 & 7.589395 & 32.008288 & 14.066987 \\ 0.010595 & 0.007552 & 9.477462 & 5.616635 & 11.557152 & 2.470735 \\ 43.944285 & 9.477462 & 22686.9873 & 9338.124775 & 22673.28104 & 6441.469264 \\ 7.589395 & 5.616635 & 9338.124775 & 6482.986216 & 12003.72706 & 2544.731919 \\ 32.008288 & 11.557152 & 22673.28104 & 12003.72706 & 26134.53842 & 6338.091277 \\ 14.066987 & 2.470735 & 6441.469264 & 2544.731919 & 6338.091277 & 2134.596132 \end{bmatrix},$$

$$\boldsymbol{\theta}\left(F_9^t, \dots, F_{43}^t \middle| s_{2_2}^t, b_1^t\right) = \left\{\boldsymbol{\mu}_{s_{2_2}^t, b_1^t}, \Sigma_{s_{2_2}^t, b_1^t}\right\}, \boldsymbol{\mu}_{s_{2_2}^t, b_1^t} = \begin{pmatrix} 0.231236 \\ 0.323838 \\ 12.920803 \\ 243.007166 \\ 174.34943 \\ 174.956048 \end{pmatrix},$$

$$\Sigma_{s_{2_2}^t, b_1^t} = \begin{bmatrix} 0.024237 & 0.027957 & -0.319945 & -9.955709 & -18.301109 & -18.091668 \\ 0.027957 & 0.09526 & -1.66069 & -19.145809 & -38.173754 & -38.198766 \\ -0.319945 & -1.66069 & 511.83414 & 237.750829 & 504.357273 & 545.426078 \\ -9.955709 & -19.145809 & 237.750829 & 8530.134555 & 14990.58837 & 14912.00879 \\ -18.301109 & -38.173754 & 504.357273 & 14990.58837 & 28433.60766 & 27978.48322 \\ -18.091668 & -38.198766 & 545.426078 & 14912.00879 & 27978.48322 & 28333.25558 \end{bmatrix},$$

$$\boldsymbol{\theta}\left(F_9^t, \dots, F_{43}^t \middle| s_{2_3}^t, b_1^t\right) = \left\{\boldsymbol{\mu}_{s_{2_3}^t, b_1^t}, \Sigma_{s_{2_3}^t, b_1^t}\right\}, \boldsymbol{\mu}_{s_{2_3}^t, b_1^t} = \begin{pmatrix} 0.795342 \\ 0.247887 \\ 18.195552 \\ 182.408735 \\ 10.043302 \\ 196.429265 \end{pmatrix},$$

$$\Sigma_{s_{2_3}^t, b_1^t} = \begin{bmatrix} 0.10742 & 0.013033 & 3.377493 & 37.374425 & -1.84495 & -43.915537 \\ 0.013033 & 0.009629 & 0.246827 & 4.008596 & -0.512561 & -4.936444 \\ 3.377493 & 0.246827 & 641.573267 & 1088.027853 & -33.239301 & -1331.726652 \\ 37.374425 & 4.008596 & 1088.027853 & 15098.11576 & -614.329686 & -16786.58226 \\ -1.84495 & -0.512561 & -33.239301 & -614.329686 & 464.409421 & 779.493917 \\ -43.915537 & -4.936444 & -1331.726652 & -16786.58226 & 779.493917 & 19891.54877 \end{bmatrix},$$

$$\boldsymbol{\theta}\left(F_9^t, \dots, F_{43}^t \middle| s_{2_4}^t, b_1^t\right) = \left\{\boldsymbol{\mu}_{s_{2_4}^t, b_1^t}, \Sigma_{s_{2_4}^t, b_1^t}\right\}, \boldsymbol{\mu}_{s_{2_4}^t, b_1^t} = \begin{pmatrix} 0.634893 \\ 0.009772 \\ 122.404276 \\ 302.298016 \\ 305.327392 \\ 326.126765 \end{pmatrix},$$

$$\Sigma_{s_{2_4}^t,b_1^t} = \begin{bmatrix} 0.014806 & -0.000021 & -0.396602 & -0.359113 & -0.353525 & -0.393714 \\ -0.000021 & 0.002432 & -0.042878 & -0.240838 & -0.270348 & -0.05813 \\ -0.396602 & -0.042878 & 883.705816 & 106.41717 & 110.454865 & 81.418118 \\ -0.359113 & -0.240838 & 106.41717 & 1166.858757 & 302.09783 & 119.537618 \\ -0.353525 & -0.270348 & 110.454865 & 302.09783 & 1116.113226 & 125.22009 \\ -0.393714 & -0.05813 & 81.418118 & 119.537618 & 125.22009 & 705.886129 \end{bmatrix}$$

$$\boldsymbol{\theta}_{F_9^t,\dots,F_{43}^t|s_{2_5}^t,b_1^t} = \left\{\boldsymbol{\mu}_{s_{2_5}^t,b_1^t} = \mathbf{0}_6, \Sigma_{s_{2_5}^t,b_1^t} = \mathbf{I}_6\right\},$$

$$\boldsymbol{\theta}_{\left(F_9^t,\dots,F_{43}^t|s_{2_0}^t,b_2^t\right)} = \left\{\boldsymbol{\mu}_{s_{2_0}^t,b_2^t}, \Sigma_{s_{2_0}^t,b_2^t}\right\}, \boldsymbol{\mu}_{s_{2_0}^t,b_2^t} = \begin{pmatrix} 0.830996 \\ 0.090047 \\ 292.783443 \\ 0.447627 \\ 158.004356 \\ 329.6378 \end{pmatrix},$$

$$\Sigma_{s_{2_0}^t,b_2^t} = \begin{bmatrix} 0.357915 & 0.007631 & 15.743036 & 0.086074 & 44.785055 & 3.441359 \\ 0.007631 & 0.009826 & -2.570279 & 0.0435 & -4.94363 & -0.269057 \\ 15.743036 & -2.570279 & 3449.412216 & -24.530217 & 4226.350474 & 643.288114 \\ 0.086074 & 0.0435 & -24.530217 & 191.819296 & -20.793373 & -5.806066 \\ 44.785055 & -4.94363 & 4226.350474 & -20.793373 & 14688.23939 & 761.456447 \\ 3.441359 & -0.269057 & 643.288114 & -5.806066 & 761.456447 & 302.306021 \end{bmatrix},$$

$$\boldsymbol{\theta}_{\left(F_9^t,\dots,F_{43}^t|s_{2_1}^t,b_2^t\right)} = \left\{\boldsymbol{\mu}_{s_{2_1}^t,b_2^t}, \Sigma_{s_{2_1}^t,b_2^t}\right\}, \boldsymbol{\mu}_{s_{2_1}^t,b_2^t} = \begin{pmatrix} 0.85674 \\ 0.107999 \\ 37.783104 \\ 0.408832 \\ 273.234789 \\ 323.42079 \end{pmatrix},$$

$$\Sigma_{s_{2_1}^t,b_2^t} = \begin{bmatrix} 0.658764 & 0.020224 & -21.082992 & -0.007118 & 47.658595 & 11.940192 \\ 0.020224 & 0.003707 & -0.682411 & 0.03931 & 1.176215 & 0.418258 \\ -21.082992 & -0.682411 & 1183.315136 & 12.982466 & -1559.791637 & -340.539708 \\ -0.007118 & 0.03931 & 12.982466 & 477.618297 & -48.349075 & -10.263017 \\ 47.658595 & 1.176215 & -1559.791637 & -48.349075 & 4317.18863 & 965.598977 \\ 11.940192 & 0.418258 & -340.539708 & -10.263017 & 965.598977 & 607.313353 \end{bmatrix},$$

$$\boldsymbol{\theta}_{\left(F_9^t,\dots,F_{43}^t|s_{2_2}^t,b_2^t\right)} = \left\{\boldsymbol{\mu}_{s_{2_2}^t,b_2^t}, \Sigma_{s_{2_2}^t,b_2^t}\right\}, \boldsymbol{\mu}_{s_{2_2}^t,b_2^t} = \begin{pmatrix} 1.103645 \\ 0.189355 \\ 146.244457 \\ 0.570633 \\ 39.062319 \\ 330.208372 \end{pmatrix},$$

$$\Sigma_{s_{2_2}^t,b_2^t} = \begin{bmatrix} 0.166934 & -0.03969 & -8.107871 & -0.135273 & 14.005111 & 2.109467 \\ -0.03969 & 0.017391 & 10.009421 & 0.01639 & -5.065516 & -0.444925 \\ -8.107871 & 10.009421 & 23908.69712 & -20.506435 & -2353.799037 & 1081.35742 \\ -0.135273 & 0.01639 & -20.506435 & 318.963941 & 4.622211 & -10.49249 \\ 14.005111 & -5.065516 & -2353.799037 & 4.622211 & 2352.797466 & 343.372568 \\ 2.109467 & -0.444925 & 1081.35742 & -10.49249 & 343.372568 & 502.52761 \end{bmatrix},$$

$$\boldsymbol{\theta}_{\left(F_9^t,\dots,F_{43}^t|s_{2_3}^t,b_2^t\right)} = \left\{\boldsymbol{\mu}_{s_{2_3}^t,b_2^t}, \Sigma_{s_{2_3}^t,b_2^t}\right\}, \boldsymbol{\mu}_{s_{2_3}^t,b_2^t} = \begin{pmatrix} 0.333467 \\ 0.079297 \\ 36.979923 \\ 0.954912 \\ 10.832667 \\ 29.548558 \end{pmatrix},$$

$$\Sigma_{s_{2_3}^t,b_2^t} = \begin{bmatrix} 0.022864 & -0.001125 & 0.519519 & 0.169205 & 0.016895 & 0.791646 \\ -0.001125 & 0.005346 & -0.107511 & 0.086557 & -0.083356 & 0.058438 \\ 0.519519 & -0.107511 & 894.25402 & 33.070347 & 16.259848 & 147.112603 \\ 0.169205 & 0.086557 & 33.070347 & 949.829709 & 41.576117 & 144.662086 \\ 0.016895 & -0.083356 & 16.259848 & 41.576117 & 826.730276 & 94.848443 \\ 0.791646 & 0.058438 & 147.112603 & 144.662086 & 94.848443 & 1034.903459 \end{bmatrix},$$

$$\boldsymbol{\theta}_{\left(F_9^t,\dots,F_{43}^t \middle| s_{2_4}^t, b_2^t\right)} = \left\{\boldsymbol{\mu}_{s_{2_4}^t,b_2^t}, \Sigma_{s_{2_4}^t,b_2^t}\right\}, \boldsymbol{\mu}_{s_{2_4}^t,b_2^t} = \begin{pmatrix} 0.252823 \\ 0.170498 \\ 15.317519 \\ 0.842103 \\ 17.282309 \\ 311.126797 \end{pmatrix},$$

$$\Sigma_{s_{2_4}^t,b_2^t} = \begin{bmatrix} 0.016896 & 0.00214 & -0.010996 & 0.193791 & -0.076299 & -0.337917 \\ 0.00214 & 0.003884 & 0.141538 & 0.040482 & -0.109133 & -0.328413 \\ -0.010996 & 0.141538 & 908.860054 & 42.783626 & 30.791135 & -30.694725 \\ 0.193791 & 0.040482 & 42.783626 & 949.861235 & 37.798671 & -17.025377 \\ -0.076299 & -0.109133 & 30.791135 & 37.798671 & 857.393711 & 26.941589 \\ -0.337917 & -0.328413 & -30.694725 & -17.025377 & 26.941589 & 700.119449 \end{bmatrix},$$

$$\boldsymbol{\theta}_{F_9^t,\dots,F_{43}^t | s_{2_5}^t, b_2^t} = \left\{\boldsymbol{\mu}_{s_{2_5}^t,b_2^t} = \mathbf{0}_6, \Sigma_{s_{2_5}^t,b_2^t} = \mathbf{I}_6\right\}.$$

Distribution $\mathrm{p}\left(\mathrm{F}_{16}^{\mathrm{t}} | \mathrm{S}_2^{\mathrm{t}}, \mathrm{B}^{\mathrm{t}} : \boldsymbol{\theta}_{\mathrm{F}_{16}^{\mathrm{t}} | \mathrm{S}_2^{\mathrm{t}}, \mathrm{B}^{\mathrm{t}}}\right)$

The distribution $p\left(F_{16}^t | S_2^t, B^t : \boldsymbol{\theta}_{F_{16}^t | S_2^t, B^t}\right)$ over the continuous variable F_{16} at time slice $t \geq 1$ is a collection of exponential distributions with an exponential distribution

$$p\left(F_{16}^t \mid s_2^t, b^t : \lambda_{F_{16}^t | s_2^t, b^t}\right) = \mathrm{Expon}\left(F_{16}^t : \lambda_{F_{27}^t | s_2^t, b^t}\right)$$

for each $\{s_2^t, b^t\} \in \mathrm{Val}(S_2) \times \mathrm{Val}(B)$, parameterized with MAP parameters

$$\boldsymbol{\theta}_{F_{16}^t | S_2^{t-1}, B^t} = \begin{Bmatrix} \lambda_{F_{16}^t | s_{2_0}^t, b_0^t}, \lambda_{F_{16}^t | s_{2_1}^t, b_0^t}, \lambda_{F_{16}^t | s_{2_2}^t, b_0^t}, \lambda_{F_{16}^t | s_{2_3}^t, b_0^t}, \lambda_{F_{16}^t | s_{2_4}^t, b_0^t}, \lambda_{F_{16}^t | s_{2_5}^t, b_0^t}, \\ \lambda_{F_{16}^t | s_{2_0}^t, b_1^t}, \lambda_{F_{16}^t | s_{2_1}^t, b_1^t}, \lambda_{F_{16}^t | s_{2_2}^t, b_1^t}, \lambda_{F_{16}^t | s_{2_3}^t, b_1^t}, \lambda_{F_{16}^t | s_{2_4}^t, b_1^t}, \lambda_{F_{16}^t | s_{2_5}^t, b_1^t}, \\ \lambda_{F_{16}^t | s_{2_0}^t, b_2^t}, \lambda_{F_{16}^t | s_{2_1}^t, b_2^t}, \lambda_{F_{16}^t | s_{2_2}^t, b_2^t}, \lambda_{F_{16}^t | s_{2_3}^t, b_2^t}, \lambda_{F_{16}^t | s_{2_4}^t, b_2^t}, \lambda_{F_{16}^t | s_{2_5}^t, b_2^t} \end{Bmatrix}$$

$$= \begin{Bmatrix} 1.802294, 3.898802, 6.793419, 8.56839, 6.293131, 2.838265, \\ 8.153475, 7.438100, 3.772352, 4.837875, 16.684276, 1.802294, \\ 1.607410, 1.430535, 2.237311, 3.569599, 5.083055, 1.802294 \end{Bmatrix}.$$

Distribution $\mathrm{p}\left(\mathrm{F}_{32}^{\mathrm{t}} | \mathrm{S}_2^{\mathrm{t}}, \mathrm{B}^{\mathrm{t}} : \boldsymbol{\theta}_{\mathrm{F}_{32}^{\mathrm{t}} | \mathrm{S}_2^{\mathrm{t}}, \mathrm{B}^{\mathrm{t}}}\right)$

The distribution $p\left(F_{32}^t | S_2^t, B^t : \boldsymbol{\theta}_{F_{32}^t | S_2^t, B^t}\right)$ over the continuous variable F_{32} at time slice $t \geq 1$ is a collection of Gaussian distributions with Gaussian distribution

$$p\left(F_{32}^t \mid s_2^t, b^t : \boldsymbol{\theta}_{F_{47}^t | s_2^t, b^t}\right) = \mathcal{N}\left(\mu_{s_2^t | b^t{}_i}, \sigma^2_{s_2^t | b^t{}_i}\right)$$

for each $\{s_2^t, b^t\} \in \mathrm{Val}(S_2) \times \mathrm{Val}(B)$, parameterized with MAP parameters

$$\boldsymbol{\theta}_{F_{32}^t | S_2^{t-1}, B^t} = \begin{Bmatrix} \boldsymbol{\theta}_{F_{32}^t | s_{2_0}^t, b_0^t}, \boldsymbol{\theta}_{F_{32}^t | s_{2_1}^t, b_0^t}, \boldsymbol{\theta}_{F_{32}^t | s_{2_2}^t, b_0^t}, \boldsymbol{\theta}_{F_{32}^t | s_{2_3}^t, b_0^t}, \boldsymbol{\theta}_{F_{32}^t | s_{2_4}^t, b_0^t}, \boldsymbol{\theta}_{F_{32}^t | s_{2_5}^t, b_0^t}, \\ \boldsymbol{\theta}_{F_{32}^t | s_{2_0}^t, b_1^t}, \boldsymbol{\theta}_{F_{32}^t | s_{2_1}^t, b_1^t}, \boldsymbol{\theta}_{F_{32}^t | s_{2_2}^t, b_1^t}, \boldsymbol{\theta}_{F_{32}^t | s_{2_3}^t, b_1^t}, \boldsymbol{\theta}_{F_{32}^t | s_{2_4}^t, b_1^t}, \boldsymbol{\theta}_{F_{32}^t | s_{2_5}^t, b_1^t}, \\ \boldsymbol{\theta}_{F_{32}^t | s_{2_0}^t, b_2^t}, \boldsymbol{\theta}_{F_{32}^t | s_{2_1}^t, b_2^t}, \boldsymbol{\theta}_{F_{32}^t | s_{2_2}^t, b_2^t}, \boldsymbol{\theta}_{F_{32}^t | s_{2_3}^t, b_2^t}, \boldsymbol{\theta}_{F_{32}^t | s_{2_4}^t, b_2^t}, \boldsymbol{\theta}_{F_{32}^t | s_{2_5}^t, b_2^t} \end{Bmatrix},$$

where

$$\boldsymbol{\theta}_{F_{32}^t|s_{2_0}^t,b_0^t} = \left\{\mu_{s_{2_0}^t,b_0^t} = 0, \sigma^2_{s_{2_0}^t,b_0^t} = 1\right\},$$

$$\boldsymbol{\theta}_{F_{32}^t|s_{2_1}^t,b_0^t} = \left\{\mu_{s_{2_1}^t,b_0^t} = 0.931409, \sigma^2_{s_{2_1}^t,b_0^t} = 0.212766\right\},$$

$$\boldsymbol{\theta}_{F_{32}^t|s_{2_2}^t,b_0^t} = \left\{\mu_{s_{2_2}^t,b_0^t} = 0.67003, \sigma^2_{s_{2_2}^t,b_0^t} = 7.866056\right\},$$

$$\boldsymbol{\theta}_{F_{32}^t|s_{2_3}^t,b_0^t} = \left\{\mu_{s_{2_3}^t,b_0^t} = 1.289185, \sigma^2_{s_{2_3}^t,b_0^t} = 0.06671\right\},$$

$$\boldsymbol{\theta}_{F_{32}^t|s_{2_4}^t,b_0^t} = \left\{\mu_{s_{2_4}^t,b_0^t} = 1.297627, \sigma^2_{s_{2_4}^t,b_0^t} = 0.263065\right\},$$

$$\boldsymbol{\theta}_{F_{32}^t|s_{2_5}^t,b_0^t} = \left\{\mu_{s_{2_5}^t,b_0^t} = 1.117723, \sigma^2_{s_{2_5}^t,b_0^t} = 0.159476\right\},$$

$$\boldsymbol{\theta}_{F_{32}^t|s_{2_0}^t,b_1^t} = \left\{\mu_{s_{2_0}^t,b_1^t} = 0.992138, \sigma^2_{s_{2_0}^t,b_1^t} = 0.172061\right\},$$

$$\boldsymbol{\theta}_{F_{32}^t|s_{2_1}^t,b_1^t} = \left\{\mu_{s_{2_1}^t,b_1^t} = 1.307334, \sigma^2_{s_{2_1}^t,b_1^t} = 0.185365\right\},$$

$$\boldsymbol{\theta}_{F_{32}^t|s_{2_2}^t,b_1^t} = \left\{\mu_{s_{2_2}^t,b_1^t} = 0.76432, \sigma^2_{s_{2_2}^t,b_1^t} = 0.270551\right\},$$

$$\boldsymbol{\theta}_{F_{32}^t|s_{2_3}^t,b_1^t} = \left\{\mu_{s_{2_3}^t,b_1^t} = 1.989994, \sigma^2_{s_{2_3}^t,b_1^t} = 0.142312\right\},$$

$$\boldsymbol{\theta}_{F_{32}^t|s_{2_4}^t,b_1^t} = \left\{\mu_{s_{2_4}^t,b_1^t} = 1.114495, \sigma^2_{s_{2_4}^t,b_1^t} = 0.034463\right\},$$

$$\boldsymbol{\theta}_{F_{32}^t|s_{2_5}^t,b_1^t} = \left\{\mu_{s_{2_5}^t,b_1^t} = 0, \sigma^2_{s_{2_5}^t,b_1^t} = 1\right\},$$

$$\boldsymbol{\theta}_{F_{32}^t|s_{2_0}^t,b_2^t} = \left\{\mu_{s_{2_0}^t,b_2^t} = 1.82755, \sigma^2_{s_{2_0}^t,b_2^t} = 0.471728\right\},$$

$$\boldsymbol{\theta}_{F_{32}^t|s_{2_1}^t,b_2^t} = \left\{\mu_{s_{2_1}^t,b_2^t} = 2.338860, \sigma^2_{s_{2_1}^t,b_2^t} = 0.117480\right\},$$

$$\boldsymbol{\theta}_{F_{32}^t|s_{2_2}^t,b_2^t} = \left\{\mu_{s_{2_2}^t,b_2^t} = 2.065790, \sigma^2_{s_{2_2}^t,b_2^t} = 0.082350\right\},$$

$$\boldsymbol{\theta}_{F_{32}^t|s_{2_3}^t,b_2^t} = \left\{\mu_{s_{2_3}^t,b_2^t} = 2.6244, \sigma^2_{s_{2_3}^t,b_2^t} = 0.346325\right\},$$

$$\boldsymbol{\theta}_{F_{32}^t|s_{2_4}^t,b_2^t} = \left\{\mu_{s_{2_4}^t,b_2^t} = 2.127334, \sigma^2_{s_{2_4}^t,b_2^t} = 0.119757\right\},$$

$$\boldsymbol{\theta}_{F_{32}^t|s_{2_5}^t,b_2^t} = \left\{\mu_{s_{2_5}^t,b_2^t} = 0, \sigma^2_{s_{2_5}^t,b_2^t} = 1\right\}.$$

Distribution $\mathrm{p}\left(\mathrm{F}_{67}^{\mathrm{t}}|\mathrm{S}_2^{\mathrm{t}}, \mathrm{B}^{\mathrm{t}} : \boldsymbol{\theta}_{\mathrm{F}_{67}^{\mathrm{t}}|\mathrm{S}_2^{\mathrm{t}},\mathrm{B}^{\mathrm{t}}}\right)$

The distribution $p\left(F_{67}^t|S_2^t, B^t : \boldsymbol{\theta}_{F_{67}^t|S_2^t,B^t}\right)$ over the continuous variable F_{67} at time slice $t \geq 1$ is a collection of exponential distributions with an exponential distribution

$$p\left(F_{67}^t \mid s_2^t, b^t : \lambda_{F_{47}^t|s_2^t,b^t}\right) = \mathrm{Expon}\left(F_{67}^t : \lambda_{F_{47}^t|s_2^t,b^t}\right)$$

for each $\{s_2^t, b^t\} \in \mathrm{Val}(S_2) \times \mathrm{Val}(B)$, parameterized with MAP parameters

$$\boldsymbol{\theta}_{F_{67}^t|S_2^{t-1},B^t} = \begin{Bmatrix} \lambda_{F_{67}^t|s_{2_0}^t,b_0^t}, \lambda_{F_{67}^t|s_{2_1}^t,b_0^t}, \lambda_{F_{67}^t|s_{2_2}^t,b_0^t}, \lambda_{F_{67}^t|s_{2_3}^t,b_0^t}, \lambda_{F_{67}^t|s_{2_4}^t,b_0^t}, \lambda_{F_{67}^t|s_{2_5}^t,b_0^t}, \\ \lambda_{F_{67}^t|s_{2_0}^t,b_1^t}, \lambda_{F_{67}^t|s_{2_1}^t,b_1^t}, \lambda_{F_{67}^t|s_{2_2}^t,b_1^t}, \lambda_{F_{67}^t|s_{2_3}^t,b_1^t}, \lambda_{F_{67}^t|s_{2_4}^t,b_1^t}, \lambda_{F_{67}^t|s_{2_5}^t,b_1^t}, \\ \lambda_{F_{67}^t|s_{2_0}^t,b_2^t}, \lambda_{F_{67}^t|s_{2_1}^t,b_2^t}, \lambda_{F_{67}^t|s_{2_2}^t,b_2^t}, \lambda_{F_{67}^t|s_{2_3}^t,b_2^t}, \lambda_{F_{67}^t|s_{2_4}^t,b_2^t}, \lambda_{F_{67}^t|s_{2_5}^t,b_2^t} \end{Bmatrix}$$

$$= \begin{Bmatrix} 0.080120, 0.073906, 0.101438, 0.072194, 0.168699, 0.530724, \\ 0.070365, 0.098471, 0.136746, 0.159795, 0.008179, 0.080120, \\ 0.128279, 0.093204, 0.096084, 0.22106, 0.351450, 0.080120 \end{Bmatrix}.$$

Appendix 3 DySAM Software

As an additional result of the project, this report is accompanied by the DySAM software appendix, comprised of executable applications (for Windows operating systems), exemplary data, and specification files that allow to utilize, test, and adapt the six models developed in DySAM. A separate document explaining the content and utilization of the DySAM software is provided as part of the DySAM software appendix.

Bisher in der FAT-Schriftenreihe erschienen (ab 2020)

Nr.	Titel
324	Methodische Aspekte und aktuelle inhaltliche Schwerpunkte bei der Konzeption experimenteller Studien zum hochautomatisierten Fahren, 2020
325	Der Einfluss von Wärmeverlusten auf den Rollwiderstand von Reifen, 2020
326	Lebensdauerberechnung hybrider Verbindungen, 2020
327	Entwicklung der Verletzungsschwere bei Verkehrsunfällen in Deutschland im Kontext verschiedener AIS-Revisionen, 2020
328	Entwicklung einer Methodik zur Korrektur von EES-Werten, 2020
329	Untersuchung zu den Einsatzmöglichkeiten der Graphen- und Heuristikbasierten Topologieoptimierung zur Entwicklung von 3D-Rahmenstrukturen in Crashlastfällen, 2020
330	Analyse der Einflussfaktoren auf die Abweichung zwischen CFD und Fahrversuch bei der Bestimmung des Luftwiderstands von Nutzfahrzeugen, 2020
331	Effiziente Charakterisierung und Modellierung des anisotropen Versagensverhaltens von LFT für Crashsimulation, 2020
332	Charakterisierung und Modellierung des Versagensverhaltens von Komponenten aus duktilem Gusseisen für die Crashsimulation, 2020
333	Charakterisierung und Meta-Modellierung von ungleichartigen Punktschweißverbindungen für die Crashsimulation, 2020
334	Simulationsgestützte Analyse und Bewertung der Fehlertoleranz von Kfz-Bordnetzen, 2020
335	Absicherung des autonomen Fahrens gegen EMV-bedingte Fehlfunktion, 2020
336	Auswirkung von instationären Anströmeffekten auf die Fahrzeugaerodynamik, 2020
337	Analyse von neuen Zell-Technologien und deren Auswirkungen auf das Gesamtsystem Batteriepack, 2020
338	Modellierung der Einflüsse von Mikrodefekten auf das Versagensverhalten von Al-Druckguss-komponenten mit stochastischem Aspekt für die Crashsimulation, 2020
339	Stochastisches Bruchverhalten von Glas, 2020
340	Schnelle, breitbandige Datenübertragung zwischen Truck und Trailer als Voraussetzung für das hochautomatisierte Fahren von Lastzügen, 2021
341	Wasserstoffkompatibilität von Aluminium-Legierungen für Brennstoffzellenfahrzeuge, 2021
342	Anforderungen an eine elektrische Lade- und Wasserstoffinfrastruktur für gewerbliche Nutzfahrzeuge mit dem Zeithorizont 2030, 2021
343	Objective assessment of database quality for use in the automotive research and development process, 2021
344	Review of non-exhaust particle emissions from road vehicles, 2021
345	Ganzheitliche Betrachtung von Rollwiderstandsverlusten an einem schweren Sattelzug unter realen Umgebungsbedingungen, 2021
346	Studie zur Abschätzung der Anwendungspotentiale, Risiken und notwendigen Forschungsbedarfe bei der Verwendung von Glashohlkugeln in Kombination mit thermoplastischem Schaumspritzguss, 2021

347 Typgenehmigungsanforderungen an Level-3-Autobahnsysteme - Hintergrundbetrachtungen zu technischen Anforderungen für eine automatisierte Fahrfunktion, 2021

348 Einfluss der Kantenbearbeitung von Aluminiumblechen auf das Restumformvermögen sowie die Festigkeitseigenschaften unter quasistatischer und schwingender Beanspruchung, 2021

349 Verstärkung dünner formgehärteter Bauteile mittels FVK-Verrippungen, 2021

350 HMI Anforderungen für den automatisierten Individualverkehr unter Berücksichtigung von Leistungsmöglichkeiten und -grenzen älterer Nutzer, 2021

351 Compatibility of polymers for fuel cell automobiles, 2021

352 Entwicklung einer gewichtsoptimierten Batteriegehäusestruktur für Volumenfahrzeuge, 2021

353 Charakterisierung und Modellierung des Deformations- und Versagensverhaltens von nicht-faserverstärkten Thermoplasten unter mehrachsiger Crashbelastung, 2021

354 Untersuchung zum thermischen Komfort im Pkw für den Grenzbereich des Luftzugempfindens, 2021

355 Anforderungen an die Güte, Verfügbarkeit und Vorausschau einer Reibwertschätzung aus Funktionssicht, 2021

356 Entwicklung einer standardisierten Prüfanordnung zur Bewertung der Übernahmeleistung beim automatisierten Fahren, 2022

357 Vorstudie zu Verkehrsemissionen - Räumlich und zeitlich aufgelöste Daten durch Schwarmmessungen, 2022

358 Produktivitätssteigerung und Kostensenkung der laser-additiven Fertigung für den Automobilbau, 2022

359 Analyse der Einflussfaktoren auf die Abweichung zwischen CFD und Fahrversuch bei der Bestimmung des Luftwiderstands von Nutzfahrzeugen mit Fokus auf den Ventilationswiderstand von Nfz-Rädern, 2022

360 Werkstoffmodelle und Kennwertermittlung für die industrielle Anwendung der Umform- und Crash-Simulation unter Berücksichtigung der thermischen Behandlungen beim Lackieren im Prozess bei hochfesten Werkstoffen, 2022

361 Compatibility of polymers for fuel cell automobiles, 2022

362 Ermüdung kurzfaserverstärkter thermoplastischer Polymerkwerkstoffe, 2022

363 Market research and definition of procedure to comparison of comfort measuring systems for a vehicle cabin, 2022

364 Methodische Ansätze zur Auswahl von Bordnetzstrukturen mit erhöhten Zuverlässigkeitsanforderungen, 2022

365 Fahrwiderstand von Lenk- und Liftachsen in Kurven und auf gerader Strecke unter realen Umgebungsbedingungen, 2022

366 Klimadaten und Nutzungsverhalten zu Auslegung, Versuch und Simulation an Kraftfahrzeug-Kälte-/ Heizanlagen, 2022

367 Experimentelle und numerische Untersuchung des selbsttätigen Losdrehens von Schraubenverbindungen mit konstanten und variablen Amplituden und Entwicklung einer Bewertungsmethode, 2022

368 Objective assessment of database quality for use in the automotive research and development process – Part 2, 2023

369 Level 2 hands-off – Recommendations and guidance, 2023

370 Funktionale Sicherheitsbewertung und Cybersecurity Analysen relevanter Use Cases für die Datenübertragung zwischen Truck und Trailer als Voraussetzungfür das hochautomatisierte Fahren von Lastzügen, 2023

371 Study on the technical evaluation of decentralization based de-identification procedures for personal data in the automotive sector, 2023

372 Legal evaluation of decentralization based de-identification procedures for personal and non-personal data in the automotive sector, 2023

373 Quantifizierung der mechanischen Belastbarkeit von Infrarot-Schweißverbindungen in zyklisch belasteten Thermoplast-Bauteilen, 2023

374 Lebensdauerbewertung von geschweißten Verbindungselementen unter Montagevorspannung, 2023

375 Einfluss verschiedener Scherschneidparameter auf die elektro-magnetischen Eigenschaften von NO-Elektroblech automobiler Traktionsantriebe, 2023

376 Automatisierte Demontage von Traktionsmotoren der E-Mobilität - Eine Studie zur Optimierung der Demontage, 2023

377 Untersuchungen zum Einfluss von feuchtem Wasserstoff auf die Spannungsrisskorrosionsempfindlichkeit von Aluminium-Legierungen für den Einsatz in Brennstoffzellenfahrzeugen, 2024

378 Diagnosekonzepte für zonale und teilredundante Bordnetzarchitekturen, 2024

379 Dynamische Erfassung und Beurteilung von Situationsbewusstsein im Kontext des automatisierten Fahrens, 2024

Impressum

Herausgeber	FAT Forschungsvereinigung Automobiltechnik e.V. Behrenstraße 35 10117 Berlin Telefon +49 30 897842-0 Fax +49 30 897842-600 www.vda-fat.de
ISSN	2192-7863

Verband der Automobilindustrie e.V. (VDA)
Behrenstraße 35, 10117 Berlin
www.vda.de
Twitter @VDA_online

Forschungsvereinigung Automobiltechnik e.V. (FAT)
Behrenstraße 35, 10117 Berlin
www.vda.de/fat

VDA | Verband der Automobilindustrie

FAT | Forschungsvereinigung Automobiltechnik